NASA TECHNICAL MEMORANDUM

NASA TM X-62,359

NASA TM X-62,359

A PRIMER IN LUNAR GEOLOGY

Edited by

Ronald Greeley
University of Santa Clara
Santa Clara, California 95053

and

Peter Schultz
Space Science Division
Ames Research Center
Moffett Field, California 94035

July 1974

FOREWORD

This "primer" is a collection of papers and reference material that was assembled for a short course in Lunar Geology conducted in April, 1974 by the University of Santa Clara at Ames Research Center, NASA, and sponsored through a grant from NASA Headquarters. The objective of the short course was to provide a foundation in lunar geology for earth-science community college instructors.

After the course, our colleagues encouraged us to put the material into a form that would be more widely available, hence, the present document. As was the case for the notebook from which this document was taken, our objective is to provide short summaries, selected illustrations, and pertinent reprinted articles dealing with primary topics in lunar geology so that the reader can more easily become familiar with the subject.

Some of the material that was in the original notebook could not be included here (maps, pamphlets, etc.). In order to make this reference complete, we suggest that the additional material be obtained, using the forms in the back.

We hope that you find the material useful and we would sincerely appreciate your comments and suggestions for its improvement.

CONTENTS

INTRODUCTION

In 1973, NASA initiated a new effort entitled "Lunar Data Analysis and Synthesis Program." The goal of this program is to derive the maximum benefit from the vast quantities of lunar data that have been collected during the preceding 15 years. Recognizing that education and information exchange is an integral part of any scientific endeavor, the Synthesis Program encourages efforts to transfer data from the lunar scientist to professionals who are not directly connected with the lunar program. Because community colleges are an important part of the educational system in most states, and California in particular, we believe that this segment of the geological community should be the first to participate in lunar geology programs.

Our intent is to provide intensive instruction in the basic concepts of lunar and planetary geology. We are particularly fortunate here in the Bay Area to conduct this course because we can draw on the expertise of NASA–Ames Research Center and the Astrogeology Branch of the U. S. Geological Survey. Many of the speakers on the program laid the foundations for planetology in the early years of modern lunar study. Although there will be a great deal of information presented, we have tried to organize the schedule to permit adequate time for discussions with each speaker.

Our hope is that you will be stimulated and motivated to the point that you will take positive means for incorporating planetology into your own Earth-Science curriculum. From the applications that you submitted, we know that you are motivated in that direction. Many of you already teach planetology in one form or another. Our task is to put the information in your hands in a way that it can be most easily assimilated, i.e., through presentations, lab exercises, and this notebook.

You will find that most of lunar and planetary geology is simply the application of basic geological concepts to the solution of the geology of other planets. The most severe constraint, of course, is the limit on field checking! More generally, a planetologist is simply an Earth scientist who draws together the fields of physics, chemistry, geology, astronomy, and meteorology in order to understand other planets. Thus, in terms of instruction, you simply take "field trips" to planets and re-ask familiar questions. It should be remembered that the various space missions have not provided answers to all problems in planetology, although the questions asked now are more detailed, more specific, and more sophisticated.

As teachers with different specialized interests, we sometimes rely on only a few articles, or review papers in order to understand new concepts, some of which may seem like gospel but are actually professional opinion. Survey topics such as planetology are particularly vulnerable to such over-simplification or dogmatism. As a result, the process of scientific inquiry, particularly in the classroom, may be lost. Yet, planetology is a relatively new field, and many of the fundamental questions being asked are still understandable to the student. Consequently, a planetology course can be a potentially valuable means to explore through student participation the interplay of opinion, fact, and scientific inquiry.

We want this notebook to be a source of information that will grow with your interests. Its organization follows the lecture sequence. Each section consists of several parts: 1) a synopsis of the speakers' presentation, 2) supplemental illustrations, and 3) supplemental references (review articles, where possible). In the pockets are additional references and resource material. We

recognize the danger of using loose leaf notebooks (too often the notebook is "cannibalized" for other uses), but we believe that you will want to expand it by adding references and material as your interests in the field develop.

Although it would have been easy to double or triple the number of participants, we want to keep a "workshop" atmosphere. Please ask questions and enter the discussions. We are particularly interested in your comments and suggestions for improving the short course, and we would like very much to hear from you after you return home.

Ronald Greeley
University of Santa Clara
and
Peter Schultz
Space Science Division
NASA–Ames Research Center

CHAPTER 1 – DATA ACQUISITION

Sources of Lunar Geological Data – *R. Greeley*

SOURCES OF LUNAR GEOLOGICAL DATA

Ronald Greeley
University of Santa Clara, Santa Clara, Calif. 95053
and
Ames Research Center, NASA, Moffett Field, Calif. 94035

I. INTRODUCTION

Geologic data for the Moon are derived from three general sources: (1) Earth-based observations, (2) remote-sensing by unmanned spacecraft, and (3) collection of data by manned lunar missions. The types of data include photographs, infrared and other "invisible spectrum" data, geophysical data from seismometers, etc., rock samples, and visual observations.

II. EARTH-BASED DATA

Prior to the introduction of lunar exploration in the mid 1960s, lunar geologic data consisted almost entirely of photographs and telescopic observations. Many rather detailed investigations were completed during this period, including geologic studies, resulting in the publication of several classic references [Fielder (1961, 1965), Baldwin (1963) and Kopal (1966) and others]. Most of the studies concerned the structure and origin of major lunar surface features, with an emphasis on craters. It is a tribute to these workers that many of their early ideas are still generally accepted, although the ordering of importance for some has changed.

In the early sixties, an ambitious photographic and cartographic program was initiated by the Defense Department that resulted in the compilation of an excellent lunar atlas (Kuiper 1960), and the LAC (Lunar Aeronautical Chart) series of 1:1,000,000 scale relief maps. These maps provided the base for the U. S. Geological Survey lunar geologic maps, compiled from observatory photographs and telescopic observations.

In addition to photographic and visual observations, Earth-based geologic data include infrared measurements of lunar thermal properties, radar data on surface properties, polarization, spectral analyses, surface roughness derived from radar scattering, and photometric data on the reflective properties of the lunar surface.

When the decision was made to send Man to the Moon, it became obvious that more detailed information was required than could be obtained from Earth-based sources. Thus, a series of unmanned lunar probes was initiated, including *Ranger*, *Surveyor*, and *Lunar Orbiter* missions. Concurrently, unmanned Soviet spacecraft of the *Luna* series provided additional data, including the first views of the lunar farside.

III. UNMANNED LUNAR MISSIONS

A. *Ranger Spacecraft*

On July 31, 1964, Ranger VII provided the first close-up images of the Moon by successfully "hard landing" on the Moon in Oceanus Procellarum. The next year Rangers VIII and IX were successfully launched, "hard landing" in southwestern Mare Tranquillitatis and on the floor of the crater Alphonsus, respectively.

Ranger spacecrafts were aimed directly at the Moon and carried batteries of television cameras to image the lunar surface at close range before crash landing. Lunar features as small as one meter could be clearly seen. One of the most obvious new geologic facts obtained by *Ranger* was that craters of all sizes (down to the limit of camera resolution) are the dominant lunar surface feature. On the assumption (now strongly supported by different lines of research) that most craters are of impact origin, the lunar surface was interpreted to be fragmental ("impact gardened") to a depth of at least several meters. Geologic maps showing volcanic features were also made from Ranger imagery.

B. *Surveyor Spacecraft*

Unlike *Ranger*, the unmanned *Surveyor* spacecraft was designed to soft-land on the lunar surface. All *Surveyors* carried television cameras to take stereoscopic images of small-scale lunar features, and some *Surveyors* had the capability to dig into the lunar soil to determine the bearing-strength of the surface, to make simplified chemical analyses of the soil, and to determine lunar surface temperatures.

From June 1966 to January 1968, five (of seven launched) *Surveyors* soft-landed on the Moon, each operating for a period of 1 to 8 lunar days. Four landed in mare areas, and the last, *Surveyor VII*, landed in the extremely rugged southern highlands on the rim of crater Tycho. At all landing sites, impact craters were observed down to the limit of camera resolution ($<$ cm). One of the most significant geological results of *Surveyor* was the determination that lunar maria are composed of basaltic rocks.

C. *Lunar Orbiter*

Lunar Orbiter missions consisted of five unmanned spacecraft placed in orbit around the Moon. Each had the primary objective of obtaining high-resolution photographs. The first three missions were in equatorial orbit and photographed mostly small areas of the mare which were potential Apollo landing sites. *Lunar Orbiter IV* was placed in polar orbit and obtained continuous photography for nearly all of the lunar surface, mostly under constant lighting conditions. *Lunar Orbiter V* was similarly placed in a polar orbit and photographed selected features of geologic interest.

The photographic system of *Lunar Orbiter* was a unique combination of two cameras (one wide angle, the other telephoto), a processing system that developed Kodak Bimat film on board

the spacecraft (Lunar Orbiter has been called a "Flying Drugstore"), an electronic system that scanned the processed film to convert the image to an electronic signal, and a transmitter to return the signal to Earth. The signals were picked up at one of three stations: Goldstone, California; Madrid, Spain; or Woomera, Australia; and placed on tape. At NASA-Langley Research Center, the tapes were played to convert the signals back to images and then placed on strips of 35 mm film. It is easy to recognize Lunar Orbiter pictures by the strips which make up the image.

Lunar Orbiter provided a tremendous wealth of geologic data that was essential to the successful manned landing and which continues to be a source for geologic studies.

IV. MANNED MISSIONS

A. *Apollo 8 and 10*

Apollo missions ushered in a new era of lunar data collection. *Apollo 8* (1968, first manned mission to the Moon) and *Apollo 10* (1969) were non-landing missions to the Moon, with the primary function of conducting spacecraft engineering tests prior to manned landings. In addition, *Apollos 8* and *10* carried cameras to derive critical information on:

1) "Approach" topography and landmarks for the early Apollo landings.

2) The scientific merit and the roughness of areas for possible follow-on Apollo landings.

3) The broad structure and characteristics of the lunar surface.

Apollos 8 and *10* obtained hundreds of Hasselblad frames (70 mm) in color and black and white, and hundreds of feet of motion picture film. Unlike the unmanned lunar missions which returned imagery via electronic signals, Apollo missions returned hard film that permitted detailed analyses not otherwise possible, such as refined topographic derivations and detection of geologic color units.

In addition, the observations of Apollo astronauts trained in geology provided data on many structures and lunar surface characteristics that were too subtle to be detected or recorded by film.

B. *Apollo 11, 12, 14*

The summer of 1969 marked one of Man's greatest achievements with his landing on the lunar surface. And for the first time, *lunar fieldwork* was possible. The primary objectives of *Apollos* 11, 12, 14 (Apollo 13 was aborted prior to landing because of spacecraft failure) were engineering feats; however, astronaut observations, sample collections, and various instruments provided vast quantities of lunar data, much of which are still being analyzed and reduced. In addition, each mission became increasingly complex and returned greater quantities of samples and data than each preceding mission.

Although most of the attention seems to go to the Apollo *landings* it must be remembered that the Apollo missions were two-part: lander and *orbiter*. The service-command module and its pilot remained in lunar orbit during the landing phase and conducted a series of important missions. During *Apollos 11, 12,* and *14*, these missions included obtaining additional Hasselblad photography and motion pictures. *Apollo 14* carried a sophisticated camera designed to obtain photogrammetric-quality photography of the lunar surface. Unfortunately, it malfunctioned early in the mission and obtained only a fraction of the imagery originally planned.

C. *Apollo 15, 16, 17*

The last three Apollo missions, termed "J" missions, carried extensive and complex instruments for both the lander and orbital phases. The addition of the *Lunar Rover* gave the astronauts mobility and permitted them to cover a much larger field area than was previously possible. Spacecraft components were thoroughly proven by *Apollos 11, 12,* and *14*, and much more attention was given to lunar scientific objectives during the "J" missions.

In addition to hand-held Hasselblad photography, "J" mission service modules obtained high quality photography with a mapping camera system and a panoramic camera system. The mapping, or metric camera (76 mm, or 3-inch lens) combined 20-m resolution terrain photography on 5-inch film with stellar camera imagery which photographed the star field in order to precisely fix the lunar scene. With a 74° square field of view, each metric frame covers about 170 km × 170 km from the nominal 111.5 km spacecraft altitude.

The panoramic cameras had 610 mm (24 inch) lenses producing either monoscopic or stereoscopic photographs of the lunar surface at a maximum ground resolution of 2 m. Each frame covered an 11° field of view along track and 108° cross track, or an area about 28 km × 334 km at nominal spacecraft altitude. The lunar surface was photographed under a wide variety of lighting conditions by both metric and panoramic cameras. Laser altimetry provided topographic profiles of the lunar surface which could be directly correlated with the photography.

Other instruments that gathered geological data from the orbiting command module included the Gamma-Ray Spectrometer, the X-ray fluorescence spectrometer, the alpha-particle spectrometer, and mass spectrometer, all to obtain chemical and geochemical data for the lunar surface. On *Apollo 16*, a bistatic radar instrument determined the electromagnetic characteristics and regolith properties of the lunar surface by directing various electromagnetic waves (radio, etc.) from orbit to the lunar surface where they were reflected back to Earth and analyzed.

Among other experiments, *Apollo 17* carried a Lunar Sounder (radar device capable of providing data on subsurface characteristics, e.g., layers of rock) and an Infrared Scanning Radiometer which measured thermal characteristics of the lunar surface.

The various types of instruments and experiments conducted during Apollo missions are described in table I.

TABLE I.

Apollo orbital science experiments	Apollo missions					
	11	12	14	15	16	17
Service module experiments						
S-160 Gamma-ray Spectrometer				X	X	
S-161 X-ray Spectrometer				X	X	
S-162 Alpha-particle Spectrometer				X	X	
S-164 S-band Transponder (CSM/LM)			X	X	X	X
S-165 Mass Spectrometer				X	X	
S-169 Far UV Spectrometer						X
S-170 Bistatic Radar			X	X	X	
S-171 IR Scanning Radiometer						X
S-209 Lunar Sounder						X
Subsatellite:						
S-164 S-band Transponder				X	X	
S-173 Particle Measurement				X	X	
S-174 Magnetometer				X	X	
SM photographic tasks:						
24 in. Panoramic Camera				X	X	X
3 in. Mapping Camera				X	X	X
Laser Altimeter				X	X	X
Command module experiments						
S-158 Multispectral Photography		X				
S-176 Apollo Window Meteoroid			X	X	X	X
S-177 UV Photography of Earth and Moon			X	X		
S-178 Gegenschein from Lunar Orbit		X	X	X		

TABLE I. – Concluded

Apollo surface science experiments	Apollo missions					
	11	12	14	15	16	17
ALSEP experiments						
S-031 Lunar Passive Seismology	X	X	X	X	X	
S-033 Lunar Active Seismology			X		X	
S-034 Lunar Tri-axis Magnetometer		X		X	X	
S-035 Solar Wind Spectrometer		X		X		
S-036 Suprathermal Ion Detector		X	X	X		
S-037 Lunar Heat Flow				X	X	X
S-038 Charged Particle Lunar Environment			X			
S-058 Cold Cathode Gauge		X	X	X		
S-202 Lunar Ejecta and Meteorites						X
S-203 Lunar Seismic Profiling						X
S-205 Lunar Atmospheric Composition						X
S-207 Lunar Surface Gravimeter						X
M-515 Lunar Dust Detector	X	X	X	X		
Other experiments						
S-059 Lunar Geology Investigation	X	X	X	X	X	X
S-078 Laser Ranging Retro-reflector	X		X	X		
S-080 Solar Wind Composition	X	X	X	X	X	
S-151 Cosmic Ray Detector (Helmet)	X					
S-152 Cosmic Ray Detector (Sheets)					X	
S-184 Lunar Surface Close-up Camera	X	X	X			
S-198 Portable Magnetometer			X		X	
S-199 Lunar Gravity Traverse						X
S-200 Soil Mechanics			X	X	X	X
S-201 Far UV Camera/Spectroscope					X	
S-204 Surface Electrical Properties						X

V. APOLLO SURFACE EXPERIMENTS

With increasing complexity, each Apollo landing set up an array of experiments on the lunar surface. Major instruments of geological interest are described below, numbers in parenthesis show Apollo missions carrying that particular instrument.

1. *Lunar Surface Magnetometer* (12, 15, 16): Designed to measure the Moon's magnetic field, which was found to be about 1/1000 as strong as Earth's magnetic field.

2. *Solar Wind Spectrometer* (12, 15): To measure the velocity, direction, and temperature of the "solar wind" (charged particles) streaming from the Sun.

3. *Suprathermal Ion Detector* (12, 14, 15): Determined the rate of ion production by the Moon's tenuous atmosphere.

4. *Cold Cathode Ion Detector* (12, 14, 15): Measured the changing density of the Moon's atmosphere.

5. *Seismic Experiments*

   A. *Passive Seismometry* (11, 12, 13, 14, 15, 16): recorded meteoritic (and spacecraft) impacts and moonquakes.

   B. *Active Seismometry* (14, 16): recorded artificial seismic events produced by grenade-like charges.

6. *Heat-Flow Experiment* (15, 16, 17): Probes placed in short bore holes measured outward heat-flow from the lunar interior. Heat flow was found to be quite high on 15 and 17 (instrument was inoperative on 16).

7. *Lunar Surface Gravimeter* (17): Determined the Moon's gravity field.

8. *Lunar Ejecta on Meteorites Experiment* (17): Determined the flux of meteoric material and the speed, direction, and mass of incoming particles.

Other experiments, many of which provided geological data, are shown in the accompanying table.

VI. APOLLO LUNAR GEOLOGY INVESTIGATIONS

The geology investigation was an integral part of all six Apollo missions. Its fundamental objective was to provide detailed geologic data in the vicinity of each landing site and to provide a "ground truth station" for the interpretation of the orbital data and of Earth-based data.

Prior to each mission, a team of geologists carefully analyzed all available data for the prospective landing site and prepared preliminary geologic reports. Concurrently, the astronauts received geological training, especially oriented for the prospective site.

Primary data for the lunar geology investigation came from Hasselblad photographs, astronaut observations, and returned lunar samples. Besides providing basic data, surface photographs documented the setting for the returned samples and were helpful during post-mission astronaut debriefings.

Sampling programs were designed to gather representative suites of lunar material, including soils, *in situ* rock, material from particular features (e.g., craters), drive-tube cores from the subsurface, etc.

During mission operations, the geology team monitored the activities of the astronauts in order to make suggestions and "real time" decisions.

After each mission, the task of reducing the tremendous quantity of data by the geology team had to reach at least a preliminary stage before the next mission. Consequently, much important data had to be left for later analysis and remain today as a vast potential source of geologic interpretation. Recognizing that *collection* of data is only the first half of any scientific endeavor, in 1973, NASA established the "Lunar Data Analysis and Synthesis" program to provide support to scientists so that maximum information can be derived from lunar data.

CHAPTER II – SOLAR SYSTEM

Formation of the Solar System – *D. Black*

Symposium on the Origin of the Solar System, Nice 1972 (Selected reprints)

Origin of the Solar System: Review of Concepts and Theories – *W. H. McCrea*

Presentation of the Models – *H. Reeves*

FORMATION OF THE SOLAR SYSTEM

David Black
Ames Research Center, NASA, Moffett Field, Calif. 94035

I. INTRODUCTION

Although the primary thrust of this lecture series is directed at the subject of lunar geology, that is the physical and chemical processes that have acted to alter the Moon from its original to its present state, it must be remembered that the Moon is a member of that collection of objects we call the Solar System. As such, an understanding of its geological history is of significance in understanding at least part of the story of the formation and evolution of the Solar System.

As subsequent lectures in this series deal with various aspects of lunar geology in detail, we shall be concerned here with a general examination of how the sun and planets may have formed, a brief consideration of the three general hypotheses for the origin of the Moon and conclude with one man's view of a likely overall scenario within which to discuss lunar geology.

II. FORMATION OF THE SUN AND THE PRIMITIVE SOLAR NEBULA

A. *Observational Evidence*

Two important and apparently general characteristics of star formation can be determined from present observational data. The first of these is that young stars are almost always found in close proximity to fairly dense clouds of gas and dust. How do we know that the stars are young? The stars in question are O and B stars, very bright and much more massive than our sun. It is well known that the more massive a star the faster it uses up its nuclear fuel and hence the faster it evolves. O and B stars "live" for 10^8 years, which is a short time astrophysically speaking. Thus the association of young stars and gas clouds is well established. This close association between young stars and dusty gas clouds strongly suggests that the stars formed from such clouds. The second piece of observational datum is that stars tend to occur in groups or clusters ranging from a few tens of stars to a few hundred. There are, of course, stars which are not presently associated with a group, but these are generally older stars which were part of a group that has gradually dispersed. These observations give rise to the general feeling that star formation initiates in gas and dust clouds, and that these clouds are fairly massive (perhaps as large as 1000 times the mass of the sun).

The conceptual framework for star formation is roughly the following. A massive gas cloud (interstellar cloud) becomes unstable to gravitational collapse; that is, the self gravity of the cloud is greater than its internal pressure. As the cloud collapses and increases its density, there will be fluctuations in density throughout the cloud. Many of these will simply be smoothed out, but some will continue to grow and attract neighboring material. These growing fluctuations, generally called fragments, are the starting points for the formation of stars. This picture is *qualitatively* consistent

with the observations, but too little is known at present of the detailed physics of the process to allow *quantitative* work.

B *Collapse of a $1M_\odot$ Fragment*

We will assume that the outline indicated above is correct, and use as the starting point of our discussion a $1M_\odot$ "fragment" which is collapsing under the influence of its own gravity. In general, calculations have assumed that such a fragment may be treated in isolation, ignoring possible interactions with neighboring fragments in the cloud. It should be added parenthetically that Dormand and Woolfson (1971) have recently suggested that such interactions are instrumental in forming the solar nebula. This revised version of a "catastrophic" theory for the formation of the solar nebula, while interesting, has not provided any quantitative results and so will be ignored for our purposes.

The first detailed attempts at computing the collapse behavior of a $1M_\odot$ fragment were done by Hayashi (1965) and co-workers in the early and mid 1960's. They assumed that the cloud was not rotating and ignored magnetic fields. Their work indicated that at some time early in its history the sun was perhaps 1000 times as luminous as it is now. This high luminosity phase is generally referred to as the "Hayashi Phase." If such a phase occurred, temperatures in the solar nebula would have been about 5 times higher than they are presently (i.e., ~2000° K at 1 A.U. as compared to ~400° K at 1 A.U. presently). Thus, any dust grains present in the nebula would be vaporized.

Subsequently, Larson (1969) has re-examined the problem and finds that Hayashi's choice of initial conditions for his calculations greatly affected his results. Using more realistic initial conditions, Larson found that the sun would *not* have gone through a high luminosity phase, and temperatures in the primitive solar nebula would have been only 2 to 3 times higher than the present values. Thus, one would expect some of the primitive dust grains to have survived (i.e., not vaporized) the formation of the Solar System. We shall return to this point later in a discussion of planet formation. As did Hayashi, Larson did not include rotation in the dynamics of the collapse. However, stars do rotate and the planets fortunately are rotating around the sun, so a realistic calculation must include the dynamical consequences of rotation.

Larson (1972) has attempted to calculate the dynamical evolution of the collapse of a rotating fragment. He was limited by available computer power to a rather coarse numerical representation of the collapse. More recently, Black and Bodenheimer (1974) have studied the problem in greater detail. One rather surprising result is that with the values of angular momentum thought to be characteristic of interstellar clouds, the fragment does not form a star! Instead, it forms a ring or toroidal configuration. The subsequent fate of this material is poorly understood, but it seems reasonable that such a configuration would be highly unstable to perturbations, and would break up into discrete blobs rotating around the common center of mass. This behavior is qualitatively consistent with binary or multiple star systems if these blobs eventually form stars. As most stars (at least 70 percent) are in multiple star systems, this result is not immediately at variance with observation. Larson has argued that single stars, such as the sun, are formed originally as part of a multiple star system and then ejected from such a system. However, if this were a correct description for the origin of the sun, it is very difficult to see how a planetary system could survive the ejection process. A more fruitful approach would seem to be in assuming that certain cloud fragments have less angular momentum than others and that these fragments are the ones that form

single stars (and planetary systems?). Even then, there are several interesting and difficult problems, which are subjects of current research. It may safely be said that we are a long way from an adequate theoretical understanding of how single, rotating stars and their nebulae are formed.

In spite of these difficulties, certain general features have emerged which afford a relatively crude estimate of some of the general characteristics of the primitive solar nebula. As is well known, the terrestrial planets are strongly depleted in volatile elements, most noticeably hydrogen and helium, when compared to the outer planets. If we argue that these planets formed from a mixture which originally had their elements in "solar" abundance ratios, we can estimate a minimum mass for the primitive solar nebula. Such an estimate appears in table I. It must be kept in mind that this is a lower limit to the mass because of the implicit assumption of 100 percent efficiency in accretion of the nonvolatile elements (table I from "Earth, Moon and Planets," Whipple).

TABLE I.

Bodies	Present mass (Earth = 1)	Factor	Original minimum mass (Sun = 1)
Terrestrial	2	400	0.002
Jupiter	318	11	.011
Saturn	95	36	.010
Uranus and Neptune	32	80	.008
Comets	1	8,000?	.024?
Total minimum original mass			0.055?

It would seem reasonable then that the solar nebula was around a few tenths of the mass of the sun.

In addition to the mass estimate discussed above, we also have theoretical and experimental evidence that some interstellar dust grains present in the solar fragment survived the formation of the Solar System. Theoretical evidence suggests that the temperature around a $1M_{\odot}$ star would only vaporize dust for distances of ~0.5 A.U. and closer, not in the region of the Earth or asteroids. Experimentally, Black (1972) measured neon isotopic compositions in carbonaceous meteorites and observed a composition which he tentatively identified as being extra-solar. Subsequently, Clayton and co-workers have measured oxygen isotopic ratios in carbonaceous meteorites which differ from any others ever measured, and which Clayton *et al.* (1973) are attributing to a distinct nuclear composition in unvaporized dust grains. In summary, the available data and theory suggest that the primitive nebula was reasonably cool and that most of the highly refractory elements were never in the gas phase.

Finally, we do have some experimental information concerning time scales in the early Solar System. As the techniques involved are of general interest and are relevant to selenology, we shall discuss these in more detail later.

III. FORMATION OF SOLID BODIES IN THE SOLAR SYSTEM

The question of how solid bodies (planets, comets, asteroids, etc.) formed in the early Solar System is as hotly debated as the question of how stars form. We will attempt to indicate the major schools of thought and inherent difficulties.

A. *Condensation Models*

The type of planetary formation model considered here is one where a fairly massive (~ mass of Jupiter) region of the solar nebula isolates itself gravitationally in a manner similar to the fragments in interstellar clouds. Such models are similar to the "proto planet" hypothesis of Kuiper. It is suggested that dust in these protoplanets will settle and form a rocky core, and that terrestrial planets formed from protoplanets which lost their gaseous atmospheres due to tidal effects from the sun. Several difficulties exist with such models, but two are of interest. It is difficult to have the fragmentation occur for such small masses. The temperatures in the primitive solar nebula would have had to be very cool indeed, a few tens of degrees Kelvin. Also, and more importantly, the formation period of the Earth, Moon, etc. would have been one of few impacts by external objects. This is not consistent with even casual observation.

B. *Accretion Models*

Most workers now feel that planets are formed by the process of accretion. Dust grains in the nebula collide and stick, forming a single massive particle. As this process continues, one expects a distribution in mass, with most of the particles being small, and progressively less particles with increasing mass. Eventually, one or two of the "particles" will be large enough to gravitationally capture objects, and not have to rely on direct impacts. This situation is unstable in the sense that bigger objects grow faster than small ones, so soon there are just a few major sized bodies surrounded by a hierarchy of bodies of various sizes. Most of the mass is contained in the few large bodies. One problem with accretion is that it is fairly slow, and one must rely on phenomena which shall not be discussed here to speed things up. Such models do provide ideal conditions for intense surface bombardment activity for the planets, a point in their favor.

IV. SOME COMMENTS ON DATING SCHEMES AND WHAT THEY MEASURE

As we remarked above, there are data which permit us to place some constraints on time scales for various processes. We will not consider here the dating of materials by measuring spallation products (cosmic ray ages), but concern ourselves with time intervals inferred from radioactive decay schemes.

Radioactive dating falls into two categories, each telling us something different about the samples studied. These two categories are (1) those where the parent nuclide is extinct in the solar system (^{129}I, ^{244}Pu) and (2) those where the parent nuclide is extant in the Solar System (^{40}K, ^{87}Rb, ^{235,238}U, ^{232}Th).

A. *Extinct Radioactivities*

The two most prominent dating schemes here are (1) the decay of ^{129}I to ^{129}Xe bv beta emission, and (2) spontaneous fission of ^{244}Pu to $^{136,134,132,131}Xe$. Both ^{129}I and ^{244}Pu are thought to be synthesized in supernovae, and once formed decay with half-lives of 17 myr and 82 myr, respectively.

Both decay schemes have isotopes of the rare gas xenon as daughter products. Measurements of the concentrations of these daughter products tell how much of the parent nuclides was present at the time the samples quantitatively retained the rare gas. Inferred ratios of $^{129}I/^{127}I$ at the time meteorites were cool enough to retain ^{129}Xe are $\sim 10^{-4}$. Knowing the half-life, and assuming an initial produced ratio in supernovae, one can calculate the time interval from the last addition of nucleosynthetic material into the Solar System until these meteorites cooled sufficiently to retain Xe. This time interval is about 10^8 yrs. Similar values are found from the $^{244}Pu - Xe$ dating scheme. There are ambiguities in how this number is to be interpreted. If the ^{129}I was added when the interstellar cloud collapsed, it means that meteorites did not form until long after the collapse was finished, because the collapse takes only about 10^6 years. On the other hand, the ^{129}I may have been added when the cloud moved through one spiral arm in our galaxy, and the collapse of the cloud did not occur until the cloud ran into the next spiral arm. The time for transit between arms is $\sim 10^8$ yrs, so one cannot say anything about whether meteorites formed quickly or slowly.

Additional work with ^{129}I dating has shown that the small spread in $^{129}I/^{127}I$ ratios at the time the meteorites were cool enough to retain xenon implies that the various meteorites all cooled to the same temperature within about $10^6 - 10^7$ years of one another.

In summary, extinct radioactivities tell us about time intervals from nucleosynthesis until meteorite (lunar?) formation. They do not say anything about how long ago meteorite formation occurred.

B. *Extant Radioactivities*

This group nicely complements the previous one in that it provides information on the time interval between the present and a point in time when the samples were chemically equilibrated. The primary dating schemes in use here are K-Ar, Pb-Pb and Rb-Sr. Potassium-40 decays to form the rare gas isotope ^{40}Ar. Dates determined with this technique indicate the time in the past when the samples cooled sufficiently to begin retaining argon. Uranium 238 and 235 decay by emission of α-particles to form ^{206}Pb and ^{207}Pb, respectively. Again. this technique indicates the time when chemical equilibrium was established between U and Pb.

A particularly powerful scheme is that utilizing the decay of ^{87}Rb to ^{87}Sr. Recent developments in high precision mass spectroscopy and the lack of pronounced terrestrial contamination problems, have made Rb-Sr dating a powerful probe of events in the history of solar system objects.

Rb-Sr measurements shed light on two important aspects of lunar geology, namely (1) crystallization ages of rocks (chemical equilibrium of Rb and Sr) and (2) geochemical differentiation. A discussion of this technique is not proper for this brief outline, but I will try to indicate how the information is obtained.

Laboratory measurements give the *present* $^{87}Rb/^{86}Sr$ and $^{87}Sr/^{86}Sr$ ratios in the samples. If samples define a straight line when these two ratios are plotted, one learns two things. First, the intercept of the line, such lines are called isochrons, with the $^{87}Sr/^{86}Sr$ axis (i.e., $^{87}Rb/^{86}Sr = 0$) defines the *initial* $^{87}Sr/^{86}Sr$ ratio for these samples. Second, the slope of the isochron is given by $e^{\lambda T}-1$, where T is the age to be determined, λ is the decay parameter for ^{87}Rb, and $^{87}Sr/^{86}Sr$ is the ordinate (fig. 1). Knowing the slope and λ, one can easily determine T. In some samples, one finds that different minerals define separate isochrons. For example, in figure 2, rock fragments define an isochron with $T = 4.52 \times 10^9$ yr, while certain fragments of this rock define isochrons of 4.0×10^9 yrs; that is, they crystallized half a billion years later than the whole rock. Also, the initial $^{87}Sr/^{86}Sr$ ratios in the fragments are higher than the whole rock value, and more importantly, they are higher than what one would expect if the whole rock Rb/Sr ratio was characteristic of the material from which the fragments formed. Thus, the fragments formed from material enriched in Rb beyond the source material for the bulk of the rock. Thus, there was geochemical differentiation involved.

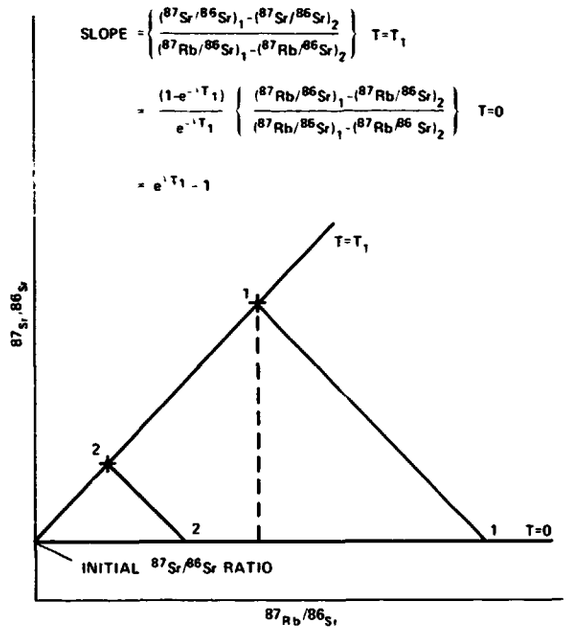

Figure 1.– Generalized Rb-Sr evolutionary diagram. Sample is characterized by a uniform $^{87}Sr/^{86}Sr$ ratio at time $T = 0$. As the ^{87}Rb decays to ^{87}Sr, it does so in direct proportion to the amount of ^{87}Rb present. At time $T = T_1$, the composition has evolved into the upper "isochron." The age, T_1, is related to the slope of the line as indicated by the equation.

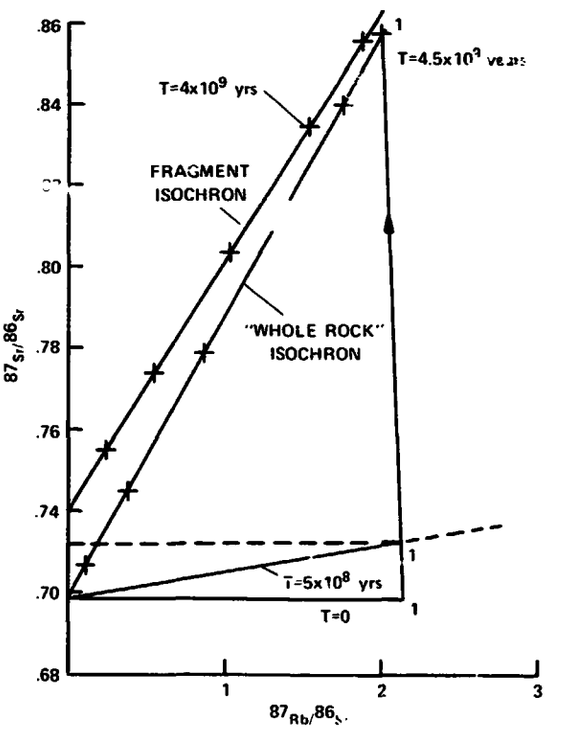

Figure 2.– Hypothetical Rb-Sr data show the types of information one can obtain from samples. It is supposed that the "whole rock" isochron was generated from the $T = 0$ system. The initial $^{87}Sr/^{86}Sr$ ratio for the 4.0 by fragment is higher than expected from 0.5 by evolution of the whole rock reservoir (dashed line), implying that the fragment came from a geochemically different reservoir than the whole rock sample.

This is not intended to be a comprehensive discussion, and hopefully these points will be more explicitly explained in the verbal presentation.

V. HYPOTHESIS FOR THE ORIGIN OF THE MOON

Perhaps the most enigmatic properties of the Moon (aside from its very existence!) are the differences in mean density and chemistry between the Moon and the Earth. Any viable hypothesis as to the origin of the Moon must account for these problems. Most hypotheses fall into one of three general categories: (1) the Moon formed when the primitive Earth fissioned due to rotation, (2) the Moon formed from a circum-terrestrial "nebula" by accretion and (3) the Moon formed at some different point in the Solar System and was captured by the Earth.

A. *Fission Hypotheses*

Most variants of this category argue that a hot, rapidly rotating young Earth underwent "fission" and separated into two pieces one of which was the Moon. The motivation behind such models is that if the fission did not occur until the Earth had its iron in a core, then the small fragment would contain primarily mantle material and would have a lower density than the Earth. The primary difficulties with such hypotheses are the large angular momentum required for the initial Earth and the orbital inclination of the Moon relative to the Earth's equator. Also, it is not clear that the details of lunar chemistry can be made compatible with a fission origin.

B. *Circum-Terrestrial Accumulation*

Again, there are several variants to be found on this hypothesis. Basically, the concept involves a swarm of bodies orbiting the Earth which eventually accreted to form the Moon. It is certainly likely that such an environment existed around the primitive Earth, but it does not seem to adequately address the compositional differences between the Earth and the Moon. If the circum-terrestrial bodies formed near the Earth, one would expect them to have iron in terrestrial abundance. Also, integrations of lunar orbits back in time indicate that it had an even higher orbital inclination in the past than it does now. This is hard to understand if the Moon formed entirely from this circum-terrestrial material.

C. *Capture Hypotheses*

Two principal variants of this school exist. One relies on gravitational capture of the Moon by the Earth, that is energy dissipation through tidal interaction only, and the second relies on collisional capture. Capture hypotheses offer natural explanations for the orbital inclination of the Moon and for differences in chemistry and density. If the Moon formed in a region of the Solar System other than that from which the Earth formed, one expects *a priori* that the compositions would be different. The major criticism of the capture hypothesis has been that it is very improbable. Such arguments should be given minimal weight.

If gravitational capture is considered, it appears to be difficult to dissipate energy sufficiently rapidly to bring about capture. Recent work by Kaula and Harris have shown that if one has a ring of material in orbit around the Earth, and if the mass of the ring is only ~1/600 that of the Moon, it could dissipate the energy of an incoming lunar mass object sufficiently to allow capture.

VI. ONE MAN'S VIEW

Here I wish to try and synthesize the preceding remarks into a working scenario within which subsequent discussions might be considered.

The available evidence strongly suggests that planets formed by accretion through a hierarchy of particle masses. The terminal stages for this process probably involved collisions between large bodies. The region of the Solar System which is known as the asteroid belt is one where for some reason this accretion process was not carried to completion and we see there a fossil example of the hierarchy in mass discussed above. The terminal phase of planetary formation was a hectic one in the sense that high velocity debris of varying sizes were moving from as far out as Jupiter into the region of the terrestrial planets. Most of the terrestrial planets were surrounded by swarms of smaller bodies during this terminal phase.

The Moon, or the bulk of it, was formed in a region of the Solar System different than that in which the Earth formed, and was captured upon close passage to the Earth as a consequence of a collision with circum-terrestrial material. Once captured, its surface was bombarded by particles in terrestrial orbit, as well as particles like the Moon which came from other regions of the Solar System.

It is very difficult to speculate on whether the duration of this bombardment phase for the Moon monitors the time evolution of particles near the Earth or bombarding particles within the Solar System generally. Additional evidence on the bombardment history of Mars and Mercury may well provide sufficient evidence to answer this question, and thereby shed light on an important time interval in the early history of the Solar System.

REFERENCES

Black, D. C.: On the origins of trapped helium, neon and argon isotopic variations in meteorites – I. Gas-rich meteorites, lunar soil and breccia. Geochim. Cosmochim. Acta, v. 36, p. 347, 1972.

Black, D. C.; and Bodenheimer, P.: The collapse of rotating interstellar clouds – I. Numerical techniques. Submitted to Ap. J., 1974.

Clayton, R. N.; Grossman, L.; and Mayeda, T. K.: A component of primitive nuclear composition in carbonaceous meteorites. Science, v. 182, p. 485, 1973.

Dormand, J. R.; and Woolfson, M. M.: The captive theory and planetary condensation. Mon. Not. R. Astr. Soc., v. 151, p. 307, 1971.

Hayashi, C.: Evolution of protostars. Ann. Rev. Ast. Astrophys., v. 4, p. 171, 1966.

Larson, R. B.: Numerical calculations of the dynamics of a collapsing protostar. Mon. Not. R. Astr. Soc., v. 145, p. 271, 1969.

Larson, R. B.: Collapse calculations and their implications for the formation of the solar system. In Proceedings of the Symposium on the Origin of the Solar System, (ed. H. Reeves), Nice, France, p. 142, 1972.

Whipple, F. L.: "Earth, Moon and Planets," 3rd Edition, Harvard University Press, Cambridge, 1971.

With permission, reprinted from Edition du Centre National de la Recherche Scientifique 15, Quai Anatole France, PARIS 75700, 1972, pp. 1–17, 28–53.

SYMPOSIUM SUR L'ORIGINE DU SYSTEME SOLAIRE.

SYMPOSIUM ON THE ORIGIN OF THE SOLAR SYSTEM.

- NICE -
3 - 7 Avril 1972

PRECEDING PAGE BLANK NOT FILMED

Edition du Centre National de la Recherche Scientifique
15, Quai Anatole France, PARIS 75700 -1972-.

Ce Symposium est un des Colloques du Centre National de la Recherche Scientifique (C. N. R. S.) :

Son organisation matérielle a été assurée par :

Melle Jeannette CARO,
(C. S. N. S. M., Orsay)

assistée pendant la durée du congrès par :

Mme Dominique MICHEL,
(Laboratoire de Minéralogie du Museum)

Melle Laure NICOULEAU,
(Accélérateur Linéaire, Orsay)

Melle Martine CADO.

La préparation des Comptes Rendus a été rendue possible grâce à l'aide de :

Melle Martine CADO.

Nous remercions en particulier Mr. Philippe DELACHE, Directeur de l'Observatoire de NICE pour l'aide qu'il nous a apportée.

Les Organisateurs : Robert KLAPISCH,
Paul PELLAS,
Hubert REEVES.

ORIGIN OF THE SOLAR SYSTEM

REVIEW OF CONCEPTS AND THEORIES

W.H. McCrea

Astronomy Centre
University of Sussex
Brighton BN1 9QH England

Abstract. A short outline is given of some of the main empirical features of the solar system. Cataclysmic theories of its origin are briefly mentioned. The general concept of a solar nebula is described. Accumulation theories of the formation of planets from the nebula are sketched with some critical comments. A proto-planet theory of the origin of planets and satellites is then considered. An attempt is made to place as much as possible of the work in a general setting and to call attention to a number of physical mechanisms that feature in one way or another in a number of theories.

Introduction

The dominant member of the Solar System is the Sun. However, the intention here is to consider largely the origin of the other members of the System and consider the origin of the Sun only so far as it elucidates, or is elucidated by, that of the rest.

Up to nearly the year 1800 the study of the Solar System (SS) was almost the whole of astronomy. Since then the scope of astronomy has expanded prodigiously. Nevertheless, at the present time there is a great resurgence of interest in the SS, partly because of the operations of space vehicles, but for many other reasons as well. Doubtless at the back of the mind of many is the hope of discovering the origin of life. For astronomers, however, there seems to be a prevalent impression that significant progress is now being made towards understanding the origin of the System itself.

If such progress is indeed being or is about to be achieved, then it is because recent developments in so many sciences are being brought to bear upon the problem — dynamics, physics, astrophysics, geophysics, cosmochemistry and so on. Fortunately, some of the contributions tell us that certain features probably have little to do with the origin of the System, so that every fresh contribution does not necessarily add to the complexity. Nevertheless, the subject has become so complicated that it would be absurd to try to make a comprehensive survey within the scope of one short essay.

I have been invited to describe the various "models". I shall attempt to do this in a way that I hope will help us to see in what [illegible] of the subsequent

particular contributions fit into the general pattern of the subject. But I do not propose to catalogue such contributions, and any I mention are to be taken only by way of illustration.

Solar System : empirical

The SS is composed of the Sun, nine planets, 32 known (natural) satellites and a ring-system, asteroids, meteoroids, comets, interplanetary dust and gas.

The Sun is an average main-sequence star which appears to be normal in every respect.

The nine planets may be classified (table 1) as:

A. Six principal planets comprising: the major planets, Jupiter and Saturn; the outer planets, Uranus and Neptune; the terrestrial planets, Venus and Earth. The planets in each pair are quite similar to each other. In passing from one pair to the next in the order stated, the mean mass decreases by an order of magnitude, and the mean density increases.

B. Three lesser planets, Mercury, Mars, Pluto. These are again about an order of magnitude smaller in mass than the terrestrial planets, but they are similar in density.

Table 1 Planets and Satellites

Principal planets	Mass	Mean density	Regular Satellites			Miscellaneous Satellites
	(Earth mass)	($g\ cm^{-3}$)	Main	Minor	Ring System	
JUPITER	318	1.4	4	1	-	7
Major						
SATURN	95	0.7	1	7	1	2
NEPTUNE	17	1.7	1	-	-	1
Outer						
URANUS	15	1.3	-	5	-	-
EARTH	1	5.5	1	-	-	-
Terrestrial						
VENUS	0.82	5.2	-	-	-	-
Lesser planets						
PLUTO	0.11	4.8	-	-	-	-
MARS	0.11	3.9	-	-	-	2
MERCURY	0.06	5.5	-	-	-	-

The satellites may be classified as:

A. Regular satellites comprising

(a) Main satellites including the Moon, the four Galilean satellites of Jupiter, the largest satellite of Saturn (Titan), and the large satellite of Neptune (Triton). These have masses about an order of magnitude less than those of the lesser planets. Their densities are similar, but they fall off somewhat with distance from the parent planet.

(b) Minor satellites including the innermost satellite of Jupiter, the seven inner satellites of Saturn (excluding Titan), the five satellites of Uranus. These all appear to be comparable amongst themselves but their masses are about two orders of magnitude smaller than those of the main satellites. Saturn's rings appear to be associated with its minor satellites.

B. Miscellaneous satellites comprising the two tiny satellites of Mars and the ten outermost satellites of Jupiter, Saturn and Neptune. It is evident that these small bodies are not in the categories mentioned in A and that they are relatively insignificant.

It may be noted that the main satellites are distributed amongst all the various sorts of principal planets, while minor satellites are associated only with planets of relatively low density and short rotation-period. Apart from the miniscule satellites of Mars, the lesser planets are devoid of satellites, so far as is known.

It may be remarked that the purely empirical features of the various satellite systems make each of them in many respects unlike a miniaturized planetary system.

As is well-known the SS possesses no known simple strict regularity. But it possesses many approximate regularities concerning the orbits, their near-circularity, their planes and their spacings, concerning the axial spins, and so on. There are also features to do with the distribution of angular momentum. In particular, there is one near-regularity that may be the most important; it may be described as follows.

The present composition by mass of the Sun is approximately hydrogen 70%, helium 28%, heavier elements 2%. It is generally accepted that Jupiter and Saturn could have about this (standard) composition. Their mean mass is $\sim 10^{30}$g. If we start with such a mass of standard composition and remove some 90% of the light elements we get bodies like Uranus and Neptune, if we remove 99% of these elements, we get bodies like Earth and Venus. In this way we can associate with the six principal planets, six standard planets of mass 10^{30}g or thereabouts made of standard material.

All the other components of the SS (asteroids, etc.) contain relatively little mass. Although they present many problems of much interest in their own right, any significance they have in the immediate context is likely to be in providing certain tests of theories of the origin of planets and satellites.

Theoretical aims

A successful theory of the origin of the SS would be expected to account for the existence and number of the planets, their total mass and the mass of the most massive planet, their composition, their axial rotations, and the spacing of their

orbits. It would be expected to account for the corresponding properties of satellites. Also it should account for any observed correlations between any of these features.

Such a theory should lead to inferences about the occurrence of other similar systems in the cosmos, and probably about connections between them and the occurrence of binary stars, multiple stars, and so on.

Raw material

Modern thinking about the origin of the planets began before much was known about the composition of the rest of the astronomical universe. So cosmogonists could start only from either a purely speculative hypothesis of a "solar nebula", as for example Laplace did, or from what appeared to be an obvious fact of observation that the only matter within reach was all in the Sun itself.

Preferring fact, as they thought, to hypothesis, for about the first half of this century cosmogonists sought persistently to show how matter could have been extracted from the Sun to form the SS.

Cataclysmic theories

Because the Sun itself is a rather pacific star, a cataclysm of some kind would be required to extract matter from it. So it appears that some dramatic intervention by a second star has to be invoked. As is well-known, distinguished astronomers have expended much ingenuity in investigating such possibilities. None of these older attempts produced acceptable theories. During the past 10 years, however, Professor Michael Woolfson[1] of York has returned to the general concept but with certain novel astronomical and computational features — and with results that are highly interesting in themselves. May I be allowed to commend Woolfson's work as worthy of the most serious study?

Solar nebula

Since the days when cataclysmic theories began to be considered, astronomers have established two simple features of the stellar system that are crucial for our problem. One is that in the Galaxy there does exist much diffuse material, and the other is that many stars, including the Sun, must have been formed after the Galaxy had reached its present state, and formed presumably from this observed material. Thus we may claim to know that the Sun was formed out of known material and to know that the same material would be the required raw material for forming planets. We are almost driven to the conclusion that the planets were formed out of the sort of interstellar material that astronomers observe every day and that this happened at the same time as when the Sun was formed from the same material, or not long thereafter.

When the planets were about to be formed, we thus infer that the raw material was in some diffuse state and retained by the gravitational attraction of the Sun (already formed or still being formed). In a general sense we come back to Laplace's notion of a solar nebula.

In figure 1 I have tried to convey an impression of the solar nebula that covers most of the features contemplated in current theories. It is a diffuse cloud of material circulating in the Sun's gravitational field and having linear extent about that of the existing Solar System. The material may be fairly evenly or very patchily distributed. The motion may be fairly regular rotation, or rotation with large vortices, or highly chaotic and turbulent. In consequence of the rotation, the system must be flattened in some way, and various possible profiles that have been discussed are sketched.

The material is taken to have standard composition. Its temperature is probably of the order of 100°K. The hydrogen and helium would be in the form of gas, the hydrogen being mostly molecular. The heavier elements would be partly in the form of gas, and partly incorporated into dust-grains — metal grains, graphite grains, silicate grains — forming altogether 1 or 2 percent of the material by mass.

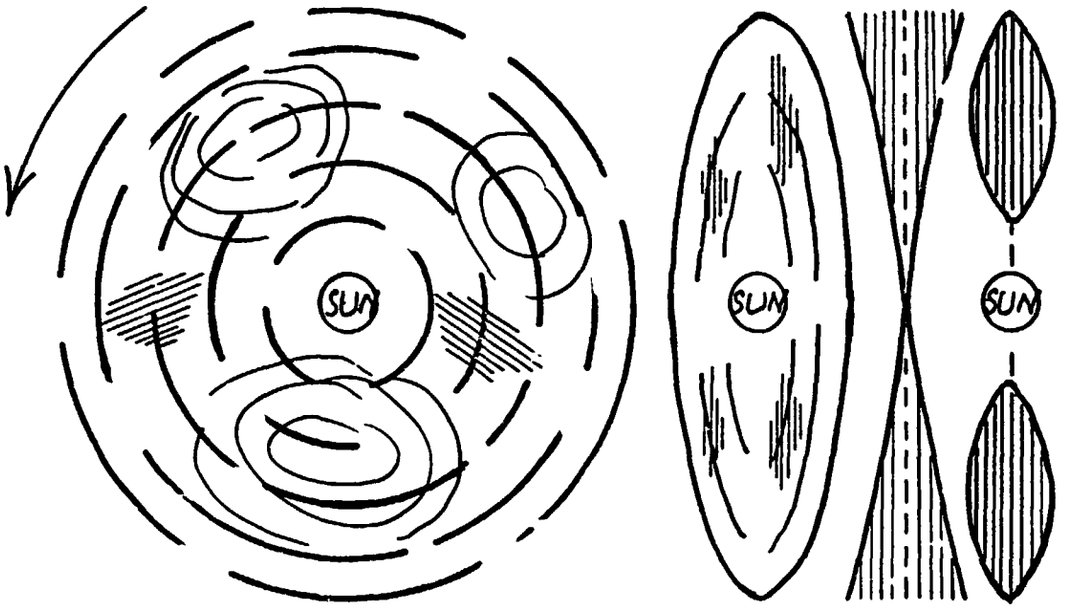

Figure 1 Solar nebula showing various suggested profiles. (The drawing indicates that the material may be patchy and that there may be large-scale eddies.)

I give this description of the solar nebula in this rather nebulous form because it can then be made the central feature in an attempt to give an overall view of present day activity in the whole field. Thus, consideration of the provenance of the solar nebula leads on to the study of the physics of the solar nebula, and this in turn leads into theories of the formation of planets and satellites.

Provenance of solar nebula

There are several views depending upon the intimacy of the connection with the formation of the Sun itself.

(a) Sun assumed to be in its final state. Here the material is considered to be

captured from an interstellar cloud either by the intervention of another star (so that we have some element of cataclysmic processes remaining), or simply by accretion so that capture results from collisions between portions of the infalling material. On this view the amount of captured material and its total angular momentum are fortuitous features depending upon the density of the cloud, the relative speed of the Sun, and so on. The spin of the Sun need have no relation to the rotation of the captured material.

It seems certain that the Sun must from time to time pass through an interstellar cloud and also that the processes contemplated could ensue. On the other hand, it seems hard to say more than this, so that there are few particular features that are testable by theory or by observation.

(I cannot refrain from offering certain critical comments as I proceed, but I do not attempt here to present detailed or systematic criticisms).

(b) Sun still being formed in interstellar cloud. Because we infer that the Sun was formed from the sort of interstellar material considered, it makes for economy of hypothesis to suppose that the solar nebula consists simply of material left over in forming the Sun. If so we might have a clue as to the density to be expected, also we should on general grounds expect such material and the Sun itself to have roughly the same axis of spin. Also the Sun may have gone through a "Hayashi" phase while the solar nebula was in position, and this may have influenced its physical state.

Again, we should think it most likely that the Sun was formed along with a few hundred other stars composing a galactic cluster (since dispersed). Certain properties, particularly the overall size of the solar nebula may depend on this circumstance.

On such a picture, the solar nebula may never had had a clear-cut identity; it could have been exchanging material with the rest of the cloud at all relevant times.

It may be that this approach has not yet served to predict quantitative properties of the solar nebula, but at the same time we can claim that the mere fact of the Sun being formed out of diffuse material is a guarantee that such material was at hand and several resulting circumstances are qualitatively advantageous in other respects. (It should be mentioned that Woolfson thinks of his process as having most likely taken place in the early stages of the history of a stellar cluster so that even here there are some common features).

(c) Solar nebula treated as part of solar condensation. Some workers go back to something even more like the original Laplace solar nebula. They think of the Sun being formed from a distinct portion of the raw material that contracts under its self gravitation. With any likely initial angular momentum, this could not contract to solar size without rotational break-up. But it is postulated that up to a certain stage there will be magnetic linking to the surrounding interstellar medium resulting in magnetic braking of the increasing spin. It is thought that the link must become severed at some stage so that there is further spin-up, with resulting equatorial break-up. Then it is supposed that there will be a magnetic link-up of the proto-Sun with the discarded material causing an outward transfer of angular momentum. On this picture, the discarded material is in fact the solar

nebula. Some such sequence of processes has been claimed, originally by D.ter Haar[2] and more recently by F. Hoyle,[3] to predict more precise properties for the solar nebula than any of the others. However, I scarcely think it has yet been established that the postulated processes would inevitably occur, or that if they did they would operate with the extreme efficiency needed in order to achieve the required distribution of angular momentum.

Physics of solar nebula

Much work is concentrated upon the study of the mechanics and physics of the solar nebula evidently on the implied belief that if a theory explains how suitable material can be produced in a suitable location there is no doubt that the planets will be formed from it.

There is now a dichotomy in the development. One type of theory regards the differentiation of material as occurring mainly in the solar nebula, from which planets are then formed with their permanent composition. Another type considers that first a number of similar condensations were formed in the raw material — proto-planets — and that differentiation then occurred within these bodies, which proceeded to evolve in different ways. The former type naturally demands the more elaborate study of the solar nebula.

This study has several aspects. It has always to be recognized that, if it is fulfilling its essential rôle of producing the planetary system, the state of the solar nebula with which we are concerned is necessarily transitory.

Hydrodynamics. The problem is that of fluid in the vicinity of a central plane in rotational motion about an axis perpendicular to the plane, under gravitational forces. Most present day treatments seem to regard fluid as turbulent — although different reasons for doing so are adduced — and in particular turbulent pressure may be important.

Thermodynamics. The aim being to infer the density and temperature distribution, the thermodynamic behaviour is important. The material is heated mainly by the solar radiation and cooled mainly by re-emission, and so the opacity has to be studied. The temperature estimated finally is usually of the order of magnitude $100^{\circ}K$ in the part near the Sun, falling to much lower values further away, but estimates differ very considerably. Densities are typically of the order $10^{-10} g\ cm^{-3}$.

Chemistry. It seems that the chemistry of material in such conditions presents novel problems. On the whole — if my impression is correct — substances condense out in the form of metal grains, silicate grains etc., much as astrophysicists estimated in the past, but apparently the details are more complicated and the variety of materials greater than had been expected. It is highly reassuring that some workers are nowadays able to check some of the predictions by laboratory tests.

The outcome of all this is the prediction of a rather complex variation of grain materials through the system.

Sedimentation. There are various mechanical actions on a grain that are not significant for atoms or molecules of the fluid. Evidently the main effect is for them to tend to fall towards the central plane of the system. Several authors have

studied this process. Some grains will adhere if they encounter each other and this property greatly affects the outcome. In the context, E.Orowan[4] several years ago concluded that metal grains would adhere, but not silicate grains. So at any stage there may be further differentiation of the material by sedimentation, in addition to the chemical differentiation already mentioned.

Other effects. Some authors infer that there is significant loss of light gases from the parts of the system remote from the Sun.

Some infer the possibility of motion which, viewed in a frame rotating with the mean motion, gives the effect of a pattern of great eddies. They think that the interesting deposition of material and condensations will occur in the interstices between these eddies. Thus there would arise a still further ordering of the materials. Here I refer to the line of thought initiated by K.F. von Weizsacker.[5]

Accumulation of planets

Hitherto a prevalent view according to this development of the subject has been that, having apparently explained how the grain material may come to be distributed in zones of different compositions (and by virtue of the way in which this material has reached the central plane it may by then consist of solid particles of centimetre dimensions or more) it can be almost taken for granted that this material must then accumulate into a few large bodies. These will have compositions determined by the zones in which they form. In the zone near which most gas remains some of it, also, may be incorporated into these bodies. It is claimed that the resulting variation of composition matches that in the actual Solar System.

Let us first of all take a comprehensive view made possible by the recent computer simulation carried out by S.H. Dole.[6]

Dole takes a solar nebula having certain assumed properties, including the assumption that the grains move in Kepler orbits of given fairly large eccentricity. In his simulation, he injects a planetary "nucleus" of a certain mass and size and supposes it picks up every grain it meets. After it has picked up everything it can, Dole injects another, at random, and lets it move under the same conditions together with the assumption that if it encounters the first, it will coalesce with it. And so on. He has also the assumption that after growing to a certain size, any of his bodies may gather gas as well by gravitational accretion. The whole process is supposed to go on until all the grain material has been swept up.

Dole has published typical sets of results of his simulation experiments showing the number, masses and spacing of his planets, compared with the actual SS. At first sight the outcome is so impressive that it looks as though the problem has been solved in all essentials and little remains to be done. However, I do not think this is how even Dole himself would view it.

He selects four parameters of the actual SS that he seeks approximately to reproduce. On my reckoning, his system has 11 disposable parameters to enable him to do it. He should thus be able to reproduce the four parameters in infinitely many ways. What his work shows is some of the requirements that would be sufficient (though not, of course, necessary) to produce a planetary system in this way. As

would be expected, it shows also that the results are sensitive to some of the assumptions and insensitive to others.

The assumptions cannot be discussed here in any detail, but obviously one of the most important is the assumption that at all intermediate stages bodies will coalesce if they meet.

The problems associated with some of the assumptions are brought out clearly in the recent extensive investigations by Alfvén and Arrhenius and by Safronov, and from somewhat different aspects in that by Cameron. In particular, they discuss this problem of the coalescence of bodies. This has led Alfvén and Arrhenius to the concept of "jet streams" produced by a process of gravitational focussing of orbits of inelastically interacting particles. It has led Safronov to a concept of "rings" of material produced in a rather similar manner. Once such a stream or ring has been formed, it is apparently possible to infer that particles composing it will coalesce, presumably as a result of some slight perturbation of the motion.

Digressing for a moment, Professor R.A. Lyttleton allows me to quote some work that will shortly appear and that is an elaboration of some he published earlier in his book Mysteries of the Solar System.[7] He infers that the grain material will settle very accurately into a plane before anything else happens. This gives a layer only a centimetre or so thick. Lyttleton calculates that a body can grow by accumulation from such a layer in a very short time.

This settling into a plane is itself a process of "gravitational focussing" and it is beautifully illustrated in practice by Saturn's rings. Whether it could operate throughout the nascent SS is perhaps more doubtful. One would expect some perturbation that would result in streams of some kind, rather than a layer, and this would be precisely the result got by the other authors I have mentioned. So this brings one back to the accumulation problem as stated.

The details of one way in which the accumulation might occur have been studied by R.T. Giuli[8] in the context of the Alfvén-Arrhenius type of theory. The work is claimed at the same time to account for the spin of the accumulating body and, incidentally, to show that the angular velocity would be always about the same. It is also claimed that such a theory leads fairly naturally to the formation of satellites as well, although I am not aware of detailed studies.

Again I must refer also to Cameron's extensive work which, I understand, he will describe elsewhere in this report.

Much ingenuity has thus gone into showing how bodies might accumulate in a solar nebula once certain starting conditions are assumed to be realized. But the work on the physical state of the solar nebula has not been shown necessarily to produce these conditions. One example is that much of the work on the accumulation process evidently requires the initial grains to move in orbits of improbably large eccentricity. Even if this requirement could be met, it seems that it would nullify the segregation of materials inferred from other assumptions. Moreover, very little of this work provides estimates of the times required to achieve the desired outcome.

Proto-planet theory

Let us now go back to the solar nebula and picture it simply as a rather haphazard assembly of fog patches drifting about (under gravity) in the vicinity of the Sun. If grains are not already present simply as surviving interstellar grains, presumably they will form fairly quickly as already envisaged except that, in a dosordered system, more or less the same mixture of grains is to be expected throughout the system. In the disordered motion, patches of the material will form and break up. But we know that, if in any chance aggregation a certain critical mass is exceeded, the body of material is bound to cohere under its self-gravitation and not to disperse again.[9)]

Let us suppose that the "standard planet" that we identified at the outset is such a mass. This is the only particular assumption I need.

Then we obtain a proto-planet with the properties shown in table 2. It is a very diffuse "fog patch," its radius being 10-20 times that of the regular satellite systems that we looked at. Any such body of matter must of course have resultant angular momentum. A rather different approach gave the value shown, but it actually could scarcely be much different since for a value several times bigger the body would not hold together, and for a value several times smaller it would have ridiculously small equatorial speed. In any case we do not need to know the value nearer than this.

Table 2 Proto-planet

Initial state : estimated typical values

Mass	10^{30} g
Radius	$1/3 \times 10^{13}$ cm
Density (mean)	$2/3 \times 10^{-8}$ g cm^{-3}
Escape speed at surface	2 km s^{-1}
Angular momentum	4×10^{46} g cm^2 s^{-1}
Corresponding equatorial speed for uniform density	1/3 km s^{-1}
Composition by mass	
Gas: hydrogen(molecular)	70%
helium	28%
heavier elements	1%
Grains: metals, graphite, silicates	1%
(possibility of some "ices")	
Temperature (kinetic) of material	100°K

Suppose such a proto-planet behaves as an effectively isolated body once it has been formed. Two processes are bound to operate:

a) It proceeds to contract under its self-gravitation.

b) Heavier material falls towards the centre through the lighter material.

At first (a) is very slow. Also (b) is slow if only the sedimentation of original grains is contemplated. But if the adhesion of grains is taken into

account it is quite a rapid process. By virtue of the properties noted by Orowan, it appears that the first effect would be the formation of a metal core, leaving silicate grains in suspension in the surrounding gas. If these proceed to settle they will produce a silicate mantle. I take it that "ice grains", or ice-coated grains, may be formed as well, and these may possibly assist the sedimentation by a sort of snow-fall.[10)]

The remaining gases would be hydrogen (because there is such an excess) and helium with other noble gases because these cannot go into chemical compounds. Of course, some gas would be trapped in the central condensation without being combined.

The formation of such a condensation releases gravitational energy but this by itself seems insufficient to drive off the gas. So if nothing else happens the whole body will now go on contracting as a whole giving a proto-major planet (still possessing the condensation around the centre.)

An actual proto-planet, however, would be under the tidal action of the Sun and for the density I inferred the Roche limit would be at $\sim 10^9$ km from the Sun or just outside Jupiter's orbit. This is somewhat excessive, but perhaps not much. It would mean that gases of the envelope would be stripped off by the tidal effect of the Sun, and we should be left with a proto-terrestrial planet. (There is independent evidence that the Earth's atmosphere is not primordial.)

Rotational instability. Once again treating the proto-planet as an independent body, we note that as it contracts with conservation of angular momentum it will naturally spin faster and faster, and so may become rotationally unstable. In the case of a proto-major-planet, the first effect would be what used to be called equatorial break-up, with the loss of material in the equatorial plane. In the light of recent investigations by J.P. Ostriker, the sequence of events may be somewhat more complicated than has hitherto been inferred, but the net result may be not much different. This process must continue until what is left of the contracting body becomes largely incompressible. It must then suffer fissional break-up. In the case of a proto-terrestrial planet, it is easy to calculate that the angular momentum remaining in the central condensation will make it rotationally unstable before it reaches its final density. So it too must suffer fissional break-up.

Lyttleton in particular has studied the consequences of such break-up. The original body breaks into two main bodies that must have mass-ratio $\gtrsim 8{:}1$. These cannot remain gravitationally bound to each other, but both remain in the SS if break-up occurs at the Earth's distance or less. If it occurs at Jupiter's distance or more, the larger of the two bodies remains in the SS, but the smaller escapes. If a "droplet" survives from the neck of fluid between the separating parts, it is likely to go into orbit about the larger body but not about the smaller.

Also Lyttleton was apparently the first to suggest that Earth and Mars might be two such main bodies resulting from a fissional break-up, with the Moon as a "droplet", while Venus and Mercury might be another such pair.

All dynamical features are compatible with this idea. Also physical features of density and composition give strong support, see table 3. Thus one of the most puzzling things about the SS, the assortment of compositions of the inner planets, would be accounted for without appeal to any differentiation within the solar

nebula itself. For the table shows that Earth + Moon + Mars and Venus + Mercury would combine to give two bodies EMM, VM having about the same iron-nickel fraction ($\sim$ 30 percent), and the same mean density ($\sim$ 5.27 g cm^{-3}, assuming no change of total volume). Thus all these diverse existing bodies could have come from the break-up of two proto-terrestrial planets of identical composition.

Table 3 Terrestrial Planets : density and composition. (The values for the iron-nickel fraction are quoted from table 9.5 of Kaula[11], the remaining fraction being treated as silicates. Particular attention is called to the results underlined.)

Body	Mass 10^{26}g	Volume 10^{26}cm^3	Mean density g cm^{-3}	Iron-nickel fraction	Iron-nickel mass (10^{26}g)
EARTH	59.74	10.83	5.52	0.315	18.82
MOON	0.73	0.22	3.36	0.06	.04
MARS	6.42	1.63	3.93	0.19	1.22
VENUS	48.69	9.29	5.24	0.265	12.90
MERCURY	3.30	0.60	5.48	0.65	2.15
EMM	66.89	12.68	<u>5.27</u>	<u>0.30</u>	20.08
VM	51.99	9.89	<u>5.26</u>	<u>0.29</u>	15.05
Total	118.88	22.57	5.27	0.30	35.13

On this view, the Moon is a Lyttleton droplet, and it is satisfactory that we have inferred that <u>all</u> the planets possessing main satellites have suffered fissional break-up. All these satellites would thus have been formed by the same mechanism, as is indicated by their properties.

In the cases of Jupiter and Saturn, we infer that the smaller parts escaped from the SS. The cases of Uranus and Neptune would have been intermediate because they have lost much of their light material, though not nearly all of it. In the case of Neptune, we infer that we have to do with the fission of a central condensation; Triton would be the droplet corresponding to the Moon. In this case, the smaller main fission-body would have had to emerge through the remaining gas, and so it may not have been lost to the SS. It is attractive to suppose that it is the planet Pluto.

As to "equatorial" break-up, in the case of any proto-planet that retained much light material, a good deal of this must have been spread in the equatorial plane, from a distance that might have been as great as 2 x 10^6km (at which instability would set in for the tabulated value of H_o) right in to near the final planet itself. The almost inescapable inference is that the minor satellites were made from this material by a process of accumulation - such as that proposed in other theories for the formation of the planets themselves. For here the conditions would be more favourable for the process since the material is more dense and it is actually deposited in the plane where it is needed. Besides, only a process of low efficiency is required. For in the case of Saturn, for instance, the minor satellites add up to $< 10^{-5}$ Saturn's mass, while the mass of material available to

make them in this way would be comparable with Saturn's mass. Also we should, of course, infer that some of the same material formed the rings of Saturn.

Comments. All such inferences together make it difficult to escape the conviction that rotational break-up has played a part several times over in giving the SS the form that we see. But the only known way of bringing about rotational instability in astronomy is by contraction of the body concerned. This means that it must be compressible (i.e. diffuse) to begin with. This argues in favour of the proto-planet concept rather than that of planets built directly with about their final densities.

General viewpoint

It seems to be possible to present a set of general ideas about the origin of stars and planets that — if it is valid — provides a framework into which any more particular theory must fit.

First it must be recalled that any coherent body of matter having mass more than about 1 percent of a solar mass will in general behave as a star, while any body of mass less than this will in general behave as a planet. This was discussed nearly 40 years ago by H.N. Russell, Kothari and others.

It is obviously the destiny of most of the material in a galaxy to form stars, and it is widely accepted that stars are normally produced in large batches or clusters. Consider then a large body of presumably diffuse material that is on the verge of forming stars. The material must fragment in some way, but the agencies that determine the sizes of the fragments are not those that determine whether those fragments will be successful in forming stars. So we can only conclude that fragments of all kinds of size will occur, but here we need to consider only those that are at least large enough to hold together under their own gravitation. At the other extreme there may at first be some fragments so large that they can form only very temporary stars, but after that the material must, so to say, try again until the largest fragments are not too great to form normal stars. There must still be a wide range of sizes of fragments moving about amongst one another. The larger ones tend to sweep up the smaller ones. By hypothesis, at the stage under consideration, almost none grows beyond the size of a normal star. But also by hypothesis we are considering the case where a considerable number of normal stars are in fact being formed. Whatever the process of formation, some fragments will acquire "stellar" mass within each others gravitational grasp so that binary, or multiple systems result. Such systems would be specially effective in sweeping up smaller fragments. In fact about the only way for a small fragment not to be incorporated into a "stellar" condensation is for it to go into orbit around a condensation of this sort that does not become a member of a multiple stellar system. From this very general point of view, that would be the start of a planetary system.

The proto-planet theory then shows how a system starting in this way could become elaborated, by segregation of materials, rotational break-up, and so on, into a planetary system like the SS.

This seems to be the most natural approach to the problem. Nature has made galaxies, clusters of stars, multiple systems, binaries, single stars — all, apparently, in one grand sequence of processes. We know that the next class of

body in the sequence are planets, and it is only an accident of mass as to whether a body is a star or a planet. The cut-off in the sequence must occur at the least initial mass that can hold together by its self-gravitation. Since we know that planets do exist, it would be odd if Nature were to impose the cut-off between stars and planets and to set about inventing a new set of processes specially in order to produce planets!

If there is one underlying set of processes as suggested by this line of thought, its operation must still be highly complex. There must be factors that limit the growth of each class of body and these must be different in each case. Nevertheless, it seems to be the most natural line of thought to pursue through the whole subject.

Other topics

My review is not the recital of a bibliography of the subject, so I hope no colleague feels neglected if I have not mentioned his contributions by name. At the same time, I do regret the omissions caused by selection effects, considerations of space, or plain forgetfulness and ignorance.

So far I have said nothing about Professor H. Urey's more particular ideas, although everyone working in the field knows that his ideas in general have been a continual stimulus for many years. I might refer especially to those suggesting that planetary bodies may have been built up out of Moon-sized objects. We can appreciate the attractiveness of the concept; fortunately Professor Urey is making a contribution about it here.

When mentioning Moon-sized objects, one recalls that the Earth-Moon system itself has been the object of much specialized study in recent times, and such work will have to be taken into account in more general studies of the SS.

Then there is the Titius-Bode law and related matters — I have scarcely mentioned them. If such apparent regularities are significant then, as I understand, they could arise in one way or another after the bodies concerned had been formed as we see them now. If so, it seems likely that they have arisen in such ways. For, had they anything to do with the formation of the bodies, we should surely expect them to be associated with other cosmogonic properties such as composition, mass, spin,..... No-one seems ever to have discerned any such association.

There are also more particular dynamical problems concerning possible effects of tidal friction. It seems, however, that the value of tidal friction may be determined by rather superficial features of any body concerned. Thus it has probably changed in unknown ways over the past history of the body so that we cannot use it to infer much about the past.

Almost every theory of the formation of the SS must have some waste material left over at the finish. In particular, there is almost certainly a surplus of light gases to be disposed of. In most theories the temporary presence of such material actually plays an essential part in rounding off orbits and, maybe, in counteracting tidal friction. But these days any problem of waste-disposal has to be treated seriously, and that applies here. For the material in question would

carry angular momentum comparable with that of the planets themselves. The problem seems to be to get rid of the angular momentum as well as the matter. The current view is that both could probably be carried away by the solar wind.

There is another class of problems that will doubtless receive special attention in the present symposium. These concern isotope-abundances in the SS. Once it is known what nuclear processes have been possible in the system, in addition to those in the Sun's interior, the measured abundances will impose exacting checks upon theories of the formation of any of the bodies concerned in these processes.

There are some more special problems. One is that of the asteroids. This cannot be solved until we know what the asteroids are. It is to be hoped that some space mission will give close-up pictures and maybe even specimens of the material.

Again, there is the problem of the origin of comets. Evidently the reservoir of comets is at the order of distance of nearby stars. This suggests to me that comets are somehow also left over from the formation of the Sun and the SS as part of the formation of a stellar cluster.

This then leads to the possible connection with the formation of binary stars. A very general view of a planetary system is simply that, while a star is the principal part of a condensation in a body of interstellar matter, the material of the associated planetary system is a component of the condensation that has too much angular momentum to allow it to fall into the principal part. But if two condensations of the matter happen to form (or grow) so that they finish by being gravitationally bound to each other, then the principal parts will ipso facto form a binary stellar system. In that case there is no rôle for a planetary system; any material bound in the system would in general be swept up by one star or the other. On this and other grounds, I should expect that stars in binary (or multiple) systems would not be attended by planets.

Physical processes

Naturally, there are many basic processes that play some part in more than one theory of the SS.

A capture process might explain how the Earth acquired its Moon, or it might explain how some other planets acquired the most insignificant of their satellites.

Tidal action has in the past been invoked to explain how matter could be pulled out of the Sun, but we have seen that it could also explain how a gaseous envelope was removed from a proto-earth by the Sun.

Accretion may explain how the Sun acquired the solar nebula, or how the great planets were constructed, or how some surplus gas was swept up by the planets.

Accumulation processes may account for the planets themselves, or merely for their minor satellites.

Rotational instability may tell us how a proto-sun discarded matter that then formed a solar nebula, or it may tell us how proto-planets broke up so as to produce all the existing planets and satellites.

Everyone now seems to agree that grains are needed in order to produce planets, and all theories seem to rely upon the same basic processes of condensation to produce the grains from the gas.

Again, most theories now invoke also processes of growth of grains, some in order to account for the concentration of grain material in the central plane of the SS, some in order to explain the concentration of heavy material in the central region of a proto-planet and at the same time to account for segregation of materials in this region, and some to account for the first stage of an accumulation process of forming planets.

Most theories nowadays appeal also to turbulence in the solar nebula to play one rôle or another. Several theories assign a key part to hydromagnetic processes. And so I might continue.

Surely this denotes progress. We may claim with some confidence that we are gradually coming to know what basic physical processes must have operated in order to produce the Solar System, even though we may still be a long way from understanding how they cooperated to this end.

References

The following are some of the most recent review articles:

MIDDLEHURST, B.M. (editor) The origin of the Earth and Planets: report of IAU Joint Discussion on 1970 August 21. Highlights of Astronomy 1971 2 193.

SCHATZMAN, E. Origin of the Solar System

WILLIAMS, I.P. and CREMIN, A.W. A survey of theories relating to the origin of the solar system. Q.Jl. R.astr.Soc. 1968 9 40.

WOOLFSON, M.M. The evolution of the solar system. Rep.Progr.Phys. 1969 32 135

The following papers are amongst those referred to in the text; only one main paper by a particular author is quoted, but that paper gives references to his earlier work. Scarcely any references are given to authors who have contributed to the present volume, since their own contributions will provide these.

1 DORMAND, J.R. and WOOLFSON, M.M. Mon.Not. R.astr.Soc. 1971 151 307

2 ter HAAR, D. Astrophys.J. 1949 110 321, 1950 111 179

3 HOYLE, F. Q.Jl. R.astr.Soc. 1960 1 23

4 OROWAN, E. Nature 1969 222 867

5 von WEIZSÄCKER, C.F. Z.Astrophys. 1944 22 319

6 DOLE, S.H. Icarus 1970 12 494

7 LYTTLETON, R.A. Mysteries of the Solar System 1968 (Clarendon Press)

8 GIULI, R.T. Icarus 1968 9 186

9 McCREA, W.H. Proc.Roy.Soc. 1960 256 A 245

10 WILLIAMS, I.P. and CRAMPIN, J. Mon.Not. R.astr.Soc. 1971 152 261

11 KAULA, W.M. An introduction to planetary physics: the terrestrial planets 1968 (Wiley, New York)

PRESENTATION OF THE MODELS

Hubert REEVES

Institut d'Astrophysique, PARIS.
Sections d'Etudes Spatiales, SACLAY.

A. SEVEN COMMONLY ASKED QUESTIONS IN RELATION WITH THE ORIGIN OF THE SOLAR SYSTEM, AND THE ANSWERS GIVEN IN THE VARIOUS MODELS.

My aim in this report is to present the various models of the solar system which will be discussed and appraised throughout this Symposium. I believe that the best way to do that is not to take in turn each model and try to summarize it, but to consider how each model answers (or attempt to answer) a number of fundamental questions which any newcomer in the field -I am a newcomer in the field- is likely to ask. These questions will be related to the various steps which, somehow, mark the way in the large road leading from the cloud of interstellar matter to the fully developed solar system as we know it now.

The most vexing uncertainty in the game relates to the probability of formation of "solar systems" in the general course of stellar evolution. Are we living on an highly improbable system -or even exceedingly improbable system- or are such systems very common throughout the galaxy ? The answer to this question has important methodological implications for the rest of the study. If the solar system is a common occurence, then we must require the physical conditions needed for its appearance to be fairly common and we must, somehow, be able to associate them with astronomical observations of interstellar clouds and young stars (as described by LEQUEUX in one of the following talks). If the solar system is a kind of a "freak" or "monster", then statistical studies of galactic observations of clouds or young stars are of little help and the problem is much more difficult. Clearly the first approach is the most reasonable one at this point (and has consequently been adopted by the modelists) but before we have actual observations of other solar systems the other possibility cannot be definitely ruled out.

Question N°1.

DO THE SUN AND THE PLANETS COME FROM THE SAME CLOUD OF INTERSTELLAR MATTER ?

This is one of the oldest debate in the game. At various times during the last three centuries the possibility that the planets represent matter ejected from a passing star, or quite gene-

rally, captured by the sun has been discussed in various scenarios. The main difficulty has always been the exceeding low probability of such encounter (which brings us back to the first point...) and furthermore the near parallelism between the angular momentum vector of the sun and of the planets would be coincidental.

Of the five models discussed here, four assume that the sun and the planets are issued from the same cloud : ALFVEN-ARRHENIUS (A + A) (this volume) on the other hand, present a capture scenario of a novel kind : the sun, already formed, has captured, through its magnetic field, a cloud of interstellar matter. The parallelism between the magnetic moment and the rotation vector of the sun accounts for rotation aligment of the planets. One observational domain which could in principle be of relevance for the subject is the chemical and isotopic composition of the sun and the planets. If, for instance a definite and systematic difference in isotopic composition of a certain chemical element could be shown to exist between the solar atmosphere, on the one hand, and the bulk of the planetary material on the other hand, and if this difference could not possibly be explained in term of chemical processes throughout the life of the solar system, then one could make a case for separate origin. There is at least one element for which such a difference does exist : it is neon. Later in the week the existence of a "planetary" and a "solar" component will be discussed. However, although we do not understand at this moment the origin of these two components, it would be rather premature to reach, from there, any conclusion regarding a separate origin... far too many possibilities exist which cannot yet be ruled out.

Question N°2.

HOW WAS THE PLANETARY MATTER SEPARATED FROM THE SOLAR MATTER ? (assuming that they come from the same cloud).

One thing that seems definitely established is that the matter of the planets has not been ejected out of the sun by some kind of tidal effect from a nearby celestial object. SPITZER (1939), considering the question, has argued quite convincingly that such an amount of matter suddenly extracted from the sun, and consequently, freed from its gravitational pull, will suddenly explode in view of its thermal energy and will not be retained in orbit around the central star.

The various modelists invoke the centrifugal force related to the initial angular momentum of the body to explain the physical separation (from the beginning) between the future sun and the "nebula".

SCHATZMAN (this volume), for instance, presents a picture in which the outer layer of a flattened disk surrounding a central star rotates at the verge of rotational instability i.e. the centrifugal force is as large as the gravitational attractive force. This way, as the nebula contracts, it sheds matter at the periphery and this matter remains in Keplerian orbit at the radial distance at which it is shed. (OSTRIKER (this volume) will discuss the hydrodynamics aspects of this model).

CAMERON (this volume), on the other hand has in his model a disk, more massive with much larger angular momentum, distributed more uniformly with radial distance.

An important characteristic of this nebula is then the absence of central condensation : the surface density of matter perpendicular to the equatorial plane varies very smoothly with radial distance. The sun, as we know it, was formed only later, through the dissipation of the disk (by the effect of circulation currents and the falling inward of a large fraction of the disk).

SAFRONOV (this volume) reckognizes all the difficulties associated with the formation of the nebular disk and does not try to solve them. He assumes, as an initial step, the existence of a protoplanetary cloud (nebula)surrounding the sun and possessing only rotational motion without radial contraction.

Question N°3.

HOW BIG WAS IT ?

A lower limit ot the mass of the protoplanetary nebula can be obtained by adding to the present total planetary mass ($\simeq 10^{-3}$ Mo) an appropriate complement of volatile elements (which have escaped from the inner and outer planets) in order to recover a "solar" composition everywhere : one obtains a value of $\simeq 10^{-2}$ Mo.

SAFRONOV argues that an upper limit can be set by the necessity of eventually evacuating the extra content of matter before the solar system takes its present shape and the consequent constraints imposed on the required mechanism. For instance, ejection of bodies by gravitational perturbations from nearby planets would result in a redistribution of angular momentum tending to bring the remaining bodies closer to the sun. (LEVIN (this volume) presents a new model in which this fact is a basic ingredient ; he postulates a 3 Mo nebula).

SAFRONOV set an upper limit of 0.5 to 0.6 Mo to the initial mass from this argument. He also sets an upper limit from the possible development of gravitational instabilities in a very dense cloud : if planets had formed through gravitational instabilities (contraction of a cloud when its gravitational energy becomes larger than its kinetic energy) they could not have, later on, been able to dissipate a large fraction of their hydrogen and helium (this argument would apply mostly to Uranus and Neptune, as we do not have definite indication that Jupiter or Saturn have "lost" any volatile). The possible importance of gravitational instability will be discussed again later. The appropriate upper limit would be $\simeq$ 0.14 Mo.

In view of these arguments SAFRONOV selects a value of $\simeq$ 0.05 Mo. This is also approximately the choice of SCHATZMAN.

One important consequence is that the gravitational effect of the central star is then largely preponderant everywhere and the gravitational field is essentially in R^{-2} everywhere in the nebula.

CAMERON makes important use of the fact that the T Tauri stars (believed to be young stars in their initial period of gravitational contraction) are known observationally to eject large amounts of their mass under the form of "stellar wind". These winds bring away matter at the rate of $\simeq 10^{-6}$ Mo a year (or $\simeq 10^{6}$ times the flux of the present day solar wind) for periods of 10^{5} to 10^{6} years. The total mass ejected may reach several tens of percent.

(It must be said, at this point, that some doubt exists on the exact interpretation of these observations on T Tauri stars. It is not clear, for instance, that the matter ejected is brought all the way out of the stellar gravitational field).

Consequently CAMERON starts with a massive nebula of 2 M⊙ (including the mass of the future sun), and counts on the wind to evacuate the extra mass, including gas and dust. Since the mechanism for matter ejection is not related to the existence of the outer planets, one of the upper limits of SAFRONOV becomes inoperant. But SAFRONOV notices that CAMERON does not consider properly the second upper limit (related to gravitational instability). We shall hear more about this point later in the week.

For A + A, the whole set-up is quite different since the nebula is not all there at the same time but the captured matter is added gradually. This way the mass of the nebula at any one time can in principle be much smaller. ($\simeq 10^{-11}$ to 10^{-12} M⊙).

Question N°4.

THREE BARRIERS TO JUMP OVER...

A cloud of interstellar matter will manage to isolate itself from the surrounding and contract into a star only if its own gravitational field becomes larger than the thermal pressure, the magnetic pressure and the "centrifugal" pressure.

The typical interstellar cloud is rather disadvantaged in this respect : it has a rather low density and consequently a low ratio of gravitational to kinetic energy. Furthermore since it partakes in the rotational motion of the galaxy, it has a rather large angular momentum. And it inherits a magnetic moment resulting from the general magnetic field of the galaxy which, upon contraction, would eventually give a very large magnetic energy density. Somehow the cloud must go over several barriers if it is to become a star. In fact, we should be rather pleased with this situation ; if the road was easy, all clouds should have become stars long ago and we would not understand why after 10^{10} years of galactic life we are still witnessing the birth of stars !

The Thermal Barrier.

This is an old problem treated first by JEANS for the infinite homogeneous case and by a number of other people for more realistic cases. The results do not differ very much and the JEANS's length criterion still describe the situation well enough for our illustrative purpose.

This criterion says that a cloud may collapse only if its free fall time is shorter than the time it takes for a sound-wave to propagate across its volume, because then the thermal motion does not have the time to react and counteract the gravitational pull !

In a cloud of mass M, radius R, density ρ and temperature T (both assumed uniform) the free fall velocity is :

$$v_{ff}^2 = GM/R$$

and the free fall time :

$$t_{ff} = 2\,R/v_f = 1340\rho^{-1/2}\ s \simeq 10^{15}\,N_H^{-1/2}\ s$$

between 10^6 and 10^7 years for most clouds.

The speed of sound v_s is given by $P = \rho v_s^2/\gamma$ (P the pressure, γ the ratio of specific heats), whence $v_s \simeq 10^4\ T^{1/2}$ cm s^{-1} (or $\simeq 1$ km/sec for most clouds). The minimum dimension of the cloud is then :

$$R > v_s\ t_{ff} \simeq 10^{19}\ T^{1/2}\ N_H^{-1/2}\ \text{cm}$$

and the mass (in unit of solar mass $M_\odot$:

$$M/M_\odot \gtrsim 10\ T^{3/2}\ N_H^{-1/2}$$

A rather similar relation is obtained if one requires that the ratio of the thermal E_T of the cloud be smaller than its gravitational energy E_G, for instance through the formal expression obtained from the virial theorem.

Typical cloud temperature are $T \simeq 100$ K and densities $N_H \simeq 10$. Hence the initial mass must be $\gtrsim 10^3\ M_\odot$ for a cloud to collapse. This is nice since we know that most stars are born in stellar clusters, but opens the need for a study of the fragmentation processes which must occur before stars are born individually (this problem was studied in particular by HOYLE in 1948).

The triggering of such collapses can probably be helped by random motions of the gas.

The possibility that these "random" motions can occasionally be helped by individual events such as nearby explosions of supernovae or light pressure by close young stars has been discussed at length.

Recently a new attractive mechanism has been proposed within the frame of the density wave theory of the spiral structure of the galaxy (FIELD. 1971).

In this theory the gas and the stars are not indefinitely attached to one galactic arm, but travel from one arm to the other in a period of $\simeq 10^8$ years. The motion is fast between the arms and slow in the interams leading to a concentration of matter in the arms and hence to the very existence of the arms which,by their gravitational field,are responsible for the state of motion described above. This is then a self-consistent theory which explains why the arms are steady features of the galaxies.

As a cloud of gas enters an arm, the deceleration of its motion is accompanied a compression resulting into an important increase of its density. Since young stars are formed in spiral arms, the temptation is great to assign to this compression a role in the overcoming of the thermal barrier.

The Magnetic Field Barrier.

Contraction of a cloud with an imbedded magnetic field will be impeded by the increasing magnetic pressure (or stresses in the lines of forces) if the matter is sufficiently ionized for the lines to be frozen-in.

Indeed, upon contraction of a cloud of radius R the total flux $\Phi = \pi R^2 B$ will remain constant, hence the field will grow up as $R^{-2} \propto \rho^{2/3}$. The magnetic pressure (or energy density) is then proportional to $B^2 \propto R^{-4}$ and the magnetic force on the matter (per cm^3) goes up as :

$$\nabla B^2 \simeq d(B^2)/dr \propto R^{-5}$$

On the other hand the gravitational force per cm^3 ($F_G \simeq GM\rho/R^2 = GM^2/R^5$) increases in the same way as R decreases. The net effect of the magnetic field is then to counteract the gravitational field by an amount which does not change during the contraction.

The virial theorem again provides us with another way of obtaining the same result. For a uniform cloud the gravitational energy term is :

$$E_G = \frac{-3}{5} \times \frac{GM^2}{R}$$

while the magnetic energy term $E_B = \int MdV = \int \frac{B^2 dV}{8\pi} = \frac{\phi_B{}^2}{3\pi^2 R}$

the ratio $E_B/E_G = \frac{5\phi_B{}^2}{9\pi^2 GM^2}$ must be smaller than one for any contraction to take place and this yields a lower limit for the condensing stellar mass Mc in a given field :

$$Mc \simeq B^3/G^{3/2}\rho^2 = 10^4\ M\odot$$

for $B = 3 \times 10^{-6}$ gauss, and $N_H = 10$, a typical cloud value. One could argue that the field does not prevent contraction along the lines of forces, but SPITZER has shown that this contraction is highly retarded by the slow increase of the gravitational potential.

For an initially spherical distribution of matter the net effect is the formation of a flattened spheroid.

A neat trick would consist in pumping a large amount of matter solely along the lines of forces. We shall describe, in a short time, how, according to CAMERON, nature may actually do it.

The problem is then : how to fragment such a massive object into objects of solar masses.

Consider an object with $E_B/E_G > 1 (M > 10^4)$ undergoing gravitational contraction. Since Mc does not change with time ($B \propto \rho^{2/3}$) it can only fragments into submits with $M \geqslant Mc \geqslant M\odot$.

The difficulty probably lies in the fact that we have assumed perfect freezing of the lines of forces in the matter and hence sufficient ionization of the matter of the cloud. One may naively imagine that, quite on the contrary, if, upon condensing, the cloud becomes opaque to all ionizing radiation (X ray, U. V. cosmic rays), the ionized component may disappear completely, in which case the magnetic field will eventually exert no effect at all.

In real life, the ionization rate will decrease gradually as the cloud contracts and the lines of forces will slowly slip out of the cloud under the pull of the magnetic pressure.

The recession of the lines of forces is retarded by the fact that the field carries with him the ionized component of the gas, through the neutral component. The velocity of recession is obtained by equating the magnetic force to the rate of momentum exchange between the neutral and the ionized component :

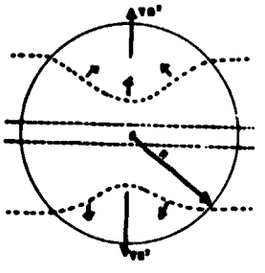

SPITZER (1968), and MESTEL (1965) have analyzed this problem. Too little is known about the intensity of the ionizing agents in dark clouds to decide whether the field will be evacuated fast enough.

LEQUEUX will talk about observation of magnetic fields in dense clouds. According to the present data, there is no clear indication that the relation $B \propto \rho^{2/3}$ is obeyed. Quite on the contrary, it seems that hardly any B increase occurs for N_H going from 10 to > 10^3 cm^{-3}. The magnetic field may, after all, be evacuated faster than we believe !

Another incidence of the same problem is, of course, through the present value of the solar magnetic field.

Assuming a dipolar field (with dipole moment $M_D = BR^3$) and assuming flux conservation, we should find $M_D(t) = B_c R_c^2 R(t)$ (where B_c and R_c are appropriate for the initial cloud) $\simeq 10^{41}$g cm^3 for the present solar value and a surface field of $\simeq 10^6$g, many orders of magnitude above the observed value. This again, points out to the need of evacuating a very large fraction of the initial magnetic energy.

In the A + A model the high initial flux is rather a benediction : the assumption is made that at, the moment of formation of the solar system, the dipole moment was larger than 10^{38}g cm^3. The whole process starts with an initial cloud of typical interstellar matter surrounding the sun and largely ionized (at least enough to impede the fall of the matter on the sun). The density is somewhat greater than $N_H = 10^5$ cm^{-3} and the radius $\simeq 10^{17}$ cm.

As time proceeds the ionization of the gas decreases (for instance through a decrease of the cloud temperature). The elements with the highest ionization energy first get neutralized and fall toward the sun. As they get closer to the sun they gain speed and become ionized again when their kinetic energy is somehow comparable to their ionization potential.

The inward motion is thereby stopped; this way the atoms will be sorted at various distances from the sun according to the value of their ionization potential.

The strength of the field needed to retain the matter at the planetary distances gives a lower limit to the product of $M_D\, t^{1/2} > 10^{46}$g cm^3 $s^{1/2}$ where t is the time duration of the whole process.

A + A choose a value $t = 3 \times 10^8$ y (no justification is given for this choice) and obtain the value of 10^{38} quoted above.

The very high surface field obtained for such a high dipole moment are eliminated in A + A's view by assuming that, at the moment of planet formation, the sun was much larger ($\sim 10^{13}$cm) How the sun could have remained at such a large radius for 10^8 years is not explained.

CAMERON has indicated a way by which the magnetic field barrier may be at least partly overcome, again in the framework of the density wave theory of the spiral structure.

Upon entering the arm regions the interstellar gas gets compressed and forms a ridge of increased density parallel to the arm, and hence parallel to the magnetic lines of forces (observationally known to follow the arms).

CAMERON combines this theory to the theory of interactions between the galactic cosmic rays and the galactic magnetic fields developped by PARKER (1966).

One effect of these interactions is the development of magnetic instabilities by which, under the pressure of the cosmic rays, tubes of magnetic fields previously contained in the plane of the galaxy (and following the arms) would curl like snakes above and below the plane (but always in the same arm). This is represented pictorially along an unfolded galactic arm :

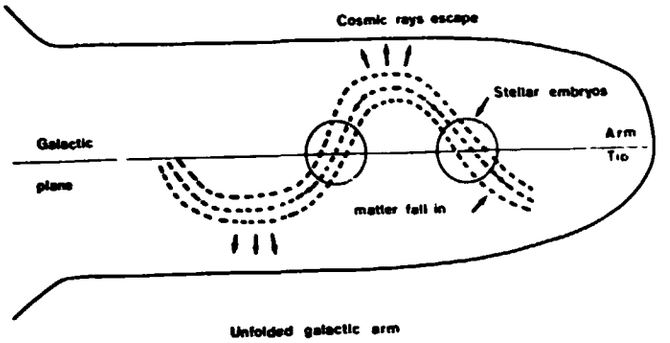

A number of arches are made this way, which channel the cosmic rays in low density regions (far above the plane) from where they presumably escape from the galaxy. Quite on the contrary, the interstellar matter contained in the tube, attracted by the gravitational field toward the plane, will slide along the lines of forces and accumulate in the plane. The crucial point here is that, since the compression takes place in a direction parallel to the field, the flux within a tube is left almost unchanged and the magnetic pressure is hardly increased (a correct discussion would show that there is some effect on the flux due to the general increase of the gravitational field -see MESTEL (this volume) for a discussion of these so called magneto-gravitational state of equilibrium-).

CAMERON expects this to be an important step in star formation but still requires in a latest stage, a phase of ambipolar diffusion to remove the unwanted field. He follows the discussion of SPITZER and concludes that when $N_H = 10^5$ the ion density becomes low enough for the field to quietly leave the stage.

The Angular Momentum Barrier.

The angular momentum of a typical interstellar cloud can be estimated in the following way. In view of the (observed) differential rotation of the galaxy we may expect it to rotate with an angular velocity of $\simeq 10^{-15}$ s^{-1}. Furthermore, as pointed out by LARSON (references in this volume), over and above this "ordered" component (aligned with the galactic angular rotation vector), the cloud will possess a "random" component which is likely to be appreciably larger. In proof of this statement LARSON mentions that, after all, the mean angular rotation vector of stars in clusters does not show preferential aligment along the galactic axis.

This random component is assign by CAMERON to turbulent motions in contracting clouds. Thus the mean angular momentum per unit mass of a large homogeneous cloud of $\simeq 10^3$ Mo with $N_H \simeq 10^3$ is :

$$L_c/M_c = 0.4\ R_c^2\ \Omega_c$$

at least 10^{22} cm^2 s^{-1} (corresponding to $\Omega_c = 10^{-15}$ s).

Unless the cloud is somehow linked to the outside, L will remain constant during the contraction. And as long as the cloud contracts homologously L/M also remains constant, and Ω increases with R^{-2} (as B for the magnetized cloud). Thus the equatorial rotational force ($\propto \Omega^2 R \propto R^{-3}$) increases faster than the gravitational force (R^{-2}) and the contraction in the equatorial plane is eventually stopped at a radius for which the forces are equal. As in the case of the magnetic effect, contraction perpendicular to Ω is also slowed down and does not really change the issue.

Equivalently we may define a total rotational energy :

$$E_R \simeq M\Omega^2 R^2 = M\Omega_c^2 R_c^4/R^2$$

which becomes comparable to the total gravitational energy at the limiting radius :

$$R_1 \simeq \Omega_c^2 R_c^4/GM \simeq 10^{16} \text{ cm}$$

for the case discussed above.

The cloud is expected to fragment into a number of stars of solar masses. The initial angular momentum of the cloud goes partly in orbital movement of the components around the center of the cloud and partly in spin components.

Since the angular momentum per unit mass goes as :

$$L/M \simeq \Omega R^2 \propto \Omega (M/\rho)^{2/3}$$

fragmentation from $M_c = 10^3$ M$_\odot$ to $M_s \simeq 1$ M$_\odot$ reduces L/M by $\simeq 10^2$ and we reach a value of $\simeq 10^{20}$ cm^2 s^{-1} for a typical spin value.

For comparison with reality we must consider two sets of objects : early types stars and late type stars.

It is well known that stars earlier than F usually rotate at a fair fraction of their maximum possible velocity ($v_{max} \simeq 400$ km s^{-1}). Observed (projected) values above 100 km s^{-1} are general occurence, and values above 150 km s^{-1} are not infrequent. Assuming more or less rigid body rotation, the corresponding L/M is $\simeq 10^{18}$, about one hundred times smaller than the initial values after fragmentation.

Stars later than F rotate at much slower rate (a few km/sec) and have L/M $\simeq 10^{16}$ cm^2 s^{-1}. In this context it has been noted that although the sun belongs to the second group ($L \simeq 10^{49}$ g cm^2 s^{-1}, unless DICKE is right !) the solar system, as a whole, really belongs to the first group ($L \simeq 10^{51}$ g cm^2 s^{-1}). From there, the suggestion that the sun has transferred most of its initial angular momentum to the planets was put forward and became an essential element of the theory of HOYLE. F., (1960).

However recent astronomical observations have casted some doubts on this issue.

Through the work of CONTI, DANZIGER, WALLERSTEIN, (see the review of WALLERSTEIN and CONTI), (1969), it has become apparent that F and G stars arrive on the Main Sequence with rather large rotation velocity and that they are gradually slowed down in a period of 3 x 10^8 - 10^9 years (obtained by comparing the rotation curve of several young galactic clusters). Furthermore the braking of the rotation is accompanied by CaII emission lines which are usually associated with non-thermal electromagnetic activity (for instance in solar flares).

This appears to give weight to the mechanism of angular momentum loss by stellar wind and

flares (as suggested by SCHATZMAN).

For a number of reasons to be discussed during the week it appears highly improbable that the formation of the solar system would have lasted so long : it seems more likely that the angular momentum lost by the sun was not transferred to the planets.

All this suggest, in our context, that while a theory of the formation of the solar system should explain the reduction from $L/M = 10^{20}$ to $L/M = 10^{18}$ ($L = 2 \times 10^{53}$ to 2×10^{51}) it needs not necessarily incorporate the second reduction from 10^{18} to 10^{16} (2×10^{51} to 2×10^{49}) during which the planets are probably mere spectators (at any rate, the present planetary system has an $L = 3 \times 10^{50}$ and if we add up the missing volatiles of Uranus and Neptune we should easily reach 10^{51} - and there may be even a lot more in the distant parts of the solar system).

One obvious qualitative explanation for the ang. momentum loss is through the interaction of the rotating cloud with interstellar magnetic field. In one variation or another, this theme comes back throughout most of the recent literature. For instance, HOYLE (1960) considers a nebula in its very early stage which is connected to surrounding interstellar clouds by the lines of forces of the galactic magnetic field. As it starts to collapse, it turns faster, and the lines of forces, wound up by the motion, exert a torque by which the angular momentum is transferred to the clouds.

This effect could be of importance only if the collapse time could correspond to several revolution periods (in order for the winding to become appreciable). However in the first stages of collapses neither the pressure nor the centrifugal force can prevent the cloud form falling-in with approximate free fall velocity. Since the free fall time is always quite close to the revolution period, very little twisting should take place at that time.

In conjonction with stellar formation SPITZER has considered the application of this process to a rotating cloud and has shown that the time for evacuation of the angular momentum must indeed be much larger than the free fall time.

One must then require that the cloud be somehow stabilized against collapse for the duration of the process. This could happen by the virtue of the centrifugal force itself : the process could start after the cloud has reached the equilibrium radius between gravitational and rotational energy. A second phase of angular momentum transfer is assumed to occur, in the model of HOYLE, when the nebula has contracted to its limiting rotational radius (at Mercury's orbit in this context). The outer part of the disk is coupled to the central condensation (protosun) by magnetic lines of forces. Through differential rotation, this coupling transfers angular momentum to the (partially ionized) disk and exerts a force (with radial component) on the gas. A ring of matter is detached from the nebula and pushed away throughout the inner solar system. This matter, after cooling, condenses into the planets. This scheme has been seriously criticized in particular by WHIPPLE (1964) and SAFRONOV (1960). The objection has to do with what happens when one adds an outward force to a nebula graviting around a central star : the net effect is an equivalent "weakening" of the attractive force and hence a decrease of the orbital velocity below the Keplerian value.

Particles orbiting with the gas would not (if they have no electromagnetic moments) feel the radial force and hence would rotate faster than the gas. The gas drag on these particles would decelerate then and move them forward, not away from the sun.

PRENTICE and TER HAAR (1971) have presented a model of the evacuation of the "interstellar" component of the angular momentum which shows some similarity with the previous paragraph.

Following the model of REDDISH and WICKRAMASINGHE (1969) they assume that, in clouds with $N_H = 10^3$ to 10^4 the temperature will be low engouh for hydrogen to condense on grains

(T ≈ 3 K). Hence we have now a nebula with a fractional mass of ≈ 70% (the interstellar hydrogen mass fraction) under the form of solids.

The most important gas component is helium, partly neutral and partly ionized. The ionized fraction is tied out to the magnetic field and rotates with it. The neutral fraction is dragged by the ionized component and by the grains, and the grains are dragged principally by the neutral gas. The net effect of the drag is that the grains spiral inward, thereby causing a redistribution of the angular momentum density throughout the nebula. Since the grains essentially fall "spoke-like" they retain their angular velocity as they approach the center and hence loose some angular momentum, which is then transmitted, via the neutral component, the ionized component and the magnetic field, to the "outside".

This way, in a period of 10^7 years, one may decrease the original L by a factor of about one hundred.

The most crucial point in this model is, of course, the assumption of a medium of low enough temperature for the hydrogen to condense on the grains. Observations of clouds with $N_H \approx 10^4$ cm^{-3} hardly confirm this assumption. It is clear that a thorough discussion of the required interstellar conditions in comparison with the observations would be needed for the model to gain plausibility.

Furthermore the separation of hydrogen and helium could raise some difficulties in later stages. A logical trend of this model would be for the central star (the sun) to contain most of the hydrogen while the helium would be left out. Then the similarity between He/H ratio in stars and in interstellar space would not be accounted for unless special care is taken to invent a later step in which the re-mixing somehow occurs.

Another way of explaining the reduction of L/M from the interstellar value ($\approx 10^{20}$) has been presented by Mc CREA.

He points out that, in the fragmentation process from a cloud of $\approx 10^4$ M$_\odot$ to solar masses, the initial angular momentum will go partly in relative motions of fragments and partly in spin motions. Off hands, one would expect that the initial angular momentum would be shared more or less equally between these two types of motions. Mc CREA assumes that the sun originates from those fragments which happen to have a low spin rotational energy. This, of course, places his theory in the realm of the "improbable" one, as discussed before.

The association of such a model has a certain aesthetic aspect which escapes a rigorous discussion. My own feeling is that one is better off if he does not have to appeal to a fortuitous set of events.

CAMERON, basing his speculations on the theory of turbulence developed in particular by LANDAU, considers the fragmentation of an initial cloud which results in a cloud of two solar masses with an angular momentum $L \approx 10^{54}$ ($L/M \approx 2.5 \times 10^{20}$)(no special assumptions are made in the partition between orbital and spin angular momentum of the fragments).

These fragments, then, collapse into a disk of 10^{15} cm, in which the surface density has been redistributed in such a way as to conserve the angular momentum of each mass element (no loss of angular momentum). In view of the large value of L the disk presents no central condensation : its surface density decreases roughly as R^{-1} as far as 10^{14} cm.

These conditions prevail throughout the life of the solar nebula (and formation of the planets).

The mechanism of redistribution of angular momentum takes place during the life of the

nebula itself and leads to its dissipation. It is associated with circulation currents induced by the dynamic structure of the nebula itself and the consequent profile of the rotation velocities as a function of height above midplane. CAMERON argues that these currents will lead to a transport of angular momentum away from the sun.

The exact fate of the initial 10^{54} g cm^2 s^{-1} is not discussed in detail but one can presume that most of it is carried away past the region of the planets, in the protocometary cloud (which he associates with satellite clouds rotating around the protosolar cloud) or even farther under the form of a T-Tauri-like stellar wind.

In the model of A + A the initial rotation of the cloud is not considered. Quite on the contrary the matter falling on the sun (as far as I can see, the motion is radial) is rotationally accelerated by the rotating magnetic field of the solar dipole at the moment that it becomes ionized (by conversion of its kinetic energy in atomic excitation) at the planetary distances. A + A consider that the absence of hydromagnetic effect in the classical Laplace nebula raises the difficulty of finding an adequate support for the cloud against the gravitational pull of the sun, before the cloud can be accelerated into Keplerian motions.

It would seem that the observed differential rotation of the galactic matter not only provides an adequate mean of support right from the beginning but even overdoes the job and raises the problems discussed in this chapter.

Finally SAFRONOV starts his model with a fully developed nebula, rotating in Keplerian orbit at planetary distances. The three barriers described here are assumed to be already surmounted when the story begins.

Question N° 5.

ON THE PHYSICAL CONDITIONS IN THE NEBULA.

One first dividing line between the models is related to the answer to the following question : do the analysis of the physico-chemistry of the meteorites show effect of ionization in the gas (indicating a gas temperature much larger than the grain temperature, hence a state of thermodynamical disequilibrium) or can we understand everything in term of chemical reactions between neutral atoms in thermodynamical equilibrium.

A + A (see references in this volume) have taken the first view ; they state that the evidence from chondrites "suggest" that the solids crystallized at low grain temperature (200 1 000 K) from the gas when it was still partially ionized ($\sim 10^4$ K).

This immediately suggests a low density gas, kept in a state of partial ionization (for instance by electric currents). A + A picture their nebula as a "super corona" - in which the physical conditions are quite similar to those of the solar corona (high degree of ionization, strong effects of the magnetic field, etc...). (The pleasant point here is that one is dealing with "familiar" conditions.

As pointed out by LINDBLAD (1935) solid grains embedded in such a gas will emit strongly in the infra-red (for which the gas is transparent) and hence will take a much lower temperature than the gas.

The degree of ionization of each atomic species in the gas will be closely correlated with their ionization potential.

The crucial point here is that the absorption properties of the grains for the atoms of the gas should be very different if the atoms are neutral or ionized and the sequence of absorption of elements, as the gas temperature decreases, should somehow be related to the ionization potential of these elements. A + A discuss the Nickel-Palladium-Platinum correlation in iron meteorites which appears to confirm the presence of ionization effects. However, as they point out themselves, the ionization potential is also correlated to the chemical bond strenght of the atoms in a solid and hence the Ni - Pa - Pd correlation may still be explained by thermal equilibrium processes.

The requirement of a low density nebula (for ionization effects) is incompatible with the so-called Laplacian ne[illegible] in which all the matter of the solar system was at the same time in a gaseous state surrounding the sun.

The alternative is, of course, a gradual addition of matter falling from far away and being kept for a certain residence time under the form of a plasma corotating with the sun. For the conditions that the authors favor the densities in the gas are 10^5 to 10^7 atoms cm^{-3} and the required time of gas addition 10^8 to 10^9 years. The trapped plasma gradually condenses in grains and these grains are then injected in the "jet streams" to be discussed later.

The dilemma : "equilibrium or not" will be discussed later by ANDERS (this volume). After years of close scrutiny of the available material, himself and his group find no strong reason why they should abandon the simplicity of equilibrium situation.

Contrary to the quasi-stationary nebula of A + A, in all other models we should expect things to be rapidly evolving. There does not yet exist calculations of the time evolution but several authors have tried to obtain an estimate of the average physical conditions during the life-time of the nebula.

In CAMERON's nebula the distribution of rotational velocity is obtained from the condition of conservation of angular momentum density during the gravitational collapse of the original gas cloud.

The temperature-density profile at mid-plane is obtained from the results of models by LARSON (references in CAMERON's text), and the effect of the consequent radial pressure gradient on the structure of the nebula is taken into account. Temperature, pressure and surface-density profiles have been calculated as a function of the radial distance. The vertical structure of the nebula has also been considered, and for this aim, studies have been made of the opacity of a low temperature gas (from 200 to 4 000 K) taking into account the formation of metallic iron grains and ice in the low T range. This study in itself is an important contribution to the subject, and its value will remain even if the model does not. The very high opacity of these solids is responsible for the generation of strong vertical convective motions in the region from 3 to 10 A.U. other convective zone appears in the center of the nebula (< 1 A. U.) due to the dissociation of hydrogen molecules.

Because of the effect of the radial gas pressure, the circular velocity of the gas in the nebula will be smaller than the Keplerian velocity (i. e. for a freely orbiting body) at the same distance. Consequently there will be a rotation velocity difference between the gas and a large solid body gravitating in the nebula.

PINE and CAMERON compute that while the Keplerian velocity is ≈ 5 to 10 Km/sec everywhere up to 10 A.U., the velocity difference between the gas and the bodies is ≈ 1 Km/sec in the same region. This will play an important role in their views of the accretional processes (gases

are swept away by solid bodies).

PINE and CAMERON also try, although in an admittedly very crude manner, to evaluate the life-time of the nebula against its dissipation by internal circulation currents.

The nebula dissipation time varies from 10^2 years at 1 A.U. to 10^4 years at 10 A.U.. CAMERON concludes that, consequently, planet formation had better be a rapid process...

The nebula of SAFRONOV rotates in Keplerian orbit around the sun (force field in R^{-2}).

Its thickness is determined by the condition of balance of vertical gas pressure against vertical component of gravitation. It increases with distance in such a way that the surface of the nebula is largely exposed to solar radiation. The heat is absorbed by the dust grains embedded in the nebula. Temperatures are ≈ 100 K in at the inner planets, and 30 K to 10 K at the outer planets. (The sun is assumed to have its present luminosity).

SCHATZMAN has a rather similar picture of the nebula. The surface density in the disk is estimated to be $\sigma \approx (10^4\ R^{-2})$ g cm^{-2} (where R is the distance in astronomical units) and, because of dust, the opacity is very large ($\approx 10^5$). The heat is absorbed in the outer surfaces and an isothermal inner layer developps with temperatures of ≈ 200 K at the earth and ≈ 50 K at Uranus-Neptune.

As for SAFRONOV the vertical structure is given by the vertical component of the gravitational field from the central body. The nebula is rather thin and flat.

For TER HAAR (this volume), the nebula appears as a cloud of ≈ 0.1 M⊙ with solar composition rotating around a sun very similar to our present sun. The density profile is obtained, taking into account the pressure gradient (mostly turbulent pressure according to TER HAAR). The density at mid-plane is given as :

$$\rho(r) = 10^{-10}\left(\frac{r}{2\ \text{A.U.}}\right) \exp\left[1 - \frac{r}{2\ \text{A.U.}}\right]$$

(with a maximum at 2 A.U.). The temperatures vary from ≈ 300° for the inner planet to ≈ 30° for the outer ones and the lifetime against dissipation processes induced by turbulence is at most 10^3 years.

The next step in TER HAAR's model describes the basic mechanisms for condensation of a gas and the crucial role played by the temperature : although the density profile presented above assign a relatively small fraction of the mass to the region of the outer planets, in view of the lower temperatures in this region, much more atomic species will manage to condense (i.e. will find their partial pressure to be larger than the local pressure). In fact, he finds the product of the density profile with the fractional mass condensation profile to match in a reasonable way the mass distribution in the solar system.

Question N°6 :

ON THE MECHANISM OF GAS CONDENSATION AND PARTICLES ACCRETION.

We enter here in one of the most obscure chapters of our book.

Some of the texts written on the subject carry a definite resemblance to the writing of the mediaeval alchemists...

Most authors agree that the initial step is the presence of interstellar grains in the gas, that these grains, after some degree of gas absorption, find themselves concentrated in the nebular plane and then somehow manage to accrete into larger bodies. The main problem of course, is the fact that the number of these bodies must eventually be reduced considerably (i.e. from swarms of small bodies we should eventually produce a few big planets), that the reduction can only take place by collisions of these bodies, and that although we know very little about the "sticking" probability of rocks in vacuo, nevertheless we have the feeling that at the typical speed expected for bodies in Keplerian orbit around the sun ($\simeq$ 10 km s^{-1}), collision of rocks is not very likely to lead to coalescence...

One further difficulty comes from the time scale required for the process, especially in the remote part of the solar system.

For instance, at the distance of Uranus and Neptune, a simple-minded calculation (with "non-educated" guesses on the basic assumptions) would yield ages larger than the age of the universe.

In the model of SAFRONOV we start with a quiet nebula in which dust particles rotate and start sinking slowly (by gravity) toward the equatorial plane. The assumption is made that all the particles it meets, on its way down, adhere to it, and, upon arriving to mid-plane, (after $\simeq 10^3 - 10^4$ years) it has reached $\simeq$ 1 cm in dimension.

The critical assumption here is the so called "cold welding" of matter which clearly represents an upper limit to the efficiency of the process. We shall hear several reports on this subject and on recent related experiments during the Symposium.

As the density of the dust layer exceeds a certain value, matter condensation would be induced by gravitational instabilities.

Critical "Jeans length" for these condensations and lower limit to their mass depend again on the density of the layer and on the mean thermal velocity of the grains (they play the same role as the gas molecules in the problem of star formation discussed earlier).

The very low velocities required could probably be found in the region of the giant planets Jupiter and Saturn, leading within $\simeq 10^5$ years to the condensation of bodies of $10^{16} - 10^{22}$ g.

In the regions closer to the sun the gas motions would have been too fast for gravitational instabilities to take place and growth of the bodies could only have taken place through aggregation during collisions. SAFRONOV argues that the relative velocities of the bodies should be determined by their gravitational perturbations at encounters and in fact should be less than 1 m/sec as long as the objects are less than 5 km in diameter. This velocity is 10^{-4} less than the Keplerian velocity and $\simeq 10^{-3}$ less than the relative velocities of bodies traveling in orbits with eccentricity difference of $\simeq$ 0.1.

The estimate is based on hydrodynamic arguments (the random motions are obtained from the dissipation of mechanical energy of a viscous fluid with a velocity gradient) which in turn assumes that the bodies are completely controled by the gas motions. This assumption is certainly correct for small bodies, clearly, however, it must break down at a certain mass.

Above this mass the motivation for the low velocities should not hold anymore and we should get our problem back.

The problem of reducing the relative velocities of colliding bodies in order to facilitate coalescence is dealt, within the model of A + A, by the introduction of the concept of "jet streams".

These authors argue that while a beam of particles shot in a medium at rest will be diffused and loose the parallelism of the initial motion, this effect will not take place if the beam is orbiting in a gravitational field, provided that collision frequency be less than the Keplerian frequency (many revolutions between each collision). In this case "collisions" lead to an equalization of the orbits of the colliding particles, with the result that the spread in space and in velocity is reduced.

It must be said right away that the validity of this new point in specific solar system circumstances has not gained general acceptance.

We shall hear more about it, in particular from WHIPPLE.

The sequence of events, then starts with a thin plasma corotating with the sun, in which grains gradually condense (as described before, in a state of strong thermodynamical disequilibrium). Mutual collisions ("viscosity") between these grains tend to focus them into a number of jet streams, with toroidal shapes centered on the sun.

The relative velocities are reduced considerably and accretion becomes possible. A + A assume that the maximum possible velocity for accretion is 0.5 km/sec and that collision at lower velocity will always lead to accretion (the cold welding again).

SCHATZMAN follows the analysis of Mc CREA and WILLIAMS (1945), (references in the text of Mc CREA). Large particles fall in the nebula and carry with them all the dust particles they meet (always the cold welding...).

CAMERON recknognized that during the lifetime of the nebula, the collision probabilities are too low for the accretion to take place in any reasonable time especially for the outermost planets.

He points out however that during the collapse phase from the interstellar cloud into the nebula the situation was much more favorable since the violent gas motions (in the form of turbulent eddies) would have considerably increased the collisions probabilities of gas and grains.

The physical conditions in the turbulent collapsing cloud are estimated qualitatively ; typical grain velocities are $\simeq$ 10 m/sec and CAMERON assumes a sticking probability of one at encounters (the cold welding...).

At the end of the collapse the nebula is formed and the turbulence rapidly decays out embedding a set of bodies "extending" up to 20 cm in radius.

As in the model of SAFRONOV, as soon as the nebula takes its shape, there is a rapid migration of particles toward the central plane. However, in view of their large size, the migration is much faster than in SAFRONOV's case,(typical duration $\sim 10^2$ years for this process.)

As discussed previously,two convective zones appear in the nebula. CAMERON studies the motion of the bodies in and out of the convective eddies. He estimates that particle velocities due to the motion of the gas should be $\sim 10^5$ cm s^{-1} and the collisions in these circumstances should lead to partial melting leading to ejection of droplets in free space. This, of course, is a pleasant thought for anyone who wants to understand the origin of chondrules. CAMERON glady forsakes his old attachment to WHIPPLE (1966) mechanism involving lightning flashes in the nebula.

Inside the eddies the relevant velocities are not the mean convective velocities discussed in connection with chondrules, but rather the turbulent velocities which should be much smaller ($\sim 10^3$ m s^{-1}). Bodies will form, embedding chondrules, which upon further collisions should tend to

form amalgamates that CAMERON likes to associate with meteorites.

Question N°7 :

ON PLANETARY FORMATION.

We resume our story at the moment that a number of bodies are happily orbiting and joyfully colliding against each other, like madly driven cars at village fairs. We still have to follow the story until we are left with a small number of large objects (planets and asteroids) orbiting in a very clean (dust and gas-free) system.

Some particularly remarkable features of the end-product (the solar system) deserves first a general discussion.

1. The Titius-Bode Law.

One of the most difficult problem in studying the origin of the solar system is to identify amongst the whealth of experimental data, those which are really relevant, and then to estimate appropriately the degree of their relevance.

Many authors, for instance, have felt that the Titius-Bode law, in its "exact" form should be a crucial key to the understanding of the system, and that consequently it should be introduced as a strict "boundary conditions" into any model. This has mostly lead to unpleasant parameter-fitting and the "beautiful agreement" between "calculated values" and "observations" has convinced very few people.

The first mistake was to call it a "law" : it is, a best, an approximate relationship which should be quoted in the form ($r_n \propto \beta^n$) where $\beta \simeq 1.7$ and not in the artificial, and in certain cases wrong, form : $r_n = 0.4 + 0.3 \times 2^n$ A.U.

The Titius-Bode relation may then be only a qualitative feature related to the scaling of the physical phenomena as one goes away from the central body (as discussed by TER HAAR).

A similar relationship holds for groups of satellites of Jupiter, Saturn and Uranus. The values of β range from 1.5 to 1.8. The real meaning of all that is still unclear, but the danger of overworking the details of this relationship is generally reckognised today. MESTEL and DERMOTT will discuss this question during this Symposium.

II. The Isochronism of Spins :

Similarly, there is the very remarkable isochronism of spins. A+ A, in particular, have noted that almost all asteroids have periods between 5 to 15 hours. Even more remarkable is the fact that the planets themselves have almost the same spin period. As a whole, for objects ranging from 10^{19} to 10^{30} gm the rotation periods hardly vary by more than a factor of four !

One fact to bring in the discussion is that the maximum rotational period is $\propto \rho^{-1/2}$, and since mean densities are all quite similar in the various objects (from ~1 to ~5) this period is about one quarter of an hour for all bodies. Thus the objects rotate at about 3% of their limits. Let us recall also that the maximum rotational velocity are, within a small factor, equal to the escape velocity.

Let us imagine that small bodies are continually being accreted by a larger body and

that their initial velocity (at "infinity") were at most comparable to this escape velocity. The angular momentum imparted will be ~ $\Delta M v_e r_i$ where r_i is the impact parameter. Let us further assume that the collision always takes place on the same side of the body, at $r_i \simeq R$ the instantaneous radius.

As R grows, the total angular momentum will correspond, very closely at least, to the maximum rotational velocity ($\simeq v_0$).

Reality will, of course, be different since collisions will take place all over the surface of the rotating body and the net effect on the imparted rotation will be related to the distribution of angular momentum as a function of radial distance from the sun. That the net effect should be a few percent seems perfectly reasonable qualitatively but to extract quantitative information from this result is a far more difficult task... (see the discussion of TER HAAR, A + A and SAFRONOV in this volume).

And is it reasonable to use this description of events in the case of the gaseous Jupiter and Saturn ?

In the following paragraphs we shall see how the various modelists have envisionned planetary formation and what explanations they have imagined to a number of problems.

SAFRONOV has studied the mass distribution of bodies following collisions for certain definite choices of the "cross sections" for coalescence or fragmentation. One interesting result which seems to emerge from these calculations is the prediction of an inverse power-law mass-spectrum of objects $N(m)\,dm \propto m^{-q}\,dm$ where $q \simeq 1.5 + 1.8$, independent of the initial distribution of masses.

The choice of the cross-sections is rudimentary (as describe elsewhere we shall need a great deal of work before we can establish realistic and physical parameters) and it is too early to decide if this important prediction will eventually be confirmed. At any rate this prediction may lend itself to test, for instance in the asteroid belt (but in my ignorance, I am not aware of existing analysis of this point).

The power law mass-distribution can clearly not be applied to the few biggest bodies. SAFRONOV argues that in various annular (circumsolar) zones, the biggest body will always, in view of its gravitational field, take the lion's share ("on ne donne qu'aux riches") and that the mass ratio between the two largest objects will rapidly reach values of tens to hundreds.

The rest of the story is, of course, the story of how this "predestinate" body managed to round up the matter surrounding itself and to become one of the planets. The rate of growth is amongst other factors, proportional to the surface density (σ_0) of condensable matter in the central plane at the corresponding distance from the sun, and inversely proportional to the rotation period T_R at that distance.

At Earth the space density of matter would decrease exponentially with a period of 2×10^7 years. The formation of the earth, as we know it now, would have then taken $\geq 10^8$ years. (> 5 mean lives).

For Jupiter and Saturn the lifetime of growth is $\simeq 10^8$ years.

SAFRONOV reckognizes at this point an important difficulty : in such a large period the proto-Jupiter would have gathered all the gases in its "orbital" (to speak like the chemists). However in view of SAFRONOV's initial choice of the nebular mass ($\simeq 0.05$ Mo), less than 10% of these gases should have been incorporated in Jupiter.

To solve the difficulty SAFRONOV appeals to the high electromagnetic activity of the

young sun and to the versatile and benevolent mighty "solar wind" of these days to have rapidly removed these unwanted volatiles before Jupiter got hold of them. The counteracting effect of the body rotation on the gas accretion is also invoked to solve this difficulty.

The low fraction of H and He in Uranus and Neptune would also find there a natural explanation : in view of the long formation time, the depletion of volatiles would have been even stronger at these large distances.

While collision of bodies has lead to embryonic growth of the planets, distant encounters in the late stage may lead to ejection of a body out of the solar system if its velocity after the encounters lies in an appropriate angular cone. SAFRONOV estimates that a mass of 10^{-3} M⊙ has been ejected this way. A much smaller fraction of 10^{-5} M⊙ would have been thrown in the elliptically elongated orbits characteristics of the comets.

One old and tentalizing problem is : why should there be an asteroid belt between Mars and Jupiter, instead of a fully grown planet ? After all even the Titius-Bode law predicts something there !

The idea of an "exploded planet" has been very much discussed by science writers and science fiction writers ; a dignified version has given rise to the idea of "parent bodies" for meteorites (ANDERS -in this volume- tells us why he likes the idea).

SAFRONOV rejects the whole idea on the ground that it could not explain the existence of families of asteroids ; in his view the process of accumulation in the asteroid belt has simply been interrupted too early. However, since the rotation period is longer at Jupiter than at the asteroid belt (recalling that the formation rate is $\propto \sigma_0/P$) we should look for a strong overcompensation increase in σ_0.

As TER HAAR, SAFRONOV likes to identify this increase of σ_0 to a temperature effect ; in the zone of Jupiter the molecules of CH_4, and NH_3 have solidified and added themselves to the dust.

Furthermore the mass of the gravitational condensation increases rapidly with distance from the sun, and their gravitational field are even made responsible for an inhibiting effect on the growth of the asteroids.

It is, of course, during that phase that the planets have acquired their rotational period. SAFRONOV makes an appropriate distinction between the "regular" direct component, associated with the rotation of the whole initial system, and the "random" component obtained after subtraction of the regular component from the observed values.

To deal with the regular component, and in particular with the isochronism of spins, SAFRONOV defines first an asymmetry parameter $\bar{\beta}$ describing the degree of asymmetry of impacts over the surface of the body, and he mentions that if $\bar{\beta}$ does not depend on the distance from the sun, the rotational periods of the planets must be approximately equal (but this description should not be applied to Jupiter and Saturn).

The "random" component is assigned to fluctuation over and above the regular asymmetry coefficient described before. Their effect will be seen through a "north-south" asymmetry in the impact distribution, resulting in a tilt of the planetary spin.

The observed tilt can be related to the largest infalling masses : for the earth the biggest object was $= 10^{-3}$ of the earth mass while for the highly anomalous Uranus we need 7% of planetary mass.

SAFRONOV, following SCHMIDT and RUSKOL, (references in the text of SAFRONOV), adopt the idea of satellite formation by solid particle accretion in the gravitational field of the simultaneously growing planet.

The initial heat of the earth was predominantly brought by the collision of infalling bodies. The central temperature is about 800 K.

He also stresses the particular effects of the impact of large bodies ($\sim 10^7$ cm). Temperatures of up to 1 500 K can be reached locally in a highly inhomogeneous fashion, which could be responsible for a large part of geochemical fractionation.

As their last step before planetary formation A + A describe the growth of an "embryo" immersed in a "jet stream" (a swarm of small particles orbiting in almost parallel orbit inside a toroidal volume surrounding the sun). The embryo sweeps up particles with a cross-section magnified by gravitational effects (gravitational Rutherford scattering).

The formation times are around 10^6 y for Mercury, Venus, Earth and Jupiter ; for the moon, Mars and Saturn, they could reach 10^8 years which is also, in their estimates, an appropriate value for the duration of the plasma injection from the outer infalling cloud. Uranus and Neptune would get, in this count, impossibly long formation times. A + A solve the problem by assuming that these planets have accreted after the end of the injection period : the jet would, then, contract. Its mean matter density would increase and the formation time would be reduced considerably. No numerical discussion of this last hypothesis are given.

In SCHATZMAN model (adapted from MAC CREA and WILLIAMS) the formation of Jupiter by collision of rocks takes $\sim 10^6$ years ; at Uranus and Neptune the formation time is again impossibly long.

As the embryo gathers matter from a rain of infalling particles, it also warms up because of the kinetic energy released at impacts. A + A make the distinction between the heat in the "accretional heat front" and the internal heat profile at the end of accretion. When an object hits an embryo, an amount of heat is suddenly released which may be large enough to melt a mass of ground material several times larger than the infalling mass, especially at the end of accretion, when the escape velocity corresponds to a few eV per nucleon. At low impact rate, the material will have time to cool before it is melted again by another impact.

After a few melting (at most) this same material is buried too deeply to feel further impacts. This way an accretional heat front follows the surface of the forming planet.

The growth rate of planets (for simplified assumtions on the feeding of matter in and out of the jet stream) has been evaluated by A + A. A maximum in the growth rate of the planet (and hence in the rate of energy release) usually appear somewhere during the process. In the case of the earth, for instance, the rate at the beginning (core formation) and at the end (mantle formation) are low enough for the matter to cool down between impacts, but for the intermediate layers the situation is opposite. Hence there should have been a maximum of temperature at around 1/2 of the radius of the earth. No numerical values are given except that this effect should account for the fact that "only an intermediate part of the Earth is melted, whereas both the core and the mantle are solid".

It is estimated that Mercury and the Moon should have been solid and cool immediately after their formation. Other planets are also qualitatively discussed.

The accretional heat front is also invoked as a factor of chemical segregation : the heavy component can only sink through the instantaneous layer but the light components are continually brought up. This way the radioactive elements may be carried to the surface even though the planet is finally left in a cool state.

After meter-sized bodies have fallen at mid-plane(in a few years)CAMERON studies their rate of growth by accretion according to a picture presented initially by WHIPPLE.

Let us remember that in view of the radial pressure, the gas rotates slower than the corresponding Keplerian velocity. According to their size the solid bodies are slowed down by the gas drag, and spiral inwards. The differential motion of large and small-size particles (due to the different gas drag) will be conducive to a sweeping up of the former by the latter and will result in an exponential growth rate, limited by the consequent clean-up of the reservoir.

The kinetic energy released is transformed in heat and radiation. In the outer (radiative part) of the nebula, where the temperature is $\sim$ 100 K, a dominant role is played by the ice. Upon melting, it forms an atmosphere of steam with a few ice clouds on top at T $\sim$ 200K. In the second convective zone (T $\sim$ 500 K) the same role is played by the silicates (with cloud temperature of $\sim$ 1 500 K). In both cases we, hence, find a very high initial core temperature surrounded by an "extensive gaseous atmosphere composed of the principal interior constituents of the body" (for the earth the total radius including the atmosphere is $\sim$ 20 times the present radius). In both cases the planets are formed in less than 10^4 years.

One important consequence is the fact that the earth would be born in a molten state. Solidification would proceed first in the center (in view of the elevation of the melting temperature with increasing pressure) and proceed upwards. Clearly the geochemistry associated with such a pattern of events would differ appreciably from what we heard about in the other models. Some implications are discussed by the author.

Satellites can be formed either by capture of secondary bodies or by formation of a subdisk around the planet, much in the same way that the planets are formed around the sun (following an idea dear to A + A).

For the giant planets, the second mechanism is invoked : the initial angular momentum in the gas of the nebula prevents the infall of matter all the way to the surface and puts the material in orbit, where it finally condenses.

For the moon, in order to account for the predominance of low density silicates, CAMERON appeals to the capture of a small body by the earth, both objects possessing a silicate atmosphere. The solid part of the smaller object is retained by the earth's atmosphere but its silicate envelope condenses into the moon. (A similar picture of lunar formation had earlier been presented by RINGWOOD and ESSENE.)

As in the model of SAFRONOV, the anomalous spins are explained by collisions with second largest bodies, late in the game.

CAMERON and PINE assume the existence of independant disks orbiting around the protosolar nebula (as left-overs from the initial collapse phase). A typical disk of this kind with M $\sim$ 4 x 10^{32} and T $\sim$ 20 K becomes the birth place of comets, through accretion mechanisms similar to those which gave rise to planets. Again the birth period does not exceed 10^3 years.

As discussed before, the nebula dissipates in 10^4 years, due to the dissipation effects of the circulation currents ; this process should be over shortly after the formation of the planets. A large fraction of the nebular mass falls inward, thus forming the sun. The solar corona, heated up by a "variety of mechanical wave process", generates, by hydrodynamic expansion, a strong T-Tauri type stellar wind which, in turn, evacuates a large fraction of the initial mass in outer space.

The interaction of this wind with planetary atmosphere gas should have played a dominant role in the making of these atmospheres as we observe them now.

The transport of matter, first from the nebula into the sun, and later from the sun into space (through the solar wind) will have important dynamical effects on the planetary distances ; the final space configuration of the orbits will be very different from the configuration at the moment of planetary accretion. For instance the planets from Mercury to asteroids were formed at 2 to 10 A. U. (where T was ~ 500 to 1 500°, and P = 10^{-3} to 10^{-4} atmosphere).

ANDERS and GAST will discuss later the geochemical information relevant to the appropriate pressure and temperature presiding at the formation of the earth, moon and meteorites.

COMMENTS.

H. C. UREY :

I proposed gravitational instability some 15 years ago. No one was interested, I should have suggested it last year, I suppose. I do not see that gravitational instability in the nebula is hopelessly incorrect though, of course, I do not regard it as certainly true.

But stickiness of grains is no problem, if dust grains settle in a gas sphere.

H. REEVES :

The difficulties met by models of planets and satellites based on gravitational instabilities, have been stressed in the recent works of ALFVEN and ARRHENIUS (reference in the text of ARRHENIUS, this volume).

D. C. BLACK :

Most of the discussion given here on the formation of stars have centered on a concept where stars form in massive clouds. However, as HERBIG as pointed out, there are cases of individual stars which appear to have formed in an isolated fashion. This possibility must be kept in mind when formulating models of star formation.

B. J. LEVIN :

1. On the Mass of the Nebula :

Recently I changed my mind and instead of a solar nebula of a small mass, I suggest that it was of about 1-2 $M_\odot$ as proposed earlier by CAMERON. Such a large mass is necessary to assure the accumulation of Uranus and Neptune within the age of the solar system. The surface density in the inner part of the nebula remains as assumed previously (below $10^4 g/cm^2$), but the nebula has to extend initially up to about 200 AU from the sun.

2. On Accretion through Jet Stream :

If we consider only a massive central body and a stream of solid particles or bodies, then ALFVEN's conclusion that the stream can form a single body is correct. But in a real solar system, gravitational perturbations from planets and encounters with stray bodies as well as the Poynting-Robertson effect will destroy the stream in a time scale short compared to the time required for its coalescence into a single body.

3. On Gravitational Accumulation of Large Bodies :

The problem of accumulation of planets includes not only the problem of sticking of small particles, but also the problem of gravitational accumulation of planets from bodies of 10-100 Km.

This stage of accumulation determines the initial temperature of the Earth and other terrestrial planets and must be discussed separately from the problem of sticking.

B. NUCLEAR PHYSICS IN THE EARLY PHASES OF THE SUN.

At the 1962 NEW-YORK meeting on the Origin of the Solar System, FOWLER presented a recent model of GREESTEIN, HOYLE and himself (usually referred to as FGH), which essentially had for effect the addition of a new dimension to the subject. The basic idea was that all the atoms of D, ^{3}He, Li, Be, B (and also the long-lived ^{129}I) in the solar system have been produced by an intense flux of high energy protons generated by the young and electromagnetically active sun, bombarding the various bodies gravitating around the sun. This idea was related to a previous work of GREENSTEIN (cf FGH) in which the lithium content of stars originated by spallation reactions in stellar flares, and also to the solar system model of HOYLE (cf FGH) in which electromagnetic effects were responsible for the rotational deceleration of the sun and rotational acceleration of the planets. By comparing the abundance ratios of the light elements and particularly the isotopic ratios of lithium and boron with their estimation of the production (no experimental data was then available) ratios in nuclear reactions,FGH were able to present a rather detailed sequence of events in which neutrons, secondaries to the spallation reactions, were thermalized and played a major role in fixing the observed ratios.

This work opened a vast field of research which first lead to the measurements of the relevant spallation cross-sections (the late Dr. BERNAS and his ORSAY group played a dominant role in this field) and second to a detailed search of minute isotopic differences in chemical constituents of meteorites (and of the moon) witnessing the occurence and the effects of this irradiation.

The cross-sections measurements did not confirm the estimation of FGH and in fact cast serious doubts on the importance of secondary neutrons (GRADSZTAJN. (1965), (BERNAS, GRADSZTAJN, REEVES and SCHATZMAN. (1967), here after called BGRS.

And the search for unambiguous proof of an early irradiation through anomalous isotopic ratios in meteorites turned out to be rather frustrating (we shall hear more about this in the talk of BEGEMAN).

Following the laboratory work of the ORSAY group,GRADSZTAJN and BGRS hypothesized that the irradiation had taken place while the nebula was still entirely gaseous and produced the isotopes of Li, Be, B. The same irradiation did produce some D and ^{3}He but the observed ratio of D/H or ^{3}He/^{4}He was found to be far too large to be accounted for by this process (mostly because secondary neutrons could not be appropriately slowed down).

In his model of the origin of the solar system, SCHATZMAN followed BGRS but assumed that the irradiation had taken place in a nebula which already lost a vast fraction of H and ^{4}He (similar work was presented by AUDOUZE (1969). Following the spirit of FGH he made important use of the physical conditions required for the model to account for D ^{3}He and Li Be B to obtain the pertinent information on which his model was based. However at that time the wind had started to change. A closed study of the physical processes involved in the production of the required amount of Li Be B by spallation reaction in stellar flares led RYTER, REEVES, GRADSZTAJN and AUDOUZE (1970), to a skeptical state of mind : the energy output needed appeared unrealistically high.

One should look elsewhere... In 1969, REEVES, FOWLER and HOYLE came to the conclusion that the most probable mechanism for the origin of Li, Be, B was simply the bombardment of the interstellar matter by the galactic cosmic rays : a rough estimate showed that the present rate of formation of these elements in the galactic gas, multiplied by the age of the galaxy would

account for the stellar observations, the idea being that when a star is made out of this gas it contains these atoms in the general "galactic" proportion and when the photosphere of this star shines up in the sky, they show up in the appropriate atomic transition lines. Detailed calculation by MENEGUZZI, AUDOUZE and REEVES (1971), and the incorporation of galactic evolution effects by MITLER (1970), and TRURAN and CAMERON (1971) have fully confirmed the plausibility of this idea.

The one negative aspect of this new theory was to decouple entirely the origin of Li Be B from processes occuring at the birth of the sun : all the Li Be B of the solar system were present in the protosolar nebula before its birth ! Nevertheless the same calculations also showed that the D and ^{3}He could not come from the galactic cosmic ray effect (factors of $\sim 10^4$ are missing). And since the solar system ratio of D/H (in earth and meteoritic water) appeared to be at least three times larger than the interstellar ratio (from radio astronomical measurements) there was still open the possibility that the solar system deuterium had originated in nuclear processes taking place in the system itself. However after an analysis of the solar wind abundance of the ^{3}He/^{4}He of the BERNE group, GEISS and REEVES (1972) came to the opposite conclusion (GEISS will talk more about it later). Hence our general conclusion :

THE ORIGIN OF D, ^{3}He Li Be B HAVE NOTHING TO DO WITH THE ORIGIN OF THE SOLAR SYSTEM.

However, we can say, since the sun must have undergone a T-Tauri phase in his young days, and since for a number of reasons (discussed by SCHATZMAN) T-Tauri stars, or stars in an even earlier phase, are believed to undergo a period of strong electromagnetic activity, the possibility of some kind of activity is still left with us.

This possibility has received a further confirmation from the establishment of a correlation between the amount of trapped rare gases and density of nuclear tracks in micrograins of meteoritic material (PELLAS, POUPEAU, LORIN, REEVES and AUDOUZE) (1969), and (LAL and RAJAN)(1969). The argument goes like this : the analysis of the emission lines in T-Tauri stars shows that these stars are emitting matter under the form of stellar winds with flux intensity of the order of 10^6 to 10^7 of the present solar wind. On the other hand, the fact that the trapped rare gases are often found to be largely surface concentrated in meteoritic grains points to the solar wind as the injection agent of these atoms in the grains. Then the correlation between gas concentration ($\sim$1 KeV particles) and tracks ($\sim$1 MeV particles) suggest that the wind was accompanied by fast particles; hence the conclusion that the increased wind had a corresponding increased high energy particles. The only weak point here is that we have no definite proof that the irradiation took place very early in history of the solar system.

What kind of limits can we set to the intensity of this early irradiation ? We must consider separately the irradiation on the nebula before the solidification of the planetesimals and the irradiation on the planetesimals itself. The later phase would generate isotopic differences between various objects since the flux will vary with distance from the sun and with the amount of matter shielding the observed sample. This subject will later on be discussed by BEGEMAN (this volume).

Since the gaseous nebula will indoubdetly have been the seat of internal motions and hence of thorough gaseous mixing we should not expect the initial phase to have left witnesses in the form of isotopic differences in stones. A limit can nevertheless be set from the fact that

some isotopic ratios are everywhere vastly different from those expected in spallation reactions; hence the spallation contribution to the abundance of these elements must be negligible. For instance, the lithium isotopic ratio $^{7}Li/^{6}Li \simeq 12$ would be reduced by a factor of two if the total integrated flux of incident particles had been larger than $10^{19} p/cm^2$. A similar flux of thermal neutrons would produce a $^{158}Gd/^{157}Gd$ ratio of $\simeq 10$ instead of the observed value of ($\simeq 1$) (REEVES, FOWLER, AUDOUZE and SCHRAMM, 1972), (approximate values of the initial Gd ratio can be obtained from a study of the physics of the s-process)

These limits are low and have an important incidence on the study of chronologies based on ^{129}I and ^{244}Pu : the intensity of the early irradiation on the gas phase was far too small to account for the abundances of these isotopes at the birth of the solar system. From the report of BEGEMAN later in the week, the same conclusion can be reached about the later irradiation on the solid phase. Hence another important conclusion :

THE ISOTOPES ^{129}I AND ^{244}Pu RESPONSIBLE FOR THE OBSERVED XENON "EXCESSES" WERE ALREADY PRESENT IN THE PROTOSOLAR CLOUD.

CHAPTER III – METEORITES – LUNAR SAMPLES

Meteorites: Clues to the Origin of the Solar System – *T. E. Bunch*

METEORITES: CLUES TO THE ORIGIN OF THE SOLAR SYSTEM

T. E. Bunch
Ames Research Center, NASA, Moffett Field, Calif. 94035

I. INTRODUCTION

What are meteorites and why do we study them? Well, to start with, meteorites are rock and metal fragments, smaller than planets and larger than molecules, of disrupted planetary bodies. Although they are commonly referred to as space debris, they are scientifically important for the understanding of Solar System origin, and possibly Earth origin. Prof. Edward Anders of the University of Chicago has referred to meteorites as "the poor man's space probes" because we receive them free and they are the only recognized extraterrestrial samples available to us other than the Apollo lunar samples. Much has been learned about their early geologic history, ages, pre-terrestrial orbits, environmental condition, organic contents, and shock events. These results have been applied in turn to interpreting the origin of the Solar System and comets.

This presentation will attempt to acquaint the reader with an introduction to meteorites and their significance. Because of the many fields of science that are involved in meteoritics (the study of meteorites), a glossary of terminology is given in appendix A. More detailed information may be obtained from Anders (1971), Keil (1969), Mason (1962), and Wasson (1973).

II. CLASSIFICATION, BULK COMPOSITIONS AND MINERALS OF METEORITES

A. *Classification*

Generally speaking, meteorites are classified on the basis of bulk chemistry and mineralogy. Further division of classes into subtypes is commonly based on textural differences and minor and trace element differences.

Meteorites are classically grouped into stones, irons, and stony-irons (table 1). Among the stones, a major distinction is made between the *chondrites* (fig. 1) which contain chondrules (rounded supercooled mixtures of silicates and glass) to a greater or lesser extent, and *achondrites*, which do not contain them. The most abundant of the chondrites, called *ordinary chondrites*, fall into three subtypes based on the amount of metallic Fe-Ni alloy present and the Fa (fayalite, Fe_2SiO_4) and Fs (ferrosilite, $FeSiO_3$) contents of the constituent olivine and pyroxene, respectively: the H (high metal) group, the L (low metal) group, and the LL (very low) metal group (fig. 2). The *main* mineral constituents of all these are olivine, low Ca pyroxene, metal, high albite, troilite, and minor chromite. An additional subdivision into petrographic subgroups is based on texture (degree of metamorphism). Ordinary chondrites with delicate chondrules, nonequilibrium assemblage, glass, etc., are designated 3 (least metamorphosed) and those where the chondrules are recrystallized, with an equilibrium assemblage and no glass are designated 6 (H6, L6 or LL6) and are most metamorphosed.

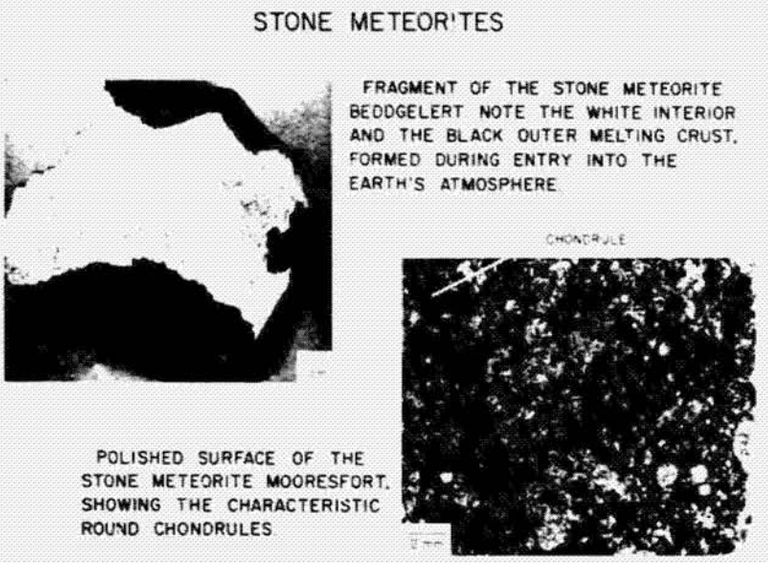

Figure 1(a). Photograph of chonarite showing black fusion crust and photomicrograph showing texture of the same stone under the petrographic microscope.

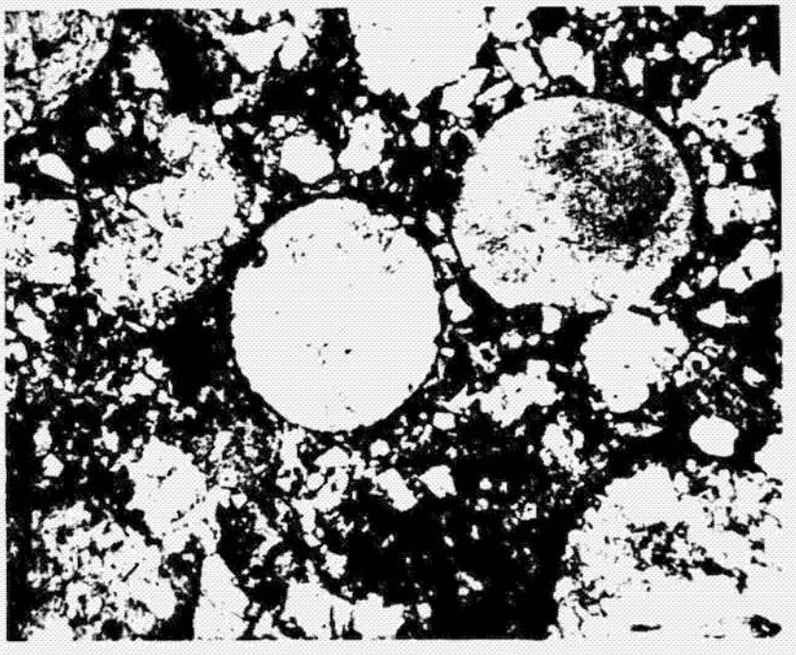

Figure 1(b). Photomicrograph of a chondrite polished thin section that shows the delicate texture of chondrules. Field diameter = 2 mm.

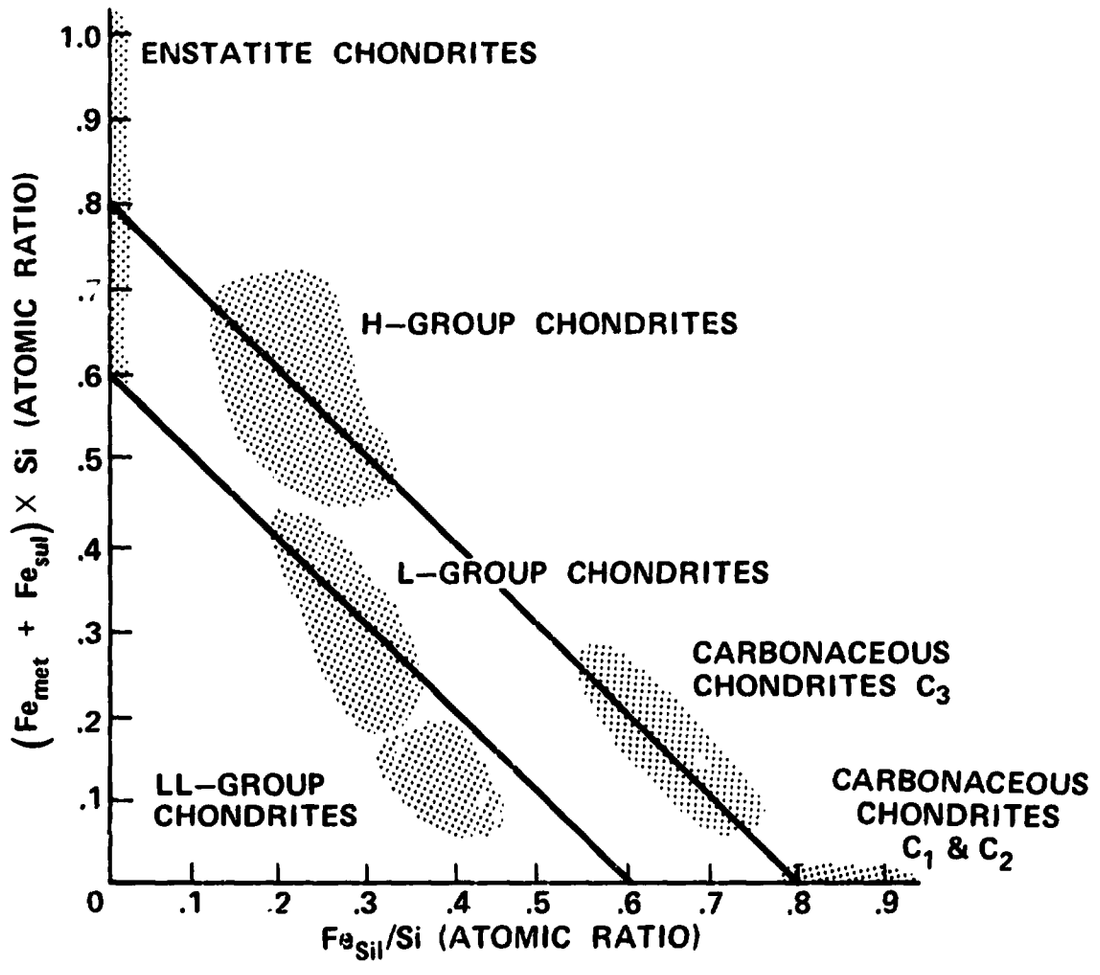

Figure 2.– Plot showing distribution of Fe between reduced metal and oxidized phases of chondritic meteorites. Solid lines show locus of points having bulk Fe/Si ratios of 0.6 and 0.8.

The nonordinary chondrites consist mainly of *enstatite chondrites* and *carbonaceous chondrites* (fig. 3). The former are composed of an extremely reduced assemblage consisting mainly of clino-enstatite (Fs=O; ferrosilite, $FeSiO_3$), Fe-Ni alloy, and troilite with a host of minor and trace phases that reflect extremely low oxidation conditions (e.g., sinoite (Si_2ON_2), oldhamite (CaS), osbornite (TiN), etc.). The carbonaceous chondrites are divided into three subtypes – C1, C2, and C3. The three are distinguished primarily by their carbon and water contents (table 1). The C1 meteorites are considered the most primitive meteoritic objects known and are the least fractionated chemically. They consist mainly of a very fine-grained layer-lattice silicate, ferric chamosite and minor magnetite. The C2 meteorites consist of a matrix (52% on the average) of ferric chamosite and inclusions (aggregate clusters and some chondrules) (48% on the average) of forsterite, enstatite, spinel, and minor Fe-Ni-Cr-Co alloy metal. The C3 meteorites have no chamosite but consist mainly of a matrix of fine-grained olivine ($\approx$ Fa 50) containing inclusions of mainly forsterite, enstatite, and spinel along with a minor amount of high Co (0.1 - 7%) Fe-Ni-Co-Cr alloy.

Achondrites consist of eight main subtypes whose major mineralogies are adequately described by their names alone (table 1).

Iron meteorites can be grouped into a moderately large number of subtypes: the octahedrites (coarse, medium, fine; fig. 4) have 6.5 - 18% Ni, the hexahedrites (fig. 5) have $\leq$ 7% Ni, and the Ni-rich ataxites have 12 to over 25% Ni. These irons commonly contain nodular to lamellar inclusions of graphite, troilite, schreibersite, and cohenite (fig. 4). Graphite and troilite inclusions contain within them, in many cases, minor assemblages of silicates (and/or phosphates), some of which are Cr-rich. These are referred to later as "silicates in ordinary irons" or SOI meteorites, which serves to distinguish them from an unusual group of iron meteorites that contain major irregular masses of silicate, troilite, ± phosphate, ± chromite assemblages, sometimes comprising 25-35 volume percent of the meteorite (fig. 6), these are called irons-with-silicate-inclusions, or simply IWSI.

The stony-iron meteorites consist principally of two subtypes: (1) pallasites (fig. 7), which have olivine (Fs=10-20) in a matrix of Fe-Ni alloy and (2) mesosiderites (fig. 8), which are mainly half Fe-Ni alloy and about half of an assemblage consisting of orthopyroxene (Fs-29-30), anorthite (An=87-97), olivine (Fa=9-10), and troilite.

B. *Bulk Compositions*

Compositions of meteorites are quite different from terrestrial and lunar rocks. Whereas major elements in ordinary chondrites are similar to solar (cosmic) abundance, many minor elements are not; achondrite compositions are even less similar to solar element abundance. Bulk compositions of various achondrites and a few representative analyses of lunar rocks are given in table 2.

C. *Meteoritic Minerals*

Over 80 minerals (table 3) have been confirmed in meteorites of which 24 are unique to meteorite assemblages. Many of these unique minerals define unusual, if not extreme, formation

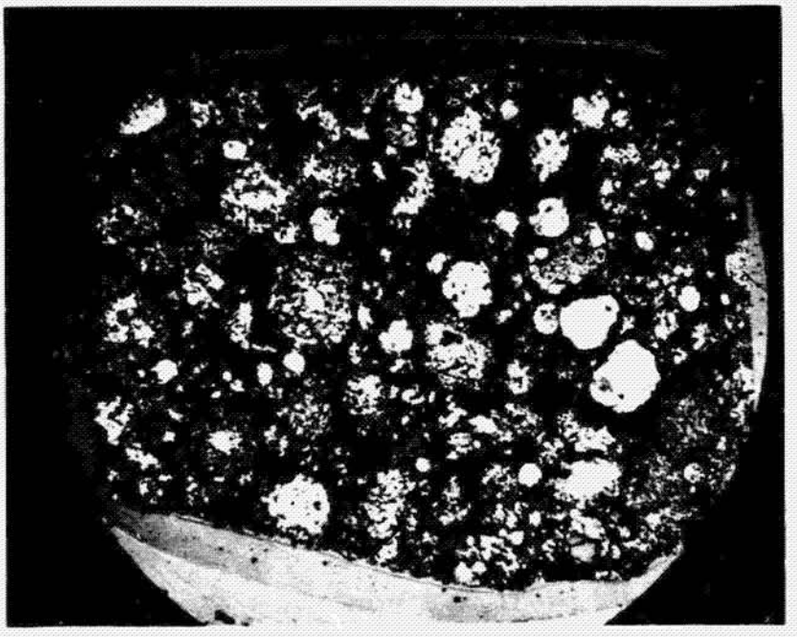

Figure 3. – Photomicrograph of the Allende C_3 chondrite. Field diameter = 2 cm.

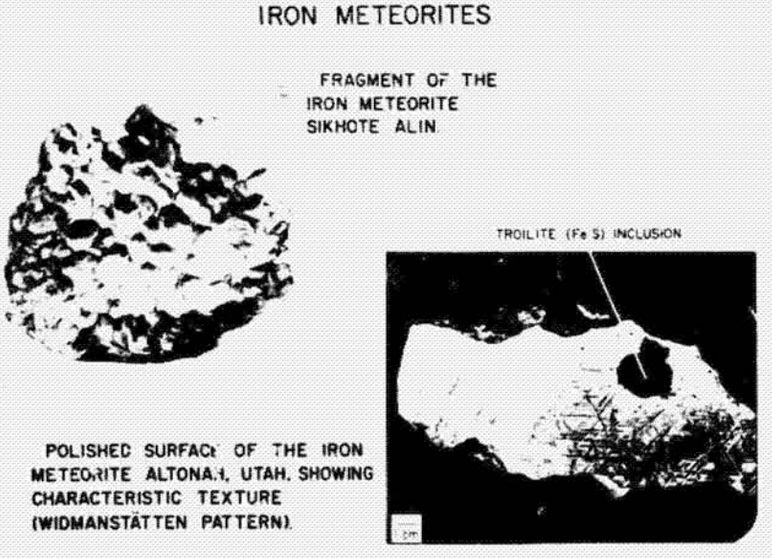

Figure 4. – Photographs of an iron meteorite abladed surface and a cut and polished surface.

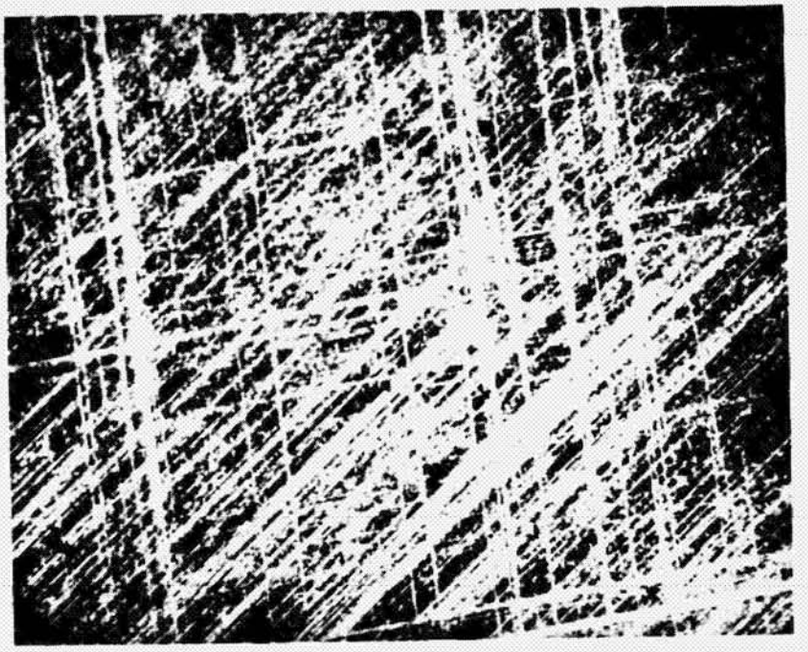

Figure 5. Photograph of a polished hexahedrite. Parallel lines are Neumann bands arising from shock events. Field diameter = 2 cm.

Figure 6. Photograph of a polished surface of the Landes iron meteorite that contains fragmented silicate inclusions.

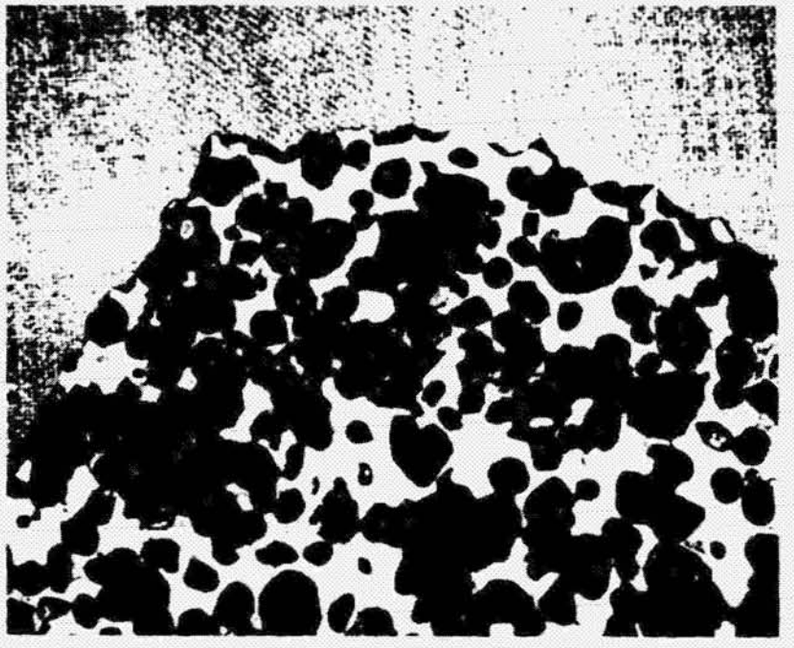

Figure 7. – *Pallasite meteorite showing metal (light) and olivine (dark). Meteorite diameter = 15 cm.*

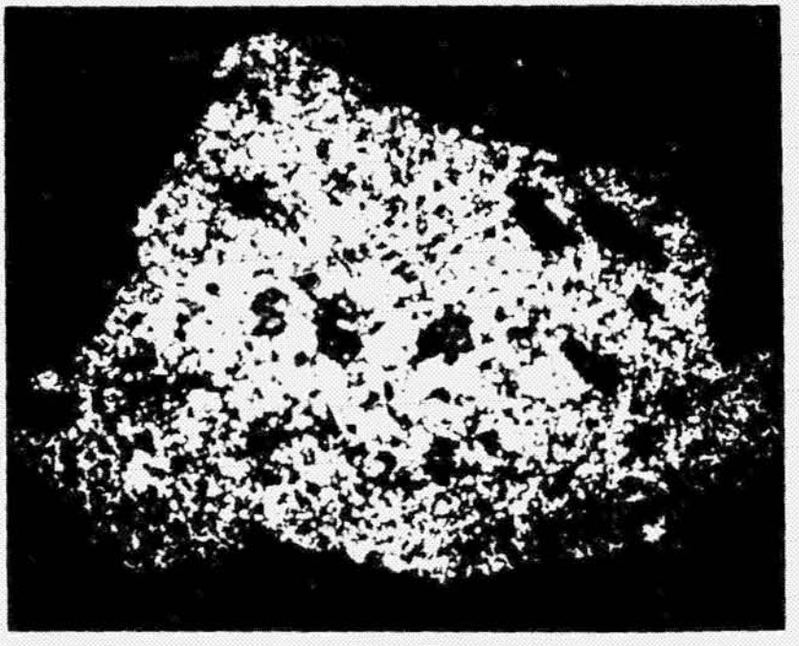

Figure 8. – *Mesosiderite meteorite consisting of 50% metal (light) and 50% silicates (dark). Meteorite diameter = 8 cm.*

environments. For example, many sulfides (CaS, Cr_2S_4, MgS, $K_3CuFe_{12}S_{14}$) indicate low partial pressures of oxygen (high reducing conditions). Brezinaite (Cr_3S_4) has been found in only one meteorite, the iron, Tucson. The apparent oxidation state of Tucson was sufficiently low to reduce virtually all Fe and Ni and some Si and Cr to the elemental form and to change V and most Cr from lithophile to chalcophile character. Other minerals indicate high shock pressure environments (diamond, C and Majorite, $Mg_3(MgSi)Si_3O_{12}$). High temperature minerals (grossular, melilite, and spinel), found in carbonaceous chondrites, support the high temperature condensation theory for meteorite origin. In addition, many common minerals in meteorites have unusual compositions or textures that aid the reconstruction of meteorite origin, thermal history, and chemical environment. An example of this application is that the petrography and composition of C2 meteoritic metal is different from other meteorite types. Metal occurs dominantly as submicron-sized beads, rarely larger than 5 microns, poikilitic within Mg-rich forsterite (and enstatite) crystals. The crystals are often euhedral or fragments of euhedral crystals. Metal in ordinary chondrites occurs interstitial to silicates, is generally ragged and irregular, and often conforms to the external shapes of silicate grains. In the C2 meteorites, the petrographic relations indicate the metal beads preceded forsterite formation and may have acted as nuclei for euhedral forsterite crystals. During the direct condensation of a solar nebula gas at $P(H_2) = 10^{-3}$ atm, metal alloys with the Fe, Ni, Cr, and Co contents observed in the metal beads of these carbonaceous chondrites (5-7% Ni, 0.3-0.5% Co, around 0.6% Cr) condense directly from 1445°-1370° K.

III. SIGNIFICANCE OF SELECTED METEORITES

A. *Chondrites*

The chondritic meteorites are the most primitive samples available for study. Some of them consist of relatively undifferentiated Solar System material and are the oldest samples so far measured in the Solar System.

There are three classes of chondrites (ordinary, enstatite, and carbonaceous) that are plotted in distinct fields on figure 2, in which the abundance of Fe in metal and FeS is plotted along the vertical axis and the abundance of Fe as FeO in silicates is plotted on the horizontal axis. Enstatite chondrites are the most reduced (no FeO) and carbonaceous chondrites are the most primitive and oxidized (little or no Fe); ordinary chondrites are intermediate and show a wide range of oxidation states. Chondrites comprise about 86% of the recovered meteorites from falls. These statistics offer a rough estimate of the relative abundance of these meteorites in earth-crossing orbits, although there is a bias against carbonaceous chondrites and other friable chondrites that cannot survive Earth entry. Moreover, our sampling is further biased by the sampling time of less than 100 years, compared to the millions of years that chondrites have traveled in space as debris.

Four independent types of chemical fractionation have been observed in ordinary chondrites; two are trends within ordinary chondrites (H, L, LL) and two are found among the petrographic subgroups (types 3, 4, 5, and 6; see classification). These fractionations and their sequence are summarized in section V.

Carbonaceous chondrites are extremely important for three reasons. (1) They contain high temperature inclusions, rich in refractory elements, and depleted in volatile elements (see sec. V) set

in a carbon, H_2O-rich matrix, of low temperature minerals. (2) They contain phases that have "non-solar" abundances of ^{16}O and neon isotopes. (3) They contain hydrocarbons and other organic compounds that may have been the starting compounds for our life forms.

B. *Achondrites*

Whereas the chondrites are primitive and relatively undifferentiated, achondrites, for the most part, are differentiated and similar in texture to terrestrial and lunar magmatic rocks. Cooling of basaltic achondrites from magmas implies planetary rock forming processes and strongly indicates at least sublunar size parent bodies. The premise for sublunar size parent bodies is further supported by the metamorphic conditions that reheated ordinary chondrites and other meteorites, the slow cooling rates of iron meteorites (see below), and the formation of lunar-like surface breccias that require a body of sufficient gravity to form (Bunch and Stöffler, 1974). Arguments against large parent bodies include improbable cooling rates (1600° C to 400° C for irons) for large bodies, difficulties in impact breakup, total mass of the present asteroids is 0.03% that of the Moon, and absence of hydrostatic high pressure phases that should form in large planetary bodies.

Several theories conclude that achondrites originated from chondrites and others conclude that chondrites originated from achondrites. The fact that some achondrites and chondrites have comparable ages of formation suggests that there is no genetic link in their formation.

C. *Irons and Stony Irons*

Iron meteorites constitute by far the largest total weight of any of the meteorite classes. The largest meteorite in the world is the Hoba iron in Southwest Africa which weighs 54 metric tons. Many irons weigh over 4 metric tons. The largest stone meteorite is in Norton County, Nebraska which weigh over 1 metric ton; most stony meteorites weigh a few kilograms or less.

Widmanstatten patterns in octahedrites (fig. 4) arise on cooling from ~ 900° C where γ-iron or taenite becomes unstable and platelets of α-iron or kamasite grow parallel to the octahedral crystal structure. Study of Ni diffusion, which is responsible for this growth, through the temperature range of 900-400° C indicates that cooling rates vary among different specimens from 1-10° C/ million years. The conclusion from this observation is that iron meteorites cooled very slowly in a parent body of sufficient size to allow for slow heat loss, but small enough to cool from the melting temperature down to ~ 400° C where some octahedrites were completely transformed into hexahedrites.

Irons with silicate inclusions (IWSI) are unusual in that they show a brecciated, angular texture of fragmented rock in a nickel-iron matrix with few silicate fragments showing any remelting signs that surely would have occurred if a molten nickel-iron melt had enveloped brecciated silicates. An alternative view is that iron meteorites formed "cold," *i.e.*, from Fe dust grains that agglomerated together and grew into large bodies via a solid state process and were heated up during the Solar System event that also metamorphosed chondrites and produced other moderate to high temperature conditions.

IV. CHEMICAL PROCESSES IN THE EARLY SOLAR SYSTEM

A. *Primordial Matter*

The Solar System was well mixed in an isotopic and elemental sense. Few isotopic differences have been found that may be attributed to incomplete mixing of material with different nucleosynthetic processes. A few deviations from this "complete" mixing process do exist and imply extrasolar system origins for their presence. Black (1972) found unusual or nonsolar isotopic ratios for neon in carbonaceous chondrites and Clayton *et al.*, (1973) discovered unusual amounts of ^{16}O in carbonaceous chondrites. Since the Earth, Moon, and other meteorites' oxygen isotope patterns all lie on a single fractionation trend, it can be concluded that they all were derived from a reservoir homogenized with respect to oxygen isotopes. The carbonaceous chondrites acquired, in addition to this homogenized material, a small excess of ^{16}O from the protosun or from outside the Solar System. It is interesting to note that both of these findings suggest that the existence of more than one type of matter (material with different isotopes) in the Solar System greatly challenge the theory of nucleosynthesis or that some portion of our Solar System came from an outside source.

Elemental differences have been observed and these differences are the basis for the classification of various meteorites and planetary bodies. These differences are explicable by chemical fractionations in the early solar nebula and postsolidification events.

B. *Condensation of Cosmic Gas*

Separation of solids from gases appears to be the best process for cosmochemical fractionation. There is good evidence for such separation during the formation of meteorites and terrestrial planets. Many of the abnormal or depleted abundances of gases for the Earth can be explained by volatility fractionation. A cooling gas of cosmic composition (at a pressure of 10^{-3} atm) could condense in the following order. Below 2000° K, the highly refractory compounds of Ca, Mg, Ti and Al appear, followed by magnesium silicates and nickel-iron and alkali-silicates (table 4). This leaves only H, C, N, O, and S of the major elements in the gas phase. At 700° K, S begins to condense on solid Fe by the reaction $Fe + H_2S \rightleftharpoons FeS + H_2$ followed by Pb, Bi, Tl, and In. Any remaining Fe reacts with H_2O to give Fe_3O_4. Lastly, H_2O is bound as hydrated silicates at some temperature below 400° K.

This is considered as the present working model among most space scientists, although one must bear in mind that other new lines of evidence indicate that the solar nebula temperature was never above ~ 1000° K, thus negating this and other high temperature condensation models. However, until this new solar nebula low temperature evidence is substantiated, the condensation model remains as the best available.

C. *Agglomeration of Condensed Solids*

Now that we have solid particles, we have to get them together to form solid bodies. Probably, the best place to begin is with chondrule formation. To form chondrules, one alternative

is that the primordial condensate was entirely dust and a fraction of it was remelted to chondrules by electric discharge of shock waves (Whipple, 1966; Cameron, 1966). At low ambient pressures, these molten droplets are unstable with respect to vapor and the droplets may freeze before they have completely evaporated. Another alternative is that condensation did not proceed under equilibrium conditions, but involved supercooling and metastability. Once nucleation of solid began, complete freezing progressed rapidly. Both dust and chondrules agglomerated into planetesimals, which in turn accreted into planetesimals and finally into parent bodies.

V. SUMMARY OF SOLAR SYSTEM EVENTS

On the premise that solar system primary solid particles condensed from a "hot" solar gas, the sequence of events, modified from a model by Wasson (1972), is given as follows:

1. An interstellar gas and dust cloud underwent slow collapse and fragmentation to form the solar nebula.

2. As a result of the dissociation of H_2 and the ionization of H and He, the solar nebula collapsed rapidly with associated conversion of gravitational energy to heat.

3. The angular-momentum content of an appreciable fraction of the nebula was such that further collapse was hindered. This material collected into a nebular disk. Heating stopped, and the temperature of the material leveled off and started to decline.

4. Evaporation of preexisting solids was incomplete in the region farther from the Sun than the formation location of the ordinary chondrites, and the gas in this outer region was therefore depleted in refractory elements.

5. There was enough turbulence in the formation region to mix the gas. Temperatures continued to decline, and after some degree of undercooling, condensation commenced.

6. Condensation of silicates began almost simultaneously, independent of distance from the sun. Metal nucleation, however, began at the edge of the formation location (presumably the edge nearer the Sun), where the most siderophilic-element-rich material ultimately formed, and the "nucleation front" moved slowly across this region.

7. The greater supersaturation of Fe-metal vapor and the lower mean condensation temperatures at the low-pressure extreme of the formation region produced higher mean Fe/(Fe + Mg) ratios at this edge, with the ratios monotonically decreasing toward the high-pressure (metal-rich) edge. Thus, the oxidation-state fractionation is tied to the same nebular properties as the siderophilic-element fractionation.

8. The temperature continued to drop, and condensation proceeded. Silicate grains formed at higher temperatures were larger and had lower Fe/Mg ratios than those formed at lower temperatures. Conditions (rate of temperature decrease, etc.) were such that the larger grains retained their initial Fe/Mg ratios.

9. Temperature approached a minimum (or better, a plateau) and condensation stopped.

10. Chondrules were produced by electrical discharges or impact. About 50-80% of the volatile and semivolatile elements were removed during this process.

11. The material agglomerated to planetesimals.

12. Agglomeration of material in the region nearer the Sun began, the opacity of this region dropped, and temperatures in the formation location of the ordinary chondrites began to rise. Accretion of planetesimals to parent bodies commenced.

13. Unaccreted planetesimals and the outer layers of parent bodies experienced metamorphism as a result of the rise in ambient temperature. This high-temperature period was relatively brief (perhaps 10^3 years), and material in the interior of larger bodies remained at essentially the temperature at which it had accreted.

14. Accretion of planetesimals to parent bodies continued, and some parent bodies coalesced to form larger parent bodies. Mixing of material from different depths and thus of different petrologic types occasionally occurred.

15. The parent bodies and their fragments experienced various breakups, as recorded in the form of cosmic-ray ages, gas-retention ages, etc.

16. Debris from three or four parent bodies was perturbed into earth-crossing orbits and was captured by the Earth.

APPENDIX A

Condensation – condensation of a vapor phase to form a solid or liquid phase.

Agglomeration – attachment of solid particles to form aggregates in the millimeter-to-meter size range.

Accretion – is the accumulation of previously condensed and agglomerated material to the size range meter-to-100 km range.

Chalcophile – elements enriched in sulfide minerals and have a weak affinity for oxygen.

Chondrites and chondrules – chondrites are stony meteorites containing *chondrules*, millimeter-sized silicate spherules that appear to be frozen droplets of a melt. They consist largely of *olivine* [$(Mg, Fe)_2 SiO_4$], *pyroxene* [$(Mg, Fe)SiO_3$], and *plagioclase feldspar* [solid solution of $CaAl_2 Si_2 O_8$ and $NaAlSi_3 O_8$]. In the more primitive chondrites, glass is often found in place of crystalline feldspar. (Special names exist for the endmembers of the Fe-Mg solid solutions: $MgSiO_3$ = *enstatite*; $FeSiO_3$ = *ferrosilite*; $Mg_2 SiO_4$ = *forsterite*; $Fe_2 SiO_4$ = *fayalite*. They are abbreviated En, Es, Fo, and Fa.)

Lithophile – elements that combine with oxygen and form silicate minerals.

Siderophile – elements that are readily soluble in iron and have a weak affinity for oxygen or sulfur.

REFERENCES

Anders, E., Meteorites and the early solar system, Annu. Rev. Astron. Astrophys., 9, 1-34, 1971.

Black, D., On the origins of trapped nelium, neon, and argon isotopic variation in meteorites – II. Carbonaceous meteorites, Geochim Cosmochim Acta, 36, 377-394, 1972

Bunch, T. E. and Stoffler, D., The Kelly Chondrite: a rent body surface metabreccia, Contr. Mineral Petrol., 44, 157-17., 1974.

Cameron, A. G. W., The ac mulation of chondritic material, Earth Planet. Sci. Lett., 1, 93-96, 1966.

Clayton, R. N., Grossman, L., and Mayeda, T. K., A component of primitive nuclear composition in carbonaceous meteorites, Science, 182, 485-488, 1973.

Grossman, L., Condensation in the primitive solar nebula, Geochim Cosmochim Acta, 36, 597-620, 1972.

Keil, Klaus, Meteorite compositions, in Handbook of Geochemistry (editor K. H. Wedepohl, Springer-Verlag), 1, 78-115, 1969.

Mason, Brian, Meteorites, John Wiley a New York, 1962.

Mason, Brian, The mineralogy of meteorites, Meteoritics, 7, 309-326, 1972.

Wasson, J. Formation of ordinary chondrites, Rev. Geophys. Space Phys 10, 711-759, 1972.

Whipple, F. L., Chondrules: Suggestions concerning their origin, Science, 153, 54-56, 1966.

TABLE 1.- SIMPLIFIED CLASSIFICATION OF MAJOR METEORITE TYPES AND SUBTYPES

Type	Major minerals
A. Stone meteorites	
Ordinary chondrites (H, L, LL)	Olivine, orthopyroxene, clinopyroxenes, metal, troilite, albitic plagioclase, chromite
Enstatite chondrites	Enstatite (ortho- and clino-), metal, troilite, ± plagioclase
Carbonaceous chondrites	
C1 $C = 3.5; H_2O = 20.1$	Ferric chamosite, magnetite
C2 $C = 2.5; H_2O = 13.4$	Ferric chamosite, olivine, enstatite, troilite
C3 $C = 0.5; H_2O = 1.0$	Olivine, enstatite, pentlandite, troilite
Achondrites	
Enstatite achondrites	
Bronzite achondrites	
Olivine achondrites	
Olivine-pigeonite achondrites	
Augite achondrites	
Diopside achondrites	
Orthopyroxene-pigeonite-plagioclase achondrites } Basaltic achondrites	
Pigeonite-plagioclase achondrites } Basaltic achondrites	
B. Iron meteorites	
Hexahedrites	Metal ($\leq$ 7% Ni), troilite
Octahedrites (coarse, medium, fine)	Metal (6.5-18% Ni), troilite, graphite
Ni-rich ataxites	Metal (12-25+% Ni), troilite, schreibersite
Irons with silicate inclusions (IWSI)	Metal, schreibersite, troilite, orthopyroxene, clinopyroxene, plagioclase, ± olivine, ± graphite
C. Stony-iron meteorites	
Pallasites	Metal, olivine
Mesosiderites	Metal, orthopyroxene, olivine, troilite

TABLE 2.– AVERAGE CHEMICAL COMPOSITION OF ACHONDRITE METEORITES (LISTED IN ORDER OF INCREASING IRON CONTENT), SELECTED TERRESTRIAL AND LUNAR ROCKS

Achondrites	SiO_2	MgO	FeO	Al_2O_3	CaO	Na_2O	K_2O	TiO_2
Enstatite achondrites	54.01	35.92	0.97	0.67	0.91	1.32	0.10	0.06
Augite achondrites	44.58	10.05	8.50	8.86	24.51	0.26	0.19	2.39
Olivine-pigeonite achondrites	50.83	37.43	12.16	0.54	0.87	0.11	0.04	0.15
Orthopyroxene-pigeonite-plagioclase achondrites	54.75	16.10	13.26	8.71	6.53	0.95	0.28	0.11
Pigeonite-plagioclase achondrites	48.17	7.10	16.00	13.91	10.94	0.67	0.13	0.51
Bronzite achondrites	52.11	25.85	16.05	1.18	1.41	0.01	0.001	0.19
Diopside achondrites	48.96	12.01	19.63	1.74	15.17	0.41	0.14	0.38
Olivine achondrites	37.12	32.05	28.82	1.26	0.56	0.19	0.09	0.16
Terrestrial (mafic)								
Dunite	40.49	46.32	8.34	0.86	0.70	0.10	0.04	0.02
Peridotite	44.94	37.21	8.50	4.87	3.61	0.64	0.21	0.10
Gabbro	47.00	8.96	10.00	17.92	11.60	2.18	0.80	1.18
Norite	50.8	8.44	10.32	16.19	9.27	2.63	0.80	1.14
Basalt	49.87	6.27	12.84	15.96	9.09	3.16	1.55	1.38
Lunar								
Apollo 11 basalt	40.2	7.1	18.4	10.2	11.2	0.75	0.15	11.4
Apollo 15 basalt	44.0	11.1	22.6	8.4	9.4	0.21	0.03	2.31
Apollo 16 troctolite	44.5	8.8	7.2	23.6	13.7	0.42	0.15	0.71
Apollo 17 basalt	37.8	9.9	18.5	8.9	10.1	0.35	0.06	13.00
Apollo 17 Dunite	39.9	43.6	11.3	1.53	1.14	---	---	0.03

TABLE 3

I. The minerals of meteorites, up to 1962 (an asterisk indicates those not known to occur in terrestrial rocks). Table modified from Mason (1972).

Name	Formula
Kamacite	α-(Fe,Ni)
Taenite	γ-(Fe,Ni)
Copper	Cu
Diamond	C
Graphite	C
Sulfur	S
Schreibersite	$(Fe,Ni)_3P$
Cohenite	$(Fe,Ni)_3C$
*Osbornite	TiN
Troilite	FeS
*Oldhamite	CaS
Pentlandite	$(Fe,Ni)_9S_8$
*Daubreelite	$FeCr_2S_4$
Chalcopyrite	$CuFeS_2$
Pyrite	FeS_2
Sphalerite	(Zn,Fe)S
*Lawrencite	$(Fe,Ni)Cl_2$
Magnesite	$(Mg,Fe)CO_3$
Calcite	$CaCO_3$
Dolomite	$CaMg(CO_3)_2$
Quartz	SiO_2
Tridymite	SiO_2
Cristobalite	SiO_2
Ilmenite	$FeTiO_3$
Spinel	$MgAl_2O_4$
Magnetite	Fe_3O_4
Chromite	$FeCr_2O_4$
Chlorapatite	$Ca_5(PO_4)_3Cl$
Whitlockite	$Ca_9MgH(PO_4)_7$
*Farringtonite	$Mg_3(PO_4)_2$
Gypsum	$CaSO_4.2H_2O$
Epsomite	$MgSO_4.7H_2O$
Bloedite	$Na_2Mg(SO_4)_2.4H_2O$
Olivine	$(Mg,Fe)_2SiO_4$
Orthopyroxene	$(Mg,Fe)SiO_3$
Clinopyroxene	$(Ca,Mg,Fe)SiO_3$
Plagioclase	$(Na,Ca)(Al,Si)_4O_8$
Serpentine (or chlorite)	$(Mg,Fe)_6Si_4O_{10}(OH)_8$

II. Minerals discovered in meteorites since 1962 (an asterisk indicates those not known to occur in terrestrial rocks).

Name	Formula
Awaruite	Ni_3Fe
*Lonsdaleite	C
Chaoite	C
*Haxonite	$Fe_{23}C_6$
*Barringerite	$(Fe,Ni)_2P$
*Perryite	$(Ni,Fe)_5(Si,P)_2$
*Carlsbergite	CrN
*Sinoite	Si_2N_2O
Pyrrhotite	$Fe_{1-x}S$
Mackinawite	FeS_{1-x}
Heazlewoodite	Ni_3S_2
*Niningerite	(Mg,Fe)S
Alabandite[1]	(Mn,Fe)S
*Brezinaite	Cr_3S_4
Djerfisherite	$K_3CuFe_{12}S_{14}$
*Gentnerite[2]	$Cu_8Fe_3Cr_{11}S_{18}$
Rutile	TiO_2
Hercynite	$(Fe,Mg)Al_2O_4$
Hibonite	$CaAl_{12}O_{19}$
Perovskite	$CaTiO_3$
Whewellite	$CaC_2O_4.H_2O$
*Stanfieldite	$Ca_4(Mg,Fe)_5(PO_4)_6$
*Brianite	$CaNa_2Mg(PO_2)$
Graftonite	$(Fe,Mn)_3(PO_4)_2$
*Panethite	$(Ca,Na)_2(Mg,Fe)_2(PO_4)_2$
Sarcopside	$(Fe,Mn)_3(PO_4)_2$
*Ringwoodite	$(Mg,Fe)_2SiO_4$
*Majorite	$Mg_3(Mg,Si)Si_3O_{12}$
Woolastonite	$CaSiO_3$
*Ureyite	$NaCrSi_2O_6$
Potash feldspar	$(K,Na)AlSi_3O_8$
Nepheline	$NaAlSiO_4$
Sodalite	$Na_8Al_6Si_6O_{24}Cl_2$
*Merrihueite	$(K,Na)_2Fe_5Si_{12}O_{30}$
*Roedderite	$(K,Na)_2Mg_5Si_{12}O_{30}$
*Yagiite	$(K,Na)_2(Mg,Al)_5(Si,Al)_{12}O_{30}$
Richterite	$Na_2CaMg_5Si_8O_{22}F_2$
Melilite	$Ca_2(Mg,Al)(Si,Al)_2O_7$
Zircon	$ZrSiO_4$
Grossular	$Ca_3Al_2Si_3O_{12}$
Andradite	$Ca_3Fe_2Si_3O_{12}$
Rhonite	$CaMg_2TiAl_2SiO_{10}$
Cordierite	$Mg_2Al_4Si_5O_{18}$
*Krinovite	$NaMg_2CrSi_3O_{10}$
Monticellite	$Ca(Mg,Fe)SiO_4$

TABLE 4.– STABILITY FIELDS OF EQUILIBRIUM CONDENSATES AT 10^{-3} ATMOSPHERES TOTAL PRESSURE (GROSSMAN, 1972)

Phase		Condensation temperature (°K)	Temperature of disappearance (°K)
Corundum	Al_2O_3	1758	1513
Perovskite	$CaTiO_3$	1647	1393
Melilite	$Ca_2Al_2SiO_7$–$Ca_2MgSi_2O_7$	1625	1450
Spinel	$MgAl_2O_4$	1513	1362
Metallic Iron	(Fe, Ni)	1473	
Diopside	$CaMgSi_2O_4$	1450	
Forsterite	Mg_2SiO_4	1444	
	Ti_3O_5	1393	1125
Anorthite	$CaAl_2Si_2O_8$	1362	
Enstatite	$MgSiO_3$	1349	
Metallic Cobalt	Co	1274	
Alabandite	MnS	1139	
Rutile	TiO_2	1125	
Alkali Feldspar	$(Na, K)AlSi_3O_8$	~ 1000	
Troilite	FeS	700	
Magnetite	Fe_3O_4	405	
Ice	H_2O	$\leqslant$ 200	

CHAPTER iV – SELENOLOGY

A Review of Lunar Surface Features – *P. H. Schultz*

A REVIEW OF LUNAR SURFACE FEATURES

Peter H. Schultz*
Ames Research Center, NASA, Moffett Field, Calif. 94035

I. INTRODUCTION

Astronomers have studied the Moon as they would other astronomical bodies: first with the lowest telescopic resolution, then with progressively higher resolutions. Their overview (fig. 1) revealed two characteristic lunar surfaces, the maria (or smooth, dark plains) and the terrae (or cratered, light highlands), and much scientific debate has centered on the origin of the gross morphologies of these terrains. Instrumentation, a turbulent terrestrial atmosphere, and 384,000 km precluded the classical approach followed by geologists: start with the simplest – and typically the smallest – structures. then examine the more complex features. During the last decade, however, lunar probes, landers, and orbiters have relayed remarkably detailed information about the Moon – information requiring the conversion of the lunar astronomer into a lunar geologist. The general questions and overview approach were suddenly changed to specific questions and a detailed approach.

The "new" lunar geologist has before him an overwhelming photographic record of different surface featu and describing these features requires a classification scheme. One scheme uses the interpretatio of the observer and incorporates them into the descriptive nomenclature. As a result we can describe a lunar impact crater, volcanic cone, lava dome, or lava tube. Another scheme avoids connotation of genesis altogether; thus, we have, respectively, a rimmed circular depression with an extensive hummocky apron, a positive-relief feature with a cone-shaped profile and summit pit, a low-relief positive-relief feature with a convex profile, and a discontinuous sinuous rille. The first scheme clearly conveys a familiar meaning but carries with it obvious observational bias. Although the second scheme avoids this genetic connotation, such descriptions can become cumbersome and perhaps seem overly cautious and timid. However, this approach is fundamental in serious morphologic studies because it forces a review of the parameters that characterize surface features. On the Earth we can directly test the validity of interpretive labels from aerial photographs; on the Moon, we cannot. A compromise is sought in the following discussions. More detailed analysis of surface features and terrestrial analogs can be found in Mutch (1972). An extensive illustrated guide to lunar surface features has been made by Schultz (1972) and is the basis for this summary.

An easy way to classify lunar features is to describe their profile as either positive or negative relief. But the abundance of lunar craters permits us to treat them separately. Thus, we have craters, positive-relief, and negative-relief features, and most surface features can be discussed as subsets of these categories.

Before looking at the Moon, we should appreciate the effects of both the harsh lighting and the absence of an atmosphere – the latter eliminating depth perception or what artists call "atmospheric perspective." Without fully appreciating these two factors, 19th-century selenologists

---

* Research Council Resident Research Associate

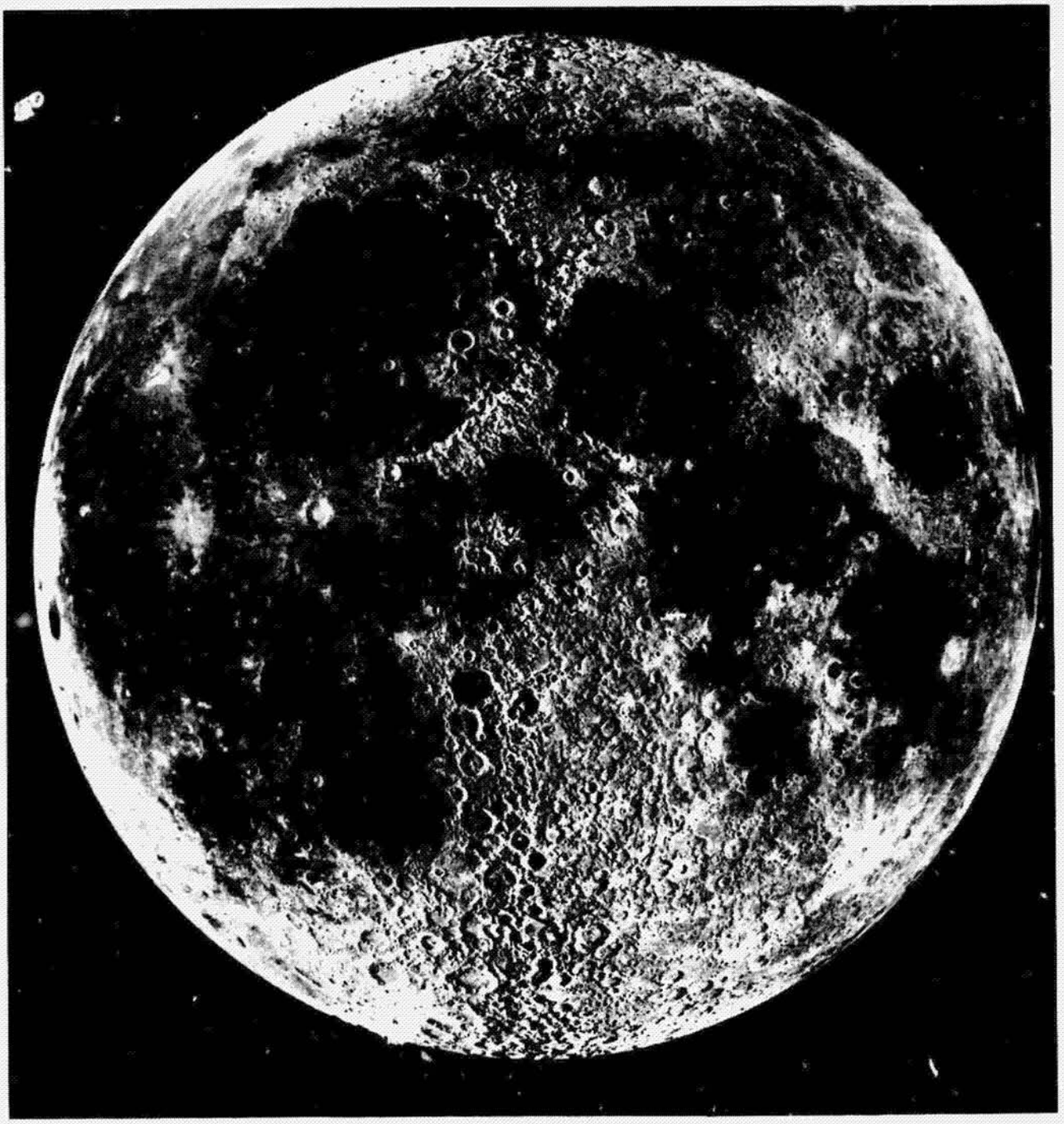

Figure 1. Composite photograph of the Moon from Earth. Note that solar illumination on the right half is from the right, but on the left side, from the left. This enhances the contrast between the heavily cratered Southern Highlands (bottom) and the smooth mare plains. Lick Observatory photograph L-9.

exaggerated craters into steep-sided pits and mountains into craggy peaks (see fig. 2). Figure 3 illustrates this exaggeration of relief owing to low illumination as well as the critical dependence of feature recognition on the angle of illumination.

II. CRATERS

The enormous variety of lunar craters reflects the morphologic differences of the *floor*, *wall*, and *rim* (beyond the rim crest) regions. The morphologic differences correspond to differences in both origin and modification. The temptation is to describe craters by type, but a more revealing first step is to consider separately these characteristic crater zones.

For example, the floors of four different craters are shown in figure 4. The crater Tycho (fig. 4(a)) exhibits a highly textured floor characterized by ribbon-like patterns, small domes and large central peaks surrounded by narrow moats, cones, flow features, and narrow crevices. In clear contrast, the crater Tsiolkovsky (fig. 4(b)) contains a smooth, dark (less than 6 percent total reflectivity) plains unit covering most of the floor, although remnants of a textured floor resembling that of Tycho occurs near the base of the walls. The plains unit resembles the maria that cover much of the visible side of the Moon. Like Tycho, Tsiolkovsky has a central peak complex; unlike Tycho, the peak rises above several portions of crater rim. The crater Abulfeda (fig. 4(c)) also contains a plains unit, but both its surface reflectivity and small crater density are much greater than those of the dark Tsiolkovsky floor. In contrast to the three preceding examples, the floor of Vitello (fig. 4(d)) is crossed by fractures arranged in concentric pattern; however, Vitello resembles Tycho and Tsiolkovsky in that it also contains central peaks.

Do these differences in floor morphologies indicate differences in crater origin or do they reflect different stages of modification? Based only on the floor morphology, we might conclude that Tycho represents a volcano. Much more likely, however, its once-molten floor is a remnant of an enormous impact event. This conclusion is based on the evidence for a devastating release of energy as indicated by rays and numerous small craters extending thousands of kilometers from the rim crest. The energy required to propel ejecta to such large distances has no counterpart in terrestrial volcanism, but more than sufficient energy is released during an impact by a large meteoroid traveling 5 km/sec. More importantly, samples returned by the Apollo missions demonstrate the importance of impact processes, and extrapolation of the frequency and size of space debris over billions of years reveals the high probability of such catastrophic encounters. Furthermore, craters resembling Tycho occur over the entire Moon without concentrations in volcanic-appearing terrains.

Because the maria are believed to be the result of basalt flows, their existence on the floor of Tsiolkovsky also could indicate a volcanic origin for this crater. However, the rim zone resembles that of Tycho. Consequently a reasonable, and generally accepted, idea is that Tsiolkovsky was also produced by an enormous impact but its floor was subsequently inundated by mare basalts during a separate epoch of volcanic modification.

The floor of Abulfeda lacks not only the features in Tycho and Tsiolkovsky but also lacks indications of an extensive ejecta blanket. The entire crater is subdued and appears to be a product of eons of exposure to meteoritic bombardment. Such repeated impacts degrade not only by the

Opposite –

Figure 2.– Comparison of telescopic view (a) of the Apennine Mountains – Archimedes region of the Moon, with a modeled reconstruction (b), under low solar illumination made by J. Nasmyth, 1885. Two imaginary views of the lunar surface from R. A. Proctor (1874): "An earth-light scene on the Moon's surface" (c); "Ideal view of mountain scenery in the Moon (Apennine Mountains)" (d). Figures (c) and (d) courtesy of Eugene Smith.

a

b

c

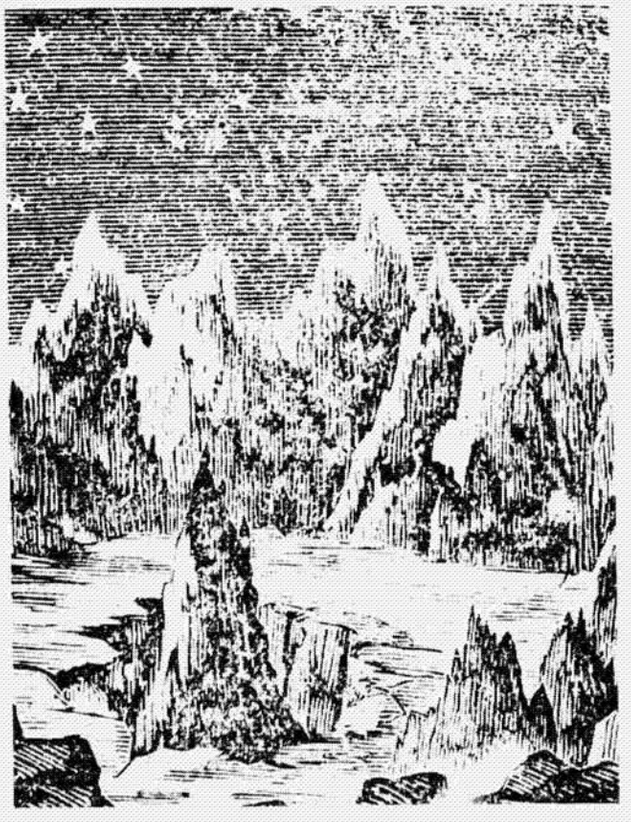

d

Opposite –

Figure 3.– Model of the lunar surface under different illuminations (courtesy of R. Greeley). Where the illumination is greater than about 20° above the horizon, much detail is lost; however, subtle reflectance (albedo) differences are lost for illumination angles below 60°.

0°
2°
4°
8°
16°
20°
45°
70°
90°

Opposite –

Figure 4. – Four craters exhibiting different floor types: volcanic-appearing floor of Tycho, (a) (LO-V-125-M); mare-inundated floor of Tsiolkovsky, (b) (III-121-H1); subdued, cratered floor of Abulfeda, (c) (V-084-M); and fractured floor of Vitello, (d) (V-168-M). Widths of respective photographs correspond to 66, 92, 51, and 58 km on the lunar surface. Solar illumination for all photographs is from the top with the north direction for (a), (c), (d), being to the left; north in (b) is to the right. Arrow in (c) identifies a small part of a long crater chain unrelated to Abulfeda.

a

b

c

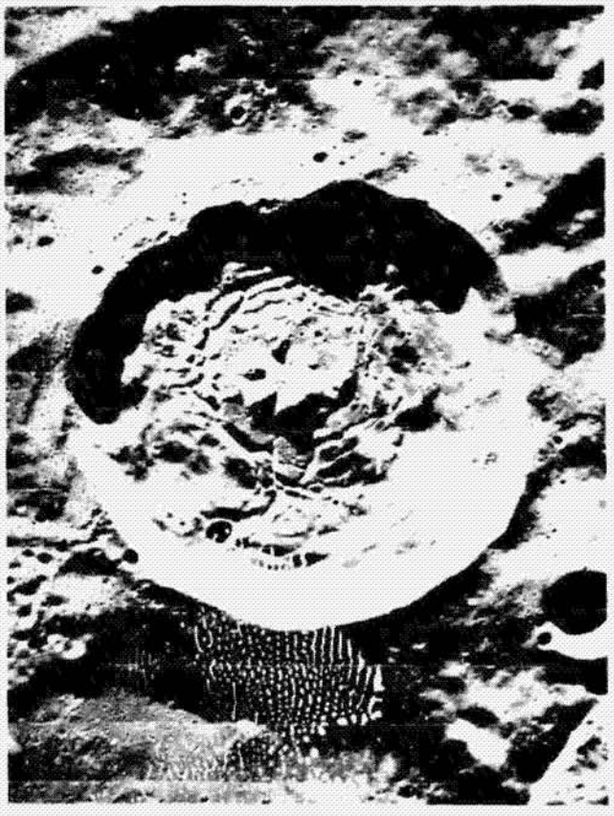

d

gradual "rounding off the edges" but also by blanketing from distant impacts, some of which produced basins as large as 1300 km in diameter (the Imbrium Basin).

The fractured floor of Vitello is typical of numerous craters that are found along the borders of the maria. The floors generally are shallow, and several contain marelike units and dark-haloed volcanic vents. Although a volcanic origin for such craters seems to be a reasonable interpretation, similar fractures and shallow floors have been recognized in craters with a rim zone resembling that around Tycho. Consequently these craters perhaps were initially produced by an impact, but the floors were modified by volcanic intrusions and eruptions associated with the volcanism responsible for the vast mare plains.

Thus, all four craters may have been originally produced by a large impact. The different appearances of their floors, however, reflect processes unrelated to crater formation (with the exception of Tycho), and the appearance of the other crater zones helps to establish which process.

Craters thought to have the same origin also change in appearance with crater *size* (fig. 5). Recently formed craters believed to be impact products exhibit increasing complexities in the morphologies of the floor, wall, and rim zones as the crater size increases. The smallest craters (less than 1 km) typically have blocky floors, blocky walls, and blocky ejecta. Differences in the crater morphologies (concentric plan, flat floor, convex floor) at this scale generally reflect differences in the competency of the lunar subsurface, and these morphologic differences have been used to estimate the depth of the lunar regolith, a surface layer of impact-produced debris extending to depths between 6 m and 10 m (see Oberbeck and Quaide, 1967). Important exceptions to the rule that well-preserved craters exhibit "crisp" and blocky appearances are *secondary craters* which are formed by ejecta thrown from a much larger impact crater (the parent or primary crater). Secondary craters typically are subdued in appearance and can be mistaken for primary craters that have been smoothed over a long period of meteoroid bombardment.

The appearance of craters larger than 1 km are summarized in the outline below.

1. Craters between 1 km and 15 km in diameter (fig. 5(b))

   a. Floor: smooth-surfaced, rubbled, or textured (once-molten floors resembling that of Tycho) floors.

Opposite –

Figure 5. – Four impact craters of different sizes: blocky 0.4 km-diameter crater northeast of Flamsteed, (a); the 4 km-diameter crater Messing C exhibiting blocky inner rim and hummocky bulk ejecta deposits, (b); the 40 km-diameter crater Aristarchus which contains a once-molten floor, central peaks, and wall slumps and which is surrounded by flow units (adjacent to rim), concentric fracturing, and dune-like terrain, (c); and the multi-ringed basin (the prominent inner ring being approximately 480 km in diameter), Orientale (d). Solar illumination in (a), (c), and (d) is from the right (east). Figure (b) is an oblique view with the Sun to the lower left (east). Lunar Orbiter photographs II-177-H2 (a), III-113-M (b), V-200-M (c), and IV-187-M (d).

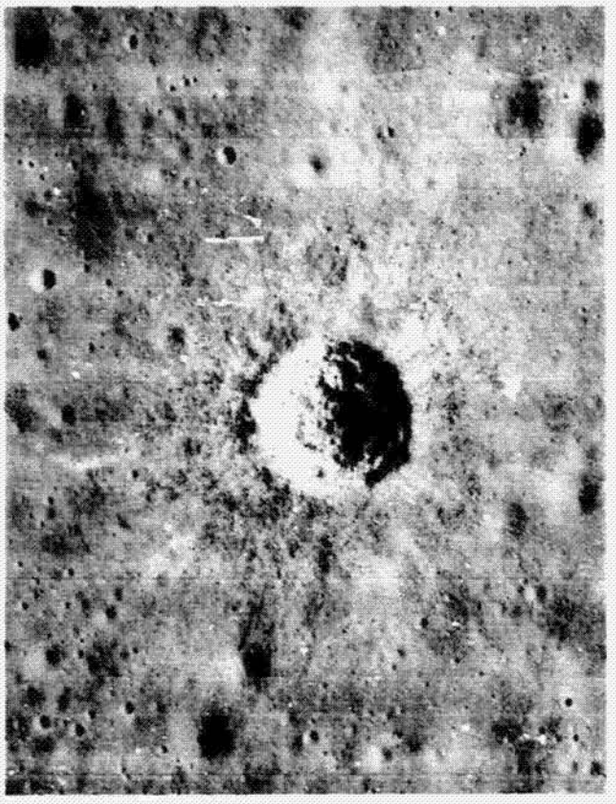

a

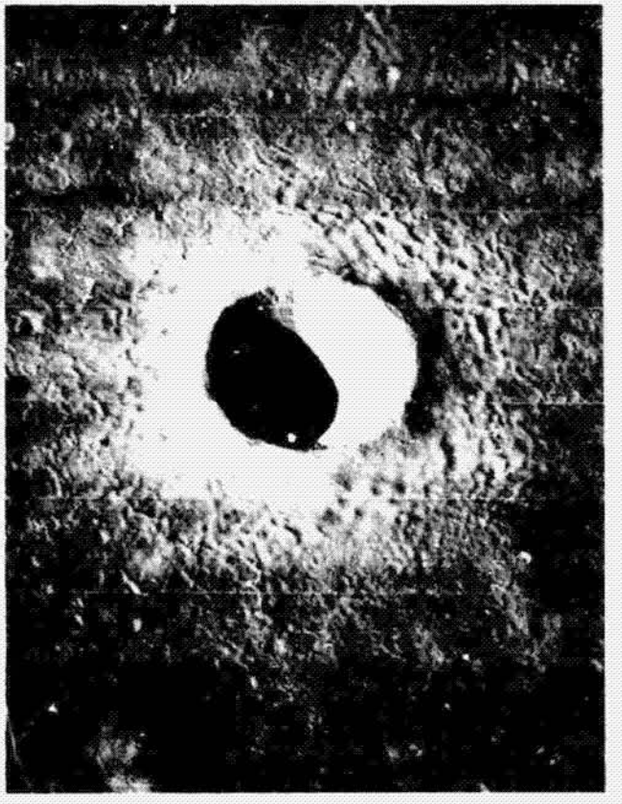

b

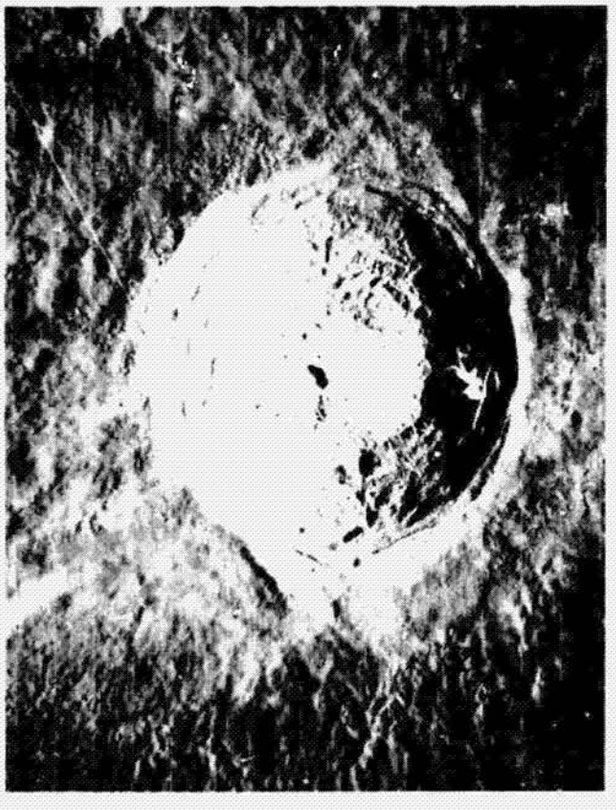

c

d

b. Wall: talus extending from near the rim crest to the floor. Differences in texture, albedo, and slope generally reflect a sorting of wall debris. Craters in this size range commonly show outcrops of strata on the upper wall.

c. Rim: division of the ejecta blanket into three relatively well-defined regions with increasing distance from the rim crest. The inner zone is characterized by blocks and concentric fractures. The middle zone exhibits a hummocky surface with radial and concentric patterns. The outermost zone contains filamentary rays and small secondary craters.

2. Craters larger than 15 km in diameter (fig. 5(c))

a. Floor: textured surface resembling once-molten units and exhibiting small volcanic features. Typically (but not always) craters of this size contain central peaks in a variety of arrangements, e.g., ridges and rings.

b. Wall: extensive wall slumps (see fig. 6) on which occur smooth-surfaced "pools" of solidified melt and across which are leveed channels from once-molten flows and debris flows.

c. Rim: division of the ejecta blanket into three zones similar to (but more complex than) those surrounding craters in the preceding size range. The inner zone exhibits remnants of flow melts, "pools" of smooth-surfaced units, and extensive annular fracturing. The middle zone contains a subdued hummocky topography with dune-like features. The outermost zone displays numerous secondaries with a characteristic herringbone pattern.

Pristine (well-preserved) craters larger than 120 km display similar features. However, above this size an inner ring of mountains may replace the central peak complex, and the larger basins may display as many as five concentric mountainous rings (fig. 5(d)). The ejecta blanket is very complex and shows clear evidence for topographic control, thus implying material traveling close to the ground during deposition. As around smaller craters, secondary craters are formed at considerable distances, but their dimensions are as large as 25 km.

The significance of the transition in crater appearance is not understood. The smaller lunar craters (less than 1 km) can be reproduced in the laboratory by high-velocity impacts (see D. Gault's summary), and such simulations reveal the details of impact mechanics. Lunar craters larger than 1 km, however, show several departures, one of which is the evidence for increasing amounts of impact-generated melts having been retained within the crater or deposited on the inner rim. In very general terms, the problem is to understand where and in what proportions are the enormous amounts of energy (the partition of energy) released during and immediately after the impact by large projectiles.

Opposite –

Figure 6.– Eight-km diameter crater, Messier B (a), in Mare Fecunditatis (AS10-29-4253) and 38 km-diameter crater, (b), on the lunar farside (AS10-28-4012). Craters smaller than 15 km in diameter generally lack the wall slumps that add to the complexity of larger craters.

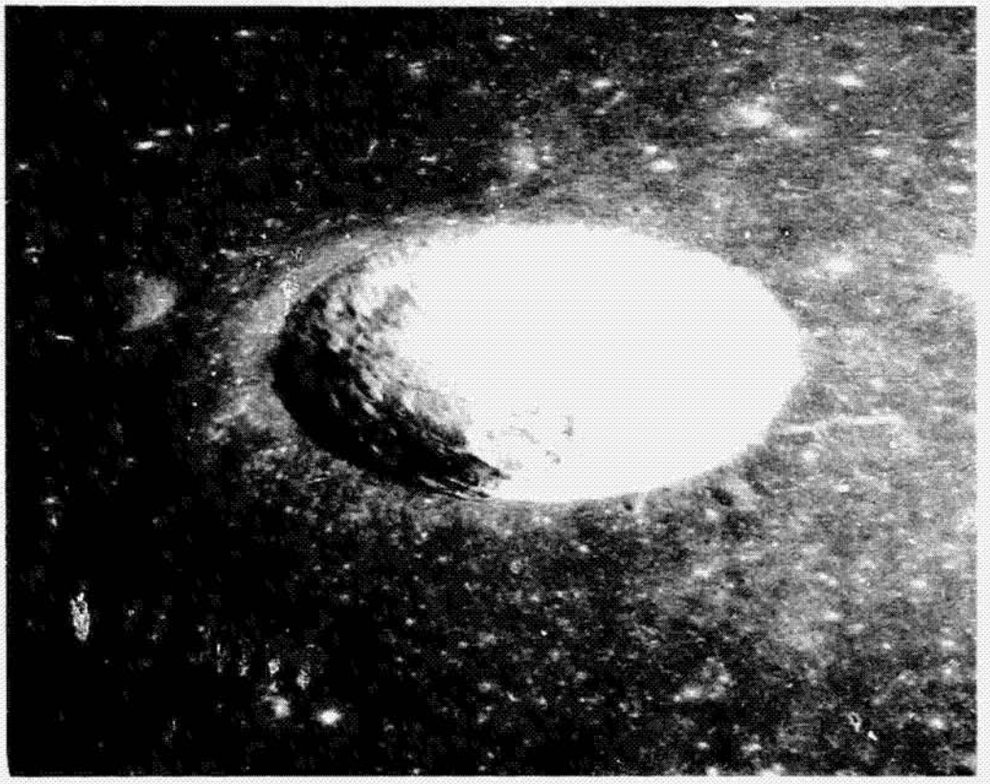

a

b

These descriptions apply only to well-preserved craters that show evidence for enormous amounts of energy release. Couple this variety with the different types and rates of modification affecting the different crater zones and we can begin to visualize the variety in lunar craters.

Not only do craters differ in their morphology, but they also display different amounts of surface reflectivity (fig. 7). Craters having the least modified surface features typically exhibit bright filamentary rays extending across the Moon (fig. 7(a)). Such rays correspond to impacts by ballistic ejecta (at velocities less than 2.4 km/sec, the lunar escape velocity), and the high reflectivity is attributed to both material thrown from the primary crater (secondary ejecta) and local material thrown from the impacting secondary ejecta (tertiary ejecta). With time, these craters lose their high reflectivity and contrast with the surrounding terrain; thus, the loss of these bright rays might be important indicators of crater age. But the use of ray darkening is not entirely reliable; in particular, figure 7(b) shows a recently formed crater with dark rays.

Numerous craters having bright ray systems exhibit a dark halo, which generally corresponds to the hummocky annulus (middle zone) of bulk ejecta deposits. Dark haloes also occur around circular and irregular craters believed to represent volcanic vents – the dark halo corresponding to relatively low-velocity mafic ejecta (around 0.05 km/sec – much lower than secondary ejecta from hypervelocity impacts). The detection of such reflectance contrasts is strongly dependent on the local elevation of the sun above the horizon (see fig. 8).

The important epochs of volcanism represented by the mare basalts also resulted in *endogenic* (internally produced) craterforms. The term "craterform" is used as an all-inclusive category that includes impact craters, calderas, collapse pits, and maars. The identification of endogenic craterforms is not as straightforward as it might seem. Although crater circularity is a useful index, volcanic craters less than 5 km in diameter can be as circular in plan as an impact crater. In fact, several Martian summit calderas, one as large as 120 km in diameter, exhibits a circularity greater than many lunar impact craters. The crater rim profile is also a useful index, but terrestrial maar explosions can show a very marked resemblance to impact craters. Morphologic criteria, for example the appearance of the ejecta blanket, can be used to distinguish between craters ejecting high-velocity projectiles (impact craters) or low-velocity projectiles (volcanic craters). However, the gradual degradation of surface features over long periods of time can mask such differences.

Opposite –

Figure 7. – Craters with ejecta facies of different albedos. The 2 km bright-rayed crater in (a) is on the rim of the crater Chaplygin; note the low-albedo blocky halo around the inner rim (AS10-33-4868). In contrast, the crater Dionysius, (b), which is 18 km in diameter, is surrounded by a bright inner halo but exhibits a dark ray system. The crater in (c) (2 km in diameter) displays a diffuse, bright halo – probably the result of mass movement destroying a once filamentary bright ray system (LO-V-93-M). The dark-haloed craters in (d) (fromelet width 12 km) probably represent impacts that excavated dark mare basalts beneath a brighter layer of secondary ejecta deposits (LO-IV-195-H2).

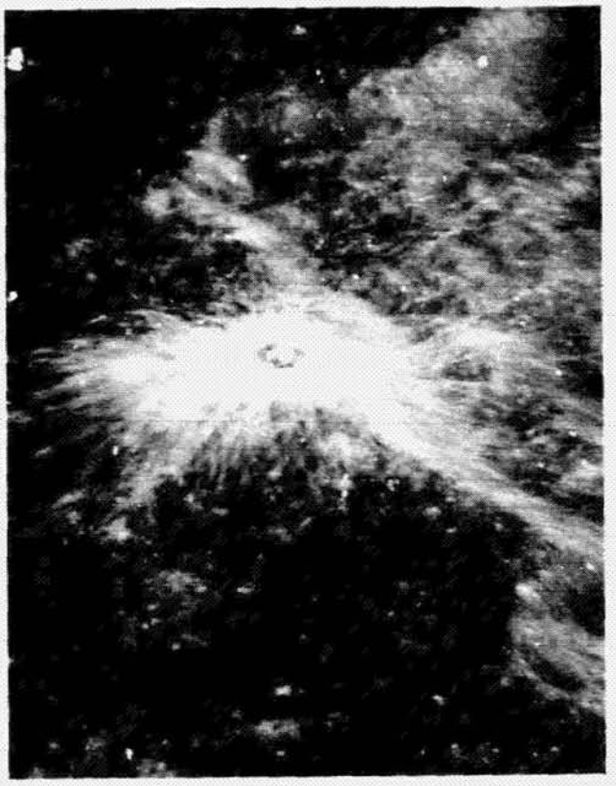

a

b

c

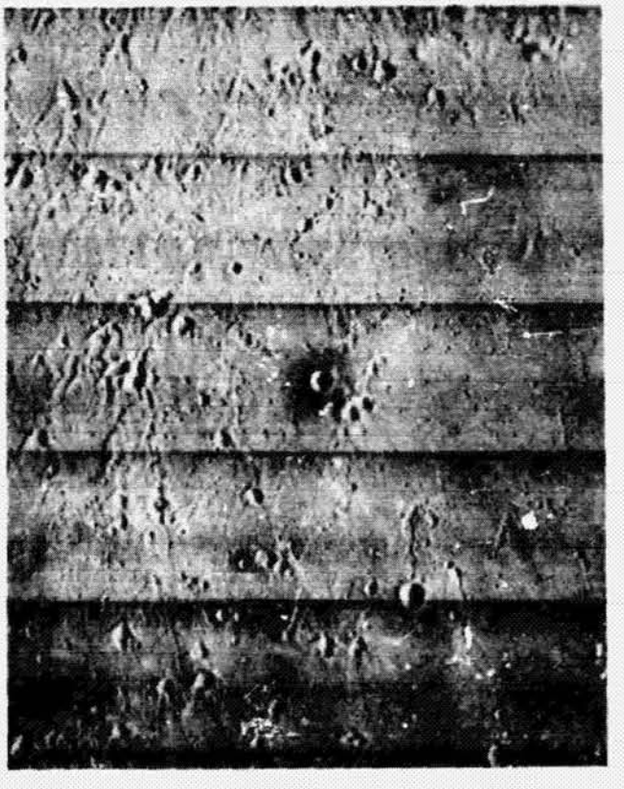

d

Opposite –

Figure 8.– Four Earth-based telescopic views of the crater Copernicus (also see fig. 10) under different angles of solar illuminations: 4°, 10°, 24°, and 90°, in (a), (b), (c), (d), respectively. Whereas surface detail is lost with increasing illumination angles, subtle albedo contrasts are enhanced (d).

a

b

c

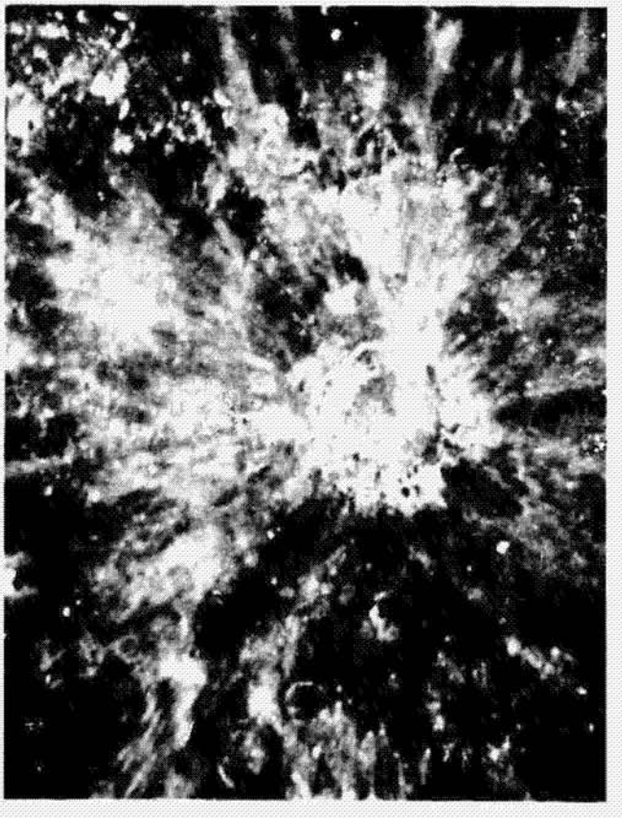

d

Perhaps one of the most reliable criteria is the association of the crater with other endogenic features, such as the crater Hyginus with the Hyginus Rille (fig. 9(a)). In this example the scalloped crater Hyginus occurs at the intersection of two rilles, i.e., linear depressions, that are believed to be grabens. Volcanic activity at the intersection of two structural trends is a common occurrence on the Earth. In addition, a chain of craterforms follows the rille plan (see fig. 9(a)) with such precision that an origin by volcanic processes is much more reasonable than an origin by fortuitously placed impacts. Other probable endogenic craterforms are shown in figures 9(b), (c), and (d).

Two important points should be made about the identification of volcanic craters. The isolation of individual crater members from the crater chain along the Hyginus Rille would leave the craters indistinguishable from many other lunar craters, generally interpreted as impact produced. Second, the volcanic *origin* of a lunar crater can be readily confused with the volcanic *modification* of a pre-existing impact structure.

Before leaving the topic of craters, we should reexamine the appearance of two different craters, Copernicus and Gassendi, with the floor, wall, and rim zones reunited (figs. 10, 11, and 12). These illustrations also permit comparison of the effects of photographic scale through nested photographs, and they reveal relative surface relief through the use of stereo pairs. Figure 11 shows an oblique view of Copernicus in order to provide perspective of true surface relief.

Opposite –

Figure 9.– Endogenic craterforms. The irregular crater Hyginus, (a), occurs near the intersection of two rilles (grabens) and is surrounded by mottled low-albedo deposits. Circular craters, which probably were volcanic vents, follow the northwestern branch of the rille (bottom of photo). The center width of (a) corresponds to approximately 45 km and illumination is from the top (LO-V-95-M).

Elongate craterforms in (b) (LO-V-182-M) occur in a chain along an extension of a wrinkle ridge (beyond photo at bottom), and remnants of this ridge may correspond to the large rims associated with several craterforms in the chain. Their relation to the crescent-shaped depression (top) and rille segments extending from this depression suggests the analogy with a partly collapsed lava tube. It is also plausible, however, that the craterforms were separate volcanic vents. The width of (b) corresponds to 30 km and illumination is from the east (right).

Three volcanic craterforms are illustrated in (c) (LO-IV-158-H1). Most noticeable is the high-rimmed crater doublet, interpreted as a pair of volcanic cones. The elongate axis of this structure aligns with the trend of the rille (lower left). Two other craterforms, above and below the doublet cone, probably were also cones but have been inundated by mare units. The width of (c) corresponds to 50 km; illumination is from the east (right).

Spade-shaped and elongate craterforms in (d) (LO-V-137-M) may represent small calderas on the mare. Note the approximate alignment of the elongate craterform with the linear extensions from the adjacent craterform. The width of (d) corresponds to 13 km; illumination is from the east (top).

a

b

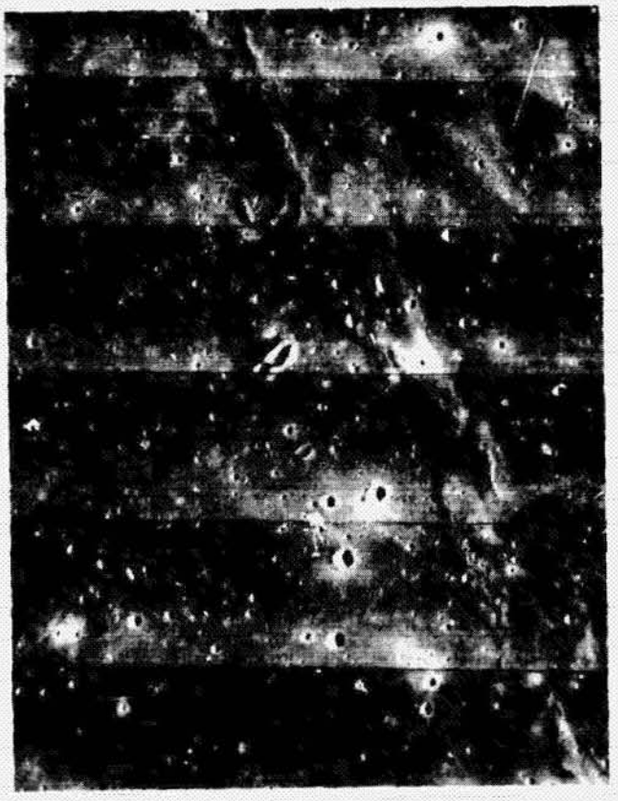

c

d

Opposite –

Figure 10.– The crater Copernicus at increasing resolutions. At the lowest resolution, (a) (width of photograph corresponding to 770 km), the bright filamentary ray system is clearly revealed. Compare this Lunar Orbiter photograph (LO-IV-126-M) to the Earth-based telescopic views in figure 8.

In (b) (LO-IV-121-H2), the three primary zones of ejecta facies – characteristic of large lunar impact craters – are shown: inner zone adjacent to the rim crest with annular fractures and flows of once-molten material; surrounding annulus of subdued, hummocky ejecta deposits; zone extending from preceding annulus with chains and clusters of herringbone-shaped secondary craters. The width of this photograph corresponds to 200 km.

The stereo pair, (c) and (d), shows at still higher resolution (vertical photo dimension, 37 km) the central ridge complex and the two contrasting floor units: the complex hillocky unit (above and to the right of the central peaks) and the plains unit (left of the central peaks) exhibiting rimless pits, volcanic cones, and fissures. Whereas (a) and (b) are oriented with solar illumination from the right (east), (c) and (d) (LO-V-154-M and LO-V-152-M, respectively) are oriented with illumination from the top (east). Compare these views with the oblique view in figure 11 in order to appreciate true surface relief.

a

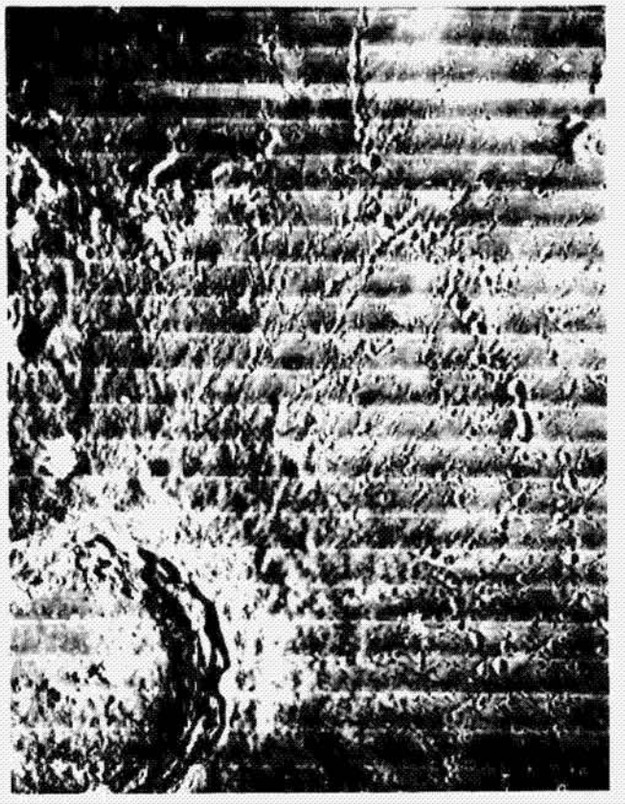

b

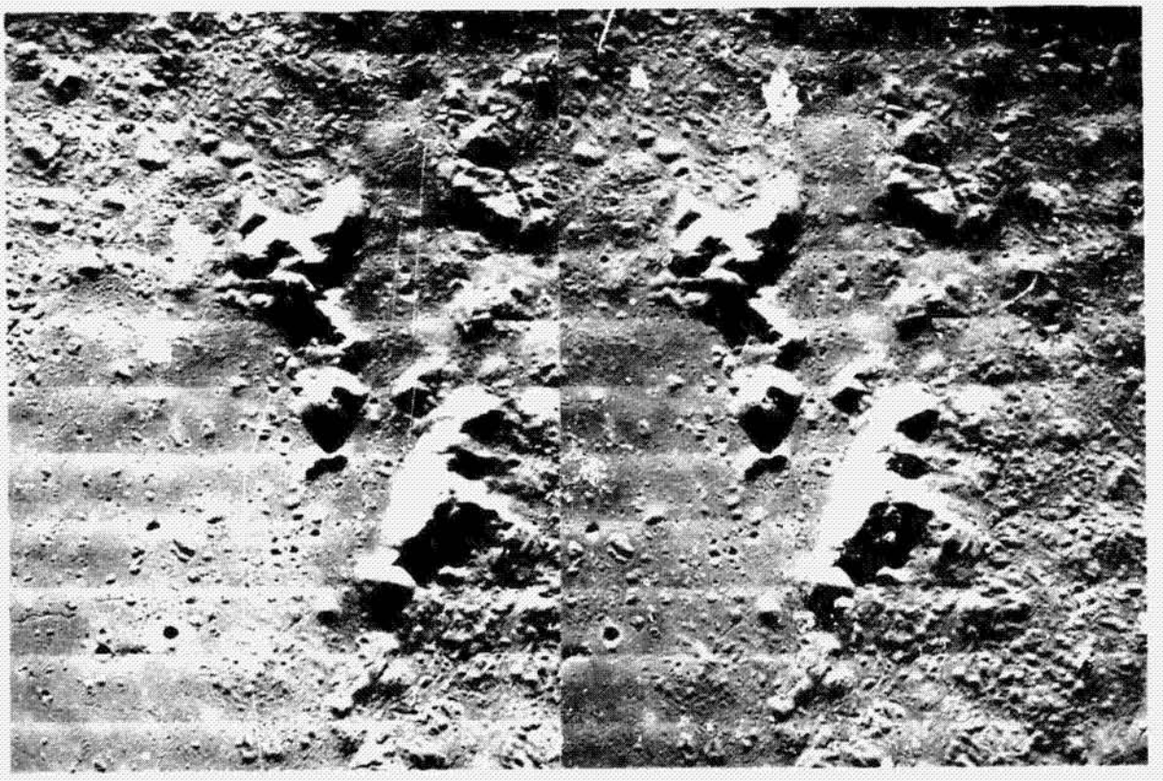

c d

Opposite –

Figure 11.– Oblique view of Copernicus from Apollo 12 (AS12-52-7742). This view is from the south of 96 km-diameter crater Copernicus and illustrates the exaggeration of depth from vertical views with relatively low solar illumination (fig. 10). The floor is about 4.5 km below the rim crest, and the peaks are about 3.5 km below the rim crest.

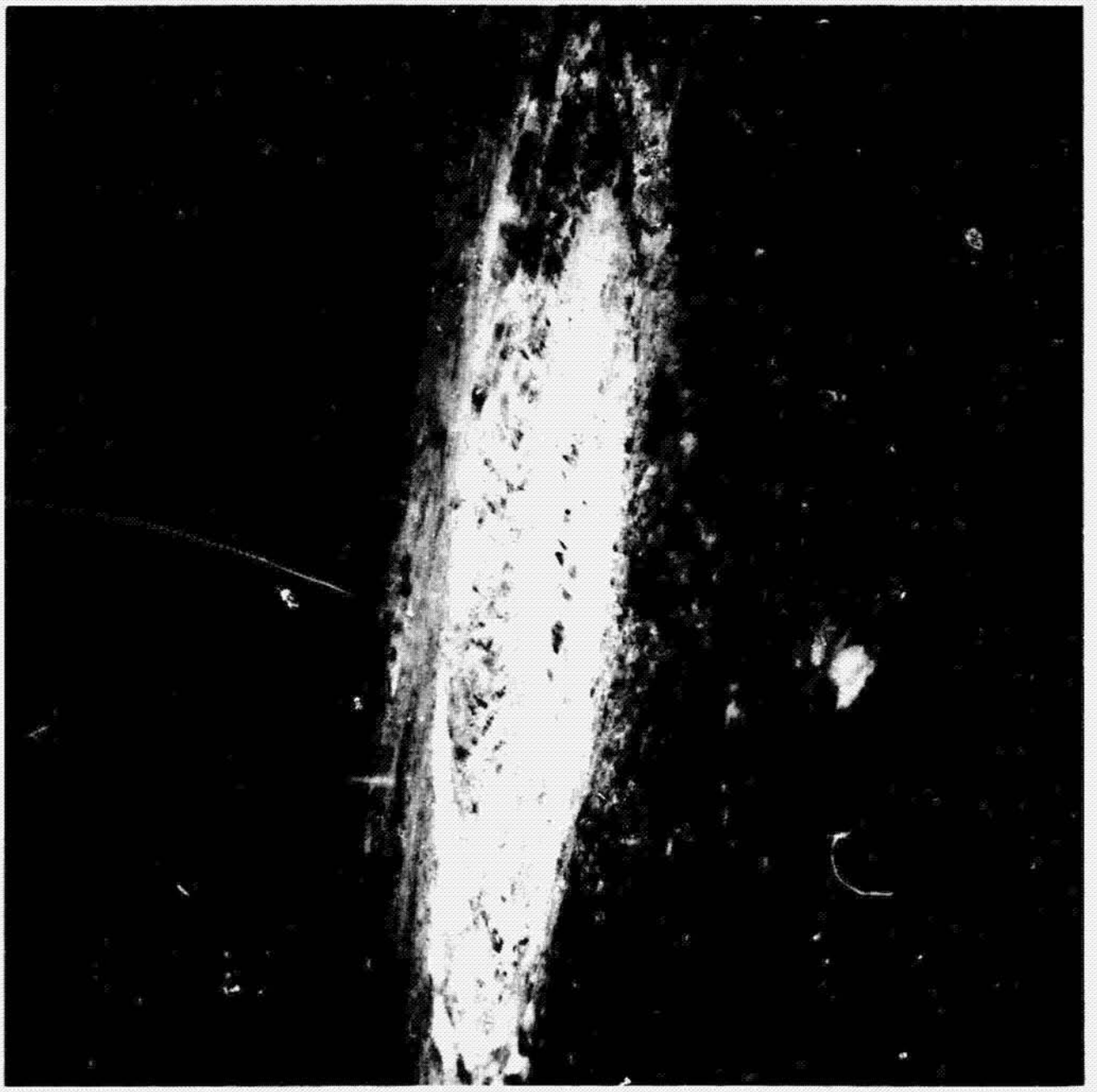

Opposite –

Figure 12.– The crater Gassendi at increasing resolutions. In contrast to Copernicus, Gassendi has a shallow, fractured floor (1.5 km beneath the rim), central peaks typically 0.3 km below the rim, and a poorly preserved ejecta blanket. It is on the northern border of Mare Humorum (a), which is an old, mare-filled, ringed basin bordered on the right (east) by concentric grabens. Two other craters with shallow fractured floors occur on the southern mare "shore." The width of (a) (LO-IV-143-M) corresponds to 770 km.

At higher resolution in (b) (LO-IV-143-H2), the floor fractures are more prominent. In addition, the southern (bottom portion) floor of Gassendi exhibits a depression adjacent to the wall/rim that has been partly filled with mare units extruded through vents on the crater floor. Compare the ridgelike wall/rim to the southeast with the subdued slumped wall and raised rim to the northwest. The width of (b) corresponds to 210 km.

The stereo pair, (c) and (d) (LO-V-179-M and LO-V-178-M, respectively), shows a portion of the floor west of the central peaks. Whereas (a) and (b) have the solar illumination from the right (east), (c) and (d) have been reoriented with illumination from the top (east). The floor appears subdued but relatively well-defined scarps bordering an irregular depression can be identified beneath the peak. Note the ridgelike rim along the fracture paralleling (left to right) the wall of Gassendi. Gassendi probably represents an old impact crater in which the floor was raised by igneous intrusions associated with the epochs of mare flooding of Mare Humorum.

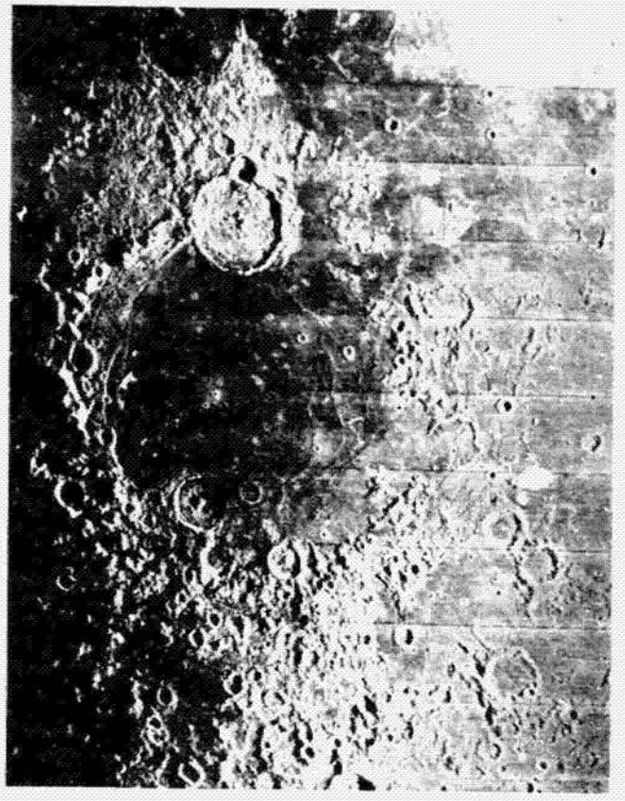

a

b

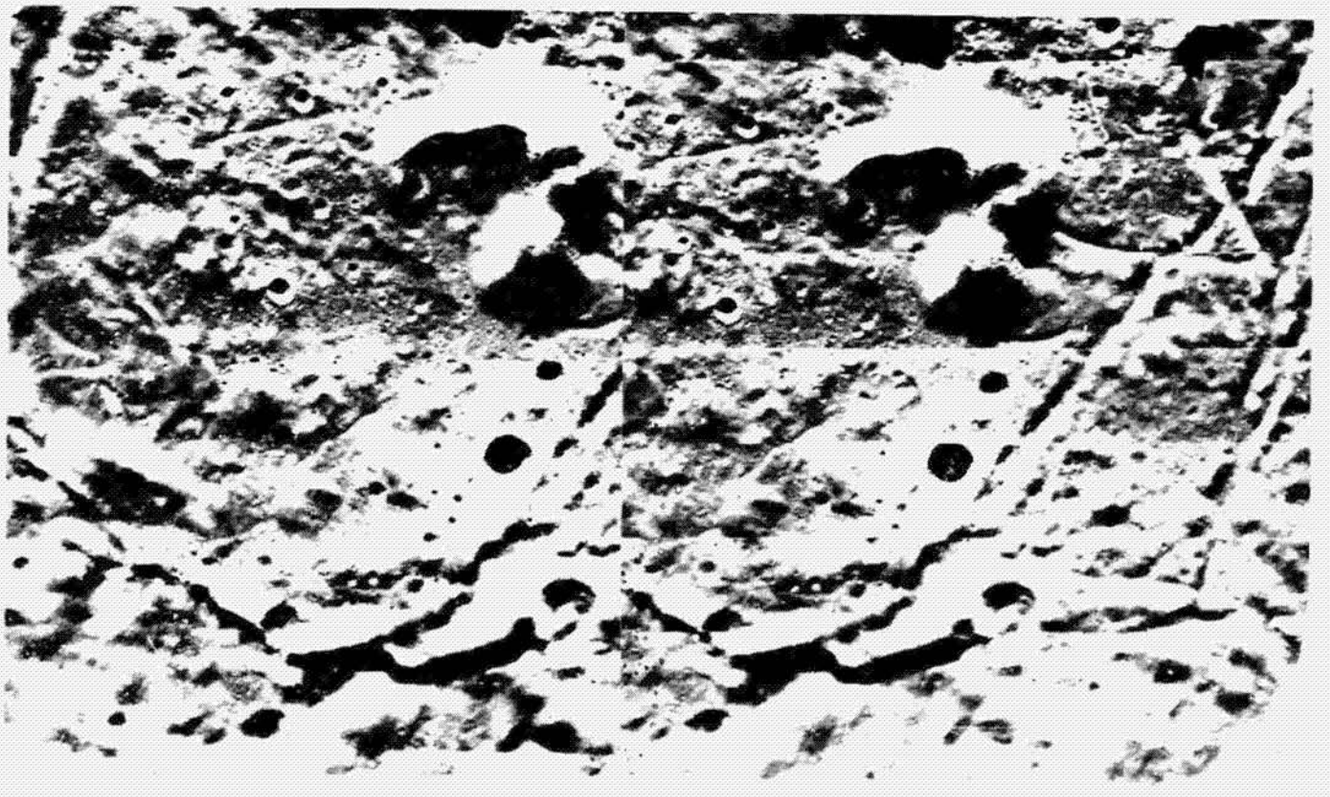

c d

III. POSITIVE–RELIEF FEATURES

Positive-relief features include plateaus, domes, cones, ridges, and massifs. Lunar plateaus are interpreted as either constructional features or relict relief features. Constructional processes include igneous extrusions and structural uplift. Relict relief plateaus are the result of the inundation by plains units, such as the maria, that isolated pre-existing structures from surrounding terrain and left them in relief. Their *relief* is not necessarily the result of a process related to mare flooding, but their morphologic *form* is the result (or at least is enhanced) by the isolation caused by the encompassing mare basalts. However, several plateaus on the maria and on crater floors appear to represent both flat-topped lava crusts and terraced pre-existing features left in relief by the removal of lava.

Figure 13(a) shows a *plateau* with a polygonal plan, which suggests a structural origin. The plateau occurs near the edge of Mare Fecunditatis but is isolated from the mare border by encompassing mare units. It is probably a remnant of the highland border and obtained its relief, at least in part, by collapse of the surrounding terrain during mare flooding.

Domes comprise a broad class of surface features and also can be viewed as constructional or relict relief forms. Figure 13(b) illustrates a cluster of low-relief domes with summit pits, which are interpreted as small shield volcanoes with summit calderas. In contrast, figures 13(c) and (d) show (in stereo) a pair of high-relief textured domes that overlap the relatively smooth-surfaced highland terrain but has been encroached by the mare units. The domes in figure 13(b) and those in figures 13(c) and (d) probably represent two different constructional processes which are common to terrestrial volcanic domes: domes created by external growth, i.e., by successive eruptions of low-viscosity lavas (shields), and domes created by internal growth, i.e., eruptions of high-viscosity extrusions and built-up from within.

Opposite –

Figure 13.– Isolated positive-relief features. Plateaus with polygonal plans are shown in (a) (III-025-M). These structures are believed to be remnants of a plains unit. Collapse of surrounding terrain (and uplift of remnant blocks) with subsequent encroachment by lava (the mare) produced the relief. Illumination is from the top (east) and the width of the photograph corresponds to 18 km.

Low-relief domes with summit pits in (b) (LO-IV-133-HI) are interpreted as small shields formed by successive eruptions of low-viscosity lavas. Also note the volcanic ridge in the upper right. The solar illumination is from the top (east) and the width of the figure corresponds to 42 km.

High-relief (1.7 km above the mare), textured domes in (c) and (d) (V-185-M and V-182-M, respectively) suggest the analogy with terrestrial lava domes, which are produced by successive internal build-ups of viscous lavas. This stereo view also reveals a sinuous rille extending from an elongate pit (center). The illumination is from the top (east) and the photo length corresponds to 62 km.

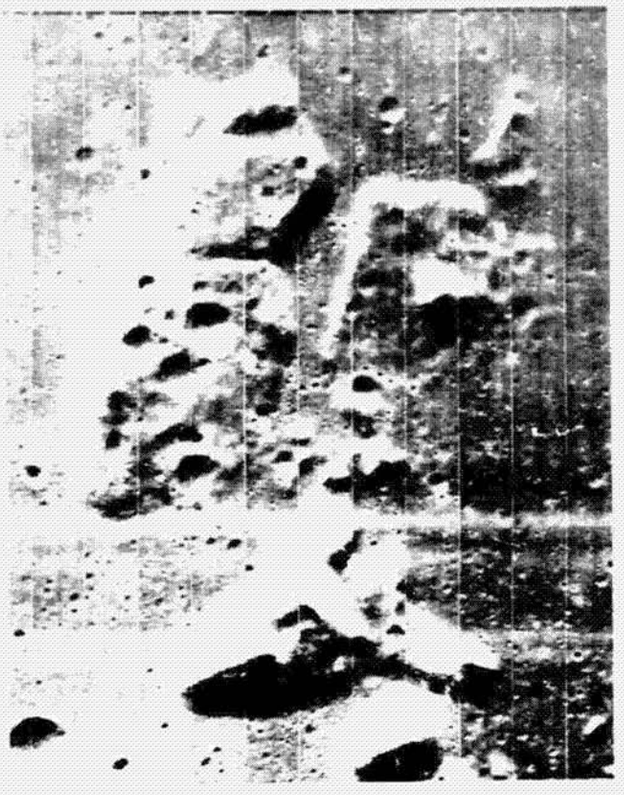

a

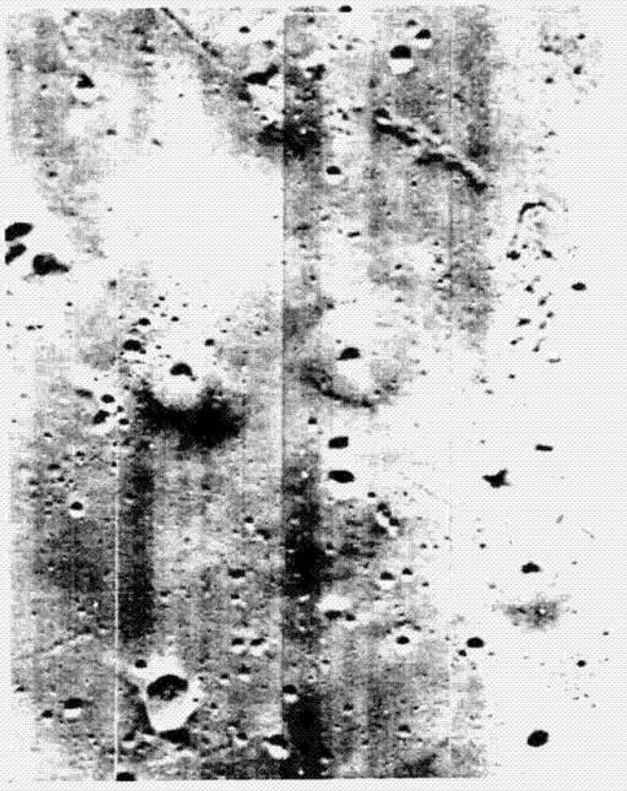

b

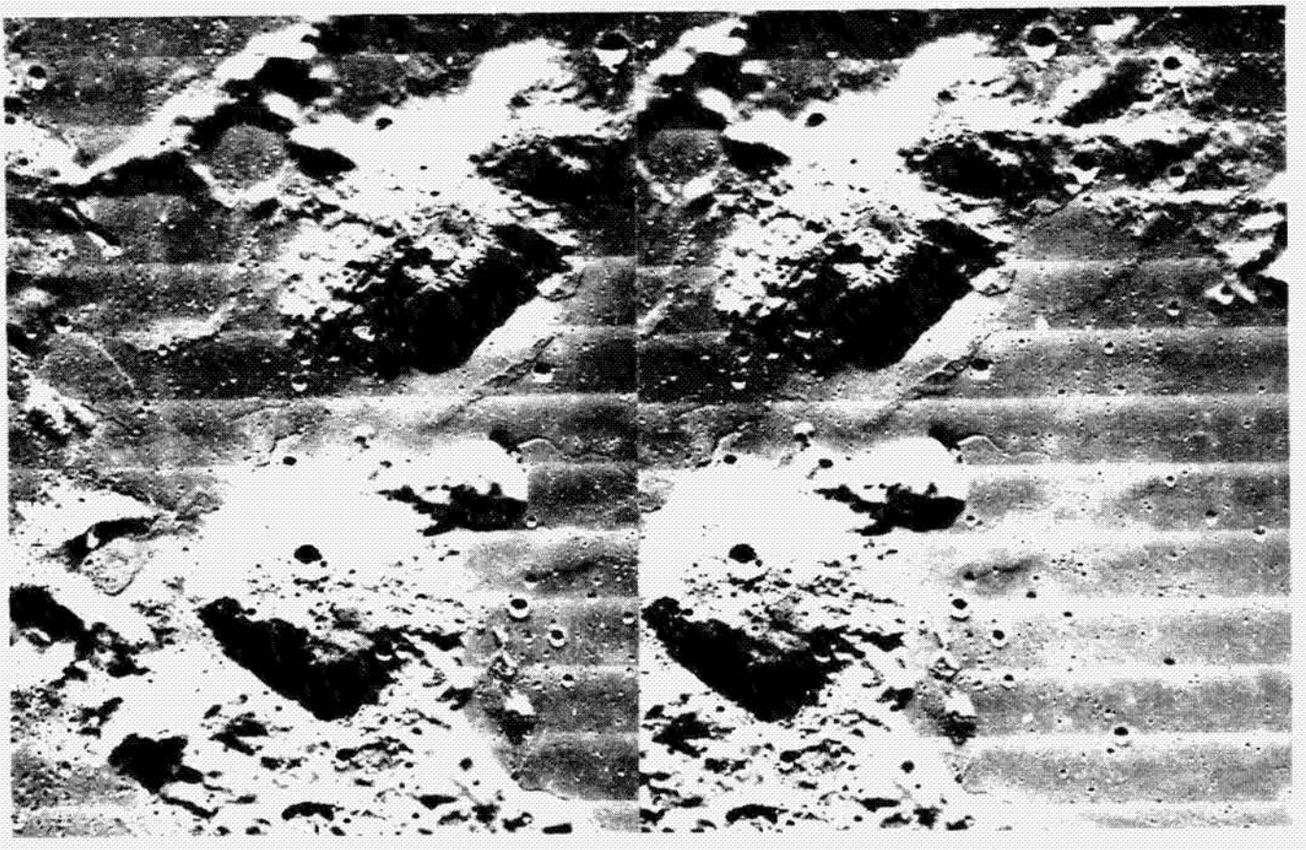

c d

In addition, we find low-relief domes called *mamelon* domes that lack summit pits and exhibit an extensively wrinkled surface texture, which is thought to be the result of slow mass movement of particulate debris. Mamelon domes are very common structures in the "shallow" regions of the maria, and many appear to be relicts of pre-existing topography that were not completely covered by the mare basalts.

Volcanic *cones* also occur in the shallow regions of mare flooding (see fig. 9(c)). In contrast to mamelon domes, which generally exhibit a higher reflectance (albedo) than the surrounding maria, the surface albedo of volcanic cones matches or is slightly lower than the surrounding maria. But not all cones have a low reflectance; for example, the cones on the floor of the crater Copernicus match its relatively high-albedo floor. Because of the low lunar gravity, the construction of thick rim deposits close to a vent, which results in a cone, requires both low-velocity ejecta and angles of ejection that depart very little from the vertical. Where these conditions are not met, the classical cone profile and summit crater may reduce to a crater surrounded by a low-relief rim (Wright *et al.*, 1963; McGetchin and Head, 1973). Consequently, large lunar cones probably represent relatively meager "last gasps" of local volcanism, although by no means the last volcanic event.

Lunar *ridges* result from a variety of processes. Figure 14(a) reveals the extensive "sculpture" that radiates from the Imbrium Basin, an enormous multi-ringed crater partly inundated by mare basalts. This sculpture is attributed to both ejecta deposits and an extensive system of closely spaced horsts and grabens. In contrast, figure 14(b) reveals a ridge that is composed of individual volcanic cones. This volcanic ridge is also radial to the Imbrium Basin and is thought to reflect eruptions following a radial system of crustal weaknesses previously created by the enormous Imbrium impact event. Another type of volcanic ridge lacks the well-defined summit vents but exhibits irregular borders and a low-albedo halo.

One of the most common types of lunar ridges is shown in figure 14(c) and is descriptively called a *wrinkle ridge*. These are low-relief structures (ranging from a few meters to a few hundreds of meters in relief) that are most obvious across the lunar maria; however, they also commonly occur in the highlands (fig. 14(d)), although less readily identified. The surface of the broad mare ridges resembles the adjacent maria with respect to crater densities and albedo. In profile, such wrinkle ridges exhibit a steep scarp on one side and a more gradual slope on the other side. The scarp commonly changes sides with the gently sloped border along the length of the ridge. In addition, a narrow ropelike ridge generally accompanies the broad ridge component and crosses back and forth, thus enhancing the wrinkle appearance (see fig. 14(c)).

Opposite –

Figure 14.– Different types of lunar ridges: ejecta ridges and horsts radial to the Imbrium basin, (a) (AS16-M847); volcanic ridge with summit pits, (b) (IV-133-H1); broad mare wrinkle ridges and narrow ropelike wrinkle ridges, (c) (V-169-M); and highland wrinkle ridge, (d) (III-132-M). Illumination in (a) is from the right (east), in (b) and (c) from the top (east), and in (d) from the left (east). The widths of (b) and (c) correspond to 26 km and 41 km, respectively. The oblique view (a) shows the flat-floored crater (top center) Flammarion, approximately 70 km in diameter. The oblique view (d) shows a small, crisp crater at center right that is approximately 0.2 km in diameter.

a

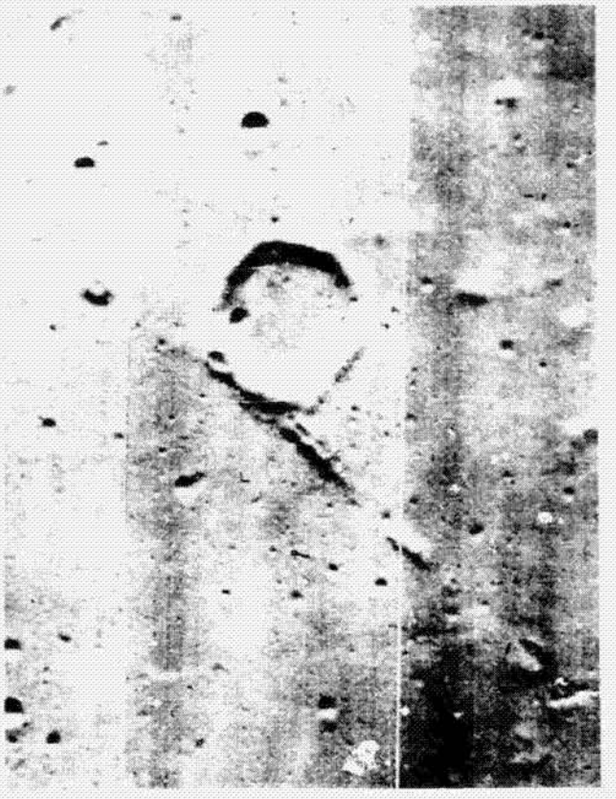

b

c

d

The term "wrinkle ridge" is usually applied to a host of different ridges which actually have subtle differences in morphology. As a result there are different origins. Many appear to be folds and surfaces elevated by low-angle thrust faulting that were produced by compressional stresses created by subsidence of the maria; however, the fact that not all ridges are restricted to the maria also indicates large-scale crustal tectonism. The association of other ridges with endogenic craters (fig. 9(b)) and sinuous rilles (fig. 15) suggests a genetic relation to volcanic intrusions; however, it is uncertain whether the ridges are products of intrusions (intrusive uplift or limited extrusions) or reflect crustal weaknesses that localized these intrusions.

The last type of positive-relief feature to be discussed is the lunar *massif*. Lunar massifs are large mountainous structures which, in most cases, appear to be remnants of one of the rings surrounding a large impact basin (see figs. 16(a) and (b)). Where these massifs are surrounded by mare units, they become prominent "peaks," particularly under low solar illumination (fig. 16(c)). Where they occur in the hummocky lunar highlands, this exaggeration is lost (fig. 16(d)). Most massifs exhibit relatively gentle slopes (less than 30°), i.e., they lack the precipitous scarps suggested by low solar-illumination.

IV. NEGATIVE–RELIEF FEATURES

Negative-relief features include rilles and irregular depressions. Prior to the availability of high-resolution photographs, the term "rille" described any linear depression without connotation of origin. Rilles are classified by their shape in plan (straight, arcuate, rectilinear, and sinuous) and profile (V-shaped, U-shaped, and flat-floored). These geometric parameters help in the recognition of rille origin although by themselves they are not reliable diagnostic criteria.

Straight and *arcuate rilles* extend over large distances (hundreds of kilometers) and typically cross a variety of different lunar terrains. Such disregard for topography strongly suggests a structural origin. In fact, where these rilles cross topographic highs, they typically widen (fig. 17(a)) – as expected for grabens with inward-dipping boundary faults (see McGill, 1971).

Many arcuate rilles are members of larger rille systems. Several systems encircle mare-filled basins, and Baldwin (1963) suggested that this association indicated peripheral tensional stresses which were produced by gravitative subsidence of the maria. The existence of mass concentrations (mascons) associated with the maria, however, indicates that this crustal adjustment remains incomplete. Perhaps the most impressive system of concentric grabens borders eastern Mare Humorum (fig. 12(a)). In contrast, western Mare Humorum exhibits a system of parallel grabens trending NE, and such asymmetry illustrates the complexity of the lunar crust.

The different profiles of arcuate rilles generally reflect different initial widths or different degrees of modification (see fig. 17(b)). For example, a narrow V-shaped rille probably represents a graben or fault zone in which the facing wall talus meet. A flat-floored rille could indicate either *en bloc* subsidence of the floor or filling of a V-shaped rille by lava or debris.

Rectilinear rilles (fig. 17(c)) clearly expose the structural influence on their formation. Note that the strong evidence for structural *influence* does not necessarily imply structural *origin*. For example, numerous terrestrial rivers trace fault systems and produce a rectilinear plan or trellis drainage patterns. The probable absence of flowing water on the Moon during its history might

Figure 15.—Wrinkle ridges near a large "ghost" crater (70 km in diameter), northeast of Gassendi, see figure 12(a). This Apollo 16 vertical metric frame (2837) illustrates the complex structure of wrinkle ridges. In particular, note the en echelon offset, the wrinkle ridge extensions of the rim of the ghost crater, and the location of the "head" pits of the two sinuous Rupes Rilles on the wrinkle ridges.

Opposite –

Figure 16.– Massifs associated with: the well-preserved Orientale Basin, (a); the degraded Humboldtianum Basin, (b); a poorly recognized basin (west of Copernicus) inundated by Imbrium ejecta and mare units, (c); and an enormous, ancient basin on the lunar farside, (d), noted by Schultz (1972). The prominent outer ring of Orientale (LO-IV-182-M) is approximately 930 km in diameter; that of Humboldtianum (LO-IV-152-M) is 600 km. The width of (c) (LO-V-164-M) is 29 km with illumination from the top (east); the width of (d) (LO-I-128-M) is 280 km with illumination from the right (west).

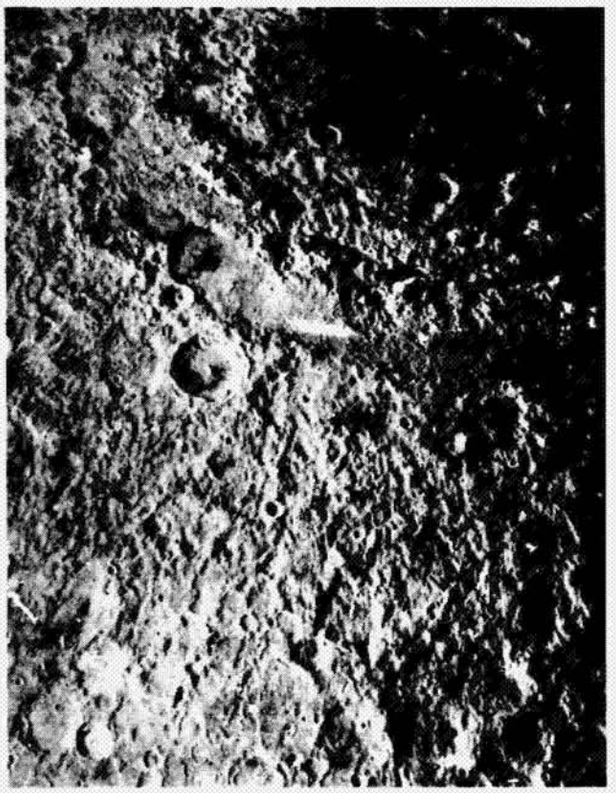

a

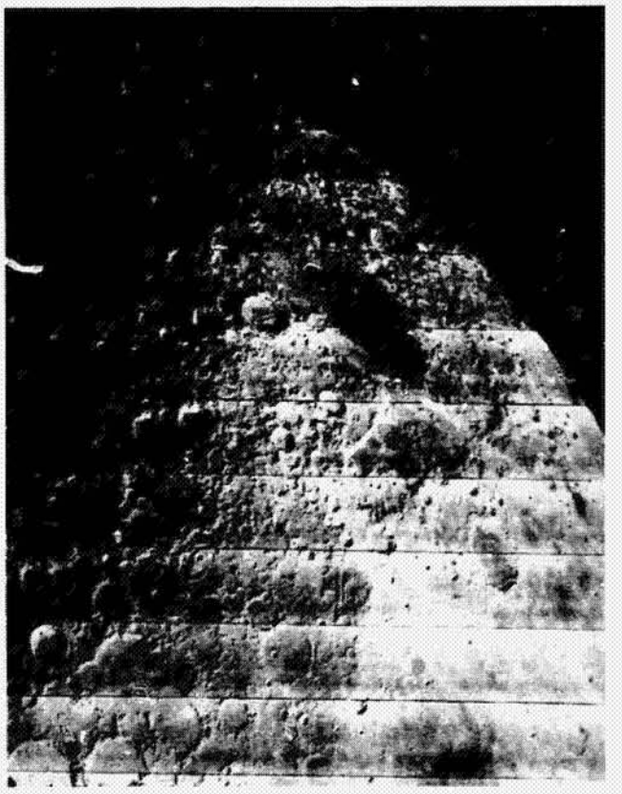

b

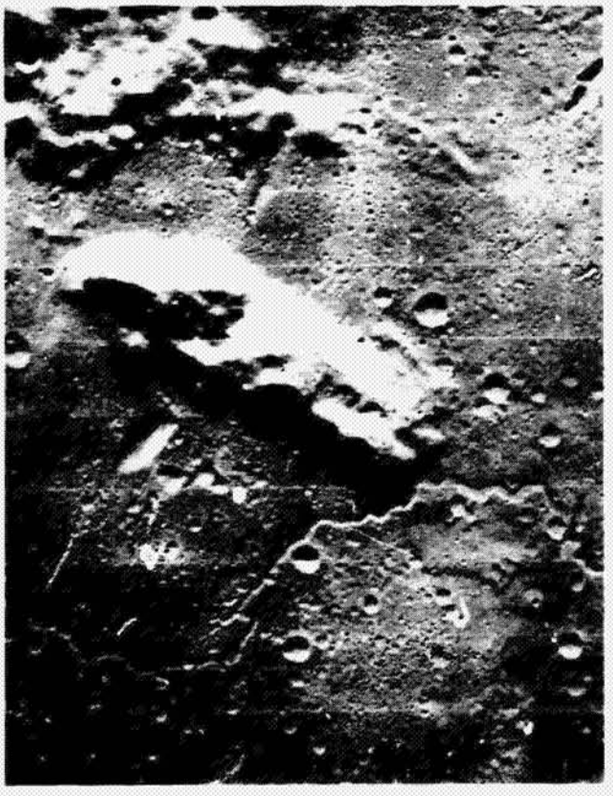

c

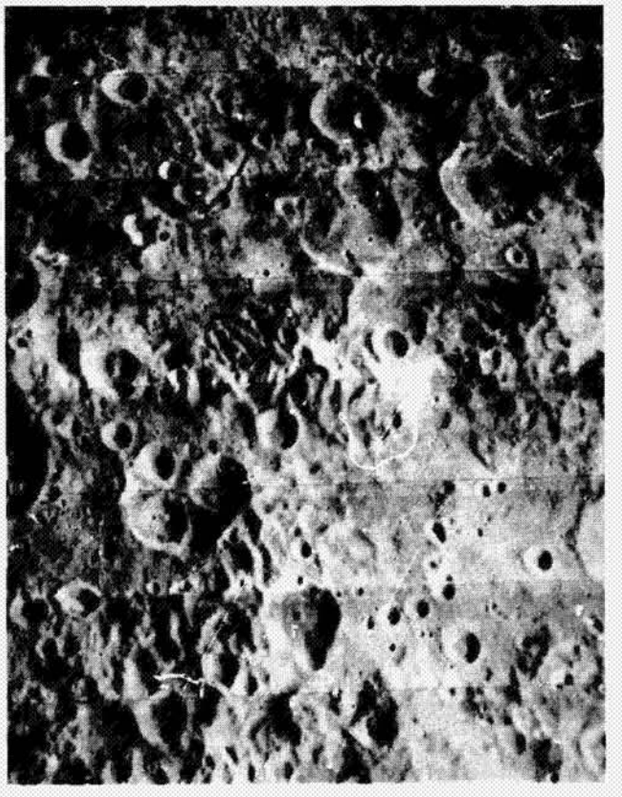

d

Opposite –

Figure 17.– Lunar rilles: 4 km-wide graben, Rima Bond I, with an en echelon *offset, (a) (AS10-31-4645); branching rille with U-shaped and flat-floored profile, (b) (AS15-11710-11); rectilinear rille that dissolves into crater chain at one end and dissolves into a volcanic cone (2.5 km in diameter) at the other end, (c) (AS11-42-6309); rectilinear and sinuous rilles in the Harbinger Mountains found in northwestern Mare Imbrium, (d) (LO-V-191-M). The width of (b) corresponds to 13 km; (d), to 50 km.*

a

b

c

d

negate a comparable origin for lunar rectilinear rilles. However, terrestrial lava channels and tubes also have been observed to follow crustal weaknesses. Most lunar rectilinear rilles, particularly highland rilles, are probably crustal fractures, but several examples found on the lunar maria appear to correspond to structurally controlled channels which once contained flows of lava (fig. 17(d)).

The preceding discussion leads to the enigmatic *sinuous rilles*, i.e., rilles that exhibit frequent curvilinear changes in plan. Sinuosity ranges from only a few curvilinear kinks with large radii of curvature to the highly sinuous "meandering" inner rille of Schröter's Valley (fig. 18). Sinuous rilles generally occur on the maria and exhibit a "head" crater or rimless elongate depression that is found, in most cases, at the highest elevation with respect to the rest of the rille. In addition, they typically lack the *en echelon* offsets that characterize structurally formed arcuate rilles, although a few rilles dissolve into crater chains.

These observations support interpretations that sinuous rilles represent ancient lava channels (Strom, 1966) or collapsed lava tubes (Greeley, 1971). Several features characteristic of sinuous rilles, however, have prompted debate. First, lunar sinuous rilles extend over enormous distances (as long as 300 km), in contrast to terrestrial examples (typically less than 5 km). Second, the sinuosity of several rilles is almost comparable to meandering terrestrial rivers. Third, several sinuous rilles occur, at least in part, within the lunar highlands. These potential objections to the analogy with terrestrial tubes or channels could reflect our lack of knowledge about the volume of lava erupted during the emplacement of the maria. The sinuosity probably reflects lava viscosity, which perhaps was as fluid as glycerin owing to the high metal content (Murase and McBirney, 1970). Thus an understanding of these structures will be important for an understanding of the period of volcanism which produced the maria.

Irregular terraced depressions are the result of structural collapse (fig. 19(a)) or are remnants of the mare-flooding epoch (fig. 19(b)). Terraces surrounding mare units are common within closed depressions, such as craters (fig. 20(b)), but also occur in the maria (fig. 20(c)). The terraces reflect previous levels of once-molten mare units, which subsequently subsided through either a volume change of the lava (devolatization) or drainage (back into the original vent or to an adjacent topographic low). Even the enormous Mare Imbrium is bordered at several locations by broad terraces (fig. 20(d)).

Opposite –

Figure 18.– Three views of Schröter's Valley: stereo pair, (a) (LO-V-204-M) and (b) (LO-V-202-M), showing the "head" crater called the "Cobra Head"; a closer view of the meandering inner rille, (c) (LO-V-202-M); and a high-resolution photograph of a "meander cutoff" partly encroached by wall talus of the containing valley, (d) (LO-V-204-H3). The framelet widths in (a), (b), and (c) are 4.3 km. The framelet width of (d) is 0.58 km. Illumination is from the top (east

a b

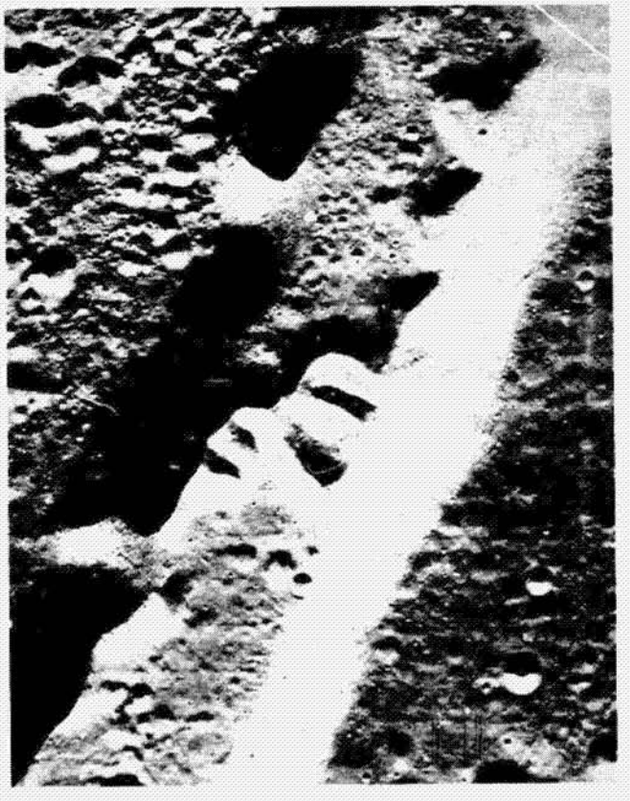

c d

Opposite –

Figure 19.– Rectilinear and irregular depressions. The rectilinear depression in (a) (LO-IV-195-H1) occurs on the southern edge of the interior Mare Orientale plains. The irregular depressions in (b) (LO-IV-161-H2) are found in highland terrain and are believed to represent receded lava (mare) lakes. The width of (a) corresponds to 216 km; and that of (b), to 55 km. Illumination in both is from the top (east).

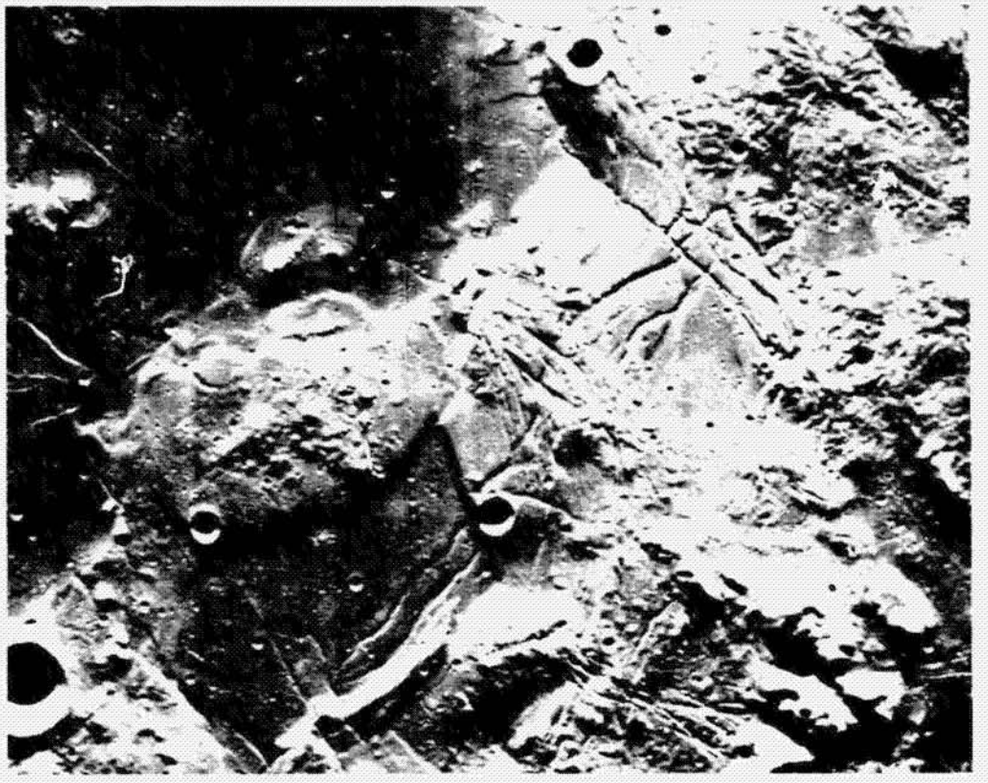

a

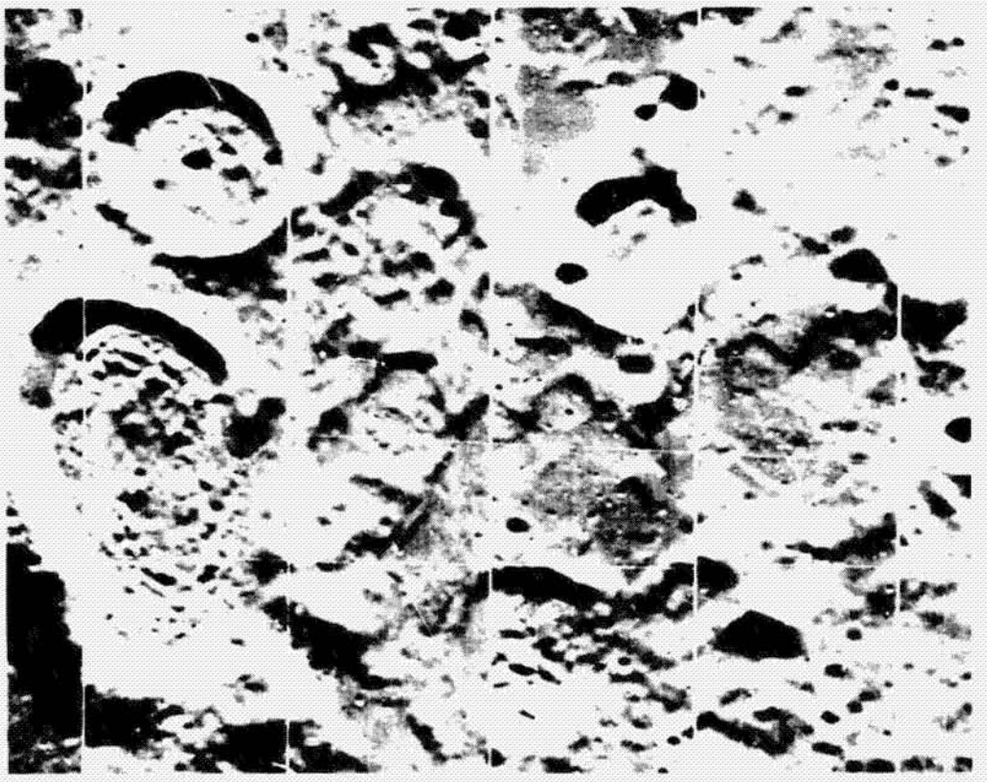

b

Opposite –

Figure 20.– Terraced depressions on the Earth (a) and on the Moon (b), (c), and (d). Terraces (a) border the basaltic floor of Kilauea-Iki crater, a 1.6 km × 0.8 km pit adjacent to Kilauea caldera, Hawaii. The lunar crater Kunowsky, (b) (AS12-_2-7746), is 19 km in diameter and also exhibits terraces along the wall and around insular hills on its marelike floor. Kunowsky is thought to be a volcanically modified impact crater which was formed prior to the last stages of mare flooding. The narrow terraces probably reflect previous levels of the mare basalts, which lowered perhaps as a result of devolatization. The irregular depressions and terraces in (c) (LO-V-209-M) occur west of the Aristarchus Plateau in Oceanus Procellarum and may be the result of either devolatization of the mare basalts during cooling or drainage of the lava. The width of this illustration corresponds to 24 km. On a larger scale, the terraces in (d) (LO-V-129-M) border northern Mare Imbrium (width of the photograph corresponds to 34 km).

a

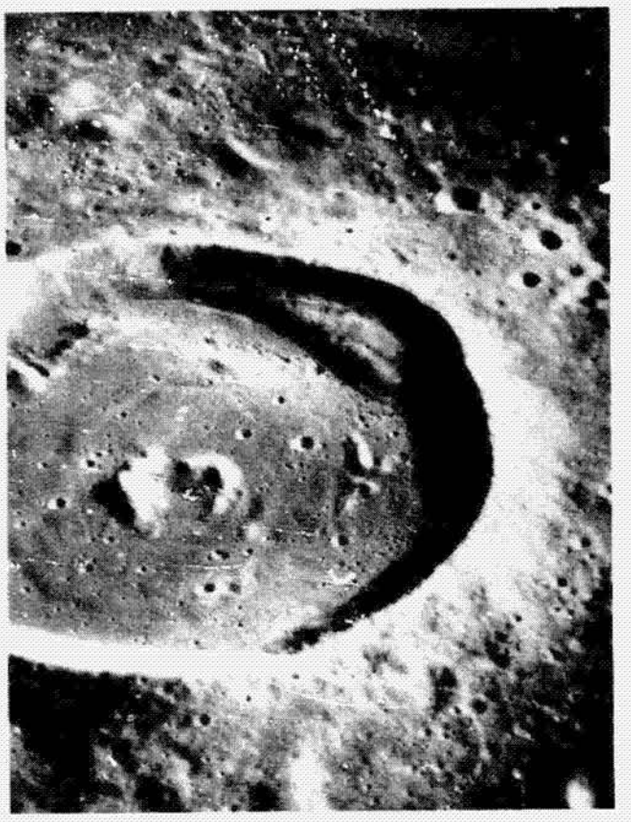

b

c

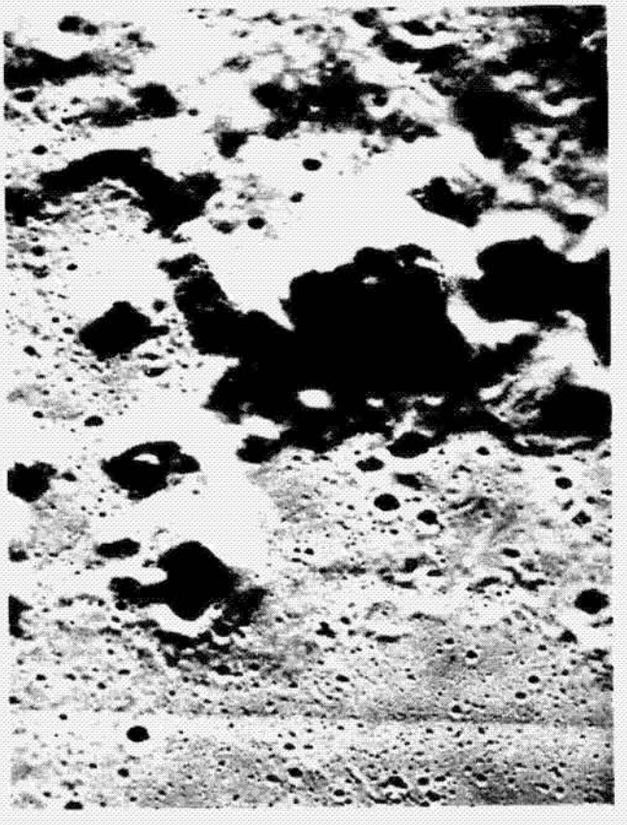

d

V. CONCLUSIONS

This very brief summary of lunar surface features should dispel the concept that the Moon is a simple planetary body because it is subject to relatively few surface processes. Perhaps the Moon's history is simple relative to the Earth's history, but in contrast to the Earth, the lunar surface has been well preserved for at least 4 billion years. Since that time, the results of both endogenic and exogenic processes have remained exposed.

The Apollo missions have returned invaluable samples of the lunar crust, but these samples generally apply to restricted regions, with the exception of locally foreign materials heaved from distant impact events. It is unreasonable to interpret findings from returned samples as strict constraints for the formation of surface features outside their geologic setting; it is also unreasonable to require terrestrial analogs for all surface features. This reminder is necessary because without manned landings in the near future, selenology based on photo-interpretation will become a fundamental approach for disclosing lunar geologic history.

REFERENCES

Baldwin, R. P.: The measure of the Moon. Chicago, Univ. of Chicago Press, 488 p., 1963.

Greeley, R.: Lava tubes and channels in the lunar Marius Hills. Moon, v. 3, p. 289-314, 1971.

McGetchin, T. R.; and Head, J. W.: Lunar cinder cones. Science, v. 180, p. 68-71, 1973.

McGill, G. E.: Attitude of fractures bounding straight arcuate lunar rilles. Icarus, v. 14, p. 53-58, 1971.

Murase, T.; and McBirney, A. R.: Viscosity of lunar lavas. Science, v. 167, p. 1491-1493, 1970.

Mutch, T. A.: Geology of the Moon: a stratigraphic view. Princeton University Press, 324 p., 1972.

Oberbeck, V. R.; and Quaide, W. L.: Estimated thickness of a fragmental surface layer of Oceanus Procellarum. Jour. Geophys. Research, v. 72, p. 4697-4704, 1967.

Schultz, P. H.: A preliminary morphologic study of the lunar surface. Ph.D. dissertation, University of Texas at Austin, 1972. Moon Morphology, Austin, University of Texas Press (in press, 1975).

Strom, R. G.: Sinuous rilles, p. 199-210. In Heacock, R. L., Kuiper, G. P., Shoemaker, E. M., Urey, H. C., and Whitaker, E. A., editors, Ranger VIII and IX, Part II. Experimenters' analyses and interpretations: Pasadena, Cal. Inst. Tech. JPL Tech. Rept. No. 32-800, 382 p., 1966.

Wright, F. E.; Wright, F. H.; and Wright, H.: The lunar surface, introduction. In Kuiper, G. P. and Middlehurst, B., editors, Moon, Meteorites, and Comets, Chicago, Univ. of Chicago Press, 1963.

CHAPTER V – IMPACT CRATERS

IMPACT CRATERING

Donald E. Gault
Ames Research Center, NASA, Moffett Field, Calif. 94035

I. INTRODUCTION

Previous discussions consider the source and condensation of the primative solar nebula, the significance to the lunar and planetary bodies of the meteorites as samples of the primative condensates, and a selenographic introduction to the major physiographic provinces and morphologic features of the Moon. This presentation illustrates that commencing in time from the initial stages of the condensation of solids from the solar nebula and their subsequent accretion into planetary objects, collisions between the condensates have played a primary role in planetary evolution in general and for the Moon in particular. Principal emphasis is focused on collisions in an excavation mode; i.e., impact cratering which represents a geologic agent for 1) major landforms and stratigraphic units; 2) metamorphism; 3) comminution; 4) erosion, transport, and sedimentation; and 5) formation and mixing of the lunar regolith.

Because an appreciation of the physics of stress waves and cratering mechanics is essential to understanding of impact processes as a geologic agent, some basic properties of stress waves with specific applications to geologic aspects and to cratering mechanics are treated in the first two sections. Parameters affecting crater size, shape, and structure are considered next, followed with examples from laboratory impact experiments and lunar and terrestrial crater forms. Lunar cratering is then considered starting from an evaluation of sources for the impacting bodies and particles, and leading into the subject of the long term (geologic) effects of impact cratering. Finally, the importance of the historical record of cratering appearing on the lunar surface is reviewed in regard to the implications to the evolution of the planets and the early history of the solar system.

The metric system will be used throughout this presentation; terminology and symbol notation are given in appendix A.

II. MECHANICS

A. *Stress Waves*

Impact of meteoroids (projectiles) against the lunar or a planetary surface (target) is fundamentally a process of an abrupt, almost instantaneous, mechanical deformation (shock compression), which is subsequently followed by a more gradual restoration (rarefaction) to ambient conditions. Figure 1 illustrates schematically a shock wave moving with a velocity U through a stationary substance producing an abrupt increase in pressure from p_0 to p with a consequent change in the specific volume and specific internal energy from v_0 to v and E_0 to E, respectively. Note that passage of the shock wave accelerates the compressed substance relative to the uncompressed substance to a particle velocity u. The compression phase is described mathematically by the classic Rankine-Hugoniot (R.H.) equations which result from applying the laws of conservation

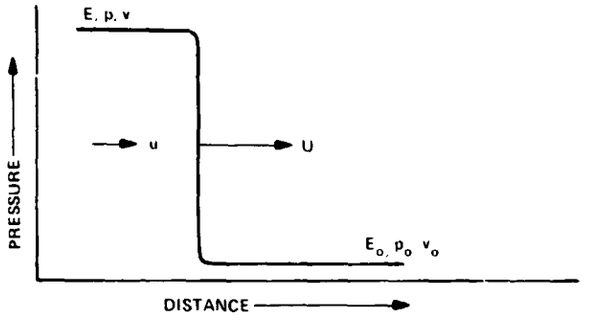

Figure 1. – Schematic of shock wave.

of mass, momentum, and energy across the shock wave. The R.H. equations are

$$U/v_o = (U-u)/v$$

$$p-p_o = uU/v_o$$

$$E-E_o = \frac{1}{2}(p-p_o)(v_o-v) = \frac{1}{2}u^2$$

The specific volume v_o and pressure p_o of the uncompressed substance are known so that the R.H. relationships provide only three equations with four unknowns, p, v, u, and U. A solution requires, in principle, a thermodynamic equation of state, which is beyond the scope of this discussion. Fortunately experiments over a wide range of pressures have revealed that

$$U = a + bu$$

with a and b constants so that solutions to the R.H. expressions are readily made. Figure 2 presents the so-called Hugoniot curve (solid line) which describes in the p – v plane the locus of points a material experiences due to a shock compression. The area in the rectangle 1-2-3-4 represents the total work done (energy expended) on the substance by the shock compression. The equal areas in the two triangles represents the work done in compression as 1) an increase in specific internal energy, and 2) accelerating the compressed substance to a specific kinetic energy of $(1/2)u^2$. The dashed line is the path followed by the substance in unloading back to ambient pressure, assumed to be an isentropic process. The area under the dashed line is a representation of the amount of useful work the expansion (unloading) of the compressed substance could perform by the expenditure of the original increase in the specific internal energy. For a perfectly elastic substance triangle 1-3-4 would be exactly equal to the area under the unloading curve. In practice the area under the unloading curve is less than triangle 1-3-4 so that some specific internal energy is trapped irreversibly in the substance after decompression; such energy appears as heat energy for melting and vaporization. Figure 2 also demonstrates that shock compression to a higher pressure p_2 increases the difference between the area under the release curve and the triangle 1-3-4 representing the original increase in specific internal energy. Thus, shocks to higher pressure cause more energy to be trapped irreversibly and be available for melting, etc. Whereas figure 2 describes conditions for a "stiff" substance such as a basalt or granite, figure 3 illustrates the conditions for a "soft" substance such as quartz sand, a crude model for the lunar regolith. Shocked to the same pressure p_1 as the "stiff" substance, the "soft" substance will experience a greater amount of irreversible energy. As a crude generalization, higher

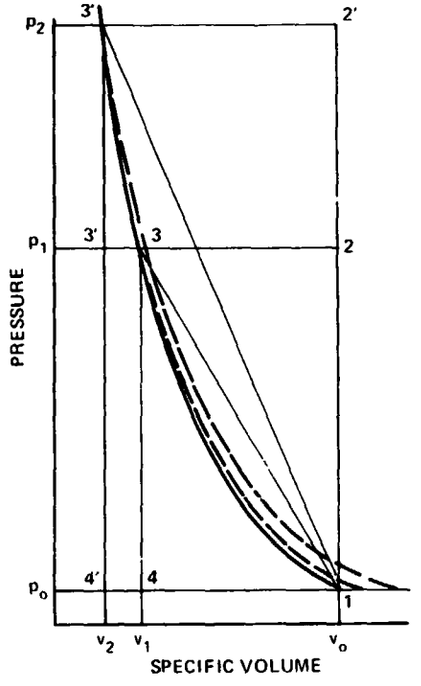

Figure 2. – Stiff Hugoniot.

pressures and lower porosity cause greater irreversible energy expenditures. A crude, but simple, procedure for determining the irreversible heating is to assume that the Hugoniot curve is an approximation for the release curves.

To calculate the pressure, specific volume, shock velocity, etc., that are produced during an impact, reference is made to figure 4 which depicts the idealized condition for one dimensional flow of a flat plate striking a semi-infinite target (Gault and Heitowit, 1963). Upon contact, two shock waves are established, one traveling down into the target and the other moving up into the platc (projectile). Because the impact velocity V_i is equal to the sum of the particle velocities in the target and projectile

$$V_i = u_t + u_p$$

it is possible to derive explicit algebraic solutions for all terms. However, equation 5 permits a simple graphical solution illustrated in figure 5 to determine the pressure resulting from an impact and, then, the remaining terms once p is established. Appendix B presents values of the constants a and b for materials of geologic interest to lunar and planetary applications.

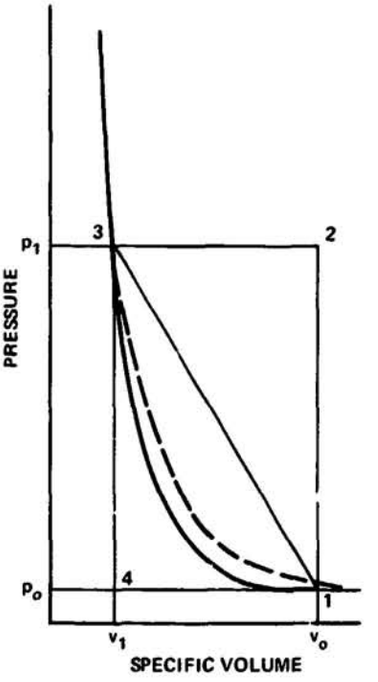

Figure 3.– Soft Hugoniot.

Results of typical calculation are included in appendix B. Even for modest impact velocities, pressures produced by impact

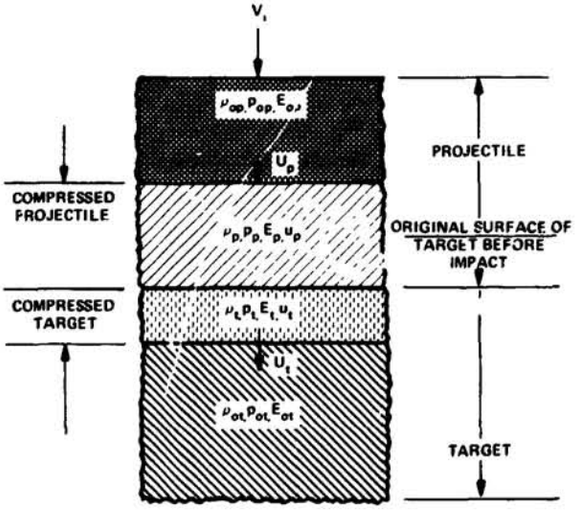

Figure 4.– Idealized impact conditions (one dimensional flow).

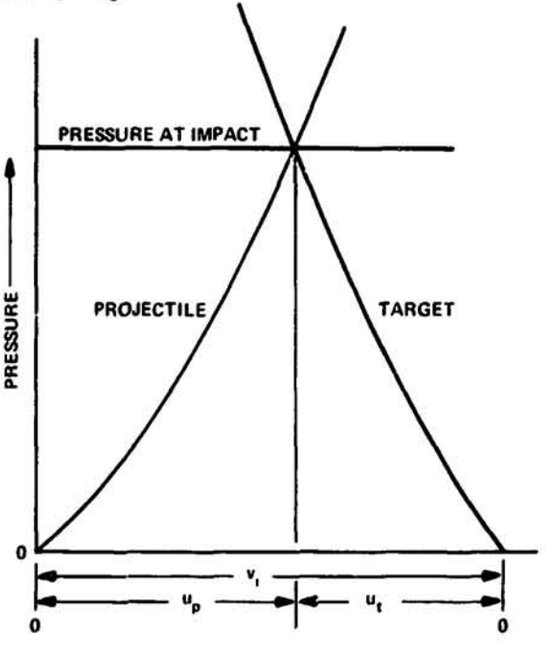

Figure 5.– Graphical determination for impact pressure.

are many orders of magnitude greater than the strength of natural materials, and cause various types and degrees of shock metamorphism. Pressures of the order of 50-100 kb are sufficient to produce deformation-lamellae in the crystal structure of feldspars and quartz. In addition, at higher pressures, polymorphic transitions can occur, the best known being the change from quartz to higher density forms of SiO_2, coesite and stishovite, which are currently accepted as a criteria for identifying old, degraded impact structures in Earth. Amorphous forms of both quartz and feldspar are also produced in a solid state transformation without passing through a melt phase. Pressures exceeding 500-600 kb are generally adequate in geologic materials to provide sufficient heating for melts; megabar pressures will cause vaporization and the onset of dissociation.

B. *Cratering Shock Wave Geometry*

Although figure 4 provides a means for calculating the initial conditions for an impact, the finite boundaries of a meteoroid control and establish the shock wave geometry during a cratering event (Gault *et al.*, 1966). Initial penetration of the meteoroid establishes shock waves running into both target and projectile that encompass a lens of compressed material. Deeper penetration causes drastic changes in the shock wave pattern due to the presence of the free surfaces on the target and projectile. Because a free surface cannot sustain a state of stress, a series of rarefaction waves develops as a means for unloading from the high impact pressures; this initiates "jetting," a hydrodynamic ejection of target and projectile material at multiples of the impact velocity. Once the projectile is consumed by shock, the shock wave pattern becomes exceedingly complex but in general has a hemispherical shape and a flow pattern dominated by a spherically expanding shell of compressed target and projectile material. The free surfaces and attendant rarefaction waves cause shocked material at and just below the surface to begin to deflect laterally outward and upward, the initial phase in the sequence of ejection of the main mass from the embryonic crater. Because impact is a conservative system in which the total energy must remain constant, the average energy density in the shocked material behind the shock front (hence, the shock pressure) must decrease as the shock engulfs more and more target material. The great bulk of material ejected from a crater is, therefore, removed in the later stages of the cratering sequence under conditions of relatively low stresses and modest ejection velocities. Particle motions during the later stages continue to be deflected outward toward the surface under the influence of rarefaction waves. Movement of target layers near the surface is predominantly in the horizontal direction; particle motions in deeper horizons and strata directly below the path of penetration of the projectile are first downward and then deflected upward. Ultimately the stresses must decay to levels equal to the material strength of the target, so that the ejection velocities decay to zero and the cratering process ceases. The stress wave, however, continues to expand and decay beyond the limits of the final crater, eventually becoming a simple elastic wave if the target has infinite dimensions relative to the scale of the crater. If the target has finite boundaries as, for example, a rock on the lunar surface, the shock waves may not decay to low levels before they encounter the geometric limits of the target. In such cases the shock wave must be reflected from the free surface boundaries as tensile waves. Because rocks are generally weaker in tension than compression, tensile fractures can occur leading to spallation failure which can disrupt the rock catastrophically.

It is important to emphasize that impact cratering is not accomplished as the result of an "explosion." Impact cratering is the manifestation of a mechanical compression which imparts kinetic energy and increases in internal energy to the target material which in turn serves to displace

the material away from the point of impact. In an explosion, gases and vapors *cause* the compression and ejection processes, gaseous constituents from an impact are a *product* of the compression and do not contribute to the excavation process. The principal products of the mechanical compression of massive rock targets are a rubble of broken and crushed target material, with lesser amounts of shock metamorphosed material including melt and vapor. The size distribution of ejecta from craters in rock appear to follow a well defined comminution law, which can be correlated with the size of the crater. Impact in particulate targets is also a comminutive process, but in addition, the particulate material may also be shock lithified into aggregates larger than the pre-impact grain size.

C. *Crater Size and Geometry*

The ultimate size and shape of craters are determined primarily by two parameters, material strength and gravitational acceleration. The relative significance of the two parameters depends on the scale (size) of the crater under consideration. Effective strengths of materials decrease with increasing volume of material involved; i.e., as the scale of an impact event increases the effective strength of the target and the forces resisting deformation decrease. On the other hand, as craters become larger the resistance forces arising from gravitational accelerations must increase. The effects of strength and gravity, therefore, tend to be dominant at opposite ends of the spectrum of crater sizes. Crater shapes and scaling laws for calculating crater size reflect the relative significance of these two parameters.

Craters smaller than a micrometer formed in glasses or individual crystals are simple glass-lined pits with only a suggestion of an encircling glassy rim. Craters larger than a few micrometers also exhibit a glass-lined pit, but are surrounded by a spallation zone about four times the pit diameter. At diameters of the order 10 cm (based on astronaut observations) the glassy central pit disappears, leaving only a shallow, rimless, conical depression centered around a zone of crushed rock. At meter to 10 meter scale, raised, upthrusted rims begin to develop and become a major structural characteristic at larger scale up to more than 100 km diameter. In sharp contrast, craters formed in particulate targets, which are most representative of the lunar regolith, do not exhibit glass lined pits at the smallest scale, and moreover, develop well defined raised rims for craters larger than a few centimeters in diameter. In addition, all other factors held constant, craters formed in low strength particulate material are larger than their counterparts formed in rock.

Subsurface structures of large craters are produced in direct response to the motions induced by reaction to the passage of stress waves. Three primary modes of response are recognized from laboratory studies using low strength (particulate) target material to simulate large events: 1) a radial displacement downward at and near the bottom of the crater; 2) an upward motion that is virtually tangential to the inner wall of the crater near the rim; and 3) a transition zone between the first two which produces large horizontal shearing displacements about midway up from the crater floor. The first contributes to downwarping of strata directly below the floor of the crater and deep underthrusts of units originally at pre-impact depths just above the final crater depth. The tangential flow near the rim is responsible for the characteristic overturned flap of the rim and consequent inverted stratigraphy. The strong horizontal movements are responsible for intense shear between adjacent strata and may result in both underthrusting at depth and overthrusting near the surface layers depending on the strength of the strata. Such deformations are normally stable and persist long after the formation of the crater, but, if the target material is unusually weak or the scale of

the crater is so large that gravitational forces are dominant, post-cratering modification will occur and alter the basic impact structure and morphology.

The dominant role of gravity at large scale is two-fold, first in affecting the dimensions of the excavation crater and, second, in contributing to post-cratering modifications. Strength, nevertheless, retains significance in that it ultimately determines the final geometry. This can be illustrated by considering an impact into a target having virtually zero strength such as water. A crater in water will be produced within the geometric limits determined by the amount of energy available to do useful work against the forces caused by gravitational accelerations. Once the limit is attained, the crater will collapse because the zero target strength fails to provide any resistance to the gravity induced forces acting on the distorted target. The water crater is, therefore, a transient event which must eventually disappear leaving no permanent record of the impact. If the target has some strength, however, collapse will still occur, but the finite strength will resist total restoration to pre-impact conditions and preclude erasure of all topographic evidence of the event. Forces and rates of collapse will depend on the size of the "transient" or "excavation" crater so that the extent of post-cratering modification is greater for the larger impact events. Thus, the interior terraces of, say, a 20 km crater are a relatively modest collapse as compared to the collapse of much larger structures ranging up to the size of the ringed basins such as Oriental and Imbrium. The excavation crater for Oriental is no larger than 300 km although its outer ring is about 900 km in diameter.

To a first approximation a minimum of three scaling laws are necessary in order to calculate crater dimensions over a range from micrometers to kilometers. The general formula is $D \propto (KE)^{\beta}$ with specific values shown in the following equations.

$$D = 0.0015\, \rho_p^{1/6} \rho_t^{-1/2} \quad (KE)^{0.37} (\sin\theta)^{2/3}$$

$$D = 0.025\, \rho_p^{1/6} \rho_t^{-1/2} \quad (KE)^{0.29} (\sin\theta)^{1/3}$$

$$D = 0.027\, \rho_p^{1/6} \rho_t^{-1/2} \quad (KE)^{0.28} (\sin\theta)^{1/3}$$

The first expression is valid for impacts against massive rock producing craters up to about 10 meters diameter. For larger craters in rock or other indurated targets, there is a gradual transition to the second expression, which is generally applicable for all cratering up to 100 meters diameter in weakly cohesive particulate material similar to the lunar regolith. The third expression is appropriate to craters of kilometer dimensions and larger regardless of the nature of the target. A transition between the last two expression occurs between about 100 meters and 1 kilometer. The size of craters is a strong function of the trajectory angle θ. Circularity of the craters is unaffected by oblique trajectories provided the impact velocity is not excessively low nor the impact is not at grazing incidence. Assymetric ray patterns around craters is indicative of oblique impacts. Tycho, Proclus, and especially Messier provide striking examples of probable oblique impact events.

D. *Impacts and Impact Craters*

Highspeed framing camera records of laboratory impacts in the Ames Vertical Gun Ballistic Range illustrate and form a basis for understanding and interpreting cratering mechanics and

structures. Comparison of the laboratory observations with terrestrial and lunar craters illustrate salient features of structures (figs. 6–18).

E. *Summary of Mechanics*

Impact cratering as a geologic process on the Moon is an agent for:

1) Extensive comminution, brecciation, and erosion

2) Ballistic transport of mass over great distances

3) Metamorphism, both solid state and thermal including melting and vaporization

4) Formation of large, complex structures

5) Formation of distinct stratigraphic units

6) Mixing of stratigraphic units

III. LUNAR CRATERING

A. *Meteoroid Population*

The sources and fluxes of meteoritic debris impacting the Moon, both past and present, is known with precision that varies from good to total ignorance and open to frequently wild speculation. The greatest uncertainty concerns the early history of the Moon, especially because we do not know its origin, whether it accreted near the Earth or at some distant part of the Solar System prior to being captured by the Earth. It is clear, however, as will be discussed later, that the Moon was subjected to an intense bombardment during its first 500-1000 million years (my) as a planetary body after which the flux decreased sharply to rates comparable or equal to current values.

Present information on the current meteoritic environment of the Moon is derived from nine sources and observational techniques: 1) satellites; 2) lunar rocks; 3) radar meteors; 4) visual and photographic meteors; 5) Prairie Network; 6) Apollo seismometers; 7) meteorites; 8) astronomical photography of comets and asteroids; and 9) lunar surface. The first four provide a basis for evaluating with good confidence (factors of 2 to 3) the flux of particles ranging in mass from the order of 10^{-15} g to 1 g, which will produce craters from about 10^{-5} cm to 50-100 cm diameter depending on whether the target is massive rock or regolith. The next three types of observations extend the mass range to the order of tons (10^{6} g), objects capable of forming craters up to 100 m diameter; the three yield widely differing result factors of 1000, for the largest bodies. The last two types of observations push the mass range upwards to the size of small planetesimals, perhaps 10^{21} - 10^{23} g, capable of producing tremendous basins the size of Imbrium and Oriental. The flux in this last category is very uncertain and speculative, and depends in part on assumptions made in trying to model and/or interpret the temporal variations in the flux since 3000-4000 million years ago.

Opposite:

Figure 6.– Time sequence photographs of an impact by a 30 caliber lexan projectile at 6.5 km/sec into a homogenecus target. By t = 0.075 sec, the basic crater shape has been established; however, ejecta remain in ballistic trajectories until after t = 0.293 sec. Bright clumps of material on the crater floor are highly shocked and shock-melted material. Note the ejecta "shadows" behind the three vertical spikes used for stereographic calibrations. The diameter of the circular plate (t = 0.003 sec) is 60 cm.

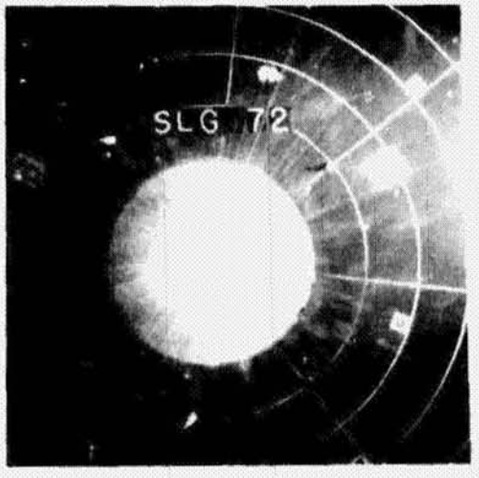

t = .003 sec

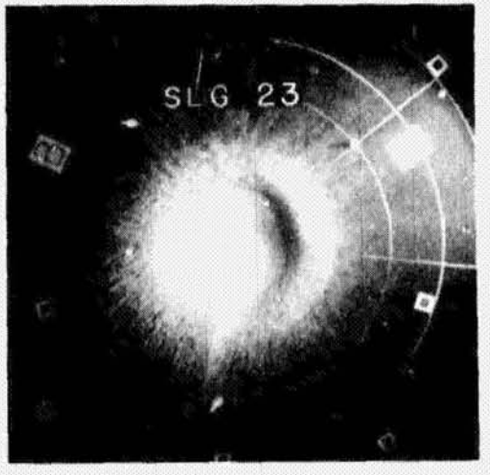

t = .075 sec

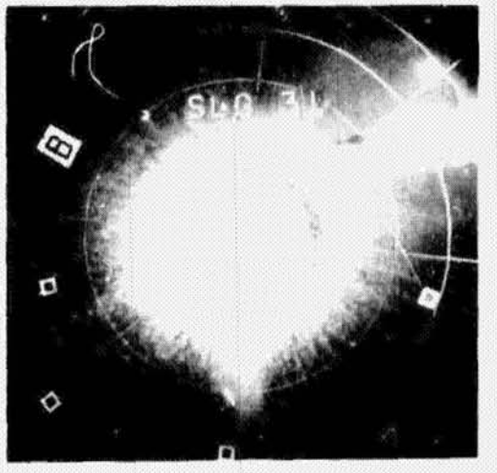

t = .104 sec

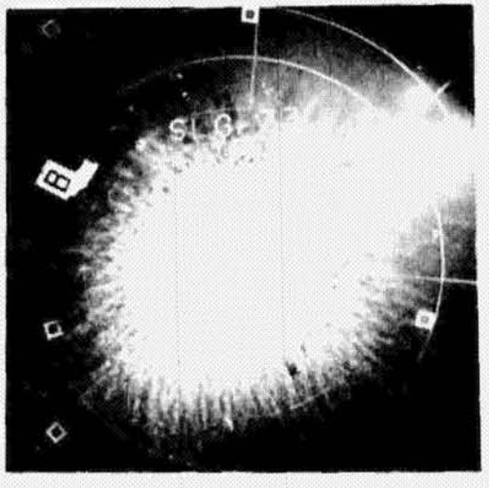

t = .176 sec

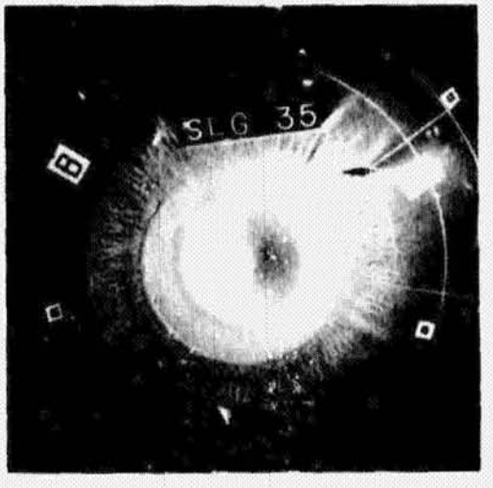

t = .293 sec

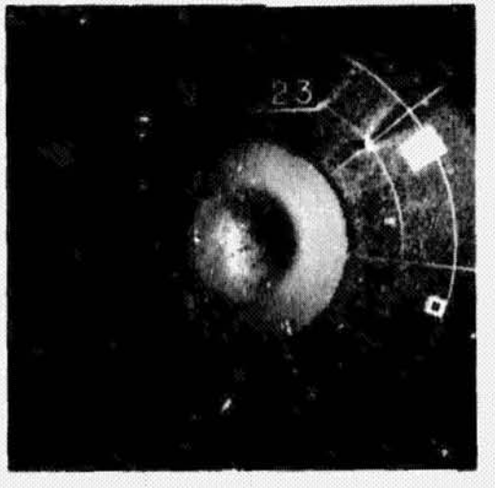

FINAL

Opposite:

Figure 7.– Profile showing the development of an impact crater. Ejecta follow trajectories approximately 40° from the horizontal, thereby forming an inverted cone. As the crater enlarges, this angle remains approximately the same. This particular impact occurred in a target containing simulated fault plains, which are responsible for loops of ejecta developing after 26 ms.

IMPACT CRATERING IN STRUCTURED TARGETS

PARALLEL FAULTS

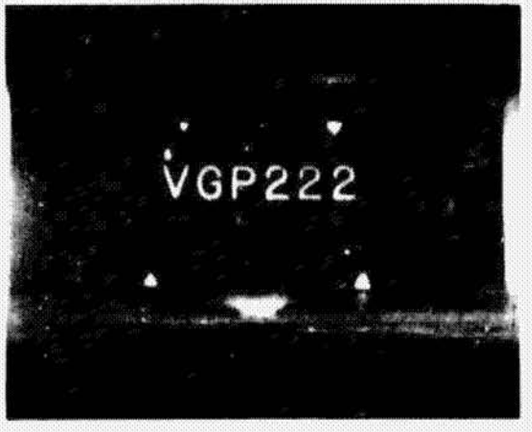

.2

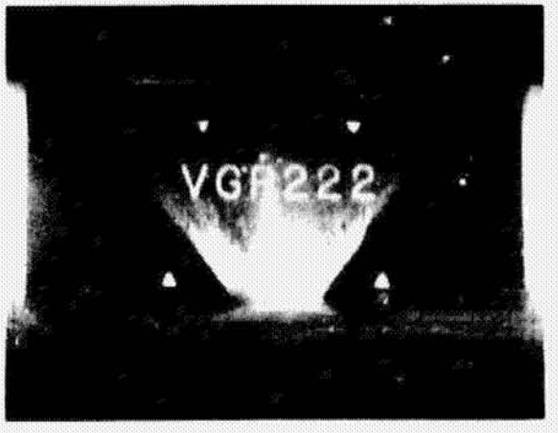

4.3

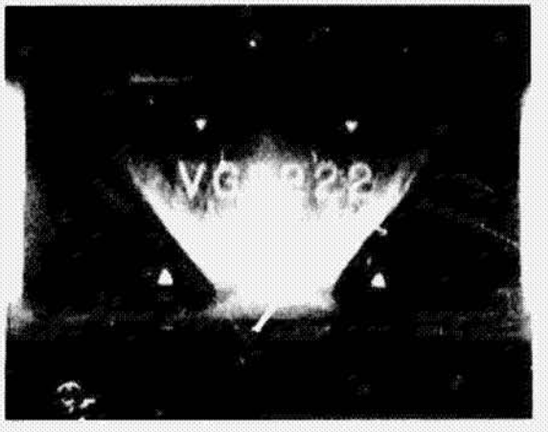

8.7

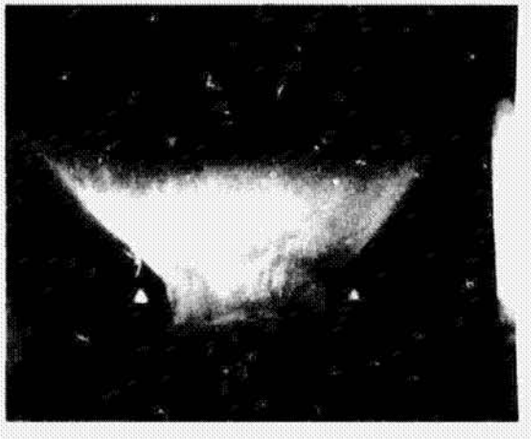

25.8

47.8

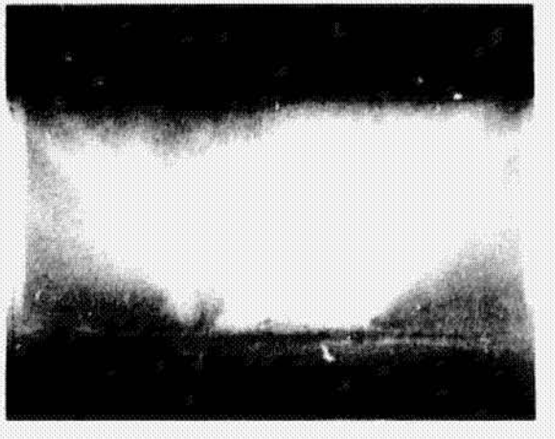

81.8

NUMBERS INDICATE TIME IN MILLISECONDS AFTER IMPACT

Opposite:

Figure 8.– Highly schematic illustration showing the formation of an impact crater based on rapid sequence photography and target cross-sections. At the initial stage, shock-melted material is ejected at multiples of the projectile velocity with angles of ejection less than 30°. The crater enlarges rapidly and is essentially complete prior to ejecta deposition (lower right). Note the overturned strata along the rim and the compressed strata directly beneath the crater.

FORMATION OF IMPACT CRATER

Opposite:

Figure 9.– Two craters formed by projectiles having identical parameters (velocity, density, angle of impact), but different target characteristics. The blocky and asymmetric crater (top) was formed in a weakly cohesive target comparable to wet beach sand, whereas the symmetric crater (bottom) was formed in non-cohesive material. The differences in morphology are intrinsic to the target.

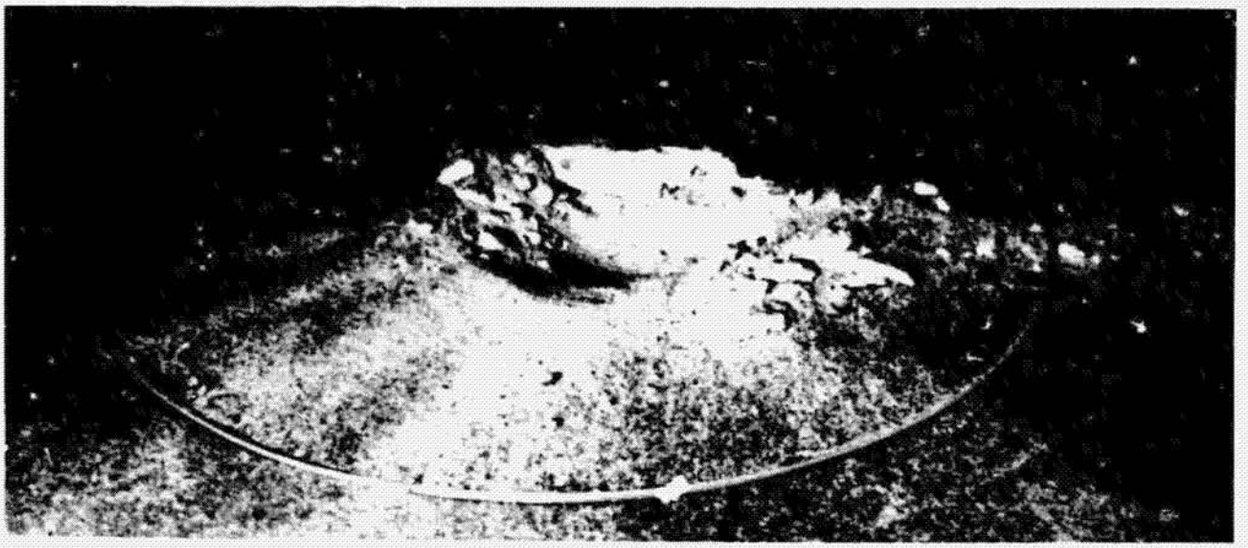

Opposite:

Figure 10.– Cross-sections of impact craters formed by high-velocity lexan projectiles traveling from right to left. Impact into a non-cohesive target of quartz sand with colored layers (a) reveals overturned strata along rim resulting from a dominant tangential flow of target material. Beneath the crater, the compressed strata (view the photograph obliquely along the strata) illustrates the radial flow; between the floor and rim, horizontal flow is dominant. Impact (b) into a target with competent layers (produced by a black lacquer coating and revealed by the black lines between strata) resulted in complex overthrusts, underthrusts, and anticlines where interbedded competent layers were shallow (left of crater center), in contrast to relatively simple alteration where the layers were deeply buried (right).

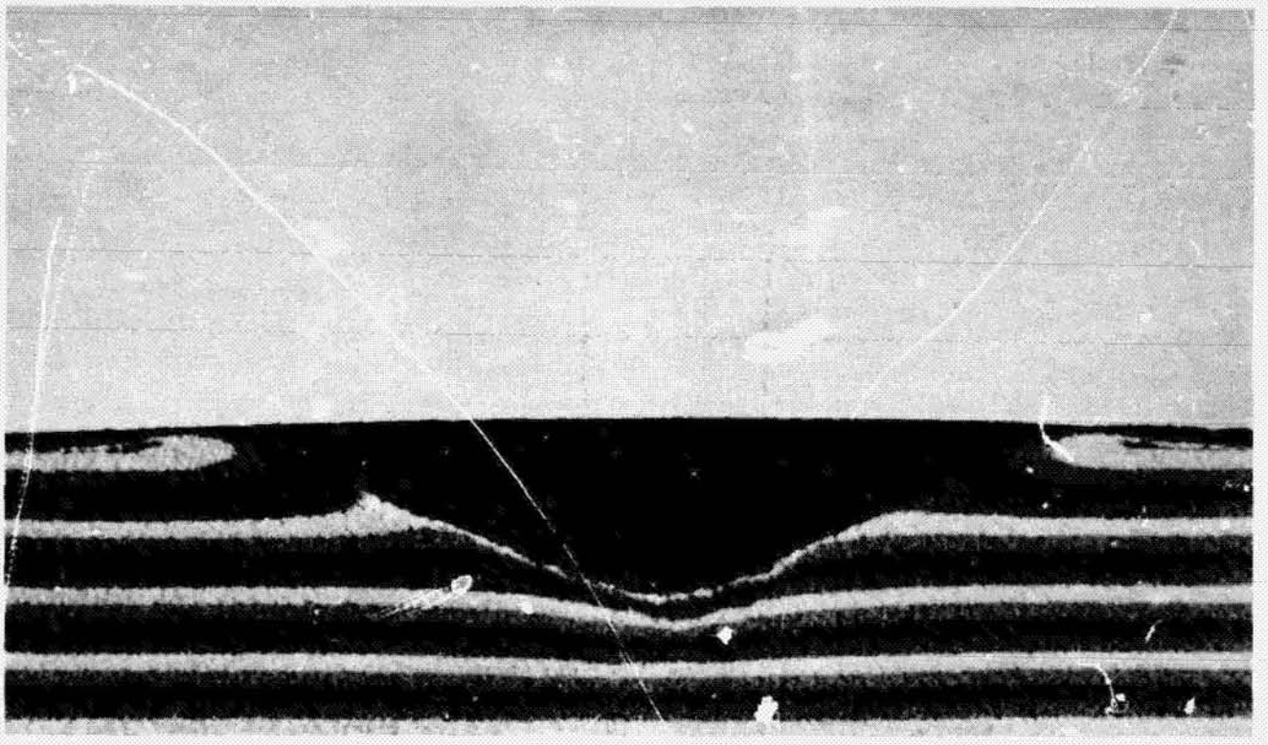

a

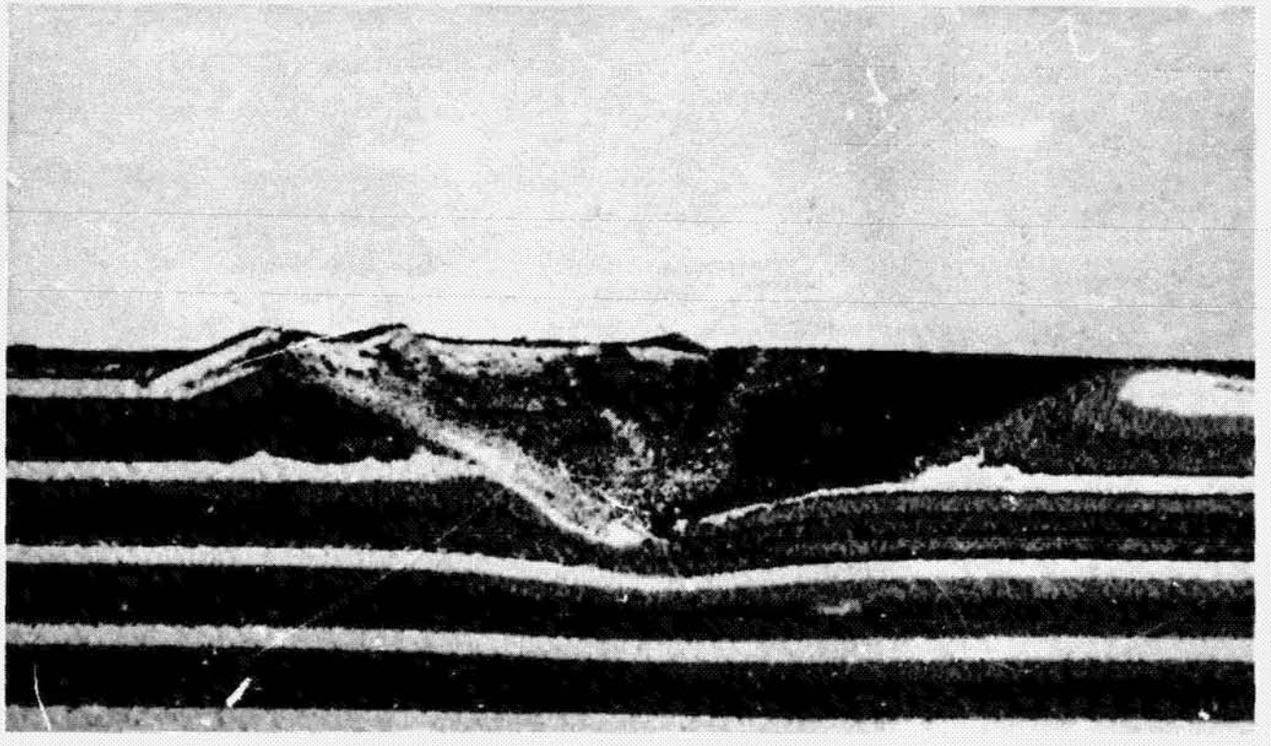

b

Opposite:

Figure 11.– Meteor Crater, Arizona, is one of the most thoroughly studied terrestrial impact craters. The raised rim, uplifted strata, blocky ejecta near the rim, and hummocky ejecta facies farther from the rim are evident in this aerial view. The present rim-to-rim diameter is approximately 1.2 km with a depth of approximately 170 m.

Opposite:

Figure 12.– Sedan crater (400 m in diameter, 100 m deep with respect to original surface) that was produced by an underground nuclear explosion. Note the incipient slump feature (upper right) and the hummocky ejecta blanket. Although Sedan is a hole in the ground and morphologically resembles an impact crater, the mechanics of its formation are drastically different from those for an impact crater.

Opposite:

Figure 13.– Examples of ancient terrestrial impact craters. Holleford Crater, Ontario, was formed 550 ±50 my ago and is the smallest of the Canadian meteorite craters (a), approximately 2 km in diameter. Brent Crater, Ontario, is dated at 450 ±40 my and is 4 km in diameter (b). Deep Bay, Saskatchewan, is the smallest Canadian crater (9 km) with a central uplift and has an age of 100 ±50 my (c). West Clearwater Lake, Quebec, is the larger (30 km in diameter) of a pair of impact craters believed to have formed nearly simultaneously by the break-up of a large meteorite 285 ±30 my ago (d). Courtesy of Michael Dence.

a

b

c

d

Opposite:

Figure 14.– Morphology of most Canadian meteorite craters all to the same scale. Courtesy of Michael Dence.

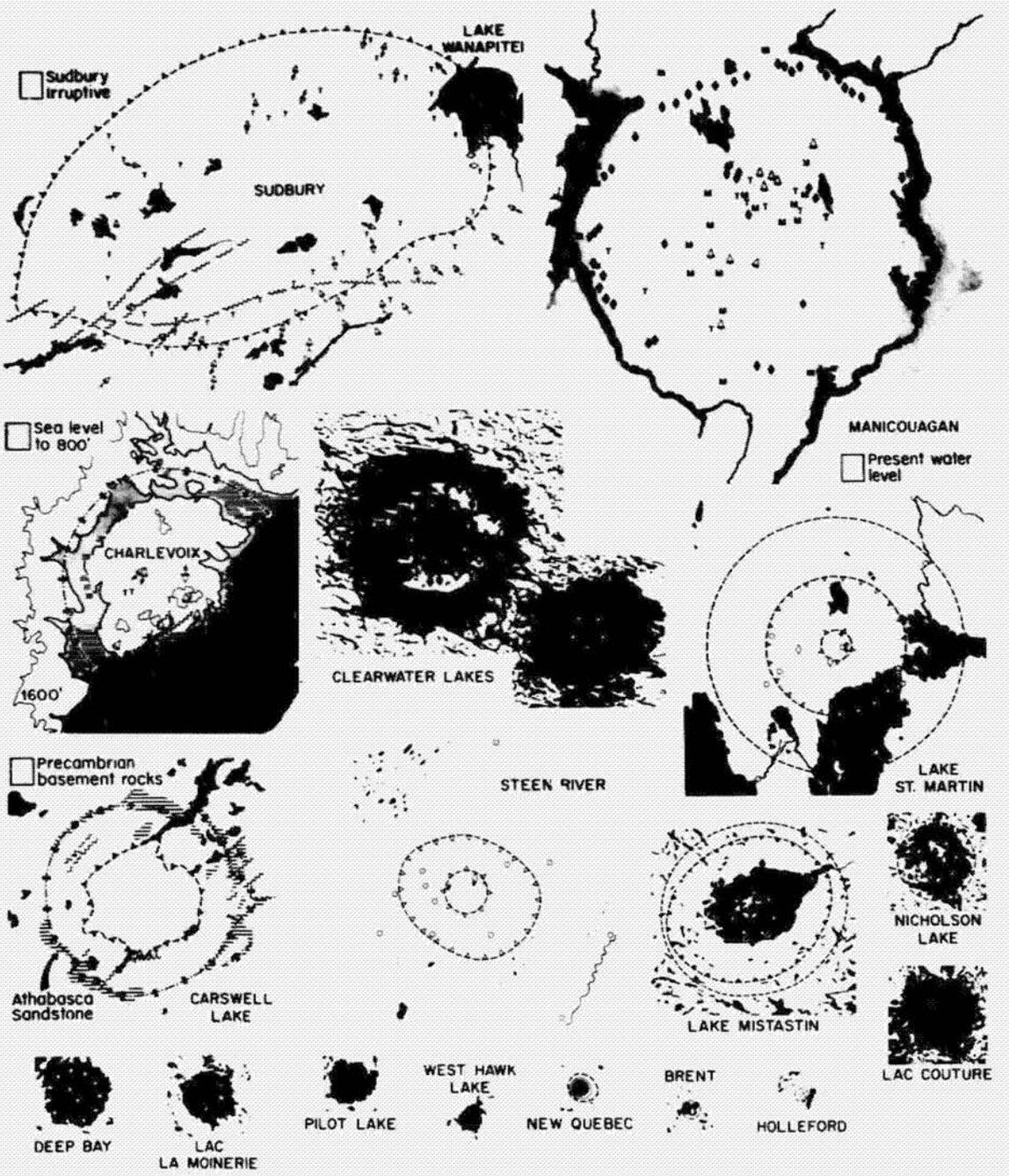
Sudbury irruptive
LAKE WANAPITEI
SUDBURY
MANICOUAGAN
Present water level
Sea level to 800'
CHARLEVOIX
1600'
CLEARWATER LAKES
LAKE ST. MARTIN
Precambrian basement rocks
STEEN RIVER
Athabasca Sandstone
CARSWELL LAKE
NICHOLSON LAKE
LAKE MISTASTIN
LAC COUTURE
DEEP BAY
LAC LA MOINERIE
PILOT LAKE
WEST HAWK LAKE
NEW QUEBEC
BRENT
HOLLEFORD
SHATTER CONE (a) orientation not determined (b) up (c) down
BRECCIA (a) outcrop (b) in drill core (c) in float
LIMIT OF STRUCTURAL DISTURBANCE
Annular trough (a) surface (b) sub-outcrop
Axis of rim syncline
Elevated rim
Dome or central uplift (a) surface (b) sub-outcrop
PSEUDOTACHYLITE
MASKELYNITE
THETOMORPHIC OR DIAPLECTIC GLASS
DRILL HOLE
LAKES
FAULT
PALEOZOIC OUTLIERS
PRECAMBRIAN INLIERS
0 Miles 15
0 Km 25

Opposite:

Figure 15.– Map of Canada with locations of most of the verified meteorite craters. The size of the dots indicate the relative size of the craters. Since this map was prepared, two additional impact craters have been added: Gow Lake and Lac La Moinerie. In addition, there are 8 more probable impact craters and 82 more possible sites. Courtesy of Michael Dence.

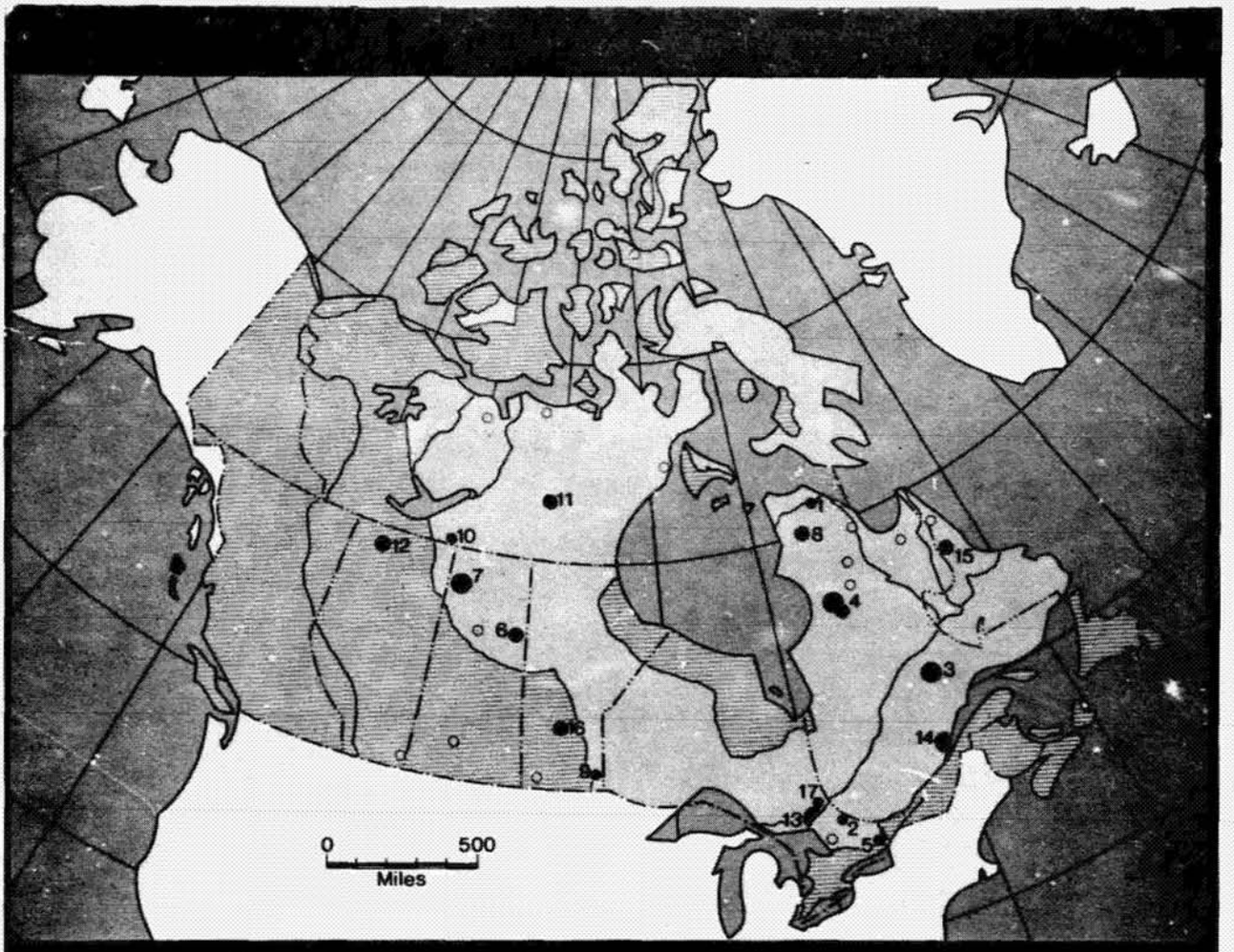

	CRATER NAME NOM DU CRATERE	DIAMETER IN KILOMETERS DIAMETRE EN KILOMETRES	AGE IN MILLIONS OF YEARS AGE EN MILLIONS D'ANNEES
1	New Quebec Nouveau-Québec	3.2	less than 1 moins de 1
2	Brent	4.0	450±40
3	Manicouagan	60	210±4
4	Clearwater Lakes	25.0 14.5	293±20
5	Holleford	2.0	550±50
6	Deep Bay Baie Profonde	9.0	100±50
7	Carswell Lake	30.4	485±50
8	Lac Couture	10	300±150
9	West Hawk Lake Lac Hawke-Ouest	2.7	150±50
10	Pilot Lake Lac Pilote	5	300±150
11	Nicholson Lake Lac Nicholson	12.5	300±150
12	Steen River Rivière Steen	13.6	95±7
13	Sudbury	100	$2000 \pm \frac{100}{300}$
14	Charlevois	35	350±25
15	Lake Mistastin Lac Mistastin	20	200±30
16	Lake St. Martin Lac St-Martin	24	225±30
17	Lake Wanapitei Lac Wanapitei	8.5	300±150

Opposite:

Figure 16.– Mare Nostrum: laboratory simulation of crater degradation. The first craters to disappear through impact erosion and sedimentation are the smallest. Eventually, the largest crater (arrows) in the upper left and lower right) is reduced to a shallow subdued depression. Comparable degradation is inferred for small craters on the lunar surface.

STAGES IN CRATER MODIFICATION

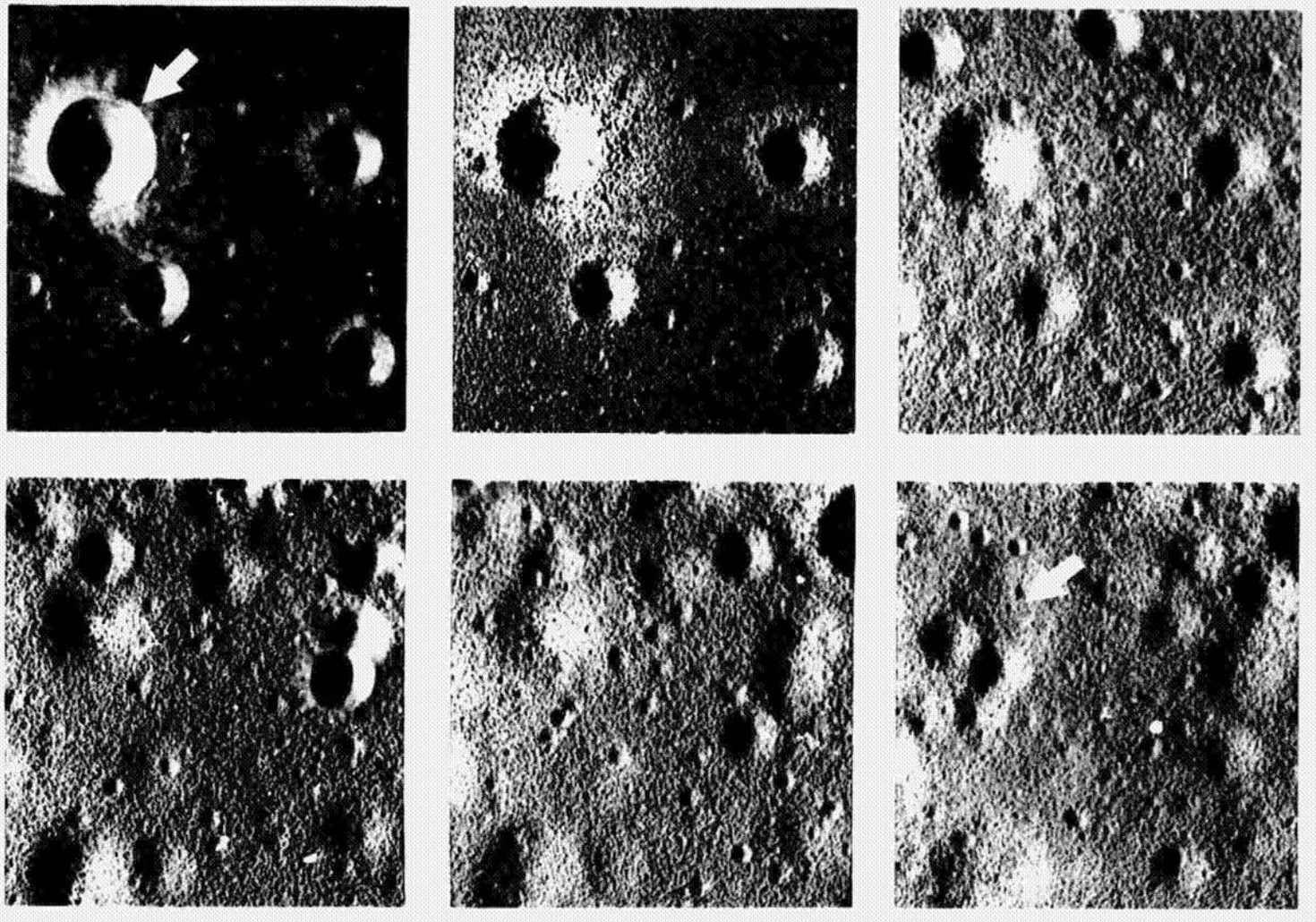

Opposite:

Figure 17.– Mare Exemplum: laboratory simulation of the development of a cratered terrain. Six different size projectiles were impacted into dry quartz sand such that 10 craters were formed in one size class for every one in the next larger size class. After a period of time, the number of craters formed balance the number destroyed, resulting in an equilibrium condition. Such a condition is believed to exist for small craters in the lunar regolith and apparently existed for much larger craters early in lunar history (preserved in the lunar highlands).

MARE EXEMPLUM

Opposite:

Figure 18.– The craters Messier (left) and Messier A (right). Messier exhibits a saddle-shaped rim (a) in which the lowest rim height occurs along the major axis (AS11-42-6304). Ejecta are asymmetrically distributed (b) in a butterfly pattern (AS15-M3-2674). These features are reproduced in the laboratory by a low-angle impact. The whisker-like rays from Messier A and the complex morphology also may be a result of an oblique impact(s).

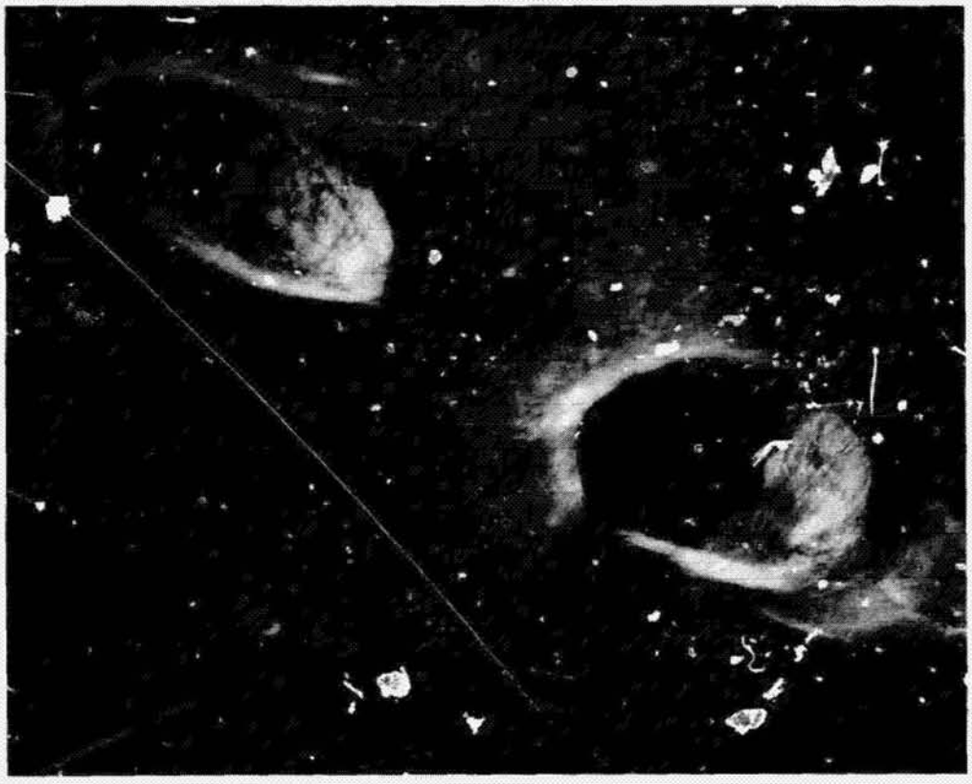

a

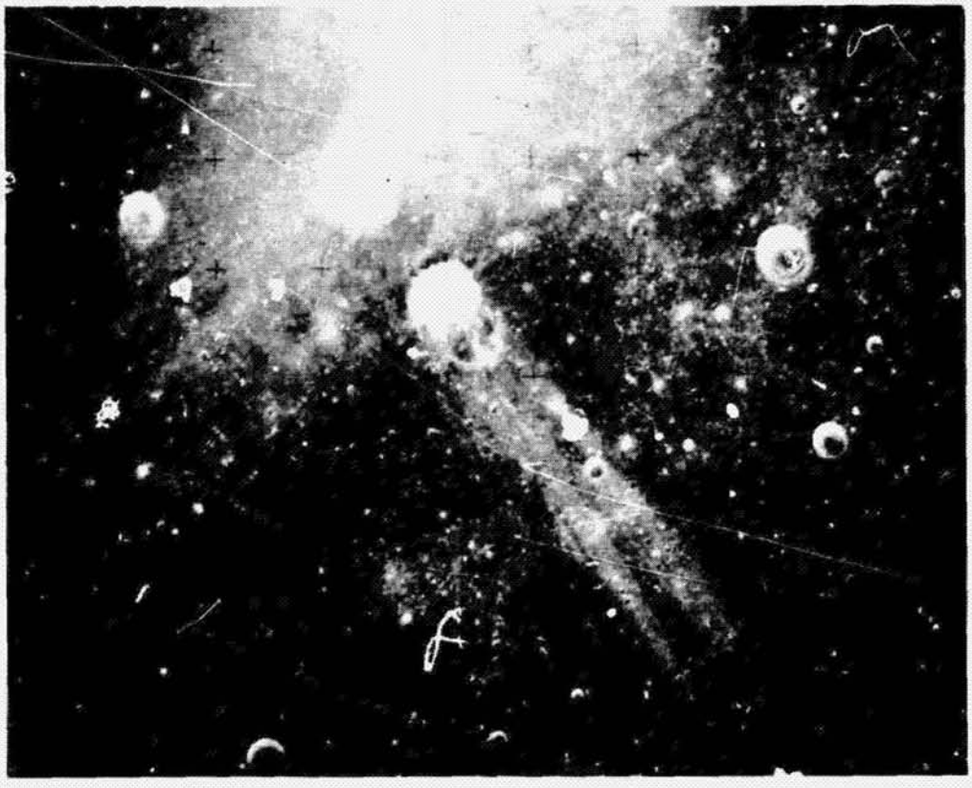

b

The population of meteoritic debris increases exponentially with decreasing mass, and is usually expressed in the form

$$N = k\, m^{-\gamma}$$

The quantities k and γ are taken to be positive constants over various ranges of the mass m. In order to depict the complete range of N and m, it is necessary for graphical presentations to employ a log-log format. Figure 19 presents a "best" estimate of the current lunar flux with the cross-hatching indicating range of uncertainty.

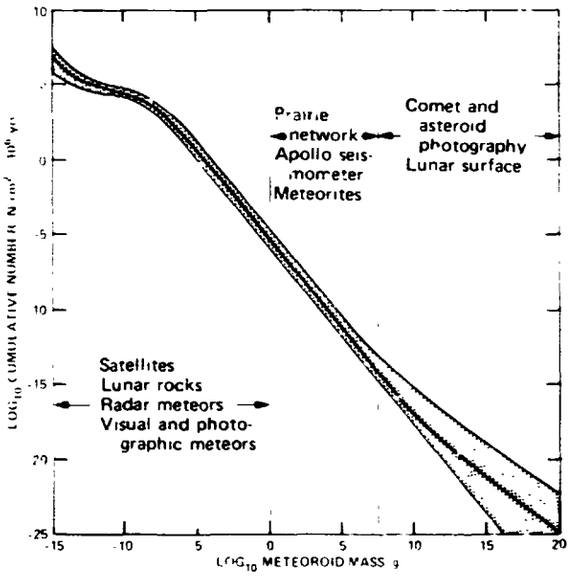

Figure 19. - Estimated lunar meteoroid flux with limits of uncertainty.

By combining crater scaling laws with the meteoritic fluxes, estimates can be made for 1) the rate at which craters of a given size are being produced, and 2) the size-frequency distributions of the primary crater population produced on the lunar surface in a given time. Thus,

$$N = c\, D^{-\gamma/\beta}$$

where the quantities c, γ, and β may be taken as constants over a limited range of the crater diameter D, and with consideration of the type of target material involved.

Impact velocities against the lunar surface range from 2.3 km/sec to 72 km/sec; the lower limit is determined by the velocity necessary to escape from the gravitational field of the Moon and the upper limit (for a member of the solar system) results from impact by a co-planar object in a parabolic retrograde orbit having its perihelion at the Earth's orbital distance from the sun. Impact velocities appear to be dependent on the mass. For masses greater than about 10^{-6} g, 20 km/sec is a representative average value; for masses less than 10^{-6} g lower velocities are appropriate, probably tending toward lunar escape velocity for the smallest particles (10^{-15} g?).

B. *Long Term Effects*

If the current flux of meteoritic debris has remained constant for the last 1000 my, each square centimeter of the Moon will have been struck 10^5 times by 10^{-6} g particles, each particle capable of forming a 0.3 cm crater in rock or a 1 cm crater in the lunar regolith (soil). Similarly, each square meter will have been struck 10 times by a 1 g object which could form a 50 cm crater in rock or a 90 cm crater in the regolith. And at the same time each square kilometer would have

experienced from 0.1 to 10 craters of 100 m diameter while the entire Moon may have been impacted by several small planetesimals or cometary bodies, the largest of which formed a 100 km diameter crater. Although less frequent, masses forming primary craters larger than about 100 m (and their secondary crater fields) excavate more total mass than the more numerous smaller members of the meteoritic population. The latter, however, are effective for erosion and catastrophic disruption of small rocks and boulders. Thus, the preceding statistics are the basis for illustrating that 1) erosion and ballistic transport of material is effected by the smallest masses of the meteoritic complex; 2) many more small craters are formed on the lunar surface than can be expressed on the surface without "erasing" by superposition previously formed craters; 3) larger craters and their secondaries excavate "fresh" rocks for the small particles to erode; and 4) only the larger craters can provide a one-for-one record of the total number of impact events that have occurred over long periods of time. Three primary types of crater populations are recognized. A surface is considered to be in a *production* state when no crater destruction by erosion or superposition has occurred and a complete record of each impact event is still recorded on the surface. A surface is considered to be *saturated* with craters of a given size when additional craters destroy existing craters. A surface is considered to be in *equilibrium* when the rate of destruction of craters is equal to the rate of production (Gault, 1970). Surfaces showing both production and equilibrium crater populations provide important quantitative information on the relative ages between different surfaces. An Ames movie "Mare Exemplum" (fig. 17) illustrates the evolution from an initially smooth uncratered surface to a surface saturated with craters in equilibrium. The movie also illustrates the manner in which craters are degraded and lose identity as a result of impact erosion and sedimentation processes.

C. *Historical Cratering Record*

It has been recognized for many years that the current meteoroid population is too low to be able to explain the heavily cratered lunar highlands, which are *saturated* with 100 km diameter craters. The generally accepted explanation was that the lunar highlands preserve a record of the terminal stages of accretion by the Moon of the larger condensates from the solar nebula, a record long since lost on Earth by its extensive geologic activity. Until the return of lunar samples by the Apollo missions, however, the time scale for terminal accretion was open to speculation. Rb/Sr ages from the lunar rocks at six Apollo sites have revealed that all the mare surfaces apparently formed between 3200 and 3800 my ago so that the highlands represent surfaces older than 3800 my. Crater-frequency determinations for the various surfaces together with the age data indicate that the meteoritic flux decayed very rapidly between 4000 to 3200 my ago and has remained relatively constant since then within the errors of present uncertainties in the flux. Dependent on the mathematical models used to represent the fluxes, the impact rates on the Moon 4000 my ago were up to 100 times greater than present flux. Interpretations of these data are varied: 1) the steep decline (assumed to be an exponential decay) in the flux between 4000 and 3200 my is the tail end of lunar accretion; and 2) the steep decline is, instead, the consequence of some catastrophic event associated in some manner with the formation of the ringed basins, especially Imbrium. If the former, the bodies must have arrived at the Moon from eccentric heliocentric orbits in order to survive colliding with the Moon at an earlier time consistent with their indicated 100 million year half life. But if such bodies represent accretionary material for the Moon, the time scale for accretion is inconsistent with the radiometric age data, which suggest the Moon accreted in several tens of millions of years. On the other hand, the second interpretation raises an awkward question of how to "store" both Oriental and Imbrium event bodies (100 km diameter??)

in the solar system for 600-800 my before they impacted the Moon. Viewed in perspective to the other terrestrial planets, the Hellas Basin on Mars and the recently discovered 1300 km circular basin on Mercury photographed by Mariner 10 would seem to suggest that such structures are a general characteristic of planetary evolution; i.e., terminal accretion may include Imbrium scale events without making it necessary to resort to special catastrophic conditions for the Moon related in some obscure manner to the Moon's proximity to Earth. Most importantly, the Moon taken collectively with Mars and Mercury would seem to indicate that extensive differentiation occurred very early in the evolution of the terrestrial planetary bodies, well before the accretionary stages were completed.

APPENDIX A

The metric system (CGS) is employed throughout the discussion; i.e., length, mass, and time are expressed as centimeters (cm), grams (g), and seconds (sec), with the usual prefixes designating fractions or multiples of ten.

p pressure (bars – 1 bar = 10^6 dynes/cm^2 = approximately 1 atmosphere)

ρ density (g/cm^3)

v specific volume (cm^3/g)

E specific internal energy (ergs/g)

U shock wave velocity (cm/sec)

u particle velocity (cm/sec)

V_i impact velocity (cm/sec)

D crater diameter (cm)

KE kinetic energy (ergs)

θ impact trajectory angle, relative to target surface, degrees

N number (bodies or craters)/cm^2 sec

APPENDIX B

Values for constants a and b in expression $U = a + bu$ for materials of geologic interest and application to lunar impacts.

Material	a	b	ρ
Basalt*	2.31×10^5	1.62	2.86
Sand†	1.30×10^5	1.4	1.65
Iron‡	3.46×10^5	1.72	7.88

*As target or simulation of stoney meteoroid projectiles
†As simulation of lunar regolith
‡Iron meteoroid projectiles

Representative pressures attained for lunar impact conditions
(pressures in megabars)

	Impact velocity, V_i (km/sec)			
	5	10	20	30
Basalt into basalt	0.45	1.49	5.28	11.38
Basalt into sand	0.29	0.98	3.54	7.69
Iron into basalt	0.77	2.48	8.65	18.50
Iron into sand	0.45	1.49	5.31	11.45

REFERENCES

Gault, D. E.; and Heitowit, E. D.: The partition of energy for hypervelocity impact craters formed in rock, Proc. of the Sixth Hypervelocity Impact Sym. Vol. 2, pp. 419-456, 1963.

Gault, D. E.; Quaide, W. L.; and Oberbeck, V. R.: Impact cratering mechanics and structures, in Shock Metamorphism of Natural Materials, Mono Book Corp. pp. 87-99, 1968.

Gault, D. E.: Saturation and equilibrium conditions for impact cratering on the lunar surface: criteria and implications, Radio Science, Vol. 5, No. 5, 1970.

With permission, reprinted from Shock Metamorphism of Natural Materials, 1968, pp. 87–99.

IMPACT CRATERING MECHANICS AND STRUCTURES

DONALD E. GAULT, WILLIAM L. QUAIDE, AND VERNE R. OBERBECK
Space Sciences Division, Ames Research Center, NASA, Moffett Field, California 94035

Hypervelocity impact craters formed in the laboratory in low- and variable-strength materials have provided insight into the mechanics of the formation and the resultant structures of meteorite craters. Three stages in the development of a crater are recognized: (1) an initial shock-wave compression of projectile and target, during which kinetic energy is transferred from impacting body to the ground; (2) an excavation stage, during which the crater is actually formed as the result of particle motions produced by the shock waves; and (3) a stage of post-cratering modification of the basic impact-basin by geologic processes. Crater structures produced in low strength target materials are remarkably similar to those found in certain large meteorite craters. Upwarped rims with inverted stratigraphy, near surface overthrusts, stratigraphically deep underthrusts, and polygonal rims have all been observed. These structures are consistent with, and are the natural consequence of, the particle motions and deformations associated with the mechanics of formation of an impact crater.

INTRODUCTION

It is a statistical certainty (e.g., Öpik, 1951) that asteroidal or cometary objects have collided—and will continue to collide in the future—with the earth and with other planetary bodies. Although geological support for this interplanetary bombardment had been lacking until recent years, the terrestrial record of such collisions is now rapidly unfolding as a steadily increasing number of structures are recognized as being very probably of impact origin (e.g., Short and Bunch, *this vol.*, p. 225). These terrestrial features, combined with the pock-marked surfaces of the Moon and Mars, attest to the possibility that collisions and the attendent cratering phenomena have been a significant, if not major, factor in the development of planetary surfaces.

Cratering as a geologic process, however, is poorly understood and subject to many uncertainties. This is to be expected, however, because general awareness of the potential role of impact cratering dates back less than a decade. Only a few natural craters are sufficiently young and well-preserved to provide any clear details of their structure, and all of these are smaller than a few kilometers in diameter. Larger craters, because of their age, have been grossly modified by erosion. In such cases, structural features are either obscure or are irrevocably lost, and this blurring of the geologic record can lead to confusion in assigning certain features to a cratering or post-cratering origin.

In the past, craters formed by explosives have been used as models for impact structures (e.g., Shoemaker, 1963; Baldwin, 1963). Although many features of impact and explosive craters appear to be similar, there are basic differences in the mechanics of formation by the two processes that can influence the final structure. Experimental investigations of impact cratering cannot be conducted, of course, on a scale that is comparable to explosive tests, but large geologic features can be studied in the laboratory by using scale models. It is the purpose of this paper to describe some results of such modeling studies that have been conducted at NASA's Ames Research Center as part of a more general program of research devoted to investigating the effects of hypervelocity impact against natural materials.

No attempt has been made to model any specific impact crater by precise scaling; the experiments have been designed only to work in the proper range of target properties, projectile properties, and impact velocities to produce craters and structures which are applicable to the large range of

1. Compression (a) Initial contact (b) Jetting (c) Terminal engulfment	Transfer of projectile kinetic energy to target and establishment of intense shock waves
2. Excavation (a) Radial expansion (b) Lateral flow (c) Ejection	Cratering process as a manifestation of shock waves and attendent rarefaction waves
3. Modification (a) Slumping (b) Isostatic adjustment (c) Erosion and infill	Potential post-cratering alterations not attributable to shock waves

Fig. 1. A summary of the sequence of events during the formation of an impact crater.

sizes exhibited by natural impact craters on earth. In this way, it has been possible to study, step by step, the effects produced by subtle changes in target homogeneity and target strength.

In the presentation that follows, the discussion is divided into three parts. In the first, a brief description is given of the experimental techniques. Then, because crater structures reflect the end product of a complex physical process, the mechanics of crater formation are discussed as an integral part of the entire problem. Finally, results from the modeling studies are presented.

EXPERIMENTAL TECHNIQUES

All cratering experiments were performed in the Ames Vertical Gun Ballistic Range. Briefly, this facility consists of a vacuum chamber, approximately 2.5 m in diameter by 3 m in height, that is straddled by a large A-frame on which light-gas guns (e.g., Charters and Curtis, 1962; Curtis, 1964) and conventional powder guns can be mounted. The A-frame can be rotated up over the vacuum chamber to permit the firing of projectiles through ports into the chamber at angles up to vertical incidence in 15° increments from the horizontal. The target surface is, thus, always horizontal and permits using noncohesive particulate material for the cratering studies. Pressure in the tank is maintained at 100 to 200 μ Hg for the cratering experiments.

The simplest targets employed for these studies consist of dry, noncohesive sand. The sand is dyed and placed in varicolored horizontal layers or in layered vertical columns to provide planes or points of reference for use in defining total deformations. Such targets are homogeneous and represent models of extremely large-scale events where target strength and inhomogeneity of target-strength variations are relatively insignificant.

Studies of the smaller natural impact craters, however, show that common inhomogeneities present in natural rocks are influential in determining crater geometries and styles of deformation. A common inhomogeneity in rocks impacted by meteorites is a variation of physical properties at various stratigraphic horizons. Various strata behave differently when deformed, depending on whether or not they are competent or incompetent. Targets simulating rocks with interlayered competent and incompetent beds have been constructed by spraying various surfaces of sand layers with thin coats of black lacquer. The lacquer cements sand layers of a few grains thickness into beds which subsequently behave competently during deformation. The black paint also provides a convenient "marker" bed for tracing out complex deformations.

Another common inhomogeneity in natural rocks that is influential in controlling crater geometry and subsurface deformational structures is the presence of joints and fractures. Faults or joint systems have been simulated in the model

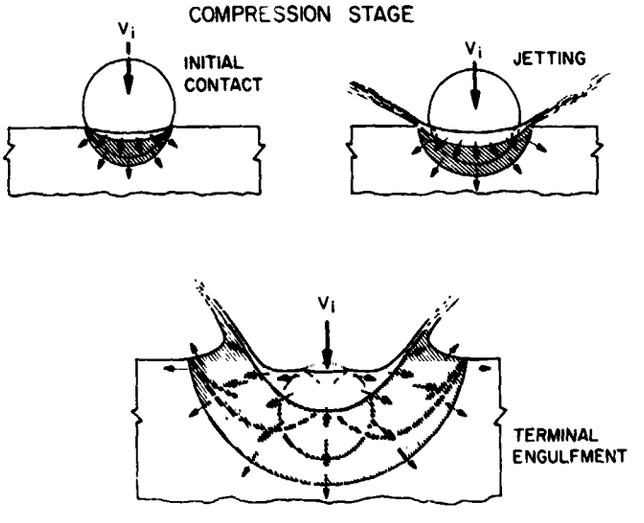

Fig. 2. Schematic representation of the compression stage of the formation of an impact crater.

targets by leaving narrow superposed gaps in the lacquer layers.

Although the bulk of the target material is dry, noncohesive quartz sand, a small amount of thermosetting plastic powder is mixed with the dry sand as a means for preserving the subsurface structure and surface geometry. All craters are formed while the sand is in the noncohesive state and then are cured at 150°C. The cured target preserves all of the impact features in rock-hard form so that the crater may be sectioned and dissected for detailed study.

CRATERING MECHANICS

It is convenient to divide the sequence of events during the formation of an impact crater into three separate stages of development that differ with respect to the physical processes taking place and the associated time scale required for the processes to come to completion. The three stages of development are, in order of their occurrence: (1) a compression stage, (2) an excavation stage, and (3) a modification stage. These stages are summarized in Figure 1 and are discussed in detail in the following paragraphs.

Compression stage.—Upon contact of the projectile against the surface of the target, a system of shock waves is established that provides the mechanism for transferring the kinetic energy of the projectile into the target material. Two shock fronts are produced, one in the projectile and the

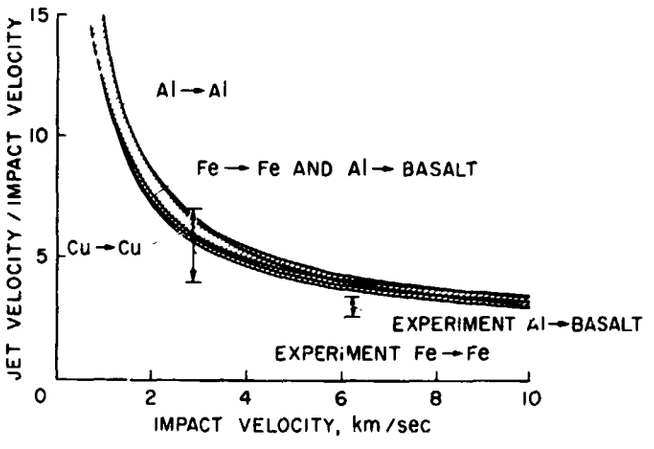

Fig. 3. Theoretical and experimentally observed jetting velocities for impact in metals as a function of the impact velocity.

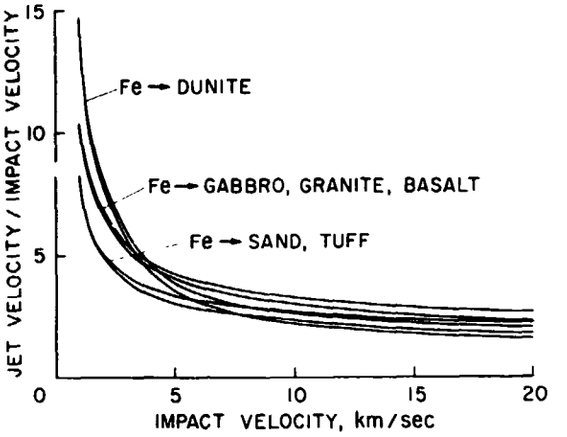

Fig. 4. Theoretical jetting velocities for impact in rocks as a function of the impact velocity.

second in the target. As the projectile penetrates into the target, the shock waves run upward and downward into, respectively, the projectile and target. Very early in this stage, the shock-compressed material is limited to a small lens-shaped mass directly below the path of penetration of the projectile (Fig. 2). Particle motion in this compressed plug of target and projectile material is predominantly downward. Reasonable estimates for the peak pressure and particle velocity in the compressed lens as a function of material properties and impact velocity (V_i) can be made on the basis of one-dimensional flow theory (e.g., Gault and Heitowit, 1963). It is sufficient to note here that, for typical geocentric impact velocities (projectiles large enough to be unaffected by the atmosphere), the particle velocities and pressures are, respectively, of the order of 10 km/sec and a few megabars. Because most natural materials have strengths less than a few kilobars, this early phase in the cratering process takes place under conditions where the deformational stresses are at least 10^3 to 10^4 greater than the material strength. Effectively, therefore, the compression stage is a hydrodynamic, or so-called fluid flow phase of cratering (Charters, 1960).

As the projectile penetrates more deeply into the target, the shock waves engulf an ever increasing mass of the target and projectile. However, the geometry of the shock wave system is drastically modified by the presence of the free surfaces on the face of the target and the sides of the projectile.

Fig. 5. An open shutter photograph of the luminosity produced by a hypervelocity impact against quartz sand. Projectile trajectory is from right to left at an angle of 30° to the target surface. Note that the long streamers of high-speed incandescent material jetted out by the collision have produced secondary impacts and incandescence on the (left) side of the vacuum chamber. 30 caliber lexan projectile, weight 0.3 gram; 6.5 km/sec impact velocity.

A free surface cannot sustain a state of stress. Therefore, as the shock waves race outward across the target face and upward along the side of the projectile (see Fig. 2), a family of rarefaction waves develops behind the shocks as the means for decompressing from the high pressure state behind the shock waves to ambient pressure. The first appearance of such rarefaction waves heralds the onset of "jetting," a hydrodynamic ejection of mass at very high velocities (Gault *et al.*, 1963). The jet emanates from the region of the interface between the compressed target and projectile. Jetting velocities that are multiples of the original impact velocity are predicted by theory and have been observed in the laboratory (Figs. 3 and 4). The material that squirts out by such a mechanism will have been subjected to the highest pressures and, hence, the highest temperatures of any of the material ejected by the impact. For nominal impact velocities in the laboratory (6 to 8 km/sec), the jetted material is in the liquidous state (Fig. 5), but at the higher typical geocentric impact velocities, the jet will also include superheated vapor.

The terminal phase of the compression stage is reached as the shock wave in the projectile reflects from the back side of the projectile. This shock transit time in the laboratory is less than 10^{-6} second, but for natural meteoritic bodies from 10 m to 1 km in diameter, the compression stage would vary from the order of 10^{-3} to 10^{-1} second. Once the projectile is consumed by shock waves, the cratering process is basically one of gradual relaxation from the high stresses produced during the initial projectile contact with the target. The stress wave geometry at this stage is exceedingly complex, with the flow pattern dominated by a spherically expanding shell of compressed target and projectile material. The

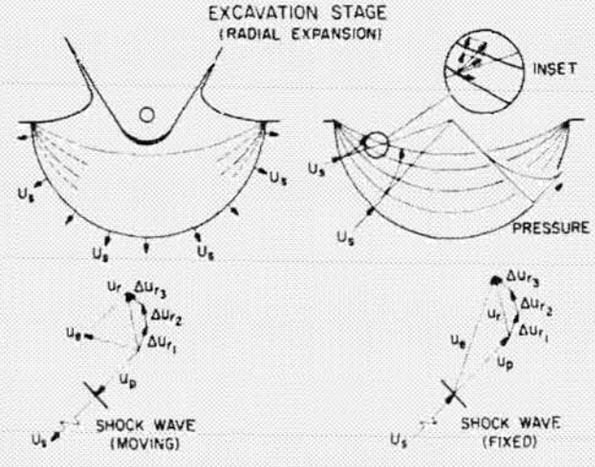

Fig. 6. Schematic representation of the radial expansion of material behind a shock wave produced by a hypervelocity impact.

presence of the free surfaces and attendant rarefaction waves causes the shocked material at and just below the surface to begin to deflect laterally outward and upward; this is the initial phase in the process leading up to the ejection of the main mass from the embryonic crater. It is worth noting that probably no more than $\frac{1}{4}$ to $\frac{1}{3}$ of the projectile (and an equivalent mass of target material) is ever subjected to the peak stresses calculated from the one dimensional theory. Rarefaction waves eat into the region of high pressure so quickly that one-dimensional flow is a valid approximation only during the initial phase of the compression stage.

Excavation stage.—Although jetting initiates the ejection of mass from an embryonic crater, the great bulk of material is removed later in the cratering sequence under conditions of low stresses and modest ejection velocities. The basic shock wave geometry for this excavation stage is illustrated in the left side of Figure 6. An approximately hemispherical shell of compressed material from the terminal phase of the compression stage is expanding radially outward, distributing the kinetic energy from the projectile over a steadily increasing mass of target material. The shock wave moves with a velocity U_s and imparts a particle motion u_p to the material through which it passes. Because this is a conservative system (i.e., constant energy) the average energy density in the shocked material must decrease as the shock front expands. For this reason, and also as a result of the irreversible conversion of internal energy to heat, the shock velocity and the particle velocity and pressure behind the shock front decrease very rapidly with increasing distance from the point of impact.

The radial movement of the shock wave along the face of the target is accompanied by a fan of rarefaction waves (dashed lines in Fig. 6) in order to fulfill the boundary condition of zero stress at the free surface. Although the rarefaction fan is shown as a series of discrete waves, the expansion from the compressed state behind the shock to ambient pressure is actually accomplished as a continuous process. The schematic representation as discrete waves, however, is useful for exposition and emphasizes that a series of connecting isobars occurs behind the shock wave. A stress wave

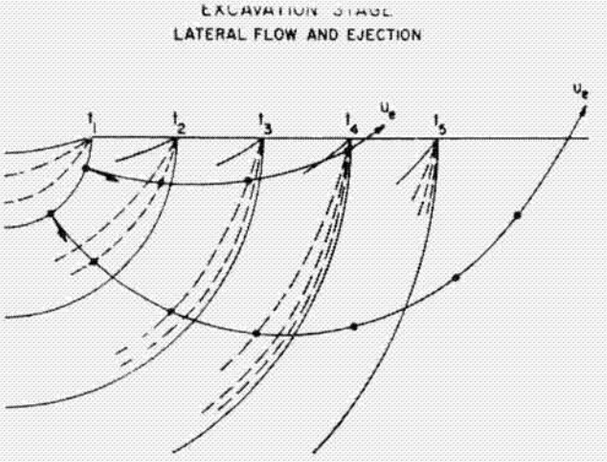

Fig. 7. Schematic representation of the lateral flow and ejection of material from an impact crater.

geometry is thereby established that tends to divert the motion of the shocked material away from the radial direction originally imparted by the shock wave.

This diversion from radial flow can be illustrated by referring to the right side of Figure 6. Here, for illustrative purposes, a stationary, hemispherical shock front and rarefaction wave system is assumed, with target material flowing radially inward with a velocity U_s. The flow first decelerates to a particle velocity u_p as the material is shock compressed, and then subsequently accelerates as the internal energy of compression is converted back to kinetic energy while flowing progressively from one isobar to another toward the region of ambient pressure. The direction of the particle motion u_p, however, is consistently oblique to the isobars. As indicated in the inset in Figure 6, only the velocity component of the particle motion that is perpendicular to an isobar will experience an acceleration as it passes into the region of lower pressure. The result is that the particle motion is continually deflected toward the direction of maximum pressure gradient. The vector diagrams depict this expansion and acceleration process for both the moving and the stationary shock wave systems. A series of incremental velocity changes Δu_r are shown as the contributions from discrete rarefaction waves. The total velocity increment u_r produced by all the expansion waves is added vectorally to u_p to yield the resultant particle velocity u_r. Figure 7

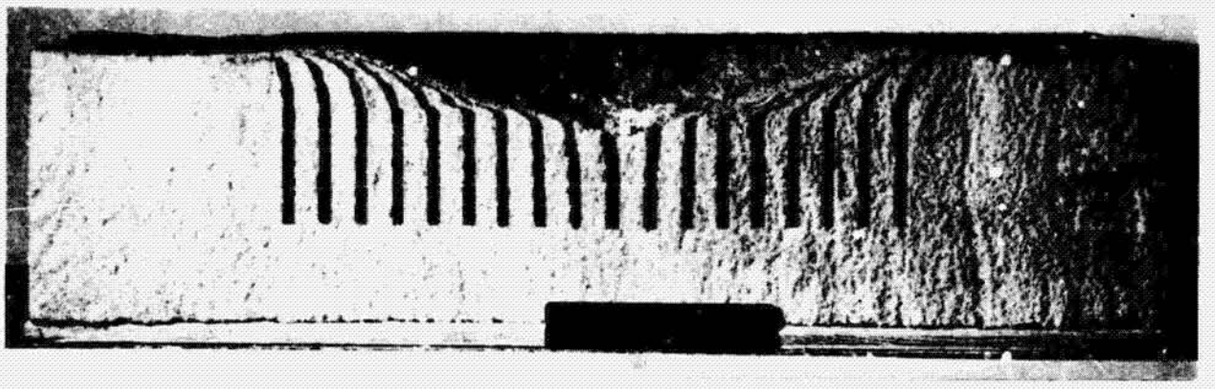

Fig. 8. Cross-section of a crater formed in homogeneous, noncohesive quartz sand, showing the deformations produced by the cratering process in originally vertical columns of colored sand. 30 caliber lexan projectile, normal incidence, 5.7 km/sec impact velocity.

shows schematically the paths one would expect for two representative point masses that are ejected from the target. As the shock wave expands radially outward, particle motions are gradually deflected upward toward the free surface under the influence of the trailing rarefaction waves. Movement of target layers near the surface is, therefore, predominantly in the horizontal direction. By contrast, deeper horizons and material directly below the path of projectile penetration are first driven downward and then deflected upward.

Although the preceding discussion is based on a highly simplified cratering model that, in particular, has neglected dissipative processes and effects of material strength, the salient features of this type of flow have been confirmed from laboratory observations of the movement of point masses around artificial impact craters formed in sand. Figure 8 presents a cross section through a crater produced in homogeneous, noncohesive quartz sand, and Figure 9 shows the total movement of point masses around the crater. The limits for appreciable deformation are indicated, and the realms where material movement is basically similar are identified. The realm of tangential flow is confined to the near surface layers and is related to the strong horizontal movements generated by the shock wave and by the trailing rarefaction waves running along the free surface. Deep in the target, the realm of radial flow correlates with the dominant radial motion imparted by the shock wave. A transition zone separates these two realms. The relationship between these flow patterns and structures in homogeneous and nonhomogeneous targets will be discussed later.

The ejection of material from an impact crater is a surprisingly orderly process. Figure 10 is a sequence of photographs for different intervals of time after impact showing the ejecta patterns and crater growth in targets of homogeneous, noncohesive sand. The embryonic crater enlarges rapidly at first and the crater attains its final size and shape while considerable ejecta is still in ballistic trajectories traveling away from the crater. It is notable that, during almost the entire period

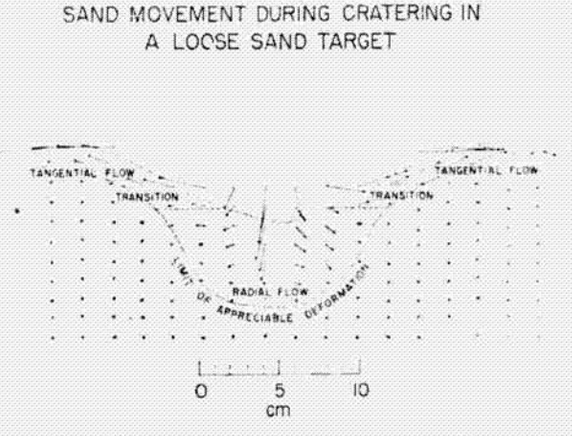

Fig. 9. Flow diagram derived from a cross-section similar to that shown in Figure 8, showing total movement produced by the cratering process in individual point masses.

of crater growth, the shape of the enlarging cavity maintains a shallow, basin-like geometry that is essentially the same as its final form. The ejecta move up and shear out from the upper wall of the growing cavity in a steady flow of material that develops into an inverted, conical-shaped curtain of debris above the surface of the target (see Fig. 11). During the early phases of ejection before crater growth is complete, it is impossible to distinguish or to define a juncture between the bottom of the conical ejecta curtain and the inner wall of the embryonic crater; there is a smooth transition from flow on the crater wall into flow in the ejecta curtain. The ejecta curtain, however, quickly tears apart into a delicate filamentary pattern that ultimately is reflected in the ray system that is so characteristic of impact events. Inhomogeneities in the target will disturb this ejection process and, as discussed later, will produce asymmetries in the throwout patterns.

It is interesting to note that the crater formation shown in Figure 10 is essentially complete by 10^{-1} second after impact, a time interval of the order of 10^5 larger than that required for the compression stage. Theoretical considerations suggest that equivalent formation times for large planetary events should scale directly with the square root of the crater dimensions. Thus, for example, it is estimated that the Meteor Crater, Arizona was formed in an interval of the order of 10 seconds. This formation time, however, refers only to the basic crater structure and morphologic features; phenomena related to atmospheric disturbances and the flight of ejecta in ballistic trajectories would continue for much longer periods of time.

It should also be emphasized that crater development and ejecta patterns for an impact event are significantly different from those for deeply buried explosive events (e.g., Johnson and Higgins, 1965). As shown schematically in Figure 12, an explosive event typically begins with a spherical compression stage from a point source of energy (chemical or nuclear). The spherically expanding shock wave is reflected from the free surface in the region of ground zero as a tension wave and imparts to these surface layers a motion that is predominantly in the vertical or near vertical direction. The central cavity that is filled with the high pressure gaseous products of the explosion (and vaporized rock or soil) soon vents to the outside through tears in the domed surface material. Ejection from the developing crater, therefore, is accomplished primarily by spallation and by aerodynamic process, neither of which have a significant role in an impact event. Thus, although there are morphological and structural similarities between some meteorite craters and craters formed by deeply buried explosives, shock wave geometry and ejection processes are fundamentally

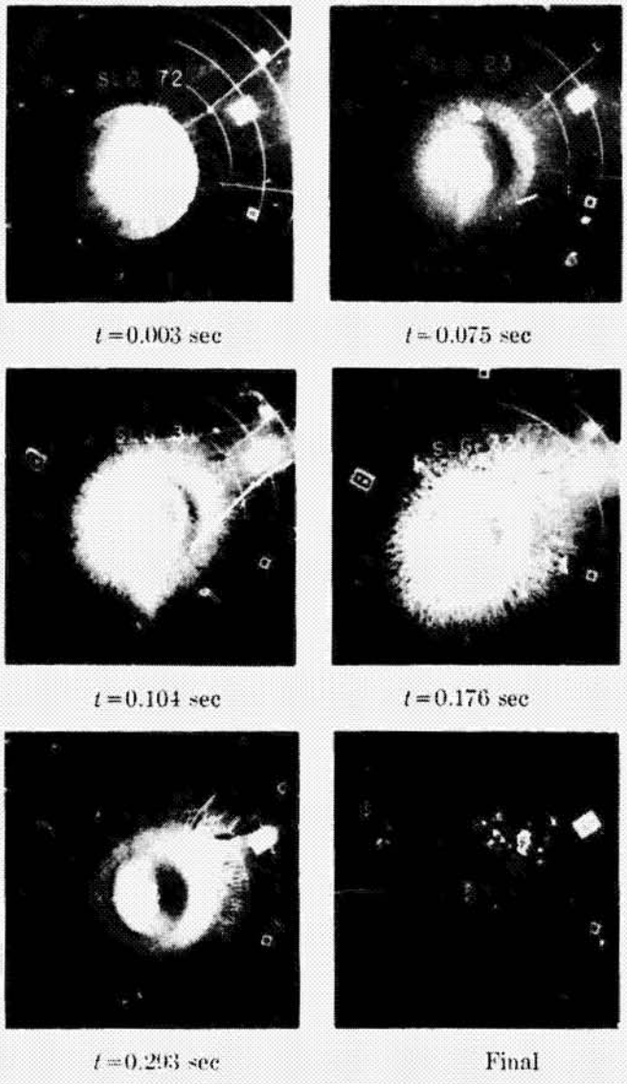

Fig. 10. Photographs of ejecta patterns and craters formed in homogeneous noncohesive sand at various intervals of time after impact. Impact at normal incidence with 30 caliber lexan projectiles. Nominal impact velocity, 6.5 km/sec.

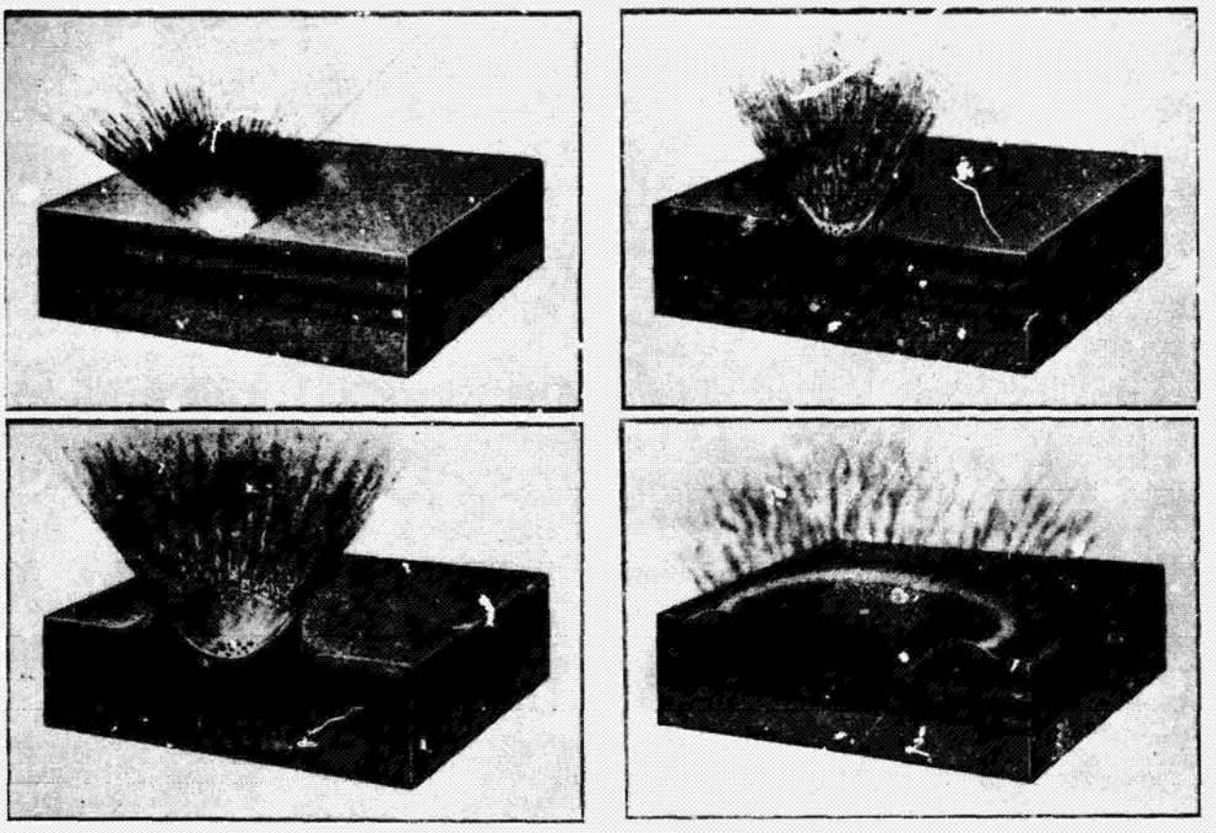

Fig. 11. Schematic representation of the ejecta patterns and progressive crater development for an impact in a homogeneous noncohesive medium.

different. On the other hand, explosions at shallow depths probably provide the best simulation of the impact shock wave geometry and, at the same time, reduce any aerodynamic effects to a minimum. Detailed studies and comparisons of shallow explosions with impact craters are required before it will be feasible to correlate features of impact and explosion events. As will be discussed later, material strength enters any such comparisons as an important variable. It is sufficient to note here that care must be exercised in the interpretation and application of explosive cratering data to natural impact structures.

Modification Stage.—As observed in the laboratory, the basic impact-crater geometry at the completion of the excavation stage is a basin-shaped depression with a depth approximately $\frac{1}{4}$ to $\frac{1}{5}$ of the rim diameter. This geometry is deeper than that observed for most large craters and, in addition, the laboratory and natural craters exhibit other significant differences in morphologic and structural features. Most, if not all, of the differences are attributable to scale effects (e.g., target strength) and to post-cratering modification by geologic processes.

The principal post-cratering modification proc-

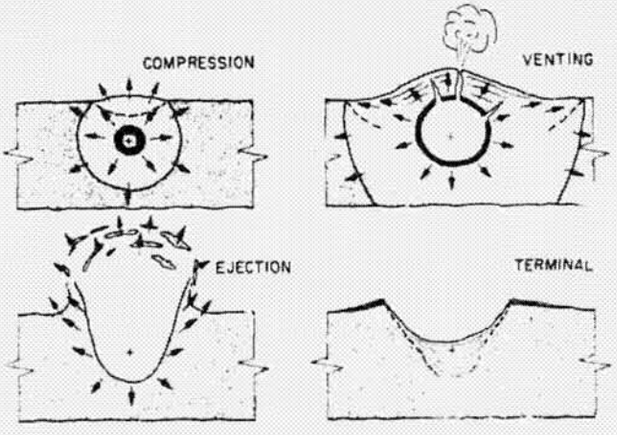

Fig. 12. Schematic representation of the formation of a crater by a deeply buried explosive.

esses (see Fig. 13) include: (1) slumping of the peripheral rim structure into the impact basin; (2) filling and possible formation of a central dome by isostatic adjustments; (3) erosion and resultant infilling; and (4) filling with material derived from internal sources.

Slumping is probably the best explanation for the interior terraced walls that characterize fresh lunar craters larger than 10 km to 12 km in diameter (Quaide *et al.*, 1965). Considering differences in gravitational acceleration, terracing in terrestrial craters should occur only in craters larger than about 1.7 km to 2 km in diameter, assuming the strengths of lunar and terrestrial "target" materials are essentially the same. The process of slumping also favors the formation of a central peak or uplift, depending to some extent on whether or not the slump is the result of slope- or base-type failure. Isostatic adjustments could further enhance any centrally positioned accumulation of slump-produced rubble. Equally probable, however, is the formation of a central uplift and raising of the entire impact basin due to isostatic processes. Elastic rebound caused by stress waves reflecting upward from strata deep below the crater (Mohorovičič discontinuity) also has been suggested as a mechanism for crater modification, but its significance and, in fact, the relative importance of all of the proposed modifying processes remains uncertain. It remains, therefore, for investigations of natural craters and suspected craters such as those described by Milton (*this vol.*, p. 115), Dence *et al.* (*this vol.*, p. 339), Roddy (*this vol.*, p. 291), and Stearns *et al.* (*this vol.*, p. 323) to clarify the understanding of post-cratering modifications.

CRATER STRUCTURES

The deformational structures in the noncohesive sand targets shown in Figures 8 and 9 reflect the relatively unconfined flow of the particulate material set in motion by the complex pattern of stress waves produced by an impact at normal incidence to the target surface. Each grain of sand moved effectively as a separate unit comprising part of an incompressible plastic mass. Near surface strata in the realm of tangential flow are

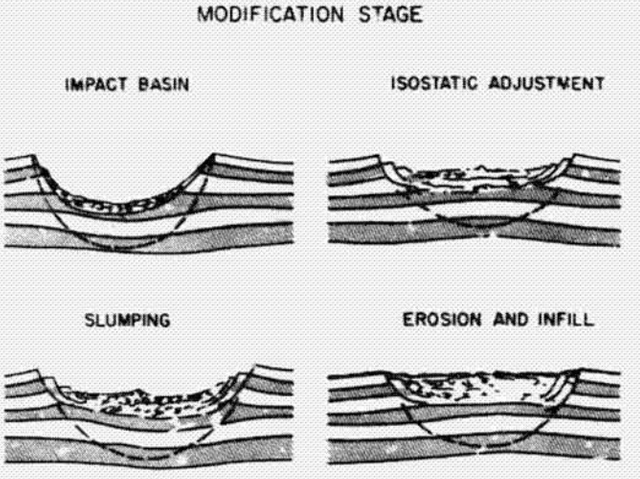

Fig. 13. Suggested processes for post-cratering modification of an impact basin.

smoothly folded upward and outward, with the topmost layers being completely overturned. All the strata, however, retain their identity. Low in the basin where radial flow predominates, the mass movements are primarily radial to the crater floor; the beds are displaced downward and outward producing the basin-like structure. Small shear folds are frequently present in the downwarped strata, resulting from movements along closely spaced discrete shear surfaces. Grain movements in the realm of transition flow (located at approximately 0.75 of the crater depth) have a resultant motion such that they are first driven outward against grains in the horizontal strata and subsequently deflected upward toward the surface. The principal structure produced in this region is an asymmetric ring anticline with an inward dipping axial surface. The hinge region of the fold is typically thickened.

Impact at oblique angles in a homogeneous target modifies the flow patterns of material set in motion from those just described, and hence, the structural deformations are different. The main effect of obliquity is the departure from axial symmetry of the structural pattern (Fig. 14). As the angle from the horizontal becomes smaller, the degree of overturning in the realm of tangential flow becomes more extensive down-range and less well-developed up-range. The change is most readily noted on the up-range side, where the original depth of the deepest beds now overturned

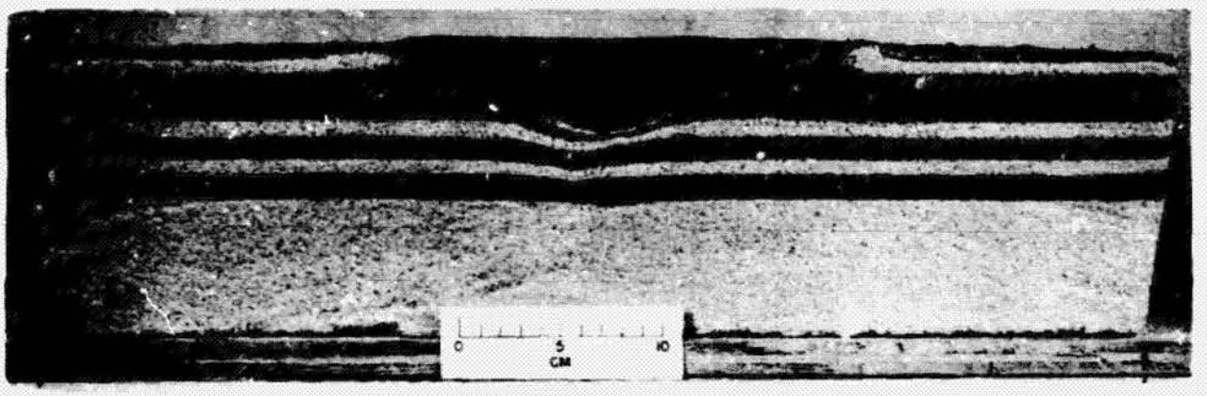

Fig. 14. Crater produced in homogeneous noncohesive quartz sand. Projectile trajectory from left to right at 30° with respect to the surface of the target. 30 caliber lexan projectile, 6.3 km/sec impact velocity.

decreases regularly from about $\frac{1}{2}$ the crater depth in the case of a 90° impact to about $\frac{1}{10}$ the crater depth in the case of the 30° impact shown in Figure 14. At 15°, only the most superficial beds are overturned. Coincident with the previous changes are the changes in amplitude and position of the anticline on the up- and down-range sides and differences in the degree of downwarping in the realm of radial flow.

Deformational structures produced by vertical impacts in inhomogeneous targets consisting of interbedded competent and incompetent strata are dependent upon the number and stratigraphic position of the competent layers as well as on the degree of competence (i.e., strength) of the individual beds. A single competent layer at or near the surface severely restricts particulate motion in the upper part of the realm of tangential flow. In one instance (Fig. 15), it has been observed that the tangential flow moved upward and under a competent surface layer producing a well-formed recumbent anticline.

More frequently, however, the surface beds are upwarped but are not inverted. The upwarping extends to a distance of approximately $\frac{1}{4}$ crater radius beyond the rim (Fig. 16). Reverse faults cut the competent bed near the crater with displacements parallel to the normal direction of tangential flow. An asymmetric ring anticline develops immediately beneath the competent bed and extends throughout that portion of the section normally characterized by inverted strata in the homogeneous target. The anticline dies out in depth in the normal place at the bottom of the transition region. The beds in the crestal region of the fold are typically thickened. In both Figures 15 and 16, the presence of the competent bed high in the stratigraphic sequence restricted the normal tangential flow and diverted the particulate motion radially away from the crater to produce the observed anticlines.

In marked contrast, however, a single competent stratum deeper in the realm of tangential flow only slightly modifies the particulate movement of the normal unconfined flow pattern of the homogeneous target (Fig. 17). The structure produced is very similar to that formed in a loose sand target in that beds above the competent horizon are overturned in a normal manner. The competent bed itself is fractured near the crater, and the segment between the fracture and the

Fig. 15. Section of crater formed by a vertical impact in inhomogeneous noncohesive quartz sand. Note recumbent anticline underlying the competent surface layer at the rim of the crater.

crater wall is rotated to a near vertical attitude, sometimes overturned, sometimes not. Reverse faulting in the competent bed does not take place, probably because there is sufficient overburden pressure at these depths to prevent upward and outward movement of the thin competent bed as a unit. Nor is there significant upwarping of the strata beyond the hinge of the overturned fold. Strata beneath the competent bed behave similarly to strata in a homogeneous target, except for those immediately adjacent to the competent layer. When the competent layer lies deep in the zone of tangential flow, the beds beneath are frequently injected in dike form through the aforementioned fracture. Mixing frequently takes place

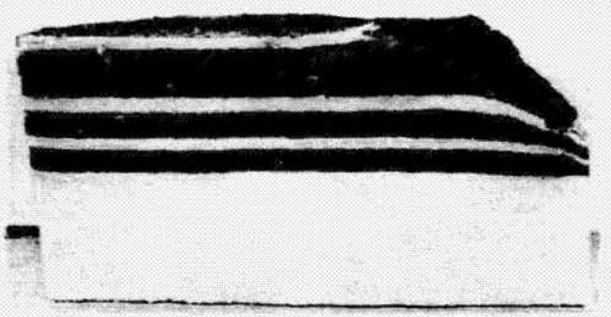

Fig. 16. Crater formed in inhomogeneous noncohesive quartz sand. Note upwarping of beds in crater wall and reverse faults cutting the competent bed near the surface.

between the intruding and host materials as a result of chaotic flow. The intruding material therefore is found in isolated pockets and stringers in the superadjacent strata.

The presence of multiple competent strata in the realm of tangential flow severely restricts the normally unconfined particulate movement throughout that zone, and the structures produced are quite unlike those found in homogeneous targets. Near surface strata are not overturned but are merely upwarped, sometimes smoothly (Fig. 17) and sometimes abruptly about fractures. Frequently, the confined incompetent beds near the crater are thickened by lateral, radial flow and are chaotically mixed. Faulting is common (Fig. 18), with underthrusting the rule in the lower levels and reverse or overthrust faults dominant at higher levels. Injection of materials through

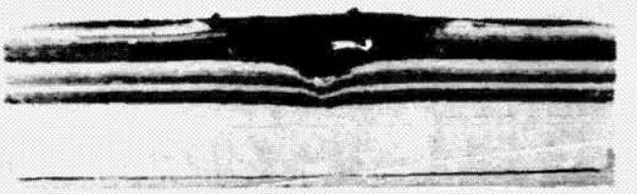

Fig. 17. Crater formed in inhomogeneous quartz sand with multiple competent layers on the left and a single competent layer on the right.

fractures in overlying competent beds is common, often producing isolated pockets and stringers of injected material.

Cratered targets with simulated fracture systems are similar to those found in targets containing interbedded competent and incompetent strata, but they have additional complexities introduced by the presence of the simulated faults. It has been observed, for example, that the presence of fractures influences the ejection process. High speed motion pictures show loops of ejecta originating from the fractures (Figs. 19 and 20). Preferential ejection begins when the expanding crater reaches a given fracture. As the cavity expands, ejection continues preferentially from the points of intersection of the fracture and the crater wall. The velocity of ejection decreases as the cavity expands, thus giving the ejecta derived from a line source a final arcuate form. The presence of fractures thus gives rise to arcuate-shaped concentrations of ejecta which can be expected to lay down on the surface to produce loops

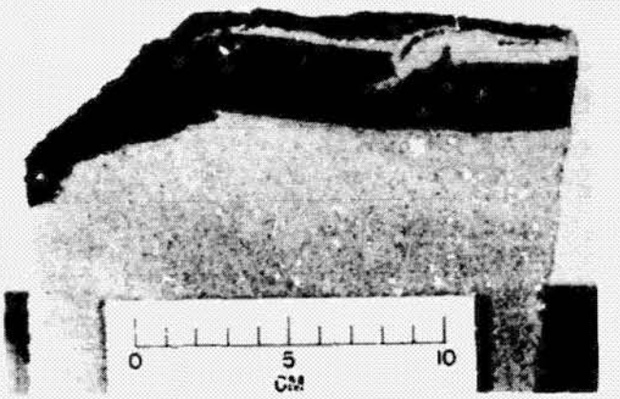

Fig. 18. Crater formed in an inhomogeneous quartz sand target, showing overthrusts in the surface layers and underthrusts in the deeper strata.

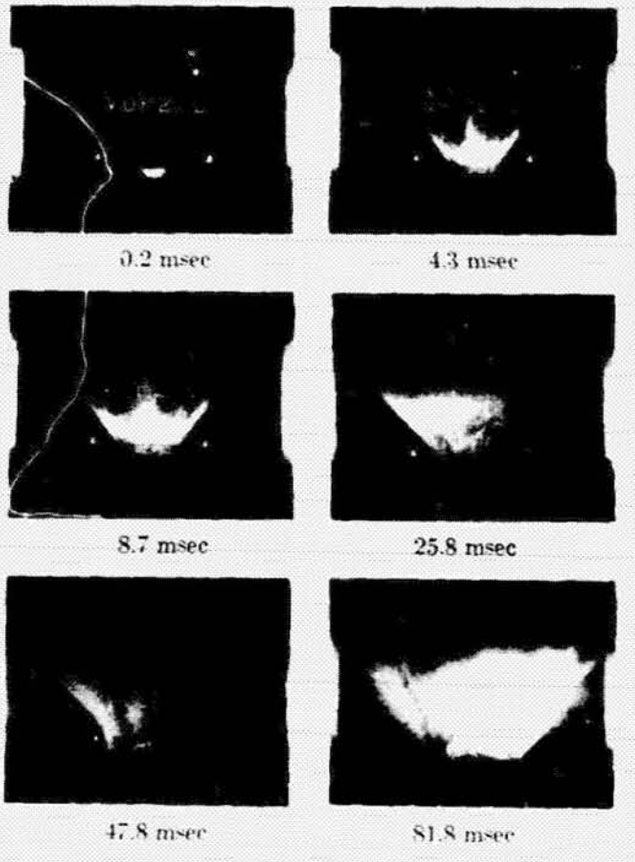

Fig. 19. Selected frames from a high-speed motion picture sequence of an impact in inhomogeneous quartz sand targets containing simulated faults oriented in a series of parallel planes. Note the loop of ejecta beginning to develop at 26 milliseconds after impact.

similar to those described at the Henbury craters (Milton, *this vol.*, p. 115) or loops of secondary craters similar to those present about the lunar crater Copernicus (Shoemaker, 1962). Ejecta loops can form in other ways, however, for they are frequently produced in noncohesive sand targets.

The location and degree of deformation within the impacted material have also been found to be influenced by the presence of fracture systems. It must be noted, however, that the fracture systems used to date have interfracture spacings of about $\frac{1}{5}$ crater diameter and can only simulate the effect of a similar ratio of fracture spacing to crater diameter in nature. The presence of such a fracture near the crater wall determines the position of underthrusts and overthrusts which occur in the realm of tangential flow. The presence of such fractures also influences the style of deformation in that true overthrusts rather than reverse faults tend to develop high in the stratigraphic sequence, with blocks between fractures moving radially from the crater center. The fault surfaces dip steeply in front of the displaced block, flatten to horizontal beneath it and steepen to root in a surface parallel to the direction of tangential flow near the crater wall. Deformation of this kind replaces the upwarping commonly found around craters in models with competent layers but without the fracture sets. Another feature common to targets with fracture systems is the injection of material along the pre-impact fracture surfaces and the chaotic mixing of this material with the overlying beds.

Since fractures influence the ejection process and modify the deformational processes, it is to be expected that they will influence the final form

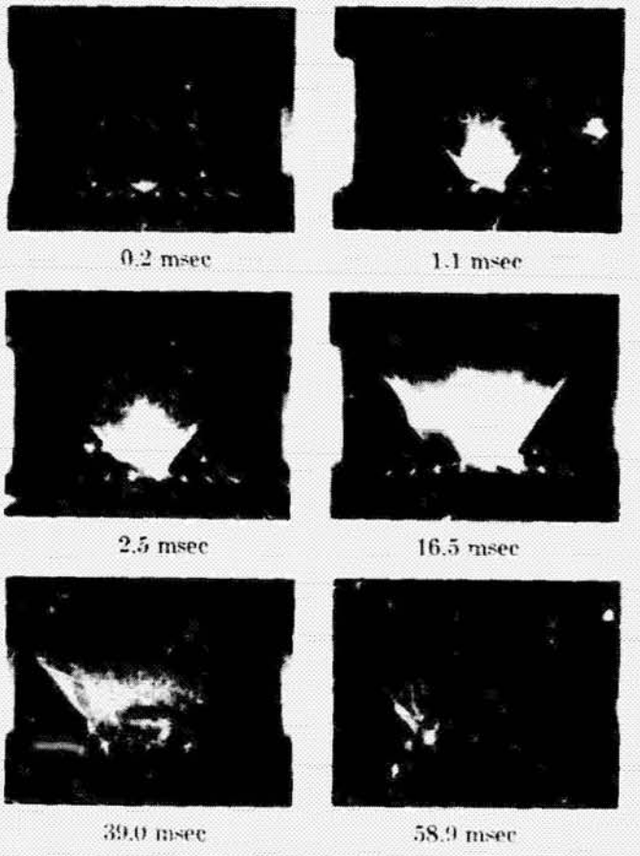

Fig. 20. Selected frames from a high-speed motion picture sequence of an impact in inhomogeneous quartz sand targets containing a checkerboard grid system of simulated faults. Note sand squirting up above surface of target through simulated faults. Grid blocks are rotated and displaced as complete units.

of the crater. Fracture systems consisting of two perpendicular sets of fracture planes have been used in two experiments (see Fig. 20). In one, a square crater was produced with the diagonals of the square parallel to the two directions of the fractures, similar to the relations observed at Meteor Crater, Arizona. In the second, a hexagonal outline was produced. Additional work is underway to relate the shape of the crater to the subsurface, pre-impact structure and to the material strength.

CONCLUDING REMARKS

The structural features of natural impact craters of the size of Meteor Crater, Arizona, and smaller have undoubtedly been influenced by the strength and inhomogeneities of the target rocks. The upper limit beyond which target strength no longer exerts a significant effect is not known. Certainly if the scale is large enough, the rocks will react as though they have essentially little or no strength. The degree and type of deformation around natural impact craters is, therefore, a function, first, of size and second, of the nature of the target rocks. That is, effective strength is an inverse function of size. Thus, the rocks around Meteor Crater reacted as though they had less strength than those around the Odessa Crater, Texas, although the pre-impact rocks in both cases exhibited similar strength characteristics. The differences in the structure of the rocks around these craters is, in part, or, perhaps, entirely an effect of scale and is not simply a result of differences in projectile penetration (Shoemaker, 1963). Structural asymmetry resulting from angular impact, however, is not dependent on scale. Only the deformation resulting from the asymmetric flow itself is determined by the effective strength of the target rock. It is reasonable to assume that, for any crater, the asymmetry of structural patterns may provide a means for identifying the direction and possibly the angle of projectile entry.

Finally, an appeal is made to geologists who are mapping impact craters: record not only the details of structural deformations and petrologic and mineralogic changes, but also record the details of the strength and degree of inhomogeneity of the pre-impact target rocks, the details of local and regional fracture systems and the scale of fracturing, and the details of local stratigraphy, including bed thicknesses and strength properties. A more thorough understanding of the formation of the natural craters will be possible when such information is available.

REFERENCES

Baldwin, R. B., *The measure of the moon*. Chicago, University of Chicago Press, 488 p., 1963.

Charters, A. C., High-speed impact. *Sci. Am.*, 203(4), 128–140, 1960.

Charters, A. C., and J. S. Curtis, High velocity guns for free flight ranges, Publication TM 62-207, General Motors Corporation Defense Research Laboratories, Santa Barbara, California, 73 p., 1962.

Curtis, J. S., An analysis of the interior ballistics of the constant base pressure gun, Publication TR 64-27, General Motors Corporation Defense Research Laboratories, Santa Barbara, California, 52 p., 1964.

Dence, M. R., M. J. S. Innes, and P. B. Robertson, Recent geological and geophysical studies of Canadian craters, *this vol.*, p. 339.

Gault, D. E., and E. D. Heitowit, The partition of energy for hypervelocity impact craters formed in rock. *Proc. 6th Hypervelocity Impact Symp., v. 2*, 419–456, 1963.

Gault, D. E., E. M. Shoemaker, and H. J. Moore, Spray ejected from the lunar surface by meteoroid impact. NASA Publication TN D-1767, 39 p., 1963.

Johnson, G. W., and C. H. Higgins, Engineering applications of nuclear explosives: Project Plowshare. *Rev. Geophys., 3*, 365–385, 1965.

Milton, D. J., Structure of the Henbury meteorite craters, Australia, *this vol.*, p. 115.

Öpik, E. J., Collision probabilities with the planets and the distribution of interplanetary matter. *Proc. Roy. Irish Acad., 54A*, 164–199, 1951.

Quaide, W. L., D. E. Gault, and R. A. Schmidt, Gravitative effects on lunar impact structures, *Annals N. Y. Acad. Sci., 123*, 563–572, 1965.

Roddy, D. J., The Flynn Creek crater, Tennessee, *this vol.*, p. 291.

Shoemaker, E. M., Interpretation of lunar craters, Chapter 8 in *Physics and astronomy of the moon*, Z. Kopal, ed., pp. 283–359, Academic Press, New York, 1962.

Shoemaker, E. M., Impact mechanics at Meteor Crater, Arizona, in *The solar system, v. 4, The moon, meteorites, and comets*, B. M. Middlehurst and G. P. Kuiper, eds., pp. 301–336, Chicago, University of Chicago Press, 1963.

Short, N. M., and T. E. Bunch, A world-wide inventory of petrologic features characteristic of rocks associated with presumed impact craters, *this vol.*, p. 255.

Stearns, R. G., C. W. Wilson, Jr., H. A. Tiedemann, J. T. Wilcox, and P. S. Marsh, The Wells Creek structure, Tennessee, *this vol.*, p. 323.

CHAPTER VI – GEOLOGIC MAPPING

Principles of Extraterrestrial Geological Mapping
– J. Guest

Geologic Mapping of the Second Planet (Reprint)
– D. E. Wilhelms

Geological Provinces of the Near Side of the Moon (Reprint)
– J. F. McCauley and D. E. Wilhelms

Two Former Faces of the Moon (Reprint)
– D. E. Wilhelms and D. E. Davis

PRINCIPLES OF EXTRATERRESTRIAL GEOLOGICAL MAPPING

John Guest
University of London Observatory
Mill Hill Park, London NW7 2QS England

I. INTRODUCTION

Although much had been accomplished in developing fundamental concepts of geology before the idea of making geological maps, the work of William Smith and some of his friends (and enemies!) allowed geological field observations to be presented in a more understandable form and the science of geology to develop in a more disciplined way; in addition, the technique of geological mapping established a stratigraphic column.

The geological map allows the geologist to represent his field observations in a form that can be understood by others and links observations made at different and separate localities into a unified form. If the map is well done, the way in which a piece of country has developed through the geological ages to its present form is clearly illustrated. The relative ages of the different rock strata can be determined by the geometrical relations and a picture of the way that different processes have operated with time can be understood. Put in another way, a geological map is like a graph to a physicist: it allows him to understand many observations in a comprehensive form that would be difficult without it.

From the preceding statements it is clear that the technique of geological mapping is equally applicable to the study of the surface of any planet with a solid surface when sufficient observations can be made. Indeed, the geological map can be of great value not only in drawing together observations of the surface but in preventing the development of concepts of surface evolution that only take into account SOME of the available evidence.

II. PRINCIPLES OF MAPPING

Despite this, many scientists – including some geologists – have argued that geological mapping is too subjective to be of any value on a planet where observations are largely made from photographs and little or no direct field observations are possible. Further, they point out that so frequently geologists cannot agree on how to map areas on Earth. Such ideas often stem from genuine ignorance of the methods and aims of geological mapping.

A good map should reliably record field observations and should distinguish between these and the interpretations which have been made from the observations. Two good maps of the same area may look different in many ways, but both may represent what is actually present and the maps differ only in – for example – the choice of geological boundaries.

With this in mind, we can look at the geological mapping of planets and in particular, the Moon. The first systematic mapping of the Moon was done by the USGS (United States Geological Survey). In order to keep their maps as objective as possible, they used a system that was close to the North American Stratigraphic Code. You will note also that interpretation is kept separate

from the descriptions in the key (e.g., Wilhelms and McCauley, 1971); consequently, the map still stands as a good map even if the interpretations of the origin of the units are wrong

At present, nearly all lunar and planetary mapping is, perforce, done from spacecraft pictures using much the same techniques as are used in normal photogeology. Of course this requires some interpretation because it is necessary to decide what represents a rock unit, the fundamental mapping unit. This is not such a great problem on the Moon as it is on the Earth or Mars because on the Moon there is no running water or atmosphere, nor are there any climatic belts. The main process that modifies the surface is that of meteoroid bombardment, which is a process that operates almost uniformly over the whole surface of the Moon. Thus, differences in surface form from one area to another relate directly to the underlying rock, age, composition, lithology and mode of formation. It should be noted that a resolution of at least 1.5 km is required to do useful stratigraphy.

III. STRATIGRAPHY

Although the principal mapping unit is the rock unit, Shoemaker of the USGS made a great advance in the study of the Moon by attempting to identify temporally distinct stratigraphic units (fig. 1). This is not at all easy to do, as can be discovered by studying the history of lunar geological mapping. Perhaps the most reliable of time stratigraphic horizons is the Fra Mauro Formation, the unit surrounding the Imbrium Basin and considered to represent the ejecta blanket that was emplaced when the Imbrium Basin was excavated. Assuming this interpretation to be correct, it would have been formed over a period of only a few minutes and is thus about the best type of time horizon that can be found. The Fra Mauro was thus defined as the base of one of the systems on the Moon known as the IMBRIAN SYSTEM. Determining a top for this system was not so easy. This was taken initially to be the base of the mare materials which were included in the next youngest system, the PROCELLARIAN SYSTEM. This division immediately gave trouble because neither the bottom nor the top of this set of rock units could be considered as being the same age over the entire Moon. Thus it was found convenient to change the Procellarian System to a group (rock unit) which forms the upper part of the Imbrian System. There is still the problem of defining the top of this system because we are still dealing with a rock unit whose top represents different ages. The next youngest system is the ERATOSTHENIAN SYSTEM. The base of this system is characterized by the oldest craters larger than about 40 km in diameter that are essentially fresh, i.e.,

Opposite:

Figure 1.– The Moon under full solar illumination (north at top). Although surface detail is lost under full illumination, the albedo contrasts are clearly shown and reveal the contacts of the major geologic units. The pre-Imbrian System includes part of the higher albedo highland terrain near the southern limb. The Imbrian System is dated with respect to the formation of the Imbrian Basin, and these units correspond to a large part of the bright highland terrain owing to enormous quantities of ejecta produced by the Imbrium event. The Imbrian System also includes most of the dark maria. The Eratosthenian System includes large craters that have lost their bright rays and dark mare units that overlap these craters. At the top of the stratigraphic column, the Copernican System includes the most recent bright-rayed craters.

retaining most of their original features, but lack the bright rays, which have been erased through degradation. Thus mare material that overlies craters of this type is considered to be Eratosthenian in age rather than Imbrian. The youngest system on the Moon, the COPERNICAN SYSTEM, includes all events that have occurred since the formation of large, rayed craters that currently are old enough just to have lost their rays. The results of the USGS mapping program for the near side of the Moon are summarized on the map by Wilhelms and McCauley (1971) and the historical development of the lunar surface based on this mapping is illustrated in figures 1–3 (Wilhelms and Davis, 1971).

IV. GEOLOGICAL MAPPING AS AN AID TO UNDERSTANDING GEOLOGICAL PROCESS

Imperfect though this system of time stratigraphy is, it helps considerably in understanding the Moon's surface evolution.

Geological mapping also can be used as an aid for detailed studies of a particular phenomenon, such as the formation of an ejecta blanket around an impact crater. Geologists are usually concerned with rock units that have been formed over long periods of geological time. In the case of an impact crater, however, all the geological units may have formed in just a few minutes. Nevertheless, the technique of geological mapping can be of great importance in determining the geometrical relations of the individual rock units that make up the ejecta blanket, relations that aid in interpreting the manner in which an impact crater is formed.

Mapping on the planet Mercury may well be much like that on the Moon. Mars, however, presents its own problems, particularly those of recognizing rock units. If one attempts to map areas that are morphologically similar, there is danger that one is mapping areas that have suffered similar geomorphological processes, and such areas may in no way represent rock units. Such a map may be termed a terrain map and should be recognized as such. It is thus important when mapping Mars to determine characteristics that allow rock units to be recognized.

V. RECOGNITION OF DIFFERENT ROCK UNITS ON THE MOON

Following the principle that on the Moon surface characteristics distinguish between rock units, map boundaries are identified by changes in appearance from one area to another. In some cases changes are gradational and the boundary must be chosen arbitrarily in much the same way as the edge for alluvium deposit is mapped on Earth. However, where a gradational boundary is mapped, the criteria chosen for the boundary must be defined and followed systematically. An example of this situation is the outer edge of a continuous ejecta blanket which grades into discontinuous ejecta. In this case a convenient position for the boundary is where the surrounding secondary craters become subdued in form at the edge of the blanket.

Mountain forming units are easily recognized, but often missed are intermountain units which often present a rugged surface and form a separate unit occupying depressed areas between the mountains. On the other hand, where mountains occur in essentially level areas, the age relations are not always clear as there may be old rocks projecting through the plains or they may be younger units emplaced above the plains. The former case can usually be detected when the mountains

become more numerous towards the outer boundary of the plains and the plains are seen to overlie a mountainous terrain.

Within plains units themselves, different surface textures will often denote separate rock units and differences in crater density will indicate different ages under most circumstances.

In dealing with craters, overlap relations will often give relative ages, but in many areas, especially in the highlands where there are few other extensive units to take as "key" horizons, other techniques must be used to obtain relative ages. The most useful method is that devised by Offield and Pohn (1970), who determined a crater denudation chronology, defining criteria for distinguishing denuded craters of different relative ages. This paper deserves careful study.

H. H. Read once said "that the best geologist was the one who had seen the most rocks." In geological mapping, experience is the best tutor and much can be learned about the Moon by attempting to construct maps for oneself as well as taking other people's maps, such as those produced by the USGS for the Moon, and comparing them with the relevant pictures. This practice of making maps is a good constructive way for students to familiarize themselves with the surface of the Moon.

REFERENCES

Offield, T. W.; and Pohn, H. A.: Lunar crater morphology and relative-age determination of lunar geologic units – Part 2: Applications. In Geological Survey Research 1970: U.S. Geol. Survey Prof. Paper 700-C, p. C 163-169, 1970.

Wilhelms, D. E.; and Davis, D. E.: Two former faces of the Moon. Icarus, vol. 15, p. 368-372, 1971.

Wilhelms, D. E.; and McCauley, J. F.: Geologic map of the near side of the Moon. U.S. Geol. Survey Misc. Geol. Inv. Map I-703, 1971.

With permission, reprinted from Interagency Report: Astrogeology 55, Geologic Mapping of the Second Planet, NASA, pp. 1–36.

INTERAGENCY REPORT: ASTROGEOLOGY 55

GEOLOGIC MAPPING OF THE SECOND PLANET

by

Don E. Wilhelms
U.S. Geological Survey
Menlo Park, Calif. 94025

Part 1: Rationale and General Methods of Lunar Geologic Mapping

Part 2: Technicalities of Map Conventions, Format, Production Mechanics, and Reviewing

Part 3: History of the U.S. Geological Survey Lunar Geologic Mapping Program

October, 1972

Prepared by the Geological Survey for the National Aeronautics and Space Administration

NASA Contract W-13,204

Introduction

This paper attempts to convey the experience accumulated in the 11 years of the U.S. Geological Survey's lunar geologic mapping program [1/] to geologists who contemplate mapping the Moon, Mars, or any other planetary body with a visible solid surface. This is done in general terms in Part I, where I stress that lunar geologic mapping is similar in philosophy and principle, as well as in many details of method, to terrestrial geologic mapping. We have transferred what we learned on the first planet mapped geologically, the Earth, to the second, the Moon. Since this transfer has been successful in advancing lunar science, we can extend the same methods to other planets without changing our approach or methods, just as we have not changed the name of our science from geology to "selenology" (see for example, Ronca, 1965). In Part II, I give detailed guidelines for constructing maps, with the intention not of dictating procedures but of avoiding re-inventions of techniques already proven to be successful or unsuccessful. The same intention led to the inclusion of Part III, a history of the Survey's lunar mapping program, which although generally successful and a worthy model for future programs, included a number of mistakes that should not be repeated.

Why do we attempt geological mapping of other planets when photographs--often very poor ones--are the only data available? Presumably we wish to learn the planet's three-dimensional make-up, its formative and modifying processes, and its history, including origin and subsequent evolution. Some kinds of data, such as chemical composition and absolute ages, have to be collected on the planet itself. But many things <u>cannot</u> be learned on the ground, given any less than an extravagant expense of resources and time, but they can be learned from photographs to a considerable extent. These include the structure of the whole planet and the geometric relations, areal distribution, and sequence of formation of its crustal elements. Besides being important in its own right, this knowledge of the planet-wide framework is essential for determining the setting of the tiny spot samples examined or collected on the surface (Carr, 1970, p. 5). This progression from gross to fine-scale analyses is actually more desirable and efficient than the opposite one used on Earth.

Requisites for Planetary Mapping

Geologic mapping is a difficult, time-consuming exercise for which some geologists are better suited than others. The answer to the question of who will be an effective planetary mapper has become increasingly clear to me in the eight years I have been examining lunar geologic maps. The best maps have been produced by experienced field geologists who understand the purpose, strengths, and limitations of geologic maps; who see their utility in lunar and planetary studies

1/ The great bulk of this program was conducted as supporting research for the National Aeronautics and Space Administration's lunar exploration program under Contract Nos. R-66 and W-13,130. The present report was prepared for the Planetology Programs Office under NASA Contract No. W-13,204.

even in the absence of final data; who are willing to apply their research methods and understanding of terrestrial geologic relations and processes to other planets; who are patient and careful; and who have no hangups about extra-terrestrial bodies. There is a close empirical correlation in quality between a geologist's lunar and terrestrial maps. Geologists who have made at least one complete and good terrestrial map from field studies generally have been able to make good lunar geologic maps, if they wanted to. Some good geologists have made inferior lunar maps because they just couldn't see the point of it or were unable to transfer what they learned on Earth to the Moon. So far, lunar mapping has been primarily inductive in its approach and based on the principles of stratigraphy, and dependent for unit definition on geometric relations and topographic properties. Fancy quantitative "remote sensing" analyses have not played an important role in the work. Planetary mapping, then, is not for non-geologists or for geologists who have rejected the traditions of their science, and expect to get real results quickly by machines and numbers; a planet is too complex to be studied exclusively by quantitative analyses, though these are of course essential for many purposes.1/ One must expect primarily to gather facts, and to advance slowly to understanding, not to suddenly comprehend the origin of the subject planet or the Solar System. If one is suited to this discipline and sufficiently patient, he can garner substantial satisfaction from his labors as order emerges and the planet at last becomes comprehensible.

Acknowledgements

For completeness, this paper has incorporated considerable material, including verbatim quotations from: 1) a summary of the telescopic phase (1960-1967) of the lunar program (Wilhelms, 1970), 2) a pamphlet that accompanies a synoptic map of the near side based both on telescopic and Lunar Orbiter data (Wilhelms and McCauley, 1971), and 3) a book which perceptively evaluates the stratigraphic approach to lunar mapping (Mutch, 1970). Much other material, especially in Parts II and III, has not been set down before and is drawn from my six-year experience as coordinator of the Survey's lunar geologic mapping program. The discussion of map explanations was prepared with the help of Rudolph W. Kopf, representative, U.S.G.S. Geologic Names Committee. Two lunar mapping stalwarts contributed valuable suggestions: John F. McCauley, currently Chief, Branch of Astrogeologic Studies, and from the start of the intensive mapping program (1963) deeply involved in its development, and David H. Scott, who, although relatively new (1969) to the program, has bypassed many of the earlier workers in mapping proficiency and productivity because of his concentrated approach, insight, and long previous experience in solving problems by geological methods. Others who contributed the valuable suggestions are G. E. McGill,

1/ All geologists can benefit from reading or re-reading the excellent collection of articles in the book, "Fabric of Geology" (Albritton, 1963), for reinforcement of their appreciation for the philosophy and methodology of the historical, primarily qualitative science of geology.

University of Massachusetts, and G. W. Colton, U.S.G.S.

Suggestions from users are welcomed and will be incorporated in a second edition of this paper should one become desirable.

PART I

RATIONALE AND GENERAL METHODS OF LUNAR GEOLOGIC MAPPING

Geologic Units and the Principles of Sequence

Lunar mapping as practiced by the Survey depends on a vital concept derived from terrestrial stratigraphic practice: That the crust is composed of discrete, three-dimensional bodies of rock called geologic units, each having limited vertical and horizontal extent. The geometric relations among units record their sequence of formation: younger rocks are deposited upon, or intrude, older rocks. Most non-geologists and even many geologists seem surprised at first that planets can be studied productively from so simple a perspective. We know, however, that no planet made of solid material can be totally homogeneous or randomly heterogeneous. Recorded on its surface in the form of discrete rock masses arranged in complex overlapping sequences are the events which have shaped that surface--impacts that threw out blankets of bedded ejecta upon older terrain, and, for large planets, the volcanism that builds stratified flows, cones, domes and the like. This concept of discrete mappable units occupying specific stratigraphic positions is an essential research tool; it reduces the enormous complexity of a planetary crust to comprehensible proportions, and allows without field examination much to be learned about the structure, history, and formative processes of a planet's surface.

The process of recognizing the geologic units which compose a planet is straightforward in principle. One tries to block out units each of which formed, relative to its neighboring units, (a) by a discrete process, and (b) in a discrete time interval. Unity of formative process is inferred from a distinctive texture--ridges, hillocks, lobes, pits, complete smoothness, etc.--that occurs uniformly over an extensive area, or varies regularly, as in a symmetrical array about a negative or positive landform. A uniform or regularly varying albedo pattern commonly accompanies the topographic pattern. For example, crater rim material, with its concentric arcuate hummocks close to the crater and radial ridges farther out, probably was formed by a single event, ejection from the crater (fig. 1a). Other types of units include a patch of mare or light plains with a smooth surface and uniform albedo, a dome with uniform ridged texture (fig. 1b), a cluster of hills and furrow-like craters having a distinctive, uniform, and repetitive pattern (fig. 1c), and a mantle of uniform albedo superposed on diverse underlying terrain (fig. 1d). The uniform or regularly varying pattern may be broken up by younger units or structures, so that the complete distribution of the unit must be mapped to identify it as a unit. One tests the likelihood of unity of formation by asking, "Can what I see be explained by laterally continuous rock bodies?"

Once units are recognized, the procedure of determining their age relative to their neighboring units is even simpler, although it is at the heart of the geologic approach, which is essentially historical and distinct from the approach of many other sciences. This procedure relies on the principles of sequence. Because temporal relations are expressed as three-dimensional spatial relations, these can commonly

a. Crater Timocharis (34 km diam.). The rim material has regular properties in concentric bands and was undoubtedly produced by a single process, ejection from the crater, so is a geologic unit. Apollo 15 metric-camera frame 1147.

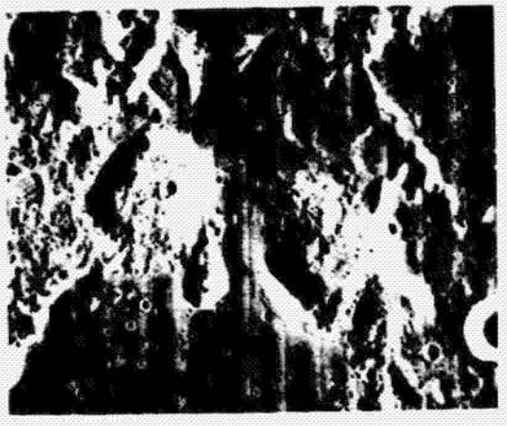

b. Possible extrusive domes, Gruithuisen γ (left, 18 km diameter) and δ (right). The complex, uniform texture of shallow overlapping pits is probably primary. Lunar Orbiter V frame M-184.

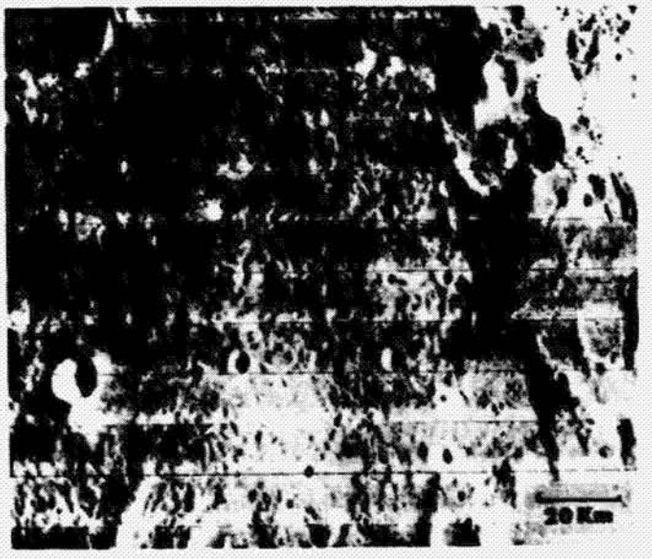

c. Descartes-type material, with repetitive pattern of furrows and hills. Mantles crater Descartes at bottom of picture. Part of Lunar Orbiter IV frame H-89.

Fig. 1.-Examples of lunar geologic units.

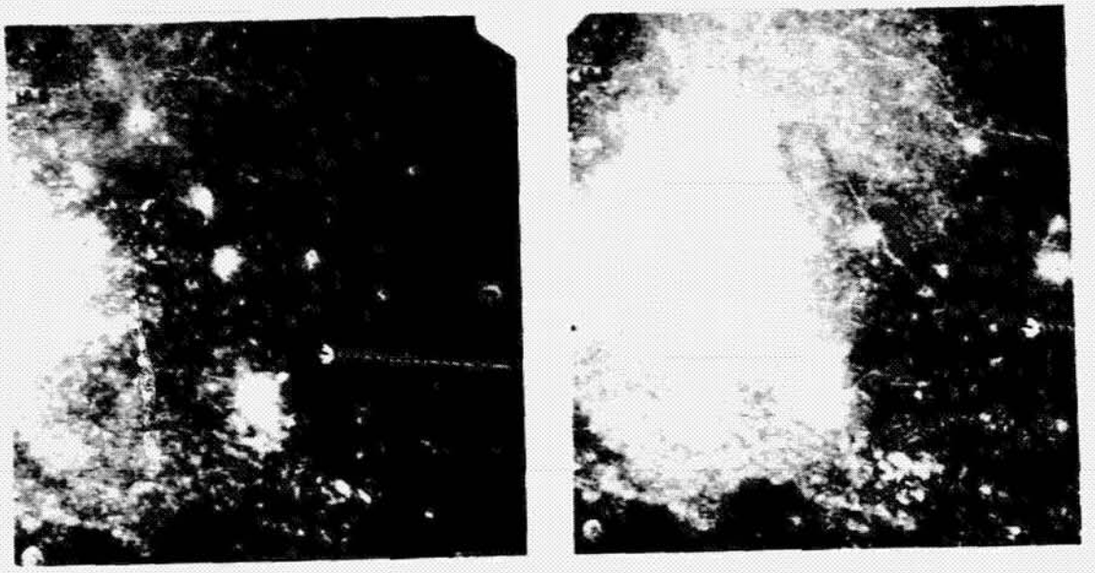

d. Dark mantle on terra, increasing in thickness to upper right (northeast). Sulpicius Gallus region, southwestern Mare Serenitatis. Parts of 2155 and 2156 Apollo 15 metric-camera frames (stereo pair). Long dimension of photos approximately 150 km.

be seen in the areal pattern of the units and their surface contact relations: a younger unit overlaps or embays an older unit; the contact of a younger unit cuts across the contact between two older units. In a commonly cited example that clearly demonstrates lunar stratigraphic methods (fig. 2) (Wilhelms, 1970, p. F7-F10): Copernicus obviously is younger than the mare material around it because its rim material, secondary craters, and rays cross the mare material in an unbroken pattern; on the other hand, mare material fills and embays Archimedes, and truncates the contact between its ejecta and the underlying plains, so is younger than Archimedes.

It is important to note that the concept that parts of a unit formed in "about the same way," is meant in very general terms: origin by ejection of material from a central source; or by emplacement as fluid flows or by viscous extrusion. One may not know whether ejection or emplacement occurred by an impact or volcanic mechanism. Details of origin and composition must await direct exploration, or sophisticated and cautious comparison of lunar features with terrestrial analogs and laboratory models (Mutch, 1970, p. 59-62 gives a list of warnings about use of analogs). Therefore units should always be mapped as objectively as possible on the basis of reproducible physical criteria. But each unit is mapped as such on the basis of a geologic judgement that it has unity of origin and age.

It should also be emphasized at this point that, although we use topographic characteristics more than any other property to define units (Wilhelms, 1970, p. F6), we attempt to map materials, not physiographic forms; the crater rim material, not the crater, which is just a hole. And similarly for plains; on Earth plains may be formed by erosion or by sedimentation but on the Moon they are probably formed by deposition of materials (lava or rock fragments) whose intrinsic mobility caused them to assume flat surfaces. So lunar mapping is not geomorphology, but rather an attempt at stratigraphy, even by its strict definition as the study of layered rocks, although few cross sections through layers can be observed (Mutch, 1970, p. 259-261) because of the nature of the Moon itself.

The degree of exactness achieved in identifying units--how "discrete" the process and time interval of formation--will vary widely with the character of units and quality of available data. The foregoing guidelines to lunar mapping can probably be applied readily by most students in well photographed, relatively fresh terranes--about late Imbrian and younger--where true stratigraphic units can be recognized from their primary characteristics such as crater rim hummocks, ridges, or mare flow lobes. It is in older, subdued-appearing terranes where this approach encounters harder going. In such terranes, primary textures and surfaces are not always visible, and we may have to be content with defining units by superposed crater populations, erosional morphology, or other secondary characteristics--a practice which is justifiably frowned on in terrestrial stratigraphy. Secondary characteristics, unfortunately, might be equally developed on quite different units, which remain undetected; that is, we might recognize and map in these situations only physiographic, not rock-stratigraphic, units.[1/] Nevertheless, partial strat-

1/ Note added in proof: Preliminary Apollo 16 rock analyses suggest that this happened at the Descartes site (fig. 1c). The distinctive pits that characterize the "Descartes-type" unit may be superposed on unrelated, older, possibly polygenetic, terrane.

a. Photograph of Copernicus-Archimedes region. Lunar Orbiter IV moderate-resolution frame 126.

Fig. 2.--Principles of sequence.

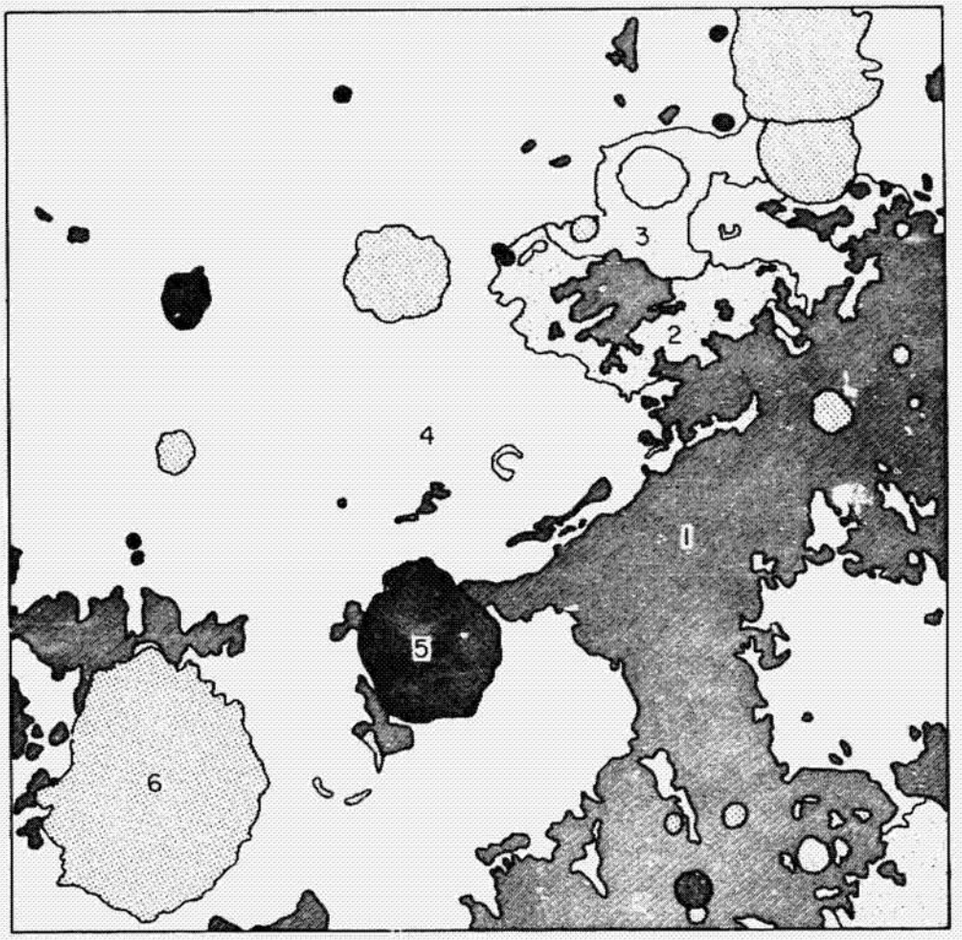

b. Geologic map of same area (after Wilhelms and McCauley, 1971). Units are numbered from oldest (1) to youngest (6). The contacts of each successively younger unit cut across those of older units. Unit 6 is known to be younger than unit 5 because its radial rays are superposed on unit 5.

igraphic sequences can usually be worked out in old terranes by overlap and transection relations, mainly among crater rims and plains. This is possible if one makes the reasonable assumption that in a general sense uniformitarianism is applicable to the Moon--that older terranes are likely to be degraded equivalents of younger, demonstrably bedded ones (fig. 3). Lunar stratigraphers will not object if the mental process that imagines the conversion of young forms to old is considered geomorphology, so long as one keeps in mind the probable bedded nature of even the oldest terrane and thinks stratigraphically.

Correlations

To build a geologic picture on a planet-wide basis, the individual, local units must be correlated and related to the total stratigraphic record. The most rigorous method in lunar stratigraphy, as in terrestrial, is use of extensive and synchronous datum planes. The best ones on the Moon are the ejecta blankets and secondary impact craters of the Imbrium, Orientale, and Nectaris basins. The mare material is also useful though not quite so synchronous. Synchronous materials of large young craters, including their secondary impact craters, are also useful over smaller but still considerable regions.[1/] Many lunar units have been dated as younger or older than these units, and the following four principal subdivisions of lunar stratigraphy, first worked out in the Copernicus-Archimedes region (Shoemaker and Hackman, 1962) and somewhat modified later (McCauley, 1967; Wilhelms, 1970), have been established: Copernican System, ray-crater material and contemporaneous materials; Eratosthenian System, materials older than ray-crater material but younger than the bulk of the mare material; Imbrian System, everything from the bulk of the mare material down through the Imbrium basin ejecta blanket (a considerable volume of material); pre-Imbrian, everything older than the Imbrium basin ejecta blanket. A move is now afoot to subdivide the pre-Imbrian on the basis of the ejecta and materials of the Nectaris basin.

Extrapolations necessary in the absence of these regional units are made by: (1) density of superposed craters, and (2) correlations of morphology with age. Relative (and absolute) age determination by means of crater population is a favorite topic in the literature (for example see Mutch, 1970, p. 263-270) and will not be discussed further here, except to caution against misleading conclusions resulting from the very large percentage of lunar craters that are secondary impact craters. Morphology of craters has come into wide use in extrapolation since the advent of Lunar Orbiter photographs (Pohn and Offield, 1970; Trask, 1970; Soderblom and Lebofsky, 1972). Age correlations are made by comparing morphology of isolated craters with morphology of craters previously dated relative to one of the regional datum planes, under the assumption that morphology partly indicates state of preservation. As noted above, a fundamental observation of lunar stratigraphy is that a kind of uniformitarianism applies: that craters and other landforms are fresh

1/ The utility of crater materials as stratigraphic datum planes is reduced by the fact that their lower and upper surfaces are randomly placed unconformities. In particular, the most extensive and easily dated crater materials, the young ones, usually have a free surface that is of little stratigraphic use (Mutch, 1970, p. 164-165).

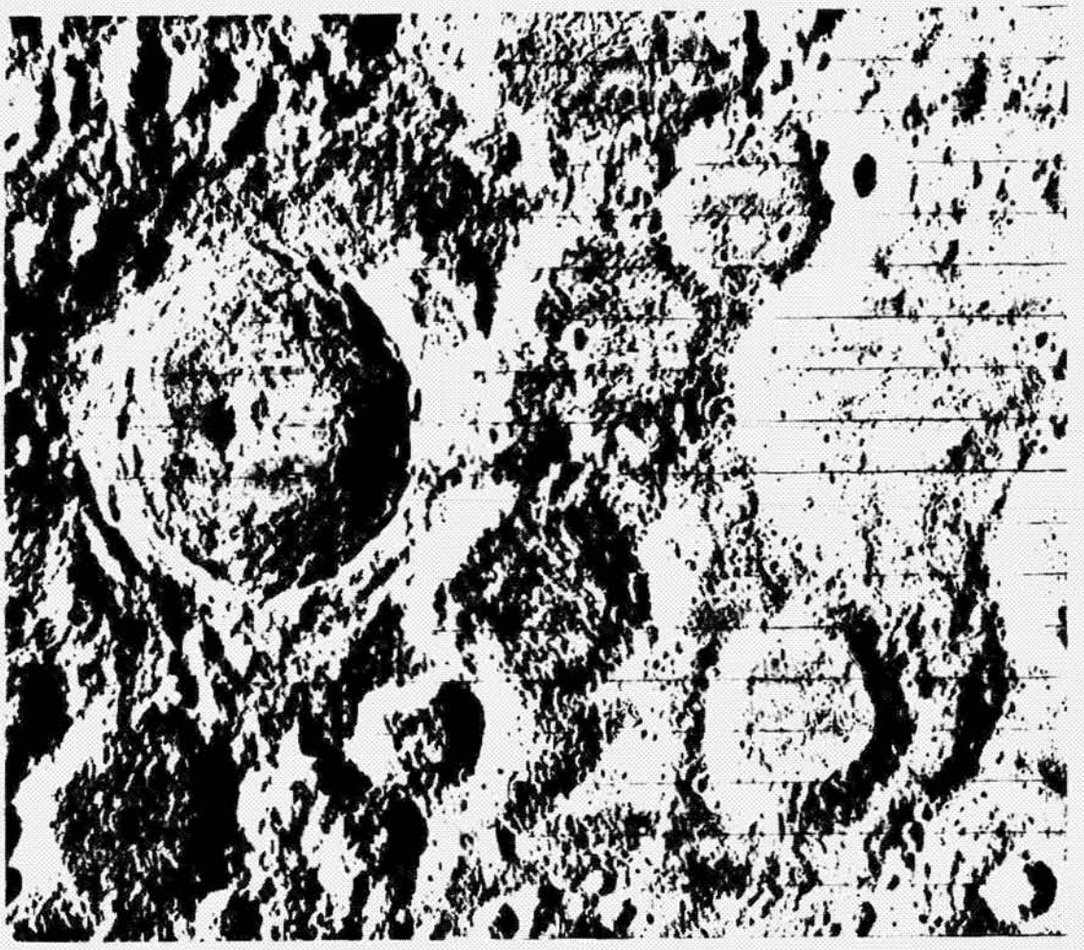

Figure 3.--Comparison of old and young terranes. The crater Tycho, left, (85 km diameter) is surrounded by a sharply hummocky rim, finely-textured radial ejecta, and swarms of secondary impact craters. These have greatly affected the topography of the nearby crater rims and of their planar floor material. Lunar uniformitarianism suggests that the Tycho-size crater on the right (Orontius) and the medium-sized craters were once surrounded by similar sharply textured materials that similarly affected their neighborhoods, but these effects have vanished. Presumably, however, the crater materials and old plains are still present but have been complexly degraded and mixed into their present characterless shape by repetitive cratering. So old terranes are composed of sequences just as complex as in young terranes, but the nature of the components must be inferred by analogy. Lunar Orbiter IV frame H-119, framelets 003-022.

when young, and become degraded with time (Wilhelms and McCauley, 1971, pamphlet). Although less desirable than more direct stratigraphic methods (using regional blankets as marker horizons or superposition and intersection relations), the dating of craters by their physiographic appearance works well in practice if age categories are not too finely drawn. Craters used this way are, in a sense, the "guide fossils" of lunar stratigraphy. The results are consistent with established stratigraphic relations where they can be tested. For example, no severely degraded craters of the type assigned to the pre-Imbrian can be identified on either the Imbrium or the Orientale circumbasin blankets, both of Imbrian age.

Avoiding the Interpretive Bias

The Survey, reacting to the sub-scientific state of much lunar geologic and parageologic literature before 1960, has made a great effort to map objectively. We have insisted on reproducible lines; the reason for their placement must be fairly obvious to other workers viewing the same photographic data. Unit names must be objective, not interpretive--"crater material," not "impact ejecta" or "volcanic rocks." Units must be objectively described on the basis of physical characteristics, so that other workers can identify them; definitions must be straightforward, not contrived to fit a tortuous interpretive maze. The description of defining characteristics must be separated clearly from discussion of genetic interpretations, in two separate paragraphs under the unit's box in the explanation. Age assignment must also be based on reproducible criteria, which must be stated. Rock and time units must be separated. Entire quadrangles or regions must be mapped, so that everything present has to be taken into account, not only objects of special interest (odd craters, sinuous rilles, lineaments, etc.) that contain only those elements which nourish special prejudices. (The Earth-analog game has very frequently been played this way, by very sloppy rules.) Cross sections, though highly interpretive, should be drawn, as on Earth, if for no other reason than to test the map relations.

To be sure, there is considerable latitude for differences of opinion even within these tight guidelines and within the constraint of mapping material units ranked stratigraphically. In fact, no two people are going to draw lines exactly the same way--though it is remarkable, perhaps, how closely similar the lines of two experienced mappers usually are (compare, even, figs. 4a and 4b). Lines might be drawn in several equally reproducible ways, because of differing opinions about which units are stratigraphically significant--for example, a thin overlying mantle or a buried, but still strongly expressed, crater rim; in this case two workers may agree exactly on the observation, but not on the map portrayal. There is, of course, some difference of opinion about relative age of units, even among people applying the same criteria. There is difference in artistic style--smooth or jagged lines--and in "lumping" versus "splitting." But all of these differences also occur in terrestrial geology. Lunar mapping has strayed unacceptably far from Survey guidelines only when a strong interpretive bias has made maps unreadable by a mapper's colleagues; two maps have been candidates for rejection for this reason.[1/]

1/ Footnote--see next page.

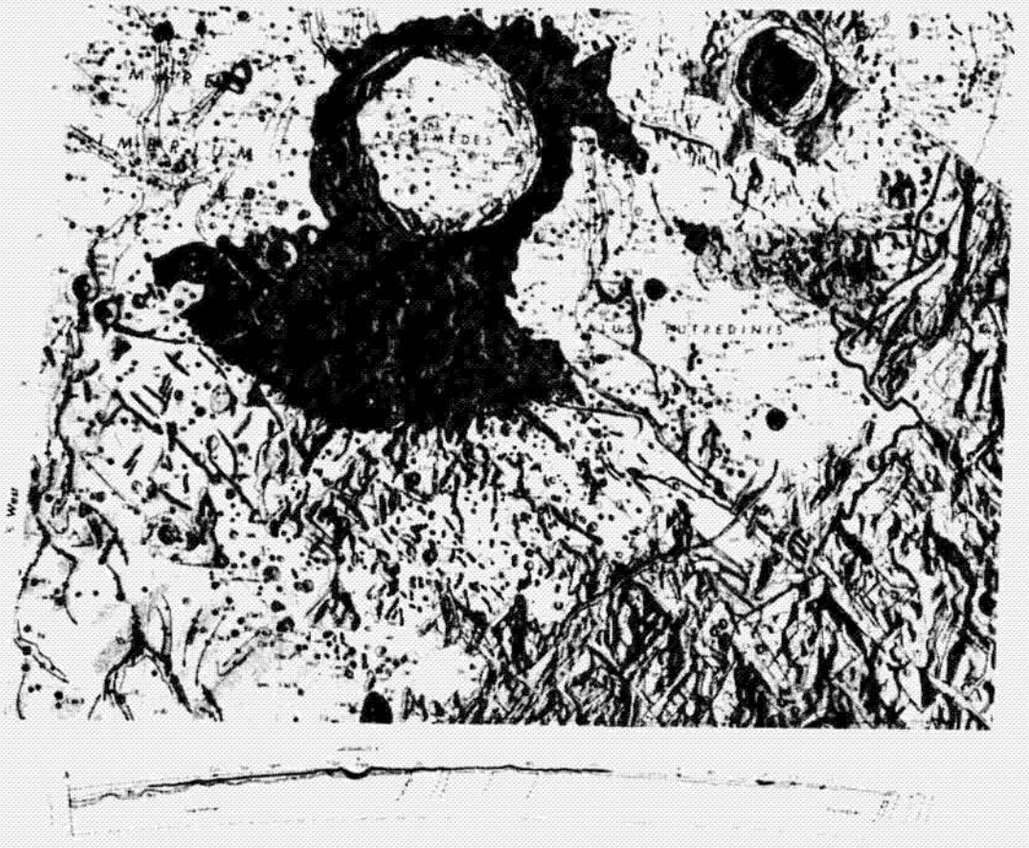

a. Geologic map and section of the Montes Apenninus region of the Moon, by R. J. Hackman (1966).

Fig. 4.--Alternative U.S. (a) and U.S.S.R. (b) maps of the same region. For (b), turn page.

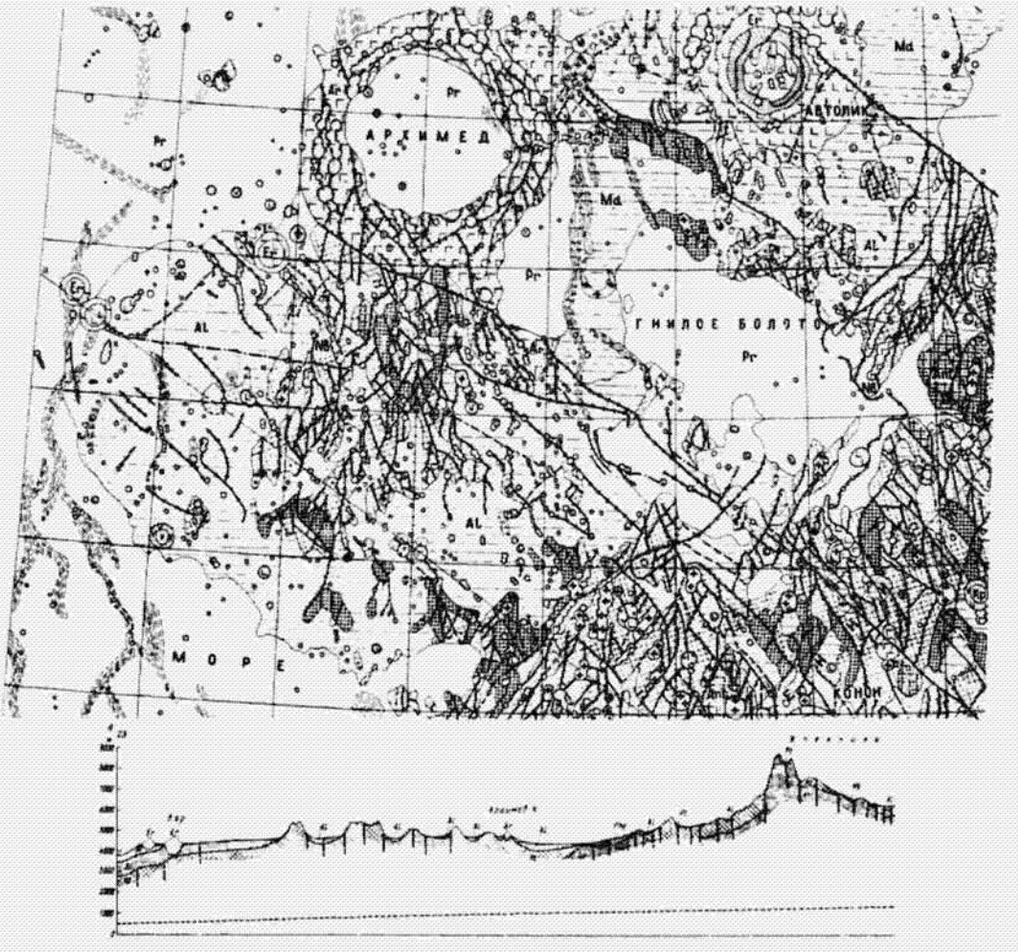

b. Geologic-morphologic map and profile of the region of the cirque Archimedes and the mountainous Apennine massif, by A. C. Sukhanov and V. G. Trifonov (in Peive, ed., 1969). Profile extends beyond map area and is at a somewhat smaller scale.

To eliminate all interpretive bias, there has been a continuing attempt to quantitize lunar properties for use in hard, reproducible unit descriptions. The most useful easily measurable property has been albedo. Pohn and Wildey (1970) photometrically distinguish 20 normal albedo steps. From 5 to 10 have been used on lunar maps. But on the 1:5,000,000-scale near-side map (Wilhelms and McCauley, 1971) only two--dark and light--were used. This dichotomy could indicate a basic two-fold compositional dichotomy--mafic and felsic. Other albedo steps may represent additional compositional variations or degree of exposure of fresh rock. In any case, albedo variations whether fully understood or not, can be used to help characterize units.

Besides albedo, possible defining properties include thermal (infrared) anomaly at eclipse, color, polarization, slope characteristics derived by photogrammetry or photoclinometry, and microwave and radar response at various wavelengths (both Earth-Moon and bistatic). Some of these--especially infrared and color--have proved informative, and others--radar--are beginning to appear interesting. But possibly we never will be able to improve much on qualitative, commonly laborious geologic mapping based on topographic properties and geometric relations. There are too many data to treat quantitatively; machines can never define units. The author's opinion of the stratigraphic utility of these properties is very well expressed by Mutch (1970, p. 58).

In all science, one is most apt to find what he is looking for; that is, his view of his subject matter is colored by the spectacles he wears. I have been describing the spectacles that the Geological Survey wears during its lunar mapping program; they have filters that pass material-geologic units, and polarizers that stack the units in stratigraphic sequence where possible. We believe that results have shown these spectacles to be better than others yet tried on the Moon, because they pass information that corresponds with the true nature of the Moon. Other spectacle prescriptions are of course possible but of such low transmissivity as not to be efficient in advancing geological knowledge in an orderly and economical way.

A Soviet group under Sukhanov (1967), partly following guidelines established by Khabakov (1962), also maps with historical spectacles, but thinks less in terms of material units and more in terms of structures. As I understand it, the Soviets recognize two kinds of lunar units, craters and maria, and believe that nearly everything now seen on the Moon is one of these, modified by structural patterns to a greater or lesser degree. For example, they, like us, recognize the maria to be younger than the Apennine Mountains, but they believe the Apennines to be old mare material that has undergone long, protracted deformation by internal forces (fig. 4b). Their "structure" spectacles predestine this different conclusion.

Another productive lunar student who wears both historical and endogenetic

1/ (From preceding page.) The main reason for outright rejection, so far, has been failure, caused by poor spatial perception or sloppiness, to transfer shapes that are clearly visible on photographs to a map. One could set up a quick semi-quantitative test for the quality of a lunar map: the amount of time it takes someone, while looking at the photographs, to locate a feature on the map.

filters on his spectacles is the English astronomer-geologist Gilbert Fielder (1965). His fundamental uniformitarian postulate is the diametrical opposite of ours: he believes that topographically sharp features are old and subdued features, young (1965, p. 146-153). He believes, for example, that Stadius and Archimedes are young craters beginning to grow up through the surface, eventually to look like their richly detailed (but, paradoxically, relatively uncratered) neighbor Copernicus.

To reiterate the thesis of the present paper in this context: use of the concept of material stratigraphic units has led the Survey in a different direction from the Soviets and Fielder, and before them, Shaler, Spurr, and von Bülow. The internal-structural model allows each small feature such as a hillock or ridge to be interpreted ad hoc, whereas our model unifies many small adjacent features as look alike, then seeks the explanation of this unity in layered units. The result is a mixed endogenetic and exogenetic interpretation. Contrary to a widespread calumny, the Survey's ruling model is not impact--as should be obvious from the many volcanic interpretations that appear on our maps. Impact as an explanation for multi-ring basins and many craters is arrived at only when a reasonable mechanism is sought for the emplacement of the extensive materials around them that appear to be layered.

Purpose of Geologic Maps

At this point, after generalizing about the lunar and planetary mapping approach and before detailing the methods of constructing a map, we should pause to consider the purpose of geologic maps. As has been stressed, planetary geological mapping is the offspring of terrestrial geological mapping. So we will know how to map a planet if we remember how we map the Earth; and if we momentarily forget why we are mapping a planet, we should recall why we map the Earth. We map to learn and to communicate. For full understanding, we must study an entire area, not selected features of interest, so we make maps to keep track of our observations economically and record them in their proper geometric relations. By mapping, we continually organize and classify the data, formulate and test multiple working hypotheses, and finally, generalize nature's complexities into a portrayal that seems consistent with available data and our accumulated knowledge.

A map must filter observations, not record all of them; otherwise it is not useful to anyone but its author. But it must also show the basis for the author's generalizations, so that other workers can test them against the facts, and either confirm them or modify them in the light of new theory. A terrestrial map made ten years ago should not be superseded by global plate tectonic theory, but rather, should be the basis for testing the theory; and a lunar map should do the same for, say, impact and volcanic theories. So in effect geologic maps are the objective, testable records and models of geology and correspond to the graphs and equations of the experimental sciences.

PART II

TECHNICALITIES OF MAP CONVENTIONS, FORMAT, PRODUCTION MECHANICS, AND REVIEWING

Map Units

A mapper usually finds that the units he has recognized and outlined require some recasting when being expressed as map units, to improve cartographic clarity or scientific rigor. This section gives some rules to be followed in setting up map units.

We should first recall the different conceptual types of units now recognized by American stratigraphers (American Commission on Stratigraphic Nomenclature, 1970). The distinctions are important in separating interpretation from observation and in keeping one's logic straight; continuing confusion of these types by European stratigraphers may impede their objective evaluation of the Moon. The Code of Stratigraphic Nomenclature distinguishes between rock-stratigraphic units--material subdivisions of the crust that are distinguished solely on the basis of lithologic properties, and time-stratigraphic units--material units which include all rocks formed in a specific interval of time. Rock-stratigraphic units are the practical mapping units and are the basis for defining time-stratigraphic units. A third unit is a nonmaterial subdivision--the geologic-time unit, which is defined in terms of time-stratigraphic units. The basic rock-stratigraphic unit is the formation; these are divided into members, and combined into groups. The basic time-stratigraphic unit is the system; these are divided into series, and combined into the era or erathem. Geologic-time units that correspond to systems are periods; to series, epochs. "Upper" and "lower" are physical terms so are applied to rock-stratigraphic and time-stratigraphic units; "late" and "early" are time terms.

Another type of unit that now might be needed on the Moon is the soil-stratigraphic unit, which might advantageously be used to codify regolith units (Mutch, 1970, p. 174-195). Other types and ranks of Earth units have no present lunar application.

The term "lunar material unit" has been proposed as the lunar parallel to the terrestrial rock-stratigraphic unit (Wilhelms, 1970, p. F11). It was defined as "a subdivision of the materials in the Moon's crust exposed or expressed at the surface and distinguished and delimited on the basis of physical characteristics." The purpose of distinguishing lunar material units from rock-stratigraphic units was to emphasize the fact that mapped lunar units, though defined by physical characteristics like Earth rock units, are not always nicely discrete, tabular, internally uniform bodies defined by true primary lithologic characteristics. That is, lunar material units may be either true rock-stratigraphic units or "terrain units." Also, the word "material" was preferred over "rock" because of a vague uneasiness at calling terrain "rock" and because we knew that most lunar units would turn out to be debris, breccias, and other crumbly stuff. But all of this is still rock and not some exotic extraterrestrial compound, so the word "rock" should perhaps come into greater use even for photogeologic units.

Another term that should be clearly understood is "map unit" itself. This is the unit that is shown on a map with its own symbol, color, and position in the box explanation. Map units may be rock-stratigraphic units (lunar material units) of any rank, or time-stratigraphic units of any rank, depending on the purpose and scale of the map.

Each limited body of material that the geologist has outlined as a unit by the principles set forth in the previous sections cannot be a map unit. Some laterally continuous formations, such as basin ejecta blankets, are sometimes used individually as map units, as is the most common practice on Earth. Very commonly, however, formations of indistinguishable appearance occur in many separated localities, and it is convenient to combine all of these as a single map unit. The individual occurrences of such a map unit have the same general age range--that is, are assigned to the same time-stratigraphic unit--but may vary in age within this range. Examples of such map units are "Imbrian plains material," which consists of thousands of separate pools of light plains material, possibly ranging in age from early to late Imbrian,[1/] and "ray-crater material," consisting of materials of a great number of individual young rayed craters, assigned to the Copernican System. These Copernican rayed craters are superposed on nearly all other materials, and may have been formed over the last half of lunar history. So a map unit can include an extensive sequence. Poorly defined lunar material units that no one would call rock-stratigraphic units are treated similarly. Thus we may have "terra material, undivided" appearing every place on a map where we don't understand the geology. (This unit may also, of course, be used on small-scale or special-purpose maps that lump well understood units.)

Two occurrences of the same map unit may be separated by a contact, with the younger shown overlapping the older (for example where materials of one Copernican crater overlap those of another); this is not done on terrestrial maps.

Two or more completely superposed units are commonly recognized (fig. 5). A thin dark or light unit may give an area its characteristic albedo, while an underlying unit may contribute the dominant topography. Or two superposed units, such as materials of two craters, may both be expressed topographically. The unit that is stressed, by being mapped in color, should be the unit that is most conspicuous at the scale of mapping being used. Ordinarily this is the youngest unit that contributes conspicuous topographic expression; but it may be the thin dark or light unit without topographic expression of its own. At low resolution, the rim material of an old crater in the southern highlands is prominent, and on maps at the 1:5,000,000-scale it is the unit mapped in color. But if high-resolution photographs show that the rim has a mantled appearance, then various mantling materials may be the units mapped in color on larger-scale maps based on these photographs. Map most conspicuously what you see most clearly.

Buried units whose textures can still be seen commonly are shown by dotted

1/ One group of the plains "formations" has been called Cayley Formation, and another, Apennine Bench Formation, but this use of formational names is disappearing.

a. Photograph of area. Crater Aristoteles, 85 km diameter. Lunar Orbiter IV frame H-98, framelets 218-247.

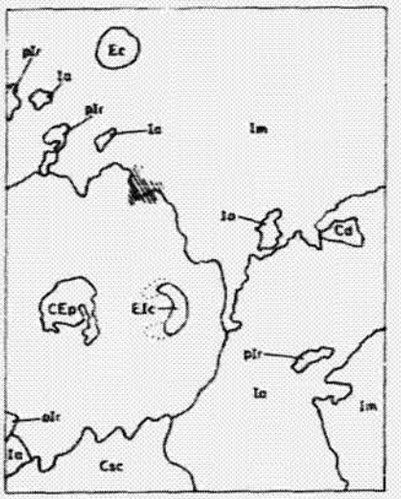

b. Most conspicuous units stressed.

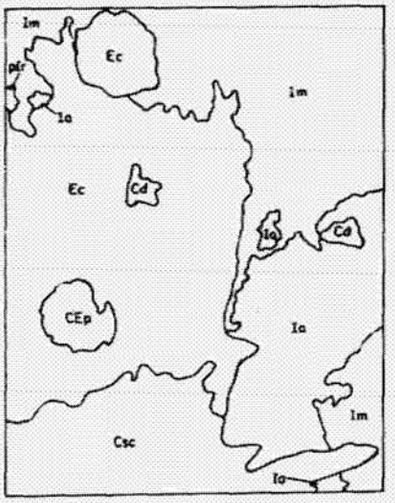

c. Surficial units stressed.

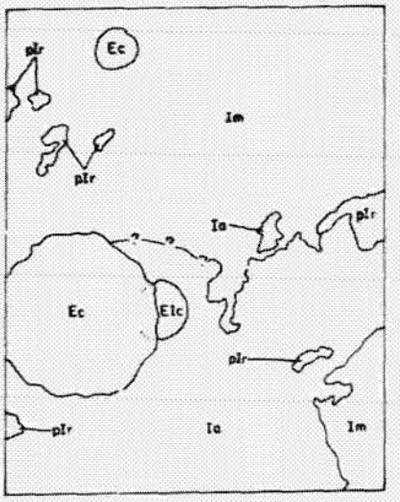

d. Deep-lying units stressed.

Fig. 5.--Alternative methods of portraying a terrane. Portrayal of (b) is ordinarily preferred. Csc--Copernican satellitic crater material; Cd--Copernican dark mantling material; diagonal line pattern--dark material; CEp--Eratosthenian or Copernican plains material; Ec--Eratosthenian crater material; EIc--Imbrian or Eratosthenian crater material; Im--Imbrian mare material; Ia--Imbrian Alpes Formation (Imbrium basin ejecta?); pIr--pre-Imbrian material of rugged terra.

contacts and symbols in parentheses; alternatively, an overprint pattern may be used for the overlying unit. Special dash-dot symbols are used for buried crater rim crests where subunits are indistinct. Buried contacts are drawn at the limit of observed topographic expression, not at the inferred or projected limits. Some units are defined to represent both the underlying and overlying layers (Milton, 1968; Wilhelms, 1970, p. F12). Provinces of quite diverse constitution can be mapped as units, provided their compound nature is explained fully and no pretense is made that they are true rock-stratigraphic units (McCauley and Wilhelms, 1972).

Crater material subunits have always played a large role on lunar geologic maps (Wilhelms, 1970, p. F40-F42; Mutch, 1970, p. 165-174). Crater materials--of rim, wall, floor, peak, etc.--were extensively subdivided, for objectivity, because they look so different. This subdivision has proved, however, to be excessively demanding on mapping time and available colors. There is sentiment now, therefore, to lump all materials of a crater. Or a more interpretive two-fold system could be used: (1) materials completely disaggregated and redistributed by crater formation (ballistic and base-surge ejecta); (2) materials structurally highly deformed but not disaggregated (inner "Schuppen" rim material, wall material, central peak material, and some hilly floor material). Materials believed formed after the crater (smooth floor materials and planar pools in rim and wall depressions) are usually mapped as separate, non-crater units, although formerly some of these were included as crater materials.

Names, Letter Symbols, and Colors

Each map unit is given a distinctive name, letter symbol, and color. Names may be formal or informal, as convenient. Formal names are given to some laterally continuous units, such as the Fra Mauro Formation, that are almost certainly true rock-stratigraphic units. Formal names may also be given to units of unwieldy description that are of special stratigraphic significance, even though the geology of the unit is not completely understood; an example is the Alpes Formation, which otherwise might be called "material forming equidimensional or slightly elongate hummocks of light albedo." Most units, well or poorly understood, are now given short descriptive informal names, followed by the word material(s); examples are crater materials, mare material, hilly and furrowed material, and dome material. All names are objective, not interpretive--"crater rim material," not "impact ejecta" or "volcanic rocks."

The symbol for a lunar map unit, like its terrestrial counterpart, consists of an abbreviation of the system to which the unit is assigned (capital letter) and an abbreviation of the formal or informal name (lowercase letters). Units that may belong with equal likelihood to either of two systems or any of three are given two capital letters representing the possible range (youngest first). If the age of a unit is unknown or only approximately known, capital letters may be omitted. The order of lower-case letters, where possible, should be: noun or formation first, adjective or member second, submember third. Ic, crater material (formation); Icr, crater rim material (member); Icrh, crater rim material,

hummocky (sub-member). Where the modifier is an integral part of the name, it may come first, especially to avoid ambiguity: pIst, structured terra material. The reason for each letter in the symbol must be apparent from the name; you cannot label "hilly material" Er because it happens to be rough. But all words of the name need not be abbreviated in the symbol; hilly and pitted material (of Imbrian age) can be abbreviated Ih if there is no ambiguity with other "h" units; but if you also have the Hevelius Formation, you must label the Hevelius Ihe; or label it Ih and label the hilly and pitted material Ihp. In other words, symbols should have the minimum number of letters to be unambiguous. A maximum of four letters may be in the symbol; pI counts as one; all other combinations count as two (CE, EI, etc.).

Use letters in preference to numbers where possible. When units are numbered, higher numbers refer to younger units (Im_2 is younger than Im_1). Numbers follow all letters, because they refer to the whole unit, not the basic formational unit ($pIcr_2$, not pIc_2r).

In all text material, the Survey prefers to refer to units by name, not symbol--"mare material," not "Im." If you must use symbols in text, say "unit Im." Symbols are newly defined on each map's explanation; symbols for the same unit may therefore vary from map to map, but we have tried to keep them as uniform as possible.

Symbols which are queried on the map should always be explained explicitly. "Queried where doubtful" is not good enough; say, "queried where could be Erathosthenian" or "queried where could be unit x." Be sparing in the use of queries; each one must be drafted on a final map. Convey only important doubts--probable departures from the defined meaning of the symbol, not just slight uncertainty as to whether you have mapped correctly.

Colors are assigned to associate like units and disassociate unlike units. Intense colors are used for small patches, weaker colors for large. The practice of using strongly contrasting colors for adjacent beds, which seems to be prevalent in terrestrial maps of the Survey, has not been followed on lunar maps in deference to the association principle. The attempt is made to express both rock-stratigraphic and time-stratigraphic relations. Age is usually shown more or less spectrally, colors toward the red for young units, toward the violet for older; oldest (pre-Imbrian) units are brown. Variations of a type of unit are shown by variations of the basic colors--muddy or mixed versus pure.

Line Symbols

A mapper should separate materials and structures clearly in his mind. Materials are mapped in color, structures with black lines. Exceptions, where structures are shown in color for one purpose or another, should be clearly labelled for what they are. (We went through an early trauma in deciding whether rilles should be shown as structures or geologic units; consensus was soon reached that linear rilles are structures (graben), and that rilles with chain craters are materials; but sinuous rilles continue to be shown both ways.)

Line symbols used on lunar maps follow terrestrial precedent as far as possible, with some additional special ones for the Moon. In explanations, all line symbols except completely closed ones, such as those for crater rim crests, are drawn straight; appurtenances, such as barbs, are drawn on top of the line. There is general consistency in style of symbol and wording of the explanation from map to map, but not slavish uniformity. One must always use symbols appropriate to his purpose and describe them in accord with his geology and his interpretations. The only unchanging requirements are clarity and appropriateness; the idea is to describe what you did.

Contacts are the thinnest lines on a map. Draw all other symbols with heavier line weights.

Structures.--The use of fault symbols should be kept to a minimum; many straight features that looked like faults on telescopic photographs are seen on better photographs to be coincidental linear--and even quite non-linear--arrangements of other features. "Inferred" fault is usually better--though unnecessary for a sharp graben. In the absence of removal or stripping of material by erosion, faults do not ordinarily form contacts between units. However, fault scarps, retreated to an unknown degree, may form some contacts by restricting the lateral extent of post-faulting material, so the fault symbol on maps includes such scarps. Faults should be drawn where the projection of the fault intersects the land surface.

A lineament is a negative feature, not an alinement of separated features (to avoid unwarranted connection of unrelated objects). Long, narrow positive features are shown by a dash-cross-dash symbol.

Dashes.--Dashed contacts are commonly overused. Dashes are expensive to draft and leave unattractive white spaces. They should be used only to convey something of interest to the reader, not to express the personality of the mapper; that is, they should express a degree of doubt, not laziness or the fact that the mapper doubts everything. If all contacts are gradational, this fact should be expressed by a blanket note, not dashes. When a mapper draws a line, he is not saying that everything within it is exactly the same, but only different from what is outside, to a degree of accuracy called for by the scale and purpose of the map. Dashes should be used primarily where the photography is exceptionally poor or the contacts especially indistinct or especially gradational. So try to use solid lines, even where you are not completely sure of location within a couple of millimeters (1 mm = 1 km at 1:1,000,000 scale). 1/

Both lunar and terrestrial maps of the Survey have distinguished different kinds of doubt by different dash lengths--long for approximately located, short for inferred or gradational, etc. We have found this tiresome and most authors of lunar maps now use only long dashes.

A reasonable practice on cross sections is: solid contacts where only thickness or position, not presence, of a unit is in doubt; dashed contacts where the

1/ Note added in proof: New Survey policy, probably based on considerations like these, is that dashes will be drafted by BTI only when absolutely necessary.

presence of a unit at that location is inferred. Where hardly anything is known, or where a unit grades with the basement, a scratch boundary is used; that is, a color boundary without a black line (indicate your desire for this type of contact by writing the word "scratch" on your manuscript).

Format

The best way to learn the format that has been used for lunar geologic maps is to study some of the maps, but some salient points should be mentioned first. The format is based on long-standing U.S. Geological Survey practice.

Items on the map sheet (fig. 6) are (1) the map, (2) unit explanation (to right of map), (3) structure-symbol and undated-unit explanation (below unit explanation or map), (4) scale (below map), (5) cross section (below scale), (6) title, author and date (below everything), (7) organization note (upper left corner of map), (8) cooperation note (above map and centered on sheet), (9) credit note and data sources (lower right corner of map), (10) notes on base (lower left corner of map; or left side of map if extensive, as on all 1:1,000,000-series maps), (11) text (left of map unless an extensive base note is there), (12) location of map area (anywhere), and (13) photographic index map (anywhere).

As discussed in the following section, details of this format will be changed for maps submitted for publication from now on. The geologist need concern himself only with the new format for the box explanation.

Explanation

Layout.--A geologic map explanation should show the age relations among the geologic units on the accompanying map, and should describe the units or refer to descriptions available elsewhere in the map package (margins or pamphlet) or in other literature. Each map unit is represented by a box, usually colored, containing its map symbol. To show age relations, these boxes are arranged in chronologic order, the youngest at the top. To show some broad descriptive classification or geographic subdivision, there may be more than one vertical column of boxes, for example, separate columns for crater materials, mare materials, and terra materials, or for a mare province and a terra province.

The Survey is currently (mid-1972) changing the format for map explanations. Formerly, on nearly all lunar maps, age relations and descriptions were shown by a single array of boxes (fig. 6). Unit titles appeared beneath the boxes, and text descriptions beneath the titles. Overlapping or uncertain age relations were shown by braces. On present Survey maps, age relations and descriptions are shown separately (fig. 7). In the upper part of the sheet, the age relations are shown by the arrangement of colored boxes, each containing a map symbol as usual, but without a title or other words outside the box. Age relations are shown partly by braces and partly by vertical overlap of rectangular boxes. Boxes that designate discrete map units should not touch; those that designate subdivisions of a map unit may touch. System and series names are written horizontally and their braces are to the right of all boxes (series braces formerly were on the left); these names should read

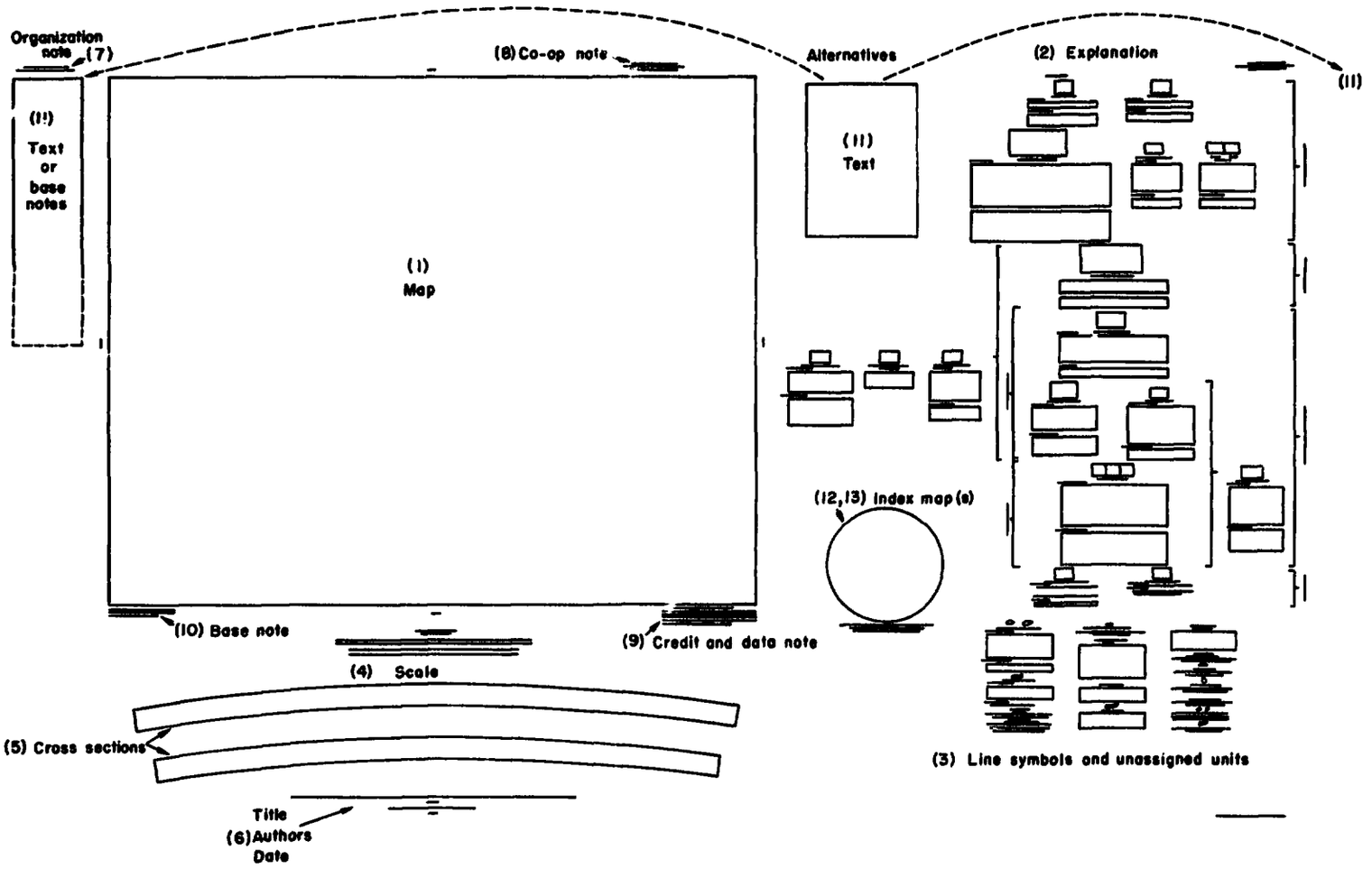

Fig. 6.--Format of typical lunar geologic map sheet.

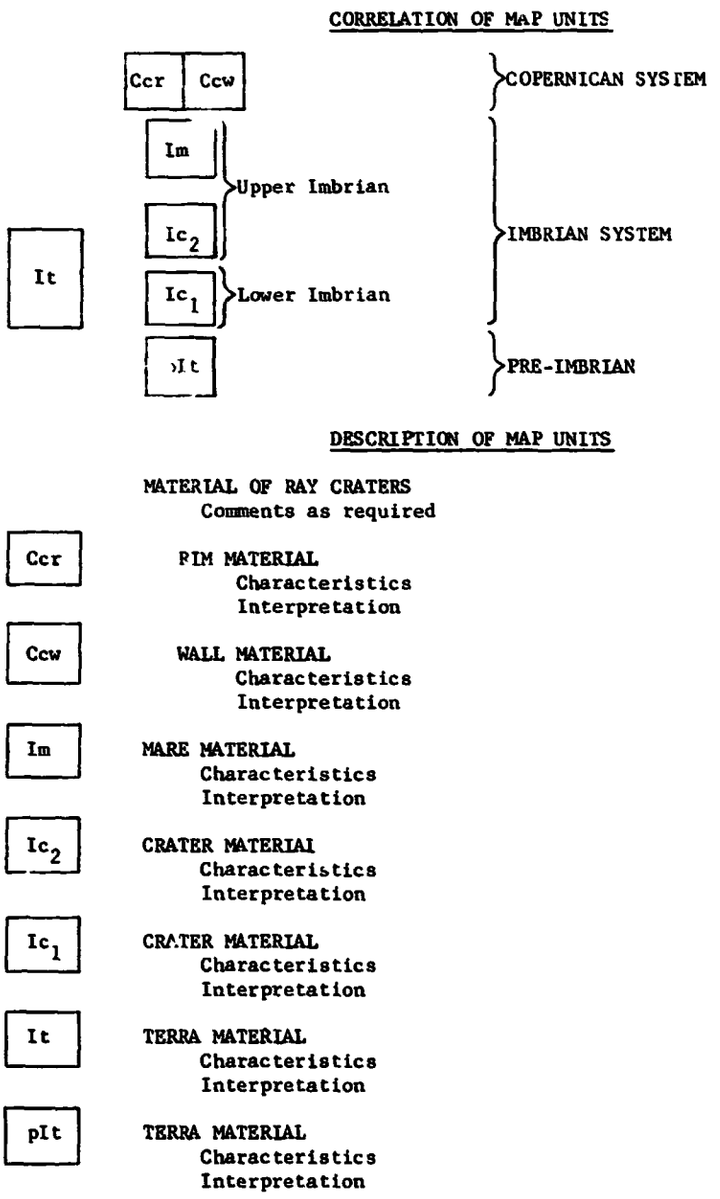

Figure 7.--New U.S. Geological Survey map-explanation format.

from youngest to oldest (ages formerly read from oldest to youngest, opposite from the order of letters in the map symbol). Entirely below this array is a second array for the unit names and descriptions. The colored boxes with the map symbol are repeated, but all are placed in a single vertical column. Box titles are to the right of these boxes, and descriptive material starts to the right of the titles and continues indented below. In both the correlation array and the description array, colored boxes should be placed as close to the map as possible, in order to utilize new electronic color-scanning devices that have a limited reach. Because details of the new format are still being worked out, it will not be described in detail here; a supplement will be sent later to recipients of this manual.

Unit descriptions.--After the box title is a paragraph on physical characteristics, followed by one on genetic interpretations, which must be clearly separated from the characteristics, though of course based on them. ("Characteristics" has come to mean "description," not the strict list of defining properties implied by the word "characteristics.")

For each major and new map unit, a type area, in which the unit is most distinctive, and if possible, where contact relations are clearest, should be given in the "characteristics" paragraph; for newly named formal units, the "should" becomes a "must." To be correlated with this occurrence, other occurrences must possess most of the characteristics of the type area. Definitions of new units should follow the Code of Stratigraphic Nomenclature, with allowances for lunar differences, and must include announcement of intent to establish a new name, bounding coordinates and description of type area, specification of the name-giving geographic feature, and relation to subjacent and superjacent units. (Defining a new formal unit is a weighty matter that should be undertaken only when a widespread stratigraphically important unit requires a name for convenient reference.)

In the explanatory material, use a telegraphic style, and particularly avoid articles and forms of the verb "to be": not, "The unit is of high albedo and has a rugged or partly smooth topographic expression," but "High albedo; rugged or partly smooth." In long descriptions, group similar characteristics in sentences--albedo in one, topography in another, distribution in another, etc. Elements of these sentences can be separated by semicolons. For some reason, the Survey does not put a period or any other punctuation at the end of an explanation paragraph, even if the paragraph includes sentences that do have periods.

Keep the explanation as short as possible, and shoot for a 3,000-word limit on text material (complete-sentence prose). The stick-up type used on maps is fantastically expensive.

Material to Submit

The following materials are required from an author when he submits a map to the Survey:

1. Stable-base copy of original drafting in ink. The base must be translucent; it is normally a plastic such as cronaflex or mylar, preferably about .004" thick (thicker sheets produce poor copies, thinner ones are insufficiently scale-stable). The relief base (imprinted photomechanically on the plastic) must not be in black, or it will interfere with the black geology lines when the two together are copied photomechanically onto the scribecoat to be scribed; we have always used brown. The best strategy is to imprint the base on the back of a double-frosted sheet ("left reading") and draft on the front, so that erasures do not affect the base.
2. A separate sheet for overlays such as ray pattern and dark mantling material. (Note: some authors, if they anticipate numerous changes, compile letter symbols and lines on separate sheets; but this makes ozaliding difficult, so combine symbols and lines before submission.)
3. A completely accurate colored ozalid of the map. This is called the "mill copy" and, after approval by the Director, is used by the Branch of Technical Illustrations (BTI) as their drafting guide; it even supersedes the author's original stable-base inked copy.
4. Text: double-spaced typed copy, preferably on 25-line manuscript paper obtainable from the Survey (ultimately the General Services Administration).
5. Explanation: two possible formats:
   a. Double-spaced typed copy like the text.
   b. Single-spaced copy on a single large sheet of paper, layed out in correct format. (I prefer this style because format and inconsistencies among unit descriptions are clarified; but it is more difficult to construct this large sheet than the page-sized package.)
6. Colored explanation layout, if not in the form of 5b.
7. Marginal notes, index maps, etc. (see section on format).
8. Cross section (optional)--stable base.
9. Cross section (optional)--colored ozalid mill copy.[1/]
10. Duplicate uncolored copies of map, cross section, text, and explanation.
11. And of course, save a copy of everything yourself. You will need these for reference in telephone discussions with reviewers; and the mails do lose things.

Note: On all material the author submits, he must label every patch of every unit. In drafting, BTI will label only as many patches as it believes necessary, because the color of a published map carries most of the story. This point is commonly not understood by authors when they check color proofs; they waste a lot of time pointing out missing labels.

Do's and Don't's

The following is a list of guidelines that will help you prepare better maps. You should consider this list and the ones that follow in all stages of your

1/ Although not always included with the final map package, cross sections (Survey editors call them "geologic sections") should always be drawn, as in terrestrial geology, to test the map relations.

mapping--before, during, and after. The listed items are not supposed to be cliches, but are derived from observations made repeatedly in the course of reviewing and editing lunar maps.

1. Make a reconnaissance of the whole area before starting, and decide tentatively on units; I do this by making a nearly complete map in pencil on a paper copy of the base, before committing ink to a stable-scale copy of the base. This reconnaissance is necessary for internal consistency.
2. Lay out and write the explanation while mapping--not after.
3. Watch embayment relations; at a triple point, the contact of the youngest unit is the continuous one; that is, the contact between the two older units must terminate abruptly at the young one.
4. Remember that you are mapping materials, not topographic forms. This means, for example, that the contact bounding materials of a crater must be drawn not at the rim crest, but at the outer limit of deposits thought to be associated with the crater; these will commonly be expressed only as a slope having no distinctive topographic texture. (if in doubt what to map in an old crater, look at a young crater.)
5. In drafting, remember that you are communicating both to other geologists and to draftsmen who know no geology.
6. You must color out your own map after you think you are finished; you will catch dozens or hundreds of errors.
7. Compare and discuss the geology on your map with authors of adjoining maps; resolve all major conflicts. This will both clarify your mapping and bring the compromise that is essential for consistent portrayal.

Or to put it negatively, following is a partial list of errors that keep cropping up on lunar maps.

1. Inconsistency between map and explanation in the following respects:
    a. Units shown on one but not the other.
    b. Different unit and structure symbols (commonly caused by a change of mind during mapping that is not completely incorporated).
    c. Age relations as shown in explanation differing from those shown on map by the overlap and embayment relations.
2. Units not fully or accurately described in explanation (usually because of being copied from other maps or written after completion of the mapping).
3. Conclusion drawn in interpretation paragraph from relations not mentioned in characteristics; or significance of a characteristic not stated in interpretation paragraph.
4. Reason for age assignment not stated.
5. Inconsistency between map and cross section.
6. Uneven portrayal in different parts of the map (commonly caused by trying to map too much detail early in a project, then giving up).
7. Too much attention to circular craters and their subdivisions, and too little to irregular craters and non-crater units.

8. Incompleteness ("leave it to the reviewer to fix").
9. Ambiguous layout of units in the explanation (very common).
10. Confusion between contacts and structural symbols, especially between dashed contacts and lineaments, and where fault and scarp symbols are at contacts.
11. Lines not closed off.
12. Joins between lines made in the space between dashes rather than on a dash (how can the draftsman tell where to close the line?).
13. Units without symbols.
14. Overprints of symbols and lines.
15. Indistinct leaders (short lines from letter symbol to unit), including confusion with contacts and structures.
16. Ambiguous dash length.
17. Queried units on the map that are not explained in the explanation (always must say "queried where could be younger" or some other specific reason for querying--not just, "queried where doubtful"--though you may say this for structures and contacts).

And as another way of describing errors, I list below two, equally wrong, extremes--because we seek happy mediums.

ONE EXTREME	THE OTHER
Excessive splitting of units that obscures the big picture.	Excessive lumping that ignores significant differences.
Excessively contorted line drawing that (while accurate) crowds the map and obscures the overall relations.	Excessive "cartooning" that ignores significant detail.
Too-careful, time-consuming line drawing.	Sloppy line drawing.
Excessive expression of doubt and qualification; for example, ignoring the great likelihood that craters like Tycho are of impact origin.	Insufficient expression of doubt and qualification; for example, assuming that all craters are of impact origin.
Too detailed or too far-out new ide - more a portrayal of the mind than the Moon.	Too few new ideas--just another map sheet like all others.
Overinterpretation that causes contacts to cross objective boundaries or to be drawn where no differences occur.	Underinterpretation that results in an "objective" terrain map.
Leroy or other time-consuming template lettering.	Unreadable symbols (too faint, too nonstandard, or too sloppy).
Recalculating positions and ignoring the base.	Attempts to match base where the base is very inaccurate.
Copying other maps.	Complete re-invention of the wheel (resulting from poor scholarship).

ONE EXTREME	THE OTHER
Not thinking of implications of the symbols and conventions for units and structures.	Developing own set of completely new conventions.
Repeating all material between text and explanation (the text should summarize and hit the highlights; the explanation is a dictionary).	No tie, or inconsistencies between text and explanation
Going back to first principles (needed once, but no longer).	Addressing work only to other lunar geologists.
Extensive list of characteristics that conveys no mental picture (especially, a list contrived to fit a tortuous interpretive maze).	Brief list of unit characteristics that conveys no mental picture.

Reviewing and Editing

The Survey has a long tradition of thorough reviewing, editing, and reworking of manuscripts.[1/] This process necessarily delays the publication of manuscripts, but usually improves them. Lunar maps, in particular, have gone through an agonizingly long period of examination and reworking--particularly the bad ones, but also the good ones, for we have tried hard to maintain consistency and achieve clarity in the face of continuing scepticism about the validity of our product. Although the job has not been pleasant for reviewers or mapping coordinators, I believe it had to be done. When you have finished a job, all the time you have spent on it is largely forgotten; but the map remains there forever with your name on it, and the name of your organization.

For lunar maps, the Survey review and edit process is as follows: (1) Branch Chief's approval of authorship, title, and scope; (2) coordinator's check of units and format; (3) at least two technical reviews, preferably sequential with author's alterations in between, but sometimes necessarily simultaneous; (4) coordinator's and Lunar Geologic Names (Standards) Committee final check; (5) Branch Chief's review; (6) Technical Reports Unit (TRU) edit of map and (usually) edit of text; (7) Survey Geologic Names Committee's check; (8) Director's approval (seldom any changes; sometimes deletion of excess material); (9) transmittal to Branch of Technical Illustrations (BTI), at which time all changes must cease or be charged monetarily against the author's project. For book reports (professional papers, bulletins, and outside publications), an additional exasperating step comes after approval: Branch of Texts edit and preparation for the printer. Book reports thus go through two independent mills--TRU (Geologic Division) and Branch of Texts (Publications Division). The Survey (Branch of Map Reproduction--BMR) prints maps; the Government Printing Office (GPO) prints book reports.[2/]

1/ Reviewing means technical reviewing for content and organization by a colleague; editing means checking for mechanical defects, spelling, grammar, format, and departure from standards.

2/ Additional information on Survey practice and standards is contained in the manual "Suggestions to Authors of the Reports of the United States Geological Survey" (U.S. Geol. Survey, 1958).

Technical reviewing is probably the most important step in this mill. Not even the best author can communicate perfectly to a reader, because he can never put himself completely in the reader's place; there is always something the author knows that he subconsciously assumes the reader knows, but doesn't. Also, authors are seldom consistent throughout the whole map, text, and explanation. For bad mappers or writers, of course, the review process will illuminate even worse shortcomings. So I cannot emphasize strongly enough the importance of thorough reviews. A review of a map is a major job; it should take several days. A review will not be complete unless the reviewer colors out the map himself while examining the photographs upon which the map was based. He must constantly go back and forth between photos, map, and explanation. So if you are going to undertake a planetary (or any) map, you must be prepared to review heavily and be reviewed heavily. Dividends are improvement of your own map by colleagues' reviews, and improvement of your own mapping by your review of other maps; you learn both the geology of other areas and the techniques of other workers.

Review comments should be helpful, not consist of query marks or sarcastic comments. If the author thought he was wrong or was not communicating, presumably he would have expressed himself differently; so tell him your objection specifically.

Comments on maps, including color proofs, are to be written in the margins, with leaders into the body of the map pointing clearly to the place in question.

All comments by reviewers must be responded to, either by accepting them or rejecting them in writing, usually in notes next to the original comment.

And finally, the faster you turn to the review job when it is given you, the faster the map will be published. Slow reviews are the biggest reason for the Survey's reputation for delayed publication. Because of this, it is now a general Survey rule that when one receives a review job, he drops all other work.

PART III

HISTORY OF THE U.S. GEOLOGICAL SURVEY LUNAR GEOLOGIC MAPPING PROGRAM

Before the space age began in 1957, most investigators concentrated on topical studies of selected lunar features (craters, lineament patterns, etc.) for the purpose of deducing their origin, or confirming a prejudice for either exclusive impact or exclusive volcanic origin of lunar features. Some whole-Moon studies were performed, including extensive ones by people with a bias for internal origin (Shaler, Spurr, von Bülow, Khabakov), and less elaborate ones by those favoring impact or mixed origins (Gilbert, Baldwin, Kuiper).[1/] Few lunar students looked systematically for stratigraphic sequences in lunar rocks, and almost all thought in terms of physiographic forms (craters) not materials (crater rim materials). What was lacking was a systematic, stratigraphically-based geologic mapping effort that incorporated as strict a separation of interpretation and observation as possible; this combination has been the charter of the Survey's program.

Two principal Survey products stimulated by the dawning space age preceded the main mapping program. In the first, for the Army Corps of Engineers, photogeologist Robert J. Hackman drew a map at a scale of 1:3,800,000 showing three stratigraphic units--pre-mare, mare, and post-mare (Hackman and Mason, 1961). This map was accompanied by maps showing rayed craters and physiographic provinces (chiefly Hackman) and by rather bold terrain evaluations and geologic interpretations (chiefly Mason). In the course of this work Hackman suspected the time lag between the formation of the Imbrium basin and its filling by mare material, because of the excess of fairly fresh (so presumably post-basin) craters on the terra (Hackman, oral communication, 1971). In a concurrent and independent effort, Shoemaker was systematically mapping the Copernicus region in greater stratigraphic detail, at the scale of 1:1,000,000. Except in its use of interpretive unit names, this map was to become the prototype for the 44 lunar quadrangles of the main Survey systematic effort. A small experimental edition was printed in color, but not released to the public, by the U.S. Air Force Aeronautical Chart and Information Center (ACIC). The base was a prototype shaded relief chart made by ACIC.[2/]

1/ In all European lunar geological publications I have seen, an internal origin is favored for all or nearly all lunar features, and the same was true in America before the space age; exceptions were the works of Gilbert, Barrell, and Dietz. It was the astronomers who favored the impact hypothesis, and they were scorned as "catastrophists" by the geologists, probably still defending themselves against bible-based pre-geology. The current acceptance among American geologists of impact as a major--but, emphatically not sole--lunar process is probably due to Shoemaker, who saw the validity of the arguments of Gilbert and Baldwin, and who helped discover new terrestrial impact craters. The Soviet and other European geologists apparently still prefer to explain nearly all lunar phenomena by analogy with terrestrial phenomena familiar to them.

2/ See next page.

(The map also appeared in color in the November 1963 edition of "Fortune.") While mapping, Shoemaker recognized the fundamental stratigraphic succession: Imbrium basin - mare material - Eratosthenes - Copernicus. This map demonstrated, against considerable skepticism and opposition, the validity of the geologic mapping approach to lunar studies. As a result of this demonstration and the active support of John O'Keefe (NASA Headquarters), Manfred Eimer (JPL), Robert Carder (ACIC), and Lorin Stieff (USGS), the systematic mapping program began under NASA sponsorship.

The stratigraphy that Shoemaker had worked out, a statement of stratigraphic principles that underlie lunar geologic mapping, and a black-and-white version of the Copernicus prototype map were published in a joint paper by the two pioneers (Shoemaker and Hackman, 1962) and in a paper on interpretation of craters by Shoemaker (1962).

The first three maps published in the systematic program--Kepler, Letronne, and Riphaeus Mountains--showed essentially three types of units--crater materials, mare materials, and terra materials; only the crater materials were extensively subdivided by age and facies. On one of the maps in an early violation of the principle of separation of interpretation and observation, smooth plains and hummocky materials were both assigned to a unit which was believed to be the ejecta blanket of the Imbrium basin.[1/] Such distinct units should always be distinguished in mapping even if they ultimately prove to have similar origins. The maps, like the early stratigraphic system of Shoemaker and Hackman (1962), also failed to separate clearly rock-stratigraphic and time-stratigraphic units, such as the rock unit "mare material" and the time-stratigraphic unit "Procellarian System." An important advance was recognition of the presence of Imbrian-age craters, those that are younger than the Imbrium basin but older than the mare material.

In late 1962 and early 1963 a group of new mappers was recruited by Shoemaker to augment and partly replace the quartet of himself, Hackman, Marshall, and Eggleton; a year later the newcomers were ready to pressure the establishment to make certain changes. (These young Turks are now, of course, the establishment.) Good agreement was reached at a stratigraphic conference of all mappers in November 1963. Rock-stratigraphic and time-stratigraphic units were firmly separated

1/ For a discussion of this unit's nomenclature history, see Wilhelms, 1970, p. F23-F27).

2/ (From preceding page). The Copernicus base chart by ACIC was the prototype of their highly useful and well executed series of 44 Lunar Astronautical Charts (LAC) which are the bases for all the Survey 1:1,000,000 geologic maps and which give their names to the maps. The airbrush technique proposed by ACIC, like our geologic mapping technique, was at first regarded as unscientific, old-fashioned, and impossible to do systematically. However, the technique was successfully demonstrated on the prototype, and ACIC began its systematic production of the maps under Robert Carder in St. Louis and William Cannell at Lowell Observatory in Flagstaff. This very productive and at times brilliantly effective effort was concluded in early 1969. The cooperation between ACIC has continued, and all Survey lunar maps have been printed on ACIC bases except a few large-scale maps of potential Apollo landing sites, printed on Army Map Service (Topocom) photomosaics.

(McCauley, 1967, p. 437; Wilhelms, 1970, p. F11, F23, F30-F32); formational names were introduced, and the splitting of units was accelerated. The basic time-stratigraphic units and the general mapping philosophy agreed on at this meeting have proved adequate for completion of the rest of the 1:1,000,000-scale program and the recent compilation of the whole area of 44 quadrangles at a scale of 1:5,000,000 (Wilhelms and McCauley, 1971). Subsequent changes in conventions became increasingly minor as the mapping progressed. Two additional meetings of all mappers were necessary to adjust some of the mapping conventions. Now, changes are handled by filtering them through the mapping coordinator, who listens to ideas and then passes them around to the other mappers for approval or rejection.

The conventions adopted at the 1963 meeting have proved flexible enough to permit a slight apparent retrogression; formational names have been down-played on recent maps and informal designations substituted. For example, the Cayley Formation and Apennine Bench Formation are now usually called "light plains material," and the Gassendi Group of crater materials, younger than the Humorum basin but older than the mare material, is now called "crater materials." This is done because it is each individual occurrence of a type of material, not the aggregate, that is equivalent to a terrestrial formation, but each cannot be given a name. So all plains patches or craters in a given time-stratigraphic system are grouped together and designated informally.

The downplaying of formational names became particularly necessary when the mapping moved from the mare and circumbasin regions, with their laterally extensive marker units useful in regional correlations, to the southern cratered highlands, which seemed to offer no such clearcut stratigraphy. Early examination, based on telescopic photography and visual observations, revealed essentially three types of topography: craters, plains, and hilly intervening terrain ("moonite"). Most authors saw no good laterally continuous units in the hilly terrain which showed a more patchwork texture than the circumbasin units, although some (Cummings, Offield) believed it to be mantled by extensive beds of volcanic material. Plains units were segregated according to crater density, but only three distinct classes of completely flat plains were recognized. An early attempt was made to set up discrete, alternating rock-stratigraphic groups of crater materials and plains materials (Cozad and Titley, unpublished), but the stratigraphy proved too complicated for this. Highland geologic studies did not progress much until Lunar Orbiter photographs became available (1967). Textures of the hilly units could then be better evaluated, and as a result, several units of possible terra volcanics and one additional distinct basin ejecta blanket (Nectaris) were distinguished; but some hilly terrain has not been separated into consistently recognizable units, and may never be (still "moonite"). One of the previously recognized plains units was found to be pre-Imbrian in age, and most other plains were seen to form a fairly uniform Imbrian assemblage. Craters came to be ranked

stratigraphically according to their morphology and to serve as "guide fossils" (Pohn and Offield, 1970; Wilhelms and McCauley, 1971). A fairly good understanding of the highlands is now in hand; although indeed without many laterally continuous units, their geology is explainable in terms of basins or absence of basins, accumulations of plains materials wherever there are depressions, and possibly, local superposition of positive volcanic landforms.

A word in retrospect about the utility of visual telescopic observations. ACIC used them to great advantage, overcoming the initial scepticism mentioned earlier, and improved greatly on the photographic data. Some geologic mappers also used them successfully to "field check" relations that appeared ambiguous on photographs, for example, the age of a crater relative to the adjacent mare material (determined from the presence or absence of secondary impact craters, which are commonly very small). And all mappers saw much more detail at the telescope than on the early primitive telescopic photographs--though not always more than on the excellent series taken by G. H. Herbig at the Lick Observatory 120-inch reflector--and got a good impression of the important effect on feature detectability of changing illumination. But as work progressed we began to realize that we were spending too much time to gain too little information. Only a few critical relations were ever tested at the telescope, and most geological insights were gained from protracted studies of large regions on photographs. And later when we compared our telescopic notes with Orbiter photographs, most of us realized that we had not seen things accurately enough for good geologic interpretation; lines of "volcanic craters" became miscellaneous semi-alined depressions or spaces between hills; "faults" became ragged scarps. Much of this was due to the rarity of good seeing. But in any case, visual observations are seldom testable; even valid observations are not scientifically acceptable unless others can confirm them.

Mapping at scales larger than 1:1,000,000 began in 1964 on the basis of Ranger photographs (Trask, in press). Four black-and-white maps were incorporated in another report, seven black-and-white ozalid preliminary maps were made, and six maps were published in color, the last in late 1971. The long time lag between the flights of the Ranger spacecraft and the publication of the last Ranger maps is due to the low priority given these maps when better data from Lunar Orbiter were acquired.[1/]

Maps based on photographs from Lunar Orbiters I, II, III, and V in support of Apollo landings were produced starting in 1966. A great many (27) were produced quickly for screening reports printed by the Langley Research Center, where the (highly competent) Lunar Orbiter Project Office was located. Seven of the areas were remapped for the Manned Spacecraft Center at two scales, 1:25,000 and 1:100,000, and in several versions each, for use in planning Apollo missions to the maria; five of these maps at 1:25,000 and seven at 1:100,000 have been

1/ Hansen (1970) and McGill and Chizook (1971) have prepared user's guides to Orbiter photographs, and Bowker and Hughes (1971) have compiled a complete atlas that includes a user's guide.

printed in color. (Two of the areas became landing sites.) The 1:100,000-scale maps have the greater scientific interest, largely because they show more stratigraphic variety and place the geology of the sites in a broader context.

Currently, maps at large scale have been or are being prepared for landings starting with Apollo 14, the (predominantly) non-mare missions. These maps are more interesting to make and read than those of the mare sites because they cover geologically more diverse terrain, and, significantly, because most of them include relatively fresh features. At large scales, most of the Moon is quite uniform and subdued-appearing and becomes diverse only in young features, whose distinctive textures have not yet become degraded.

Another way of seeing a diverse Moon is to look at it from a distance. The mapping based on Lunar Orbiter IV photographs (starting May 1967) has probably been the most interesting and productive of all. These photographs have been used to modify 20 of the 36 1:1,000,000-scale quadrangles partly mapped at the telescope and to map 8 more quadrangles in their entirety. The 1:5,000,000-scale near-side map (Wilhelms and McCauley, 1971) was satisfying to make and is a good medium of communication for the important things, though it is a little crowded. The time, money, and base maps that are available coincide with this preference, and mapping of the two-thirds of the Moon not covered by the near-side map is being done at the 1:5,000,000-scale.[1/]

A short account of the effectiveness of the early quick-look work versus the later, drawn-out, inductive mapping will be of interest to mappers attacking a new planet. Some of the basic facts about the Moon's structure and evolution were thought out early in the game by Gilbert (1893), Hackman and Mason (1961), Shoemaker (1962), Baldwin (1949, 1963), and Kuiper (1959). They saw that most craters and the basins were of impact origin, but that the basins were filled in a relatively brief time by volcanic mare material. Also, quite early, Baldwin (1949), Shoemaker, and Hackman (see above) perceived the important fact that a time gap intervened between basin formation and filling. Important contributions of the later mapping were the recognition of the light terra plains as a major unit that apparently belonged neither to the basins or the maria, and the tentative recognition, on Lunar Orbiter photographs, of terra volcanics (bright, positive relief). The impact origin of the basins was clinched by studies of the Orientale basin and the discovery, through systematic mapping, of the Orientale, Imbrium, and Nectaris secondary craters. Moreover, the fundamental role played by the basins in nearly every way became clearer, including their influence on volcanism and the major contributions by buried and degraded basin ejecta to the total volume of lunar surface materials. Apollo radiometric dates have shown that the "relatively brief time" of mare formation is brief if the total number of lunar feature-forming events is taken as the scale, but that substantial mare formation actually occupies a con-

1/ Given the best possible photography I believe that a scale of 1:2,500,000 would be optimum for mapping the Moon. Smaller scales are crowded and do lose some data of interest, such as small fresh features, whereas the information that can be shown at larger scales is not very significant in most regions, because of the smooth appearance of most terrain.

siderable portion (half a billion years) of the total most active part of lunar history (the first 1 1/2 billion years). The impact-volcanic controversy for crater origin has shifted in favor of impact, but some craters are certainly of volcanic origin.

In summary, the early work deduced some origins, and the later work documented these origins, charted the extent of the various units, deduced the three-dimensional structure over much of the crust, and discovered new fundamental units. This has resulted in a good model of the structure and evolution of the Moon that puts each crustal component in perspective of the whole. The problem with emphasizing origins is that nearly everyone plays with only certain ones. Several people that did this may have been right, but many others were wrong for one reason or another--including selection of analogs that contain only those elements that nourish special prejudices. So insight can establish working hypotheses, but these must be tested, modified, and amplified by systematic study, which forces examination of the geometric relations, areal distribution, and sequence of formation of all crustal elements.

REFERENCES

Albritton, C. C., Jr., 1963, Fabric of geology: Reading, Mass., Addison-Wesley, 372 p.

American Commission on Stratigraphic Nomenclature, 1970, Code of stratigraphic nomenclature: Am. Assoc. Petroleum Geologists. Reproduced in "Stratigraphic nomenclature in reports of the U.S. Geological Survey," 1970.

Baldwin, R. G., 1949, The face of the Moon: Chicago, Univ. Chicago Press, 239 p.

_____ 1963, The measure of the Moon: Chicago, Univ. Chicago Press, 488 p.

Bowker, D. E., and Hughes, J. K., 1971, Lunar Orbiter photographic atlas of the Moon: Natl. Aeronautics and Space Admin. SP-206.

Carr, M. H., ed., 1970, A strategy for the geologic exploration of the planets: U.S. Geol. Survey Circ. 640, 37 p.

Fielder, Gilbert, 1965, Lunar geology: London, Lutterworth Press, 184 p.

Gilbert, G. K., 1893, The Moon's face--a study of the origin of its features: Philos. Soc. Washington Bull., v. 12, p. 241-292.

Hackman, R. J., 1966, Geologic map of the Montes Apeninnus region of the Moon: U.S. Geol. Survey Misc. Geol. Inv. Map I-463.

Hackman, R. J., and Mason, A. C., 1961, Engineer special study of the surface of the Moon: U.S. Geol. Survey Misc. Geol. Inv. Map I-351 (3 maps and expl.).

Hansen, T. P., 1970, Guide to Lunar Orbiter photographs: Natl. Aeronautics and Space Admin. SP-242, 125 p.

Khabakov, A. V., 1962, Characteristic features of the relief of the Moon--Basic problems of the genesis and sequence of development of lunar formations, in Markov, A. V., ed., The Moon, a Russian view (translated from the Russian edition of 1960 by Royer and Royer, Inc.): Chicago, Ill., Univ. Chicago Press, p. 247-303.

Kuiper, G. P., 1959, The exploration of the Moon, in Vistas in astronautics, v. 2: New York, Pergamon Press, p. 273-313.

McCauley, J. F., 1967, The nature of the lunar surface as determined by systematic geologic mapping, in Runcorn, S. K., ed., Mantles of the Earth and terrestrial planets: New York, Interscience, p. 431-460.

McCauley, J. F., and Wilhelms, D.E., 1971, Geological provinces of the near side of the Moon: Icarus, v. 15, no. 3, p. 363-367.

McGill, G. E., and Chizook, P. A., 1971, Use of Lunar Orbiter photographs in Earth Science courses: Jour. Geol. Education, v. 19, no. 1, p. 21-26.

Milton, D. J., 1968, Geologic map of the Theophilus quadrangle of the Moon: U.S. Geol. Survey Misc. Geol. Inv. Map I-546.

Mutch, T. A., 1970, Geology of the Moon--A stratigraphic view: Princeton, J. J., Princeton Univ. Press, 324 p.

Peive, A. V., ed., 1969, Problemi geologii luni (problems of lunar geology): Nauka, Moscow, 291 p. (in Russian).

Pohn, H. A., and Offield, T. W., 1970, Lunar crater morphology and relative age determination of lunar geologic units--Pt. 1: Classification, in Geological Survey Research 1970: U.S. Geol. Survey Prof. Paper 700-C, p. C153-C162.

Pohn, H. A., and Wildey, R. L., 1970, A photoelectric-photographic study of the normal albedo of the Moon: U.S. Geol. Survey Prof. Paper 599-E, 20 p.

Ronca, L. B., 1965, Selenology vs. geology of the Moon, etc.: Geotimes, v. 9, no. 9, p. 13.

Shoemaker, E. M., 1962, Interpretation of lunar craters, in Kopal, Zdeněk, ed., Physics and astronomy of the Moon: New York, Academic Press, p. 283-459.

Shoemaker, E. M., and Hackman, R. J., 1962, Stratigraphic basis for a lunar time scale, in Kopal, Zdeněk, and Mikhailov, Z. K., eds., The Moon--Intern. Astron. Union Symposium 14, Leningrad 1960 Proc.: New York, Academic Press, p. 289-300.

Soderblom, L. A., and Lebofsky, L. A., 1972, Technique for the rapid determination of relative ages of lunar surface areas from orbital photography: Jour. Geophys. Research, v. 77, no. 2, p. 279-296.

Sukhanov, A. L., Trifonov, V. G., and Florenskiy, P. V., 1967, Geologic and physiographic mapping of the Moon and some structural features of the lunar surface: Geotectonica, no. 5, p. 327-332 (translated from the Russian).

Trask, N. J., 1970, Geologic maps of early Apollo landing sites: Suppl. to U.S. Geol. Survey Misc. Geol. Inv. Maps I-616 to I-627.

_____ in press, Ranger photographs of the Moon: U.S. Geol. Survey Prof. Paper 599-J.

U.S. Geological Survey, 1958, Suggestions to authors of the reports of the United States Geological Survey: Government Printing Office, Washington, D. C., 255 p. (fifth edition).

Wilhelms, D. E., 1970, Summary of lunar stratigraphy--Telescopic observations: U.S. Geol. Survey Prof. Paper 599-F, 47 p.

Wilhelms, D. E., and McCauley, J. F., 1971, Geologic map of the near side of the Moon: U.S. Geol. Survey Misc. Geol. Inv. Map I-703.

With permission, reprinted from ICARUS, vol. 15, no. 3, December 1971, pp. 363–367.

Geological Provinces of the Near Side of the Moon[1]

J. F. McCAULEY AND D. E. WILHELMS

U.S. Geological Survey, Center of Astrogeology, Flagstaff, Arizona 86001

Received July 23, 1971; revised August 2, 1971

Systematic geologic mapping of the near side of the Moon has provided the basis for defining and delineating the major geological provinces of the near side. From the nature of the provinces and their distribution patterns a general historical sequence evolves. Five main surface-shaping periods are recognized: (1) one of intense early impact cratering; (2) another, probably overlapping the first, during which the impact basins were formed; (3) a prolonged period of varied terra volcanism; (4) a short period of mare volcanism that resulted in filling of the multiring basins; and (5) a period of diminishing volcanic activity continuing up to the time of formation of the last ray craters.

The relative sequence in which most of the Moon's major surface features formed has been determined from systematic lunar geologic mapping begun by the U.S. Geological Survey in 1961 (Shoemaker and Hackman, 1962; McCauley, 1967; Wilhelms, 1970). The data used were almost exclusively photographic, starting with the best available telescopic photographs and later supplemented by the Ranger, Surveyor, and Lunar Orbiter photographs. The most productive of these flights from the standpoint of an improved regional understanding of the Moon was Orbiter IV which provided nearly uniform 80-m resolution coverage of most of the near side. Preparation of a geologic map of the near side at 1:5,000,000 scale commenced with the final acquisition of the Orbiter IV data late in 1967. This map (Wilhelms and McCauley, 1971) is a synthesis built upon the results from the 44 quadrangles of the U.S. Geological Survey's 1:1,000,000 scale systematic program and it summarizes our current understanding of the regional geology of the near side. It was completed in manuscript form prior to Apollo 11; preliminary Apollo 11 and 12 results were, however, incorporated during manuscript processing. These data are consistent with the previously determined relative stratigraphy and the lithologic interpretations presented in the text that accompanies the map.

Various derivative products that depict certain aspects of the Moon's crustal evolution have been prepared from the near side map. One of these to be published at the 1:10,000,000 scale shows the major geologic provinces as now recognized (McCauley and Wilhelms, in preparation). It is reproduced in generalized form and at reduced scale in Fig. 1 which represents an interim product pending review and publication of the 1:10,000,000 scale map.

As in the case of terrestrial geologic province maps, each unit consists of a related rock assemblage and is characterized by a similar inferred origin or a distinctive history. The provinces differ markedly in relative age and regional distribution pattern; it is these differences that lead to a general understanding of the sequential evolution of the near side.

A descriptive name and a generalized order of formation, from the youngest to the oldest, is given in the caption of Fig. 1. The younger provincial units lie mostly in depressions and are interpreted as volcanic in origin. These include the dark mantles (dm) which cover terra units of lighter albedo and frequently lie across mare-terra contacts. They are interpreted as thin veneers of pyroclastic materials that formed contemporaneously with some

[1] Publication authorized by the Director, U.S. Geological Survey.

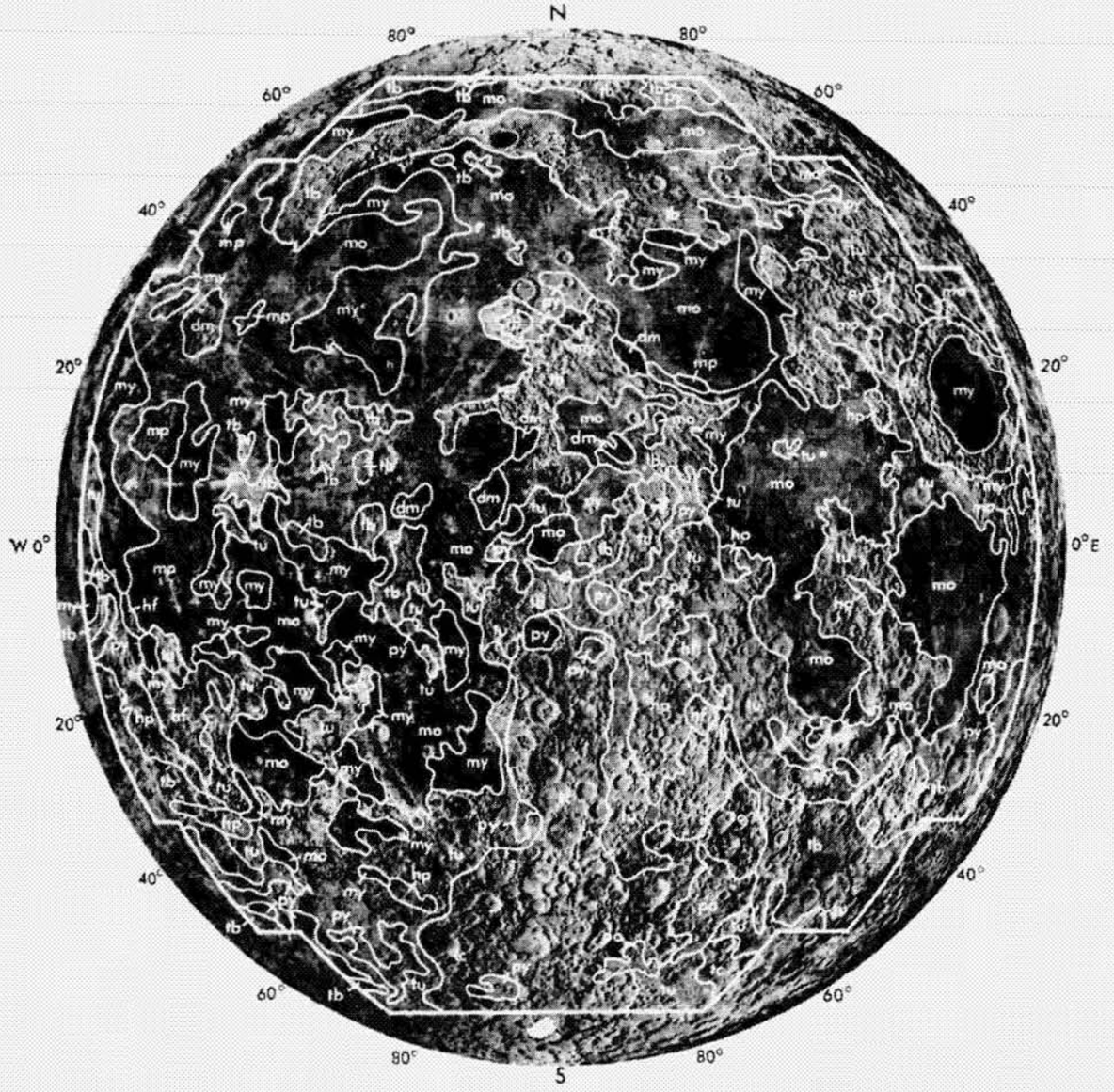

FIG. 1. Geologic provinces of the near side of the Moon. Approximate scale 1:25,000,000. Base is Mosaic LEM-1, 3rd edition, 1966, prepared by the U.S. Air Force Aeronautical and Chart Information Center. Explanation of geologic symbols: dm—dark mantles; mp—mare plateaus; my—mare, young; mo—mare, old; py—plains, young; hf—hilly and furrowed; hp—hilly and pitted; tb—terra of younger basins; po—plains, old; tu—terra, undivided; tc—terra, cratered. Solid line indicates province boundary, dashed where obscured by younger (unmapped) deposits.

of the mare basalts but which are mostly later than the main pulse of mare flooding. Their very dark albedo suggests a distinctive composition and possibly a more deep seated origin than for the maria. The plateau units (mp) within the maria, of which the Marius Hills region is the largest and best example, consist predominantly of aggregates of cones and domes that lie on broadly elevated plateaus or shield-like structures. These plateaus are later than the adjacent maria and are interpreted to consist of pyroclastics and relatively viscous flows of the same or more probably slightly different composition than the maria (McCauley, 1969). They may represent the late stage fractionation products of mare flooding, and thereby be more felsic in composition. The younger mare (my) is generally darker, less cratered, and more patchy in its distribution than most of the older mare exposed on the near side. Contacts tend to be gradational or are diffuse because of superposed ray cover. Some boundaries, however, are coincident with faint color differences (McCord, 1969). This unit is interpreted to consist of relatively thin flows with possible subordinate pyroclastic deposits present. The unit mapped probably resembles petrologically the rocks sampled by Apollo 12. The older mare (mo) is of dark to intermediate albedo and lies almost exclusively within the major near side multiring basins or in concentrically positioned structural troughs that are part of their associated "ring" systems. The surface of this unit marks the end of the main pulse of mare flooding and it defines the top of the Imbrian System (Wilhelms, 1970). Representative samples of this unit were collected during the Apollo 11 mission. The young plains (py) of light albedo partly fill some of the basins, irregular terra depressions, and the floors of large ancient terra craters. Where in contact with the mare they are embayed and, therefore, older than the mare; they also show a demonstrably higher frequency of small craters. This unit, although subordinate in areal extent to the mare materials on the near side, is of considerable significance as a Moon-wide depression filler; on the far side it occupies the floors of most of the multiring basins and large craters. Its origin remains unclear. It could consist mostly of impact-lightened older mare or compositionally distinct volcanic flows that preceded the main pulse of near-side magmatic activity.

Two distinct types of terra that appear to modify older more densely cratered surfaces are now recognized and their distribution pattern shown on the map (units hf and hp). The first, which is described mostly as hilly and furrowed, consists of closely spaced linear structures with interspersed equidimensional hills. The linear structures show furrows along their crests and closely resemble terrestrial fissure cones. The second unit consists of rolling plains and plateaus which show numerous closely spaced rimless or smooth rimmed pits, mostly in the 2–6km size range. Within these provinces few large pre-Imbrian craters are present; those that do occur appear to be embayed or partly covered by these units. Both are interpreted as volcanic in origin and as the products of a pre-mare episode of terra volcanism that is probably compositionally distinct from the later basalt flooding of the near side basins (Wilhelms and McCauley, 1969). One patch of hilly and furrowed material in the Descartes region is the current target for Apollo 16.

The terra of the younger basins (tb) consists of the recognizable ejecta blankets, the elevated and most prominent parts of the encompassing structural rings, and the radially lineated terrain surrounding the three youngest near-side basins—Orientale, Imbrium, and Nectaris. Also included is the most prominent ring around the Crisium basin although it does not show a now recognizable ejecta blanket. This unit is interpreted as a lithologically complex mixture of shocked and unshocked breccias excavated from deep within the central parts of the basin and redistributed as much as a 1000km or more over the Moon's surface. Rocks of this type were sampled in the Fra Mauro region during the Apollo 14 mission. They clearly should consist of relatively primitive lunar materials—some

of which may be magmatic—and the reworked ejecta of the older basin blankets and impact craters that were located within the region of the crater produced during multiring basin formation. Heavily cratered plains (po) fill several large depressions in the southeast quadrant of the near side. Most of the superposed craters appear to be of Imbrian age and many are probable secondary impact craters of the Imbrium basin. These plains generally resemble those of unit py but were emplaced before the Imbrium event whereas unit py truncates many Imbrium related structures. These older plains are, however, younger than the Nectaris event which is of pre-Imbrian age. Their general similarity to the younger plains suggests a common origin.

The most extensive near-side terra province (tu) consists of nondescript blocky hills and unevenly filled irregular to sometimes linear depressions along with what appear to be segments of mantled craters. Probable volcanic landforms are sparsely distributed and the unit most likely consists largely of erosionally degraded, interlayered ejecta from the more ancient near-side basins such as Crisium, Humorum, and Serenitatis. Cratered terra (tc) occupies most of the south-central part of the near side. This unit was named the macro-crater province by Hackman and Mason (1961). It consists mostly of closely spaced 50–150km craters of early pre-Imbrian age; probable volcanic materials, except for the terra plains in crater floors, are absent as are recognizable basin related deposits. The almost shoulder to shoulder array of ancient craters which characterizes this province suggests that it represents a very primitive surface little modified by later internal activity or basin-forming events. It lies outside the range of deposition and structural dislocation associated with multiring basin formation, which probably accounts for its preservation.

The definition and delineation of these major near-side provinces yields the following general historical sequence: (1) An early period of intense bombardment that produced a surface essentially saturated with craters in the 50–150km size range. (2) A period of impact basin formation, probably overlapping the first period, during which ejecta blankets were emplaced around all of the multiring basins; older basin structures and blankets were catastrophically aged by the newer. (3) A period of terra volcanism which began during basin formation and continued at least until after the Imbrium event. Some of the younger plains, appear to postdate Orientale. (4) A main pulse of basaltic volcanism, also of relatively short duration, which flooded the depressed parts of the near-side basins to varying levels. (5) Diminished volcanic activity, possibly of distinct composition, continuing up through the time of formation of the last ray craters. Contemporaneously with these last four major evolutionary episodes, impact cratering continued but probably at a progressively diminishing rate, for simplicity these craters have not been included; where present and of large size (on the order of 100km) the major provincial boundaries have been extrapolated beneath these younger features.

References

Hackman, R. J., and Mason, A. C. (1961). Engineer special study of the surface of the Moon. *U.S. Geol. Survey Misc. Geol. Inv.* Map I-351.

McCord, T. B. (1969). Color differences on the lunar surface. *J. Geophys. Res.* **74**, 3131–3142.

McCauley, J. F. (1967). The nature of the lunar surface as determined by systematic geologic mapping. *In* "Mantles of the Earth and Terrestrial Planets" (S. K. Runcorn, Ed.), pp. 431–460. Interscience, New York.

McCauley, J. F. (1969). The cones and domes of the Marius Hills region. *Trans. Amer. Geophys. Union* **50**, 229.

McCauley, J. F., and Wilhelms, D. E. (in preparation). The geologic provinces of the near side of the Moon.

Shoemaker, E. M., and Hackman, R. J. (1962). Stratigraphic basin for a lunar time scale. *In* "The Moon—Symposium 14 of the International Astronomical Union" (Z. Kopal and Z. K. Mikhailov, Eds.), pp. 289–300. Academic Press, New York.

WILHELMS, D. E. (1970). Summary of lunar stratigraphy—Telescopic observations. *U.S. Geol. Survey Prof. Paper* 599-F, 47.

WILHELMS, D. E., AND MCCAULEY, J. F. (1967). Volcanic materials in the lunar terrae—Orbiter observations. *Trans. Amer. Geophys. Union* 50, 230.

WILHELMS, D. E., AND MCCAULEY, J. F. (1971). Geologic map of the near side of the Moon. *U.S. Geol. Survey Misc. Geol. Inv.* Map I-703.

Two Former Faces of the Moon

DON E. WILHELMS AND DONALD E. DAVIS[1]

U.S. Geological Survey, Menlo Park, California 94025

Received July 23, 1971; revised July 30, 1971

Systematic geologic mapping of the lunar near side has resulted in the assignment of relative ages to most visible features. As a derivative of this work, geologic and artistic interpretations have been combined to produce reconstructions of the Moon's appearance at two significant points in its history. The reconstructions, although generalized, show the Moon (1) as it probably appeared about 3.3 billion years ago after most of the mare materials had accumulated, and (2) about 4.0 billion years ago after formation of the youngest of the large multiringed basins, but prior to appreciable flooding by mare material.

Two reconstructions of the visual appearance of the Moon at geologically significant points in its evolution have been derived from the results of the U.S. Geological Survey's lunar geologic mapping program as recently summarized in a 1 : 5,000,000-scale map of the near side (Wilhelms and McCauley, 1971; McCauley and Wilhelms, 1971). Geological and artistic interpretations have been combined to produce these geological visualizations. The present Moon and the features discussed in this paper are shown in Fig. 1. The artist, Davis, working principally under the guidance of Wilhelms, used the 1 : 5,000,000 geologic map to identify features younger than the top of the mare basalt sequence that fills to varying levels the near side multiring basins. These younger features were then removed from the Moon's present face for the first reconstruction (Fig. 2). An older stratigraphic datum—the top of the Orientale ejecta blanket (the Hevelius Formation)—was similarly used for the second reconstruction (Fig. 3). Features older than these stratigraphic horizons were enhanced or freshened according to their position in the relative stratigraphic sequence determined during the geologic mapping. Most of the older major craters are assumed to have had an initial morphology like that of the young craters Copernicus or Tycho. In the second reconstruction, where visible evidence was lacking because of mare flooding, the interior parts of the multiring basins were assumed to be similar to those of the youngest of these structures, Orientale, the geology of which has been summarized by Mutch (1970, pp. 143–156). Also by analogy the nature of the now partly buried ejecta blankets recognized around the Imbrium (Fra Mauro Formation) and Nectaris (Janssen Formation) basins were assumed to be similar to the better preserved blanket around Orientale.

The first reconstruction (Fig. 2) represents the Moon after deposition of most of the mare material but before the formation of the major post-mare deposits and craters—that is, at the end of the Imbrian Period or the beginning of the Eratosthenian Period. Dating of Apollo 11 and 12 rocks, whose relative stratigraphic position had previously been determined photogeologically, suggests that this time was about 3.3 billion years ago. The Moon's appearance at this time is relatively easy to reconstruct because post-mare materials obscure only a small percentage of the surface. The underlying topography is partly visible through all but the innermost deposits of the Eratosthenian (rayless) and Copernican (rayed) craters, and these collectively cover only about

[1] Publication authorized by the Director, U.S. Geological Survey.

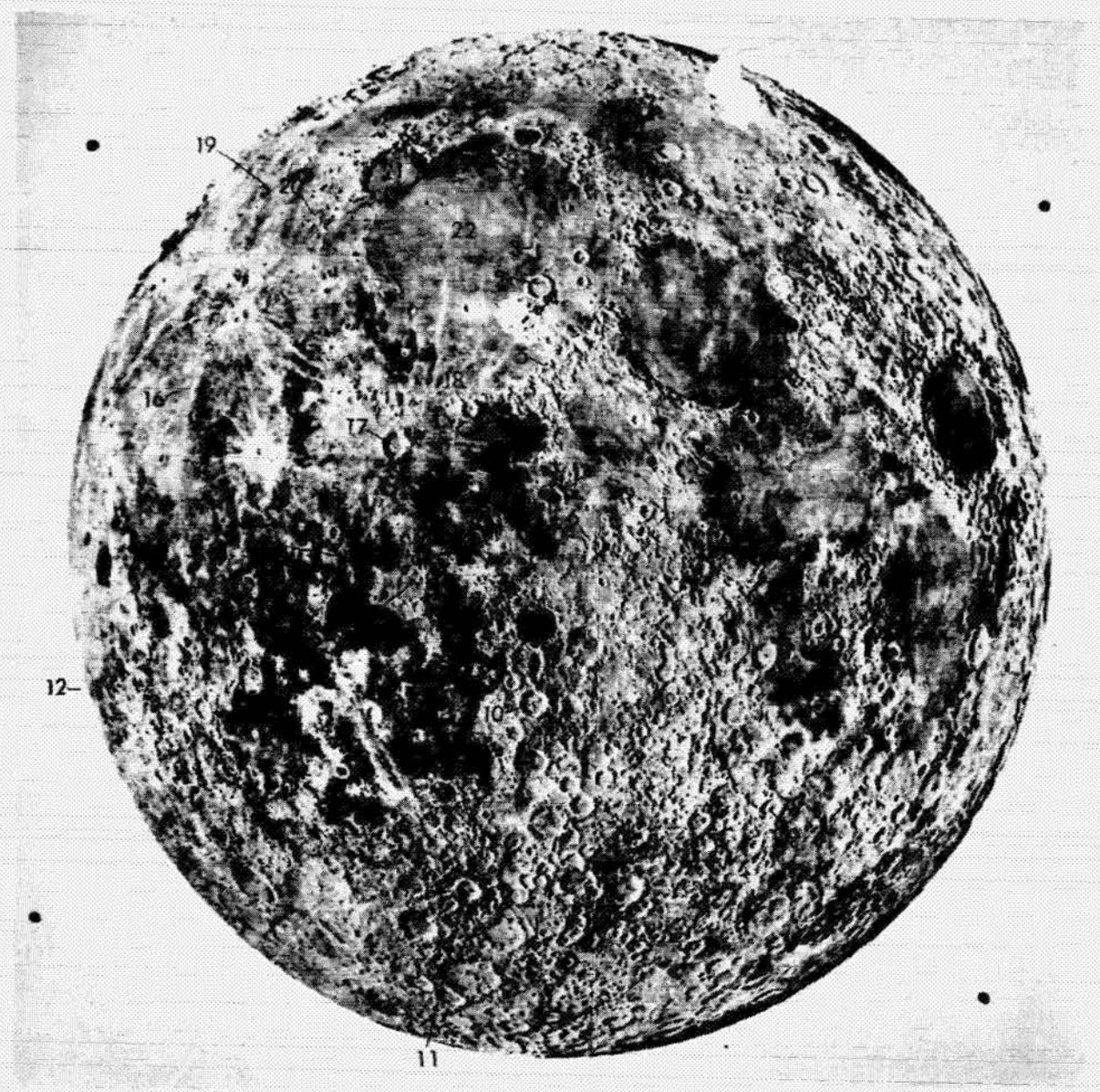

FIG. 1. The present Moon. Mosaic LEM-1, 3rd edition, 1966, made from telescopic photographs by U.S. Air Force Aeronautical Chart and *Information Center*. Places or features mentioned in the text are: 1, Plato; 2, Archimedes; 3–6, Imbrium basin rings; 7, Apollo 11 landing site; 8 Mare Nectaris; 9, Piccolomini; 10, Arzachel; 11, Tycho; 12, Orientale basin; 13, Fra Mauro; 14, Apollo 14 landing site; 15, Apollo 12 landing site; 16, Marius hills; 17, Copernicus; 18, Eratosthenes; 19, Rümker; 20, Gruithuisen domes; 21, Sinus Iridum; 22, Mare Imbrium.

2% of the near side. Post-mare deposits unrelated to craters are even rarer; the artist had to remove only the steep bright domes near Gruithuisen, the low mare domes, the mare plateaus such as the Marius and Rümker hills, and the dark deposits that thinly mantle the terra at the edges of some maria. Craters formed just before the main pulse of mare flooding, such as Archimedes and Plato, were freshened so that the exposed parts of these late Imbrian craters resemble Copernican craters. Everything on this reconstruction thus represents something now visible,

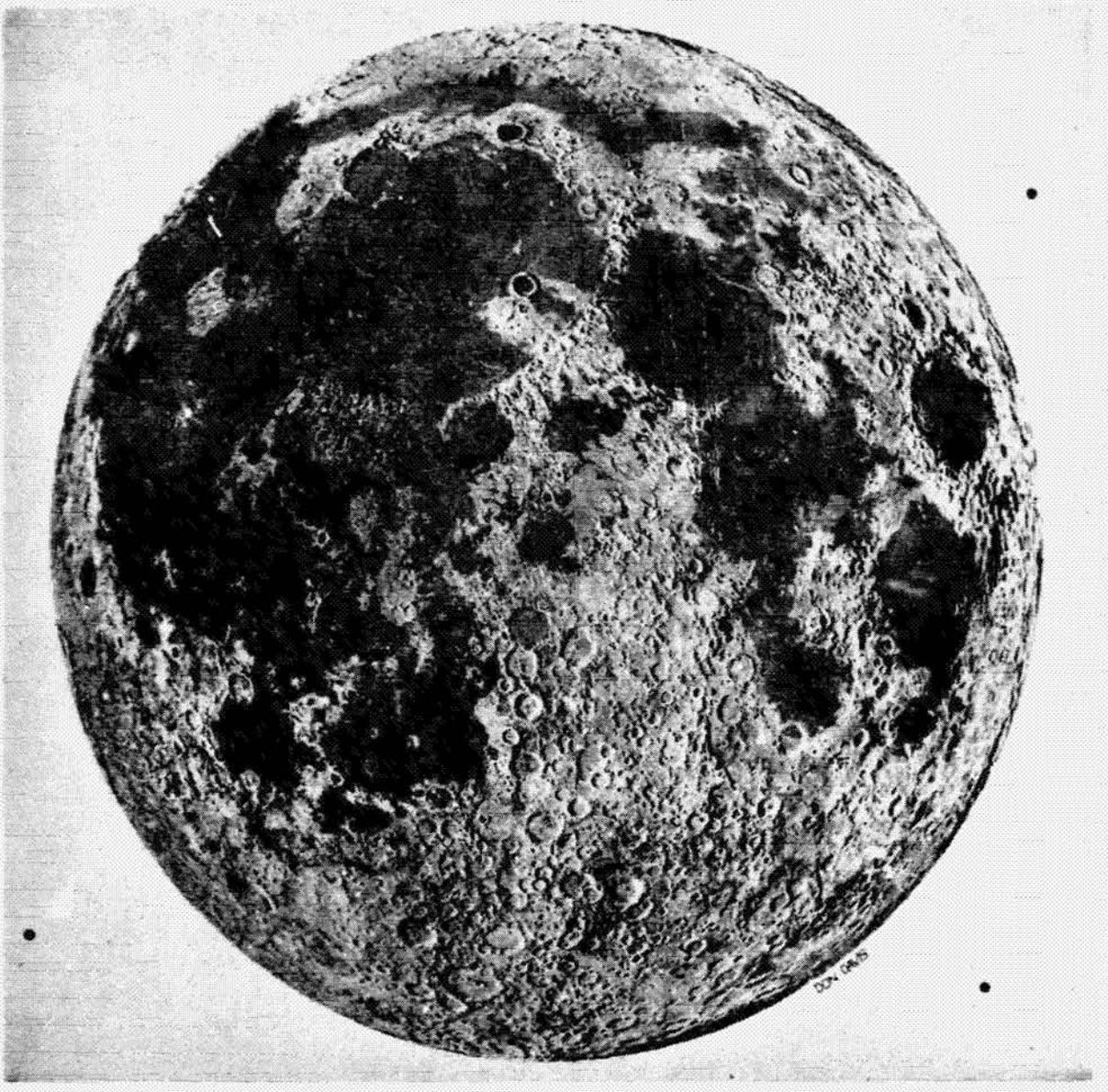

FIG. 2. The Moon at the end of the Imbrian Period, soon after the formation of most of the mare material approximately 3.3 billion years ago. Note the absence of such young craters as Tycho, Copernicus, and Eratosthenes from the otherwise not too unfamiliar scene.

but altered in appearance according to relative age.

The mare surfaces are shown darker and with sharper contacts than for the present Moon mainly because of the absence of overlying crater rays. Rays are not shown because for simplicity it is assumed that all the late Imbrian mare material formed after all the late Imbrian craters, thereby covering the rays which these craters had when first formed. However, pre-Apollo studies of crater frequencies and the somewhat divergent dates of the Apollo 11 and 12 samples (3.6–3.7 and 3.3 b.y., respectively) show that all mare material did not form exactly at the same time although the peak of mare generation appears to have occurred in late Imbrian time. The most significant feature of this reconstruction is that in

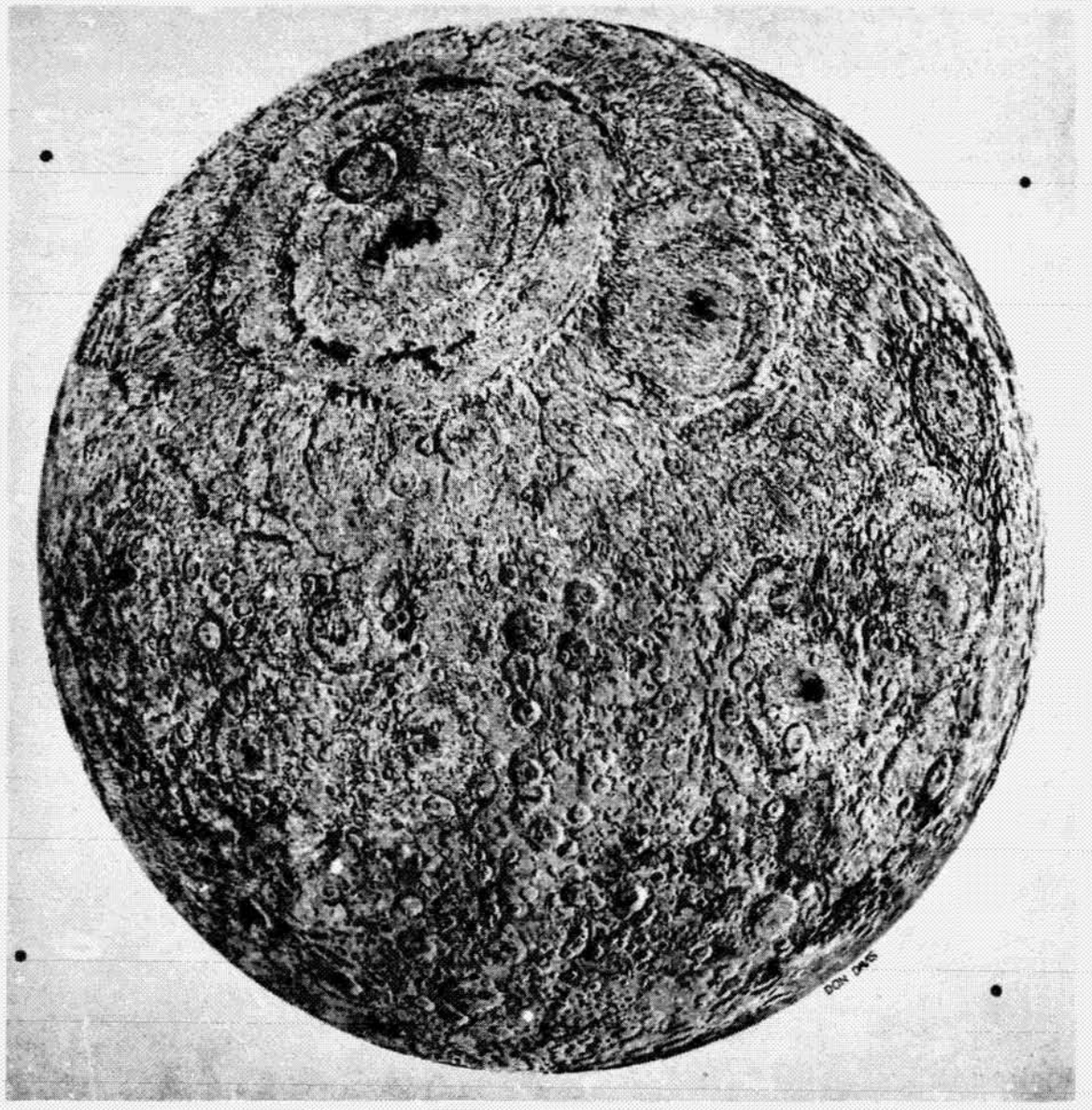

FIG. 3. The Moon in the middle of the Imbrian Period, before the formation of the present mare surface material and after the formation of the last of the mare basins, Mare Orientale (partly in view on the west limb). Features exhumed by the artist include the fully developed, yet unburied Iridum crater, perched on one of the rings of the Imbrium basin.

spite of the very ancient time represented—less than half way through the history of the Moon—the Moon's surface looks much like the present Moon and people unfamiliar with its surface details must look carefully to detect the differences.

The second reconstruction (Fig. 3) shows the Moon at a still earlier time in its history, before the rocks of the present mare surface were emplaced and shortly after the youngest multiringed basin, Orientale, was formed. This is approximately in the middle of the Imbrian Period, perhaps four billion years ago. The artist, therefore, removed most mare material and late Imbrian craters and freshened early Imbrian craters such as Arzachel and Piccolomini. Without the mare cover and other deposits, the geological dominance of the structures and

blankets of the multiringed basins is strikingly revealed. Predominant among these is the Imbrium basin whose deposits, the Fra Mauro Formation, were probably sampled during the Apollo 14 mission. Although the artist necessarily had to add details for which there is no direct evidence, the pre-mare appearance of the Imbrium basin can be reconstructed with a fair degree of accuracy from the present appearance of the relatively nonflooded Orientale basin. Those features associated with the Imbrium basin now exposed at the surface appear to be the erosionally degraded equivalents of similarly positioned features of the Orientale basin.

Craters shown in regions now covered by mare materials were reconstructed where a partial rim crest or ghost-ring structure is present. Incipient mare fill is shown where the greatest present concentrations presumably exist—in the deepest depressions, especially those basins that contain "mascons." The amount of mare material portrayed in Fig. 3 is dependent on the depth of the basin or depression, not upon the age, because several lines of stratigraphic evidence imply that mare age is independent of basin age.

Light plains, which appear to be mostly older than the maria, are shown at each locality where now present but in somewhat diminished amount. Some light plains are also shown in deep places now buried by mare material in the multiringed circular basins. Possibly more light material is present than is shown. This would be true if the plains were formed by extensive Moon-wide eruptions of "terra-type" (felsic) magmas. In this case even this very ancient lunar face would closely resemble the present-day Moon, except for the higher albedo of the basin-filling plains.

Reconstructions farther back into the Moon's past are possible, though they would be increasingly speculative in details, particularly because of our present ignorance of the role of volcanism in early lunar history. A reconstruction in pre-Imbrian time would show a Moon much like that of Fig. 3, but without the Imbrium basin and with the older basins appearing considerably fresher. Successively older faces would lack increasingly more of the presently known basins and craters, and would contain others now obliterated or unrecognized.

References

McCauley, J. F., and Wilhelms, D. E. (1971). Geological provinces of the near side of the Moon. *Icarus* **15**, 363–367.

Mutch, T. A. (1970). "Geology of the Moon—A Stratigraphic View." Princeton Univ. Press, Princeton, N.J.

Wilhelms, D. E., and McCauley, J. F. (1971). Geologic map of the near side of the Moon. U.S. Geol. Survey Misc. Geol. Inv. Map I-703.

CHAPTER VII – LUNAR BASINS

MULTI-RING BASINS AND MASCONS

Keith A. Howard
U. S. Geological Survey, Menlo Park, Calif. 94025

The significance of huge circular or multi-ring basins on the Moon was pointed out by G. K. Gilbert (1893). He interpreted the basins as impact scars, and all the most recent evidence agrees. Gilbert was followed by several volcanic enthusiasts, but an impact origin was again favored for the basins by the detailed descriptions of Baldwin (1963) and Hartmann and Kuiper (1962). Apollo samples of breccias from basin-related materials seem to confirm an impact origin. The distribution of identifiable basin ejecta, as mapped by Wilhelms and McCauley (1971), is shown in figure 1.

The Soviet spacecrafts Lunik 3 and Zond 3 showed that dark maria were uncommon on the lunar far side, but as shown in figure 2, basins are as common there as on the near side (Stuart-Alexander and Howard, 1970). This relation emphasizes the important concept (Shoemaker and Hackman, 1962; Wilhelms, 1970) that basins are distinct from the mare rocks that fill them. Post-basin filling by mare rocks has hidden much of the Imbrium Basin from view. The sequence of modification of Imbrium is depicted by figures 3–6. The early geography of the Imbrium Basin (fig. 3) was reconstructed by comparison with a fresher and less flooded example, the Orientale Basin (fig. 7).

The Orientale Basin has served as a type example for studies of basin stratigraphy and structure (McCauley, 1967, 1968; Masursky, 1968, Mutch, 1970). Older basins are similar but more degraded and more heavily cratered (fig. 8) (Stuart-Alexander and Howard, 1970; Hartmann and Wood, 1971). Geologic mapping of Orientale (fig. 9) reveals several stratigraphic units. Crackled floor material in the inner basin may be a thick layer of impact melt (fig. 10(a)). Knobby material between the third (Rook) and fourth (Cordillera) mountain rings is puzzling but may represent slumped ejecta. Radially lineated ejecta outside the basin is named the Hevelius Formation. The Hevelius covers pre-existing craters and is distributed widely, thus demonstrating a catastrophic origin for the basin. Parts of the Hevelius have been compared in texture to turbidites, to avalanches, and to pyroclastic flows. Patterns in the Hevelius thus suggest deposition as a ground-hugging flow, likened to a base surge by McCauley (1968) and Masursky (1968). This base-surge concept remains controversial because the source of any interstitial fluids is unknown. Lunar samples of probable basin ejecta at the Apollo 14 and 17 sites (table 1) show evidence of high temperature and suggest the ejecta was hot. Many hundreds of kilometers outside the basin, the Hevelius grades outward to smooth mantles and plains deposits. Clusters of craters 5 to 25 km across radiate from the basin and are confidently interpreted as secondary impact craters. The basin formed quickly and required such enormous energies (estimates range from 10^{31} to 10^{32} ergs) that any internal origin is inadequate. The basin must be the product of a very large impact.

The bullseye structure of Orientale is made by several concentric mountain rings with steep inward-facing scarps (figs. 7, 10(a)). The two main hypotheses for these rings are that they are fault scarps formed by collapse into the transient basin (Hartmann and Kuiper, 1963; McCauley, 1968) or that they are frozen tsunamilike waves (Van Dorn, 1968; Baldwin, 1972); possibly both hypotheses are correct.

Uplift of the rim (Baldwin, 1972) favors a wave origin, whereas the steepness and freshness of the wall scarps favor a fault origin. A fault origin for at least the outer scarp is also favored by comparison with small 2-ring basins such as Schrödinger and Antoniadi (fig. 11(a)). At these small basins, the wall scarp clearly represents a series of slump terraces, just as in large craters (fig. 11(b)). Peak rings in the center seem to be transitional with central peaks of large craters (fig. 11) and may be bedrock uplifts. Experience with terrestrial impact and explosion craters shows that downward and inward movements along slump faults at the crater margin are expressed in the substructure. These displacements are matched by inward and upward movement under the center of the crater. These adjustments apparently occur during or immediately following crater formation (Milton and Roddy, 1972). If the analogy can be extended to multi-ring basins (Dence, 1972; Howard *et al.*, 1974), then downfaulting at the basin margins may go together with huge uplifts of the lunar mantle under the basin center (fig. 10(b)). Such a geometry would be consistent with the observed gravity profile at Orientale (fig. 10(b)).

Large positive gravity anomalies characterize all obvious mare-filled circular basins on the near side. The gravity field was identified from anomalous accelerations of Lunar Orbiters (Muller and Sjogren, 1968). The positive free-air anomalies represent mass concentrations nicknamed mascons. Most mascons seem best explained as thin discs of dense mare basalt (Conel and Holstrom, 1968); the relative contributions of mantle uplifts (Wise and Yates, 1970), such as is depicted in figure 10(b), is uncertain. Mascons represent loads in excess of isostasy that have existed since the undeformed mare lavas were emplaced approximately 3.5 b.y. ago. Recent studies of mare stratigraphy and structure in the Serenitatis basin reveal that the early mare lavas (c.a. 3.7 m.y. old) sagged into the basin but the youngest lavas are relatively undeformed (fig. 12). This sequence may record a progressive stiffening or thickening of the lunar lithosphere.

Recent geologic mapping of the lunar limbs and far side, together with Apollo results, appear to confirm that multi-ring basins account for most or all pre-mare regional deposits and structures expressed in the lunar landscape (Howard *et al.*, 1974). Highland deposits of plains, furrowed and pitted terrain, and various hills, domes, and craters that were interpreted before the Apollo missions as volcanic can now be interpreted as basin-related. A province map of the whole Moon (fig. 2) shows that the relatively young Orientale and Imbrium basins imprinted and rejuvenated much of the Moon's surface; older basins must have also. The most primitive cratered surface remaining is mostly on the far side, distant from Imbrium and Orientale and other large relatively young basins. All five lunar landings in the highlands sampled stratigraphic units probably related to basins (table 1).

Several nearly obliterated basins have been discovered recently, including a deep one on the far side that is as wide as the Moon's radius. The presence of these ancient basins suggests that the surface is effectively saturated by basins and that many others were completely destroyed by later impacts. The visible basins formed after solidification of the lunar crust. Basin impacts may have churned the crust to large depths. Now that multi-ring basins are known on the Moon, Mars (Wilhelms, 1973), and Mercury, it seems likely that such basins were important in shaping the early Earth's crust also.

REFERENCES

Baldwin, R. B.: The measure of the Moon. Chicago, Univ. of Chicago Press, 488 p., 1963.

Baldwin, R. B.: The Tsunami model of the origin of ring structures concentric with large lunar craters. Phys. Earth Planet. Interiors, v. 6, p. 327-339, 1972.

Conel, J. E.; and Holstrom, G. B.: Lunar mascons – a near-surface interpretation. Science, v. 162, n. 3860, p. 1403-1405, 1968.

Dence, M. R.: Meteorite impact craters and the structure of the Sudbury basin. Geol. Assoc. Canada, Spec. Paper No. 10, 18 pp., 1972.

Hartmann, W. K.; and Kuiper, G. P.: Concentric structures surrounding lunar basins. Arizona Univ., Lunar Planetary Lab. Comm., v. 1, no. 12, p. 51-66, 1962.

Hartmann, W. K.; and Wood, C. A.: Moon: Origin and evolution of multi-ring basins. The Moon, v. 3, no. 1, p. 3-78, 1971.

Howard, K. A.; Carr, M. H.; and Muehlberger, W. R.: Basalt stratigraphy of southern Mare Serenitatis, *in* Apollo 17 preliminary science report, NASA SP-330, p. 29-1 to 29-12, 1973.

Howard, K. A.; Wilhelms, D. E.; and Scott, D. H.: Lunar basin formation and highland stratigraphy. Reviews of Geophysics and Space Physics (in press), 1974.

McCauley, J. F.: The nature of the lunar surface as determined by systematic geologic mapping, *in* Runcorn, S. K., ed., Mantles of the earth and terrestrial planets, Interscience Publishers, John Wiley & Sons, p. 431-460, 1967.

McCauley, J. F.: Geologic results from the lunar precursor probes. AIAA Jour., v. 6, n. 10, p. 1991-1996, 1968.

McGetchin, T. R.; Settle, M.; and Head, J. W.: Radial thickness variation in impact crater ejecta: Implications for lunar basin deposits. Earth Planetary Sci. Lett., v. 20, p. 226-236, 1973.

Masursky, Harold: Preliminary geologic interpretations of Lunar Orbiter photography, *in* Hearings before the Subcommittee on Space Science and Applications of the Committee on Science and Astronautics, U.S. House of Representatives, Ninetieth Congress, Second Session, on H.R. 15086, p. 665-691, 1968.

Milton, D. J.; and Roddy, D. J.: Displacements within impact craters. 24th Internatl. Geol. Congress, Montreal, Sect. 15, p. 119-124, 1972.

Muller, P. M.; and Sjogren, W. L.: Mascons: Lunar mass concentrations. Science, v. 171, no. 3842, p. 680-684, 1968.

Mutch, T. A.: Geology of the Moon: a stratigraphic view. Princeton, N.J., Princeton Univ. Press, 324 p., 1970.

Shoemaker, E. M.; and Hackman, R. J.: Stratigraphic basis for a lunar time scale, *in* Kopal, Zdeněk and Mikhailov, Z. K., eds., The Moon – Symposium No. 14 of the Internatl. Astronom. Union. London, Academic Press, p. 289-300, 1962.

Stuart-Alexander, D. E.; and Howard, K. A.: Lunar maria and circular basins – a review. Icarus, v. 12, p. 440-456, 1970.

Van Dorn, W. G.: Tsunamis on the Moon? Nature, v. 226, no. 5172, p. 1102-1107, 1968.

Wilhelms, D. E.: Summary of lunar stratigraphy – telescopic observations. U.S. Geol. Survey Prof. Paper 599-F, 1970.

Wilhelms, D. E.: Comparison of Martian and Lunar multi-ringed circular basins. Jour. Geophys. Res., v. 78, n. 20, p. 4084-4095, 1973.

Wilhelms, D. E.; and McCauley, J. F.: Geologic map of the near side of the Moon. U.S. Geol. Survey Misc. Geol. Inv. Map I-703, 1971.

Wise, D. U.; and Yates, M. T.: Mascons as structural relief on a lunar "moho." Jour. Geophys. Res., v. 75, n. 2, p. 261-268, 1970.

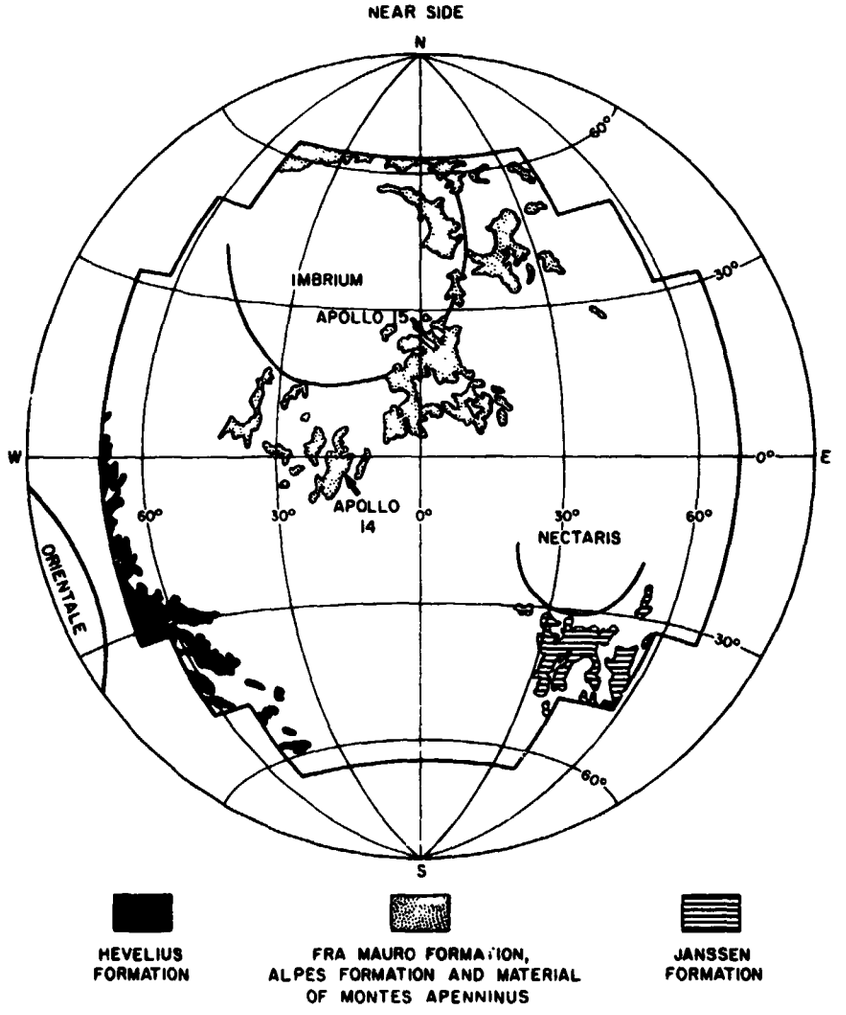

Figure 1.– Near side of the Moon showing textured basin ejecta as identified by Wilhelms and McCauley (1971) of the three freshest basins. Lambert equal-area projection.

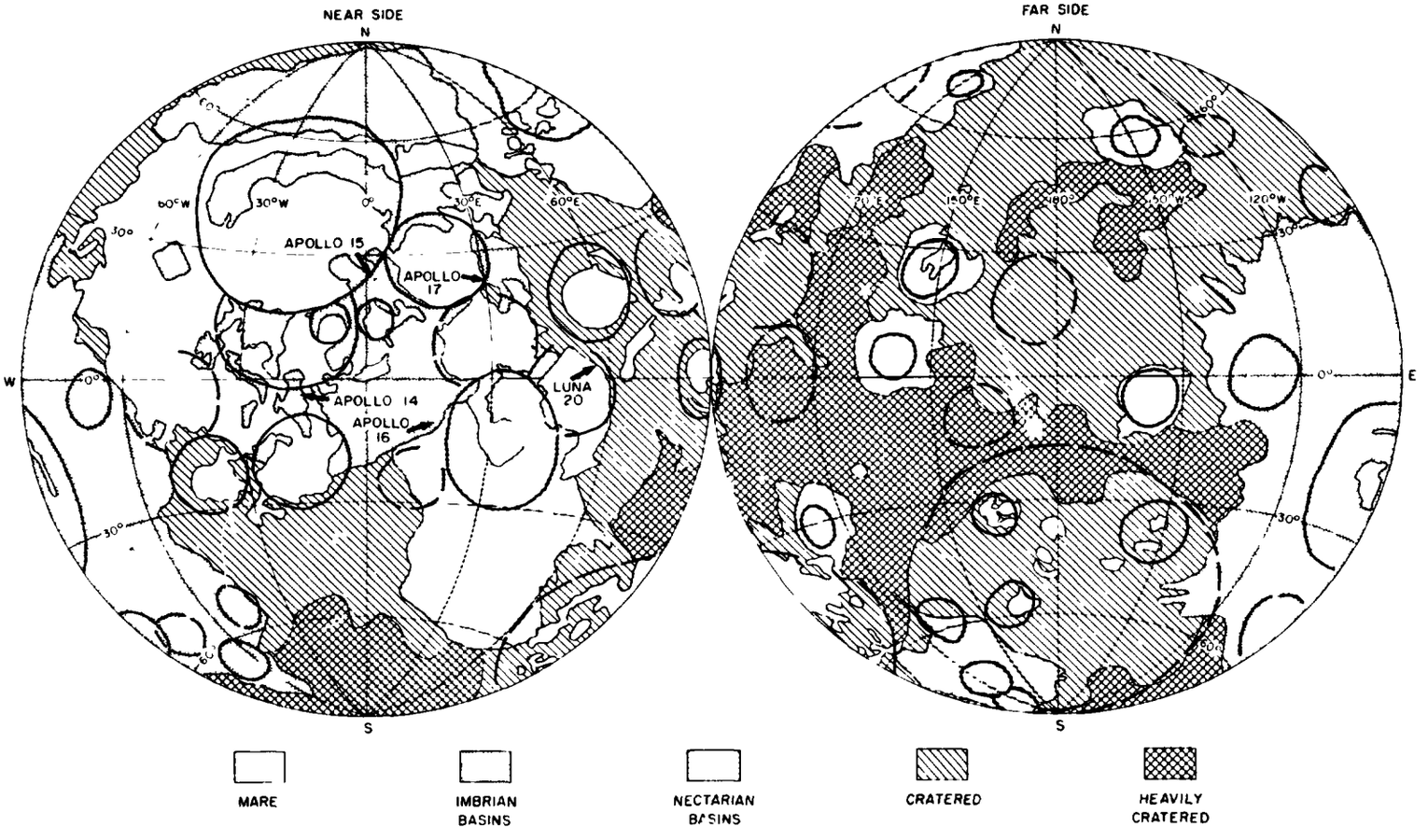

Figure 2. – Preliminary province map of the lunar highlands, based on liberal interpretations of basin-related terrain. Recognized basins and landing sites in highlands are indicated. Imbrian Basin *and* Nectarian Basin *provinces are terrains recognized to have been rejuvenated by basin-forming events of Imbrian and Nectarian age (Nectarian is a new formal stratigraphic term that encompasses the upper part of the pre-Imbrian). The province designated* cratered *includes numerous older basins. The* heavily cratered *province consists of overlapping craters and basins and is the most primitive lunar terrain; it occurs mainly on the far side distant from the rejuvenating influence of the Nectarian and especially Imbrian basins. From Howard* et al. *(1974).*

Opposite:

Figu. 3.– The first of a series of four views of the northern hemisphere (turn illustration so that the limb is at the top) of the Moon. This and the following sketches by Don Davis under the direction of Don Wilhelms (U.S.G.S., Menlo Park, Calif.) are based on geologic maps made at the U. S. Geological Survey. The lunar surface is shown as it appeared approximately 4 billion years ago. The most prominent feature is the Serenitatis Basin (upper right) and a slightly larger and older multi-ringed basin near the center. Courtesy of Don Wilhelms.

Opposite:

Figure 4. – The northern hemisphere (turn illustration so that the limb is at the top) approximately 3.8 billion years ago. The Imbrium Basin (top) was formed by a gigantic impact approximately 3.9 billion years ago. Through analogy with the partly mare-filled Orientale Basin, mare units were initially emplaced within the central basin and along the base of the mountainous rings. These mare units are believed to reflect a period of internal heating, probably related to the decay of radiogenic nuclei. Note the bright-rayed crater, Archimedes, on the second outer Imbrium ring and the Iridum crater on the same ring near the limb. Also note the two small multi-ringed basins (center right, see fig. 3) that have been inundated by Imbrium ejecta; these eventually will correspond to Sinus Aestuum and Mare Vaporum. Illustration courtesy of Don Wilhelms.

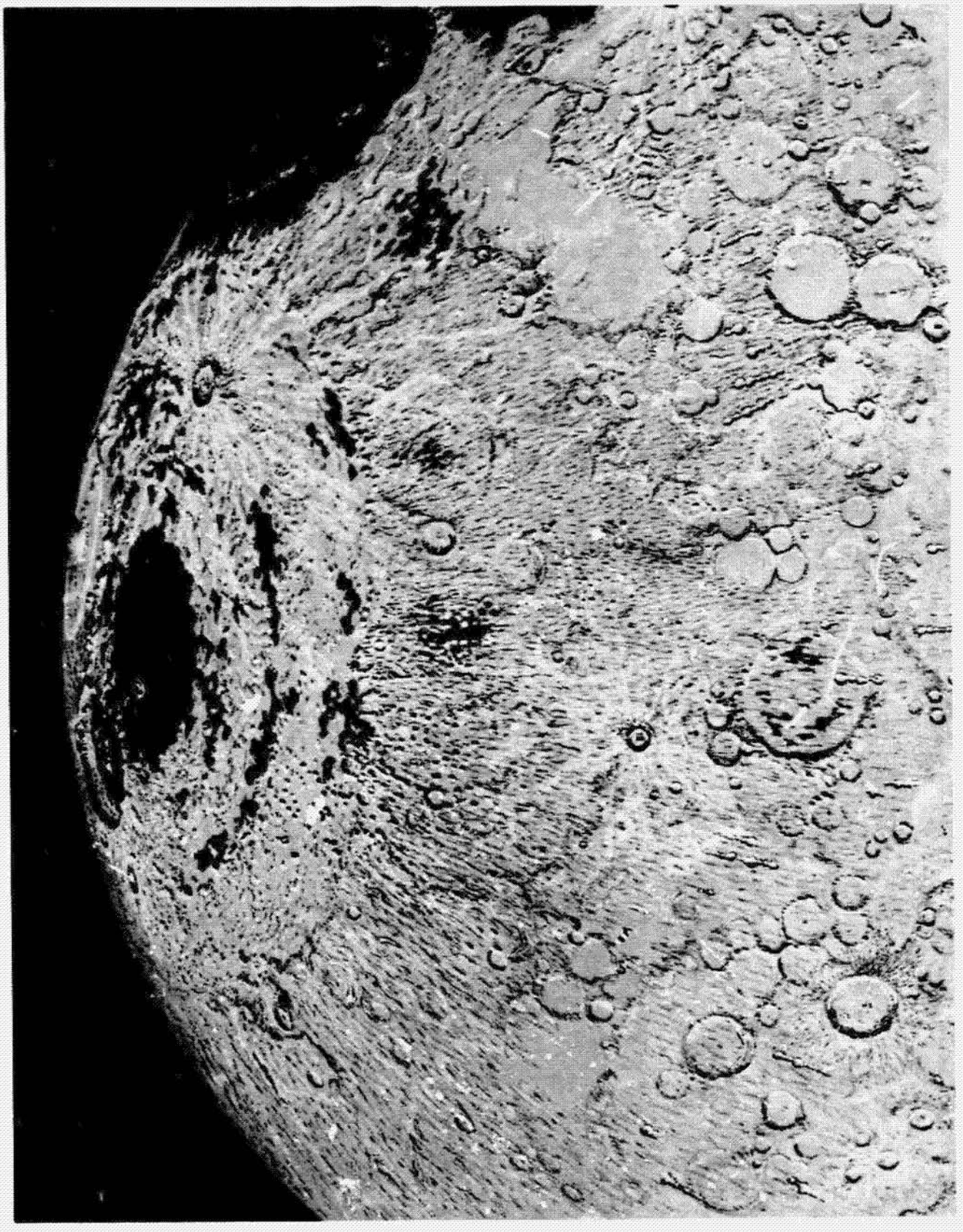

Opposite:

Figure 5.– The last eruptions of mare units, approximately 2.5 billion years ago (turn illustration so that the limb is at the top). Between 3.8 b.y. and 3.0 b.y., most of the lunar maria were emplaced. Note the inundation of the craters Archimedes and Iridum. The last major flows occurred within Mare Imbrium northwest of the crater Tobias Mayer, and these are the flows recognized in Earth-based telescopic photographs and vividly displayed in Lunar Orbiter V photographs (see Volcanism, fig. 6(a)) and Apollo 15 (see Volcanism, fig. 12). Several bright-rayed craters, for example, Eratosthenes, Euler, and Flamsteed, have been superimposed by the lava flows. Illustration courtesy of Don Wilhelms.

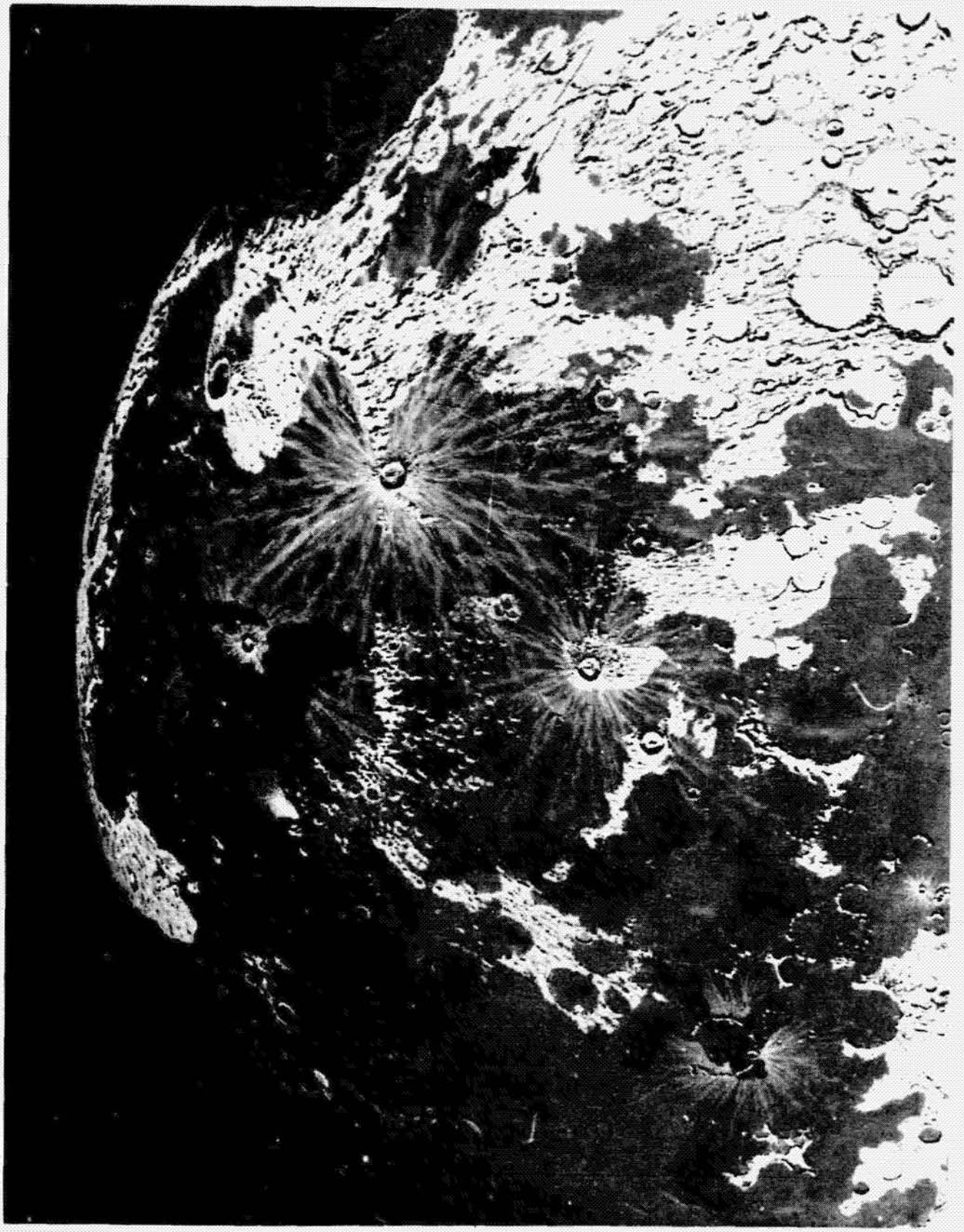

Opposite:

Figure 6.– The present-day lunar surface (turn illustration so that the limb is at the top). The rays associated with Eratosthenes, Euler, and Flamsteed have lost their high reflectivity and the dark mare flows have lightened. More recent craters, such as Copernicus (center), Aristarchus (upper left), and Kepler (left) exhibit ray systems extending over the maria. Illustration courtesy of Don Wilhelms.

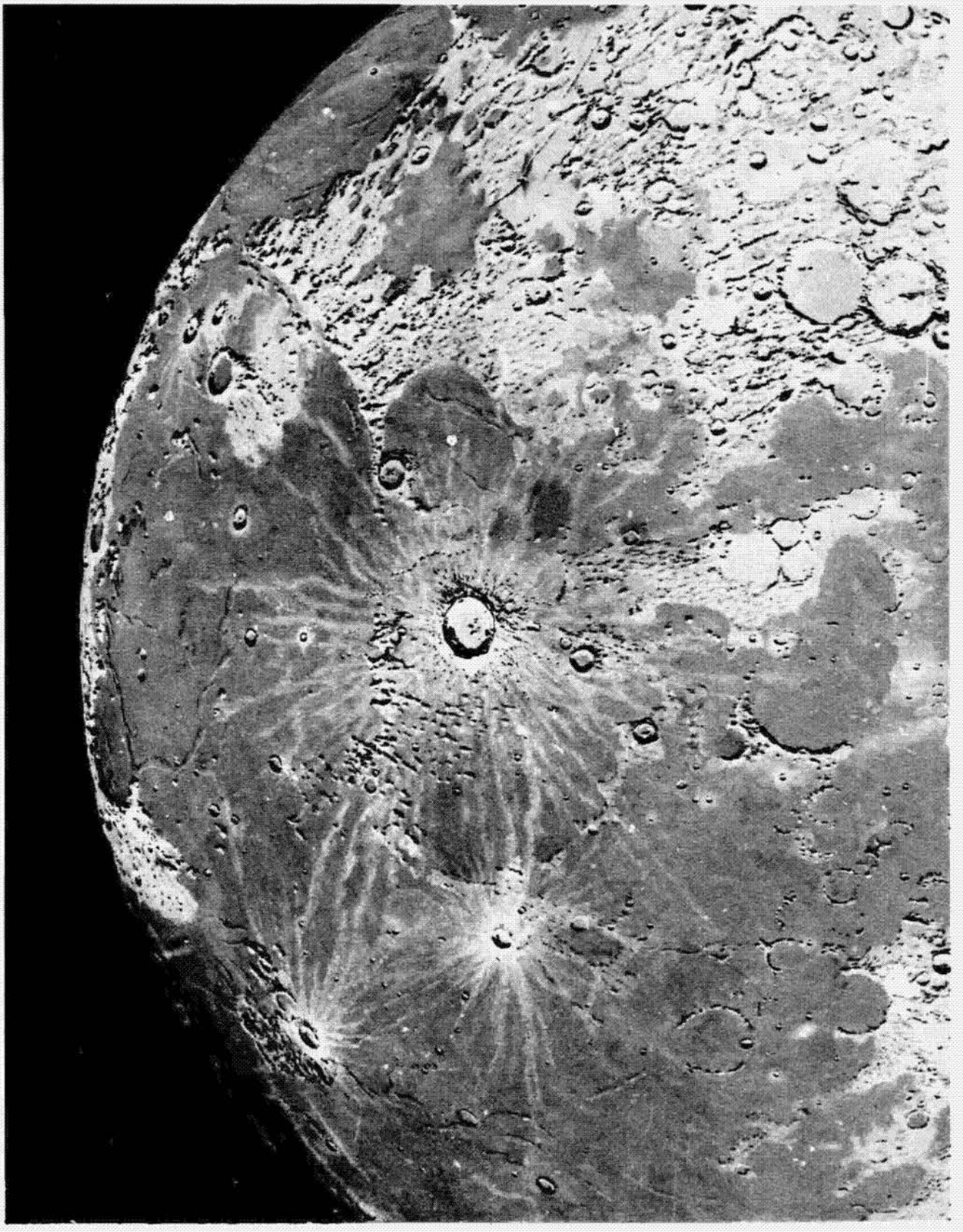

Opposite:

Figure 7.– Orientale Basin: The last major multi-ringed basin to form on the Moon. As many as five rings can be recognized, the most prominent rings correspond to the Cordillera Mountains (930 km in diameter) and the next interior ring, the Rook Mountains (620 km in diameter). The Orientale Basin exhibits minor eruptions of mare basalts relative to the inundated Imbrium Basin. This is evidence that the mare units were not directly the result of impact-generated melt. As a result of the minor mare flooding, the locations of the major vents are exposed: within the inner basin and along the base of the concentric mountains. The distribution of volcanic features across Mare Imbrium suggests analogous concentrations of vents. This overview reveals the complexly striated ejecta facies that resemble those around smaller craters.

Opposite.

Figure 8.– Comparison of the irregular and circular maria along the eastern limb of the Moon. Mare Crisium (top) is a circular basin with a major mountainous ring 450 km in diameter. In contrast, Mare Smythii (lower left center) is contained within one of the oldest basins (450 km in diameter), which lacks a well-defined mountainous ring (AS14-75-10304).

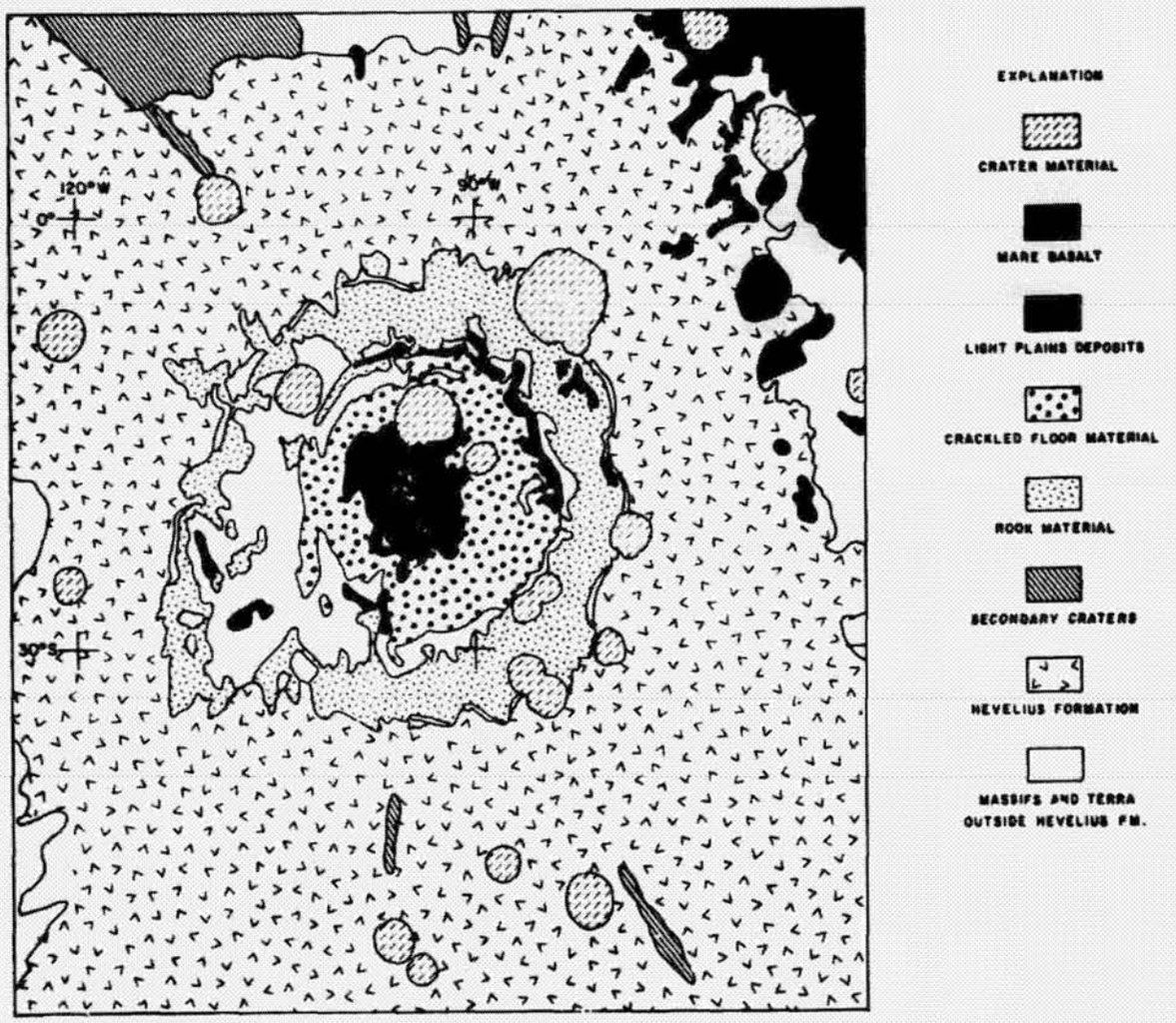

Figure 9.– Generalized geologic map of the Orientale Basin adapted from a map of the west side of the Moon in preparation by D. H. Scott, M. West, and J. F. McCauley. The basin is 900 km across and its ejecta blanket (Hevelius Formation) covers a tenth of the Moon. Mercator projection; lower edge of map is 50° S.

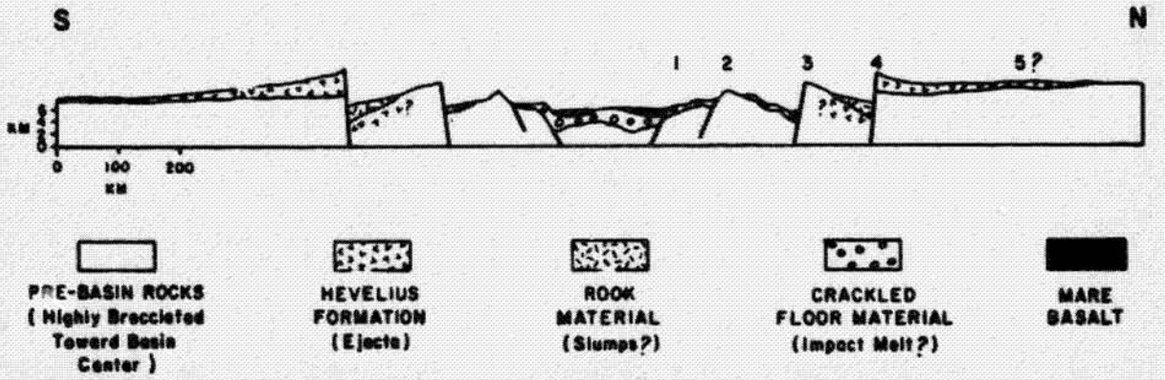

Figure 10(a).– Schematic cross section of the Orientale Basin to illustrate stratigraphy and generalized topography. Mountain rings are numbered. Ring 3 is Rook Mountains, ring 4 is Cordillera Mountains. A possible fifth ring is questionable. Massifs of inner rings may expose ejecta or fallback. 10X vertical exaggeration. An interpretive cross section at true scale showing substructure is shown below.

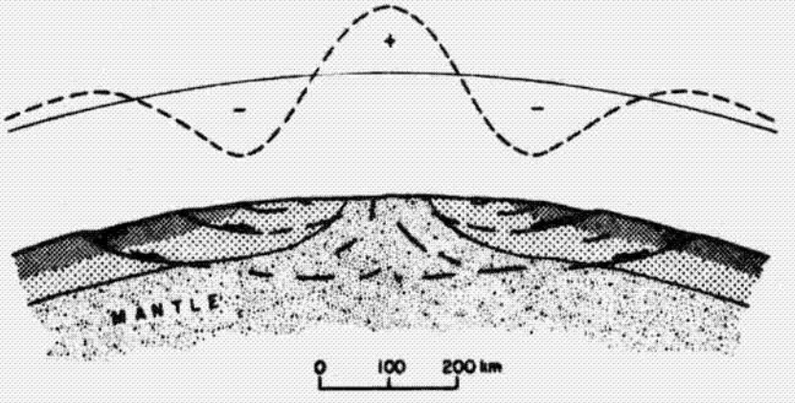

Figure 10(b).– Suggested cross section of the Orientale Basin with no vertical exaggeration. Gravity profile is diagrammed above. Exposure of the mantle at the surface implies that some mantle material was excavated. A shallow moat in the mantle can account volumetrically for a high uplift. Crust, assumed 75 km thick, is shown with arbitrary layering.

Opposite:

Figure 11.– The multi-ringed craters (basins) Schrödinger and Antoniadi, (a), and a large crater, Humboldt (b). Schrödinger is approximately 320 km in diameter and contains an inner mountainous ring 155 km in diameter. Antoniadi (upper right in (a)) is only 140 km in diameter and exhibits a 65 km diameter inner ring within which is a small central peak. Although Humboldt (b) is 170 km in diameter, it does not display a comparable inner ring. Thus, the formation of ring structures may reflect local properties.

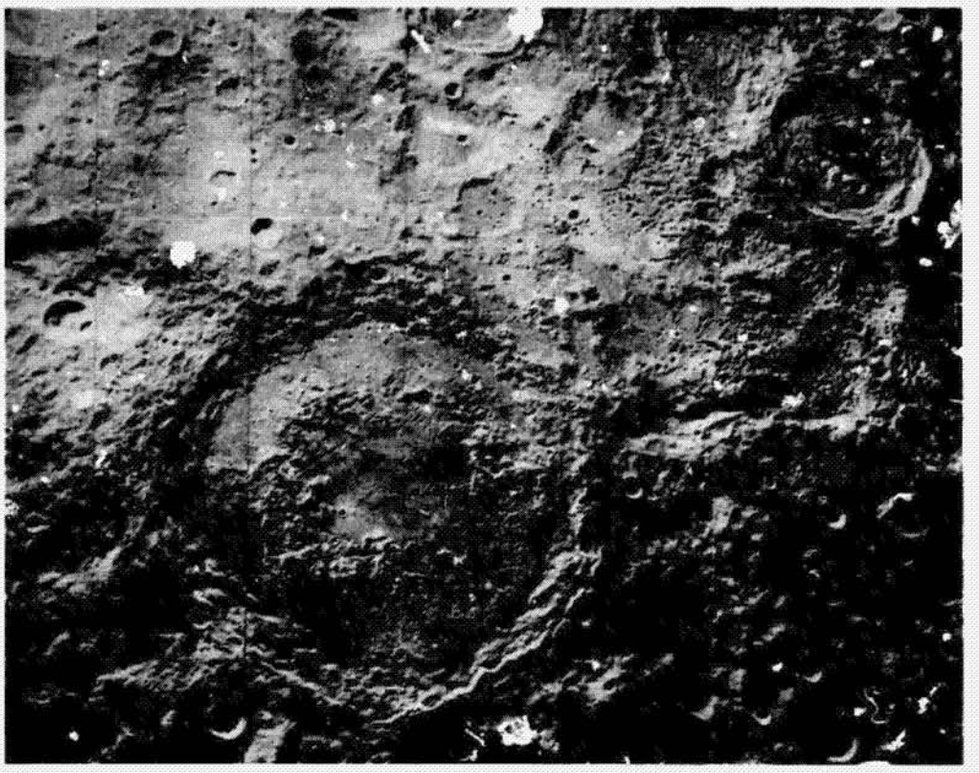

a

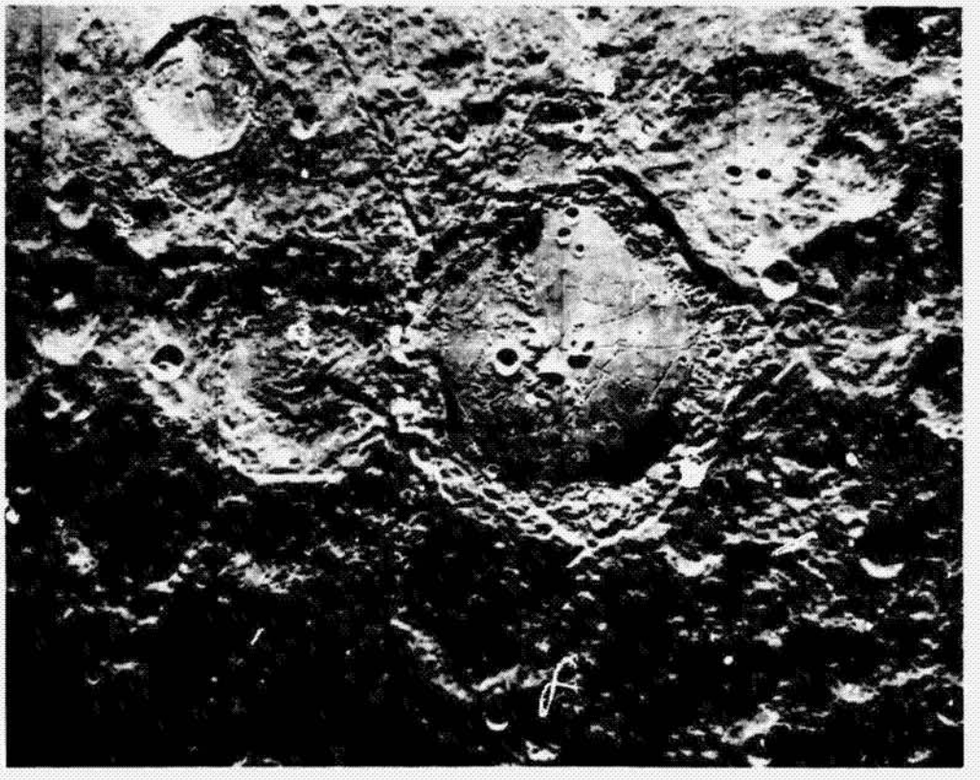

b

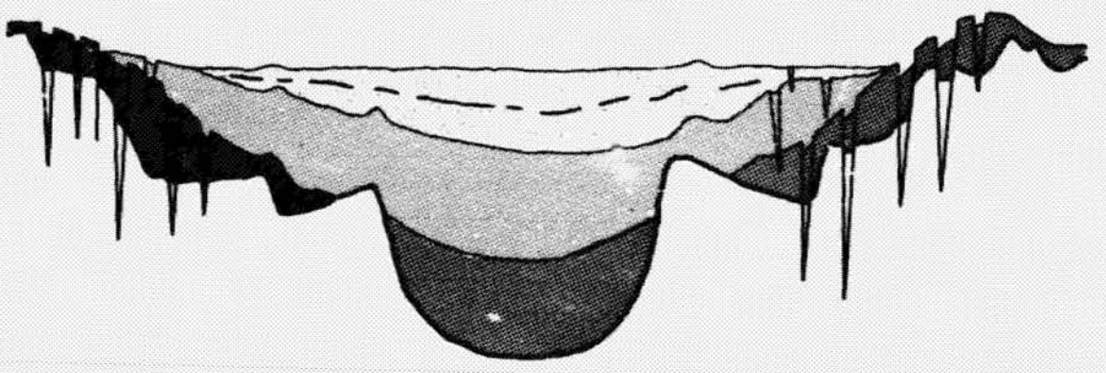

Figure 12.– Schematic cross section of Mare Serenitatis showing progressive sagging of three successive fills of mare basalt (greatly exaggerated vertical scale; from Howard, Carr, and Muehlberger, 1973). Arcuate graben (rilles) are in the older, tilted basalts exposed at the basin margin. By the time the youngest basalt was emplaced, the lunar lithosphere had stiffened enough to support the mascon as a superisostatic load.

TABLE 1. HIGHLAND STRATIGRAPHIC UNITS AT LANDING SITES, GIVING SOME POSSIBLE BASIN–RELATED ORIGINS (HOWARD *ET AL.*, 1974). MC GETCHIN *ET AL.* (1973) GIVE THEORETICAL ESTIMATES OF THE AMOUNT OF BASIN EJECTA EXPECTED AT EACH SITE.

Site	Distance from basin margins (basins listed youngest to oldest for each site)	Geologic unit	Possible basin-related origins
Apollo 14	550 km from Imbrium	Fra Mauro Formation	Imbrium ejecta
Apollo 15	Imbrium margin 100 km from Serenitatis	Massif material	Imbrium ejecta over Serenitatis ejecta
Apollo 16	3000 km from Orientale 1100 km from Imbrium 150 km from Nectaris	Cayley Formation	Fluidized ejecta from Imbrium and/or Orientale, or mainly local material redistributed by basin secondaries
		Descartes material	Nectaris or Imbrium ejecta, perhaps sculptured by Imbrium event
Luna 20	400 km from Nectaris 200 km from Crisium	Hilly and furrowed material	Crisium or Nectaris ejecta
Apollo 17	800 km from Imbrium 600 km from Crisium Serenitatis margin	Massif material	Serenitatis ejecta and/or overlying Imbrium ejecta
		Sculptured hills material	Serenitatis ejecta (?) faulted by Serenitatis, Crisium, or Imbrium events

With permission, reprinted from ICARUS, vol. 12, 1970, pp. 440–456.

Lunar Maria and Circular Basins—A Review

DESIREE E. STUART-ALEXANDER AND KEITH A. HOWARD

U.S. Geological Survey, Menlo Park, California 94025

Received December 9, 1969; revised January 20, 1970

Lunar Orbiter data make it possible to examine the distribution and relations of maria and large circular basins over the entire Moon. The restricted distribution and age of the maria are in marked contrast to the apparently random distribution in time and place of the circular basins, some of which contain mare fillings. The circular basins are believed to be impact scars, and the maria to be volcanic fills which in each case are younger than the structures they fill.

Twenty-nine circular basins 300 km wide or wider are recognized. They are placed in an age sequence because successive stages of degradation can be recognized from the fresh Orientale basin to the almost obliterated basin containing Mare Australe.

The maria were emplaced during a short span of lunar history, although some light plains of the highlands may be older maria lightened through age. The present maria are topographically low, tend to be associated with large circular basins, and lie in a crude global belt of regional concentrations; 94% are on the hemisphere facing the Earth. Possible explanations offered for these patterns of mare distribution include impact-induced volcanism, volcanic extrusion to a hydrostatic level, isostatic compensation, lateral heterogeneity in the lunar interior, suberustal convection, and volcanism due to disruption by Earth's gravity.

Introduction

Moon-wide distribution of maria and major structural features can now be studied in detail with the photography of the Lunar Orbiters. Maria, the dark plains of the Moon, commonly occur in circular multiringed basins, and whether these basins and the mare material are genetically related and how they are distributed are of fundamental importance to interpretations of lunar history and processes. This paper compares the morphology and relative ages of circular basins 300 km wide or wider and examines the relations between these basins and mare material on both the near and far sides of the Moon.

An excellent description of the basins on the near side of the Moon is that of Hartmann and Kuiper (1962). The distribution and origin of maria have been discussed often in the literature. New stimulus to the discussion was added by the Russian pictures returned from Luna 3 and Zond 3 that showed a scarcity of maria on the far side, and later by gravimetric data from Lunar Orbiters (Muller and Sjogren, 1968) that indicated large mass concentrations under some of the circular maria on the near side. Pre-Orbiter summaries of the distribution of basins and maria have been made by Hartmann (1966*a*) and Lipskiy *et al.* (1966). Large basins devoid of maria have been called thalassoids by Lipskiy (1965).

Our observations support the view that the maria are volcanic fields, and the circular basins impact scars that in all cases predate the maria that occupy them. Although the great ages of the rocks returned by Apollo 11 (Lunar Sample Preliminary Examination Team, 1969) suggests that the differences in absolute age of events and rocks may be small, the sequence of events is clear and remains an important key to understanding how the basins and maria developed. Too much confusion has developed in the literature from the failure of some authors to distinguish between circular basins and the mare

rocks that fill them. Because of the age differences between maria and basins, and also because the degree of mare filling varies considerably from basin to basin, it is useful to consider the basins independently first, and then to examine their relationship to mare rocks.

The photographs accompanying this report emphasize far-side features because the near-side basins have been well illustrated by Hartmann and Kuiper (1962) and Hartmann (1964). Photographs from the NASA Lunar Orbiters are available from the National Space Science Data Center, Code 601, U.S. Goddard Space Flight Center, Greenbelt, Maryland 20771.

Circular Basins

Large circular basins are fundamental elements of the lunar tectonic framework, and the major lunar mountain ranges are circumferential to these basins. The basins

Table I

Circular Basins[a]

Name	Location		Representative Lunar Orbiter photos	Diameter (km)	Age Group
	Longitude	Latitude			
1. Orientale	−95	−20	IV M-187	900	IV
2. —	130	−70	IV M-4	300	
3. Imbrium	−19	37	IV M-115, M-134	1250	
4. Crisium	59	17	IV M-60	450	III
5. —	−129	3	V M-24, M-26	490	
6. —	−158	−3	I M-30, M-38	450	
7. Moscoviense	145	25	V M-103, M-124	460	
8. Bailly	−69	−67	IV M-179	310	
9. —	141	5	I M-116, M-117	330	
10. Humorum	−39	−24	IV M-137	430	II
11. Nectaris	34	−16	IV M-71, M-84	840	
12. —	160	−53	V M-65	300	
13. —	165	−35	II M-75	370	
14. near Schiller	−45	−34	IV M-142	350	
15. —	−148	58	V M-29	300	
16. Grimaldi	−68	−5	IV M-161	430	
17. Serenitatis	19	26	IV M-91, M-97	680	
18. —	−153	35	V M-26, M-30	480	
19. —	−98	35	IV M-189	320	
20. Humboltanium	81	58	IV M-23	640	
21. Pingré	−79	−56	IV M-180	300	
22. Smythii	84	−3	IV M-12, M-17	370	I
23. Fecunditatis	51	−3	IV M-52	480	
24. —	130	−78	IV M-94	370	
25. W. Tranquillitatis	27	9	IV M-72, M-84	550	
26. E. Tranquillitatis	38	11	IV M-72, M-84	500	
27. Nubium	−17	−19	IV M-120	750	
28. —	162	−11	II M-75	480	
29. Australe	90	−45	IV M-9, M-106	900	

[a] Listed in approximate order of increasing age, based on degree of modification. Diameters and locations are subject to revision. Identification of some basins included in age group I is questionable. Photographs referred to are of the Lunar Orbiter project of the National Aeronautics and Space Administration. The roman numerals refer to the number of the Lunar Orbiter Flight, the M refers to moderate resolution photograph, and the arabic numbers to the frame number.

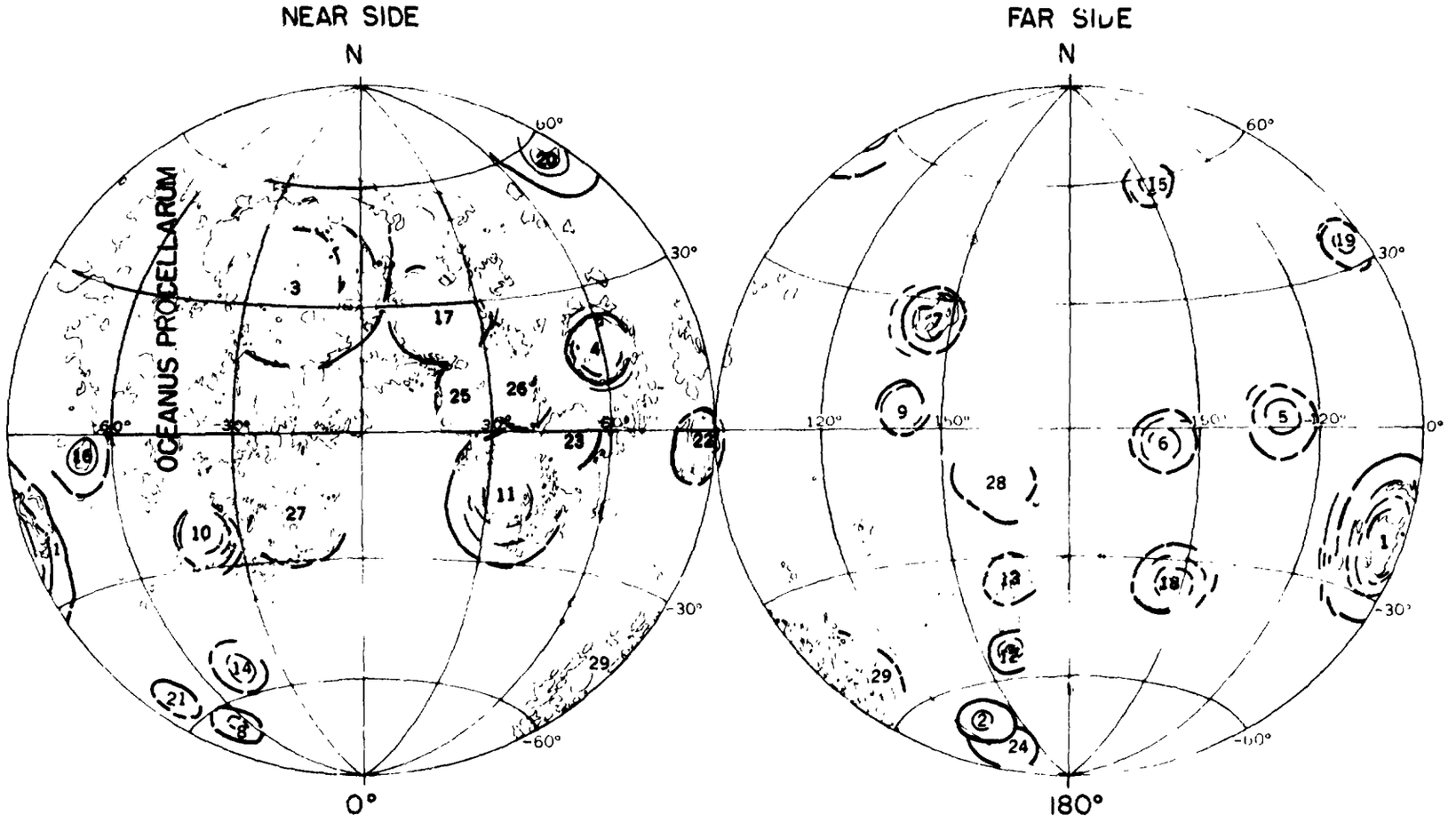

FIG. 1. Distribution of maria and large circular basins, Lambert equal-area projection; basins 300 km or more in diameter. Mare areas are shaded. Basins numbered as in Table 1. The highest mountain ring of each basin is shown by a heavy line; secondary mountain rings are shown by light lines. Location and size of far-side features are taken from ACIC provisional Lunar Farside Chart (LFC-1), 2nd edition, 1968.

(Table I and Fig. 1) vary considerably in size and appearance, but a close inspection reveals that they have many features in common which are only more obscure or obliterated in more heavily cratered basins interpreted to be older. The range in form

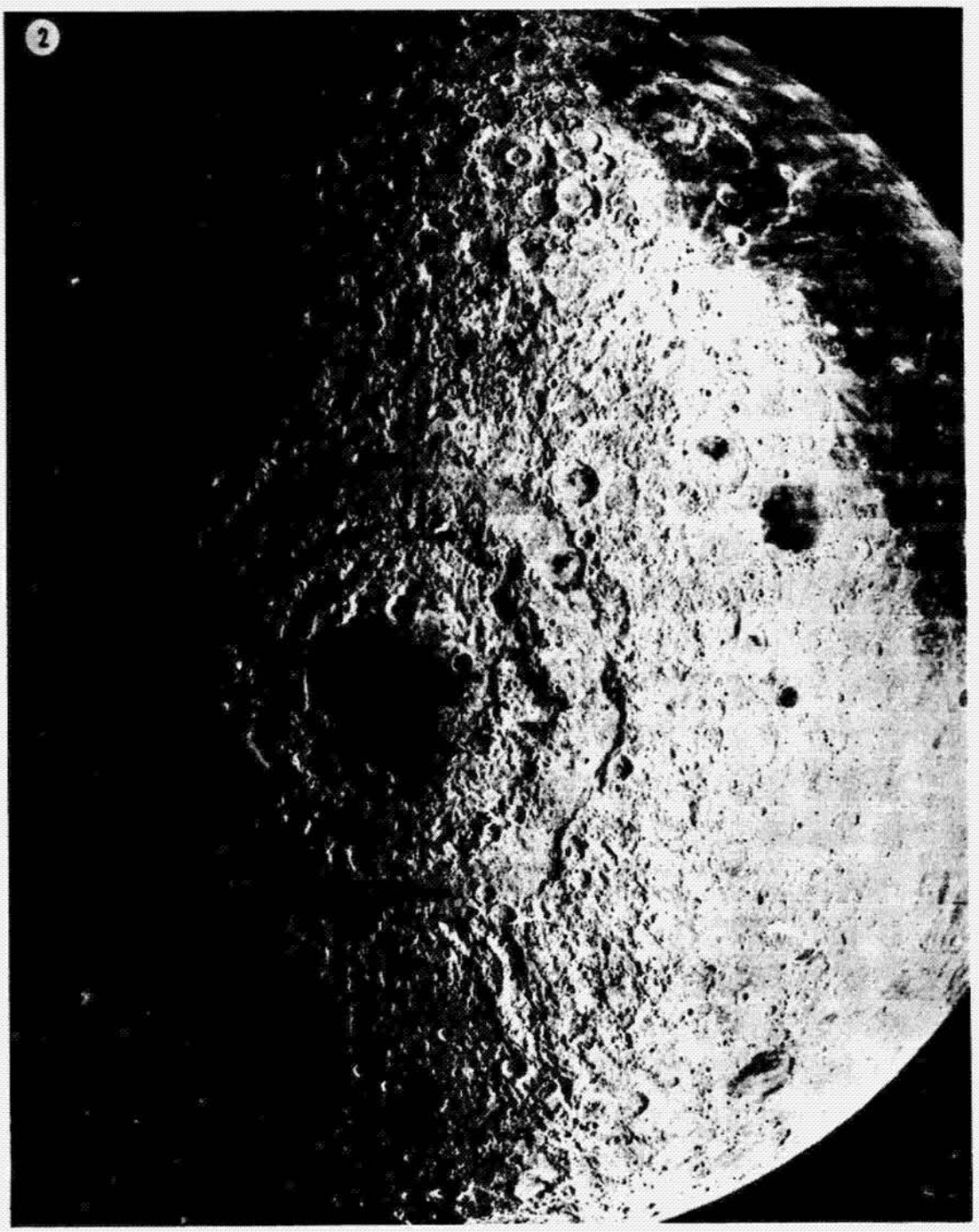

FIG. 2. Orientale basin and concentric mountain systems, age group IV (no. 1 in Fig. 1). Outer mountain ring (Montes Cordillera) is 900 km across. Mare rocks make up the smooth dark area within the inner basin and scattered small patches at the foot of the mountains. Radial texture of rim deposits is well developed. (Photograph LO IV, M-187.)

of apparently similar features leads us to believe that progressive modification has taken place and that the initial forms of basins of like size were similar. The major features are well shown in two fresh examples: The Orientale basin, 900 km

FIG. 3. A small (300-km diameter) fresh-appearing basin near the south pole on the far side, age group IV (no. 2 in Table I and Fig. 1). The inner ring is less well developed than those of the much larger Orientale basin. Radial valleys are clearly evident, but the texture of rim deposits is not well preserved. Light plains material fills the inner basin, except for a large dark halo that may be incipient mare around an elongate crater (Photograph LO IV, M-8.)

across (Fig. 2), and a basin 300 km across on the far side near the south pole (Fig. 3).

Form

A high mountain ring forms the outermost boundary of most basins and one or more lower mountain rings occupy concentric positions within the basin. A scarp generally makes the outer mountains asymmetric, with the steep side facing inward toward the main basin. Lowlands within the basin typically consist of an inner basin flooded by plains-forming material and hummocky benches between the concentric mountain rings. Some of these benches are flat; others slope gently outward. Outside the rim crest of the freshest basins are rim deposits (McCauley, 1968; Saunders, 1968; Wilhelms, 1970; Shoemaker and Hackman, 1962), satellitic craters, and radial valleys (Baldwin, 1949; Hartmann, 1963, 1964).

The number of inner mountain rings is a function of basin size: large basins, such as Orientale, have two or more (Hartmann and Kuiper, 1962), nearly all basins below 600 km in diameter have only one inner ring, and fresh examples below 150 km have no inner mountain ring but instead a central peak or peaks. Basins or craters in the diameter range 300 to 150 km are transitional; some have multiple mountain rings and some have central peaks. To ensure that only one major structural type is considered, we will discuss only basins 300 km wide or wider.

Gentle exterior rises and depressions encircle the large Imbrium and Orientale basins and also the smaller Crisium and Humorum basins (Baldwin, 1949, Chap. 2; Hartmann and Kuiper, 1962; Wilhelms, 1964, 1968); the rises may be incipient scarp-bounded mountain rings. Crisium is atypical by being less circular than most basins of comparable freshness and by having an unusually small spacing between concentric scarps. Thus while most basins were formed similar to those shown in Figs. 2 and 3, some deviations occurred. Conceivably, Crisium may have a different origin from the rest.

Origin

An impact origin was suggeted for the Imbrium basin by Gilbert in 1892 and is generally favored for the basins today, although some workers still take exception (Lipskiy *et al.*, 1966; Khabakov, 1962; Green, 1967). Compelling arguments for an impact origin of the 90-km crater Copernicus were presented by Shoemaker (1962), and it is now apparent that there is a gradation in form from craters like Copernicus to larger basins such as shown in Fig. 3 and to very large basins like Orientale (Fig. 2). The salient features favoring an impact origin can be summarized as follows: The extensive blanket of coarsely braided rim deposits around the Orientale basin suggests rapidly deposited ejecta (McCauley, 1968; Saunders, 1968). Beyond the rim deposits are numerous smaller craters, many arranged in radial rows, that have the character expected of secondary craters produced by ejecta flung from the basin. The radial sculpture or lineaments around many of the basins, whether they are fractures (Hartmann, 1963, 1964) or gouges made by projectiles (Gilbert, 1893), suggest a very violent event in the center of each basin. Other factors favoring an impact origin are the vast size and symmetry of the basins compared with know volcanic structures, and the general similarity in form between so many of the lunar basins.

The sequence of events upon the collision of a large comet or asteroid with the Moon is thought to be as follows (McCauley, 1968); excavation of a deep crater, formation of small secondary craters by material ejected at fairly low angles, deposition of a thick ejecta blanket by material ejected at very low angles or transported in a base surge, and gravitational collapse of the crater along normal faults to produce a wide basin with concentric fault scarps.

Aging

Continuous modification of basins through time is indicated by a range in the extent to which similar structures are degraded in various basins, by differences

in frequency of superposed craters,[1] and by the stratigraphic evidence of the ejecta from the three youngest basins superposed on older basins. Figures 2 through 6 illustrate successive stages in modification of large circular basins. The Mare Australe area (Fig. 6) is included here because we believe that it represents the oldest discernible impact basin. We concluded that Australe was initially like the other basins because (1) its mare patches occupy a circular area that appears to be depressed (Mills and Sudbury, 1968), and (2) high mountains rim a short section of the southeast perimeter.

The processes that subdue and eventually obliterate old basins and their encircling mountain rings are varied and the rates are unknown. The most significant processes appear to be superposed impact cratering[1] and, for some basins, flooding by plains-forming materials, especially mare. Other processes that probably are important are deposition of ejecta flung from other impacts, mass wasting (McCauley, 1968; Gold, 1955; Rowan, 1968), building of volcanic landforms (Wilhelms and McCauley, 1969), isostatic rebound (Masursky, 1964), and perhaps tectonic deformation. The absolute rate of the aging is uncertain; even interpretations of the rate of impact events differ widely. If most of the Moon's features formed early in its history, as suggested by the 3 ± 0.7 b.y. ages reported for rocks from Tranquility Base (Lunar Sample Preliminary Examination Team, 1969), then the flux of colliding objects was highest early in the history, as suggested by Urey (1956) and Hartmann (1965*a*, *b*, 1966*b*), and the difference in absolute age between the oldest and youngest basins is small.

The basins can be arranged in an approximate relative age sequence (Table I) based on the degree of modification from those basins of Figs. 2 and 3, assuming similar initial forms. We have ranked them by evaluating several factors that suggest age: completeness of the outer mountain ring; circularity; recognition of rim deposits, of inner mountain ring or rings, and of a scarp on the outer mountain ring; size of the largest superposed craters[2]; and a subjective estimate of the overall degree of destruction. Each factor was assigned a numerical rating from 10 (fresh) to 0 (obliterated); the total of these numbers indicates approximately the relative youth of each basin. Although this technique yields a range of numbers, the basins are here grouped into four broad age categories (Table I) to avoid a misleading impression of precision. In any case, revisions can be expected with the application of more refined techniques such as morphology of superposed craters (Offield and Pohn, 1968) or detailed crater counts.

The sequence of morphologic changes follows a general pattern, although individual basins do not fit perfectly all aspects of the pattern. Among the first features to become obscure are rim deposits. They are prominent around the basins in Figs. 2 and 3, but have not been recognized around basins regarded as older (age groups I–III). Secondary craters also are obliterated quickly; clear examples are present only around Orientale. Radial valleys are associated with the youngest (group IV) basins and have been recognized only around a few older basins.

Mountain rings are persistent features. The prominent outer mountain ring lasts longest; it generally remains intact until broken by craters more than 50 km wide, and only in the oldest basins is it nearly obliterated. The steep inward-facing escarpment of the outer mountain ring degenerates more rapidly than the mountains themselves; it is vague in group II basins and unrecognizable in group I. The scarp appears to degrade rather steadily, and its state of preservation is probably a

[1] We share the common belief (e.g., Shoemaker, 1962; Baldwin, 1963; Hartmann, 1966*b*), suggested by crater distributions and morphologies that most lunar craters are of impact origin, and thus frequency counts can be used as age indicators. Chain craters and other craters of probable volcanic origin appear to be considerably less numerous.

[2] We arbitrarily measured the nine largest craters superposed on each basin not flooded by mare, discarded the largest as accidental, averaged the diameters of the remaining eight, and compared this average to the basin diameter.

FIG. 4. A 490-km basin on the far side, age group III (no. 5 in Table I and Fig. 1). Two concentric mountain rings are prominent, although interrupted by large craters. Light plains in the inner basin are more sparsely cratered than the rest of the basin and so are younger. No radial texture or rim deposits are readily identifiable.

reliable criterion of age. The inner mountain rings are destroyed more rapidly than the higher outer ring so that only vestiges remain in group II. Inner mountain rings are not visible in several mare-filled basins, presumably because they are buried; they may be represented by circular patterns of mare ridges and low scarps. In some basins the filling even covers part of the outer mountain ring, giving a false appearance of age. Finally, old basins are generally less circular in outline than young basins, apparently due to disruption of the rim by younger craters and by volcanic flooding,

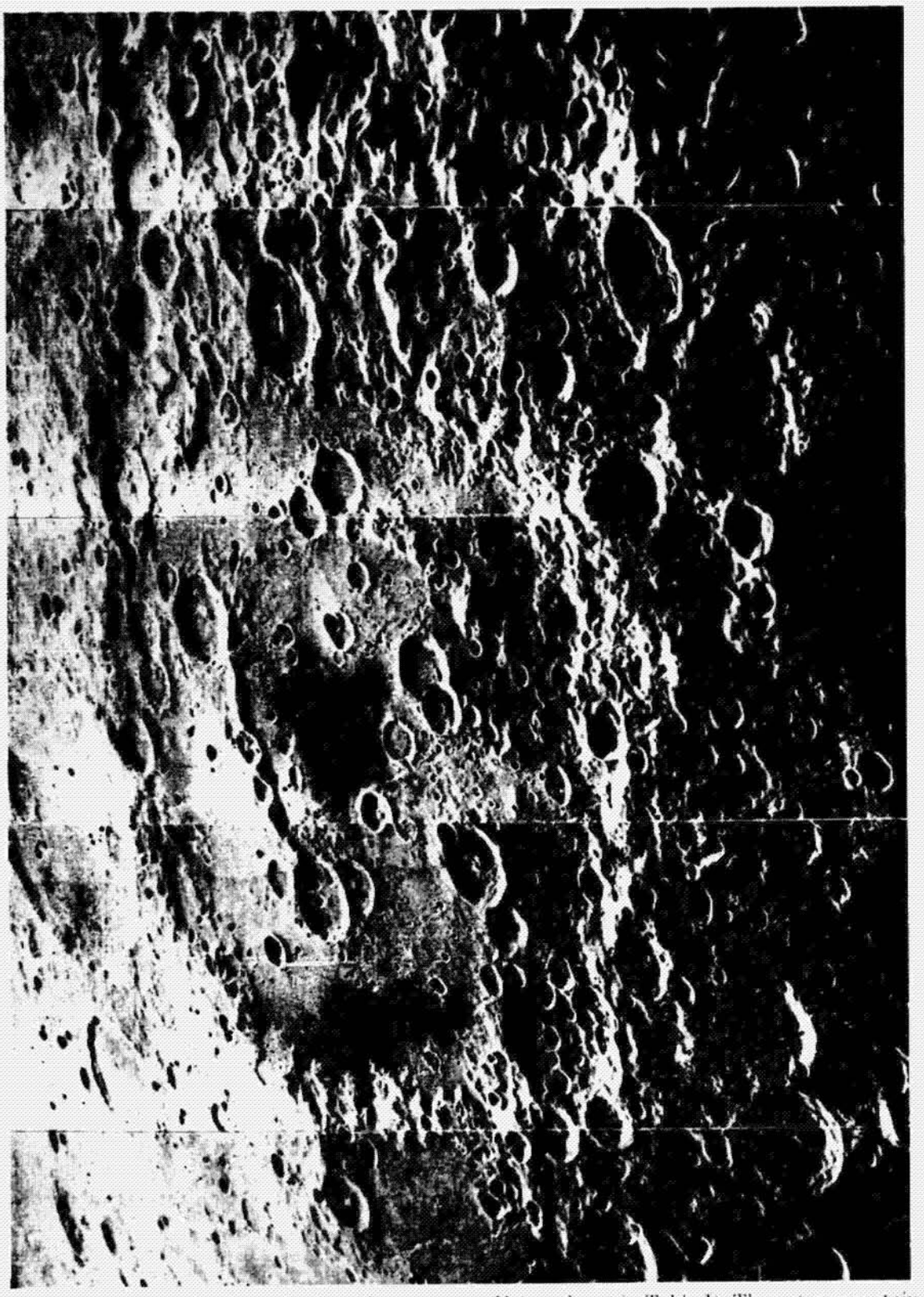

FIG. 5. A 480-km basin on the far side, age group II (number 8 in Table 1). The outer mountain ring is fairly subdued and broken by many large craters; the innermost ring is distinct but incomplete. Mare rocks form the dark patches within the inner ring and just inside the southern and western parts of the outer ring. (Photograph LO V, M-30.)

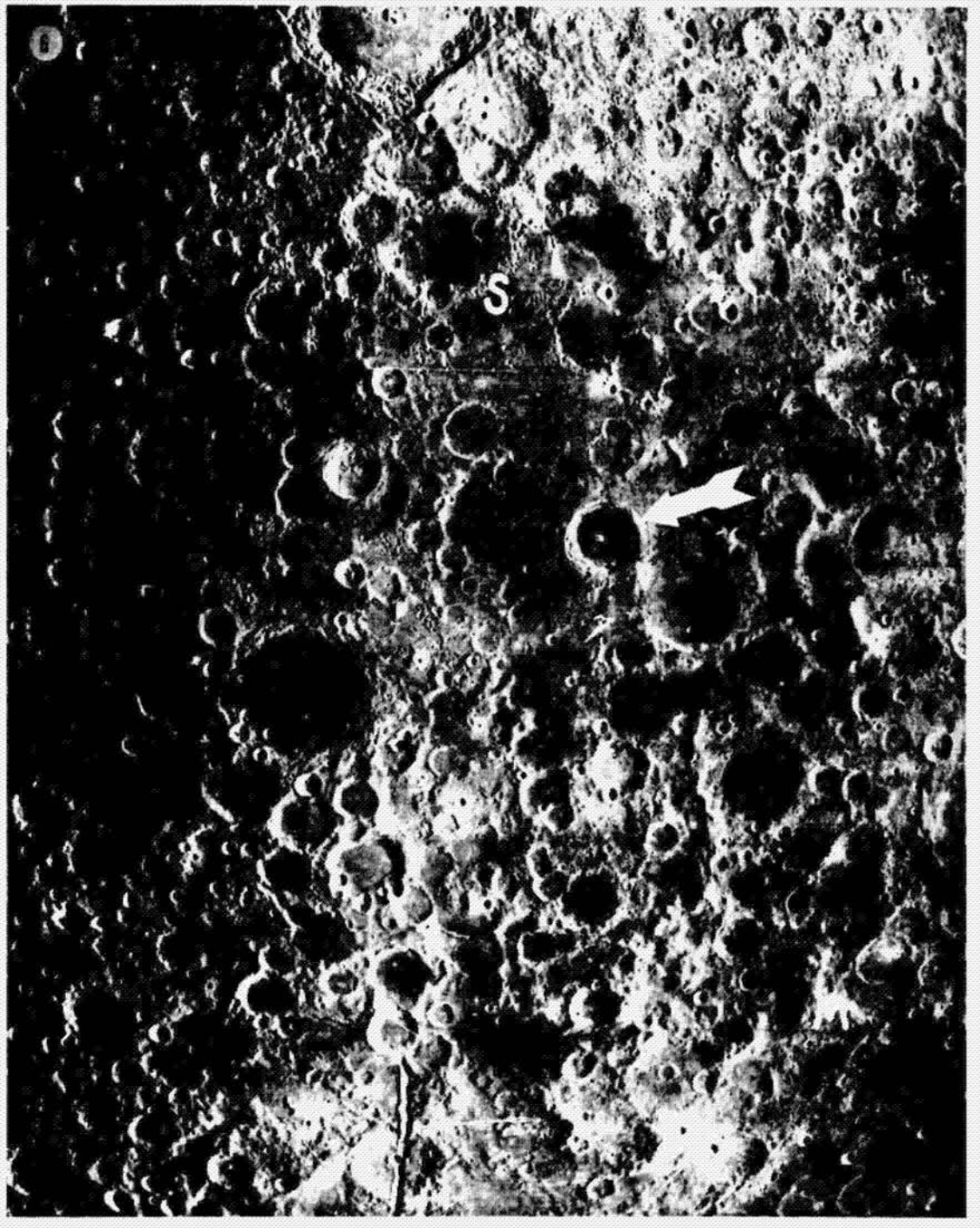

FIG. 6. Mare Australe with the western sector in partial shadow. The circular pattern of mare patches, and high mountains in the southeast (M lower right) that may be the remnants of an outer mountain ring, suggest this is the site of an ancient (age group I) circular basin, 900 km across (almost the width of the picture) (no. 29 in Table I and Fig. 1). Intricate superposition relations of younger craters and mare patches are well displayed. Large crater partly shown at top is Humboldt; S in satellitic crater field. Valley at bottom is radial to basin shown in Fig. 3. (Photograph LO IV, M-9.)

and perhaps by tectonic deformation such as blockfaulting. However, some irregularities in outline—such as the birfurcation of the southwestern part of the outer scarp in Orientale (Fig. 1) and the asymmetry of Crisium—appear to be original.

Distribution

Twenty-nine basins wider than 300 km have been recognized by us (Table 1). Most are clearly circular basins, but a few are so extensively modified that their identity as such is questionable, particularly Fecunditatis, East and West Tranquillitatis, and Nubium. The existence of several other questionable basins has been proposed by Baldwin (1949, p. 38; 1963, p. 194), Hartmann and Kuiper (1962), and Campbell *et al.* (1969). The distribution (Fig. 1) appears random to us, contrary to pre-Orbiter suggestions (Lipskiy *et al.*, 1966; Khabakov, 1962; Alter, 1956) that the basins are distributed mainly in a broad girdle.

A histogram of relative age as a function of basin size (Fig. 7) summarizes the basin distribution and shows that there is no marked concentration on the near or far side with regard to age or total number. The number of basins is too small for statistical analysis, and the apparent size discrepancy between the near and far sides would be reduced if the questionably identified basins were excluded. The distribution on near and far sides has no definite pattern, and seems most easily explained by random impact events.

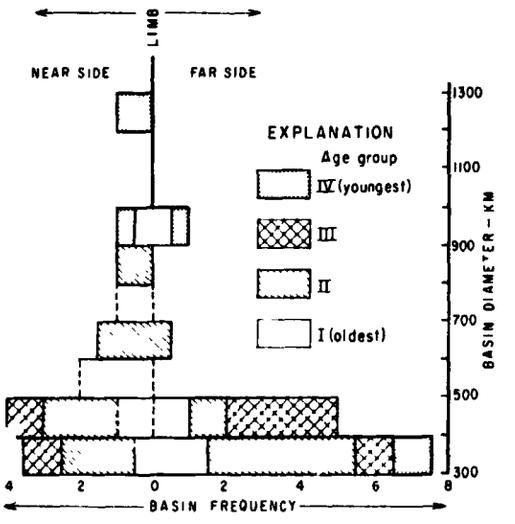

FIG. 7. Histogram of the size frequency of circular basins on the near side, left and far side, right. Age of basins indicated by patterns. Dashed lines indicate questionable basins.

MARIA

The dark or low-albedo plains known as maria form one-sixth of the Moon's surface, mostly in the prominent patchy dark band across the near side (Fig. 1). Mare rock occupies depressions and has obviously embayed and flooded older structures through some kind of surface emplacement. Most authors agree that the maria represent volcanic rocks, though a sedimentary origin has also been suggested. Dark domes and plateaus closely associated with the maria are commonly interpreted as shield volcanoes (Pickering, 1908; Baldwin, 1963; McCauley, 1967). Lobate scarps in Mare Imbrium are interpreted as flow fronts (Strom, 1965; Kuiper, 1965; Whitaker, 1966; Fielder and Fielder, 1968). The crystalline rocks returned from Mare Tranquillitatis by Apollo 11 have igneous textures, and compositions similar to terrestrial basalt but enriched in some refractory elements, particularly Ti and Zr, and depleted in alkalies and some volatile constituents (Lunar Sample Preliminary Examination Team, 1969). An approximately basaltic composition is also indicated for mare rocks at the Surveyor V site in Mare Tranquillitatis and the Surveyor VI site in Sinus Medii (Turkevich *et al.*, 1968, 1969; de Wys, 1967, 1968). The nearly uniform appearance of the various maria suggest they are all similar in origin and composition, and an approximately basaltic composition for all mare rocks is supported by remote sensing (Hapke, 1968; Vinogradov *et al.*, 1968; Adams, 1968). Thus the accumulated evidence indicates that maria are volcanic fills of basaltlike composition.

A map of the mare areas on an equal-area projection (Fig. 1) shows that they are distributed unevenly. Thirty percent of the near side is mare in contrast to only 2% of the far side. In 1903 Shaler had predicted a significantly lower quality of mare on the far side than on the near side based on his observations that the quantity of mare decreases on the near side as the limbs are approached. The great maria concentration on the near side lies mostly north of the equator, whereas the small mare areas of

the far side lie mostly south of the equator. The north polar area and the adjacent northeast quadrant of the far side lack mare altogether, and a smaller empty area caps the south pole and covers the southern highlands of the near side. The maria tend to be concentrated along a crude global belt that approximates a great circle (Lipskiy *et al.*, 1966).

Maria occupy depressions, and their surface elevations, though variable, average lower than the terra (Arthur, 1966; Mills and Subdury, 1968). Some deep depressions, however, contain no mare. Many maria occupy large circular basins but the largest mare area is the irregular Oceanus Procellarum which is not circumscribed by ring structures (Fig. 1). Smaller mare patches occur in smaller craters and irregular depressions.

Superposition relations indicate that all mare surfaces are relatively young compared to other lunar features even though their absolute ages may be great. These relations include the filling and embayment of relatively fresh features by mare material and the youthfulness of all craters that are superposed on maria. Crater counts, starting with Young's in 1933, show that the maria are all of similar age and are younger then most highlands. Subsequently many mare surfaces have been separated into relative age sequences (Lyubarski, 1961; Dodd *et al.*, 1963; Fielder, 1963; Carr, 1966; Wilhelms, 1968). By extrapolation from the lunar geologic maps published by the U.S. Geological Survey, the oldest surfaces that are usually classified as mare are probably younger than the Orientale basin. The restricted range in age of the maria suggests that they were produced during a relatively short period of extensive mare volcanism.

Differences in reflectivity in mare areas are clearly visible at full Moon (the albedo ranges from 0.07 to 0.12; Pohn and Wildey, in press). In many local areas the darker maria are concluded to be the youngest (Carr, 1966; McCauley, 1967; Morris and Wilhelms, 1967), suggesting that albedo can increase with time. Good examples of this age relation are seen in Mare Australe (Fig. 6), which is an area of partly coalescing patches mainly of relatively light mare. The dark mare covering the floor of the well-formed crater with a central peak (arrow, Fig. 6) is younger than the crater it fills, and that crater in turn is clearly superposed on surrounding lighter mare. Also, some satellitic craters from the large crater Humboldt (top center, Fig. 6) are superposed on light mare (S) and yet others are inundated by dark mare. Evidently there was a relatively prolonged sequence of mare formation in the Australe area. Although accurate albedo values are not known for the far side, most mare patches there appear to be comparatively light, like most of Mare Australe, suggesting that they are among the older maria; a notable exception is the floor of Tsiolkovsky.

Older equivalents of maria may be some light plains that are similar to mare except for a higher albedo and greater crater density. Lighter plains such as the floor of Ptolemaeus are not included as mare, nor are dark uplands, but both these types of terrain may be closely related to mare. If some of the light plains were maria that have been lightened by age, then the distribution of maria has varied through time (Sukhanov *et al.*, 1967; Wilhelms, 1970) and what we call maria may represent only the youngest deposits of a more complicated crustal flooding sequence.

Relations between Maria and Circular Basins

Most major maria occupy large circular basins, but not all basins contain mare (Fig. 1). The histogram shown in Fig. 8 reveals that all basins wider than 500 km and most basins wider than 400 km contain some mare, whereas two-thirds of those between 300 and 400 km contain none. However, the quantity of mare is disproportionately distributed among like-sized basins: nearly all near-side basins within the mare belt are flooded whereas similar basins outside the belt and on the far side are only partially flooded or unflooded. Most of the mare areas on the near side are in circular basins or near them. The mare material of Oceanus Procellarum is continuous with that which fills the Imbrium basin, but the vast area of Procellarum suggests it is not related to the Imbrium

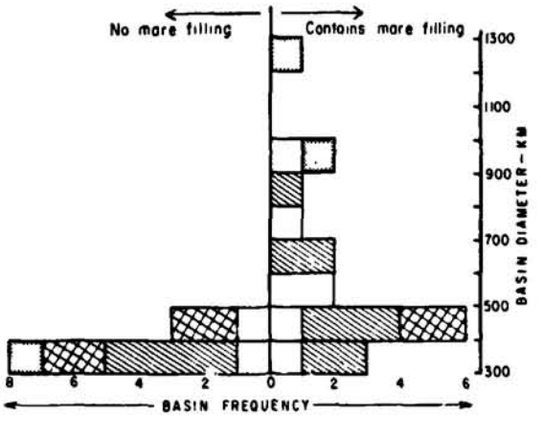

FIG. 8. Histogram of the size frequency of circular basins with and without mare filling. Patterns indicate basin age as in Fig. 7.

basin. Furthermore, the crude east–west band of mare patches across the south-central far side (Fig. 1) also shows independence from large circular basins and indicates some other control on the generation of mare.

Among the circular basins, the partly filled basins show a preference for mare to be located first centrally in the inner basin and second in concentric valleys between mountain rings (e.g., Figs. 2, 5), suggesting this was the order of filling of the more completely flooded basins also. The initial stage of mare flooding in smaller craters such as Humboldt (at the top center of Fig. 6), is generally along the outer and apparently lowest part of the crater floor. Thus mare is emplaced preferentially in certain structural positions of craters and basins, and these positions coincide with the lowest depressions.

Large positive gravity anomalies indicate mass concentrations, "mascons," in those large mare-filled basins having well-developed ring structures on the near side (Muller and Sjogren, 1968). However, no mascons are associated with the maria Tranquillitatis, Nubium and Fecunditatis, which we suggest may occupy nearly obliterated circular basins (Table I), nor with Oceanus Procellarum. These areas must differ in some respect from the mascon basins, the possibilities varying with the interpretations placed upon the cause of the gravity anomaly. The mascons may be dense metallic objects (Muller and Sjogren 1968; Urey, 1956), layers of dense mare rock (Conel and Holstrom, 1968), dense subcrustal rock (ultrabasic?) at a shallow level beneath the basin (Wise and Yates, 1969), or some combination. The circular mare areas that lack mascons may record impacts of low-density bodies. They may instead merely contain a lesser thickness of mare than the well-formed circular impact basins, either because they are old impact scars that rebounded before the mare flooding, or, alternatively, because they are not due to impact.

The wide range in age of the large circular basins contrasts with the general concordance in age of their mare fillings. It is particularly interesting that mare rocks occur unpreferentially in basins of any age, and conversely that there are both old and young basins that contain no mare (Fig. 8). However, the light plains-forming materials that occur in the basins devoid of mare (e.g., Fig. 4) could have been mare material now lightened through aging. On the other hand, basins can apparently remain as potential loci for mare flooding long after they are formed. Mare Australe, for example, occupies a very ancient circular basin (Fig. 6). Although the mare patches of Australe vary in age, all are considerably younger than the impact scar, whose topographic expression has been nearly obliterated. It is conceivable, though unlikely, that even Oceanus Procellarum is analagous to Australe and occupies an even older and larger impact scar.

POSSIBLE EXPLANATIONS OF MARE DISTRIBUTION

The following distribution patterns of mare rocks have become apparent: (1) Maria are associated with circular basins of all ages. (2) Maria are topographically low. (3) Maria tend to lie in a crude global belt that contains regional concentrations such as that in the south central part of the far side. (4) Most of the mare area is on the hemisphere facing Earth. Several explanations for these patterns can be entertained as working hypotheses that will have to be tested critically as more data become

available. It seems likely that some combination of processes functioned together, as none by itself seems sufficient to explain all the known features of mare distribution.

Delayed volcanism induced by impact was suggested by Carr (1964) and is attractive because it can account for both the concentration of mare rocks in large basins and for the apparent youth of the mare compared with the enclosing basins. An impact produces transient heat so that local melting might easily occur (Carr, 1964; Ronca, 1966). Carr concluded, however, that long after the impact very extensive melting might occur as a result of a slow rise in geothermal gradient caused by the insulating effects of breccia and of high transient temperatures caused by the impact. Thus as much as a billion years might have elapsed between the Imbrium event and the formation of Mare Imbrium.

The low elevations and apparent common level of many nearby mare surfaces that are not connected have suggested to Shoemaker (1964) and Sukhanov (1968) that mare material was emplaced as a fluid to an approximate hydrostatic level during widespread melting. Exemplifying this apparent hydrostatic equilibrium is the crater Archimedes, whose interior is filled with mare rocks to nearly the same level as adjacent Mare Imbrium (Turner, 1961). Exceptions are the reported limb height difference of 3 km between Mare Smythii and nearby Mare Marginis (Arthur, 1966), and some deep unflooded pre-mare craters such as Lansberg. Whether most maria share a common low hypsometric level remains to be shown by better selenodetic data than are now available.

Isostatic compensation may account for the low elevation of the maria (Baldwin, 1949, 1963, 1968; O'Keefe 1968) if the maria are thinner or denser than the highlands. Such a density difference is suggested by the Surveyor chemical analyses (Gault *et al.*, 1968) as well as the high densities of mare rocks from Tranquillity Base (Lunar Sample Preliminary Examination Team, 1969), and perhaps by the presumed greater brecciation in the older and more heavily impacted highlands. The great lunar mascons (Muller and Sjogren, 1968) do not appear to be compensated, but the lack of free-air gravity anomalies over Oceanus Procellarum and the maria Tranquillitatis, Fecunditatis, and Nubium (Muller and Sjogren, 1968) suggest these maria may be compensated with respect to adjacent highlands.

Regional concentrations of maria might be accounted for by lateral heterogeneities in the Moon, such as might be due to accretion of chemically different lumps of material (Urey *et al.*, 1959) or to some internal processes. Volcanic provinces of compositions different from maria seem likely in the highlands, where a variety of probable volcanic landforms such as the Kant plateau (Milton, 1968) are now recognized on Orbiter photos (Wilhelms and McCauley, 1969). Surveyor analyses also suggest some differences in chemical makeup for highland and mare rocks (Jackson and Wilshire, 1968). The differences between mare and highland volcanism may reflect different source compositions.

Convection in the lunar interior (Runcorn, 1962, 1967; Fielder, 1964) might explain some regional volcanic differences such as the concentrations of mare rocks within a crude global belt (Fig. 1). It has been suggested to explain a province of ridges and volcanic plateaus along the northwest axis of Oceanus Procellarum (McCauley, 1968). However, the Moon lacks tectonic mountain chains such as are commonly interpreted as products of mantle convection on Earth (Dietz and Holden, 1965) so that convection, if it existed, may have been very sluggish.

The concentration of maria facing the Earth suggests a terrestrial influence in their emplacement, although Nash (1963) postulated that the uneven distribution might predate and be responsible for the Moon's present orientation. Kopal (1966) suggested that the near-side lunar surface was disrupted by the Earth's gravity at a time when the Moon so closely approached Earth that the Moon's near side dipped within the Roche limit—that distance from a planet within which a satellite cannot approach without disruption. Any close approach, even if not to the Roche limit, would generate considerable heat (Alfvén

and Arrhenius, 1969). The generally concordant age of most maria supports the concept of a brief interval of mare volcanism during a close approach to Earth.

Thus the mare distribution patterns seem to require some combination of two or more causes. The association of maria with circular basins can be explained by impact-induced volcanism. The generally low elevations of mare surfaces suggest that the mare rocks were extruded approximately to a hydrostatic level; some may be low because they are isostatically compensated. Regional concentrations of mare rocks unrelated to impact basins, and the contrast between maria and probable volcanic landforms in the highlands, suggest volcanic provinces related to compositional differences in the subsurface, or perhaps subcrustal convection. Finally, the nearside concentration of mare rocks is so striking that it strongly suggests an influence of Earth's gravity in mare volcanism.

Acknowledgments

We thank M. D. Crittenden, R. E. Eggleton, J. F. McCauley, and H. G. Wilshire for critical review of the manuscript, and M. F. Kane for discussions on gravity anomalies. Lunar Orbiter photographs were supplied by Langley Research Center, NASA. Publication was authorized by the Director, U.S. Geological Survey. The work was supported by NASA contract R-66.

References

Adams, J. B. (1968). Lunar and Martian surfaces—petrologic significance of absorption bands in the near-infrared. *Science* **159**, 1453–1455.

Alfvén, H., and Arrhenius, G. (1969). Two alternates for the history of the Moon. *Science* **165**, 11–17.

Alter, D. (1956). The nature of the lunar maria. Publ. *Astron. Soc. Pacific* **68**, 38–45.

Arthur, D. W. G. (1966). The validity of selenodetic positions. *Commun. Lunar Planetary Lab.* **5**, 19–30.

Baldwin, R. B. (1949). "The Face of the Moon," 239 pp. Univ. of Chicago Press, Chicago, Illinois.

Baldwin, R. B. (1963). "The Measure of the Moon," 488 pp. Univ. of Chicago Press, Chicago, Illinois.

Baldwin, R. B. (1968). Lunar mascons—another interpretation. *Science* **162**, 1407–1408.

Campbell, M. J., O'Leary, B. T., and Sagan, C. (1969). Moon—two new mascon basins. *Science* **164**, 1273–1275.

Carr, M. H. (1964). Impact-induced volcanism. *In* "Astrogeologic Studies Annual Progress Rept., July 1, 1963 to July 1, 1964, pt. A." U.S. Geol. Survey open-file Rept., 52–65.

Carr, M. H. (1966). Geologic map of the Mare Serenitatis Quadrangle of the Moon. *U.S. Geol. Survey Map I-489.*

Conel, J. E., and Holstrom, G. B. (1968). Lunar mascons—a near-surface interpretation. *Science* **162**, 1403–1405.

de Wys, J. N. (1967). Surveyor V magnet experiment. *Science* **158**, 632–635.

de Wys, J. N. (1968). Surveyor VI magnet experiment. *J. Geophys. Res.* **73**, 1915–1924.

Dietz, R. S., and Holden, J. C. (1965). Earth and Moon; Tectonically contrasting realms. *In* "Geological problems in lunar research." *New York Acad. Ann.* **123**, 631–640.

Dodd, R. T., Jr., Salisbury, J. W., and Smalley, V. G. (1963). Crater frequency and the interpretation of lunar history. *Icarus* **2**, 466–480.

Fielder, G. (1963) Nature of the lunar maria. *Nature* **198**, 1256–1260.

Fielder, G. (1964). A case for convection on the Moon. *Nature* **4**, 171.

Fielder, G., and Fielder, F. (1968). "Lava flows in Mare Imbrium." Boeing Document D 1-82-0749, 36 pp. Boeing Sci. Res. Lab., Seattle, Washington.

Gault, D. E. *et al.* (1968). Lunar theory and process. *In* "Surveyor VII a Preliminary Report." *NASA SP-173*, pp. 233–276.

Gilbert, G. K. (1893). The Moon's face. *Phil. Soc. Washington Bull.* **12**, 241–292.

Gold T. (1955). The lunar surface. *Monthly Notices Roy. Astron. Soc.* **115**, 585–604.

Green, J. (1967). The volcanic origin of the Orientale Basin. *In* "Alternate Interpretations of the Orientale Basin" (R. A. Orti and J. Green). *Griffith Obs.* **31**, 122–123.

Hartmann, W. K. (1963). Radial structures surrounding lunar basins, I. The Imbrium system. *Commun. Lunar Planetary Lab.* **2**, 1–16.

Hartmann, W. K. (1964). Radial structures surrounding lunar basins, II. Orientale and other systems, conclusions. *Commun. Lunar Planetary Lab.* **2**, 175–192.

Hartmann, W. K. (1965*a*). Terrestrial and lunar flux of large meteorites in the last two billion years. *Icarus* **4**, 157–165.

HARTMANN, W. K. (1965*b*). Secular changes in meteoritic flux through the history of the solar system. *Icarus* **4**, 207–213.

HARTMANN, W. K. (1966*a*). Lunar basins, lunar lineaments, and the Moon's far side. *Sky and Telescope* **32**, 128–131.

HARTMANN, W. K. (1966*b*). Early lunar cratering. *Icarus* **5**, 406–418.

HARTMANN, W. K., AND KUIPER, G. P. (1962). Concentric structures surrounding lunar basins. *Commun. Lunar Planetary Lab.* **1**, 51–67.

HAPKE, B. W. (1968). Lunar surface—Composition inferred from optical properties. *Science* **159**, 76–79.

JACKSON, E. D., AND WILSHIRE, H. G. (1968). Chemical composition of the lunar surface at the Surveyor landing sites. *J. Geophys. Res.* **73**, 7621–7629.

KHABAKOV, A. V. (1962). Characteristic features of the relief of the Moon—Basic problems of the genesis and sequence of development of lunar formations. *In* "The Moon—A Russian view" (A. V. Markov, ed.), pp. 247–303. Univ. of Chicago Press, Chicago, Illinois.

KOPAL, Z. (1966). On the possible origin of the lunar maria. *Nature* **210**, 188.

KUIPER, G. P (1965). Interpretation of Ranger VII records. *In* "Ranger VII, Part II—Experimenters' analyses and interpretations." *Jet Propulsion Lab. Calif. Inst. Technol., Tech. Rept.* **32-700**, 9–73.

LIPSKIY, YU. N. (1965). Zond-3 photographs of the Moon's far side. *Sky and Telescope* **30**, 338–341.

LIPSKIY, YU. N., PSKOVSKIY, Y. P., GURSHTEYN, A. A., SHEVCHENKO, V. V., AND POSPERGELIS, M. M. (1966). Current problems of morphology of Moon's surface. *Kosmicheskiya Issledovaniya* **4**, 912–922 [in Russian]; translated U.S. Goddard Space Flight Center, ST-LPS-10, 547, 16 pp.

LUNAR SAMPLE PRELIMINARY EXAMINATION TEAM. (1969). Preliminary examination of lunar samples from Apollo 11. *Science* **165**, 1211–1227.

LYUBARSKY, K. A. (1961). An attempt to determine the absolute age of lunar formations. Translated from Russian (1956) by J. L. Zygielbaum. *Jet Propulsion Lab. Calif. Inst. Technol. Transl.* **26**, 12 pp.

MASURSKY, H. (1964). A preliminary report on the role of isostatic rebound in the geologic development of the lunar crater Ptolemaeus. *In* "Astrogeologic Studies Ann. Rept., July 1, 1963 to July 1, 1964, pt. A." *U.S. Geol. Survey Open-File Rept.*, pp. 102–134.

MCCAULEY, J. F. (1967). The nature of the lunar surface as determined by systematic geologic mapping. *In* "Mantles of the Earth and Terrestrial Planets" (S. K. Runcorn, ed.), pp. 431–460. Interscience, London.

MCCAULEY, J. F. (1968). Geologic results from the lunar precursor probes. *AIAA J.* **6**, 1986–1991.

MILLS, G. A., AND SUDBURY, P. V. (1968). Absolute coordinates of lunar features: III. *Icarus* **9**, 538–561.

MILTON, D. J. (1968). Geologic map of the Theophilus Quadrangle of the Moon. *U.S. Geol. Survey, Map* **I-546**.

MORRIS, E. C., AND WILHELMS, D. E. (1967). Geologic map of the Julius Caesar Quadrangle of the Moon. *U.S. Geol. Survey Map* **I-510**.

MULLER, P. M., AND SJOGREN, W. L. (1968). Mascons—Lunar mass concentrations. *Science* **161**, 680–684.

NASH, D. B. (1963). On the distribution of lunar maria and the synchronous rotation of the Moon. *Icarus* **1**, 372–373.

OFFIELD, T. W., AND POHN, H. A. (1968). Lunar crater morphology and relative-age determinations; Part II, Ramifications [Abs.]. Program, *64th Ann. Mtg. Geol. Soc. Am. Cordilleran Sect., April* 11–13, p. 89.

O'KEEFE, J. A. (1968). Isostasy on the Moon. *Science* **162**, 1405–1406.

PICKERING, W. H. (1908). L'origine de la Lune et la probleme des volcans. *Soc. Belge Astron. Bull.* **13**, 71–74.

POHN, H. A., AND WILDEY, R. L. (In press). A photoelectric photographic map of the normal albedo of the Moon. *U.S. Geol. Survey Prof. Paper* **599-E**.

RONCA, L. B. (1966). Meteoritic impact and volcanism. *Icarus* **5**, 515–520.

ROWAN, L. C. (1968). Mass wasting on the lunar surface. Program, *64th Ann. Mtg., Geol. Soc. Am., Cordillerian Sect.*, p. 104.

RUNCORN, S. K. (1962). Convection in the Moon. *Nature* **195**, 1150–1151.

RUNCORN, S. K. (1967). Convection in the Moon and the existence of a lunar core. *Proc. Royal Soc. (London)* **A296**, 270–284.

SAUNDERS, R. S. (1968). Problems for geologic investigation of the Orientale region of the Moon. *In* "Advanced Systems Traverse Research Project Report" (G. E. Ulrich and R. S. Saunders) *U.S. Geol. Survey Interagency Rept.—Astrogeology* **7**, 59 pp.

SHALER, N. S. (1903). A comparison of the features of the Earth and Moon. *Smithsonian Contribs. to Knowledge* **34**, 1–130.

SHOEMAKER, E. M. (1962). Interpretation of lunar craters. *In* "Physics and Astronomy of the Moon" (Z. Kopal, ed.), pp. 283–359. Academic Press, London.

SHOEMAKER, E. M. (1964). The geology of the Moon. *Sci. American* **211**, 38–47.

SHOEMAKER, E. M., AND HACKMAN, R. J. (1962). Stratigraphic basis for a lunar time scale. *In* "The Moon" (Z. Kopal, ed.), pp. 289–300. Academic Press, New York.

STROM, R. G. (1965). Map of flows photographed in Mare Imbrium. *In* "Ranger VII. Part II—Experimenters' Analyses and Interpretations" *Jet Propulsion Lab., Calif. Inst. Technol. Tech. Rept.* **32-700**, Fig. 18.

SUKHANOV, A. L. (1968). The mechanism of origin of the lunar seas. *Akad. Nauk SSSR Doklady* **181**, 309–312 [in Russian]. Translated E. R. Hope, Canada Defense Sci. Information Service transl. T507R, 4 pp.

SUKHANOV, A. L., TRIFONOV, V. G., AND FLORENSIKY, P. V. (1967). Geologic–geomorphic mapping of the Moon and structural features of the lunar surface. Translated from Russian in *Geotectonica* **5**, 327–332.

TURKEVICH, A. L., FRANZGROTE, E. J., AND PATTERSON, J. H. (1968). Chemical analysis of the Moon at Surveyor VI landing site—Preliminary results. *Science* **160**, 1108–1110.

TURKEVICH, A. L., FRANZGROTE, E. J., AND PATTERSON, J. H. (1969). Chemical composition of the lunar surface in Mare Tranquillitatis. *Science* **165**, 277–279.

TURNER, G. (1961). Measurements of the height of the walls of the crater Archimedes. *In* "Studies in lunar Topography" (Z. Kopal, ed.). *U.S. Air Force, Cambridge Res. Lab. GRD Res. Notes* **67**, 150–160.

UREY, H. C. (1956). The origin and significance of the Moon's surface. *Vistas in Astronomy* **2**, 1667–1680.

UREY, H. C., ELSASSER, W. M., AND ROCHESTER, M. G. (1959). Note on the internal structure of the Moon. *Astrophys. J.* **129**, 842–848.

VINOGRADOV, A. P., SURKOV, YU. A., CHERNOV, G. M., KIRNOZOV, F. F., AND NAZARKINA, G. B. (1968). Gamma investigation of the Moon and composition of the lunar rocks. *In* "Moon and Planets." (A. Dollfus, ed.), Vol. II, pp. 77–90. North-Holland Publ. Co. Amsterdam.

WHITAKER, E. A. (1966). The surface of the Moon. *In* "The Nature of the Lunar Surface" (W. N. Hess, D. H. Menzel, and J. A. O'Keefe, eds.), pp. 79–98. Johns Hopkins Press, Baltimore, Maryland.

WILHELMS, D. E (1964) Major structural features of the Mare Vaporum Quadrangle. *In* "Astrogeologic Studies Ann. Prog. Rept., July 1, 1963 to July 1, 1964, pt. A." *U.S. Geol. Survey Open-File Rept.*, pp. 1–16.

WILHELMS, D. E. (1968). Geologic map of the Mare Vaporum quadrangle of the Moon. *U.S. Geol. Survey, Map* **I-548**.

WILHELMS, D. E. (1970). Summary of lunar stratigraphy—telescopic observations. *U.S. Geol. Survey Prof. Paper* **599-F** [in press].

WILHELMS, D. E., AND MCCAULEY, J. F. (1969). Volcanic materials in the lunar terrae—Orbiter observations [abs.]. *Trans. Am. Geophy. U.* **50**, 230.

WISE, D. U., AND YATES, M. T. (1969). Mascons as structural relief on a lunar moho [abs.]. *Trans. Am. Geophy. U.* **50**, 125.

YOUNG, J. (1933). Preliminary report of a statistical investigation of the diameters of lunar craters. *British Astron. Assoc. J.* **43**, 201–209.

CHAPTER VIII – VOLCANISM

VOLCANISM AS A PLANETARY PROCESS

Ronald Greeley
University of Santa Clara, Santa Clara, Calif. 95053

I. INTRODUCTION

Planetary surfaces result from the complex interplay of several geological processes, including impact cratering, igneous activity, tectonism, and gradation. These are general processes that probably are operative on all terrestrial planets, but their relative importance varies with the environment and evolutionary history of each planet. Thus, a thorough knowledge of these processes, their relative importance, and resulting surface features is required to understand the geological history of the terrestrial planets.

Although the role of volcanism on Earth has long been recognized as important, it was not until data were gathered for the ocean basins, showing extensive basaltic lava flows, that its full significance was realized. The role of volcanism on other planets is also beginning to emerge. Data from unmanned lunar missions, returned samples, photographs, and astronaut observations show that volcanism also played a significant role in shaping the surface of the Moon. In addition, *Mariner* missions to Mars have shown that volcanism dominated several regions of Mars, evidenced by tremendous shield volcanoes, dome volcanoes, flood-type lava flows, and fissures. Thus, it is obvious that for at least three out of the five major terrestrial planetary bodies, volcanism as a planetary process is very important.

Comparative geologic studies offer one means for understanding geological processes on other planets. Three steps are involved in such comparative studies: 1) determine the morphology and the conditions of formation for possible terrestrial analogs (e.g., impact craters); 2) through theoretical considerations, determine the ways in which the morphology and process of formation might be different under different planetary conditions (e.g., gravity differences, presence of an atmosphere, etc.); and 3) apply the results to the interpretation of features on extraterrestrial bodies. Unfortunately, most geological processes are too complex to be completely understood, even on Earth. Comparative field studies, however, can result in diagnostic criteria for the identification of extraterrestrial surface features and provide clues to formative processes.

This paper is a brief review of the more common volcanic features that have been identified on the Moon and Mars and offers some possible terrestrial analogs. The features described include volcanic vents, flood-type lava flows, volcanic rilles, and lava domes.

An excellent descriptive and illustrated catalog of terrestrial volcanoes is *Volcanic Landforms and Surface Features: A Photographic Atlas and Glossary*, by N. Short and J. Green (1972). This reference is particularly useful for comparing terrestrial and planetary volcanic features.

II. VOLCANIC VENTS

Prior to the recognition of impact cratering as a significant geological process (before about 1900), most scientists believed that craters on the Moon were volcanic. Later, selenologists were split into two camps, the "impactors" and "volcanists." With the tremendous wealth and quantity of data returned by the Apollo missions, most investigators now recognize that both processes were important on the Moon but that the majority of craters are *impact-produced*. The belief, however, does not exclude some volcanic craters. The problem depends on the ability to recognize and distinguish various types of craters. A further distinction to be made is that between volcanic and tectonic events – both processes are responsible for crater-like depressions. Because the selenologist works mostly from photographs, identification of crater types must be based primarily on morphologic characteristics.

On Earth, volcanic vents occur in a wide variety of forms and sizes, depending primarily upon type, duration, and magnitude of eruption. The resulting landform is typically an irregular crater that has developed through multiple events. In contrast, impact craters result from single events and are usually symmetrical. The following table summarizes the *general* differences between impact craters and volcanic craters:

Impact
1. Circular or symmetrically elongate
2. Floor lower than surrounding plain
3. Symmetric ejecta blanket
4. Overturned rim (inverse stratigraphy)
5. Shatter cones
6. High temperature-high pressure minerals
7. Central peak(s) (some cases)

Volcanic
1. Non-circular
2. Often aligned with similar craters
3. May not have raised rims
4. Normal stratigraphy
5. Lack of shatter cones and high temperature-high pressure minerals
6. Small (typically less than a few kilometers)

Common to both
1. Base-surgetype deposits
2. Brecciation
3. Secondary craters
4. Concentric fractures
5. Rock-melt flows

One quantitative technique to aid in separating craters is to determine their *circularity*. Although this technique is not definitive in itself, it can be used with other criterion for separating impact craters of other origins. Known impact craters and most lunar craters tend to be [illegible] in contrast to terrestrial calderas and ring complexes which deviate widely

from a circle. Murray and Guest (1970) discuss the different techniques for describing crater circularity and present circularities for 215 craters including artificial explosion craters, terrestrial volcanic craters, and various types of lunar craters.

A. Calderas

Calderas are basin-shaped volcanic depressions with diameters that are many times greater than their included vent or vents. They may result from *collapse* of the magma chamber roof (as a result of either magma extrusion or magma withdrawal), *explosive* removal of the upper part of the volcanic cone, *erosion*, or some combination (e.g., Crater Lake caldera, Oregon). On Earth, calderas develop in lavas of all compositions. Because they usually result from multiple events, they generally are irregular in outline (non-circular), display multiple vents, and show post-caldera structures such as flows, rifts, and pit craters (fig. 1).

Several lunar calderas have been tentatively identified. These include the crater Kopff in the Orientale basin, the crater at the head of Schröter's Valley, Wolf Crater, and the summit pits on the Hortensius domes. Most of the identified lunar calderas have typical caldera morphologics and are associated with other volcanic features.

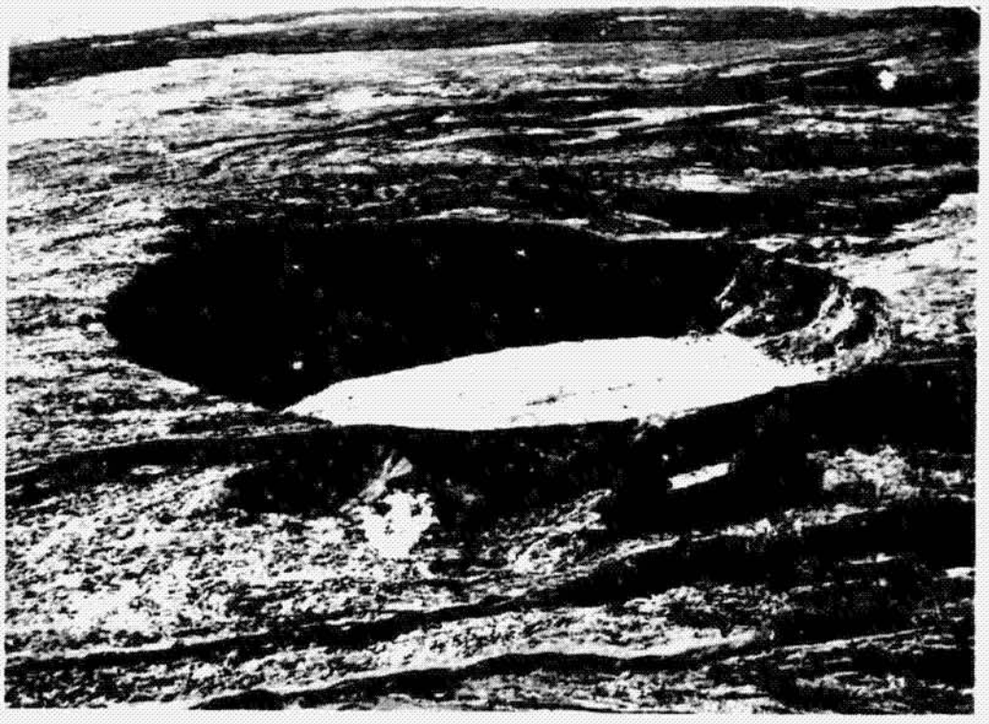

Figure 1. – Rimless pit (approximately 0.5 km in diameter) on the flank of Mauna Loa.

The best examples of extraterrestrial calderas are on Mars (fig. 2). Imagery from Mariner 9 shows several martian volcanic regions (Carr, 1973), including Olympus Mons, the Tharsis mountains, and the Elysian area where classic summit calderas occur on enormous shield volcanoes, some of which rise more than 25 km above the surrounding terrain. The diameter of Olympus Mons is about 600 km and is the largest known shield volcano on both Mars and Earth. Its summit caldera is about 75 km in diameter and is composed of multiple, coalesced craters. Most martian shield volcanoes display various volcanic flow features on their flanks.

B. Maar Craters

Maar craters are low relief depressions typically lacking raised rims (cones), formed by generally single, explosive eruptions (fig. 3). They usually result from the interaction of magma and ground water. Of the various volcanic craters, maars are the most likely type to be confused with impact craters because of their similar morphologies. Both types form through single, short-lived releases of energy. Normal rim stratigraphy distinguishes maars from impact craters which have inverse rim stratigraphy; however, it is not possible to determine rim stratigraphy from most imagery of extraterrestrial structures and we must rely on other criteria for their separation. For example, lunar Rima Hyginus includes a series of circular, cone craters aligned within a graben. They lack the characteristics of secondary impact crater chains and from their morphology and setting, the craters of Rima Hyginus are possible maars. However, even this interpretation may be over-simplified because cone formation on the Moon will result in low-relief rims in comparison to terrestrial volcanic cones because of the lower lunar gravity (Wright *et al.*, 1963).

Because ground ice and possibly ground water are present, Mars is a much more likely planet to have maars than the Moon. None thus far, however, have been positively identified.

Opposite:

Figure 2.– (a) An enormous shield volcano on Mars. Olympus Mons is a mountain 600 km wide at its base and over 25 km in elevation. The summit caldera is approximately 75 km in diameter and is the result of multiple stages of eruptions. (b) The high-resolution image reveals a long lava channel and numerous lava flows. For comparison, the largest shield volcano on Earth, Mauna Loa in the Hawaiian chain, is less than an eighth the diameter of Olympus Mons and less than half its height. Shield volcanoes of comparable size are absent on both the Earth and the Moon and should provide clues for the evolution of planetary interiors.

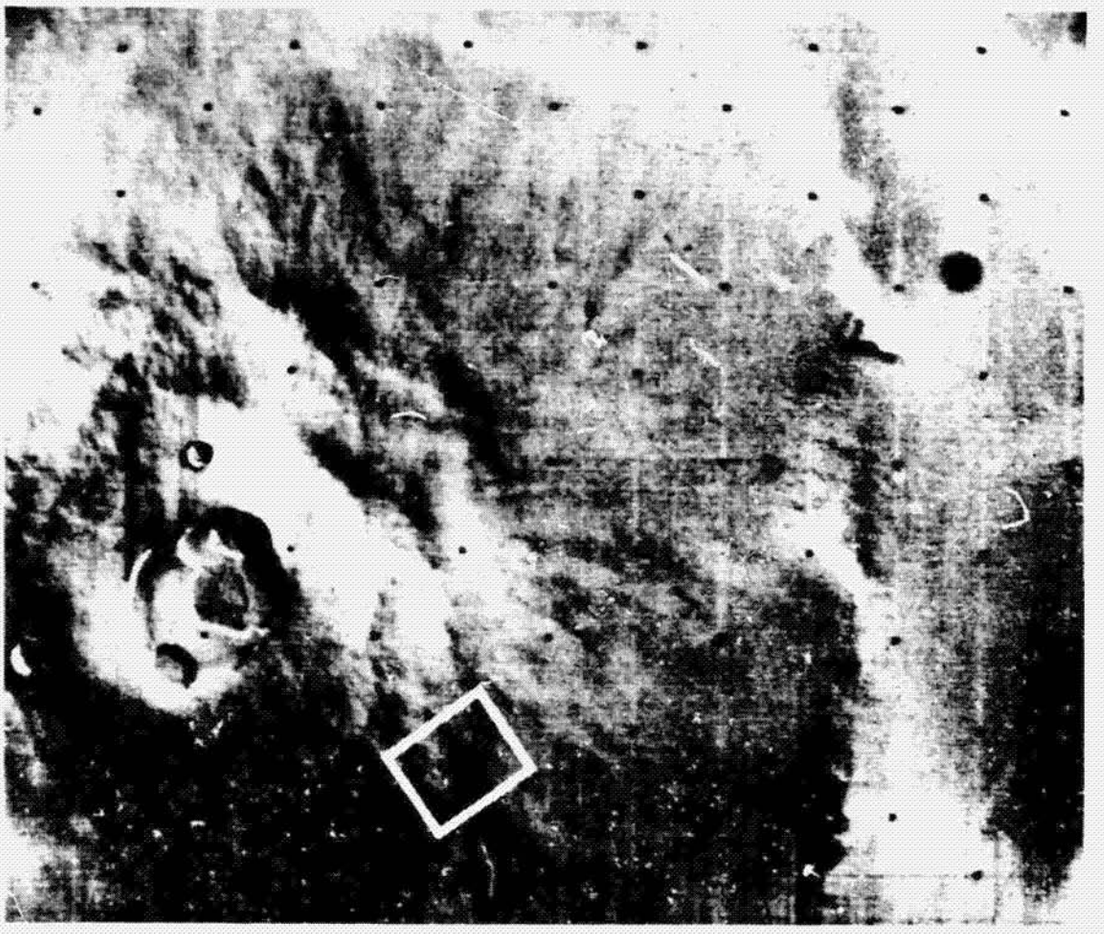

a

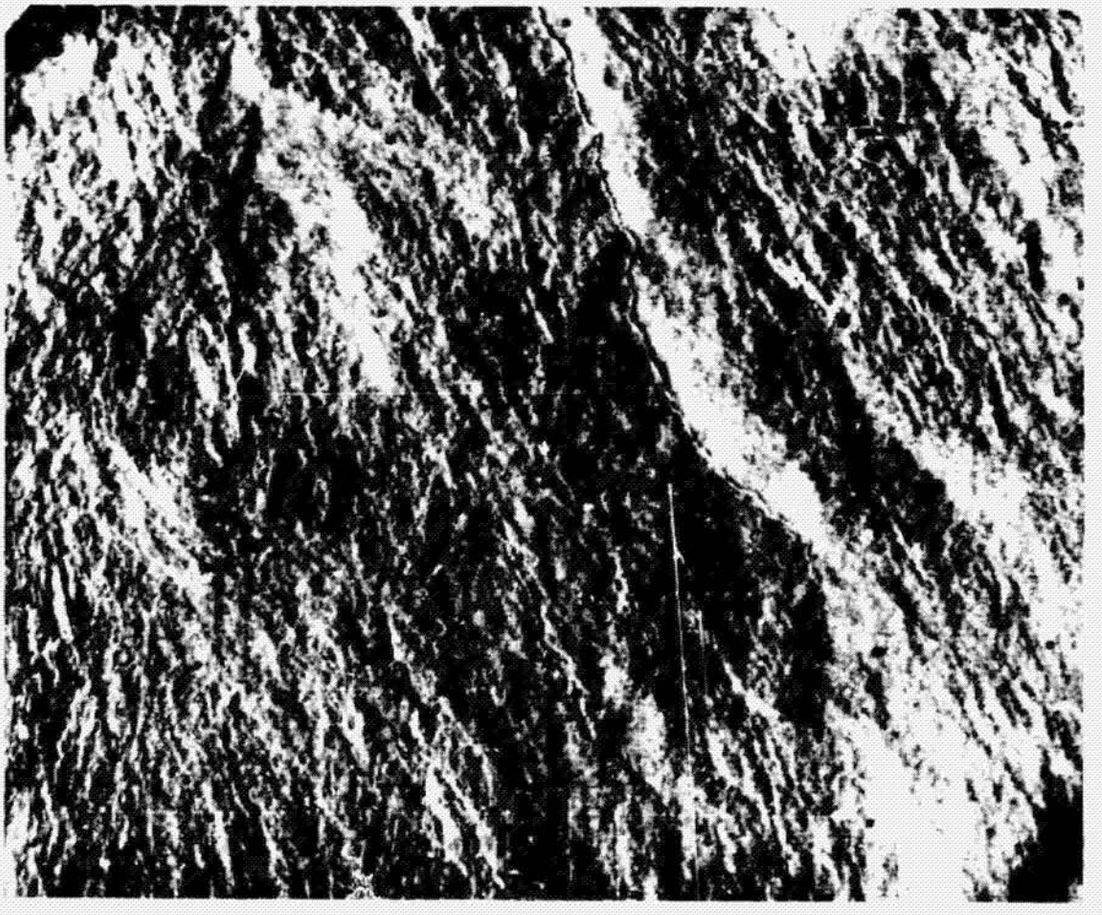

b

Figure 3. – *Terrestrial maar, Elegante Crater (1.5 km in diameter), in the Pinnacate volcanic field of northern Mexico.*

C. Fissure Vents

Fissure vents develop along fissures or rift zones, with lava erupting from a series of "point" sources, or as sheets of flows (or both). Fissure eruptions can involve higher rates of eruption than shield-forming vents and typically produce flood basalt flows. Often, the precise positions of fissure vents are masked by their own products, or by younger flows from other sources. The youngest fissure vents, however, are sometimes visible as fractures (e.g., King's Bowl Rift, Idaho), a chain of elongate depressions, or a chain of spatter cones. The lunar crater Aratus CA in Mare Serenitatis, fractures on the floor of Copernicus, and an unnamed martian structure are possible examples of fissure vents that compare favorably with similar structures in the Snake River Plain, Idaho (fig. 4).

Opposite:

Figure 4. – *Basaltic flow channel extending approximately 2.5 km from a volcanic crater* Inferno Chasm, *in the central Snake River Plain, Idaho.*

III. LAVA FLOWS

Lava flows are lateral bodies of magma extruded from vents or fissures. During active flow, a variety of surface features may develop which are large enough to be visible from the air. Some of the features are diagnostic of specific flow properties and hence their identification can provide clues to the nature of the lava.

A. Flood-Type Flows

Flood-type flows are usually erupted at extremely high rates and involve fluid types of lava. Basalt is the only lava commonly fluid enough to permit the formation of long, thin units characteristic of flood-type flows. Examples are lavas of the Columbia Plateau, the Snake River Plain, and the Modoc Plateau. Mare material that fills lunar basins is composed of basaltic lavas that were erupted (at least partly) as very long, thin, extremely fluid flows. Low illumination photography obtained during Apollos 15, 16, and 17 show the long, thin character of the upper (Eratosthenian) marial lava flows (figs. 5,6(a)).

Similar lava flows have been identified in several plains areas on Mars (Masursky, 1973), notably in the Amazonis basin (fig. 6(b)).

Pressure ridges are surface features that develop on some flood-type flows. They result from deformation of partly cooled crust on top of still-molten and mobile lava. A few small-scale lunar and martian wrinkle (or mare) ridges may have formed by similar processes, although Strom (1971) presents a good case for some lunar mare ridges to have resulted from a combination of extrusive and intrusive processes. Other mare ridges are probably tectonic, resulting from compressional forces (Baldwin, 1963).

B. Collapse Depressions

Some basalt flows, or parts of flows, fill depressions and are ponded. As cooling and degassing occurs, the volume of lava shrinks (shrinkage greater than 40% has been observed in Hawaii, R. Holcomb, per. commun.), leaving "high" lava marks on the sides of the basin. Such bench marks are visible in many lunar regions (Holcomb, 1971; West, 1972). Occasionally, only the center of the pond may collapse, resulting in a highly irregular, flat-floored depression, as seen on the Earth, Moon, and Mars (fig. 7).

Some lava ponds are not *completely* contained in basins, but may collapse by drainage through lave tubes or by withdrawal down the vent; however, the same type of features can develop on temporarily ponded flows as those described above. Collapse craters often form on pahoehoe lava flow surfaces. The craters lack raised rims, are subcircular, and average about 10 m in diameter Similar features were inferred in suspected lava "pools" on the rim of Copernicus by analysis of crater statistics (Greeley and Gault, 1971). An anomolously high frequency of small craters was found in the "pools," which, coupled with the setting and surface morphology, was interpreted to mean that collapse craters were present, along with the normal impact craters.

Figure 5.—Successive lava flows in Mare Imbrium: flow 1 being the youngest, flow 3 the oldest. Note the arcuate wrinkle ridge system that encircles Mare Imbrium.

Opposite:

Figure 6.– Lunar lava flows in Mare Imbrium, (a) (LO-V-161-M) and Martian lava flows, (b) (MTVS 4179-30: DAS 6966608), on the floor of the Amazonis basin. The sheets of lava indicate low viscosities of the flows.

b

a

Opposite:

Figure 7. – Terraced lava pools on the Moon (a) and on the Earth (b). The lunar example (AS15-M3-2358) occurs on the farside west of the crater Scaliger and is contained within a breached craterform approximately 35 km across. It is part of a small mare-filled region adjacent to Mare Australe. The terraces are believed to reflect previous levels of the mare basalts. The terrestrial example is a basaltic pool (less than 1 km across) on the flank of Mauna Loa.

b

a

C. Channels and Lava Tubes

Observations of active basalt lava flows and field investigations of solidified basalt flows and lava tubes indicate that lava tubes can form by several mechanisms (figs. 8–10).

Lava tubes form in pahoehoe basalt flows that have partly cooled to form a surface crust, with flow of fluid lava continuing beneath the crust. As cooling progresses, active flow is restricted to a conduit within the flow. Toward the flow front, the conduit subdivides into smaller, multiple distributaries termed *feeder tubes* that lead molten material to the advancing flow front. As the supply of lava from the vent diminishes, molten lava drains from beneath the free-standing crust and leaves a hollow void, or lava tube. Most feeder tubes do not drain, or are sealed with lava from subsequent flows. Lava tubes also develop from open channels, or lava rivers (Greeley, 1971, 1972), which develop surface crusts.

Lava tubes occur on slopes ranging from about 0.4° to 6.5°. In contrast, channels appear to form on slopes over a much wider range and develop in both viscous (aa) basalt and fluid (pahoehoe) basalt. Apparently, if flow velocity is high (as on steep slopes), then the flow may become turbulent, or if the flow is too viscous (aa basalt), then open channels may form instead of lava tubes. However, sections of turbulent channels may become roofed by accretion of splashed lava along the banks. Channels also may form as a result of drainage of molten lava from beneath the crust before the crust has cooled and solidified to a thickness sufficient to support its weight. The width of the channel also may exceed the maximum span attainable by a free-standing basalt roof. In either case, the cooled or partly cooled roof collapses as the supporting fluid drains. This type of collapse often occurs in terrestrial structures and typically results in sinuous channels with smooth sides or as a series of elongate drainage craters. Thus, channels may develop in preference over tubes when (1) the gradient is steep, (2) the lava is viscous (precise limiting viscosities are not known), or (3) the crust over the molten lava is not free standing after drainage of the lava. Thus, the distinction between the tubes and channels can be made in regard to the crust: If the roof is free standing after drainage of molten lava, the structure is a tube; if the crust only partly develops, or collapses during drainage, the structure is a channel. Some resulting structures alternate from tube to channel to tube, etc.

Active lava flows containing tubes and channels with surface crusts are closed hydrostatic systems. As an advancing flow encounters a topographic obstruction, such as a ridge, the flow may ride up and over the obstruction; the contained tube or channel then may act as a siphon operating under hydrostatic pressure to carry molten lava to the advancing flow front.

Cross sections perpendicular to lava tubes and channel axes show that lava flows typically form topographic highs, or ridges, along the axes. Lava channels are aggradational features and the channel floor is often elevated considerably higher than the surrounding ground level. This condition results from accretion of lava that spills over the bank of the channel. Multiple surges of lava, or individual flow units, may spread laterally from the main channel through distributary channels or tubes. Multiple eruptions will continue to elevate the channel and adjacent area by accretion. Tubes and possibly channels also can be erosive structures. Lava tubes in southwest Washington and northern California show areas in which the lava tube and flow apparently undercut the pre-flow valley wall.

Figure 8.—Southwest rift zone on Mauna Loa, Hawaii, with channeled pahoehoe flows. Cones and spatter ramparts have built up along the rift from fire fountain eruptions. Note the channel sinuosity, the merging channels, and the braidlike pattern (the result of successive flows).

Opposite:

Figure 9. – Stereo pair of Mammoth Crater (400 m across) and Lava Tube, Lava Beds National Monument, California.

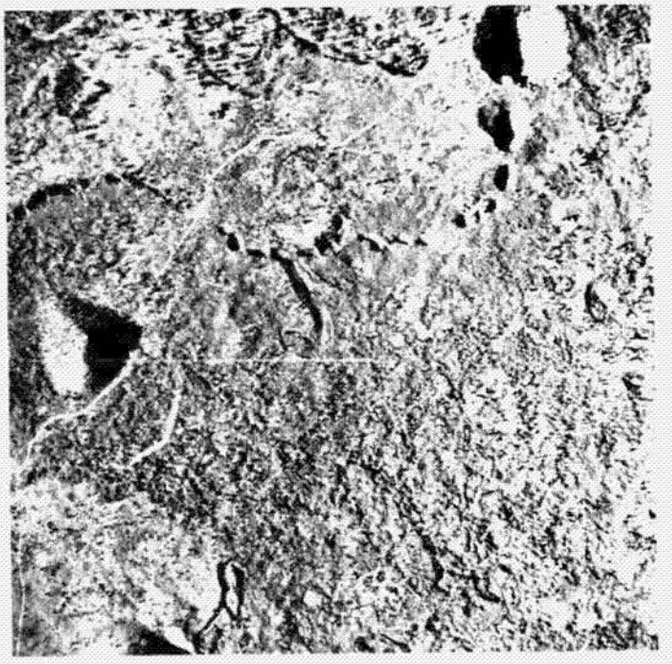

Opposite:

Figure 10.– Lava River Cave (Tube) near Bend, Oregon. This is one of the longest uncollapsed lava tubes in the area. The roof is relatively uniform in thickness (as thick as 22 m) throughout its length. The tube wall displays multiple flow lines.

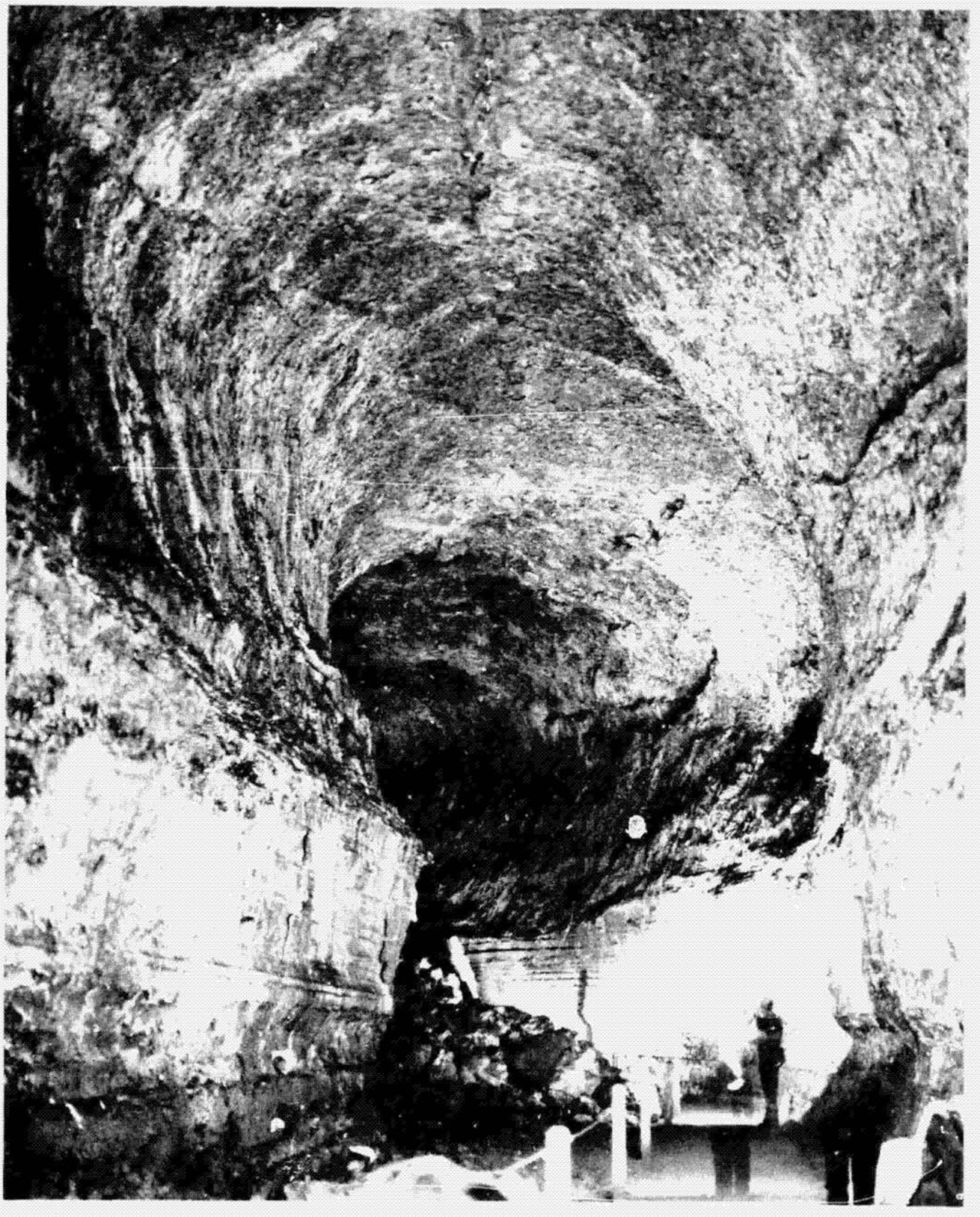

Lava tubes and channels commonly form cut-off branches along the main structure. Cut-offs may be at higher, lower, or the same level as the main structure. Collapse of the roof results in an "island" surrounded by lava trenches. As collapse progresses, large blocks parallel to the tube axes can break away from the wall and slump into the collapsed tube.

Width of lava tubes may be fairly constant throughout their course or they may vary in width. The trench resulting from lava tube roof collapse usually reflects the original configuration of the tube. Lava channels, on the other hand, are fairly constant in width; however, they often become progressively shallower down slope.

Lava tubes and channels have been identified in several lunar and martian regions on the basis of their geomorphology and geologic setting. Many lunar sinuous rilles (figs. 11–14(a),(b)) originate in craters, trend down slopes, are generally (but not always) restricted to mare material (basaltic lava flows), are controlled by pre-mare topography, have cut-off braces, and lateral leeves. Many martian channels, particularly those associated with the shield volcanoes, have these same characteristics. The primary problem in comparing lunar and martian rilles to terrestrial lava tubes or channels is the disparity in size. The extraterrestrial features are commonly 3-10 times larger than their earthly counterpart. However, laboratory determinations of the viscosity and thermal conductivity of lunar basalts indicate that lunar lava flows could be extremely long (confirmed by Apollos 15, 16, and 17 photography) and it seems likely that associated flow features would be correspondingly large.

IV. LAVA DOMES

Lava domes are constructional volcanic landforms that develop from the eruption of viscous varieties of lava, such as rhyolite and dacite. In contrast to shield volcanoes and other fluid lava features, domes are small and steep-sided. Lava flow textures are blocky and domes lack flow channels and lava tubes. Examples are the domes near Mono Crater, California. Lunar domes (figs. 14(c),(d)) occur in several areas, notably near Gruithusen in the Rümker Hills and on the floor of Copernicus. These and other examples are discussed by Smith (1973) along with possible terrestrial analogs. Hecates Tholus is an example of a martian volcanic dome.

Opposite:

Figure 11.– Lunar sinuous rille characteristics. Although many sinuous rilles resemble terrestrial lava channels and tubes, they are typically much longer. This difference in scale may be the result of greater volumes of erupted lunar lavas with very low viscosities.

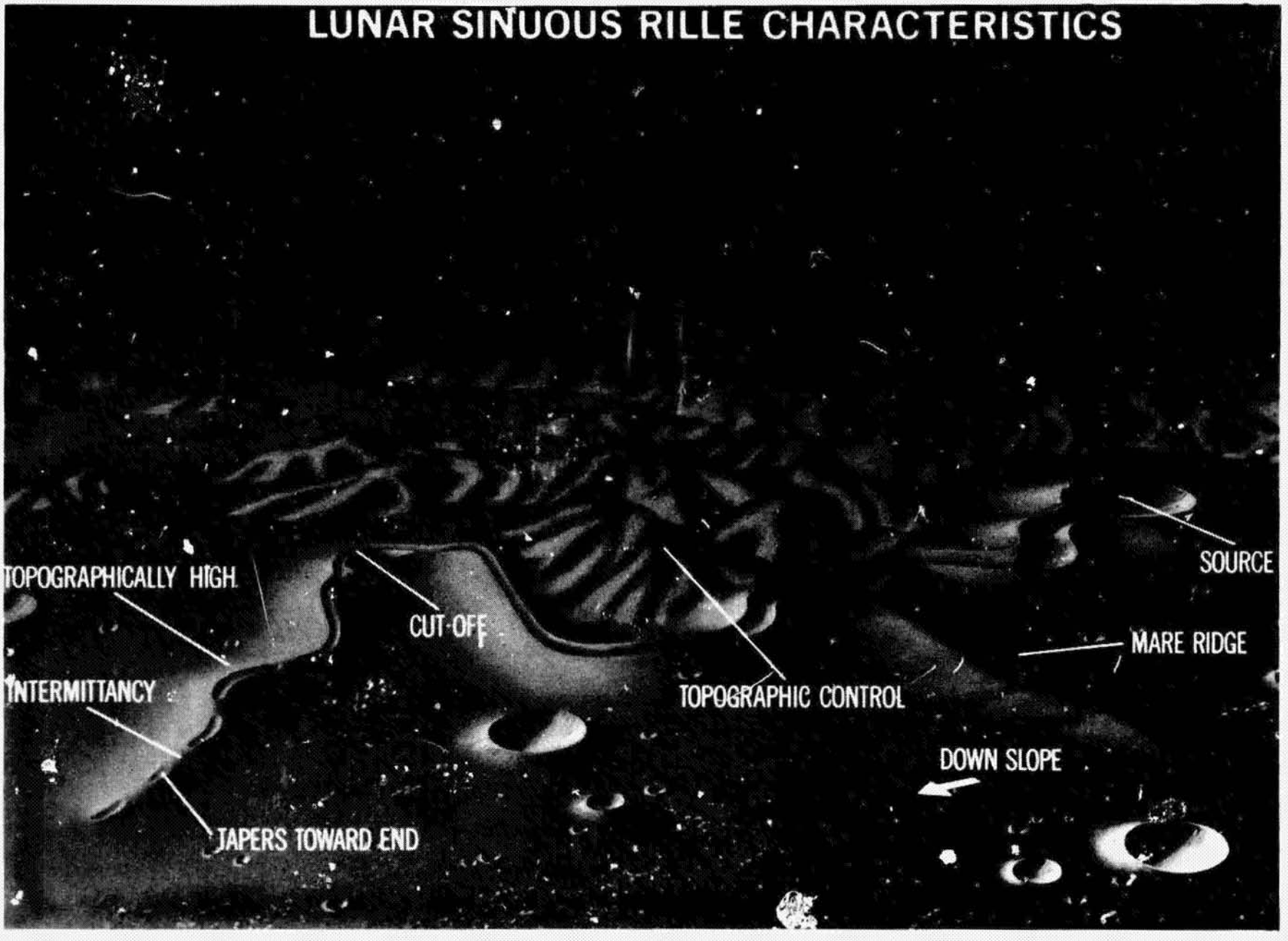
LUNAR SINUOUS RILLE CHARACTERISTICS
TOPOGRAPHICALLY HIGH
CUT-OFF
SOURCE
MARE RIDGE
INTERMITTANCY
TOPOGRAPHIC CONTROL
DOWN SLOPE
TAPERS TOWARD END

Opposite:

Figure 12.– An oblique view of lunar sinuous and rectilinear rilles in the Harbinger Mountains. The rectilinear part probably represents structural control of a portion of the flow path. Note the merging of rilles extending from the Aristarchus Plateau (to the right). The Harbinger Mountains are believed to represent massifs forming part of an inner ring of the Imbrium Basin. Sinuous rilles typically occur in such ring zones and suggest eruptions along deep faults originally produced by the formation of the basin.

Opposite:

Figure 13.– Stereo views of the volcanic Marius Hills. The top pair, (a) (LO-V-211-M) and (b) (LO-V-210-M), reveals irregular plateaus, low-relief domes, wrinkle ridges, and a discontinuous rille (partly collapsed lava tube?). The region shown in (c) (LO-V-215-M) and (d) (LO-V-212-M) is adjacent and to the north (left) of the region in (a) and (b). Two sinuous rilles cross the wrinkle ridge. Note that the rille at left splits into smaller rilles at its terminus whereas the rille at right abruptly ends at the edge of a broad, low-relief terrace. This stereo pair also reveals breached and elongate cones, textured plateaus, and collapse pits. The vertical length of these photographs corresponds to 70 km.

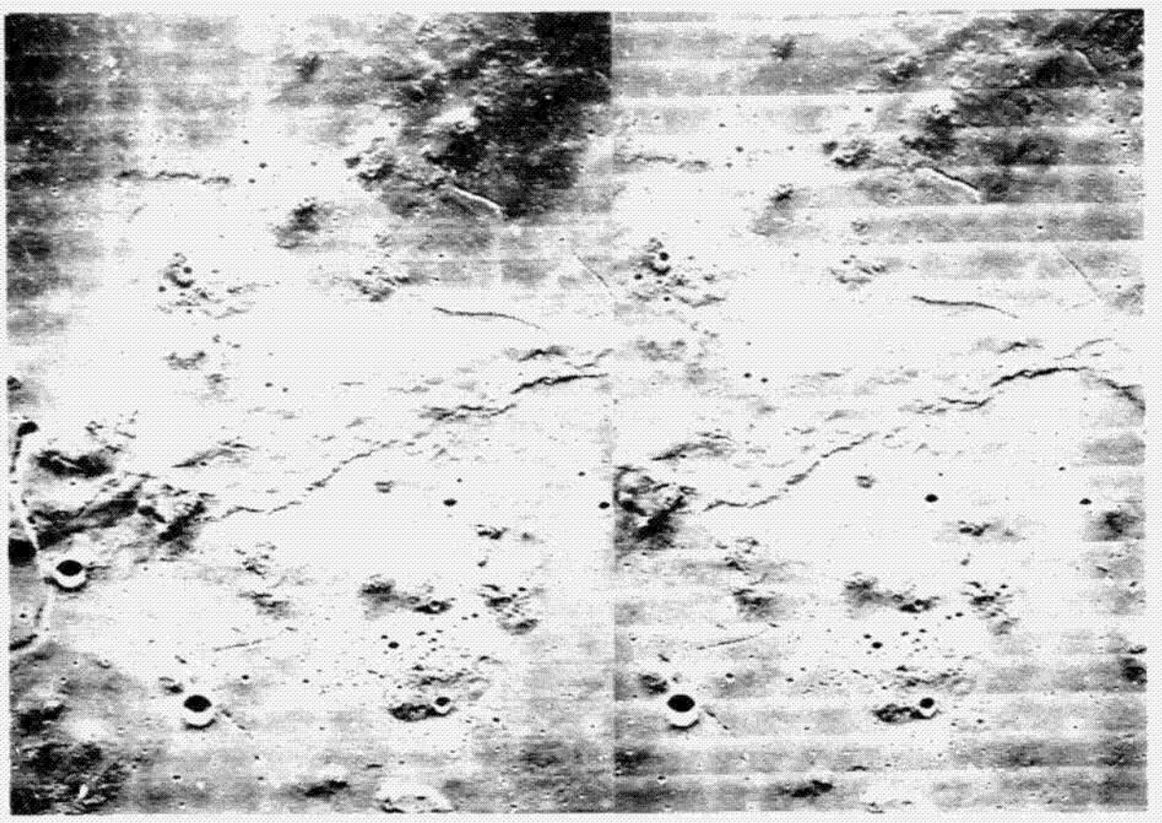

a b

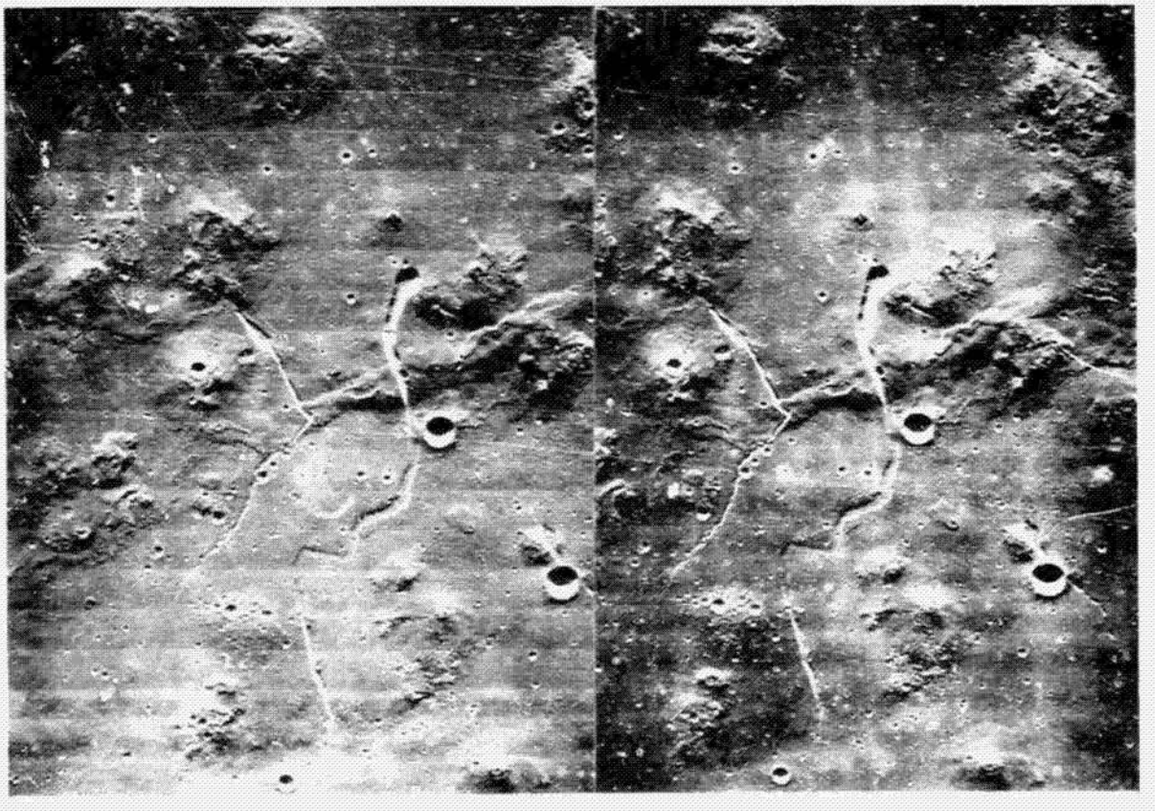

c d

Opposite:

Figure 14.– Close-up views of the Marius Hills. Volcanic cones are clearly shown in (a) (LO-V-215-M); in particular, note the breached cone (lower left), the elongate cone (center), and the smaller cones. In addition, the branching rille terminus noticed in figures 9(a) and (b) is shown in the lower right. Another view, (b) (LO-V-215-M), includes the other end of the rille where it is connected with a wrinkle ridge and appears to be related to the corrugated surface across the summit of the irregular dome. The width of both (a) and (b) corresponds to 15 km. The stereo pair, (c) (LO-V-215-M) and (d) (LO-V-212-M), shows a textured dome (approximately 8 km in diameter) surrounded, in part, by irregular terraces.

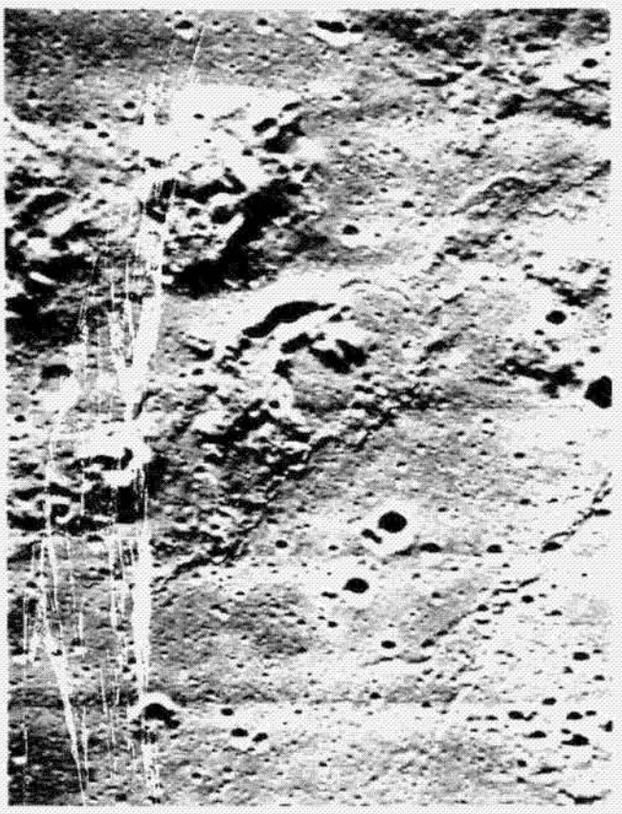

a

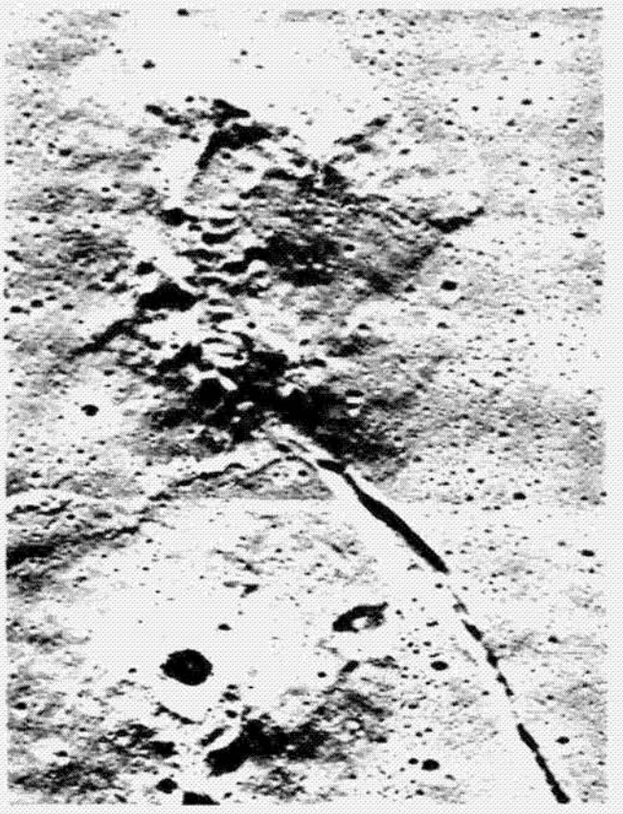

b

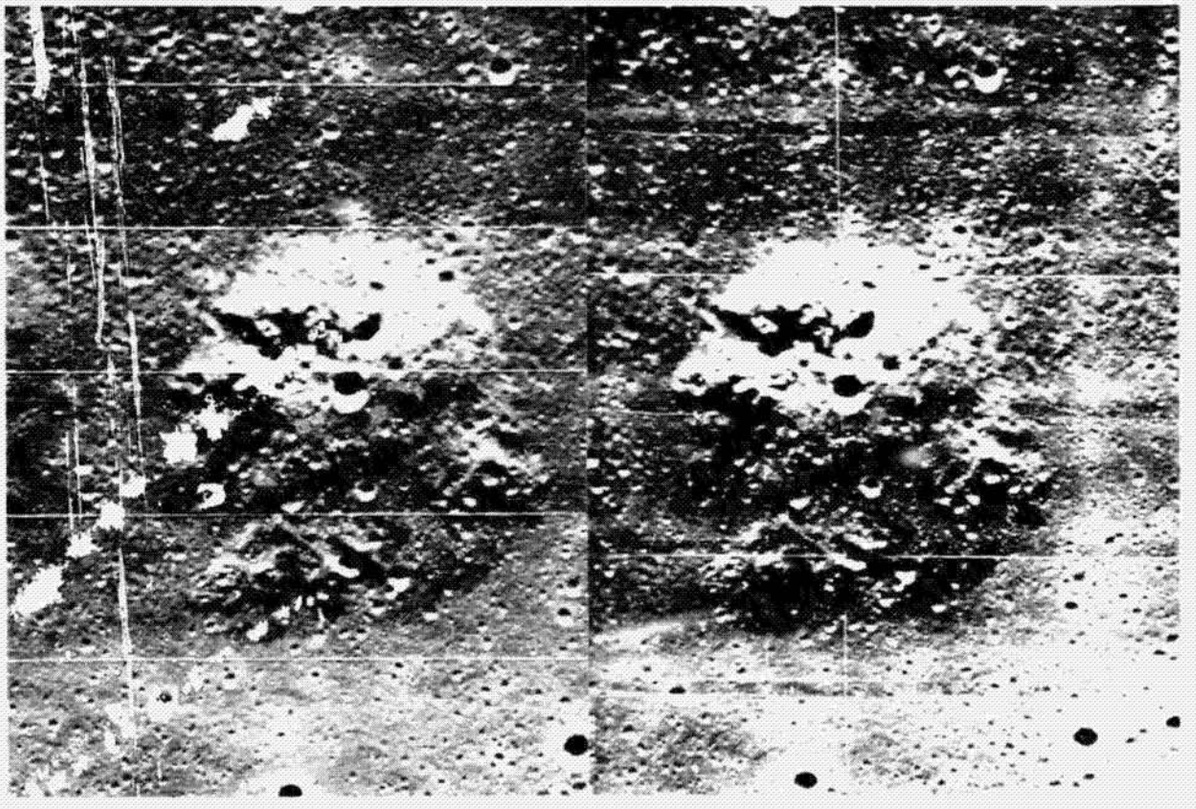

c d

V. CONCLUSIONS

Volcanic features have been identified on the Earth, Moon, and Mars. Through comparative studies, it is possible to interpret the form, structure, and origin of many extraterrestrial volcanic features, whose identification and classification are essential to the derivation of regional geology and the general geological evolution of planets.

REFERENCES

Carr, M. H., 1973. Volcanism on Mars. Jour. Geophys. Res., v. 78. pp. 4049-4062.

Greeley, R. 1971. Observations of actively forming lava tubes and associated structures, Hawaii. Modern Geology, v. 2, pp. 207-223.

Greeley, R. 1972. Additional observations of actively forming lava tubes and associated structures, Hawaii. Modern Geology, v. 3, pp. 157-160.

Greeley, R. and Gault, D., 1971. Endogenetic craters interpreted from crater counts on the inner wall of Copernicus. Science, v. 171, p. 477-479.

Green, Jack and Short, Nicholas M., editors, 1971. Volcanic landforms and surface features, a photographic atlas and glossary. Springer-Verlag, New York.

Holcomb, R., 1971. Terraced depressions in Lunar Maria. Jour. Geophys. Res., v. 76, pp. 5703-5711.

Masursky, H., 1973. An overview of geological results from Mariner 9. Jour. Geophys. Res., v. 78, pp. 4009-4030.

Murray, J. B. and Guest, J. E., 1970. Circularities of craters and related structures on Earth and Moon. Modern Geology, v. 1, pp. 149-159.

Smith, E. I., 1973. Identification, distribution and significance of lunar volcanic domes. The Moon, v. 6, pp. 3-31.

Strom, R. G., 1971. Lunar mare ridges, rings and volcanic ring complexes. Modern Geology, v. 2, pp. 133-157.

West, M., 1972. Selected volcanic features in Apollo 15. Preliminary Science Report. NASA SP-289, pp. 25-81 – 25-83.

Wright. F. E., Wright, F. H., and Wright, H., 1963. In Moon, Meteorites and Comets, ed. G. Kuiper and B. Middlehurst. Univ. Chicago Press, Chicago, pp. 38-43.

With permission, reprinted from The Moon,
vol. 6, 1973, pp. 3–31.

IDENTIFICATION, DISTRIBUTION AND SIGNIFICANCE OF LUNAR VOLCANIC DOMES*

EUGENE I. SMITH**
Dept. of Geology, University of New Mexico, Albuquerque, N.M., U.S.A.

(Received 21 March, 1972)

Abstract. Over 300 previously unrecognized volcanic domes were identified on Lunar Orbiter photographs using the following criteria: (1) the recognition of land forms on the Moon similar in morphology to terrestrial volcanic domes, (2) structural control, (3) geomorphic discordance, and (4) the recognition of land forms modified by dome-like swellings. Many terrestrial volcanic domes are similar in morphology to lunar domes. This analogy suggests that some lunar hills are in fact extrusive volcanic domes. Many of the domes identified in this paper seem to be related to basins and craters, and with the exception of local tectonic grid control few domes are related to any observable Moon-wide pattern. Domes are not uniquely found on maria. Dome formation probably spans a wide range of lunar time and activity in areas where domes are located may be continuing to the present as revealed by the close correlation of dome distribution with the distribution of lunar transient events. The overall morphology of a lunar dome is a poor indicator of the composition of the rock that forms the dome.

1. Introduction

The form and distribution of lunar volcanic domes bear on the problem of the nature of lunar volcanism. Furthermore the distribution of domes and other probable volcanic features may provide clues to structural patterns controlling volcanism.

The Lunar Orbiter missions provided good high resolution photographs of most of the Moon and revealed over 300 previously unrecognized domes and other probable volcanic land forms. This paper discusses the criteria established for identification of lunar volcanic domes and the significance of dome distribution. Domes identified by methods presented here vary greatly in morphology from broad mare domes to irregular steep-sided cratered domes. The irregular steep-sided features are of particular interest because many resemble extrusive volcanic domes in terrestrial volcanic fields. For example, Holocene rhyolite domes in the Mono Craters in California are similar in morphology to some steep-sided lunar land forms. This analogy suggests that extrusive volcanic domes are indeed present on the Moon. Many lunar domes seem to be associated with basins and craters, and with the exception of local tectonic grid control few are related to any Moon-wide pattern.

Apollo orbital photography is now being studied to re-examine domes identified on Lunar Orbiter photographs and to survey areas where high resolution Lunar Orbiter coverage was not satisfactory. Most interpretations have not changed by viewing domes on Apollo photographs.

* Contribution No. 33 Planetary Geology Group, University of New Mexico.
** Present address: Division of Science, University of Wisconsin – Parkside, Kenosha, Wis. 53140, U.S.A.

In this paper, I have adopted the definitions of mare material, mare and basin established by Hartmann and Wood (1971). They define *mare material* as "relatively smooth dark material... can occur in basins, craters or irregular depressions". *Mare* is defined as "a large deposit of mare material whether in a circular basin or irregular depression", and *basin* "is used to designate the largest circular depressions... Basins may or may not be flooded by mare material".

2. Definitions of Terrestrial and Lunar Domes

On Earth, the term *volcanic dome* has been broadly applied to basalt shield volcanoes, Pelean spines, tumuli and felsic extrusions. Williams (1932a), however, restricted the definition to include only "steepsided, viscous protrusions of lava forming more or less dome-shaped masses around their vents (Williams, 1932a)". Examples of volcanic domes of this type are in the Mono Craters, California (Putnam, 1932; Smith, 1970) (Figure 1). These rhyolite domes vary in diameter from less than 100 m to more than 2 km and are commonly associated with flows and craters. Flows rarely travel more than 2 km from their source. Collapse craters are shallow sags with depth-diameter (d/*D*) ratios varying from about 1:5 to about 1:10. Explosion craters on the other hand are deep cone-shaped craters (d/*D* about 1:3) up to 2 km in diameter.

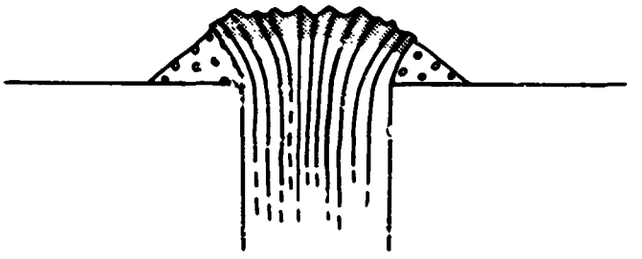

Fig. 1. Diagramatic cross section of a terrestrial volcanic dome.

In this paper, the term *lunar volcanic dome* is used in its broad sense. That is swellings on the maria, irregular swellings and steep-sided hills are referred to as domes, even though many of these features may not be true volcanic domes. Some, in fact, may be cinder cones, stratovolcanoes and shield volcanoes.

Previous lunar dome definitions are inadequate in that they only describe mare domes (Westfall, 1964). A typical mare dome is a low blister-like feature, circular to irregular in shape with diameter ranging from the limit of telescopic resolution to

about 35 km. The average mare dome diameter is about 4 km (Brungart, 1964). Slope angle rarely exceeds 5° on the flanks of mare domes.

3. Literature Review

Previous studies of lunar domes were based primarily on telescopic observations and detailed studies of Earth-based photographs. Most of these studies described broad mare domes and various hypotheses were presented for their origin. Shaler (1903) and Spurr (1944) indicated that domes might be formed by trapping gas beneath the surface, uparching surface layers. Pickering (1903) and Baldwin (1963) showed similarities between basaltic shield volcanoes and mare domes, and Herring (1960) and Fielder (1962) advanced the idea that domes were laccolithic intrusions. Beswick (1962) suggested that domes may develop into craters. Domes mapped by the U. S. Geological Survey, Branch of Astrogeology, were interpreted as laccoliths, shield volcanoes and extrusive domes.

Arthur (1962) and Baldwin (1963) stated that domes are on the maria and noticeable clustered on both sides of the lunar equator, and Brungart (1964) substantiated this observation. Bülow (1964) indicated that domes probably existed on the lunar highlands, but could not be seen from Earth. Lunar domes were catalogued by Moore and Cattermole (1957), Abbey and Both (1958), Brungart (1964), Rae (1963, 1966) and Jamieson and Rae (1965).

Features other than mare domes were interpreted as endogenic land forms on Ranger, Orbiter and Apollo photography. Kuiper *et al.* (1965) on Ranger photographs compared several domes to tumuli on basalt flows, and Elston (1967) interpreted spines with summit pits on the northeast wall of Alphonsus as extrusive morphologies. On Lunar Orbiter photographs, McCauley (1967, 1969) interpreted hills in the Marius Hills as domes and cinder cones. O' Keefe *et al.* (1967) suggested that the Flamsteed structure was the surface expression of a ring dike, with domes and flows exposed, and Smith (1969) interpreted the Rümker Hills as a dome complex and suggested analog of domes in the Mono Craters, California to some lunar cratered domes (Smith, 1970). Eggleton (1970) suggested that several features in the Rümker and Montes Riphaeus quadrangles are stratovolcanoes. Apollo Orbital photography has revealed several probable domes (El Baz and Wilshire, 1969; El Baz, 1971; Scott *et al.*, 1971).

4. Criteria for Identification of Lunar Volcanic Domes

A. INTRODUCTION

Domes on Lunar Orbiter photographs were identified by application of a set of objective criteria which are based on (1) the recognition of land forms modified by dome-like features, (2) structural control and geomorphic discordance, and (3) characteristic surface morphology and the shape and dimensions of summit pits. Features identified by these criteria are interpreted as endogenic and not as features

related to meteorite or asteroidal impact. The number of domes identified as volcanic by these criteria is probably a conservative estimate of the total number of lunar domes, because dome identification is extremely difficult in the lunar highlands where many positive topographic features occur. A summary of criteria used to identify domes is given on Table I.

TABLE I

Summary of Criteria for Identification of Lunar Volcanic Domes

A. Land forms modified by dome-like swellings
   1. Swellings on crater walls, rims and floors.
   2. Swellings on mare ridges, and associated with rilles.

B. Structural control
   1. Swellings at the intersection of mare ridges.
   2. Swellings at the intersection of rilles.
   3. Swellings at crater intersections.

C. Geomorphic discordance
   1. Land forms superimposed on regional trends.
   2. Land forms with fresh looking appearance in areas where other features are subdued.
   3. Land forms atypical of the local terrain.

D. Morphologic criteria
   1. The presence of analogous land forms on Earth and Moon.
   2. Identification of volcanic craters associated with positive topographic features by depth-diameter technique (Smith, 1971) or crater circularity (Murray and Guest, 1970).

B. LAND FORMS MODIFIED BY DOME-LIKE SWELLINGS

Deviation from typical crater morphology, that is a distinct deviation from the shape which is typical of the majority of craters of the same size and age, is considered evidence for modification by endogenic processes. Examples are oversized central peaks, large swellings on crater walls and rims, and hills on a crater floor not related to the central peak or wall slump blocks. Swellings on mare ridges probably have an endogenic origin, since mare ridges themselves are interpreted as intrusive and/or extrusive features (Strom, 1971). Strom (1971) also noted the presence of swellings and small hills on mare ridges and interpreted them as post-mare volcanic hills. Swellings associated with rilles are also interpreted as domes.

Examples of domes in craters are: (1) a crater 8.9 km in diameter north of Mare Serenitatis enclosing a cratered central dome 3.5 km in diameter (Figure 2); (2) a crater in western Oceanus Procellarum 5.6 km in diameter with a cratered dome 2.8 km in diameter (Figure 3); (3) craters in Aitken filled with bulbous domes (boytroidal fill) (Figure 4); (4) domes in large fresh craters (Tycho, Aristarchus, Copernicus). An example of a swelling on a mare ridge is in southeastern Oceanus Procellarum (Figure 5) and domes associated with rilles are in southern Oceanus Procellarum (Figure 6) and near the crater Gruithuisen.

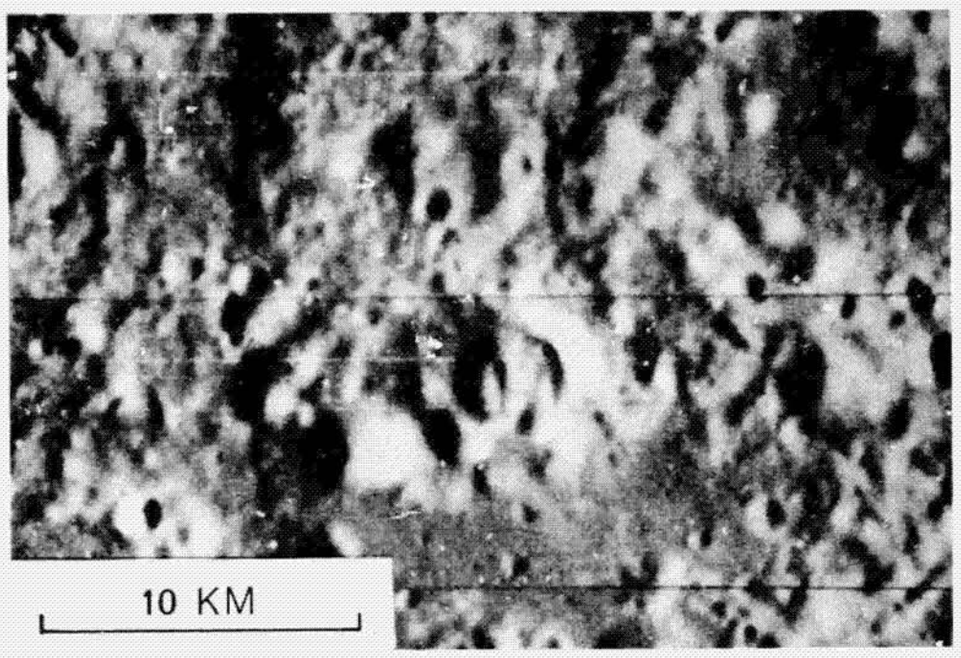

Fig. 2. A crater 8.9 km in diameter north of Mare Serenitatis which encloses a cratered dome (Lunar Orbiter 4).

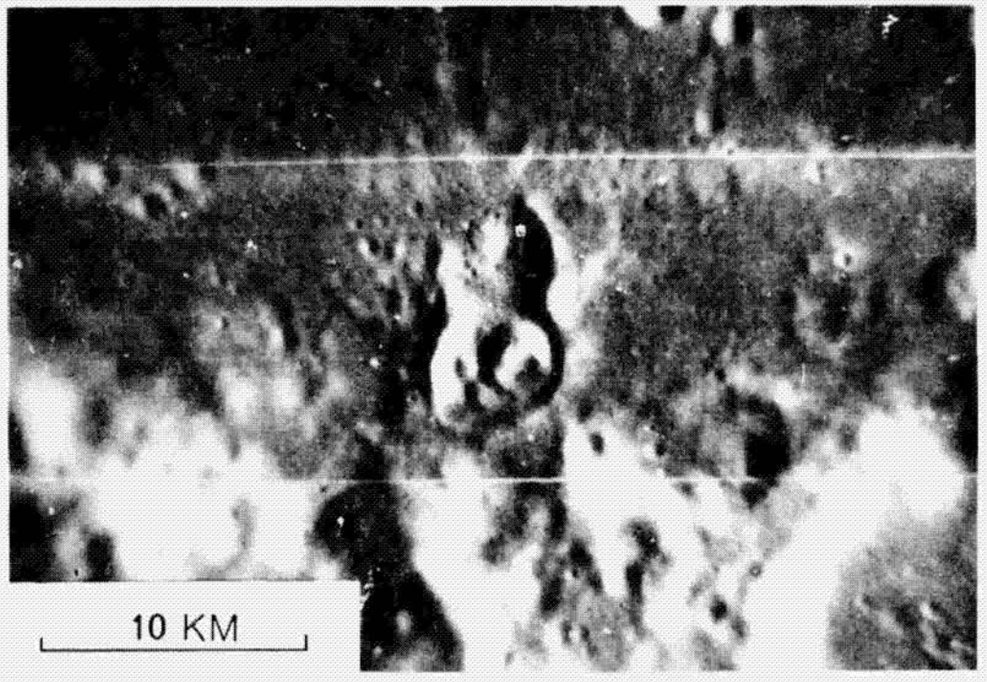

Fig. 3. A crater in western Oceanus Procellarum 5.6 km in diameter enclosing a cratered dome 2.8 km in diameter (Lunar Orbiter 4).

C. STRUCTURAL CONTROL AND GEOMORPHIC DISCORDANCE

Intersection of structural elements often controls the location of domes. For example bulbous forms at the intersection of mare ridges (Figure 7), at the intersection of rilles (Figure 8), and at the intersection of two craters (Figure 9) are interpreted as volcanic domes. Domes also may be aligned in a common direction, for example, the Hortensius domes.

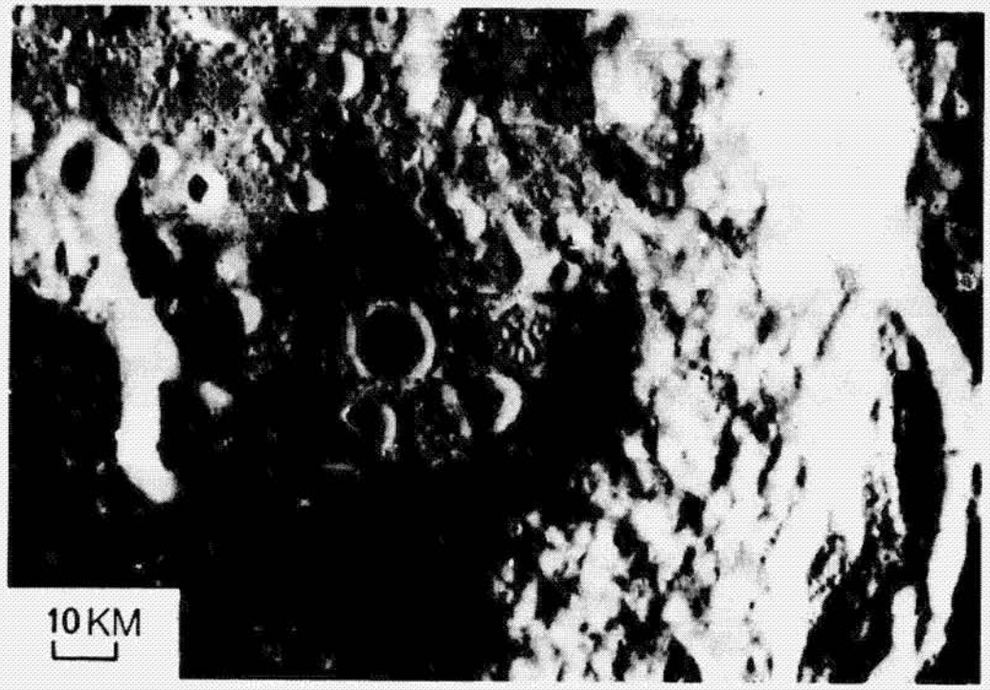

Fig. 4. Craters in Aitken filled with bulbous domes (botryoidal fill) (Lunar Orbiter 3).

Geomorphically discordant land forms are those which cut or are superimposed on regional trends, or have a sharp and fresh-looking appearance in areas where other features are subdued or those features which are atypical of the local terrain. Examples are the Gruithuisen domes (Figure 10) and a large cratered hill in an unnamed crater on the far side of the Moon (Figure 11).

D. MORPHOLOGIC CRITERIA

Information gained from study of Holocene terrestrial volcanic domes can be used as criteria for lunar dome identification. For example, Holocene rhyolite domes in the Mono Craters, California (Putnam, 1938; Smith, 1970) have characteristic surface morphologies. Their surfaces are irregular and covered with blocks; locally spines of breccia and massive rock protrude through debris (Figures 1 and 12). Flanks of the domes stand at the angle of repose (35°) and are mantled by ash, lapilli and blocks.

The overall shape of these features is due to debris resting at or near the angle of repose and not to shape or structure of the central plugs (Putnam, 1938; Smith, 1970). Similar shapes are found in domes of dacite (Williams, 1932b) and andesite (Georgala 1962).

Fig. 5. A swelling on a mare ridge in southeastern Oceanus Procellarum (Lunar Orbiter 4).

Several lunar domes are covered by debris and may be analogous to domes in the Mono Craters. For example, on the floor of Copernicus there are irregular hills and cratered cones covered by blocks which are in places arranged in circular patterns (Figure 13). It is suggested that these rubble-covered hills on the floor of Copernicus are lava extrusions surrounded by debris and hence are analogous to domes in the Mono Craters.

In the Mono Craters, there is a distinct eruptive sequence (Smith, 1970) which accounts for the wide diversity of domal forms. The sequence has the following

stages (1) formation of explosion crater, (2) extrusion of a dome in the explosion crater, (3) cratering of the dome by collapse and explosions, and (4) extrusion of a dome on the floor of the crater formed in stage 3 and its subsequent cratering producing a double crater. Flows are associated with stages 2 and 4 of the sequence (Figure

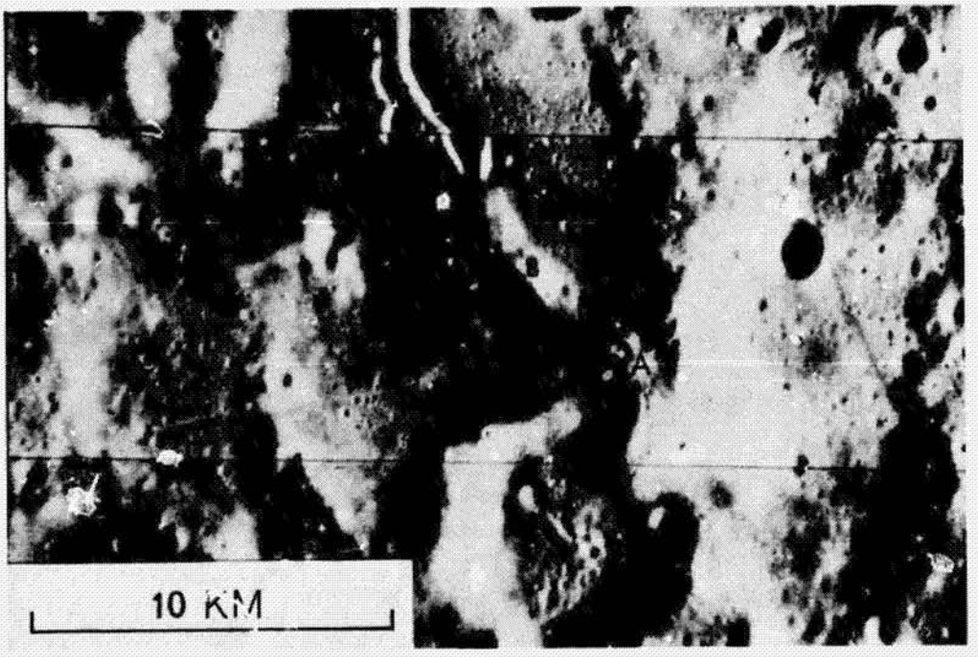

Fig. 6. A cratered dome (A) and ridge (B) associated with a rille in southern Oceanus Procellarum (Lunar Orbiter 4).

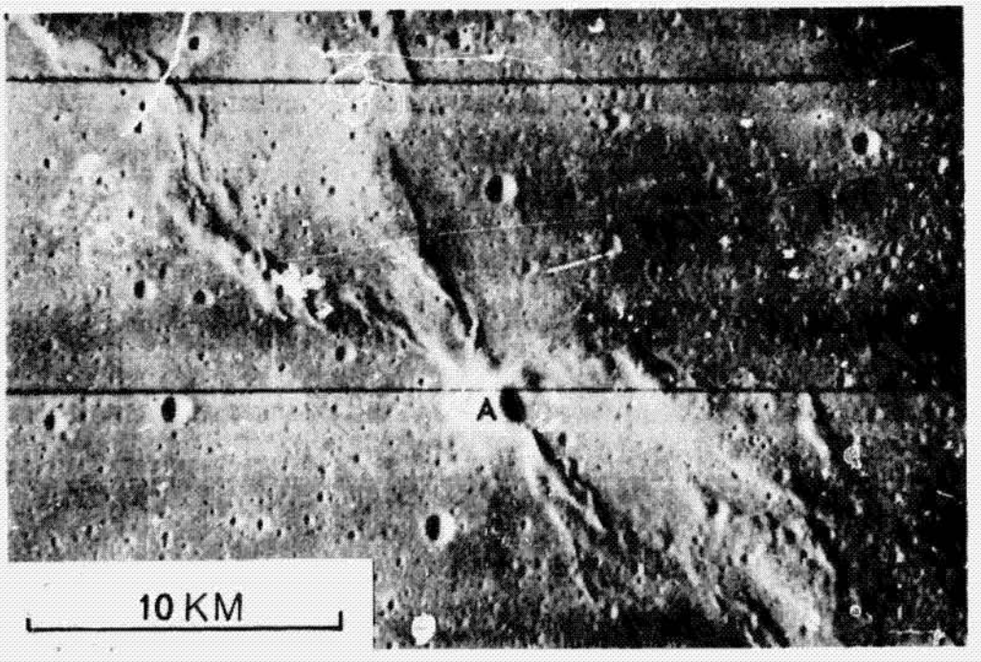

Fig. 7. A swelling (A) at the intersection of mare ridges in Oceanus Procellarum (Lunar Orbiter 4).

14). The development of a particular dome may be arrested at any stage. Parts of this sequence are well documented in dacite and andesite terrains (Smith, 1970). On the Moon, many morphologies similar to those in the Mono Craters are found associated together, for example, domes, cratered domes and double craters are observed to the west of Lacus Mortis, in Mare Frigoris and near the Alpine Valley (Figure 15).

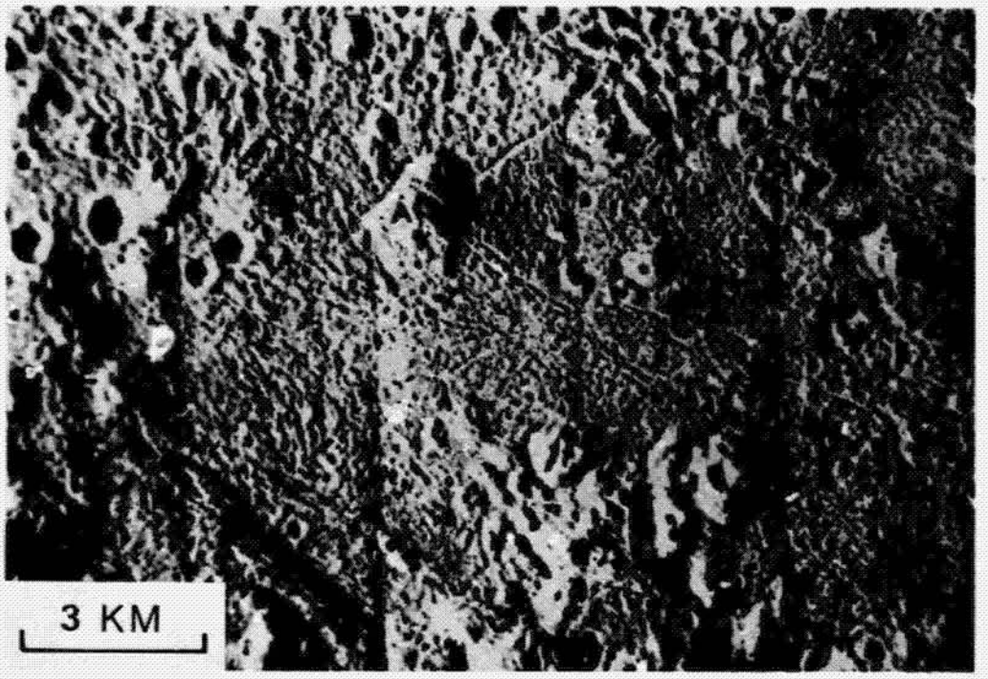

Fig. 8. Irregular hill (A) at the intersection of rilles on the floor of Copernicus (Lunar Orbiter 5).

Many lunar examples are larger than most terrestrial domes, but the difference is usually less than an order of magnitude and is not considered to be a major difficulty in making these comparisons. The fact that similar land forms exist on the Earth and Moon is evidence that some lunar domes are indeed viscous extrusive domes.

In lunar and terrestrial photographs cratered viscous extrusions may be difficult to distinguish from cratered basaltic cinder cones because the outward appearance of both features is controlled by debris on the flanks of the extrusions resting at or near the maximum angle of repose. The maximum angle of repose is dependent on particle size, shape and packing and is independent of rock composition and force of gravity. Overall shape of some volcanic hills is therefore a poor indicator of the composition of the rock composing the hill. Distinction between domes and cinder cones may be possible by the fact that they are associated with different land forms and that their crater diameter-dome diameter ratios differ. McCauley (1968) has observed similarities between cratered cinder cones and breached cones in the San Francisco volcanic field, Arizona and cones in the Marius Hills. Basaltic cinder cones in the San Francisco field may be a source of voluminous lava flows which

travel up to 20 km. Flows commonly contain well developed lava tubes and collapse depressions. On the other hand volcanic domes are associated with stubby flows which rarely flow more than 2 km and these flows are not associated with lava tubes. Domes are commonly associated with other land forms of the Mono Craters eruptive sequence (double craters, uncratered domes, dome and crater morphologies) and

Fig. 9. Dome-like forms (A) at the intersection of two craters (Lunar Orbiter 4).

rarely with breached cones. Detailed inspection on photographs with resolution greater than 1 m will probably resolve the problem because in detail cinder cones and cratered domes differ considerably. For example, cinder cones have smooth outer slopes and bedding within the summit crater, and volcanic domes commonly have rough flanks and bedding is rare in central craters.

In photographs it may also be difficult to distinguish domes from stratovolcanoes. On the flanks of stratovolcanoes successive flow fronts and aligned craters may be

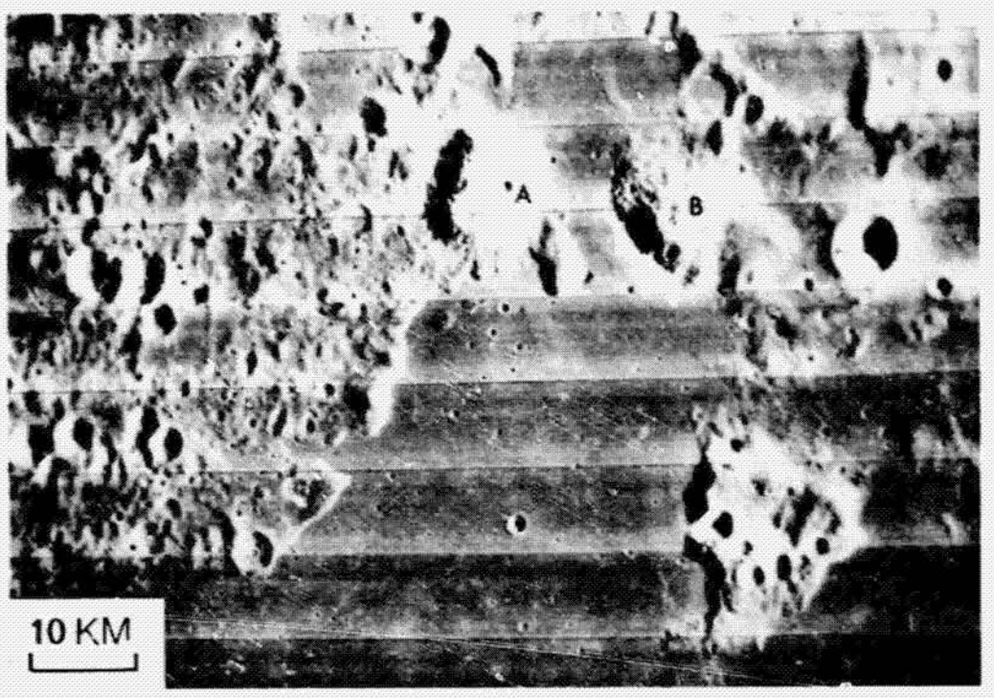

Fig. 10. The Gruithuisen domes (A and B) west of Mare Imbrium. These hills are unlike most land forms in surrounding terrain and are interpreted as volcanic domes (Lunar Orbiter 5).

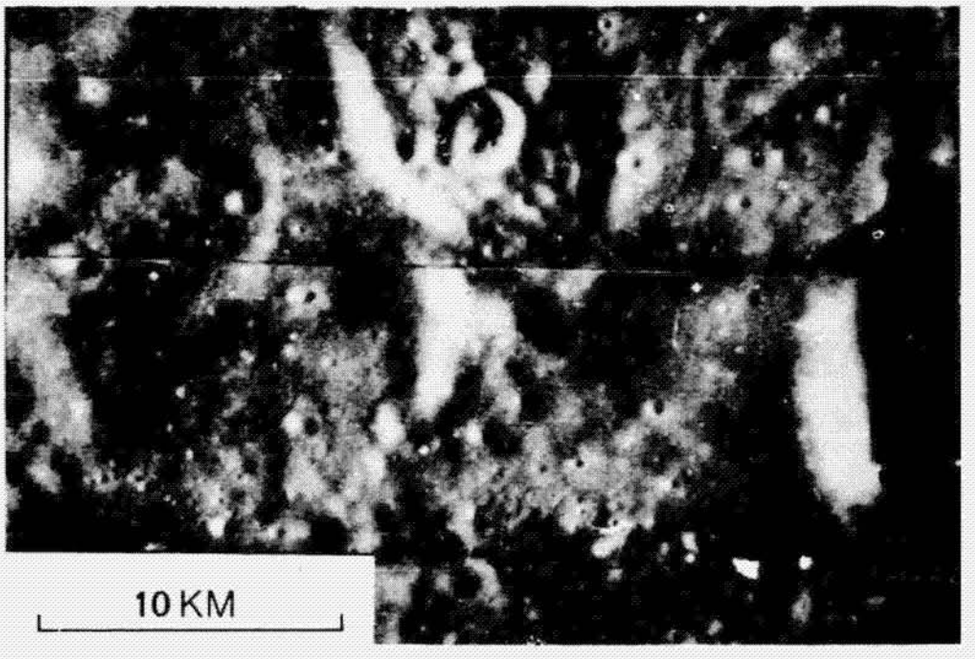

Fig. 11. A large cratered hill in an unnamed crater on the far side of the Moon. This hill is distinctly different from land forms in surrounding terrain and is interpreted as a volcanic dome (Lunar Orbiter 3).

Fig. 12. An oblique aerial photograph of Wilson Butte; a rhyolite dome in the Mono Craters, California. This dome has a shape which is typical of uncratered volcanic domes.

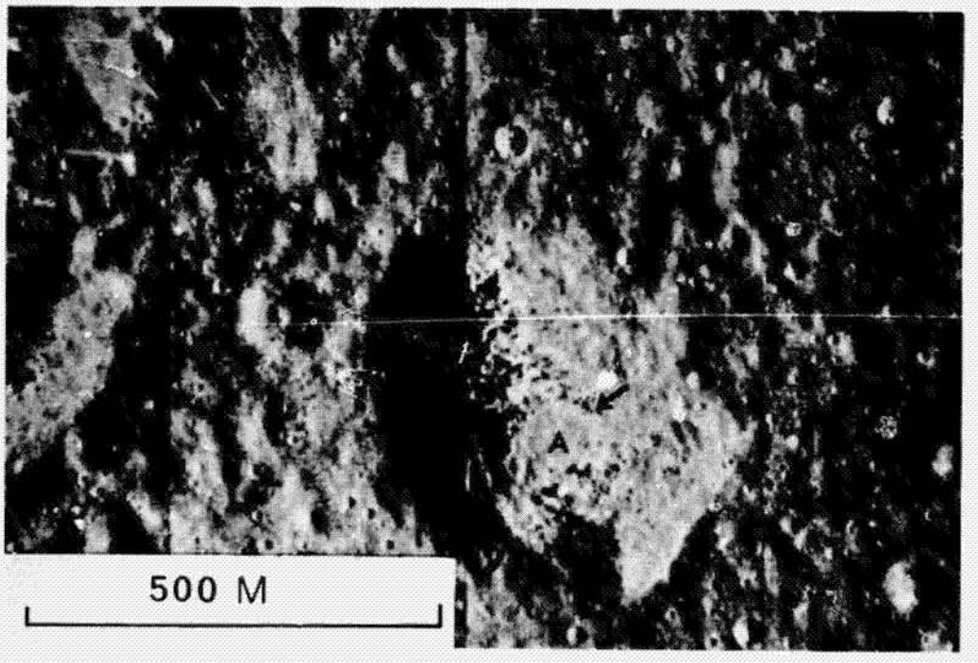

Fig. 13. An uncratered hill on the floor of Copernicus interpreted as a volcanic dome. Note ring of blocks (arrow) which may represent the margin of a circular extrusive plug (A). This plug may be surrounded by an apron of debris in the same manner as domes in the Mono Craters, California.

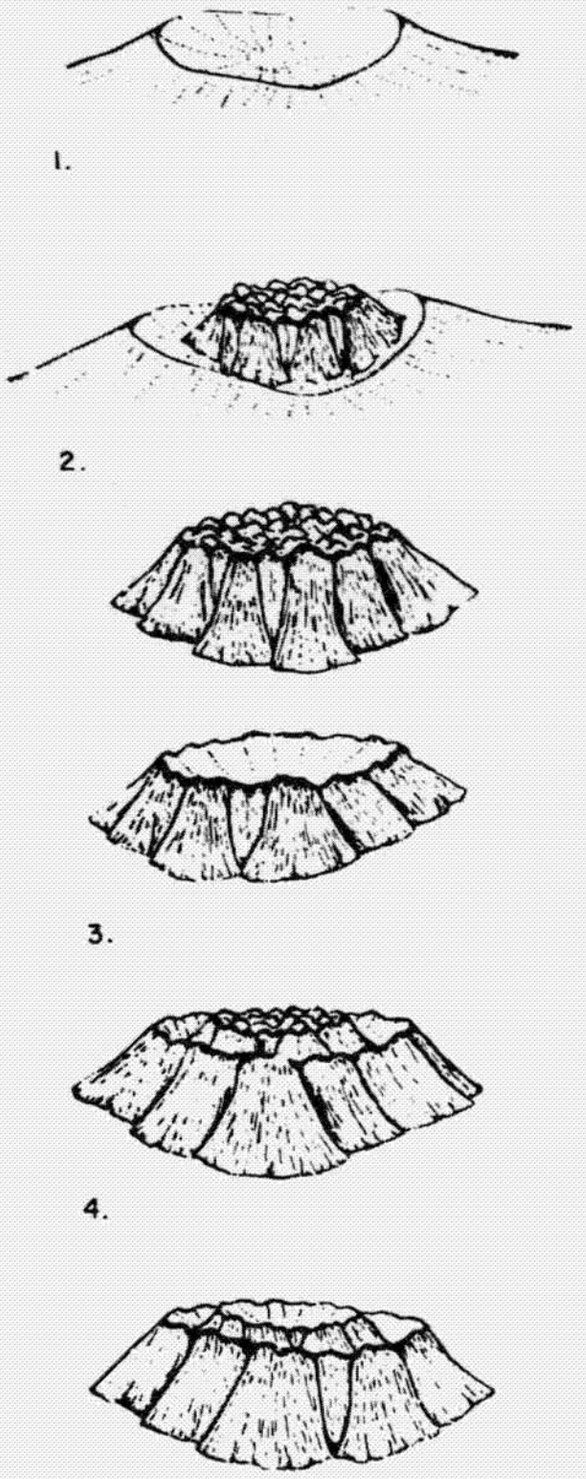

Fig. 14. The Mono Craters developmental sequence: 1. formation of an explosion crater, 2. extrusion of a dome on the explosion crater floor, 3. cratering of the dome by collapse and explosions, and 4. extrusions of a dome on the floor of the crater formed in stage 3 and its subsequent cratering producing a double crater.

present. These features are rare on the flanks of domes. An example of a possible lunar stratovolcano is in the Rümker Hills (Figure 16). Other examples are in the Rümker and Montes Riphaeus quadrangles (Eggleton, 1970).

The base-diameter/summit-crater-diameter ratio may be used as a criterion to distinguish between cratered domes, cinder cones and stratovolcanoes on photographs even though fields overlap. The ratio for five domes varies from 0.4–0.7. This compares to values of 0.17–0.5 for 35 basaltic cinder cones and 0.05–0.20 for eight strato- and shield- volcanoes. The ratio for lunar cratered hills varies from 0.2–0.9.

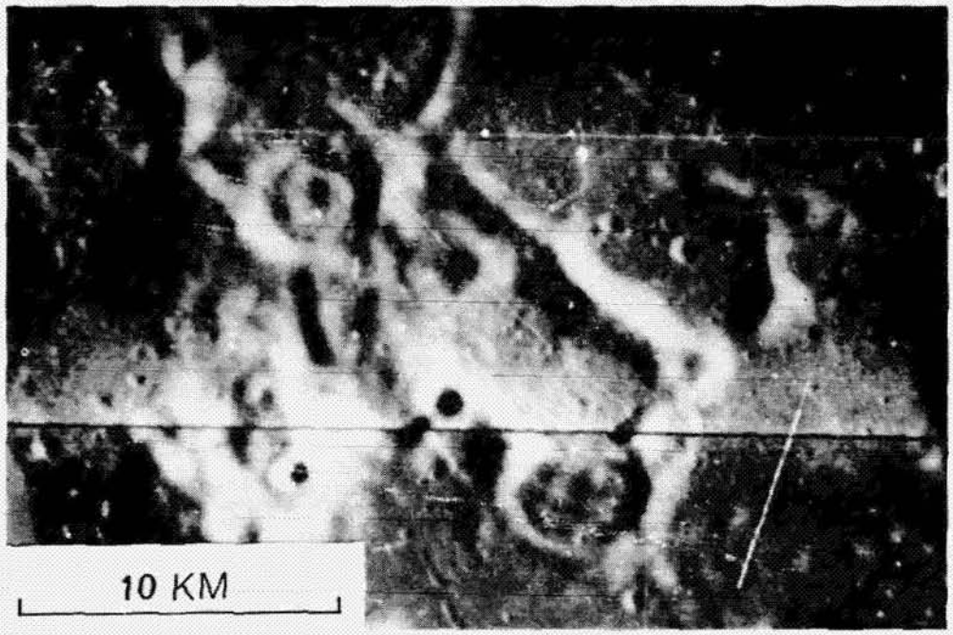

Fig. 15. Associated domes, dome in crater and cratered domes in Mare Frigoris. These features may be analogous to domes in the Mono Craters and may develop through stages similar to those of the Mono Craters developmental sequence.

Quantitative morphologic criteria include the depth-diameter ratio of craters 3.5 km in diameter (Smith, 1971). Terrestrial and lunar craters show consistent differentiation into two fields *i.e.*, a low depth/diameter field of impact craters and a high depth/diameter field of volcanic craters. If a summit crater on a lunar hill is identified as a volcanic crater, it is probable that the hill itself has a volcanic origin. The technique of Murray and Guest (1970) based on crater roundness can be used to suggest origin of large lunar craters. If a crater is interpreted as volcanic by this method, bulbous features associated with the crater may have an endogenic origin.

5. Distribution of Lunar Domes

Domes identified in this study, previously identified domes, sinuous and straight rilles and dark halo craters are plotted on Figure 17 and listed in Table II. Density

of domes and other endogenic features is plotted on Figure 18. On Table II each dome is graded A to E indicating the level of its documentation (*i.e.*, grade A indicates a well-documented dome, and E a poorly-documented dome). Land forms which are now poorly documented are an obvious choice for re-examination when high quality photography becomes available. The following conclusions are based on Figures 17 and 18.

Fig. 16. The Rümker Hills, a volcanic dome complex in the Oceanus Procellarum. A possible stratovolcano is at A. Possible lobate flow fronts associated with the stratovolcano are at B (Lunar Orbiter 4).

(1) Dome distribution is not random; domes are preferentially found (a) about the margins of basins and irregular depressions both on mare and marginal highlands materials; (b) on crater floors, walls and rims; (c) in the highlands on isolated smooth material not clearly associated with recognizable basins and in mountainous highland terrain.

(2) Domes are closely associated with sinuous rilles and dark halo craters. The

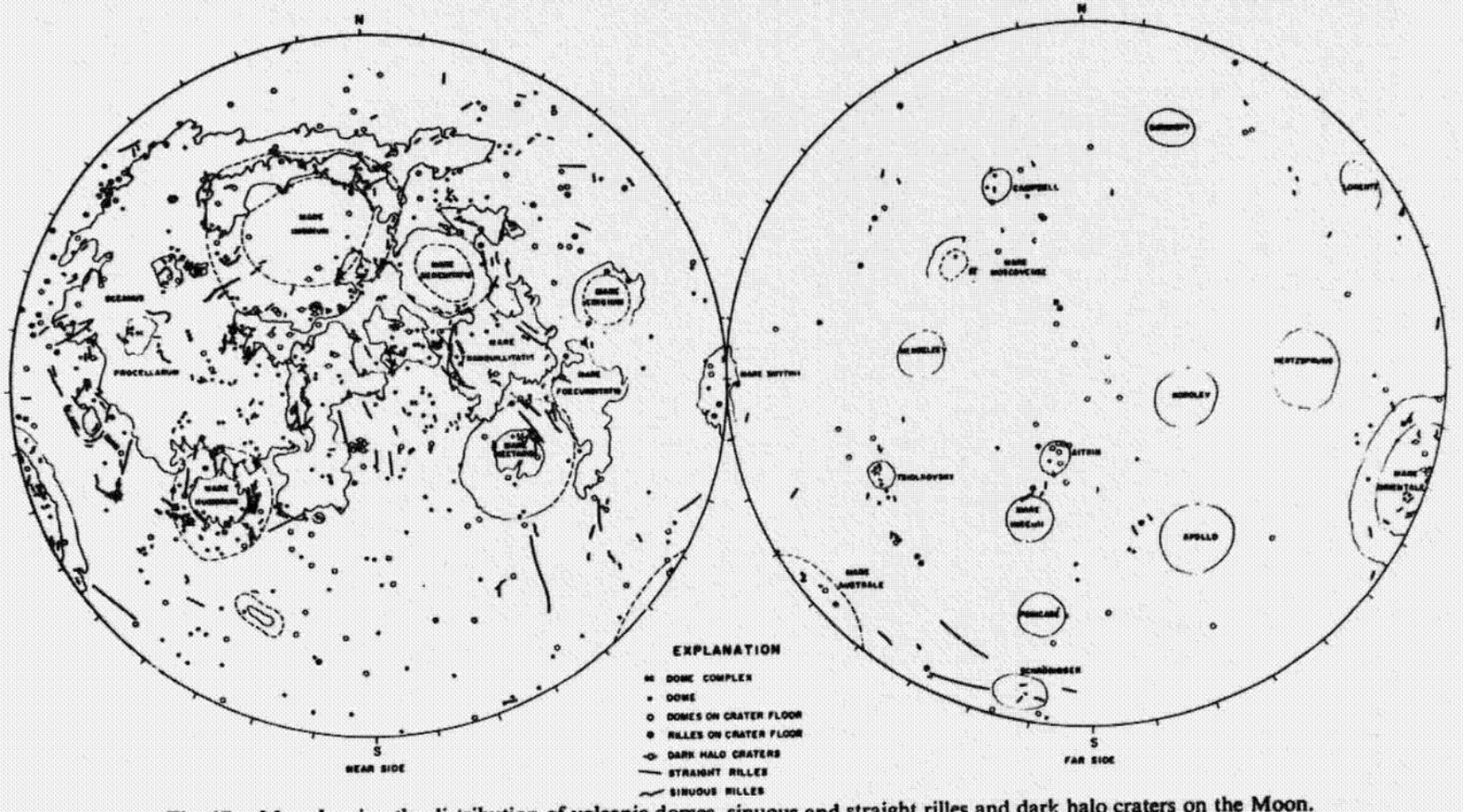

Fig. 17. Map showing the distribution of volcanic domes, sinuous and straight rilles and dark halo craters on the Moon.

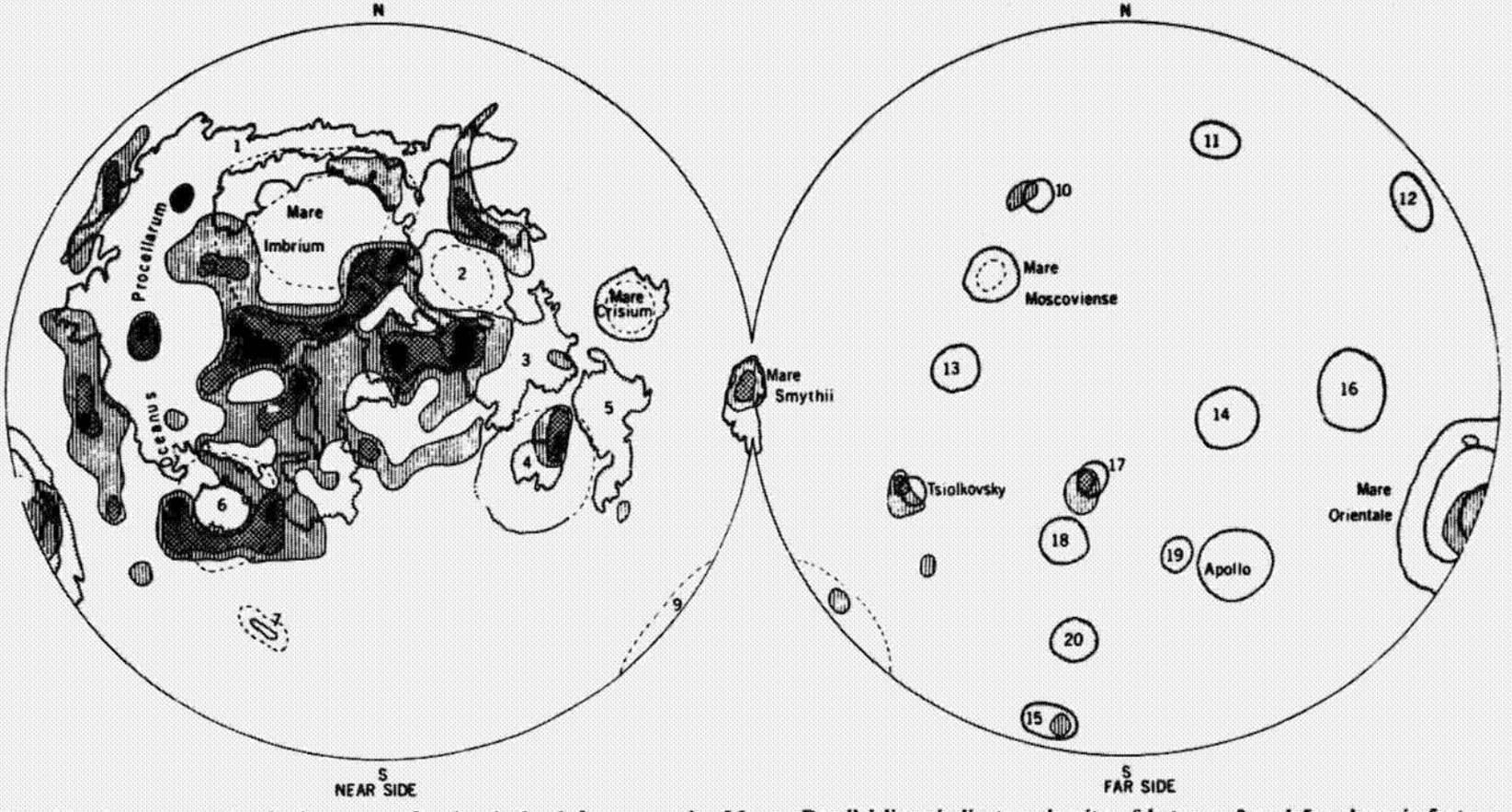

Fig. 18. Contoured distribution map of volcanic land forms on the Moon. Parallel lines indicate a density of between 3 and 5 endogenic features /40000 km²; squares, a density between 6 and 10; and the dark pattern over 10 endogenic features/40000 km². Base map is a Lambert azimuthal equal-area projection. – 1. Mare Frigoris, 2. Mare Serenitatis, 3. Mare Tranquilitatis, 4. Mare Nectaris, 5. Mare Foecunditatis, 6. Mare Humorum, 7. Schiller, 8. Grimaldi, 9. Mare Australe, 10. Campbell, 11. Birkhoff, 12. Lorentz, 13. Mendeleev, 14. Korolev, 15. Schrodinger, 16. Hertzsprung, 17. Aitken, 18. Mare Ingenii, 19. Oppenheimer, 20. Poincaré.

TABLE II

List of Lunar Domes

Location – IV H108 (988, 19 L) indicates that the feature is located on Lunar Orbiter 4 high resolution photograph 108, framelet 988, 19 cm from the left margin of the photograph.

R – Reliability of dome identification on A to E scale.

	Location	Description	R
	Orbiter 2		
M33	(946, 19.5L)	Hills on crater floor	C
	(941, 19.5L)	Botryoidal fill	B
M75	(446, 7.2L)	Double ring	B
	(439, 8.4L)	Hills on crater floor	D
	(443, 18.6L)	Double ring	D
	Orbiter 3		
M120	(762, 13L)	Two cratered cones with summit pits	C
M121	(900, 21L)	Cratered cones and botryoidal fill	B
	(724, 11.9)	Cratered cones on floor of Tsiolkovsky	C
	(711, 17.4L)	Cratered cones on floor of Tsiolkovsky	C
	(692, 5.5L)	Dome in crater with sinuous rille	A
	(658, 20L)	Cratered cones	A
H199		Flamsted Ring	A
	Orbiter 4		
H5	(20, 5L)	Dome on mare ridge	A
H6	(180, 16.3L)	Dome on crater wall	B
	(182, 9L)	Cratered cone	C
	(201, 19L)	Domes on crater floor	C
	(227, 10.5R)	Isolated flat-topped domes	C
H8	(483, 9R)	Domes on crater floor	C
H9	(578, 12.7R)	Flat dome within irregular crater	A
H10	(672, 5L)	Domes on mare ridge	C
	(696, 14l)	Cratered cone within crater	C
H17	(623, 5.5L)	Textured dome in crater	D
H18	(755, 3L)	Cratered cones	D
H27	(983, 5L)	Hill on rille	C
	(983, 9.5L)	Hill at intersection of three rilles	C
H38	(415, 20L)	Dome on mare ridge	B
H52	(216, 11.5L)	Cratered flat-topped dome in crater	C
	(262, 21.5L)	Domes in three craters	A
	(265, 17L)	Rounded ridge in crater	D
H53	(373, 19.5L)	Aligned domes in crater	B
	(385, 16.5L)	Domes in crater	C
H60	(283, 9L)	Dome in crater	C
	(285, 23L)	Dome on mare ridge	B
	(277, 17L)	Double crater	A
H65	(935, 7L)	Dome associated with rille in crater	C
H66	(040, 10R)	Hummocky mass on crater floor	D
	(157, 19L)	Dome in the Palus Somnii	D
H67	(148, 17L)	Elongated domes in crater	C
	(169, 6L)	Double crater with domes in moat	A
	(255, 10R)	Flat-topped dome in crater	C
	(214, 18L)	Cratered dome	B

Table II (Continued)

	Location	Description	R
H68	(322, 16R)	Cratered cone on crater wall	A
	(368, 13.5R)	Double crater	A
	(368, 4.8L)	Broad dome on ridge	A
H70	(548, 4.5L)	Dome in crater	C
H71	(714, 9L)	Domes in Fabricus associated with rille	B
H72	(813, 10L)	Cratered domes associated with rille	B
	(815, 19L)	Domes in crater	B
	(818, 3.4)	Dome at crater intersection	A
	(819, 13.5L)	Large dome on crater floor	A
	(887, 15.5L)	Cratered cone	D
	(889, 5.7L)	Cratered cone	C
	(816, 15L)	Cratered cone associated with rille	C
	(816, 2R)	Dome field	D
	(838, 4.5L)	Dome in double crater	C
	(839, 16.5L)	Six domes on mare ridge	A
	(855, 10L)	Dome on crater rim	A
H74	(072, 20.5L)	Three peaks in crater	D
H76	(378, 2.5L)	Oversized central peak	D
H77	(526, 8R)	Irregular domes associated with rille	D
H78	(637, 19L)	Dome on mare ridge	A
	(593, 10L)	Pear shaped dome on mare ridge	C
	(611, 16R)	Cratered hill on crater wall	A
	(643, 7L)	Domes on mare ridge	B
H83	(259, 15L)	Swelling on ridge in crater	D
H84	(411, 7.5R)	Domes on floor of Theophilus	C
	(432, 8L)	Domes on crater rim	D
	(397, 18.7)	Cratered ellipsoidal hill	A
H86	(641, 14L)	Dome field	E
	(699, 3L)	Aligned hills	E
	(678, 8.5R)	Small domes	D
	(681, 13.5L)	Dome at crater intersection	D
	(682, 19.7L)	Cratered hill	D
	(683, 1.52L)	Cratered cone on crater wall	D
	(699–685)	Lacus Somniorum Dome Field	C-A
H88	(924, 9L)	Cratered hills in crater	D
	(904, 15.5R)	Cratered hill on crater wall	C
H89	(0.35, 9.5L)	Pear-shaped hill with summit crater	C
	(046, 14L)	Domes in crater	D
	(0.39, 7.5L)	Cratered cone	D
	(0.53, 4.5L)	Cratered hills on crater wall	C
	(059, 10.5L)	Three aligned hills	D
	(063, 2L)	Hills on crater wall	D
	(099, 9R)	Dome at crater intersection	C
	(074, 5L)	Domes on crater floor	C
H90	(200, 12R)	Domes associated with rille	C
	(215, 14L)	Domes in crater	D
H91	(324, 10L)	Dome Field, Lacus Mortis	B
	(336, 7L)	Dome Field, Lacus Mortis	C
	(357, 2L)	Dome associated with ridge	B
	(357, 6L)	Cratered dome in crater	A
	(349, 5.5L)	Cratered cone	A
	(345, 2L)	Dome associated with ridge	C

Table II (Continued)

	Location	Description	R
	(318, 19L)	Cratered cone in crater	C
	(343, 2.5L)	Cratered cone	B
	(322, 14.2L	Cratered cone	B
	(324, 14.7L)	Cratered cone	C
	(329, 5.2L)	Pear shaped cratered hill	C
	(338, 8.5L)	Cratered cone	D
	(349, 7L)	Cratered cone	C
	(321, 2L)	Cratered cone	B
	(364, 5.5L)	Cluster of irregular hills	E
H94	(717, 9.5L)	Off-center central peak	C
H95	(840, 0.5L)	Dome on crater wall	C
	(838, 0.5L)	Dome on crater wall	C
	(859, 4L)	Dome in crater with fracture	B
H96	(010, 3L)	Flat topped hills	E
	(014, 2L)	Cratered hill on crater wall	C
	(0.28, 12R)	Double crater	B
	(940, 12L)	Cratered cones	B
	(958–956)	Dome Field	C
	(993, 6L)	Domes in crater, dome cratered	B
H97	(99–104)	Dome Field	C
	(127, 4L)	Mare dome, cratered	D
	(128, 10.5L)	Cratered cone	D
	(155, 18L)	Domes in craters	C
	(168, 5L)	Four domes in crater	D
H98	(23,	Botryoidal fill	
	(266, 9L)	Dome in crater	B
	(270,	Dome in crater	
H101	(621, 13L)	Double crater	B
	(623, 5.5L)	Flat topped dome with summit sag	B
	(671, 17L)	Cratered central peak	C
H102	(762, 18L)	Dome field	C
	(788, 6R)	Swelling on mare ridge	B
	(810, 6L)	Domes in crater	C
H103	(888, 13L)	Low hills	E
	(909, 13L)	Cratered hills	C
	(928, 11L)	Cones to southeast of Cassini	D
	(953, 1L)	Three domes	D
H108	(577, 10L)	Oversized central peak	D
	(583, 12.5L)	Dome on wall of Arzachel	C
H109	(676)	Dome field	C
	(683, 19R)	Cratered dome	D
	(716)	Dome field	C
	(713, 14.5L)	Cratered cone	C
	(737, 12L)	Double crater	A
H110	(807, 7L)	Cratered cone	E
	(867, 3L)	Dome associated with rille	D
	(821, 2L)	Cratered cone	C
	(808, 1.5L)	Flat topped dome on crater wall	C
H112	(091, 16R)	Dome associated with rille	C
	(092, 11R)	Domes on crater floor	C
	(063, 19L)	Cratered central peak	C
H113	(188, 1L)	Dome associated with rille	A

Table II (Continued)

	Location	Description	R
	(188–193)	Five elongated domes	D
	(225, 14L)	Cratered cone	A
	(238, 11L)	Dome on mare ridge	B
	(240, 10.5L)	Swelling on mare ridge	A
	(263, 15L)	Flat topped irregular dome	C
	(269, 1L)	Three domes on crater floor	C
H114	(317, 10R)	Hemispheric dome	D
	(317, 7.5R)	Cratered cone	C
	(341, 16L)	Oversized central peak	C
	(340, 10L)	Cratered dome	D
	(350, 1.5L)	Cratered hill associated with ridge	D
	(354, 14L)	Domes in Eratosthenes	D
	(362, 10.5L)	Domes associated with ridge	D
	(366, 5L)	Oversized central peak	E
	(376, 1.5L)	Flat topped dome	D
	(405, 13R)	Irregular hill with summit sag	B
H115	(464, 8.2L)	Cratered cone	B
	(470, 22.5L)	Double crater	B
	(520, 17.5L)	Domes on mare ridge	D
	(507, 18.5R)	Cratered cone	C
	(510, 19.5R)	Dome associated with ridge	B
	(472, 6R)	Cratered cone	D
	(471, 21L)	Cratered cone	C
	(468, 16R)	Cratered cone	B
	(471, 5R)	Cratered cone	B
	(461, 6.5L)	Cratered cone	B
	(443, 8.5R)	Hummocky terrain	E
H116	(639, 12L)	Dome associated with ridge	D
	(641, 19R)	Cratered cone	C
	(604, 12L)	Dome cluster	C
H119	(010, 7L)	Domes on floor of Tycho	B
H120	(159, 17.5L)	Swelling on mare ridge	C
	(101–108)	Dome field in Fra Mauro Fm.	C
	(111, 15.5L)	Cratered cone	A
	(107, 1.5L)	Four cratered domes	C
H121	(304, 14L)	Cratered cone	B
	(209, 2L)	Domes on floor of Copernicus	B
	(299, 9R)	Elongated domes	C
	(307–318)	Dome field	C
H122	(402, 19.5L)	Dome on mare ridge	D
H124	(636, 4.5R)	Cratered dome in double crater	B
	(640, 17L)	Domes on crater floor	C
	(647, 4.5R)	Dome associated with rille	B
	(649, 7L)	Cratered hills and noncratered hills	B
	(654, 4.5L)	Cratered cone	B
H125	(836, 3.2L)	Cratered cone	C
	(773, 16R)	Dome on mare ridge	B
	(786, 5.5R)	Cratered ridge on mare ridge	B
	(798, 3L)	Dome with summit rift	B
H126	(941, 1.6L)	Cratered cone	C
	(942, 0.6L)	Two cratered cones	B
	(941, 1.8L)	Cratered cone	B

Table II (Continued)

	Location	Description	R
	(933, 11.5L)	Cratered cone	B
	(940, 4L)	Cratered cone	C
	(942, 0.5L)	Cratered cone	B
	(944, 9L)	Irregular dome	B
H127	(044, 10L)	Dome associated with mare ridge	D
	(017, 11R)	Swelling on mare ridge	C
H130	(440, 7.8L)	Cratered cone on crater rim	D
	(441, 5.5L)	Cratered cone	C
	(445, 8.4R)	Chain of domes in Moretus	B
	(433, 7R)	Irregular domes	B
H131	(542, 4.3L)	Cratered cone	C
H132	(686, 27L)	Small hemispheric hill with depression	C
	(693, 17.8L)	Swelling at mare ridge intersection	A
	(741, 13.5L)	Cratered cone at rille-crater intersection	B
H133	(863, 13L)	Mare dome, Milichius Dome	A
	(863, 10L)	Flat topped domes	B
	(838, 19.5L)	Six irregular hills	B
	(868–871)	Hortensius Domes	A
	(865, 14L)	Dome on mare ridge	B
	(879–888)	Hummocky Terrain	D
	(862, 9L)	Mare dome	A
H133	(860, 5L	Mare dome	A
	(854, 13L)	Mare dome	A
	(871, 1.7L)	Cratered cone	D
H134	(968, 6.8L)	Dome on mare ridge	B
	(224, 14L)	Dome-in-crater morphology	B
H137	(383, 2L)	Domes in Gassendi	B
	(353, 11.2R)	Dome on mare ridge	B
	(353, 7R)	Hill on mare ridge	B
	(353, 15.5R)	Irregular dome	C
H138	(544, 13.5L)	Dome on mare ridge	A
	(513, 7L)	Three domes	D
	(528, 18L)	Hummocky Terrain	D
H139	(598, 2R)	Oversized central peak	D
H142	(989, 11L)	Ridge associated with rille	A
	(985, 13L)	Dome associated with ridge	B
	(995, 8L)	Mare dome associated with rille	B
	(008, 4L)	Flat topped dome	B
	(012, 5L)	Cratered hill, textured	B
	(992, 9L)	Four aligned hills	B
H143	(134, 17.5L)	Four elongated domes	A
	(125–128)	Crater rim	B
	(139, 9.4L)	Mesa on mare ridge	A
	(140, 10L)	Flat topped hills forming circular pattern	A
	(255	Harbinger Mountains	C
H145	(488, 1L)	Domes in moat of double crater	A
	(444, 7L)	Gruthuisen domes	A
	(443, 24.5L)	Domes on mare ridge	C
	(445, 12.7L)	Domes on mare ridge	C
	(387, 7L)	Flat topped domes	D
H148	(784	Domes in crater	
	(773	Textured dome	

Table II (Continued)

	Location	Description	R
H149	(966, 15L)	Dome in Mersenius	C
	(992, 10.5L)	Flat topped domes in crater	C
H150	(044	Aristarchus Plateau	A
	(077	Marius Hills	A
H151	(164, 8.5L)	Double crater	C
	(165, 7L)	Elongated hill	D
	(166, 19L)	Flat topped hill	D
	(230, 21L)	Domes associated with rille	A
	(232, 13.2L)	Cratered cone	B
	(224, 4L)	Mare dome	B
	(164, 7.6L)	Double crater	A
	(164, 16L)	Double crater	B
	(165, 9.5L)	Dome in crater	B
H154	(598, 12.3L)	Crater with summit sag	D
H155	(697, 6.5K)	Flat topped hill	C
	(758, 19.8R)	Elongated dome	B
	(692, 0.7R)	Dome in rille	C
H156	(836, 5L)	Botryoidal fill	C
	(837, 15L)	Swelling on mare ridge	B
	(860, 15R)	Swelling on mare ridge	C
	(862, 12R)	Irregular hill	B
	(872, 13L)	Dome associated with ridge	B
	(891, 11R)	Cratered cone	C
H157	(999, 8.2R)	Cratered cone	A
	(998, 5.3R)	Cratered cone	A
	(999, 4L)	Cratered cone	A
H158	(090, 3L)	Three hills associated with ridge	D
	(100, 4.5L)	Irregular hill	D
	(131, 17L)	Mairan T, Cratered cone	B
	(156, 7L)	Elongated cones	A
	(127, 9.5L)	Textured dome	A
H160	(419, 11L)	Two cratered cones	D
	(363, 12L)	Irregular Hills	E
	(363, 15.5R	Cratered hills	C
	(356, 13.5R)	Irregular hills	E
	(406, 21L)	Flat-topped hill	D
H161	(504, 13.4L)	Flat-topped cratered hill	D
	(541, 6L)	Dome on floor of rille	C
	(497, 17L)	Domes on crater wall	C
	(497, 9L)	Dome on crater wall	B
	(488, 10L)	Hills on crater rim	C
	(485,	Hummocky terrain	C
H162	(690, 7L)	Cratered cone	B
	(679, 6L)	Domes in Cavalerius	B
	(667, 7R)	Mare dome	B
	(660, 7.5R)	Mare dome	C
	(663, 0.5R)	Mare dome	B
H163	(760, 15.4L)	Cratered hill	E
	(763, 4.8L)	Swelling at crater intersection	C
	(768, 19.5L)	Botryoidal fill	B
	(789,	Rümker Hills	A
	(808, 15.5L)	Mare dome	B

Table II (Continued)

	Location	Description	R
	(798, 19.5L)	Mare dome	B
H165	(072, 6L)	Six cratered cones	B
	(066, 11L)	Textured domes in crater	C
	(067, 3L)	Hummocky terrain	D
	(010, 13.5L)	Flat-topped dome	C
	(011, 17L)	Flat-topped domes	C
H166	(148, 8.5L)	Cratered dome	D
	(148, 13L)	Cratered cone on crater rim	C
H167	(279, 10.5L)	Domes within crater	D
	(299, 8L)	Flat-topped domes in crater	C
H168	(426, 10.5L)	Aligned hills	D
	(423, 6L)	Dome on crater floor	D
	(409, 8R)	Flat-topped hill	D
	(406, 16.5R)	Domes in crater	D
H169	(595, 12.5L)	Cratered cone associated with rille	B
	(584, 13.5R)	Domes in crater	D
	(573, 5L)	Domes floor of Kraft	C
H174	(237, 15.7R)	Large cratered cone	B
	(205, 13.5L)	Dome on crater wall	C
H175	(379, 16L)	Mare dome	B
	(378, 20L)	Aligned hills	C
H176	(505, 10L)	Domes in Pythagoras	B
	(506, 14L)	Dome in Pythagoras	B
	(491, 11L)	Dome in crater	B
H177	(624, 19.5L)	Flat dome	C
	(740 13L)	Large dome in crater	C
H178	(762, 15L)	Dome at intersection of rille and crater	B
H179	(899, 8L)	Cratered hill	D
	(890, 7.5L)	Hill at crater intersection	E
	(888, 10L)	Dome on crater wall	C
H181	(118, 19L)	Cratered domes	C
	(154, 4L)	Flat-topped domes	A
	(167, 7.5)	Dome in crater	B
H182	(238, 9.5R)	Five aligned domes	B
	(267, 7L)	Domes in crater	C
	(265, 17L)	Domes in crater	C
	(285, 3.5L)	Hill at rille intersection	D
	(282, 5L)	Cratered cone on ridge	B
	(305, 14.5L)	Domes in crater	B
H183	(423, 0.5L)	Dome in crater	D
	(422, 1.3L)	Cratered cone	B
	(416, 6.5L)	Double crater	C
	(385, 11L)	Domes in crater	D
	(409, 7L)	Cratered dome	B
	(420, 1.5L)	Textured dome	A
	(433, 13L)	Botryoidal fill	B
	(446, 14.5L)	Aligned domes in crater	C
H184	(549, 5R)	Central peak Petavius	C
H186	(759, 5R)	Domes in crater	B
	(770, 22L)	Domes in crater	B
	(806, 15L)	Domes in crater	B
	(838, 16L)	Domes on mare ridge	C

Table II (Continued)

	Location	Description	R
H187	(928, 22L)	Domes in crater	D
	(938, 7L)	Mare dome	C
	(938, 8L)	Mare dome	C
	(943, 5L)	Mare dome	C
	(951, 9L)	Cratered domes	B
H188	(051, 17L)	Domes in Einstein	B
H189	(203, 21.5L)	Double crater	B
	(211, 24L)	Textured hill	D
	(154, 14.5L)	Botryoidal fill	C
H191	(456, 10.5L	Flat-dome in crater	C
	(460, 4.5L)	Flat-topped dome in crater	C
H192	(555, 9.5L)	Cratered cone	C
	(556, 11L)	Cratered cone	C
	(572, 15L)	Dome in crater	C
	(579, 17L)	Domes in Geminus	C
H193	(718, 12L)	Domes in crater	C
H195	(978, 15L)	Domes in crater	C
	(999, 14L)	Dome and flow, Mare Orientale	A
	(002, 13L)	Layered mare dome	A
	Orbiter V		
H6	(295, 14L)	Dome at crater intersection	D
H18	(869, 14R)	Dome in crater	D
H20	(122, 8.4L)	Cratered cone	C
M40		Domes on floor of Stevinus	C
M43	(304, 10.5L)	Domes in crater	E
M65	(189, 11.5L)	Domes on mare ridge	B
	(180, 13L)	Dome in crater	B
	(187, 11L)	Dome in crater	C
H79	(811, 4.3L)	Cratered cone	C
H103	(944, 21L)	Two double craters	C
H151	(252, 18L)	Cratered cone	B
	(250, 17L)	Hill associated with rille	C
M152		Domes on floor of Copernicus	A
M177	(901, 12L)	Domes on mare ridge	B
M179	(147, 8L)	Dome at rille intersection	C
	(154, 26L)	Dome in crater	C
M183	(451, 18L)	Three domes in crater	C
M201		Domes on floor of Kepler	A

origin of sinuous rilles is controversial; but their origin is probably related to an endogenic process (Greeley, 1970; Schumm, 1970) and dark halo craters have been interpreted as volcanic features (Kuiper *et al.*, 1966). The association and similar distribution of domes, sinuous rilles and dark halo craters suggests that they have a similar origin (all are related to endogenic processes).

(3) Domes are rarely found in the central portions of the circular basins (for example, Mare Imbrium and Humorum).

(4) Domes are in general concentrically arranged about circular basins. Few domes are related to radial sculpture. This suggests that concentric patterns may be related

to deep-seated fractures which are in places controlled by the lunar tectonic grid (see point 5). Radial sculpture, on the other hand seems to represent a surficial layer with no deep-seated connections. Hartmann and Wood (1971) reached a similar conclusion by observing that radial structure is obscured faster than concentric structure as a basin ages. This occurs because radial systems are primarily surficial, of low relief and easily blanketed by ejecta and regolith whereas concentric systems have greater relief and possibly deep-seated structural control, and as a result retain topographic relief longer (Hartmann and Wood, 1971).

(5) Domes are locally controlled by the lunar grid (Strom, 1964). Domes are on mare ridges and rilles elongated in a grid direction; in several places domes themselves are aligned in a grid direction and in places location may be controlled by grid intersections. Grid control around basins may be secondary, that is grid lineaments were present before the formation of the basins and were subsequently rejuvenated or activated by basin formation. With more data, concentric patterns about basins may resolve into grid directions. For example, concentric mare ridge patterns in Mare Imbrium can be resolved into segments controlled by the lunar grid (Elston *et al.*, 1971).

(6) Dome formation spans a wide range of lunar time. Presently observed domes are associated with old mare materials in Mare Smythii and Tsiolkovsky and are on the floors of young craters such as Tycho and Copernicus. Domes were probably not formed during one great lunar effusive event, but each dome-forming episode is probably related to the formation of individual craters and mare basins and to basin-filling episodes. Activity in areas where domes are located may be continuing to the present as seen by the close correlation between dome distribution and the distribution of lunar transient events. Middlehurst (1967) concluded that lunar transient events occur (a) near the border of the maria especially about Mare Imbrium, Serenitatis, Crisium and Humorum; (b) associated with ray craters (e.g., Tycho, Copernicus, Aristarchus and Kepler); (c) in ring craters with dark mare or partially dark floors (e.g., Plato, Grimaldi and Alphonsus). Transient lunar events have not been reported from the central parts of the circular basins. Transient events therefore occur in the same general areas as domes, rilles and dark halo craters. Middlehurst and Moore (1967) previously recognized the correlation of sites of lunar events with the distribution of dark halo craters. Moore (1971) added 313 additional events to Middlehurst's list of 400; however these additional data do not change the distribution. This correlation does not necessarily infer that domes, sinuous rilles and dark halo craters are presently active; however one may speculate that the areas where these features occur are the sites of recent activity; perhaps in the form of isolated gas discharges.

(7) Domes are not restricted to the equatorial areas of the Moon or maria as suggested by Arthur (1962) Baldwin (1963) Brungart (1964) and others. This illusion was due to the fact that on Earth-based photographs domes were more easily observed on the maria and the fact that more mare material is present near the equator than elsewhere on the Moon's Earth-side.

(8) Dome distribution does not correlate well with gravimetric and acceleration

data (Muller and Sjorgen, 1968), deviation from the best fitting ellipsoid (Runcorn and Shrubshall, 1968) or infrared thermal anomalies (Shorthill and Saari, 1966). Domes are on the margins of basins with gravity highs of 60 mgals. Other than this, no other agreement between dome distribution and gravimetric data is obvious. A poor correlation exists between dome distribution and deviation from a best fitting ellipsoid (Runcorn and Shrubshall, 1968). Domes are on highs (positive deviations from the ellipsoid) in Oceanus Procellarum, Sinus Medii and Mare Tranquillitatis; otherwise no obvious correlation is observed. The alignment of the Rümker Hills, Aristarchus Plateau and Marius Hills along the axis of the Oceanus Procellarum on a 0.5–1.5 km bulge has been suggested as evidence that the area overlies an up-welling convection cell (McCauley, 1967). The distribution of domes does not correspond to locations of infrared thermal anomalies other than the fact that fresh craters which contain domes may be hot spots and vice versa.

(9) Domes at times group into volcanic complexes; for example the Rümker Hills, Aristarchus Plateau and Marius Hills. In these complexes, domes are commonly associated with flows, rilles and dark halo craters.

6. Conclusions

This paper presents criteria for the identification of lunar domes based on modification, location and morphology and shows:

(1) Many terrestrial volcanic extrusive domes are similar in morphology to some lunar domes. This analogy suggests that extrusive volcanic domes are indeed present on the Moon.

(2) Over 400 domes are present on the lunar surface, and are interpreted as having formed by endogenic processes.

(3) Many domes and other endogenic features on Figure 17 are related to basins and craters, and not to any observable moonwide pattern. Local control by the tectonic grid is, however, an exception. Domes are not uniquely found on maria.

(4) Activity in areas where domes are located may be continuing in the form of gas emissions to the present as revealed by the correlation of dome distribution with reported transient lunar events.

(5) The rock type and chemistry of domes is difficult to ascertain from study of Orbiter photographs. Earlier workers (McCauley, 1967, for example) assumed that low mare-type domes were basaltic and that lunar domes with steeper slopes and textured surfaces were formed by intermediate and felsic rocks. Even though this relationship may be true in some instances, a general rule can not be applied. For example, on Earth both basalts and rhyolites form broad shields and both form cone-shaped extrusions with slope angles on the flanks between 30–35° (Smith, 1970). Many domes are composed entirely of debris or mantled by rubble which stands at or near the angle of repose and controls the outward appearance of the dome. In these, morphology is essentially independent of composition. Too many variables exist therefore to make suggestions about dome rock type based on photogeologic studies alone.

Acknowledgments

This paper reports on a portion of a study which compares volcanic domes in the Mono Craters in California, and a dome complex in southwestern New Mexico with lunar volcanic features. I thank Wolfgang E. Elston of the University of New Mexico for reviewing the manuscript and offering many helpful suggestions. Research was supported by NASA grant NGL-32-004-011.

References

Abbey, L. B. and Both, E. E.: 1958, *Strolling Astron.* **12**, 96.
Alter, D.: 1957, *Publ. Astron. Soc. Pacific* **69**, 245.
Arthur, D. W. G.: 1962, *Commun. Lunar Planet. Lab.* **1**.
Baldwin, R. B.: 1963, *The Measure of the Moon*, University of Chicago Press, 488 pp.
Beswick, J. D.: 1962, *British Astron. Assoc. J.* **72**, 119.
Brungart, D. L.: 1964, 'The Origin of Lunar Domes', Thesis, Air Force Institute of Technology, MECH/GSF-64-32, 191 pp.
Bülow, Kurt Von: 1964, *Geologie* **13**, 449.
Eggleton, R. E.: 1970, 'Recognition of Volcanoes and Structural Patterns in the Rümker and Montes Riphaeus Quadrangles of the Moon', Ph.D. dissertation, University of Arizona, Tucson, 266 pp.
El-Baz, Farouk: 1971, *Apollo 14, Preliminary Science Report*, NASA SP-272, 267–274.
El-Baz, Farouk and Wilshire, H. G.: 1969, *Apollo 8, Preliminary Science Report*, NASA SP-201, 32–33.
Elston, W. E.: 1967, *Am. Astron. Soc.* **14**, 213.
Elston, W. E., Laughlin, A. W., and Brower, J. A.: 1971, *J. Geophys. Res.* **76**, 5670.
Fielder, G.: 1962, *British Astron. Assoc. J.* **72**, 24.
Greeley, Ronald: *Science* **172**, 722.
Hartmann, W. K. and Wood, C. A.: 1971, *The Moon* **3**, 3.
Herring, A. K.: 1960, *Sky Telesc.* **20**, 219.
Jamieson, H. D. and Rae, W. L.: 1965, *Brit. Astron. Soc. J.* **75**, 310.
Kuiper, G. P., Strom, R. G., and Le Poole, R. S.: 1966, in *Ranger VIII and IX*, Part 11, NASA Technical Report No. 32-800, 35–248.
McCauley, J. F.: 1967, in S. K. Runcorn (ed.), *Mantles of the Earth and Terrestrial Planets*, Interscience, New York.
McCauley, J. F.: 1968, *Amer. Inst. Aeron. Astron. J.* **6**, 1991.
McCauley, J. F.: 1969, *Trans. Amer. Geophys. Union* **50**, 229.
Middlehurst, B. M.: 1967, *Rev. Geophys.* **5**, 173.
Middlehurst, B. M. and Moore, P.: 1967, *Science* **155**, 449.
Moore, P.: 1971, *British Astron. Assoc. J.* **81**, 365.
Moore, P. and Cattermole, P. J.: 1957, *J. Intern. Lunar Soc.* **1**, 16.
Muller, P. M. and Sjogren, W. L.: 1968, *Science* **161**, 680.
Murray, J. B. and Guest, J. E.: 1970, *Modern Geology* **1**, 149.
O'Keefe, J. A., Lowman, P. D., and Cameron, W. S.: 1967, *Science* **155**, 77.
Pickering, W. D.: 1903, *The Moon*, Doubleday, Page and Co., New York.
Putnam, W. C.: 1938, *Geograph. Rev.* **38**, 68.
Rae, W. L.: 1963, *Brit. Astron. Assoc. J.* **73**, 165.
Rae, W. L.: 1966, *Brit. Astron. Assoc. J.* **76**, 319.
Runcorn, S. K. and Shrubshall, M. H.: 1968, *Phys. Earth Planetary Interiors* **1**, 317.
Schumm, S. A.: 1970, *Geol. Soc. Am. Bull.* **81**, 2539.
Scott, D. H., West, M. N., Lucchitta, B. K., and McCauley, J. F.: 1971, *Apollo 14, Preliminary Science Report*, NASA SP-272, 274–283.
Shaler, N. S.: 1903, *Smithsonian Contrib. Knowledge* **34**, 1.
Shorthill, R. W. and Saari, J. M.: 1966, in W. N. Hess, D. H. Menzel, and J. A. O'Keefe (eds.), 'The Nature of the Lunar Surface', *Proceedings of the 1965 IAU-NASA Symposium*, Baltimore, p. 215.
Smith, E. I.: 1969, *Trans. Amer. Geophys. Union* **50**, 229.

Smith, E. I.: 1970, 'A Comparison of Selected Lunar and Terrestrial Volcanic Domes', Ph.D. dissertation, University of New Mexico, Albuquerque, 200 pp.
Smith, E. I.: 1971, *J. Geophys. Res.* **76**, 5683.
Spurr, J. E.: 1944, *Geology Applied to Selenology*, Vol. 1, Science Press Printing Co., Lancaster, Pa., 112 pp.
Strom, R. G.: 1964, *Commun. Lunar Planet. Lab.* **205**, 39.
Strom, R. G.: 1971, *Modern Geology* **2**, 133.
Westfall, J. E.: 1964, *Strolling Astron.* **18**, 15.
Williams, H.: 1932a, *Univ. Calif. Pub., Bull. Dept. Geol. Sci.* **21**, 51.
Williams, H.: 1932b, *Univ. Calif. Pub., Bull. Dept. Geol. Sci.* **21**, 195.

With permission, reprinted from The Moon,
vol. 3, 1971, pp. 289–314.

LAVA TUBES AND CHANNELS IN THE LUNAR MARIUS HILLS

RONALD GREELEY

Space Science Division, Ames Research Center, National Aeronautics and Space Administration, Moffett Field, Calif., U.S.A.

(Received 19 May, 1971)

Abstract. The Marius Hills region, a volcanic plateau in Oceanus Procellarum, contains numerous rilles, rille-like structures, and chains of elongate craters. Most of these structures characteristically: (1) originate on or near irregular shaped craters associated with features previously interpreted as volcanic domes, (2) trend downslope onto Plateau Plains, (3) generally taper in width and become shallower, (4) are often discountinuous, (5) occupy the center, or apparent crest of a broad ridge, (6) may contain cut-off branches and distributary structures, and (7) may have local reversals in longitudinal slope. Structures having these characteristics are interpreted to be lava channels or partly collapsed lava tubes. Terrestrial lava tubes form exclusively, and commonly, in fluid basalt flows. Recent evidence indicates that viscosities of lunar mare 'basalt' lava flows were conducive for lava tube formation.

Terrestrial analogs are offered for structures described in the Marius Hills. The analogs are comparable in qualitative and quantitative geomorphic aspects, excluding that of width. Scaling consideration of lunar reduced gravity accounts for increased width of the lunar structures. Linear and curvilinear rilles trending along equal elevations are interpreted to result from fracturing or faulting.

1. Introduction

This paper presents quantitative and qualitative geomorphic evidence for the existence of lava channels and partly collapsed lava tubes in the Lunar Marius Hills region. Analogs are offered as terrestrial counterparts to the lunar structures described.

Marius Hills is one of several lunar areas of inferred igneous and volcanic activity. McCauley (1965) described the area as a southward-dipping volcanic plateau comprising about 35 000 km^2 in the middle of Oceanus Procellarum (Figures 1 and 2). McCauley later (1967) proposed the Marius Group as new rock unit and assigned it to the Eratosthenian System. He described the area as a smooth undulating region of low, uniform albedo with prominent ridges, scarps, and local plateaus. Two types of domes (the Marius 'hills') were described (Figure 2): *low domes* with convex profiles and gentle slopes (2–3 degrees), and *steep domes* with steep concave slopes (6–7 degrees). Steep domes are often situated on low domes and both types may be elongate in a NNE–SSW orientation and have small summit pits. McCauley attributed the difference between the two dome types as possibly resulting from magmatic differentiation, with low domes as mafic and steep domes as intermediate to felsic. He also considered the possibility that they resulted from different eruptive processes with lavas of the same composition.

Because the region offers a variety of inferred volcanic structures, Marius Hills is considered a prime Apollo landing site. Karlstrom *et al.* (1968) and Elston *et al.* (1969) presented detailed exploration plans for about 75 km^2 of the Marius Hills region

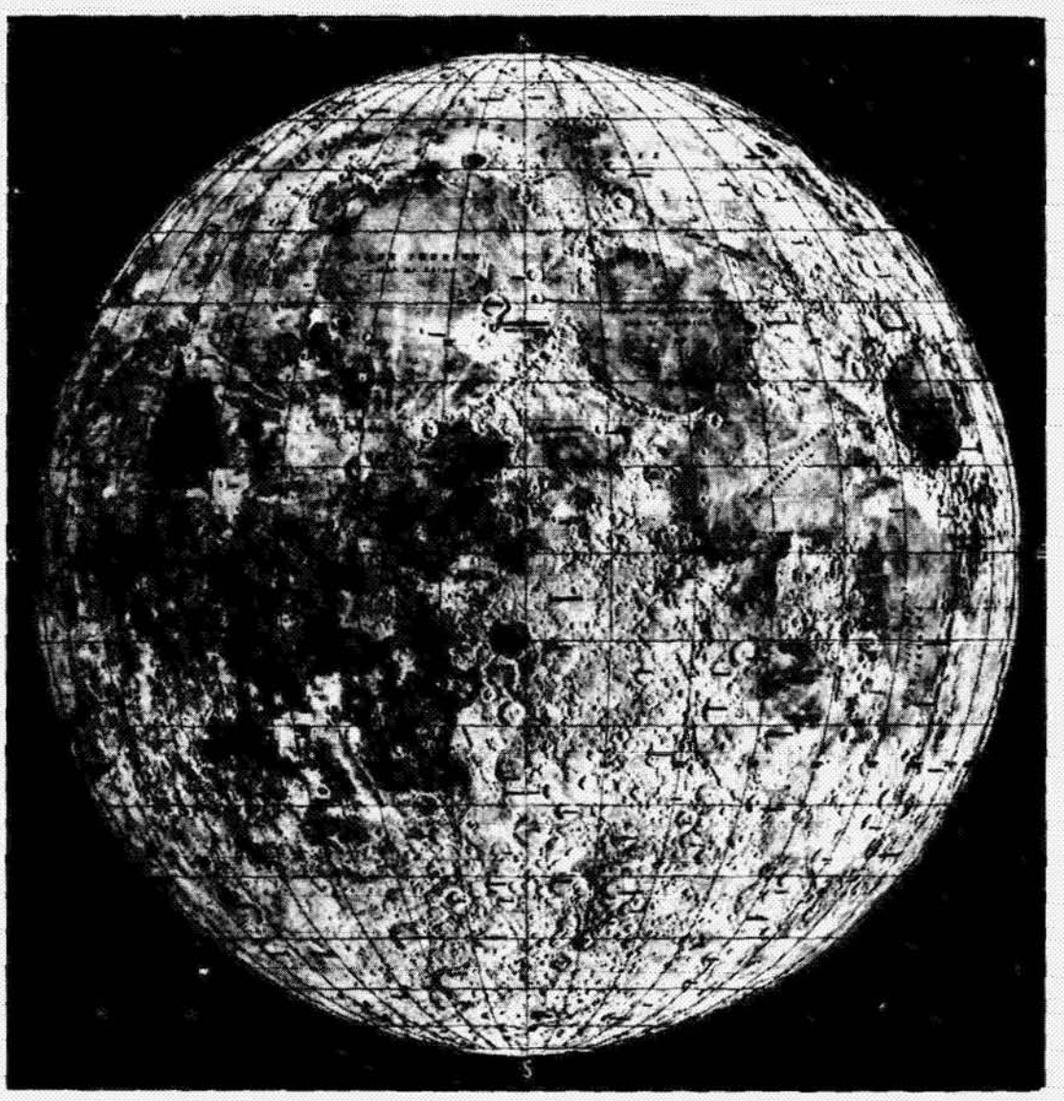

Fig. 1. Location of the Marius Hills region and outline of area covered by Lunar Orbiter 5 photography, MR frames 210-216.

(Figures 2 and 7). They described domes of several types, ridges, endogenous craters, exogenous craters, and rilles, and proposed that many of these structures be visited, examined, photographed and sampled by the astronauts. Although they discussed possible rock types in the area and interpreted many of the structures, the rilles were somewhat neglected, though two rilles were proposed as primary investigation stations. Because rilles are prominent structures in the Marius Hills and other lunar areas and some rilles may be visited and sampled within the next few years, an understanding of rille morphology and consideration of their origin are significant to lunar geology.

Fig. 2. Part of Marius Hills showing rilles and described areas. Craters described or shown on Figure 3 are identified by numbers. Location of cross sections (Figure 4) are indicated by letter. Photograph from LO 5 frame MR-213.

2. Rille Descriptions

Lunar rilles can be separated morphologically into at least three types: linear rilles, sinuous rilles, and tightly meandering rilles. Linear rilles are generally large (often tens of kilometers long and more than 5 km wide) and appear to be controlled by deep-seated structures that cut across crater rims, mare and highland areas. Some

linear rilles, however, are much smaller and may represent small faults, fractures, or fissures. Large linear rilles are probably analogous to terrestrial grabens. In contrast, sinuous rilles appear to be topographically controlled and generally trend around topographic highs. Sinuous rilles range in size from less than a few kilometers long and less than a hundred meters wide to structures exceeding tens of kilometers long. Tightly meandering rilles are charcaterized by their extreme sinuosity and often resemble old age fluvial channels. The three types may grade one into another (particularly linear and sinuous rilles) and there appear to be numberous sub-types, each with a distinctive morphology. It is likely that there are several different modes of origin, each producing different types of rilles.

A. DESCRIPTIVE TECHNIQUE

1. *Sinuosity*

Meandering is a salient characteristic of sinuous rilles. Leopold and Wolman (1960) described a quantitative means of comparing sinuosity of individual channels:

$$S_1 = a/\tfrac{1}{2}L$$

where S_1 = sinuosity, a = arc length and L = meander or wave length for individual segments of a channel. Thus, a straight segment would have a sinuosity of one. Overall sinuosity of a channel from end to end may be defined as:

$$S_2 = d_2/d_1$$

where S_2 = overall sinuosity, d_1 = straight-line distance and d_2 course-line distance, end to end. A straight channel would have an overall sinuosity of one.

2. *Cross Sections*

Cross sections perpendicular to the channel axis and longitudinal profiles aid in describing rilles. Most lunar areas lack topographic control suitable for detailed cross sections. However, the Army Topographic Command (TOPOCOM) has performed preliminary photogrammetry for the Marius Hills from stereoscopically overlapping Lunar Orbiter 5 photographs. The cross sections presented in Figures 4 and 5 were prepared from TOPOCOM data. Errors in elevation, attributable to photographic resolution and inherent uncertainties in spacecraft parameters, range from ± 126 m to ± 162 m in the area considered. A manuscript topographic map (contour interval, 200 m) prepared by TOPOCOM was employed for regional topography. TOPOCOM data was supplemented by height determinations from shadow measurements on steep slopes.

3. *Crater Circularity*

Murray and Guest (1970) showed that circularity of craters may give an indication of endogenetic or exogenetic origin for craters and described several techniques for determining circularity. They noted that terrestrial impact structures and explosion craters

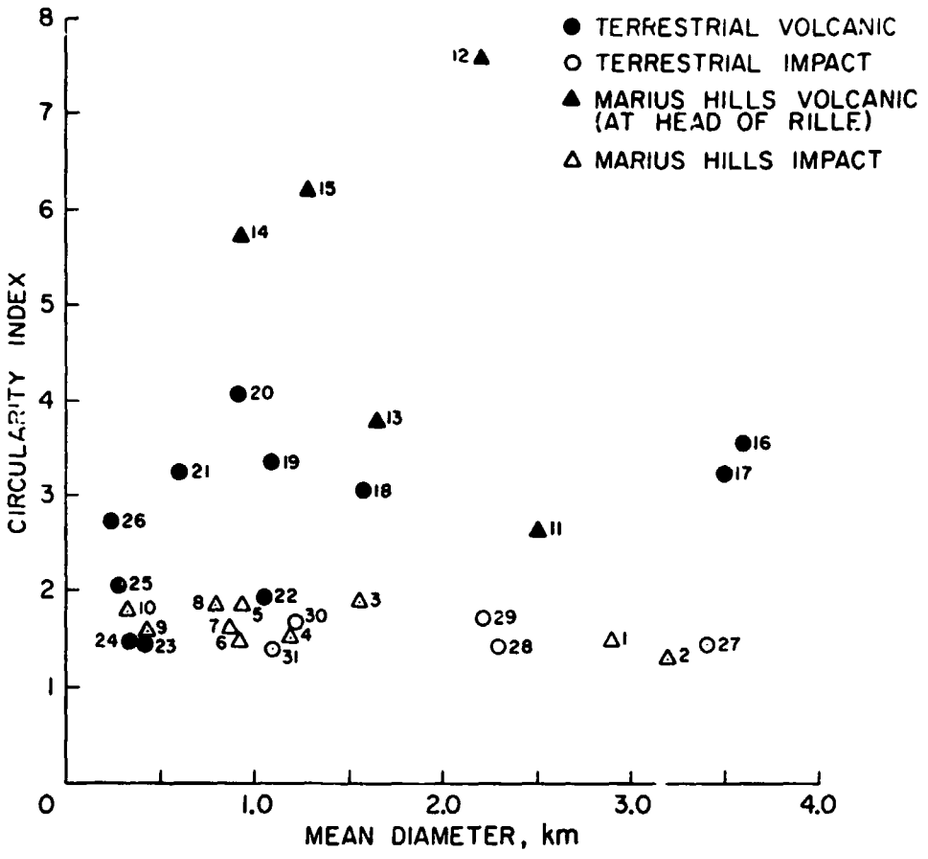

Fig. 3. Circularity index (after Murray and Guest, 1970) for terrestrial impact and volcanic craters compared with craters in the Marius Hills. Circularity index of 1.9 generally separates internally and externally produced craters. Data for some terrestrial craters from Murray and Guest (1970). Crater identification: 1–10, Marius Hills (identified in Figure 2); 11, head of Rille A; 12, head of Rille B; 13, head of Rille C; 14, summit crater, Fissure Cone 1; 15, summit crater, Fissure Cone 2; 16, Mauna Loa; 17, Kilauea; 18, Menengai, Kenya; 19, Makaopuhi; 20, Deep Crater, Calif., 21, Alae; 22, Haiemaumau; 23, Mammoth Crater, Calif.; 24, Pauialua; 25, Modoc Crater, Calif,; 26. Giant Crater, Calif.; 27, New Quebec, Canada; 28, Brent, Canada; 29, Holleford, Canada; 30, Meteorite, Arizona; 31, Wolf Creek, Australia.

are more circular (lower circularity index) than terrestrial endogenous craters. Circularity indexes (Method C1, Murray and Guest, 1970, p. 149–150) were obtained for the large craters in the area, including craters associated with, or at the head of, sinuous rilles. Circularity values are shown in Figure 3 for Marius Hills craters and terrestrial craters. Of the terrestrial examples, all craters with a circularity index above 2 are endogenetic.

Crater circularities are not considered definitive in separating impact craters from endogenous craters. Some impact craters produced in the laboratory by projectiles fired into targets at oblique angles are noticeably noncircular (personal communication, D. E. Gault). However, when considered with other factors, circularity may aid in determining crater origin.

4. *Photographic Coverage*

Lunar orbiter 5 provided photographic coverage of the Marius Hill region with 8 stereoscopically overlapping Medium Resolution Frames (MR 210–216) at a scale of about 1 : 202000 (ground resolution ~2.5 m). Sun angle at time of exposure, about 15.2° above the horizon, is rather low and many interior crater and rille structures are in shadow. The photographs are slightly oblique with the camera axis tilted about 10° from the nadir; however, this amount is negligible in determining crater circularities.

B. RILLE A

This rille (Figure 2), the longest channel in the area (Table I), originates in an irregu-

TABLE I

Rille dimensions and characteristics

Rille	Length km	Width, m		Depth ave. m	Sinuosity		Gradient
		Max.	Min.		S_1 (ave.)	S_2	
A, total	48.0	1400	560	56	1.21	1.17	0°38′
A, upper	35.7	1400	750	80	1.21	1.42	0°29′
A, lower	12.3	980	560	29	–	1.08	1°08′
B, total	36 0	665	66	35	1.16	1.28	0°32′
B, upper	6.8	665	415	95	–	1.02	1°10′
B, lower	29.2	450	66	30	1.16	1.17	0°25′
C	12.5	895	187	46	–	1.04	1°30′
C-1	6.3	146	83	11	–	1.32	–
D	4.1	171	–	15	1.09	1.15	–
E	0.8	40	–	5	–	–	–
F	2.6	160	140	17	1.26	1.22	–

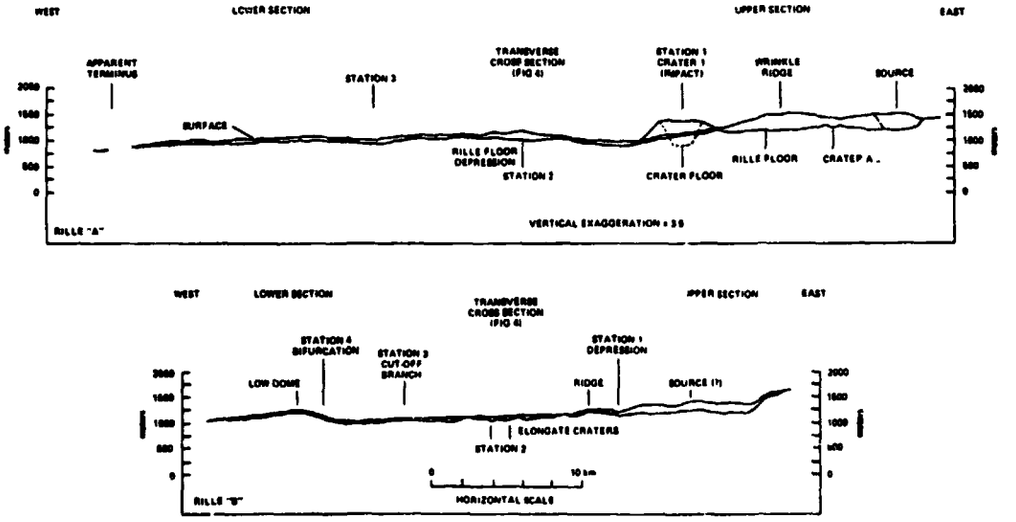

Fig. 4. Topographic profile along axes of Rilles A and B; vertical exaggeration X3.5. Topographic control from unpolished TOPOCOM data and from photographic detail (±126 to 162 m).

lar, 2 km in diameter crater (circularity index = 2.59) formed in Plateau Plains lava flows adjacent to a low dome (McCauley, 1968) on the east side of a prominent wrinkle ridge. Rille A passes through the ridge, trends westward downslope with the regional dip of the Marius Hills Plateau and terminates indistinctly in the mare plains. The terminal end of the channel is less than half the width of the channel at the source. Rille A can be divided into two parts, an upper sinuous section and a lower linear section.

In profile (Figure 4), the rille maintains about the same elevation as it passes through the wrinkle ridge. West of the ridge (Station 1), the rille is partly buried by ejecta from Crater 1 (circularity index, 1.49) interpreted to be impact (McCauley, 1968). There is a slight depression about 4 km long in the floor, about midway down the rille (Station 2). The depression coincides with a segment of the channel that is sub-perpendicular to the regional topographic slope. At Station 3, the channel makes a 98° turn to the south and continues downslope 15 km in a fairly straight course comprising the lower section. Overall slope along the rille floor is 4.3 m km^{-1}(0°15′); overall slope along the channel rim is 11 m km^{-1}(0°38′).

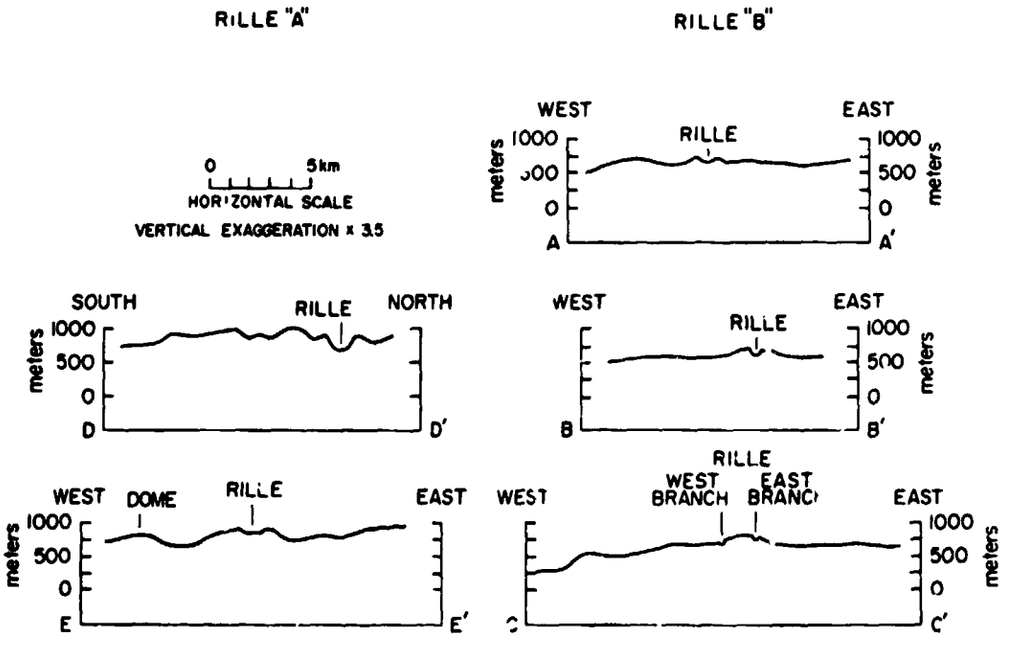

Fig. 5. Transverse cross sections for Rilles A and B, showing rille on or near a ridge crest and development of levees near the rille source. Topographic control from unpublished TOPOCOM data (accuracy ± 126 to 162 m) photographic detail (rille depths determined from shadow measurements), and from McCauley (1968, section D–D′).

Figure 5 shows cross sections perpendicular to the channel axis, constructed from photogrammetically derived elevations (TOPOCOM, and McCauley, 1968). Near the source (section D–D′), the channel is rather deep and has prominent levels along both sides. Downchannel at the next cross section (E–E′), the rille is centered on a ridge and

the channel floor is well above the general ground level. The rille floor is flat along most of the course. However, the upper section from the source through the wrinkle ridge has a more 'V' shaped cross section, probably resulting from slumping of the higher channel walls.

C. RILLE B

Rille B is the second largest rille in the area (Table I) and as with Rille A, originates in Plateau Plains lava flows on the east side of the wrinkle ridge, skirts around (or crosses) the ridge, then trends northwest. The rille can be divided into two parts, an upper section on the east side of the ridge and a lower section to the west of the ridge. The upper section is fairly straight, wide, and appears to originate in an elongate cleft. The cleft has an irregular, hummocky floor and a prominent rim on the southeast side.

In profile (Figure 4) the floor of Rille B does not maintain the same elevation at the juncture with the ridge; rather, it appears to ride up and over the ridge. This may be due, in part, to slumping of the end of the ridge into the rille. Station 1 marks a shallow depression in the rille floor, upslope from the ridge. As the rille crosses the ridge, the channel turns abruptly northwest into the lower section. The lower section of the rille is slightly narrower than the upper section and is locally more meandering ($s_1 = 1.30$, maximum). Station 2 marks two elongate craters in the rille floor that may be of endogenetic origin. At Station 3 the channel displays a small cut-off channel about 1.6 km long on the northeast side of the main channel. The subsidiary channel is about half the width of the main channel and is on a higher elevation. The lower section of Rille B trends generally downslope to Station 4 within 7 km of its apparent terminus. Here, the slope reverses and the rille occupies a low dome. At this same point, the rille divides into at least two small (about 180 m wide) channels, East Branch and West Branch, both of which become discontinuous and fade into the mare plains.

In cross section (Figure 5) many segments of Rille B occupy ridge crests or have lateral levees, similar to Rille A. In the upper section near the apparent source-cleft the rille has prominent levees (section A–A'). Below the ridge the rille is centered on a broad topographic high (section B–B'). Near the terminus East Branch and West Branch cross a low dome (section C–C').

Walls along Rille A and Rille B have slumped over the channel floor. Sections of the walls exhibit boulders up to 40 m in diameter that have weathered from their apparent outcrop source very near the surface.

D. RILLE C AREA

This area (Figure 6) contains at least five distinct structures: (1) a combination sinuous rille – elongate crater chain (Rille C) (2) an inferred impact crater, (3) a prominent steep dome superposed on a low dome, (4) a small sinuous rille, and (5) a small linear rille.

Rille C originates in an irregular shaped crater (circularity index = 3.76), about 1.66 km in diameter on the southeast flank of a cratered dome complex. There is no indication of a raised rim on the southeast side of the crater (the rest of the crater rim

intercepts other structures) and the interior rim has a 'tree bark' texture possibly resulting from soil creep. The crater floor is somewhat hummocky and has normal, round bottomed craters. One exception is a 235 m in diameter (largest crater on the floor) funnel, or dimple shaped crater in the northwest quadrant of the floor near the rim. Boulders up to 8 m in diameter have apparently weathered from the main crater rim and rolled to the bottom of the dimple crater.

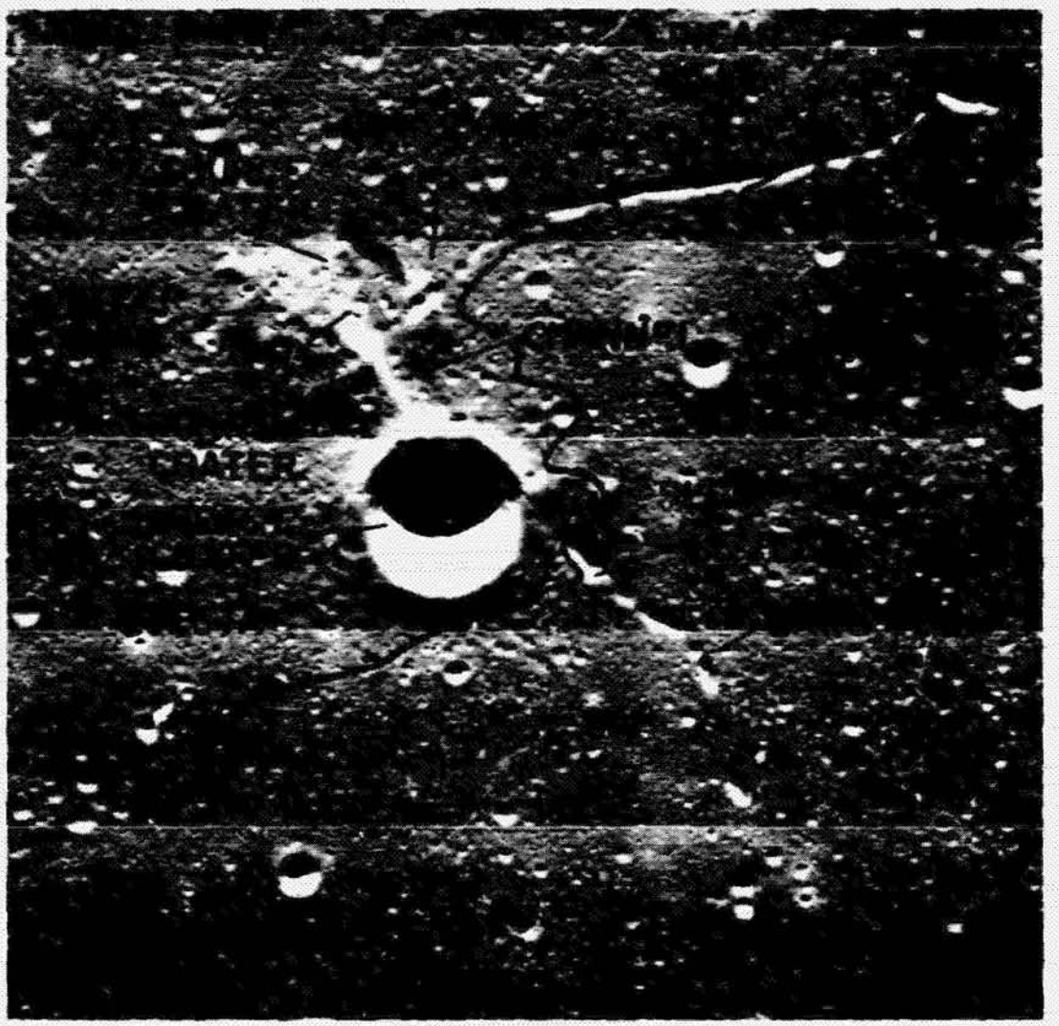

Fig. 6. Rille C area. Crater 2 (circularity index, 1.38, interpreted to be impact origin) and its ejecta cover Rilles C and C-1; 4000 m contour line from TOPOCOM manuscript map. The upper part of Rille C, originating in Source Crater 13 (circularity index 3.76), is considered a lava channel (compare with Figure 14). Below the ejecta blanket of Crater 2, Rille C is considered to be a collapsed lava tube. Rille C-1 is discontinuous and is also considered to be a collapsed lava tube, possibly a distributary structure for the main rille. Photograph from LO 5 frame MR-214.

Rille C leads southwest 1.45 km and is blocked by ejecta from Crater 2, interpreted to be impact (circularity index, 1.38). This section of the rille is 83 m wide, 33 m deep, and has a flat floor pocked with craters up to 31 m in diameter.

Southwest of the impact crater, the Rille C structure continues as a series of elongate craters, identified A through G beginning nearest the ejecta. Crater A has a prominent fracture extending along its southern rim forming a 100 meter-wide block that may have slumped toward the crater.

A 334 m in diameter crater (G), 12.5 km from the apparent source, is the last structure considered part of the rille system. The rille system may continue southwestward through a few elongate craters an additional 14.5 km to a 300 m wide sinuous rille. Although this small rille is on the same general trend as Rille C, there is not sufficient surface evidence to warrant its connection with Rille C.

Crater 2 is 3.12 km in diameter, at least 505 m deep, and has rims about 200 m above ground level. Continuous ejecta extends at least 940 m radially from the rim and there are no discernible ray elements. Ejecta fills part of the upper part of Rille C and part of a smaller rille (Rille C-1) which may be genetically related to Rille C. Unfortunately, the crater covers the area of possible junction. Rille C-1 is 6.25 km long, averages 125 m in width and is about 11.3 m deep. It is discontinuous and, like other rilles in the Marius Hills, ends by fading out on the mare surface.

The fourth structure in the area is the dome associated with the source crater of Rille C. McCauley (1968) described the dome as a compound structure composed of a low dome and superposed steep dome. The structure is subcircular, about 4.5 km in diameter, and has craters up to 270 m in diameter on the surface. Some craters on the dome appear to be funnel or dimple shaped; however, shadows prevent conclusive determinations of the morphology.

Cross cutting Rille C and the dome is a small linear rille. The rille is paralell to the major ridge system in the Marius Hills and preliminary topographic determinations indicate that the rille is nearly horizontal (paralleling the 4000 m contour line, Figure 6). The linear rille consists of two parts, a northern section 3.9 km long × 415 m wide (maximum) × 34 m deep (maximum) and a southern section 9.6 km long × 520 m wide (maximum) × 38 m deep. The northern section is composed of subcircular craters, some of which are connected by fractures. The structure intersects the southern rim of Rille C crater, apparently passes without surface expression across the crater floor and northern rim, and intersects the steep dome. The southern section is better defined than the northern section and is comprised of deep elongate craters and clefts connected by fractures. At the southern terminus, the rille hooks toward the southwest in a large, deep (96m) elongate crater.

E. PROPOSED APOLLO SITE

The proposed landing site (Figure 7) is north of Rille B on relatively smooth Plateau Plains material interpreted to be lava flows and (or) pyroclastics in a small, NNW–SSE trending basin situated between domes (McCauley, 1968). The domes bounding the basin to the west were described by McCauley (1968) as fissure or punctured cones and interpreted to be pyroclastic deposits surrounding structurally controlled vents. There are at least three rilles in the general area, two of which (Rilles D and E) are scheduled as investigation stations (Elston *et al.*, 1969).

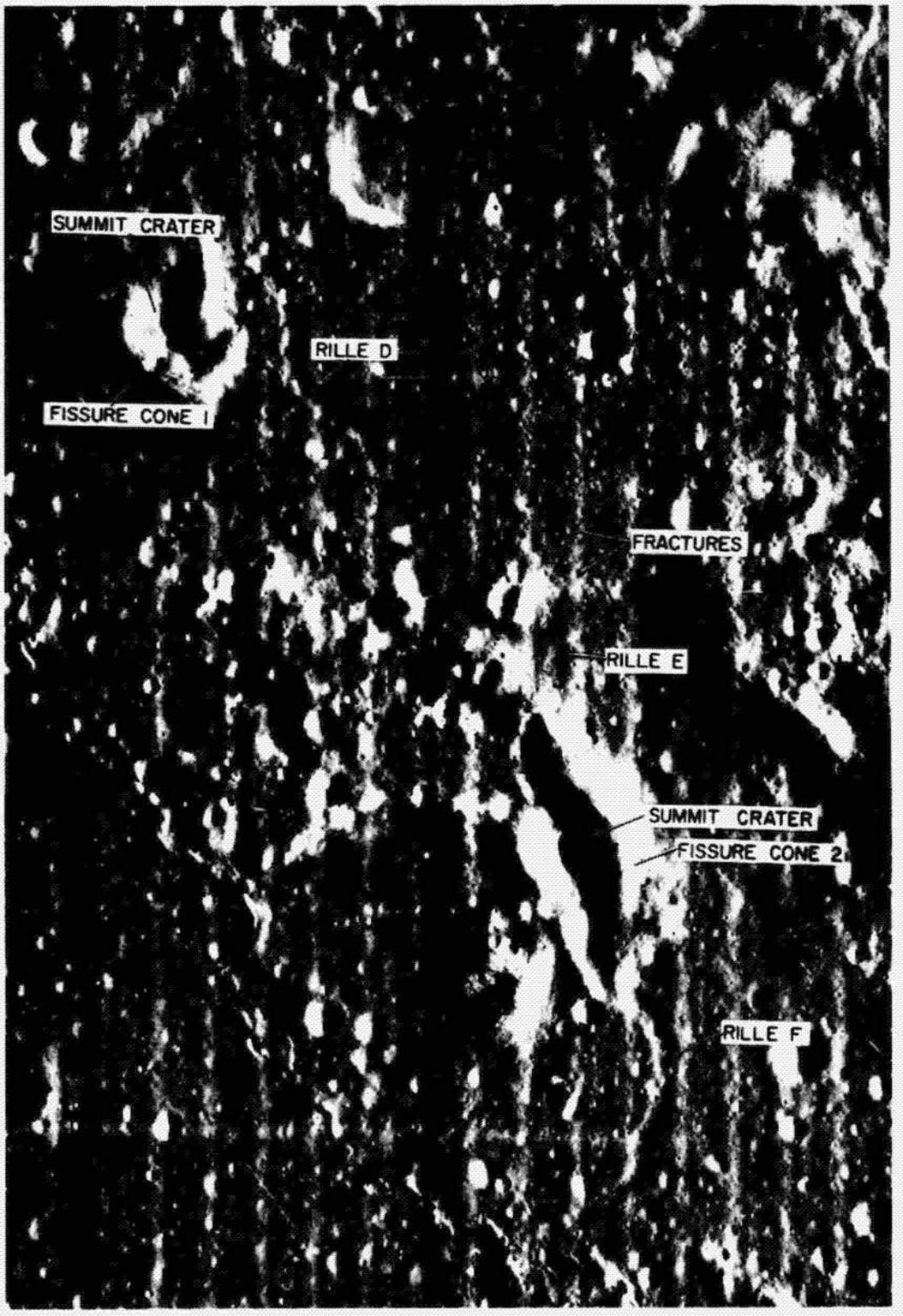

Fig. 7. Proposed Apollo landing site. Rille D is interpreted to be either a lava tube or lava channel; Rille E is considered to be a fracture or fissure; Rille F is interpreted to be a nearly completely collapsed lava tube, probably originating from Fissure Cone 2 (compare with Figure 16). Photograph from LO 5 frames HR-216 and 217.

Rille D marks the contact between McCauley's (1968) Plateau Plains unit and the low dome on which Fissure Cone 1 is situated. The rille is at least 4.07 km long and 171 m wide. In cross section the rille is broadly rounded without a well defined wall-floor contact. Depth appears to be variable and is difficult to determine because the walls are not steep enough to cast sharp shadows. In one area, however, the rille appears to be about 15 m deep. Although the exact rille termini are not readily apparent, the west end is at a higher elevation than the east end and is about halfway between Fissure Cone 1 and a shallow 1.21 km in diameter crater.

Fissure Cone 1 is about 2.6 km long × 1.85 km wide and has an irregularly shaped summit depression about 1170 m long × 650 m wide × 85 m deep (maximum). The north end of the crater has a low rim with a broad depression trending from it north 500 m before hooking toward the northeast.

Rille E was described by McCauley (1968) as a 'subdued trough or rille-like depression'. Similar to Rille D, it is on the dome-Plateau Plains contact and is scheduled as an Apollo investigation station. The rille is 790 m long × 39.5 m wide × about 5 m deep. It is composed of three fairly linear or curvilinear segments meeting at angles, and does not have the usual appearance of a smoothly meandering sinuous rille. The middle of the rille is at a lower elevation than the ends.

About 400 m northeast of Rille E is a series of NNW-SSE trending fractures. The fractures are about 2 m wide and are in discontinuous, en echelon sections, with the longest section about 1.8 km. Although McCauley (1968) described these structures as sinuous rilles, the linear, en echelon character of the structure is not typical for sinuous rilles.

Fissure Cone 2 is in the southern sector of the proposed landing site. It is 1.6 km wide × 3.4 km long and has a central linear depression with a depth exceeding 135 m in the deepest area. The south end of the depression has a very low rim leading toward (but separated from) Rille F by a gentle topographic swale about 240 m long. Interior and exterior walls of Fissure Cones 1 and 2 are steep and exhibit 'tree bark' textures.

Rille F is a sinuous structure about 2.6 km long × 160 m wide × 17 m deep, leading downslope away from Fissure Cone 2. It tapers to about 104 m and becomes shallower toward the south where the rille ends nearly perpendicular to a wrinkle ridge. The wall-floor contact is better defined than in Rille D and the floor in places is wide and flat

3. Terrestrial Analogs Compared with Lunar Features

Several hypotheses on the formation of lunar sinuous rilles have been proposed in the last several years. Oberbeck *et al.* (1969) discussed some of the various proposals and presented evidence that at least some sinuous rilles result from collapse of lunar lava tubes; possible formation by other mechanisms, particularly that by lava channel formation, were not excluded. Morphological similarities between certain lunar rilles or rille-like structures and terrestrial lava tubes and channels are supported by recent evidence on the estimated viscosity and composition of lunar mare material. Apollo 11 and 12 mare samples closely resemble terrestrial basalt (Hess and Calio, 1969; and

LSPET, 1970). Laboratory simulation of molten lunar lavas by Murase and McBirney (1970) indicated that viscosity is an order of magnitude less than the closest terrestrial counterpart and on this basis, predicted the probable existence of many large, long lunar lava tubes. Lava tubes from exclusively and commonly in basalt lava flows and it is reasonable to assume that tubes have formed in lunar basalt. Under multiple impacts at least some lunar lava tube roofs would collapse, resulting in sinuous trenches similar to collapsed terrestrial lava tubes.

A. LAVA TUBE AND CHANNEL FORMATION

Observations of active basalt lava flows (Jagger, 1947; Finch and Macdonald, 1953) and field investigations of solidified basalt flows and lava tubes (Ollier and Brown, 1965; and Greeley and Hyde, 1970) permit speculation on lava tube and channel formation (Greeley, in press).

Lava tubes form in fluid basalt flows that have cooled on the surface (forming a crust) with flow of fluid lava continuing beneath the crust. As cooling progresses, flow is restricted to a conduit-shaped structure within the flow. Toward the flow front, the conduit subdivides into smaller, multiple distributaries termed *feeder tubes* that lead molten material to the advancing flow front. As the supply of molten lava from the vent diminishes, the molten lava drains from beneath the free-standing crust and leaves a hollow void, or lava tube. Most feeder tubes do not drain, or are sealed with

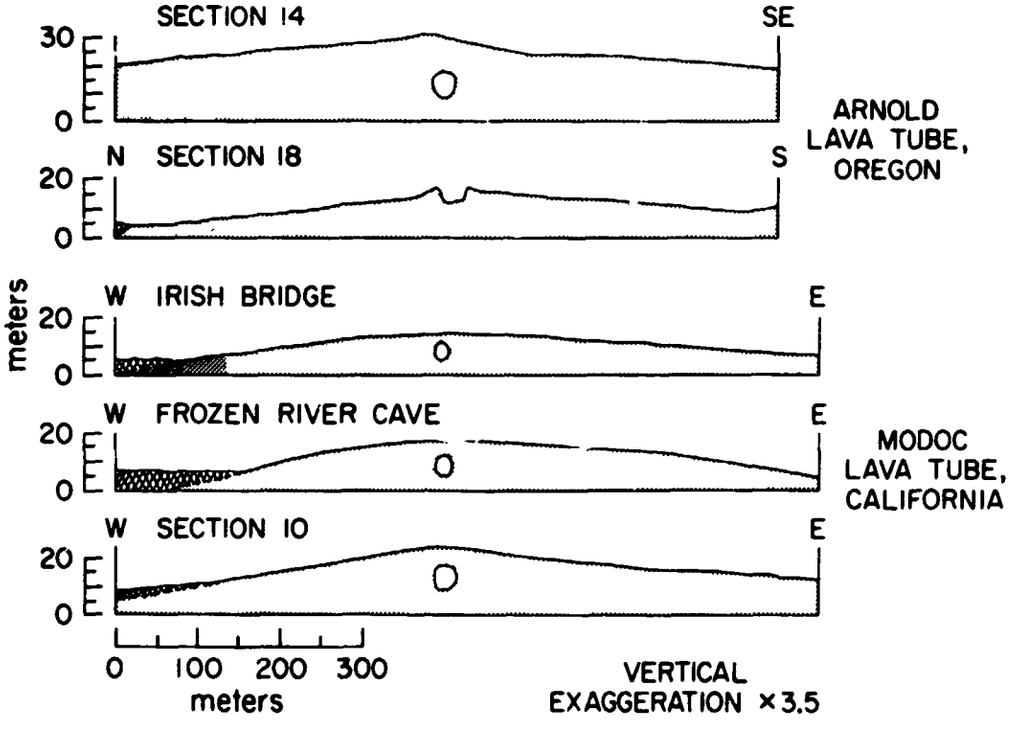

Fig. 8. Cross sections along two lava tubes (Arnold Lava Tube, Deschutes Co., Oregon, and Modoc Lava Tube, Lava Beds National Monument, Calif.) illustrating formation of topographic high along the tube axis.

lava from subsequent flows. Some terrestrial lava tubes exceed 25 km in length and 30 m uncollapsed diameter.

Lava tubes occur on slopes ranging from less than 0.4° to more than 6.5°. Basalt flows as long as 48 km with an overall slope of 0.61 m km^{-1} (less than 0.1°) are known to contain lava tubes (1881 Lava Flow, Mauna Loa containing the Kaumana Lava Tube). In contrast, channels appear to form on slopes over a much wider range and develop in both viscous (aa) basalt and fluid (pahoehoe) basalt. Major lava tubes, in contrast, form only in laminar, fluid flows, possibly through shear plane development (Ollier and Brown, 1965). If flow velocity is high (as on steep slopes) or the flow is too viscous (aa basalt), then the flow may become turbulent, losing the shear planes, and open channels may form instead of lava tubes. Channels may also form as a result of drainage of molten lava from beneath the crust before the crust has cooled and solidified to a thickness sufficient to support its weight. The width of the channel may also exceed the maximum span attainable by a free standing basalt roof. In either case, the cooled or partly cooled roof collapses as the supporting fluid drains. This type of collapse often occurs in terrestrial structures and may result in sinuous channels with smooth sides or as a series of elongate drainage craters (Greeley, 1970). Thus, channels may develope in preference over tubes when (1) the gradient is steep, (2) the lava is viscous (precise limiting viscosities are not known), or (3) the crust over the molten lava is not free standing after drainage of the lava. The distinction between the tubes and channels can, thus, be made in regard to the crust: if the roof is free standing after drainage of molten lava, the structure is a tube; if the crust only partly develops, or collapses during drainage, the structure is a channel. Some structures alternate from tube to channel to tube, etc.

Active lava flows containing tubes and channels with surface crusts are closed hydrostatic systems. As an advancing flow encounters a topographic obstruction, such as a ridge, the flow may ride up and over the obstruction; the contained tube or chan-

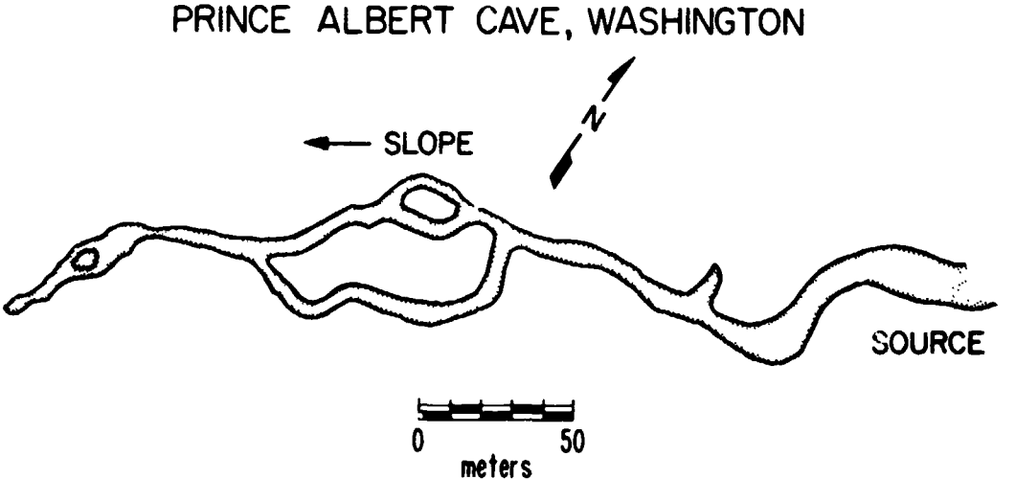

Fig. 9. Diagram of uncollapsed part of Prince Albert Cave (lava tube) in Skamania Co., Wash., illustrating cut off branches.

nel may then act as a siphon operating under hydrostatic pressure to carry molten lava to the advancing flow front.

Cross sections perpendicular to lava tube axis show that lava flows often form topographic highs, or ridges, along the axis (Figure 8). Lava channels also develop topo-

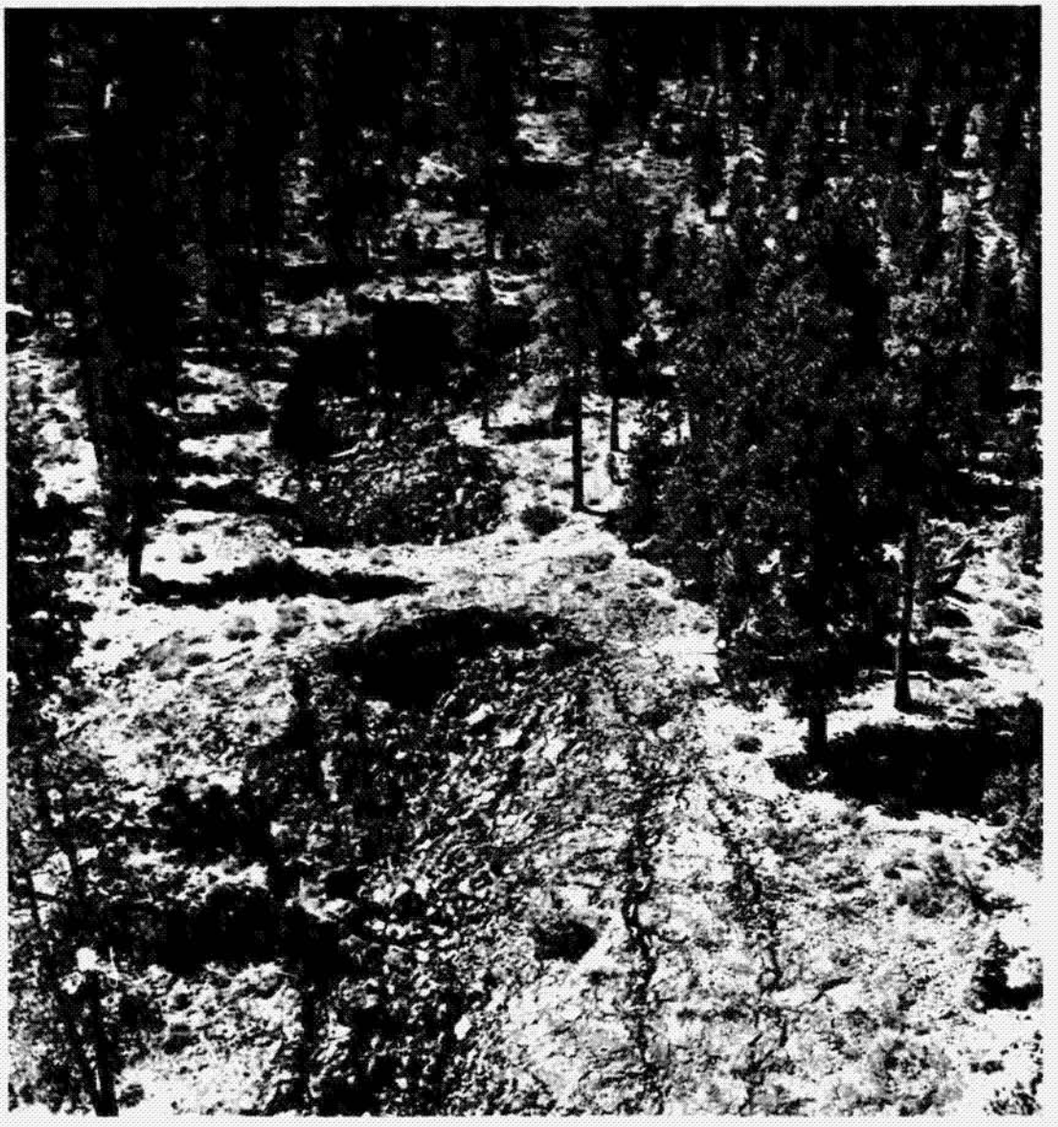

Fig. 10. Aerial oblique view of part of Hambone Lava Tube, Siskiyou Co., Calif. Large lateral blocks parallel to the tube have slumped toward the tube, similar to the structure along the collapse depression in Rille C.

graphic high regions, with the slope generally away from the axis of the structure. Lava channels are generally aggradational features and the channel floor is often elevated considerably higher than the surrounding ground level. This condition results from accretion of lava that spills over the bank of the channel. Multiple surges of lava,

or individual flow units may spread laterally from the main channel through distributary channels or tubes (Greeley, 1969). Multiple eruptions may continue to elevate the channel and adjacent area by accretion. Tubes and possibly channels may also be erosive structures. A lava tube in southwest Washington shows areas in which the lava tube and flow apparently undercut the pre-flow valley wall (Greeley and Hyde, 1970).

Lava tubes and channels form cut-off branches along the main structure, as illustrated in Figure 9. Cut-offs may be at higher, lower, or the same level as the main structure. Collapse of the roof results in an 'island' surrounded by lava trenches. As collapse progressed, large blocks parallel to the tube axes may break away from the wall and slump into the collapsed tube (Figure 10).

Width of lava tubes may be fairly constant throughout their course (Hambone Lava Tube, Siskiyou Co., Calif.) or may be variable. The trench resulting from lava tube roof collapse usually reflects the original configuration of the tube. Lava channels, on the other hand, are generally fairly constant in width; however, they may become progressively shallower.

B. RILLE A

Rille A originates in a crater lacking raised rims and ejecta and that has a high circularity index, all indications of internal origin. Rille rims near the source (Figure 5) form prominent levees. Downslope the rille occupies the crest of a ridge at least 200 m above the surrounding terrain. It is unreasonable to assume that the rille eroded its channel along the center of the ridge by fluvial or nuée ardent mechanisms. Levees and ridges are considered constructional features of the rille, analogous to structures formed in association with lava channels. Although it may be argued that small levees can result from fluvial processes, an origin by water does not explain the large ridge underlying the axis of Rille B, reversals in slope along the channel floor (Figure 4), absence of tributaries, or tapering of channel width toward the terminus.

Morphologically, Rille A is identical to many lava channels and collapsed lava tubes. Its great width probably exceeds that of a free standing lava tube roof, even under lunar conditions (Oberbeck *et al.*, 1969). Lava channels, however, are not restricted in width. Formation of a thin crust during active flow permits hydrostatic flow conditions and allows the structure to cross topographic highs. The ridge appears lower at the junction with Rille A and the rille possibly passed through a gap, overriding small topographic obstructions. Contemporaneously, lateral channels and tubes distribute accretional lava to form levees and to elevate the overall structure. Length of Rille A is comparable to terrestrial basalt flows containing tubes and channels. Slope along Rille A is similar to that of terrestrial basalt flows (Rille A = 0°31′, Horse Cave System, Oregon = 0°28′ [Greeley, in press]).

Although quantitative and qualitative morphologic evidence and compositional evidence strongly support origin by lava channel formation, other mechanisms cannot be entirely excluded. The lower part of the rille consists of fairly straight segments which meet at rather sharp angles rather than forming meandering bends, and the rille floor is flat, suggestive of linear rilles and possible formation by block faulting.

C. RILLE B

The upper section of this rille, consisting of an elongate cleft and curvilinear rille, appears to be structurally controlled and may be analogous to a fissure. Figure 11 illustrates part of the Southwest Rift Zone of Mauna Loa and the associated basalt flows and channels controlled by the rift. The lower part of Rille B is meandering, occupies a ridge crest, has an irregular floor, a cut-off branch at a higher elevation than the main

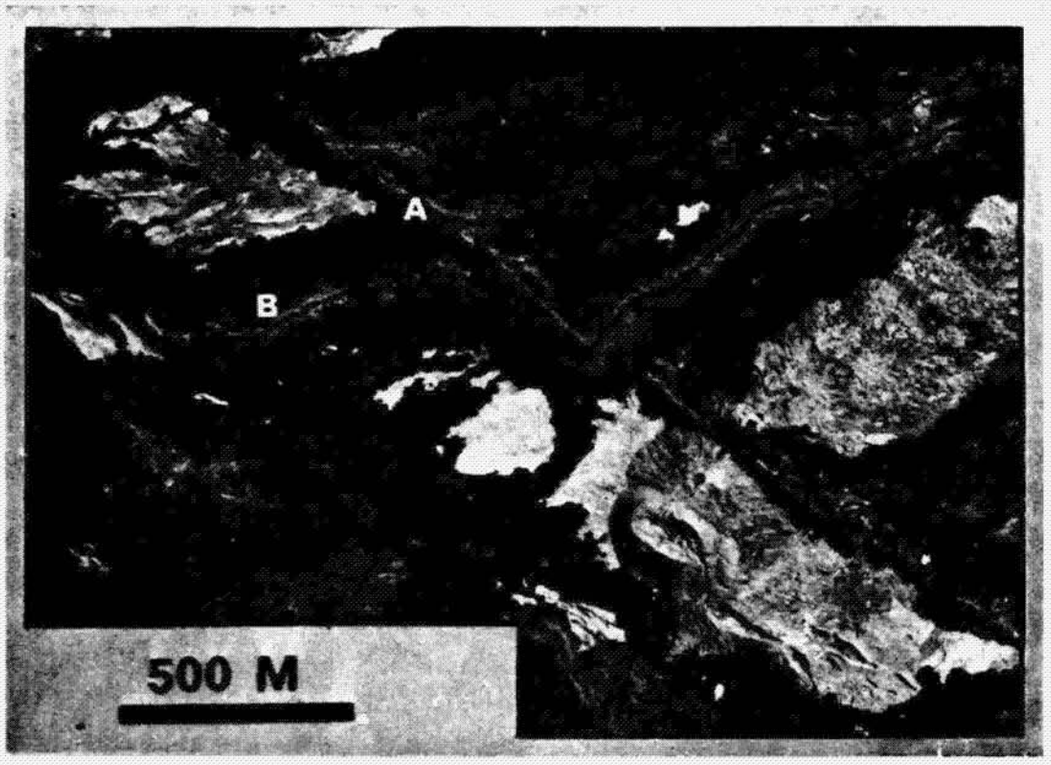

Fig. 11. Southwest Rift Zone, Mauna Loa, Hawaii. The rift (A) has controlled the course of the lava channel (B).

trench, crosses a low dome, and has terminal distributary channels. These structures are best explained as parts of a collapsed lava tube network. The irregular floor and discontinuous channel (between Stations 2 and 3) may represent piles of collapsed blocks and uncollapsed sections of a lava tube roof of variable thickness, similar to that of Arnold Lava Tube, Oregon (Greeley, in press). The cut-off branch at Station 3, occupying a higher elevation than the main trench is typical for cut-off, subsidiary lava tubes (Figure 9). At the western terminus of Rille B, the branching and discontinuous smaller channels are analogous to feeder tubes and distributary channels frequently found in lava tubes (Figure 12). The lower section of Rille B, therefore, is interpreted as a nearly completely collapsed lunar lava tube. The upper section may represent a fissure zone and (or) lava channel.

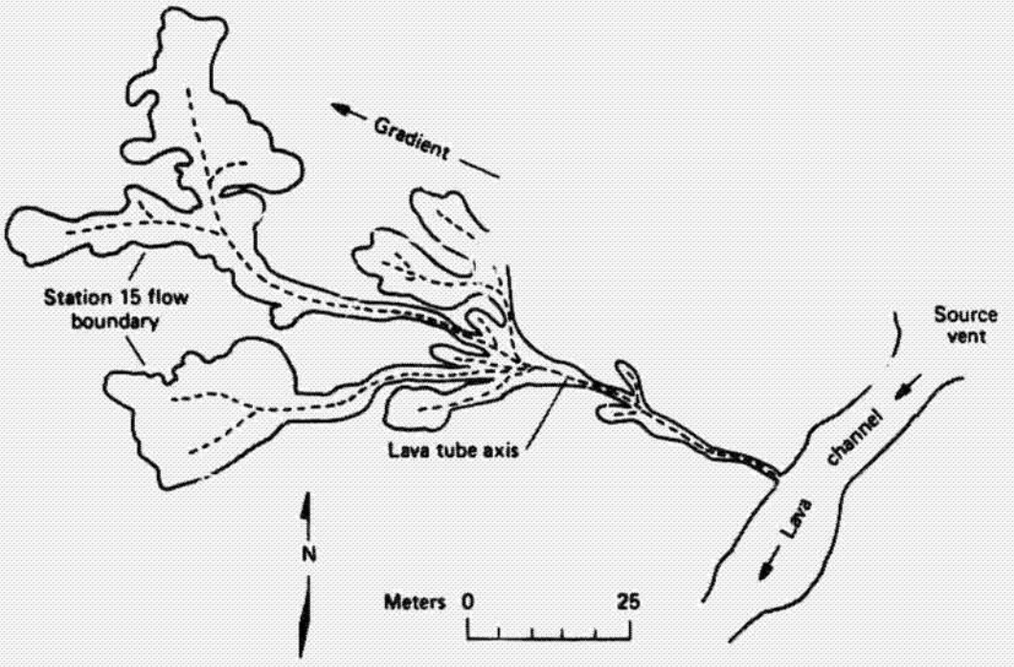

Fig. 12. Diagram of a small distributary lava tube system leading from a larger lava channel-tube. Distributary systems deposit lava along major channels and tubes thus elevating the system.

D. RILLE C AREA

Rille C is a classic example of a partly collapsed lava tube. Unfortunately, precise topographic control is not available for detailed quantitative geomorphic analysis. However, preliminary topography and qualitative geomorphology provide ample evidence for its interpretation. Comparisons can be made with Giant Crater, Modoc Crater, and Mammoth Crater Lava Tubes, Northern California (Figures 13 and 14). Like these three structures, Rille C originates in an irregular crater (high circularity index, Figure 3) indicative of internal origin. The source craters of all the structures are situated in upland areas associated with domes (pyroclastic cones and lava flow domes for terrestrial examples, 'extrusive structures' of McCauley [1968], for Rille C). Rille C crater has on its floor prominent funnel-shaped crater suggestive of drainage to the subsurface. Similarly, Giant Crater has internal craters (Figure 13) which resulted from subsidence and withdrawal of the magma (Anderson, 1941, p. 381). The upper channel leading from the source crater of Rille C is probably similar to the elongate trough leading from Giant Crater. Both structures have flat floors and probably did not have free standing roofs; thus, the upper sections are considered lava channels.

Giant Crater tube passes through a series of elongate collapsed sections separated by nearly solid sections of layered and multiple basalt flows. Some solid sections have small, multiple lava tubes connecting the large collapse depressions. this configuration probably resulted from sporadic eruptions of flow and intermittant drainage of the tube. The lower end of Rille C also consists of a series of elongate depressions. Because the impact of Crater 2 probably generated a strong seismic wave, it is reaso-

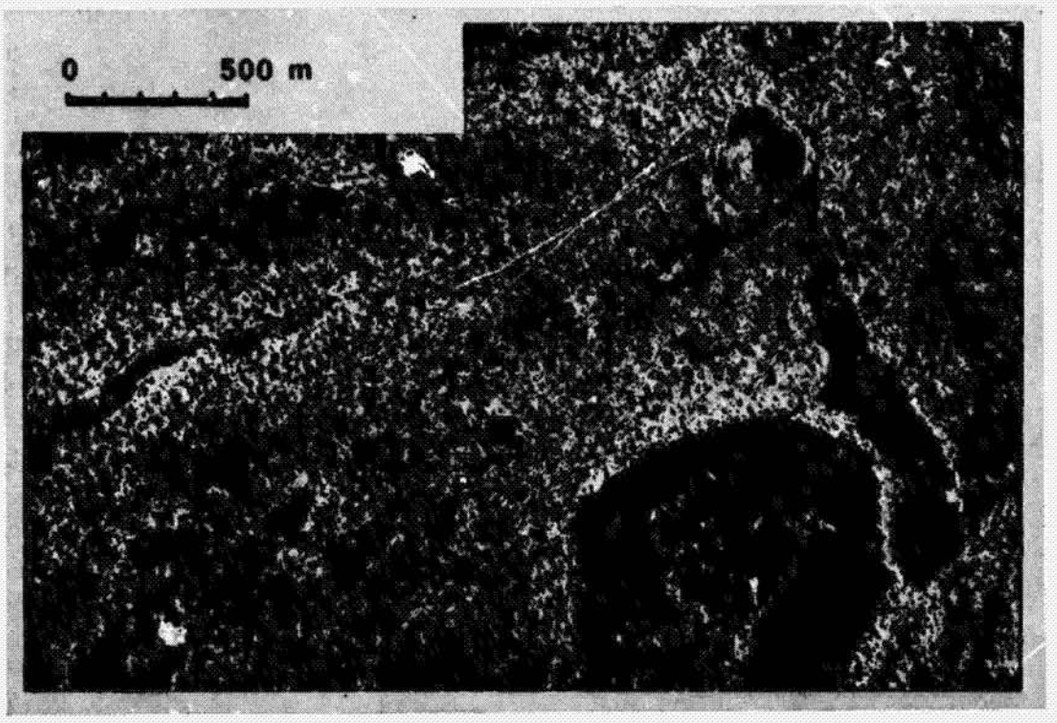

Fig. 13. Aerial photograph of Giant Crater and Lava Tube, Siskiyou Co., Calif. The upper part of the system, near the source crater, may not have had a free-standing roof after drainage of the fluid lava, and this may be considered a lava channel. The lower part of the tube is composed of collapse depressions separated by relatively solid masses of basalt. Giant Crater has several interior craters which resulted from collapse and drainage of fluids back down the vent.

nable to assume that a lava tube roof within one crater diameter would be completely collapsed. However, this part of the rille is considered analogous to Giant Crater tube, with intermittant solid sections. Degradation of the rille is shown by the large slump block on the first depression. This structure is similar to collapse blocks common in many lava tubes (Figure 10).

The largest collapse depression of Rille C is about 420 m wide, or about 3 times wider than the widest known collapsed lava tube on earth (Bear Trap Lava Tube, Idaho). Oberbeck, *et al.* (1969) demonstrated that reduced lunar gravity would permit collapsed lunar tubes up to 500 to 1000 m wide, depending upon lateral slumping. Rille C width is well within this range. Overall length of the rille, 12.5 km, and estimated slope of 1.5° are analogous to many terrestrial lava tubes.

Rille C-1 leading from Rille C tapers and becomes slightly shallower toward its lower end. It is discontinuous and interrupted in at least three places (Figure 6). Rille C-1 is interpreted to be a distributary lava tube associated with the main rille. Unfortunately, Crater 2 is superposed over Rille C at the juncture of the channel, collapsed tube, and the distributary channel, and it is impossible to determine the relationships between the structures. Although ejecta from the crater has altered the pre-impact topography, preliminary topography from a manuscript topographic map of the

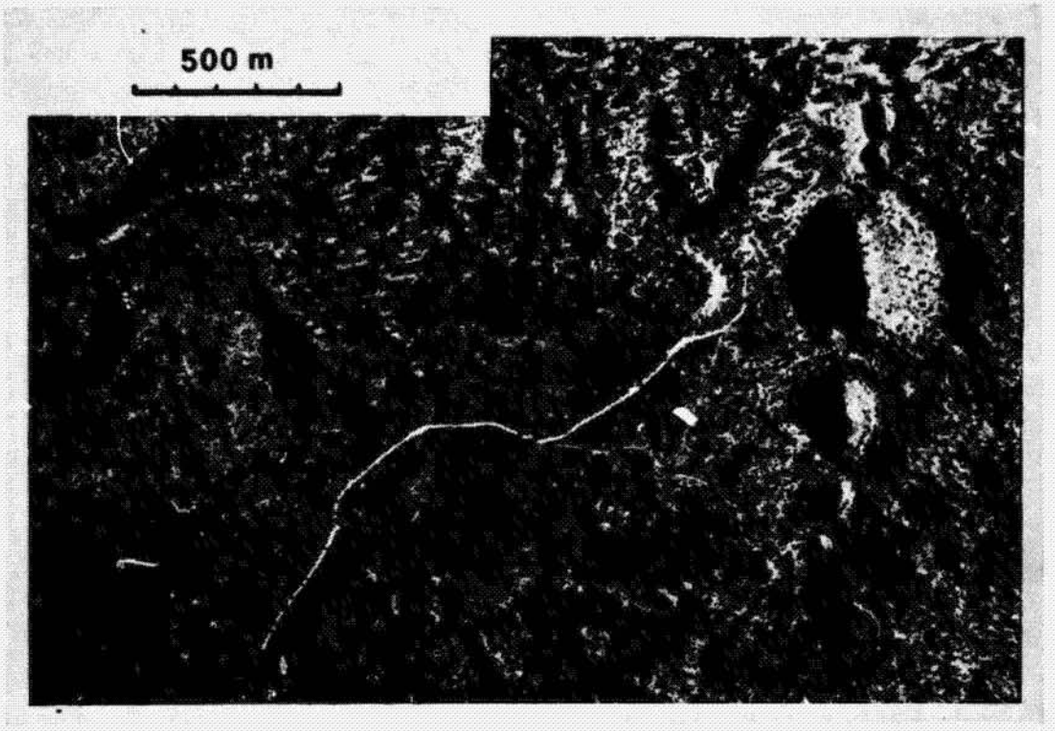

Fig. 14. Mammoth Crater and Lava Tube, Lava Beds National Monument, Calif. The lava tube can be traced through a series of collapse depressions. Like Giant Crater and Tube, Mammoth Crater is adjacent to pyroclastic cones and domes.

Marius Hills (TOPOCOM) indicates a slight rim along both sides of Rille C (see the 4000 m contour line, Figure 5).

The cross-cutting relationship of the linear rille to the mare, Rille C, and the dome indicates that it is younger than these features and is structurally controlled. Because the structure is nearly horizontal (parallel to the 4400 m contour line) it is unlikely that it resulted from fluid flow. It is interpreted to be a fault, or fault block, through which fragmental surface material has drained to form elongate craters.

E. APOLLO LANDING SITE

This area contains structures interpreted to be lava tubes and channels. Rilles D and F originate in or near cratered domes interpreted to be pyroclastic structures which are situated on low domes possibly representing flows or laccolithic structures (McCauley, 1968). These structures are analogous to Hawaiian shield volcanoes with superposed pyroclastic domes having common vents (Stearns, 1966, p. 45). Associated with the Hawaiian structures are fluid basalt flows containing lava tubes and channels. In other areas, pyroclastic cones are built from essentially the same vent as source craters for tubes and channels. Examples include Bandera Crater and lava tube, New Mexico and Deep Crater and tube, California. Deep Crater (Figure 15) is considered analogous to the fissure cone and Rille F in the Apollo site.

It is difficult to determine whether Rilles D and F are collapsed lava tubes or are

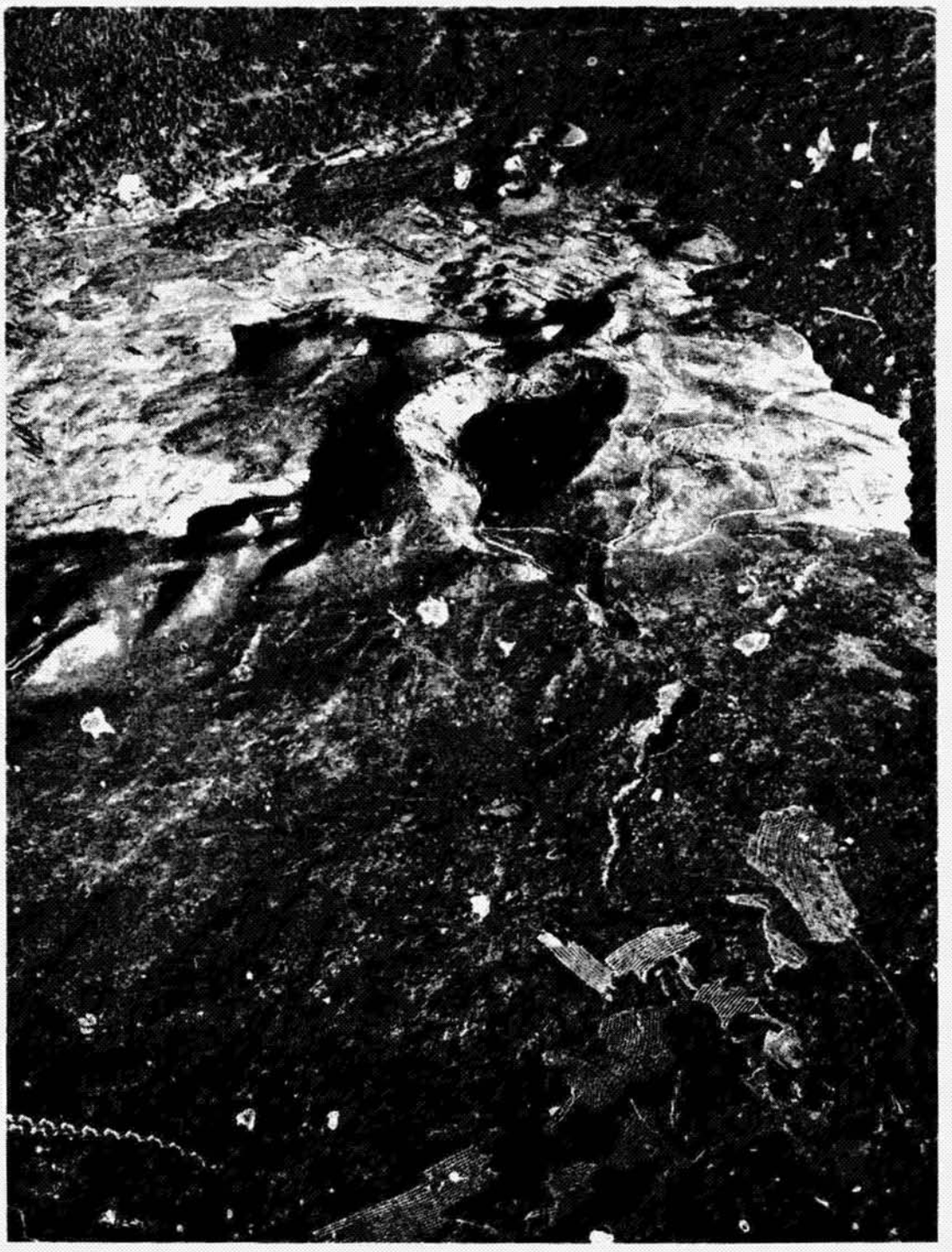

Fig. 15. Deep Crater and Lava Tube, Siskiyou Co., Calif. The lava tube originated in or near the crater formed in a pyroclastic cone, then flowed down the flank of the cone onto the lava plains. Deep Crater is approximately 1 km in diameter. Compare with similar structures in the Proposed Apollo landing site (Figure 7).

lava channels. The depth of Rille E is fairly constant and the rille is continuous; thus it may not have been roofed. Rille F, on the other hand, is discontinuous and may represent uncollapsed, or sealed parts of a lava tube.

Rille E, composed of three linear sections, appears to traverse a slight valley, with each end at a higher elevation than the middle. Rille E and the en echelon linear depressions to the north and northeast are interpreted to be faults, fractures, or fissures.

4. Summary and Conclusions

The Marius Hills region has been previously described as a volcanic province exhibiting many common volcanic structures. The mare area (Plateau Plain material of McCauley, 1968) is considered composed of volcanic flows and interbedded pyroclastics. Results from Apollo 11, Apollo 12 and Surveyors 5 and 6 indicate the mare rocks are similar to basalts. From viscosity determinations of postulated lunar lavas, Murase and McBirney (1970) predicted the existence of many long lunar lava tubes. Lava tubes and channels are common features of terrestrial basalt flows and it is reasonable to assume that lunar lava tubes and channels exist. Under prolonged impact, many of the tube roofs would collapse, leaving sinuous trenches. The softening effect of impact would smooth surface irregularities in the trenches and channels.

Thus far, no lunar mission has yielded photographs showing structures that can be conclusively described as lunar cave entrances, although Kuiper (1965) posed some possible examples. Although to some workers, this is a criticism against the existence of lunar lava tubes, there are three points to consider: First, terrestrial lava tube entrances generally are not visible in aerial photographs. For example, Figure 16 shows a collapsed lava tube and entrance to the uncollapsed interior taken under various conditions. Figure 16a is a conventional vertical photograph taken at an altitude of 30000 ft with vertical illumination; ground resolution is 37 cm. Figure 16b is the same area, taken from an altitude of 24000 ft, with the Sun 18° above the horizon (similar to Lunar Orbiter lighting conditions) and a ground resolution of 29 cm. Finally, Figure 16c is an oblique aerial view, taken 200 ft above ground, under good lighting conditions. Lunar Orbiter pictures, in contrast, are made at altitudes of about 370000 ft (Marius Hills Site) producing photographs with ground resolution of 2.5 m (Marius Hills photographs). If cave entrances do not show (or seldom show) in terrestrial photographs, it is unlikely that they will be visible in spacecraft photographs. Lava tubes generally begin to collapse where the roof is thinest, and where the tube tends to rise toward the surface. Collapsed roof sections often block or nearly block the entrance. Thus, lava tube entrances are considerably smaller than the uncollapsed interior. In aerial photographs the entrances are usually lost in shadow, too small to be clearly distinguishable, or appear as irregular shadows.

Second, in many cases uncollapsed lava tubes are intermittantly blocked completely by collapse and surface detritus. The tube continues through a series of disconnected collapse depressions, none of which display cave entrances.

Third, if most mare areas are as old as Apollo 11 and 12 indicate, then lava tubes

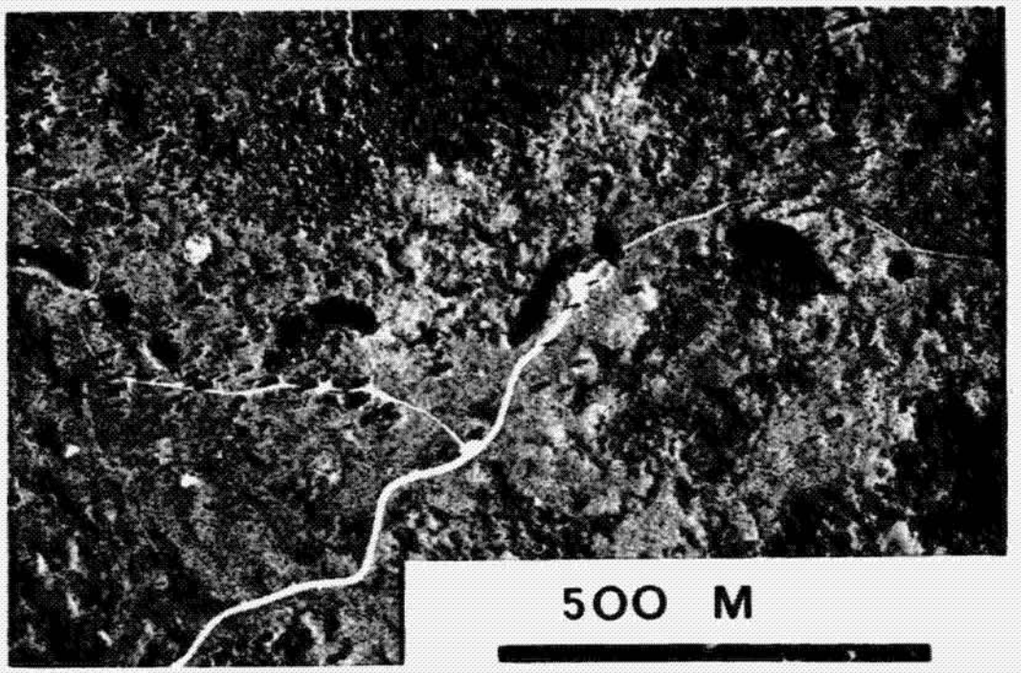

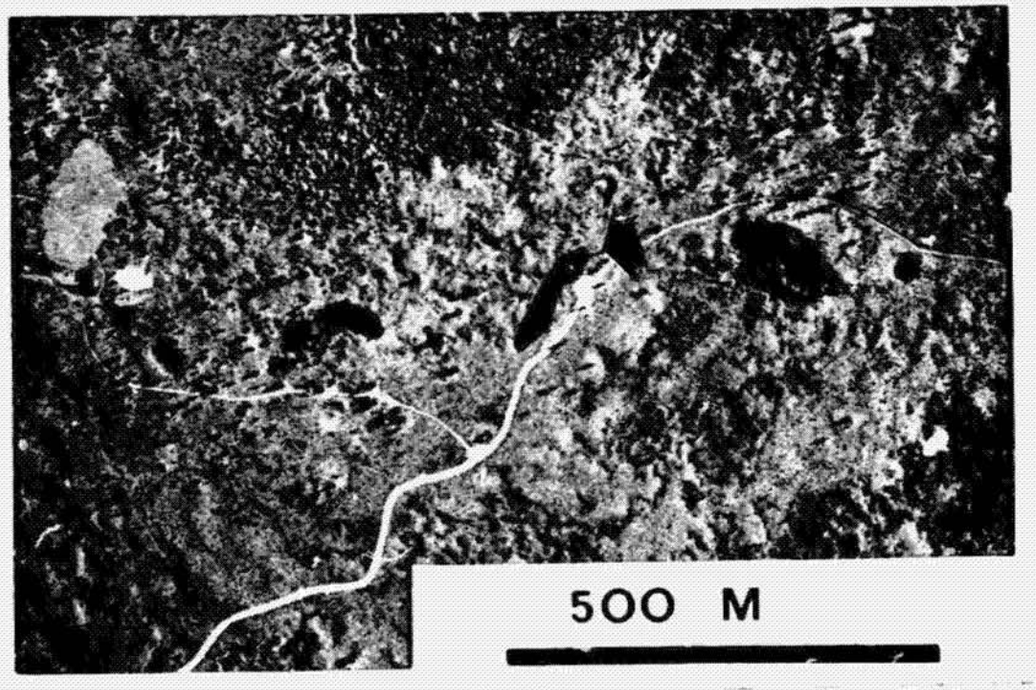

Fig. 16a and 16b.

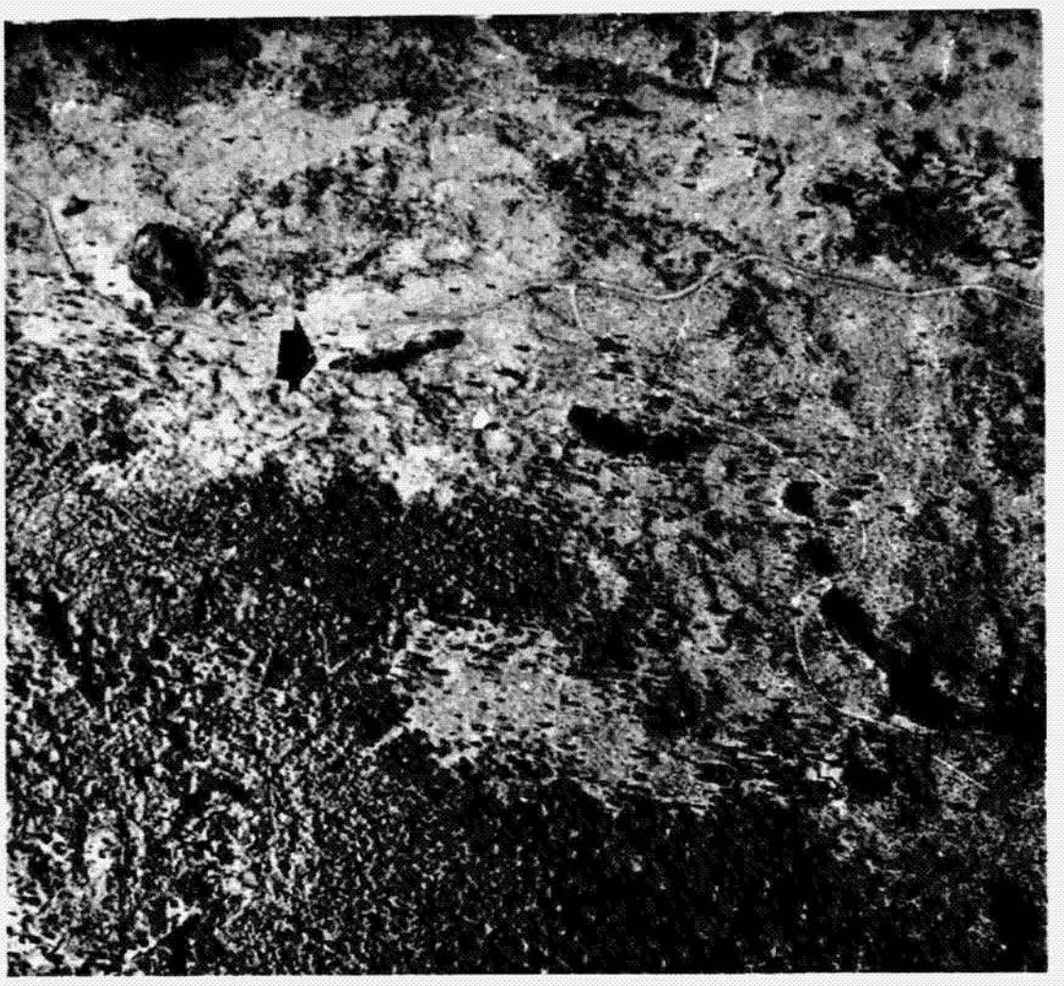

Fig. 16c.

Fig. 16. Aerial photographs of part of Modoc Lava Tube and Skull Cave entrance (uncollapsed tube exceeds 27 m in diameter), Lava Beds National Monument, Calif. Series illustrates the difficulty in detecting cave entrances from the air: 16a-vertical photograph, vertical illumination, ground resolution 37 cm from altitude of 30000 ft; 16b-vertical photograph, oblique illumination (Sun approximately 17 above horizon, similar to Lunar Orbiter photography), ground resolution 29 cm at altitude of approximately 24000 ft; 16c-oblique aerial photograph, oblique illumination, from altitude of about 200 ft. Only in the last photograph, under condition superior to present lunar imagery, is there any indication of cave entrance.

and channels would be significantly degraded. All but the deepest tubes would be collapsed, thus reducing the number of tube, or cave, entrances.

All the structures in the Marius Hills interpreted to be lava tubes or channels originate in topographically high areas, often in or near McCauley's 'steep' or 'low' domes and often in irregular shaped craters. The rilles then trend downslope into the plateau plains, generally decreasing in width and depth. One has a cut off branch at a different elevation than the main channel and one rille bifurcates near its terminus. Structures for which topographic control is available are shown to be situated along or near the

crest of a topographic high, or to have pronounced levees. The rille floor is well above general ground level, indicating the structures were aggradational.

Rilles C, F, and part of B are discontinuous and interpreted to be collapsed lava tubes. Because of its width and continuous channel, Rille A is considered to be a lava channel. It is considered to have passed through the wrinkle ridge at a relatively low region and have carried over topographic obstructions. Rille D is also continuous, but is in a size class attainable by lava tubes. Its origin, whether lava tube or lava channel, is not determined. Some of the rilles, particularly Rille B, appear to have been structurally controlled by fissures and fractures.

Rille E and the linear rille near Rille C because they are straight, cut across other structures, and do not trend downslope, are considered to be faults, fractures, or fissures. They may have been modified by slumping and drainage of surface material into the subsurface.

Although the lines of evidence presented here in support of origin by lava tube and channel formation can be applied to similar lunar structures in other areas, particularly in regions of suspected volcanic activity, it is not suggested that all sinuous rilles have formed by this mechanism. As stated previously, there appear to be many subtypes of sinuous rilles, each of which may have formed in a different way. It is also conceivable that different mechanisms could produce similar appearing structures. However, in the Marius Hills, most of the rilles appear to have resulted from lava flow activity.

Acknowledgements

Grateful acknowledgment is made of M. Lovas for field and laboratory assistance in studies of terrestrial analogs. I wish to thank R. Reynolds and R. Wrigley for their comments and suggestions in regard to the manuscript. This study was conducted while on tenure as a National Research Council-NASA Research Associate.

References

Anderson, C. A.: 1941:, *Bull. Dept. Geol. Sci.* **25**, 247.

Elston, D. P. and Willingham, C. R.: 1969, *Five-day Mission Plan to Investigate Geology of the Marius Hills Region of the Moon*, Astrogeology, 14, U.S. Geol. Survey, open eport, 55 pp.

Finch, R. H. and Macdonald, G. A.: 1953, *Hawaiian Volcanoes During 1950*, U.S. Geol. Survey, Bull. 996-B, p. 27.

Greeley, R.: 1969, *Trans. Amer. Geophys. Union* **50**, 678.

Greeley, R.: 1970, *Moon* **1**, 237.

Greeley, R. and Hyde, J.: 1970, Lava tubes of Mount St. Helens, Washington (abstract). *Geol. Soc. Amer. Abstracts Progr.* **2**, 96.

Greeley, R.: 1971, 'Geology and Morphology of Selected Lava Tubes in the Vicinity of Bend, Oregon', State of Oregon, Dept. of Geology and Mineral Industries, in press.

Hess, W. N. and Calio, A. J.: 1969, *Summary of Scientific Results in Apollo II – Preliminary Science Report, NASA SP-214*, 1.

Jaggar, T. A.: 1947, *Geol. Soc. Amer. Mem.* **21**, 508 p.

Karlstrom, T. N. V., McCauley, J. F., and Swann, G. A.: 1968, *Preliminary Lunar Exploration Plan of the Marius Hills Region of the Moon*, Astrogeology 5, U.S. Geol. Survey open-file report 42 p.

Kuiper, G. P.: 1965, *Ranger VII, Part 2, Experimenter's Analysis and Interpretations, Jet Propulsion Lab., Calif. Inst. Technol., Tech. Rept.* 32-700, 9.
Leopold, L. B. and Wolman, M. G.: 1960, *Bull. Geol. Soc. Amer.* **71**, 769.
LSPET: 1970, *Science* **167**, 1325.
McCauley, J. F.: 1965, in *Astrogeologic Studies*, Ann. Prog. Rept , July 1, 1964 to July 1, 1965, pt. A: U.S. Geol. Survey open-file report, p. 115.
McCauley, J. F.: 1967, *Geology of the Moon, Hevelius Region*, U.S. Geol. Survey Map I-491 (LAC-56).
McCauley, J. F.: 1968, in T.N.V. Karlstrom *et al.* (eds.), *Preliminary Lunar Exploration Plan of the Marius Hills Region of the Moon*, Astrogeology 5, U.S. Geol. Survey open-file report, Plate 1.
Murase, T. and McBirney, A. R.: 1970, *Science* **167**, 1491.
Murray, J. B. and Guest, J. E.: 1970, *Modern Geol.* **1**, 149.
Oberbeck, V. R., Quaide, W. L., and Greeley, R. :1969, *Modern Geol.* **1**, 75.
Ollier, C. D. and Brown, M. C.: 1965, *Bull. Volcanolog.* **28**, 215.
Stearns, H. T.: 1966, *Geology of the State of Hawaii*, Pacific Books, Publ. Palo Alto, Calif., 266 p.

CHAPTER IX – GEOPHYSICS

LUNAR GEOPHYSICS

Curtis W. Parkin
University of Santa Clara, Santa Clara, Calif. 94053

I. INTRODUCTION

During the Apollo missions, geophysical instruments were deployed on the lunar surface (fig. 1) and in orbit around the Moon to study geophysical properties of the Moon's interior and its near environment. In this section a summary will be presented concerning some of the findings of these geophysical experiments. Though several experiments have yielded extremely interesting results concerning extralunar properties, emphasis in this report will be placed on the experimental results pertaining to the lunar interior and atmosphere. Results will be presented for the following experiments: passive and active seismometers; magnetometers; heat flow experiment; laser altimeter; gamma ray, X-ray, and alpha-particle experiments; and mass spectrometer experiments.

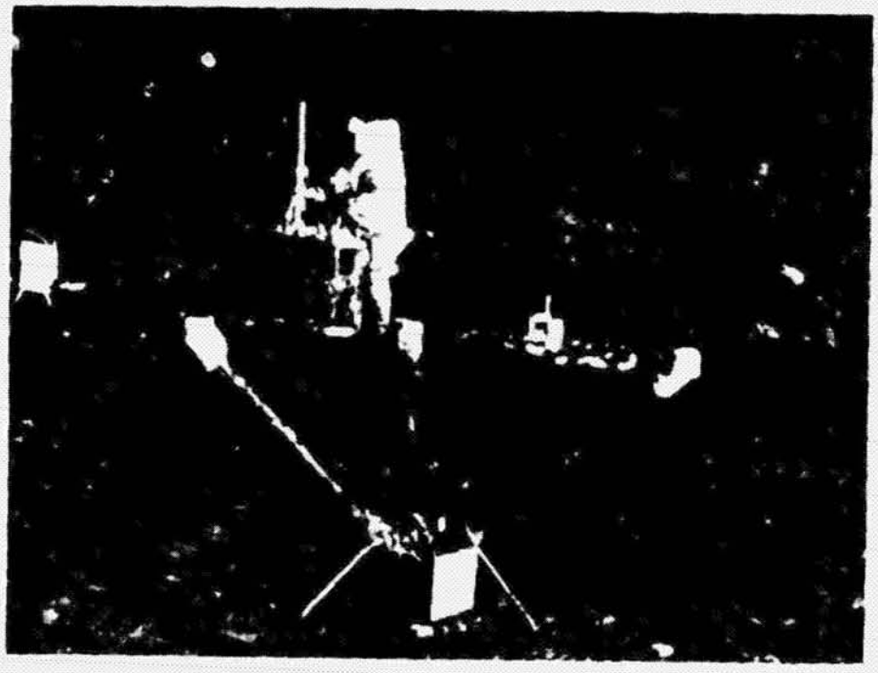

Figure 1. Geophysical experiments deployed on the Moon at the Apollo 12 site in Oceanus Procellarum. The lunar surface magnetometer is shown in the foreground. The passive seismometer is to the astronaut's left. These and other instruments not shown, are powered by the radioisotope thermoelectric generator, the black object at the far left rear.

II. LUNAR INTERIOR PROPERTIES FROM SEISMOMETER RESULTS

Results of passive seismic experiments show that the Moon is seismically much quieter than the Earth. Seismic data indicate that the interior of the Moon can be divided into two major regions: a rigid, seismically inactive outer shell about 1000 km thick (the lunar lithosphere), and a relatively less rigid core zone (the lunar asthenosphere) in which partial melting is likely (fig. 2, and Toksöz, 1973). The transition between the two regions is gradual. Small moonquakes, extremely low in magnitude relative to the Earth, originate near the base of the lithosphere about 800 km deep in the Moon (whereas nearly all seismic activity in the Earth occurs in the upper 25 km or so). Tidal energy due to the Earth's gravitational attraction is the dominant source of energy released to moonquakes (fig. 3, and Latham *et al.*, 1973); therefore, moonquakes receive a large portion of their energy from an external source. It is unlikely that Earthlike tectonic activity is occurring at present.

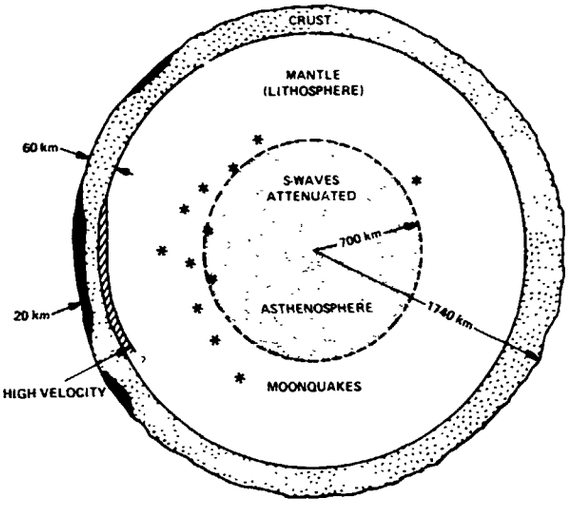

Figure 2.– Schematic representation (not to scale) of lunar structure, as deduced from lunar seismometer data. Earthside of the Moon is to the left. Maria basalt filling is shown in black, and the possible high-velocity zone at 60 km depth is indicated by stippling. From Toksöz (1974).

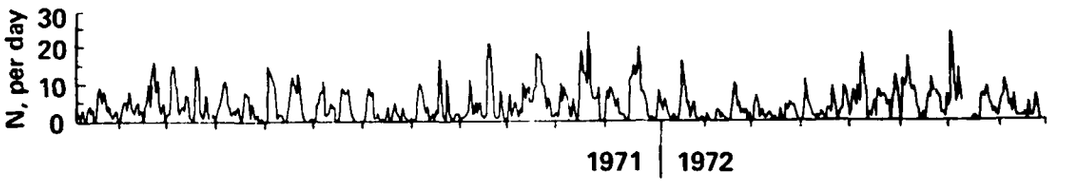

Figure 3.– Moonquake activity, recorded by the Apollo 14 passive seismic experiment (from Latham et al., *1973), for the time period February 7, 1971 to July 27, 1972. Times of peak activity occur when the Moon is nearest to the Earth in its orbit (perigee) and farthest from the Earth (apogee).*

Seismic data have yielded information about the composition of the outer 150 km of the Moon (fig. 4). The structure of the shallow crust has been obtained by the active seismic experiment, which has measured sound velocity profiles generated from vibrations which were originated by an astronaut-held "thumper" and by mortar-launched grenades. It is found that the outer 1 km has very low seismic velocities, appropriate for loosely packed rubble rather than consolidated rock (Kovach *et al.*, 1973). For depths down to 25 km the velocity increases (Toksöz, 1973), appropriate for consolidated rubble or an extensively fractured igneous rock such as basalt. The increase of velocity with depth perhaps is a function of greater consolidation and fewer cracks with depth. A transition occurs at about 25 km depth, where the velocity rapidly increases to a value similar to that of lunar anorthositic gabbros. Thereafter the velocity is relatively constant down to a depth of 60 km. At that depth another transition occurs indicating that material similar to terrestrial pyroxenites exists from 60 km depth to at least 150 km depth in the Moon. There are also indications that a high-velocity (9 km/sec) layer may exist at 65 km depth, but results are not conclusive. Such a layer would be quite unusual by Earth standards, since very few terrestrial minerals have such high velocities.

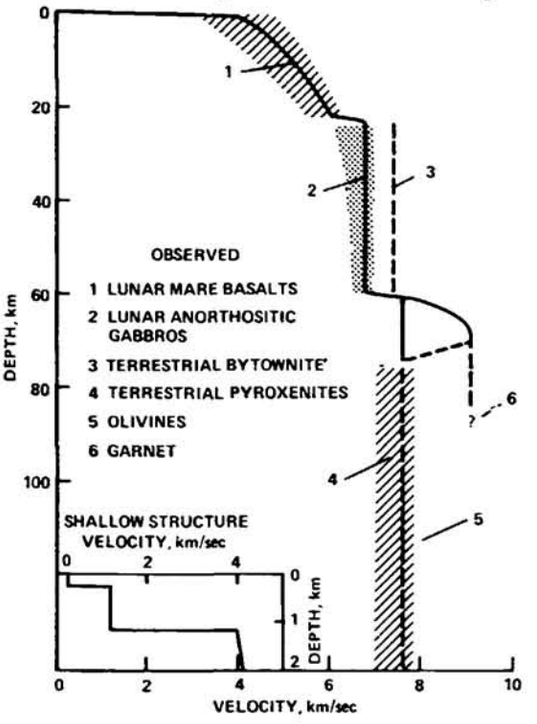

Figure 4.– Seismically calculated velocity profiles for the near-surface region of the Moon, showing comparisons with velocities measured in the laboratory for samples of selected material composition (from Toksöz, 1974). Shallow structure at the Apollo 17 Taurus Littrow site are shown in the inset (from data of Kovach et al., *1973).*

Seismic results have also been used to propose a thermal evolutionary model for the lunar interior (Töksoz, 1973), assuming an accretional origin of the Moon whereby during its early history the outer portions of the Moon were hotter than its interior. During the first two billion years of the 4.6 billion year lunar history, the lunar upper mantle underwent sufficient melting to account for the differentiation of the crust and the subsequent lunar volcanism and mare filling. Later the mantle crust cooled while the deep interior temperature increased. Seismic results indicate that the deep interior may be hot enough at the present time to be partially molten.

III. LUNAR INTERIOR PROPERTIES FROM MAGNETOMETER RESULTS

Magnetic fields have been measured at a total of nine locations on the lunar surface. The magnetic field measurement at any site is a sum of the external (solar or terrestrial) field, the permanent lunar field, and the fields induced in the Moon by changes in the external field. These different types of magnetic fields can each have relatively large magnitudes at different times, in contrast to the case of a magnetic measurement on the Earth, which is generally dominated (in magnitude) by the Earth's permanent field. The permanent lunar field measurements (figs. 5 and 6)

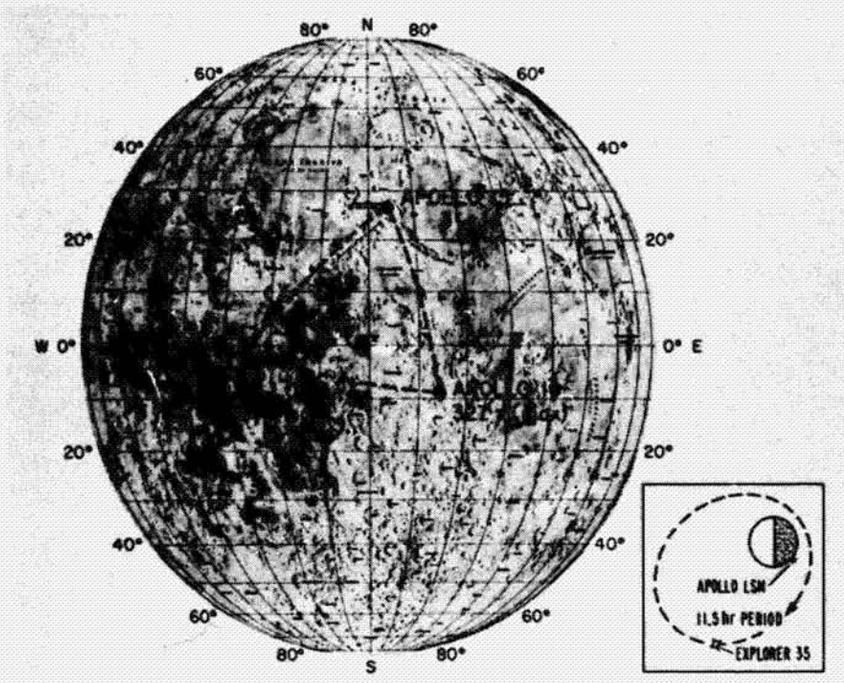

Figure 5.– Remanent magnetic field measured at four Apollo sites on the lunar surface, ranging from 5 γ to 327 γ in magnitude (1 γ = 10^{-5} gauss). Inset schematically shows lunar surface and orbiting magnetometers; simultaneous data from these magnetometers are analyzed to determine magnetic and thermal properties of the lunar interior.

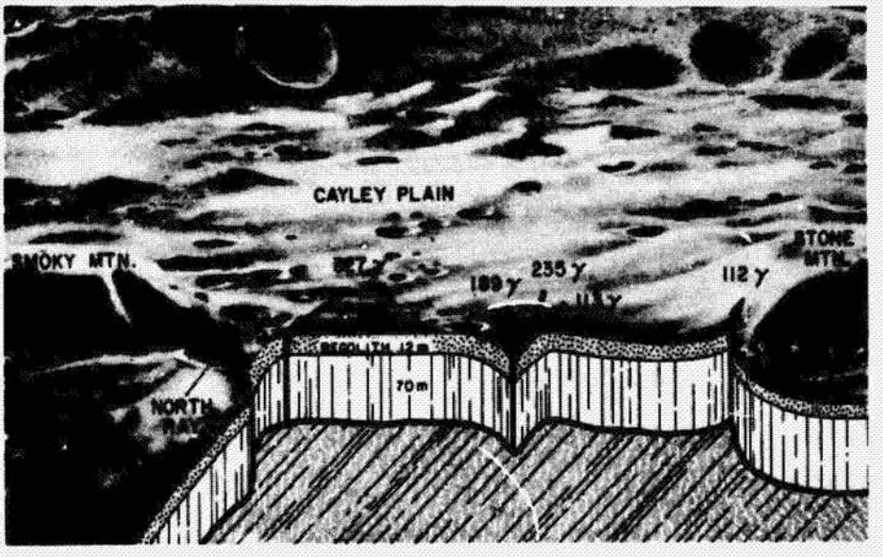

Figure 6.– Remanent magnetic field measurements at five locations of the Apollo 16 Descartes site. Arrows schematically show the magnetic field directions measured at the surface locations (from Dyal et al.*, 1973).*

range (Dyal *et al.*,1973) from 3 γ to 327 γ in magnitude (1 $\gamma = 10^{-5}$ gauss), much smaller than the field of the Earth, which ranges from 30,000 to 60,000 γ. Satellite maps of magnetic fields and surface magnetometer measurements show strong evidence that the lunar crust is magnetized over much of the lunar globe (Sharp *et al.*, 1973). Magnetic fields are stronger in lunar highland regions than in mare regions, and stronger on the lunar far side than on the near side. The origin of the lunar remanent field remains an enigma. Possibilities are generally grouped under three classifications: a strong external (solar or terrestrial) field in the lunar past, an ancient intrinsic field of global scale such as the Earth's dynamo field, and localized field sources.

Magnetic field measurements have yielded calculations of the iron abundance in the Moon (fig. 7, and Parkin *et al.*, 1974). The free iron abundance of the whole Moon is determined to be 2.5 percent by weight. Total iron abundance is dependent upon the composition of the lunar interior. Calculations have been carried out for lunar compositions of olivine and orthopyroxene; the average calculated total iron abundance is 9 percent by weight.

Magnetic measurements (Dyal *et al.*, 1974) have also allowed an indirect calculation of the temperature profile of the lunar interior. The calculated temperature rises rapidly with depth to 1200° K at 250 km depth, then more slowly to about 1800° K at 850 km depth (fig. 8).

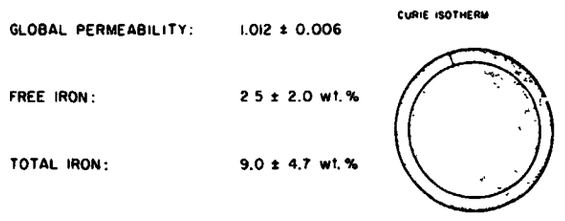

Figure 7.– Lunar iron abundance and magnetic permeability, calculated from lunar magnetometer measurements (from Parkin et al., *1974).*

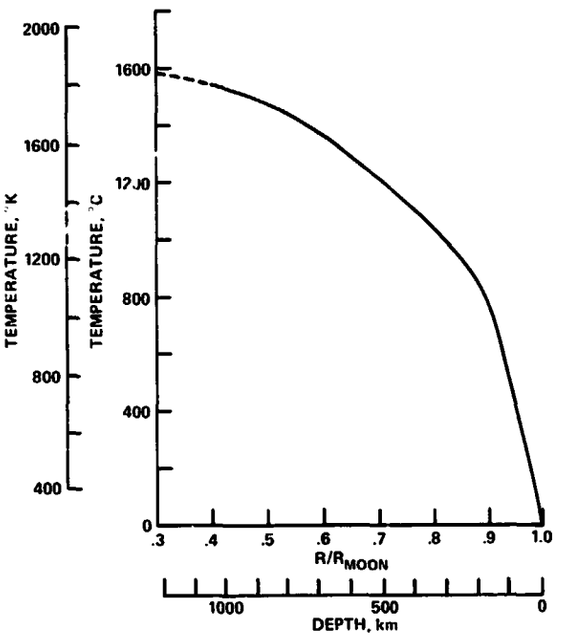

Figure 8.– Lunar temperature profile calculated from lunar magnetometer measurements (Dyal et al., *1974).*

IV. HEAT FLOW EXPERIMENT RESULTS

Two heat flow measurements have been made on the lunar surface during the Apollo missions (Langseth *et al.*,1973). The measurements have yielded a lunar heat flow of about 3×10^{-6} W/cm^2, which is approximately one-half the heat flow average for the Earth. This value is somewhat larger than the predicted value (~1/5 that of the Earth). Assuming the lunar heat value is representative of the whole Moon, then the measured heat flow requires that the lunar interior heat production per unit mass be more than twice that of Earth. This in turn implies that the abundance of lunar uranium (which, through radioactive decay, is probably the major heat source in the Moon's

interior) exists in quantities two to three times richer than in the Earth's interior. The radioactive isotopes of uranium, ^{235}U and ^{238}U, and potassium (^{40}K) and thorium (^{232}Th) probably are concentrated in the Moon's outer 100 to 200 km.

The heat flow experiment temperature sensors measure the mean surface temperature at the Apollo 17 site to be 216° K. A large temperature gradient with depth is found at the site, which is attributed to a strongly temperature-dependent thermal conductivity of the surface material, at least in the upper few centimeters.

V. LASER ALTIMETER RESULTS

The laser altimeter, flown three times in lunar orbit aboard the command and service module, measured precise altitudes above the Moon's surface by means of transit times of a ruby laser beam down to the lunar surface and back. The latest results (Kaula *et al.*, 1974) show that the mean radius of the Moon is 1737.7 km and that the maria are very level and smooth, with slopes less than one-tenth of a degree over distances of hundreds of kilometers so that mare topographic features generally deviate less than 150 m from the mean. Elevation differences in the highlands, however, are often greater than 3 km, and the highland's mean altitude is about 4 km above that of the maria. The Moon is found to deviate from a sphere in that it is flattened on the side facing the Earth, and the center of mass is offset from the center of figure about 2.4 km toward the Earthside, 24° east longitude. The best value for lunar moment of inertia is $I/MR^2 = 0.3953 \pm 0.0045$.

VI. OTHER ORBITAL EXPERIMENTS: GAMMA–RAY SPECTROMETER, X–RAY FLUORESCENCE EXPERIMENT, ALPHA–PARTICLE SPECTROMETER EXPERIMENT

The gamma-ray spectrometer (Arnold *et al.*, 1972), sensitive to gamma rays produced by radioactivity in the lunar soil, has revealed that the western maria on the Moon's near side are more radioactive than other lunar regions. The eastern maria are less radioactive, and the lunar highlands are regions of lowest radioactivity.

The X-ray fluorescence experiment (Adler *et al.*, 1973) has measured characteristic secondary X-ray emissions produced when solar X-rays impinged on the lunar surface. Generally, the highlands have been found to be high in aluminum and low in magnesium, whereas for the maria, the reverse is found to be true. The X-ray experiment has yielded evidence supporting the idea that the lunar highlands are portions of an ancient crust with composition between anorthositic gabbro and gabbroic anorthosite.

The alpha particle spectrometer (Bjorkholm *et al.*, 1973; Gorenstein *et al.*, 1973) is sensitive to radioactive radon gas emerging from the Moon's surface. Local areas have been found on the lunar surface which have high radon (^{222}Rn) emanation rates, the most conspicuous being the Aristarchus crater region. Radon emission has also been seen in varying amounts around the edges of the maria, implying that radon emission is a time-dependent phenomenon. If there were presently regions of strong volcanic activity on the Moon, the alpha-particle experiment would probably detect it; however, no present-day volcanic activity has been identified.

VII. THE LUNAR ATMOSPHERE

The mass spectrometer (Hoffman *et al.*, 1973) has measured helium, neon, argon, and possibly molecular hydrogen as constituents of the lunar atmosphere. It is expected that the helium and neon originate in the solar wind. Argon isotopes vary in abundance over the lunar day, implying that they condense into the lunar surface at night and release into the atmosphere at dawn. The total gas concentration of all molecules at lunar night (when the instrument is shielded from incoming particles from the sun) in the atmosphere is 2×10^5 molecules/cm^3.

VIII. DISCUSSION

Considerable analysis has been carried out to date in lunar geophysics, and much information has been gained concerning properties of the Moon. Although it is often said in lunar research that more questions than answers have emerged in the five years since the first Apollo landing, the future looks bright for continued lunar research. NASA has launched the post-Apollo lunar synthesis program, inviting new scientists to synthesize the great quantities of lunar scientific data which have been gathered by separate experiments. The next few years may well bring a much fuller understanding of the origin and evolution of our Moon and the solar system.

REFERENCES*

Adler, I.; Trombka, J. I.; Schmadebeck, R.; Lowman, P.; Blodget, H.; Yin, L.; Eller, E.; Podwysocki, M.; Weidner, J. R.; Bickel, A. L.; Lum, R. K. L.; Gerard, J.; Gorenstein, P.; Bjorkholm, P.; and Harris, B.: pp. 2783-2791, 1973.

Arnold, J. R.; Metzger, A. E.; Peterson L. E.; Reedy, R. C.; and Trombka, J. I.: In Apollo 16 Preliminary Science Report, NASA SP-315, pp. 18-1 to 18-8, 1972.

Bjorkholm, P. J.; Golub L.; and Gorenstein, P.: pp. 2793-2802, 1973.

Dyal, P.; Parkin, C. W.; and Daily, W. D.: pp. 2925-2945, 1973.

Dyal, P.; Parkin, C. W.; and Daily, W. D.: Submitted to Proc. Fifth Lunar Sci. Conf., Geochim. Cosmochim. Acta, Suppl. 5, vol. 3, 1974.

Gorenstein, P., Golub, L.; and Bjorkholm, P. J.: pp. 2803-2809, 1973.

Hoffman, J. H.; Hodges, R. R., Jr.; and Johnson, F. S.: pp. 2865-2875, 1973.

Kaula, W. M.; Schubert, G.; Lingenfelter, R. E.; Sjogren, W. L.; and Wollenhaupt, W. R.: Lunar Science V, part 1, The Lunar Science Institute, Houston, pp. 399-401, 1974.

Kovach, R. L.; Watkins, J. S.; Nur, A.; and Talwani, P.: In Lunar Science IV, ed. J. W. Chamberlain and C. Watkins, The Lunar Science Institute, Houston, pp. 444-445, 1973.

Langseth, M. G., Jr.; Keihm, S. J.; and Chute, J. L., Jr.: In Apollo 17 Preliminary Science Report, NASA SP-330, pp. 9-1 to 9-24, 1973.

Latham, G.; Dorman, J.; Duennebier, F.; Ewing, M.; Lammlein, D.; and Nakamura, Y.: pp. 2515-2527, 1973

Parkin, C. W.; Daily, W. D.; and Dyal, P.: Submitted to Proc. Fifth Lunar Sci. Conf., Geochim. Cosmochim. Acta, Suppl. 5, vol. 3, 1974.

Sharp, L. R.; Coleman, P. J., Jr.; Lichtenstein, B. R.; Russell, C. T.; and Schubert, G.: The Moon, v. 7, p. 322, 1973.

Toksöz, M. N.: Preprint. Submitted to Ann. Rev. Earth Planet. Sci., 1973.

*Unless otherwise noted, the reference is in Proc. Fourth Lunar Sci. Conf., Geochim. Cosmochim. Acta, Suppl 4, vol. 3, Pergamon Press, 1973.

With permission, reprinted from Physics Today, March 1974

The interior of the Moon

As a result of the Apollo program we know that the lunar crust is much older than we had suspected, but the interior temperature remains a puzzle, as does the problem of the Moon's origin

Don L. Anderson

Full Moon from Apollo 17, showing (on right) part of the farside. Figure 1

The Moon is one of the more obvious of our neighbors in space and is certainly the most accessible. In spite of intensive analysis and probing by virtually every conceivable chemical and physical technique, the maneuvering room for speculation on lunar origin has scarcely diminished as a result of the Apollo program. This is not primarily due to lack of information but to the unexpected and confusing nature of the newly acquired data, most of which is open to multiple interpretations.

The Moon's unique characteristics have become even more unique as a result of lunar exploration. This strange body, shown particularly well in the Apollo 17 photograph (figure 1), is like no other in the solar system that we know about, either presently orbiting the Sun or having fallen on the Earth. It is similar to no planet or meteorite. Curiously, it is most like some tiny white inclusions in a meteorite that fell spectacularly to Earth in Mexico during the midst of the lunar exploration program.

The most immediate scientific and public-interest aspects of the lunar exploration programs have been the photographs and the returned lunar samples. The orbital and surface photographs form the basis of detailed morphological, historical and structural geological studies of the lunar surface. The samples have been subjected to a battery of chemical, petrological and physical measurements that has resulted in volumes of primary data and thousands of pages of interpretation. Less publicized, and less tangible to the layman, is the wealth of data that has been returned and is still being returned by the scientific instruments that accompanied the astronauts around and to the Moon (see figure 2).

These scientific observatories, more sophisticated by far than any that are operating on Earth, have measured the shape of the Moon, its gravity field, the electromagnetic fields in its vicinity, heat flow through the surface, the seismic activity and velocities in the interior and the composition of the surface and the tenuous lunar atmosphere.

From these measurements we can draw conclusions about the composition, temperature and history of the Moon; some of these conclusions confirm what we had already guessed from Earth-based observations, but others are unexpected. For example, we already knew that the Moon was deficient in iron (in comparison with the proportions of iron in the Earth and in the other terrestrial planets), but from examination of surface samples we now know that it is deficient also in all elements and compounds more volatile than iron. We had guessed that the Moon must have a low-density crust, but the great age and thickness of this crust were quite unexpected. The temperature of the interior is still a puzzle, with new evidence confirming neither the hot-core nor the cold-core theories—though I believe the hot-interior model is the more likely. Likewise we can still not be certain precisely how the Moon was formed, but we can make a scenario that not only fits the evidence we have for the Moon but also has useful things to say about the formation of the inner planets.

Don L. Anderson is professor of geophysics and director of the seismological laboratory, California Institute of Technology, Pasadena, California.

Bulk chemistry

It has long been known that the density of the Moon is considerably less than that of the other terrestrial planets, even when allowance is made for pressure. The terrestrial planets contain about 30% iron, which is consistent with the composition of stony meteorites and the nonvolatile components of the Sun. They therefore fit into any scheme that has them evolve from solar material. Because iron is the major dense element occurring in the Sun, and presumably in the preplanetary solar nebula, the Moon is clearly depleted in iron. Many theories of lunar origin have been based on this fact, and numerous attempts have been made to explain how iron can be separated from other elements and compounds. Density, magnetic properties and ductility have all been invoked to rationalize why iron should behave differently than silicates in early solar-system processes.

Once samples were returned from the Moon, however, it became clear that the Moon was not only deficient in iron but in a number of other elements as well. The common characteristics of these elements and their compounds is volatility. The returned samples showed that the Moon is depleted in compounds more volatile than iron and that, to a first approximation, the Moon could be considered a refractory body. Calcium, aluminum and titanium are the major elements involved in high-temperature condensation processes in the solar nebula; minor refractory elements include barium, strontium, uranium, thorium and the rare-earth elements. The Moon is enriched in all these elements and we are now sure that more than simply iron-silicate separation must be involved in lunar origin.

The abundance of titanium in the returned lunar samples was one of the first surprises of the Apollo program. Titanium is not exactly rare on Earth, but it is usually considered a "minor" or "trace" element. The first samples returned from the Moon contained 10% of titanium-rich compounds. The surface samples were also remarkably depleted in such volatile elements as sodium, potassium, rubidium and other elements that, from terrestrial and laboratory experience, we would expect to find concentrated in the crust. Water, sulfur and other volatile elements and compounds were also sparse. The refractory trace elements—such as barium, uranium and the rare-earth elements—were concentrated in lunar surface material to an extent several orders of magnitude over that expected on the basis of cosmic or terrestrial abundances.

Some of these elements, such as uranium, thorium, strontium and barium, are "large-ion" elements, and one would expect them to be concentrated in melts that would be intruded or extruded near the surface. However, other volatile large-ion elements, such as sodium and rubidium, are clearly deficient, in most cases by at least several orders of magnitude from that expected from cosmic abundances. The enrichment of refractory elements in the surface rocks is so pronounced that several geochemists proposed that refractory compounds were brought to the Moon's surface in great quantity in the later stages of accretion. The reason behind these suggestions was the belief that the Moon, overall, must resemble terrestrial, meteoritic or solar material and that it was unlikely that the whole Moon could be enriched in refractories. In these theories the volatile-rich materials must be concentrated toward the interior. In a cooling-nebula model of planetary formation, the refractories condense before the volatiles and it was therefore proposed that Moon was made inside out!

However, it now appears that the depletion of iron and volatiles can be taken at face value and that the whole Moon is deficient in elements and compounds more volatile than iron. Petrological considerations show that not only the surface rocks but also their igneous source regions, deep in the Moon, are also depleted in volatiles. The Moon is probably enriched in calcium, aluminum, titanium and the refractory trace elements throughout. This composition would explain the mean density of the Moon and the high heat flow, and it would help to explain why the Moon melted and differentiated very rapidly.

The interior

In view of the abundant geological evidence that the surface rocks resulted from melting processes in the interior, it was no surprise that the geophysical evidence indicated that the Moon has a low-density crust. Its great age, as measured by geochemical techniques, and great thickness, as re-

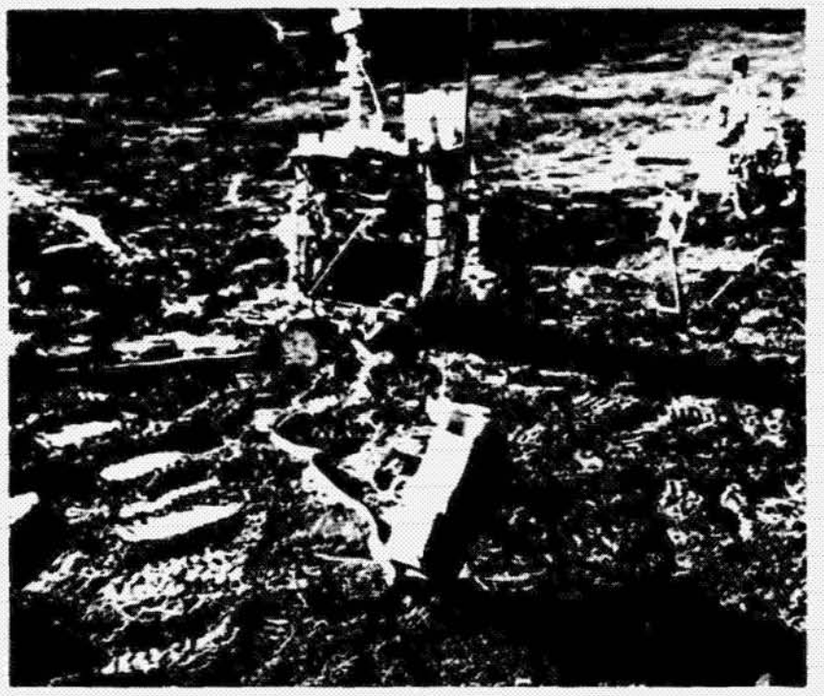

Scientific instruments taken to the Moon and left there by Apollo-14 astronauts are telemetering data back to Earth. (This photo and figure 1 from NASA.) Figure 2

quired by the physical evidence, were, however, unexpected. These are important boundary conditions on the origin and composition of the Moon.

The Moon's principal moments of inertia indicate that crustal thickness varies from about 40 km at the poles to more than 150 km on the lunar backside.[1] Large variations in crustal thickness are also required to satisfy gravity data and the noncoincidence of the centers of mass and figure of the Moon. The present orientation of the Moon and the restriction of basalt-filled maria to the Earth-facing hemisphere are undoubtedly the result of this asymmetry in crustal thickness.

The laser altimeter flown on some of the later Apollo missions provided details of topography as well as clarifying major problems such as frontside-backside asymmetry, offset of center-of-mass, elevation differences between maria and highlands and relative roughness of highlands compared to maria basins.[2] The maria are remarkably smooth and level; slopes of less than one tenth of a degree persist for hundreds of kilometers and topographic excursions from the mean are generally less than 150 meters. By contrast elevation differences in the highlands are commonly greater than 3 km. The mean altitude of the terrace, or highlands, above maria is also about .

The center of mass is displaced toward the Earth and slightly toward the east by about 2 km. This gross asymmetry of the Moon has long been known from consideration of the principal moments of inertia. The differences between the principal moments of inertia are more than an order of magnitude greater than can be accounted for by a simple homogeneous body, rotating and stretched by Earth tides. The simplest interpretation is in terms of a crust of highly variable thickness, an interpretation supported by nearside gravity results.

Asymmetry is not a unique characteristic of the Moon; the asymmetric distribution of continents and oceans on the Earth is well known, and Mars, likewise, is very asymmetric both in its topography and gravity field. Large-scale convection associated with early gravitational differentiation could lead to the observed asymmetries and may be one common characteristic of all the terrestrial planets.

In the case of the Earth and the Moon, and probably for Mars as well, the physical asymmetry correlates well with, and is probably the result of, chemical asymmetry. The lunar highlands are dominately plagioclase feldspar-rich rocks with densities considerably less than the frontside mare basalts and the mean density of the Moon. These feldspars crystallize at higher temperatures than basalt does and can therefore be expected to float to the surface of their parent liquid. The residual liquids would likely be the source region of the mare basalts, which erupt to the surface later.

This scenario not only explains the physical measurements but also some subtle details of the chemistry. Large-ion refractory elements are preferentially retained by the liquid, and therefore such elements as barium, strontium, uranium and thorium would be concentrated in the last liquid to crystallize. These elements are concentrated in the lunar-mare basalts by several orders of magnitude over the highland plagioclase-rich material, with the notable exception of europium, which is retained by plagioclase. Compared to the other rare-earth elements europium is depleted in basalts and enriched in anorthosites. The "europium anomoly" was one of the early mysteries of the lunar sample-return program and implied that plagioclase was abundant somewhere on the Moon. The predicted material was later found in the highlands.

Seismic evidence

Seismology is one of the most powerful tools for studying the interior of a planet, providing as it does information relevant to structure, composition and tectonics. In the case of the Earth, the major regions such as the crust, mantle and core and the sites of most earthquakes were discovered in the early days of seismology. At that time only a few seismic stations were in operation, and seismic waves were used not only to determine velocities but to determine the locations of the earthquakes as well. When earthquakes became better located, with networks of seismic stations, the structure of the Earth could be refined. As the velocity distribution in the Earth became better known the earthquake could be located with more certainty. Even today, with hundreds of seismic stations and thousands of well located earthquakes and large explosions, the refinement of Earth structure continues.

Currently four seismic stations are operating on the Moon, although two of them are so close together that the information they provide is partially redundant. For the problem of locating moonquakes this is a minimum network. In a homogeneous sphere four parameters are required to specify the location and time of occurrence of an unknown event. If the propagation velocity in the sphere is unknown more parameters are required. In general each seismic station, if appropriately placed, provides one parameter—usually the arrival time of the fastest phase, the direct compressional wave arrival. If the sphere is not homogeneous, additional parameters and seismic stations are required. For these reasons the locations, particularly the depths, of moonquakes must be considered tentative.

But it is clear that the seismic activity of the Moon is much less than the Earth, both in numbers of quakes and

their size, or magnitude. Their times of occurrence appear to correlate with tidal stresses caused by the varying distance between the Moon and the Earth. Compared with the Earth they seem to occur at great depth, about half the lunar radius (but we must keep in mind the reservations on location accuracy mentioned above). Both the age-dating evidence and the seismic data indicate that the Moon today is a relatively inactive body. This conclusion is consistent with the absence of obvious tectonic activity and with the low level of stresses in the lunar interior implied by gravity and moment-of-inertia data.

On the Earth, most, if not all, seismic and tectonic activity is associated with the movements of large plates on or near the Earth's surface. The driving mechanism of plates is only vaguely understood, but the extreme mobility of plates is probably related to their thinness relative to the radius of the Earth; the mass and thermal inertia of the lithosphere are negligible compared to the Earth as a whole. The ability of plates to break and slide past, or drive beneath, one another are consequences of their thinness. A variety of observations can be explained if the lunar lithosphere is much thicker than its terrestrial equivalent. Because the depth of the lithosphere is believed to be controlled by the intersection of the temperature-depth curve with the "solidus" (the temperature at which partial melting occurs), a thick lithosphere means either higher melting temperatures, or a shallow temperature gradient, or both. Both, in fact, are probable for the Moon. The Moon, being a smaller body than the Earth, will cool faster; the rarity of volatiles, including water, means that melting temperatures will be greater, and the refractory nature of the bulk of the lunar crust would drive melting temperatures even higher. The lunar heat-flow values are less than terrestrial ones, and this reduction is also consistent with a shallower temperature gradient.

The travel times of seismic waves generated by artificial impacts have been used to determine the structure of the outer 150 km of the Moon.[3] To produce useful impacts, Saturn IV-B booster and lunar-module ascent stages were programmed to strike the surface of the Moon at distances as far as 1750 km from the lunar seismic stations. The resulting velocity structure applies roughly to the central portion of the lunar frontside. We should keep in mind our previous discussion of inhomogeneity, particularly the rather strong evidence that crustal thickness varies substantially. Lateral changes in structure and velocity also complicate seismic interpretations.

The shallow crustal structure has been determined by the active seismic experiment,[4] which used thumper and mortar-launched grenade sources, and by surface gravity traverses. The outer kilometer has extremely low velocities, less than 1 km/sec. This value is more appropriate for rubble than consolidated rock. The velocities increase from 4 km/sec at 1 km depth to 6 km/sec at 20 km (see figure 3). The lower velocity is appropriate for consolidated rubble or extensively fractured igneous rock, such as basalt. The increase of velocity with depth is probably primarily the result of consolidation and crack closure. The 6-km/sec velocity at the base of this layer is consistent with laboratory measurements on returned samples of lunar basalt.

At 20 km depth the velocity increases abruptly to about 6.7 km/sec, and it remains relatively constant to 60 km depth. The constancy of velocity means that most cracks have been eliminated and also that the effects of temperatures and pressure gradients are either small or they cancel. In this region the velocities can be matched by anorthositic gabbro, a plagioclase-rich rock type that is low in iron and has relatively low density (about 2.9 gm/cm^3). This layer may be similar in composition to the lunar highlands.

At 60 km the velocity jumps, at least locally, to about 9 km/sec. When all the seismic data are considered together we may find that this layer is very thin (less than 40 km) or it occurs only locally, or both. Perhaps it occurs only as pods or lenses under maria basins or only under mascon basins; at the moment we have no way of telling. In any event, such high velocities were unexpected and are unusual by any standards. They may also be fictitious, because seismic waves refracted by dipping interfaces can give apparent velocities slower or faster than real velocities. A velocity of 9 km/sec is much greater than the 8 km/sec velocity typical of the Earth's upper mantle and of rocks thought to be common in the upper lunar mantle. Only a few minerals, exotic by terrestrial standards, have such high velocities. These include spinel ($MgAl_2O_4$), corundum (Al_2O_3), kyanite (Al_2SiO_5) and Ca-rich garnet ($Ca_3Al_2Si_3O_{12}$). These are all calcium- and/or aluminum-rich minerals and occur as the dense residual crystals when a Ca–Al-rich liquid partially solidifies. The 9-km/sec layer may therefore be related petrologically to the overlying crustal layer.

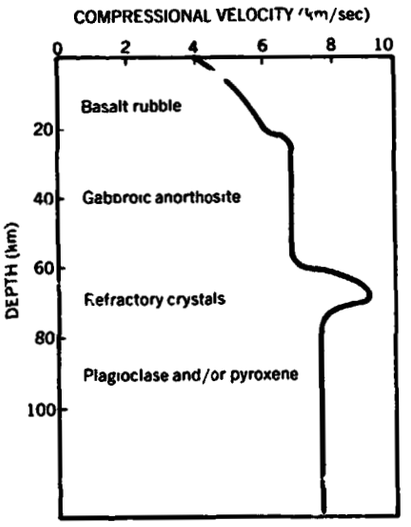

Compressional velocity plotted against depth in the Moon, with an indication of possible mineral assemblages present at different depths (From ref 3.) Figure 3

The apparent seismic velocity at greater depth is only 7.7 km/sec—intermediate between the velocities we usually associate with the crust and the mantle. This velocity continues to a depth of at least 150 km (the deepest depth of penetration of seismic energy from artificial impacts) and is appropriate for pyroxene or plagioclase-rich rocks. In the latter case we would still be monitoring the crust and therefore would have only a lower bound, 150 km, on its thickness. It should be recalled that the crust is thicker on the backside. Even if the crust is only 60 km thick, the conventional interpretation of the seismic results, it is much thicker than the average terrestrial crust, particularly in relative terms; this great thickness indicates that the Moon was extensively differentiated. In combination with the age data this means that the Moon was extensively melted early in its history. The source of this early heat is a matter of some controversy.

Evidence for the constitution of the deeper interior is very sketchy. Seismic shear waves apparently cannot pass efficiently below some 1000 km depth. This can be taken as tentative evidence for at least a hot, if not molten or partially molten, deep interior.

Is the Moon hot or cold?

One of the long-standing controversies regarding the Moon is whether its interior is hot or cold. Most of the newer evidence is ambiguous and fails to resolve the controversy that originated with the earlier data. The widespread occurrence of basalt certainly indicates that it was at least partially molten early in its history, but we are not sure that this happened since then. Conduction alone is only efficient in lowering the internal temperatures of the outer 300 km; on the other hand the process of basalt extrusion is an efficient mechanism for removing heat. However, basalts are unlikely to have

originated deeper than 500 km, and they represent only a small fraction of the Moon. Therefore they are ineffective in cooling the deep interior. The anorthositic highlands are probably also the result of igneous and differentiation processes. But their emplacement mechanism would be plagioclase flotation, resulting in a thick insulating blanket for the remaining liquid. The age of maria material indicates that melts still existed at moderate depths for more than 10^9 years after creation of the plagioclase-rich highlands.

It is quite possible that the mare-forming igneous episodes were a result of thermal, tidal and impact stresses, all of which were intense in the earliest history of the Moon. Igneous activity may have ceased when stresses were no longer adequate to breach the thick lithosphere. If this is true, then the Moon below some 300 to 1000 km may still be partially molten. A lithosphere of this thickness could easily support the stresses implied by the nonhydrostatic shape of the Moon and the presence of mascons.

The nonequilibrium shape of the Moon, the offset of the center of mass from the center of figure and the presence of large surface concentrations of mass (mascons) have been used as arguments that the Moon is a cold, strong body. However, when viewed more carefully, all of this evidence suggests just the contrary. The stresses required to support the nonequilibrium shape are only some tens of bars, and a relatively thin, strong, outer layer would suffice to support these stresses. The Earth, by contrast, supports stress differences of hundreds of bars, and stresses at kilobar levels are required to break rocks in the laboratory. Thus, taken at face value, the lunar data suggest that the Moon is a hot weak body. This conclusion is consistent with the lunar heat-flow values, the low level of seismic stresses and the high radioactivity inferred for the interior. Figure 4 shows the cross section of the Moon according to this picture.

If a small body such as the Moon formed hot it is likely that the other planets also formed hot, and that they too are differentiated. This is an important boundary condition on the vaguely understood processes of planetary formation. The accretion of planetesimals into planets must have been extremely rapid, at least in the time scale of cooling of the nebula. Otherwise the gravitational energy of accretion would be conducted to the surface and radiated away. A rapid time scale of accretion is consistent with modern theories of planetary accretion in a collapsing gas-dust cloud. High initial temperatures are also consistent with the hypothesis of accretion during condensation, which has been proposed to explain the differences in composition of the terrestrial planets. Briefly, this hypothesis states that the planets formed rapidly while the nebula was still cooling and that the nebula was dissipated before cooling or condensation was complete (see figure 5). The outer planets would be rich in volatile materials because of their distance from the Sun. Mercury would be the most refractory-rich terrestrial planet, insofar as distance from the Sun is the main variable. Its high density suggests that the nebula was dissipated shortly after iron condensed in its vicinity.

How can we explain the early high-temperature history of the Moon and at the same time its rapid death as an active body? Prior to lunar exploration the preferred theory for the formation of the planets involved the gradual accretion of cold particles with subsequent heating, melting and differentiation resulting from decay of radioactive elements. Because the first 10^9 years of terrestrial history are inaccessible to us there was no compelling reason to suppose that the Earth was initially hot. Some indirect clues, however, point to a high-temperature origin. The oldest terrestrial rocks are clearly the result of igneous processes, and they contain evidence that the Earth had a magnetic field when they crystallized. This suggests that the Earth had a molten core early in its history. Many ancient meteorites also have clearly gone through a high-temperature event (are the result of magmatic processes that predate the oldest traceable magmatic events on the Earth. These processes must have taken place in a body much smaller than the Earth.

Age dating of lunar material indicates that most of the differentiation of the Moon occurred in the first 10^9 years of its existence. For the Earth most of this early record is lost because of subsequent igneous and volcanic activity and rapid erosional processes. The Moon, unlike the Earth, has been remarkably quiescent for the last 3×10^9 years. This is true not only for internal processes but also for the external bombardment processes that are mainly responsible for the surface features of the Moon. Both the internal structure and exterior morphology were apparently the result of an extensive early history of activity.

Many sources have been proposed as early heating processes. These include short-lived radioactive elements, solar radiation high temperatures associated with the early nebula, and energy of gravitational accretion. For any of the latter three processes to be effective the bodies in the solar system must have assembled very quickly. Gravitational collapse of a gas-dust cloud is an

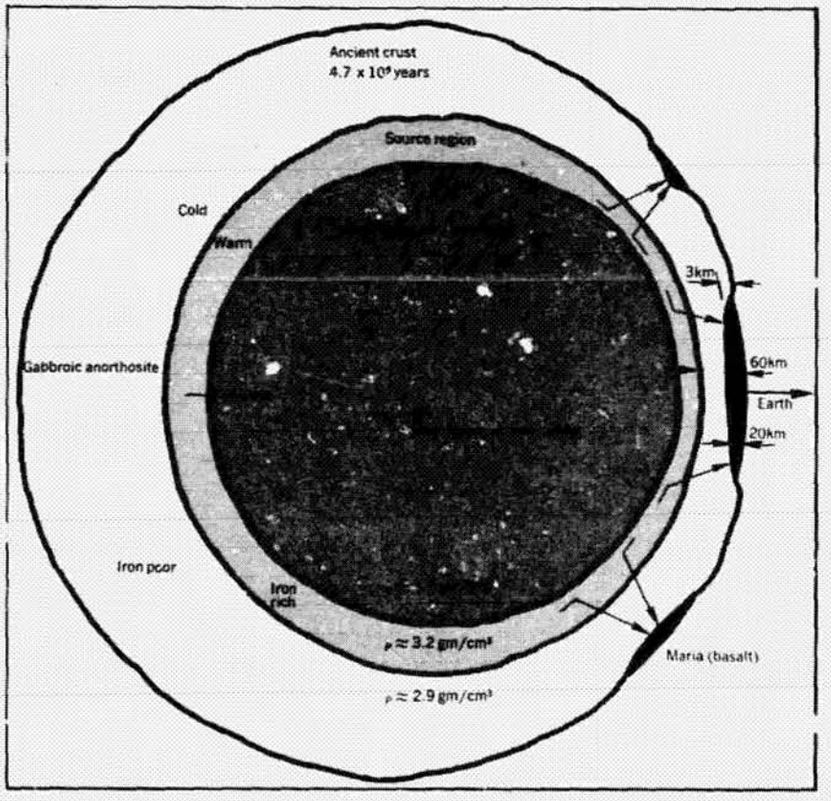

Schematic cross section of the Moon, showing the variations in crustal thickness required to satisfy gravity data and the offset position of the center of mass. Figure 4

attractive way both to localize protoplanetary material and to have initially high temperatures. The main problem is to be able to build planetary nuclei to a size big enough that they can effectively scavenge the remaining material in their vicinity.

The origin of the Moon

Some of the most obvious facts about the Moon may also be among the most relevant for our attempts to understand its origin. It is small, light and is close to a more massive body. These simple facts may all be related, for it is unlikely that preplanetary processes resulted in a single nucleus for each of the present planets. The nebula probably evolved from a disc to a series of rings; each ring in turn collapsed to a series of local gas-dust concentrations that collapsed further to form protoplanets, the building blocks of the planets.

Variations in the eccentricities and inclinations of the orbits of protoplanets at this stage of development ensure that they periodically approach each other; encounter velocities between bodies in a ring are low, and concentration rather than dispersal is the natural result. It is not difficult to believe, although certainly difficult to prove, that eventually one body will predominate; the remaining bodies will impact, orbit temporarily before impact, or orbit permanently. The scenario repeats for those bodies in orbit about the primary body. The largest nucleus, the Earth in this case, grows at the expense of the smaller particles and, if all this is happening in a cooling nebula, it will inherit most of the later, lower-temperature condensates.

In a cooling nebula of solar composition the first compounds to condense are calcium-, aluminum-, and titanium-rich oxides, silicates and titanates. These compounds comprise approximately 6% of the nonvolatile composition of the nebula, which is roughly everything but hydrogen, helium, carbon and that oxygen which is not tied up in the refractory compounds. Carbonaceous chondrites are usually taken as an approximation to the "nonvolatile" content of the nebula. Planetesimals formed at this point will be deficient in iron, magnesium, silicon, sulfur, sodium and potassium, all of which are still held in the gaseous phase. Solid particles will rapidly concentrate toward the median plane to accrete into refractory-rich planetary nuclei. While cooling of the nebula continues, iron and magnesium silicates condense; these are the most abundant constituents of meteorites and of the terrestrial planets. The largest body at any distance from the Sun will obtain the major share of these later condensates. In this scenario the Moon is one of the original smaller bodies that avoided impact with, or expulsion by, the Earth. It may also represent the coagulation of many smaller bodies that were trapped into Earth orbit from Earth-crossing solar orbits. In this hypothesis many of the satellites in the solar system may be more refractory than their primary bodies.

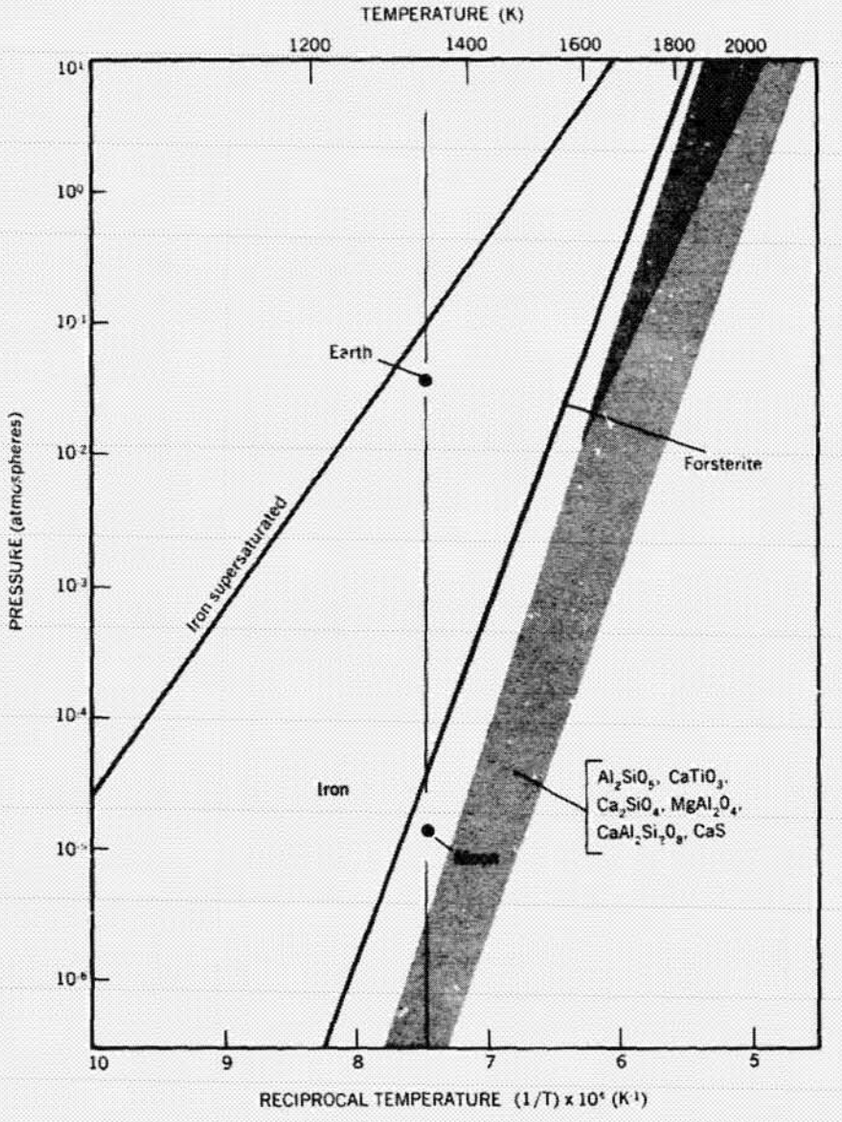

Condensation temperature versus pressure in a nebula of solar composition, to illustrate the hypothesis of planetary formation discussed in the text. (From ref. 5.) Figure 5

Type I and II carbonaceous chondrites contain about 10% of unique white inclusions, composed primarily of exotic Ca-Al-rich minerals such as gehlenite, spinel and anorthosite. These inclusions are rich in barium, strontium and uranium and the rare-earth elements, and they have most of the properties that have been inferred for the Moon. They are also very ancient. This material, together with the Moon, may represent the most primative material in the solar system and be the initial building blocks of the planets.

* * *

This article is contribution number 2447 of the Division of Geological and Planetary Sciences, California Institute of Technology, Pasadena, California. It was supported by NASA Grant No. NGL 05-002-069.

References

1. J. Wood, in *Abstracts of the Fourth Lunar Science Conference* (J. Chamberlain, C. Watkins, eds.), page 796 (1972).
2. W. Kaula, in *Abstracts of the Fourth Lunar Science Conference* (J. Chamberlain, C. Watkins, eds.), page 432 (1972).
3. N. Toksoz, Ann. Rev. Earth and Planet. Sci., 1974 (in press).
4. R. Kovach, in *Abstracts of the Fourth Lunar Science Conference* (J. Chamberlain, C. Watkins, eds.), page 444 (1972).
5. D. L. Anderson, Earth Planet. Sci. Lett. 18, 301 (1973). □

CHAPTER X – APOLLO MISSIONS

GEOLOGY OF THE APOLLO LANDING SITES: A SUMMARY

W. L. Quaide
Ames Research Center, NASA, Moffett Field, Calif. 94035

I. INTRODUCTION

This discussion is about the geology of the Apollo sites. In it, findings at each site are related to a generalized picture of lunar geologic history. Such a brief attempt as this can be only partly successful. It is hoped, however, that by highlighting the most significant findings, the present state of knowledge (and lack of knowledge) can be appreciated more fully. For those who wish to follow-up on this subject, only one source of information need be consulted at the outset: publications of the proceedings of the five lunar science conferences. These publications consist of three volumes, each for every conference, and represent the most thoroughly documented studies of rock suites ever assembled.

For the understanding of discussions presented here, standard geological backgrounds are adequate. Most terminology used in lunar studies has been adapted from standard geoscience usage. Only a few specialized terms have grown from this work. Definitions of certain of those terms are given in the appendix.

II. THE APOLLO SITES

The six Apollo sites are illustrated in figure 1. The first three visited, 11, 12 and 14, are equatorially located in Mare Tranquillitatis, Oceanus Procellarum, and in the Fra Mauro region, respectively. Their equatorial position was dictated by early mission safety constraints. Their precise locations within this belt were selected partly on the basis of surface characteristics necessary for landing and partly on the basis of geological considerations. Both Mare Tranquillitatis and Oceanus Procellarum are typical mare terrains. They differ mainly in age and composition of the lavas, physical characteristics of the surface and regolith that are age dependent, and in the character and relative abundances of exotic components. Tranquillitatis basalts are richer in titanium and much older than Procellarum counterparts (2.5 to 6.5 $\times$ 10^8 years older). Furthermore, two different flow units were sampled in Tranquillitatis with different ages (3.65 and 3.8 B.Y.) and different chemistry (low K and high K types). Physical characteristics of the two surfaces differ, when large areas are considered, in that Mare Tranquillitatis is more densely populated with impact craters, has a thicker regolith, and contains more products of impact (agglutinates) than does Procellarum – facts that are consistent with the crystallization ages of the rocks. Exotic components are present in both, but for still incompletely known reasons, the Apollo 12 site contains an excess abundance of these. Exotic fragments in the Apollo 11 regolith indicated that an extensive source of anorthosite, troctolite, and norite existed on the Moon, and it was speculated that these rocks were characteristic of the lunar highlands. Exotic components at the Apollo 12 site were found to be dominated by KREEP type material, often in the form of breccias. The abundance of KREEP materials at this locality may be a function of provenance or it may relate to the fact that this site is crossed by a prominent ray from Copernicus. Some have speculated that these materials represent Copernicus

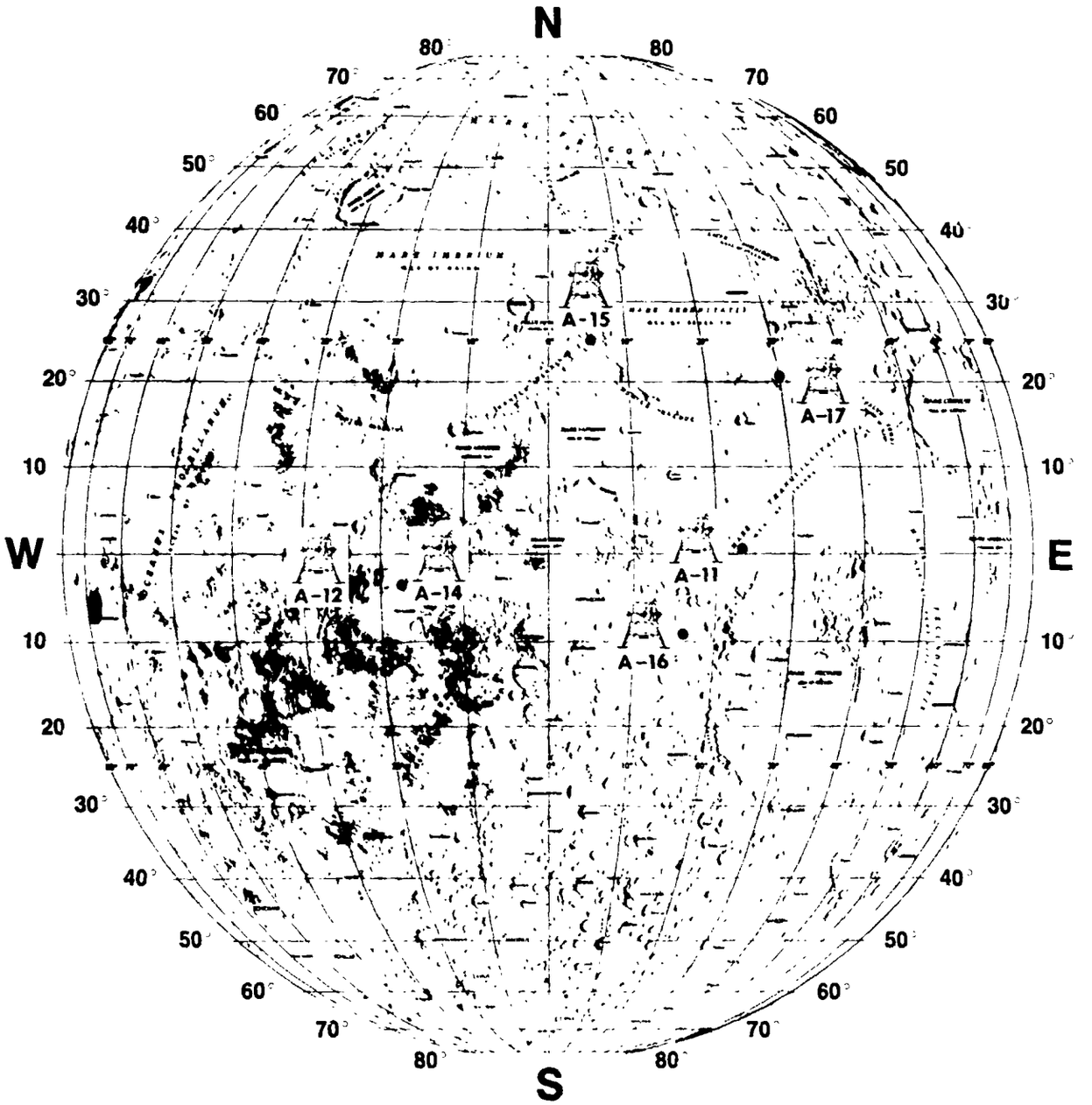

Figure 1.– Apollo landing sites.

ejecta, whereas others maintain that it may have been derived locally by large cratering events that excavated material from beneath thin mare lavas. Whatever the source – and it now appears to be in debris marginal to Procellarum or spread over its surface – this material has provided evidence of possible early differentiation of crustal material (4.4 B.Y.).

The Apollo 14 site, in contrast to Apollos 11 and 12 sites, is significantly different in that it is not located on mare units but on terrain of the Fra Mauro Formation, a unit thought to represent ejecta, or intermixed locally derived material and ejecta, from the Imbrium Basin. Samples collected are dominated by a class of annealed polymict breccias containing fragments of noritic breccias, micronorites, anorthosites, troctolites, olivine-rich microbreccias, and a few basalts. It is conceded that these samples were derived, at least in part, from a complexly cratered pre-Imbrium terrain containing an abundance of impact breccias (and some basalts) enriched in siderophile elements, unlike post-mare impact debris which perhaps are derived from impacting iron-rich planetesimals. Studies of these samples have provided extensive evidence that early crystalline rocks were rich in anorthosite, norite, and troctolite, that they had been extensively modified by impact processes prior to the Imbrium event, and that the Imbrium impact occurred between 3.9 and 3.95 B.Y. ago, resetting the radioactive clocks of the ejected debris. Whether or not the thermal metamorphism of the Fra Mauro rocks occurred before or after the Imbrium event is debated. Evidence appears strongest that the deposits were annealed after deposition at the Fra Mauro site.

Apollo missions 15, 16, and 17 were more explorative in nature than previous ones with the selection of sites based on geologic and geophysical criteria. The Apollo 15 site was selected to sample both Imbrium mare material in the vicinity of a sinuous rille and Apennine Front material, thought to represent deep ejecta from the Imbrium Basin. The Apollo 16 site in the Cayley Plains of the highlands was selected to study what was thought at that time to be highland volcanic products. The Taurus-Littrow site of Apollo 17 was chosen to sample juxtaposed Serenetatis ejecta and mare-like fill thought to be extremely youthful. Although premission criteria turned out faulty, a wealth of information was obtained from these explorations. Studies at Hadley (Apollo 15) revealed that the age of the last basaltic activity in that area, 3.3 B.Y., and the composition of the lavas were more like Procellarum rocks than like Tranquillitatis lavas, and that the mare there was composed of a sequence of flows with thickness in tens of meters. A volcanic origin of the rille was not proven but strongly supported by the visual studies. Components of the Apennine Front were found to be enriched in anothosites, troctolites, and norites – a finding which confirms earlier less direct evidence that these rocks are characteristic of the highlands and premare crustal materials. Again, a confirmation of the 3.9–3.95 B.Y. age of the Imbrium event was obtained, and resetting of atomic clocks was found to be the rule. One anorthosite fragment, that apparently survived impact resetting of the clock, was found with a crystallization age of 4.1 B.Y.

The mission to the Cayley Formation site in the highlands (Apollo 16) revealed that these deposits are not volcanic plains but are accumulations of highland-type breccias with reset atomic clocks. Initial considerations of their origin suggested that they may have been derived from the Imbrium or Orientale Basins. Recent studies suggest strongly, however, that these often highly-shocked breccias were derived locally through long periods of time but with significant quantities of debris having been produced locally by heavy, temporally restricted bombardment by secondary projectiles produced by the Imbrium impact.

The mission to Taurus-Littrow (Apollo 17) revealed that lavas there were not youthful, nor was a youthful mantle of volcanic ejecta found as suspected, but rather were comparable in age and compostion to Tranquillitatis basalts. Studies of returned samples also demonstrated that Serenitatis ejecta proved to be similar compositionally to Imbrium ejecta and similar in age (about 3.97 B.Y.) although Serenitatis is one of the oldest of the mare basins. Relative ages of formation of the major mare basins based on superpositional evidence are, oldest to youngest, Fecunditatis, Serenitatis, Nectaris, Humorum, Crisium, Imbrium, and Orientale. The near simultaneity of formation of Serenitatis and Imbrium Basins implies the nearly simultaneous formation of all and is strong evidence of either a cataclysmic bombardment within a period of 10^8 years at about 3.95 B.Y. ago, or a termination of a set of conditions at that time which has almost completely obliterated evidence of more ancient history.

Relative to the bombardment history, an approximate reconstruction is possible based on crater frequencies in deposits of known crystallization age. This reconstruction is presented in figure 2 where the cratering rate is estimated relative to the present. The main points of these data are that the early flux was extremely high and that maria flooding took place during a time when flux was changing rapidly. The slope of the cratering rate (Hartmann, 1970), in fact, suggests that the population of producing bodies has a half life of 10^8 years, suggesting that they were solar orbiting, low eccentricity planetesimals with impact velocities in the range 2–10 km/sec.

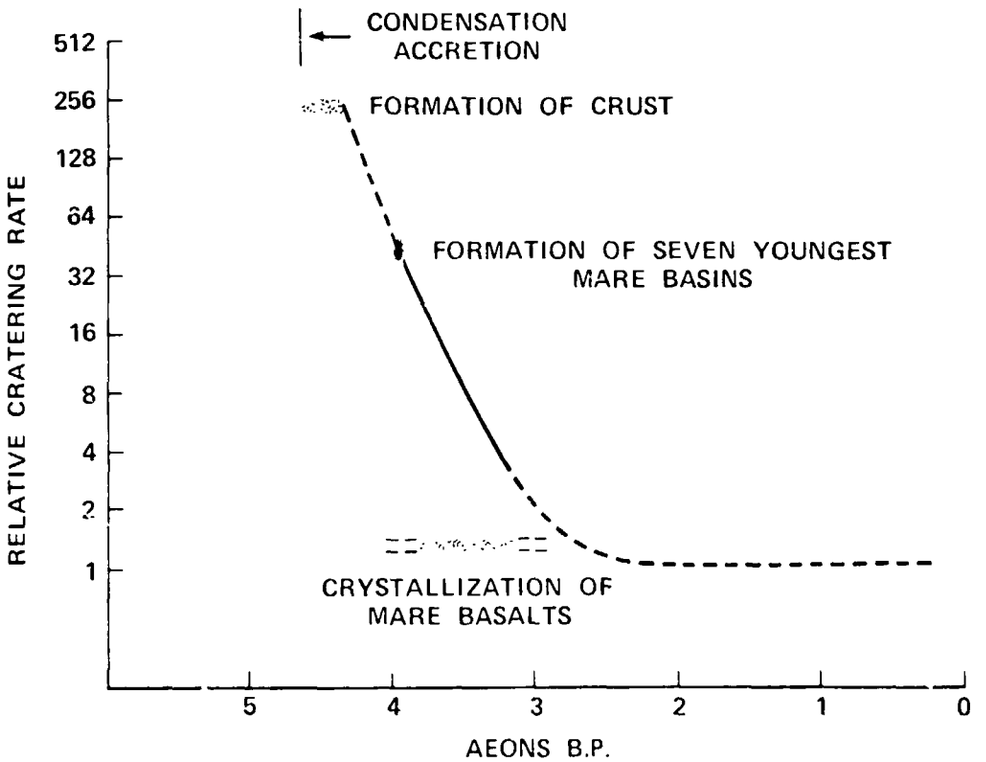

Figure 2.– Links in the chain of lunar events.

The igneous history of the Moon, shown minimally in figure 2, is reconstructed in more detail in figure 3 along with a model that has been proposed to account for known facts (McConnell and Gast, 1971). The most significant points of the model are that, to account for all known geological, geochemical, and geophysical aspects, it had to be assumed that the Moon accreted inhomogeneously and that surface melting gradually progressed to deeper levels. Aspects of the model and other significant points not discussed here will be considered at length in the formal presentation.

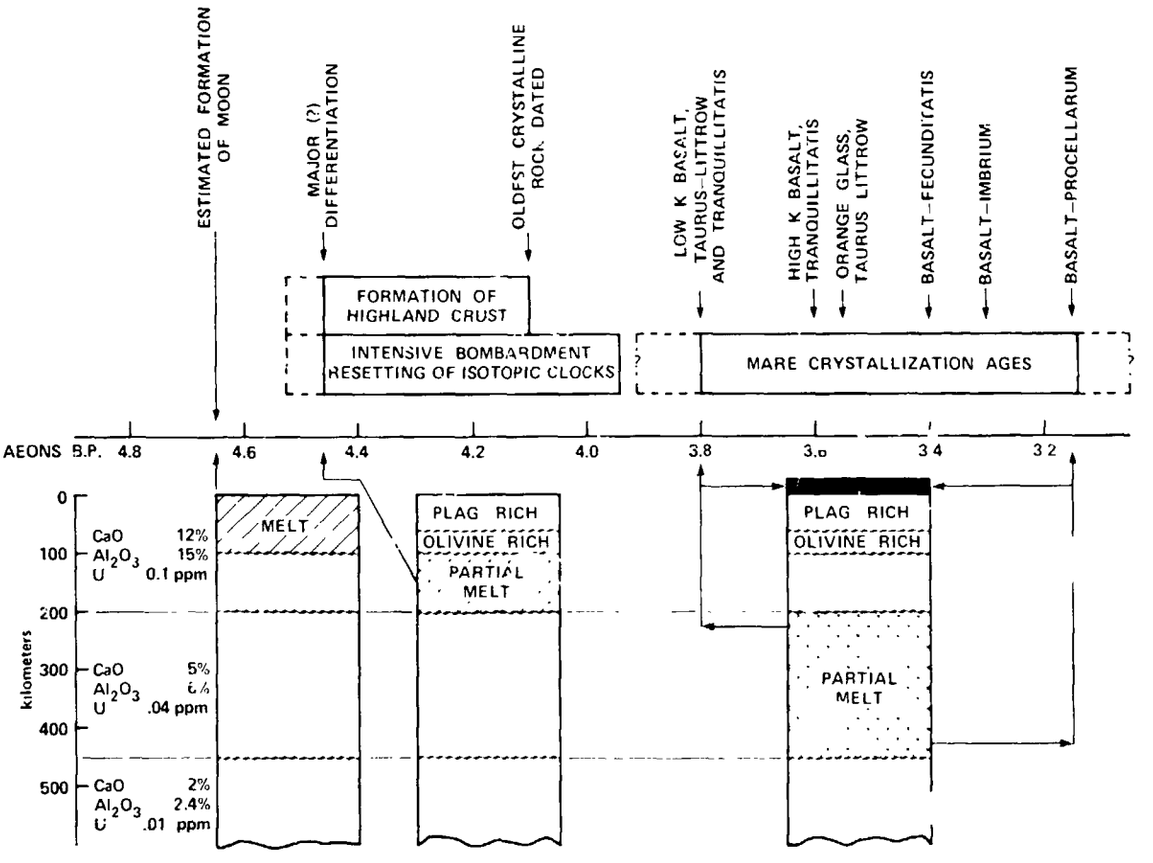

Figure 3.– Igneous history of the Moon.

APPENDIX

LUNAR SCIENCE TERMINOLOGY

Most of the terminology used in lunar science is straightforward and easily recognizable by all geoscientists. There are a few terms that are unique to lunar or meteoritic studies, however, the most common of which are listed below.

Agglutinate – delicately branching assemblages of fragments cemented by crusts and filaments of glass. Found in lunar "soils" and considered to be products of meteoritic impacts.

Ballistic transport – process by which particles are launched into ballistic trajectories by cratering processes and transported across the surface, the major form of transport on the Moon.

Chondrule – a spheroidal body (millimeter sized) often radially crystallized, consisting chiefly of olivine and/or orthopyroxene, and occurring in many stony meteorites and lunar "soils" and breccias.

Cosmogenic nuclide – a nuclide (such as Na^{22}, Al^{26}, etc.) produced by the action of cosmic radiation (very high energy sub-atomic particles, e.g., atomic nuclei).

Exotic – a straightforward use of a common term to describe certain particles in lunar "soil" thought to have been formed in regions distant to the site where found.

Exposure age – the length of time a rock or particle has existed at or near the lunar surface during which time it has been subjected to the various processes by which exposure age is determined.

Fines – a term describing the less than one centimeter fraction of lunar "soil." Coarse fines refers to the 1-cm to 1-mm fraction. Fine fines refers to the less than 1-mm fraction.

Galactic cosmic rays – very high energy sub-atomic particles from galactic sources (non-solar sources).

Highland terrain – the higher, older portions of the lunar surface (contrasted to maria), now thought to be compositionally distinct from maria. Also called Terrae.

Impactite – a glassy to finely crystalline material, often vesicular, produced by fusion or partial fusion of target rock by heat generated from the impact. Impactites are composed typically of mixtures of melt and rock fragments and sometimes contain traces of meteorite material.

Impact metamorphism – a type of shock metamorphism in which the shock waves and the observed changes in rocks and minerals result from the impact of a body such as a meteorite.

KREEP – an acronym applied to a group of rocks found in lunar samples that are enriched in potassium (K), rare earth elements (REE), and phosphorus (P).

Mare – one of several dark, low-lying, level, relatively smooth, plains-like areas of considerable extent on the surface of the Moon, now known to consist of basic lavas overlain by a fragmental soil-like layer, the regolith.

Mascon – a large-scale, high density, lunar mass concentration.

Microbreccia – a terrestrial rock term applied to lunar rocks characterized by clastic texture, thought to be the product of impact fragmentation and lithification. Several types are recognized according to composition, type of component clasts, state of aggregation or degree of metamorphism.

Microcrater – small craters, generally less than few mm to micron size found on surfaces of mineral grains and rocks that have existed at the lunar surface. Sometimes called micrometeorite craters or zap pits.

Micrometeorite – a very small meteoritic particle (diameter < 1 mm).

Particle tracks – tracks left in minerals or other media by the passage of highly energetic particles. In lunar samples, tracks result from radioactive decay of natural radioactive atoms and from passage of galactic and solar particles.

Planetesimals – large bodies of the solar system, but less than planet size.

Ray (crater ray) – long, relatively bright streaks, loops or lines that radiate from lunar craters.

Regolith – an old term that has been applied to lunar geology in the strict sense: the entire layer or mantle of fragmental and loose (incoherent or unconsolidated) rock material, of whatever origin, and of very varied character that nearly everywhere forms the surface of the land and overlies or covers the more coherent bedrock.

Rille – trench-like valleys on the Moon's surface. Rilles are subdivided according to plan shapes as straight or arcuate (both of which are long and narrow, probably tectonic in origin), sinuous (generally found on lava surfaces and thought to be lava channels or collapsed lava tubes) or irregularly branching (in large, lava-filled craters where the rilles apparently results from fracturing).

Ringed basin – large, crater-form basins such as the Imbrium Basin, Crisium Basin, etc., on the lunar surface that contain one or more topographic rings outside the basin. They are thought to represent scars of ancient, impact, low-velocity planetesimals.

Secondary crater – crater produced by a projectile ejected from a (primary) crater produced by the impact of a meteoroid.

Shock metamorphism – synonymous with impact metamorphism for lunar cases where metamorphism is accomplished by the passage of a shock wave.

Smooth plains – lunar terrain in highland depressions in highly cratered (not mare) areas characterized by relatively smooth surfaces. Smooth plains are now considered to consist of accumulations of impact ejecta.

Solar flare – flare of the Sun, particularly of interest to lunar geology in that solar flares produce extremely high quantities of highly energetic sub-atomic particles that strike the lunar surface.

Solar wind – the motion of interplanetary plasma or ionized particles away from the Sun.

REFERENCES

Hartmann, W. K.: Preliminary note on lunar cratering rates and absolute time scales. Icarus, v. 12, p. 131-133, 1970.

McConnel, R. K., and Gast, P. W.: in a paper delivered at the conference on lunar geophysics at the Lunar Science Institute, Houston, Texas, 18 to 21 October, 1971.

With permission, reprinted from Apollo 11: Preliminary Science Report, NASA SP-214, 1969.

Summary of Scientific Results

W. N. Hess and A. J. Calio

The scientific objectives of the Apollo 11 mission, in order of priority, were the following:

(1) To collect early in the extravehicular activity (EVA) a sample, called the contingency sample, of approximately 1 kg of lunar surface material to insure that some lunar material would be returned to Earth.

(2) To fill rapidly one of the two sample return containers with approximately 10 kg of the lunar material, called the bulk sample, to insure the return of an adequate amount of material to meet the needs of the principal investigators.

(3) To deploy three experiments on the lunar surface:

(a) A passive seismometer to study lunar seismic events, the Passive Seismic Experiment Package (PSEP).

(b) An optical corner reflector to study lunar librations, the Laser Ranging Retroreflector (LRRR)

(c) A solar-wind composition (SWC) experiment to measure the types and energies of the solar wind on the lunar surface

4) To fill the second sample return container with carefully selected lunar material placed into the local geologic context, to drive two core tubes into the surface, and to return the tubes with the stratigraphically organized material, called the documented sample.

During these tasks, photographs of the surface were to be taken using a 70-mm Hasselblad camera and a close-up stereoscopic camera (the Apollo Lunar Surface Closeup Camera (ALSCC)). The scientific tasks and a variety of other tasks were planned for a 2-hr and 40-min time period.

According to mission plans, the time allotted for the collection of the documented sample, which had the lowest priority, would be shortened if time were insufficient. All the scientific tasks were completed satisfactorily, all instruments were deployed, and approximately 20 kg of lunar material were returned to Earth. The documented-sample period was extremely short, however, and samples collected during this period were not carefully photographed in place or documented in other ways.

Nature of the Lunar Surface

The Apollo 11 lunar module (LM) landed in the southwestern part of Mare Tranquillitatis, approximately 50 km from the closest highland material and approximately 400 m west of a sharp-rimmed blocky crater approximately 180 m in diameter. Rays of ejecta from this crater extend past the landing site. Rays from more distant craters, including the crater Theophilus, are also in the landing region.

Surface material at the landing site consists of unsorted fragmental debris ranging in size from approximately 1 m to microscopic particles, which make up the majority of the material. This debris layer, the regolith, is approximately 5 m thick in the region near the landing site, as judged by the blockiness of material near various-sized craters.

The soil on the lunar surface is weakly cohesive, as shown by the ability of the soil to stand on vertical slopes. The fine grains tend to stick together, precluding clods of material that crumpled under the astronauts' boots. The depth of the astronauts' footprints and the penetration of the LM landing gear correspond to static bearing pressures of approximately 1 psi. The surfaces were relatively soft to depths of 5 to 20 cm. Deeper than these depths, the resistance of the material to penetration increases considerably. In general, the lunar soil at the landing site was similar in appearance, behavior, and mechanical properties to the soil encountered at the Surveyor equatorial

landing sites. Although the lunar soil differs considerably in composition and in range of particle shapes from a terrestrial soil of the same particle-size distribution, the lunar soil does not appear to differ significantly from similar terrestrial soil in mechanical behavior.

Both rounded and angular rocks appear on the surface in profusion. All degrees of burial are present, and fillets on the sides of rocks, caused by the powdery surface material being piled up by some erosional process, were common. At least three of the rocks returned to Earth have been identified in photographs of the lunar surface. On what appears to be the upper surface of several rocks, a thin rind of altered material approximately 1 mm thick is found. This rind is lighter colored than the remainder of the rock and appears to be caused by shattering of mineral grains.

One outstanding feature of the surfaces of the rocks returned to Earth is the existence of several glass-lined pits 1 mm or smaller in diameter. These glass-lined pits appear only on the surfaces of rocks. (More of these pits are observed on the top surfaces of rocks with known orientations.) Quite clearly, these pits are of external origin. The glass overlaps of the surface of the rock and the resulting features clearly resemble hypervelocity impact craters. However, the pits do not resemble craters made in the laboratory by hypervelocity particles, and the origin of the pits is presently unknown.

The most interesting and unexpected surface features discovered and photographed by the astronauts are glassy patches on the lunar surface that are described by the astronauts as resembling drops of solder. These patches were observed only inside several raised-rim craters approximately 1 m in diameter. These glassy blebs may be formed by low-velocity molten material splattering into the craters, or they may be formed from material that has been melted in place. The section of this document entitled "Lunar Surface Closeup Stereoscopic Photography" presents an interesting theory of the origin of the blebs, based on radiation heating. This theory postulates that within the last 100 000 years, the Sun had a superflare or mininova event that heated the lunar surface to a temperature that caused material inside the craters to melt, but did not cause surface material to melt. According to the theory, the reason that material inside the craters melted while surface material did not is that a focusing effect caused the temperature inside the craters to increase. This radiation-heating theory is certainly not yet proved, but no other plausible theories have been advanced to explain the blebs' being located only in the bottoms of craters. None of the blebs photographed by the astronauts were returned in the sample containers, and no blebs have been identified in the samples.

The Passive Seismic Experiment

Since the time of the Ranger 1 mission, scientists have been trying to land a seismometer on the surface of the Moon to search for moonquakes. Successful operation of a seismometer is extremely important for understanding of the internal structure of a planet and to a search for possible layering or discontinuities. On the Apollo 11 mission, a seismometer was placed on the surface of the Moon, and the instrument operated satisfactorily for 21 days. The instrument contained four separate components. Three long-period (LP) (approximately 15-sec resonance) seismometers were alined orthogonally to measure surface motion both horizontally and vertically. A single-axis, short-period (SP) seismometer, with a resonant period of approximately 1 sec, measured vertical motion. The system had tilt adjustment motors to level the system upon command from Earth. The instrument was deployed on the lunar surface approximately 16 m from the LM and was turned on while the astronauts were on the lunar surface. Signals were received when the crewmen climbed the LM ladder, used a hammer to pound on the core tubes, and jettisoned equipment, including the portable life support systems (PLSS).

Actual maximum instrument temperature (approximately 190° F) exceeded the planned maximum instrument temperature by approximately 50° F. Even at this elevated temperature, the instrument worked satisfactorily during the first lunar day and during part of the second. However, near noon of the second lunar day, the instrument no longer accepted commands from Earth stations; therefore, the experiment was terminated.

The LM appears to have been a rich source of seismic noise. One class of repeating signals of nearly identical structure that was observed gradually died out over a period of many Earth days. These signals seem to be related to events on the LM such as fuel venting, valve chatter, or other mechanical motion. The signals had a dominant frequency of 7.2 Hz before LM ascent and of 8.0 Hz following ascent. These frequencies appear to be characteristic frequencies of the LM structure.

Several events showing dispersion and having the appearance of surface waves were detected on the LP seismometers. These wave trains often occurred simultaneously with a series of pulses on the SP seismometer. It is not yet certain, but these waves are probably not the result of real seismic events but are of instrumental origin.

Several other classes of events of unknown origins were observed. The following are possible source mechanisms for these observed seismic signals:

(1) Venting gases from the LM and circulating fluids within the LM

(2) Thermoelastic stress relief within the LM and the PSEP

(3) Meteoroid impacts on the LM, the PSEP, and the lunar surface

(4) Displacement of rock material along steep crater slopes

(5) Moonquakes

(6) Instrumental effects

It is unclear whether any of the received signals were actually of lunar-seismic-event origin. One of the most important results of the PSEP is the discovery that the background noise level on the Moon is extremely low. At frequencies from 0.1 to 1 Hz, the background seismic-signal level for vertical surface motions is less than 0.3 mμm. This level is from 100 to 10 000 times less than average terrestrial background levels in the frequency range of 0.1 to 0.2 Hz for microseisms. Continuous seismic background signals from 10 to 30 mμm were observed on the records of the horizontal seismometers. These signals decreased considerably near lunar noon and may have been due to lunar surface-temperature changes which tilted the instrument.

Of the many seismic signals recorded, several were produced by the LM. Many of the signals may be a result of real seismic events and may be generated by moonquakes, impact events, or movement of surface rocks. However, none of the events can be clearly identified as real, and none of the observed signals has patterns normally observed on recordings of seismic activities occurring on Earth. Clearly, the Moon is not a very seismic body. Artificial seismic sources, such as the impact on the lunar surface of the Saturn IVB stage or the spent LM ascent stage, will be useful for future lunar seismometers.

Laser Ranging Retroreflector

The LRRR consists of an array of finely machined quartz corners deployed on the lunar surface and aimed at the Earth. The array is used as a reflector for terrestrial lasers. By measuring the distance from the laser to the reflector, small changes in the motion of the Moon or the Earth can be measured. The goal, when the system is fully operational, is an uncertainty of 15 cm (6 in.). The LRRR will allow studies to be conducted on (1) the librations of the Moon, both in latitude and longitude, (2) the recession of the Moon from the Earth caused either by tidal dissipation or by a possible change in the gravitation constant, and (3) the irregular motion of the Earth, including the Chandler wobble of the pole. The amplitude of the Chandler wobble seems to vary in time with relation to major earthquake events.

On the same day the LRRR was deployed satisfactorily on the surface of the Moon, attempts were made to range on the reflector from the Lick Observatory in California and from the McDonald Observatory in Texas. Some time was required for the ranging attempts to be successful because, initially, there was some uncertainty as to the location of the landing site. After a few days, this problem was solved, but ground-instrument difficulties and weather problems caused further delays. In approximately a week, both observatories had received signals reflected by the LRRR. The signals, although weak, were clearly identifiable. By using this technique, the distance to the Moon from the Earth has been measured to an accuracy of approximately 4 m. It should be noted that the distance to the Moon is actually uncertain to a few hundred meters

because of uncertainties in the velocity of light. However, the distance expressed in light seconds is accurate to approximately one part in 10^8, which is consistent with the 4-m accuracy discussed previously.

The LRRR experiment will continue for months or years before final data are obtained on many of the detailed measurements to be undertaken.

The Solar-Wind Composition Experiment

For some time, direct measurements have been made of the solar wind, establishing the presence of approximately 5 percent helium ions in the solar-wind stream, which is composed predominantly of protons. The solar wind is expected to contain many heavier ions, probably representative of solar composition, but no direct measurements of these heavier species have yet been made. It now seems quite likely that the rare gas measured in the powdery lunar samples is of solar-wind origin, but this rare-gas source may be confused with other gas sources. The measured rare gas represents an integration of the solar wind into the soil over a period of many millions of years.

An experiment was conducted during the Apollo 11 mission to measure heavier elements in the solar wind directly. A thin aluminum foil of 4000 cm^2 was deployed on the surface of the Moon facing the Sun. The solar-wind particles were expected to penetrate approximately 10^{-5} cm into the foil and to be firmly trapped there. The foil was collected after 77 min, placed inside one of the sample-return containers, and brought to the NASA Manned Spacecraft Center (MSC) Lunar Receiving Laboratory (LRL).

Approximately 1 ft^2 of the foil was removed in the LRL, sterilized by heat at 125° C for 39 hr, and sent to Switzerland for analysis. Several small pieces of the foil, each approximately 10 cm^2, were cleaned by ultrasonic methods, and the noble gases were then extracted for analysis in a mass spectrometer. Helium, neon, and argon were found, and their isotopic composition was measured. The results correspond generally to solar abundances and are clearly nonterrestrial. More complete results will be presented when the major portion of the foil has been analyzed.

The Lunar Samples

Of the 22 kg of returned lunar material, 11 kg are rock fragments larger and 11 kg are smaller than 1 cm in size. This material may be divided into the following four groups:

Type A – fine-grained vesicular crystalline igneous rock.

Type B – medium-grained crystalline igneous rock.

Type C – breccia.

Type D – fines (less than 1 cm in size).

The crystalline rocks contain mineral assemblages, crystal sizes, and gas cavities, indicating that the rocks were crystallized from lavas or near-surface melts. It is uncertain whether the lavas were impact generated or of internal origin. Twenty crystalline rocks were found in the returned sample, 10 rocks of type A and 10 of type B. Individual rocks weighed up to 919 g. The type A rocks contain vesicles of 1 to 3 mm in diameter faced with brilliant crystals. (Most vesicles are spherical but some are ovate.) There are also irregular cavities, or vugs, into which crystals and other groundmass minerals project. The percentages of the minerals present in type A rocks are clinopyroxene, 53 percent; plagioclase, 27 percent; opaques (including abundant ilmenite, minor troilite, and native iron), 18 percent; and other translucent phases, and a minor amount of olivine, 2 percent. Except for the high content of opaques, which reflects the high iron and titanium content, the mineralogy and chemistry of the rocks resemble terrestrial olivine-bearing basalts.

The dark-brownish-gray speckled type B rock is granular in texture and generally resembles terrestrial microgabbros. The grain sizes are from 0.2 to 3 mm. The percentages of minerals in type B rocks are as follows: clinopyroxene, 46 percent; plagioclase, 31 percent; opaques (mainly ilmenite), 11 percent; cristobalite, 5 percent; and other minerals, 7 percent. No olivine is present in type B rocks. Other unidentified minerals have been found. The complete absence of hydrous mineral phases in type A or type B rocks and the presence of free iron places a low limit on the amount of water present in the melt from which the rocks crystallized. The water content in the lunar

material is considerably lower than the water content in terrestrial basalts.

All the breccias are mixtures of fragments of different rock types similar to type A or type B rocks and are mixtures of angular fragments and sphericles of glass of a variety of colors and a variety of indices of refraction. Evidence of strong shock is present in many type C rocks. These rocks vary from being very friable and soft to being as hard as the crystalline rocks. Evidence points to the breccias being formed by shock cementing or by lithification of the powdery lunar surface material. Both techniques of breccia formation are probably the result of impact events.

Fines were returned to Earth in the bulk-sample container and in the core tubes. The core tubes showed no stratification of fines, and the material was, in general, similar to the bulk-sample fines. The type D material consists of a variety of glasses, plagioclase, clinopyroxene, ilmenite, and olivine. A few Ni-Fe spherules up to 1 mm in diameter were found. Glasses, which make up approximately 50 percent of type D material, are of three types: (1) vesicular, globular dark-gray fragments; (2) pale or colorless angular fragments with refraction indices of approximately 1.5 to 1.6; and (3) spheroidal, ellipsoidal, dumbbell-shaped, and teardrop-shaped bodies. Most of these glass types are smaller than 0.2 mm and range in color from red to brown to green to yellow with refraction indices ranging from 1.55 to 1.8. Unlike most terrestrial magnetic glasses, many single glass particles are inhomogeneous. Like the Ni-Fe spherules, the type 3 rounded glass bodies seem to indicate melting induced by strong shock. In fact, evidence for shock is common in the fines and in the breccias. However, only a few crystalline rocks show evidence of strong shock in places other than near the surface pits.

A chemical analysis of several samples of all four types of glass was made using optical emission spectroscopy. A few samples were also analyzed using atomic absorption procedures. All four types of lunar material samples have been studied, and all types appear to be quite similar chemically. There is no similar material common on Earth. Several of the refractory metals are very prominent. On Earth, a deposit containing from 5 to 10 percent titanium is rare and might be considered a titanium mine. Zirconium, yttrium, and chromium are also present in amounts substantially larger than might be expected in terrestrial basalts.

Another characteristic of the samples is that they are low in alkali and volatile elements such as sodium, potassium, rubidium, lead, and bismuth. Aside from this characteristic and the very low water content mentioned previously, the material might be considered to be similar to terrestrial basalts. Because of the enrichment of the refractory elements and the depletion of the volatile elements, it is tempting to consider the material to be similar to a cinder, being the end product of a high-temperature environment, to explain these modifications.

The rare-gas content of lunar samples has been measured by mass spectroscopy. The content of beryllium, neon, argon, krypton, and xenon has been measured in several samples. The total rare-gas content in the fines and breccias is approximately 0.1 cc/g, which is quite high. These gases were found in the outside layer of the crystalline rocks, but the gas content found inside these rocks was very low. The gases were found throughout the breccias, further indicating that the breccias are formed, probably by shock, from the fines. Quite clearly, most of the measured rare gas is from the solar wind. Although no isotopic ratios have been measured previously for solar rare gases, the values obtained from the preliminary examination compare well with the values that would theoretically be expected.

Several of the rocks measured contained radiogenic ^{40}Ar, which, when coupled with data on potassium abundance, enables dating of the time of crystallization of the rocks by using the decay process

$$^{40}Ar \longrightarrow {}^{40}K + e^{+} \qquad (1)$$

This process gives an age of $3.0 \pm 0.7 \times 10^{9}$ yr, which shows that the surface of the maria is older than had been expected.

Age dating can also be accomplished by measuring the amount of certain isotopes that are produced by cosmic ray bombardment of the lunar surface. This technique yields the time that the rocks within a few feet of the lunar sur-

face have been exposed to cosmic rays. The rocks studied had cosmic-ray-exposure ages from 20×10^6 to 160×10^6 yr.

The organic content of the samples was studied by two techniques: (1) pyrolysis with flame ionization detection and (2) mass spectroscopy. The amount of extractable organic material with temperatures to 500° C is less than 1 part per million (ppm). Some organic contaminants were introduced into the samples by recovery and processing in the LRL, and it is uncertain whether an indigenous organic material exists in the samples.

Several samples have been counted in the LRL Radiation Counting Laboratory. The gamma rays measured show the presence of several cosmic-ray-induced radionuclides and the presence of thorium, uranium, and potassium. The uranium and thorium concentrations are near the concentration values of these elements found in terrestrial basalts; however, the amount of potassium present in the lunar samples is lower than that in terrestrial basalts and is comparable to the amount found in chondritic meteorites.

Conclusions

The major findings have been as follows:

(1) By using a fabric and mineralogy basis, the rocks can be divided into two genetic groups: fine- and medium-grained crystalline rocks of igneous origin and breccias of complex origin.

(2) The crystalline rocks, as shown by their modal mineralogy and bulk chemistry, are different from terrestrial rock and meteorites.

(3) Erosion has occurred on the lunar surface in view of the fact that most of the lunar rocks are rounded, and some of the rocks have been exposed to a process that gives them a surface appearance similar to sandblasted rocks. There is no evidence of erosion by surface water.

(4) The probable presence of the assemblage iron-troilite-ilmenite and the absence of any hydrated phase indicate that the crystalline rocks were formed under extremely low partial pressures of oxygen, water, and sulfur. (Pressures are in the range of equilibrium pressures found within most meteorites.)

(5) The absence of hydrated minerals suggests that no surface water has existed at Tranquility Base at any time since the rocks in this region were exposed.

(6) Evidence of shock or impact metamorphism is common in the lunar rocks and fines.

(7) All the rocks have glass-lined surface pits that may have been caused by the impact of small particles.

(8) The fine material and the breccia contain large amounts of all the noble gases which have elemental and isotopic abundances indicative of origin in the solar wind. The fact that interior samples of the breccias contain these gases implies that the samples were formed at the lunar surface from material previously exposed to the solar wind.

(9) $^{40}K-^{40}Ar$ measurements on igneous rocks show that they crystallized from 3×10^9 to 4×10^9 yr ago. The presence of nuclides produced by cosmic rays shows that the rocks have been within 1 m of the surface for periods of 20×10^6 to 160×10^6 yr.

(10) The level of indigenous organic material capable of volatilization or pyrolysis, or both, appears to be extremely low, that is, considerably less than 1 ppm.

(11) Chemical analyses of 23 lunar samples show that all rocks and fines generally are chemically similar.

(12) The elemental constituents of lunar samples are the same as those found in terrestrial igneous rocks and meteorites. However, the following significant differences in composition were observed: some refractory elements (for example, titanium and zirconium) are notably enriched, and the alkali and some volatile elements are depleted.

(13) Elements that are enriched in iron meteorites (i.e., nickel, cobalt, and the platinum group) were not observed; such elements are probably low in abundance.

(14) Of 12 radioactive species identified, two were cosmogenic radionuclides of short half life, namely ^{52}Mn (5.7 days) and ^{48}V (16.1 days).

(15) Uranium and thorium concentrations are near the typical concentrations of these elements found in terrestrial basalts; however, the potassium-to-uranium ratio determined for lunar surface material is much lower than such ratios determined for terrestrial rocks or meteorites.

(16) No evidence of biological material has

been found to date in the lunar samples.

(17) The lunar soil at the landing site is predominantly fine grained, granular, slightly cohesive, and incompressible. The hardness of the lunar soil increases considerably at a depth of 15 cm. The soil is similar in appearance and behavior to the soil encountered at the Surveyor equatorial landing sites.

(18) The PSEP deployed on the Moon operated satisfactorily for 21 days and detected several seismic signals, many of which originated from astronaut activity or mechanical motions of the LM. It is uncertain whether any actual lunar seismic events were detected. The seismic-noise background is much less on the Moon than on Earth.

(19) The LRRR was deployed on the Moon and has been used as a target for Earth-based lasers. The distance to the Moon has now been measured to within an accuracy of approximately 4 m. Future studies will be made on the variation of this distance to study in detail the motion of the Moon and the Earth.

(20) Preliminary analysis has been made on part of the aluminum SWC foil. Helium, neon, and argon have been found in the analysis, and the isotopic composition of each element has been measured.

With permission, reprinted from Apollo 12: Preliminary Science Report, NASA SP-235, 1970.

Summary of Scientific Results

Gene Simmons[a] *and A. J. Calio*[b]

The Apollo 12 mission provided the first opportunity in the scientific exploration of the Moon to sample extensively the rocks within a radius of ½ km of the landing site, to obtain geologic data from firsthand observations made on the Moon, to measure on the surface of the Moon the vector components of the lunar magnetic field, to measure the pressure of the lunar atmosphere, and to collect seismic data on the interior of the Moon from the impact of the lunar module (LM) ascent stage. During the two extravehicular activity (EVA) periods, a total duration of 7.5 hr, the astronauts collected three core tubes of lunar soil and additional surface samples along a geologic traverse. They obtained material from the bottom of a shallow trench and brought back several items from the Surveyor 3 spacecraft. The astronauts caught some of the solar wind in an aluminum foil, and they obtained extensive photographs of the lunar surface and of crew activities by using 70-mm Hasselblad cameras and a closeup stereoscopic camera.

The Apollo 12 LM landed on the northwest rim of the 200-m-diameter Surveyor Crater in the Ocean of Storms. The landing site was at 23.4° west longitude and 3.2° south latitude, approximately 120 km southeast of the crater Lansberg and due north of the center of Mare Cognitum. The landing site is near a ray associated with the crater Copernicus, which is situated approximately 370 km to the north. The landing site is characterized by a distinctive cluster of craters that range in diameter from 50 to 400 m. The traverses during the two EVA periods were generally made on or near the rims of these craters and on deposits of ejecta from them. Therefore, the samples returned to Earth contain a variety of material ejected from local craters. Some of the fine-grained material was derived locally, and some probably from distant sources.

The Apollo 12 results obtained to date are summarized in this section. The reader should understand that these results are preliminary and that the interpretation, especially, is likely to change in the future.

Surface Experiments

Geology

Igneous rocks, breccias, and soils were collected from a variety of local geologic features that included a mound and several craters. Along several parts of the traverse made during the second EVA period, the astronauts found fine-grained material of relatively high albedo that, at some places, was buried in the shallow subsurface and, at other places, was situated on the surface. This light-gray material was specifically reported to be at the surface near Sharp Crater and a few centimeters below the surface near Head, Bench, and Block Craters. It is possible that some of this light-gray material may constitute a discontinuous deposit that is observed telescopically as a Copernican ray.

Small linear patterns similar to those at the Apollo 11 site were noted in the surface. These patterns are probably caused by drainage of fine-grained material into fractures in the underlying bedrock. This interpretation implies northeast- and northwest-trending joint sets in the bedrock of the Apollo 11 site and north- and east-trending joint sets in bedrock of the Apollo 12 site. The lineated strips of ground reported by the crew probably reflect joint sets within larger fracture zones in the bedrock.

[a] NASA Manned Spacecraft Center and Massachusetts Institute of Technology.

[b] NASA Manned Spacecraft Center.

Darker regolith material that generally overlies the light-gray material is only a few centimeters thick at some places, but probably thickens greatly on the rims of some craters. The regolith varies locally in the size, shape, and abundance of constituent particles and in the presence or absence of patterned ground. Most of the local differences are probably the result of local cratering events.

The Apollo 12 site is younger than the Apollo 11 landing site as suggested by the fewer number of kilometer-size craters. The Apollo 11 site has about 2.37 times as many kilometer-size craters as does the Apollo 12 site.

One of the notable differences between the set of rocks collected at the Apollo 12 site and that collected at the Apollo 11 site (Tranquility Base) is the ratio of crystalline rocks to breccias. At the Apollo 12 site the rocks collected are predominantly crystalline, whereas at Tranquility Base, approximately half the rocks collected are crystalline and half are microbreccia. This difference exists probably because the rocks from the Apollo 12 landing site were collected primarily on or near crater rims. The regolith is thin on the crater rims, and many of the rocks are probably derived from craters that have been excavated in the bedrock that lies well below the regolith. Tranquility Base was on a thick, mature regolith, where many of the observed rock fragments were produced by shock lithification of regolith material and were ejected from craters too shallow to excavate bedrock.

Two mounds were situated in the area north of Head Crater. Both mounds are visible on the high-resolution Lunar Orbiter photographs. These mounds are probably clumps of regolith material that were slightly indurated by impact and ejected from one of the nearby craters—possibly from Head Crater. Bombardment by meteoritic material and by secondary impacts and, possibly, the effects of diurnal temperature changes have probably caused sloughing of the sides of the mounds, which has resulted in their present rather smooth form.

The lunar surface materials near the Surveyor 3 spacecraft were examined for measurable changes that might have occurred in photometric properties during the 30 months since the Surveyor landing. None occurred, within the limits of the measurements. The optical properties indicate that the lunar surface in the area of the Surveyor spacecraft has not received a new covering of dust nor been mechanically altered by the lunar environment during the 30 months. A significant change occurred in the reflectance of the Surveyor footpad imprint over the 30-month span; the change may have been caused by microscopic mechanical alteration of the compressed surface.

In spite of local variations in soil texture, color, grain size, compactness, and consistency, the soil at the Apollo 12 site is similar in appearance and behavior to the soils encountered at the Apollo 11 and Surveyor 3 equatorial landing sites. Although the deformation behavior of the surface material involves both compression and shear effects, the conclusion drawn earlier from the Surveyor 3 mission results—that the soil at the Surveyor 3 landing site is essentially incompressible—is consistent with the consistency, compactness, and average grain size of the soil at the Surveyor 3 site, as assessed during the Apollo 12 EVA. There appears to be no direct correlation between crater slope angle and consistency of soil cover. The latter depends mainly on the geologic history of the terrain feature and on the local environmental conditions.

Seismology

No seismic signals with characteristics similar to terrestrial signals have been observed for the Moon. This fact is a major scientific result. The high sensitivity at which the lunar instruments were operated would have resulted in the detection of many such signals if the Moon were as seismically active as the Earth and had the same transmission characteristics as the Earth. Thus, the data obtained to date indicate that either seismic energy release is far less for the Moon than for the Earth or the interior of the Moon is highly attenuating for seismic waves.

The LM ascent stage was impacted approximately 80 km E 24° S from the seismometer. The event was recorded on all three long-period seismometers. The signal amplitude increased slowly and then decreased slowly. The signal continued for approximately an hour. The coherence between various signal components was quite low. None of the signal features was typical of anal-

ogous terrestrial events. The velocity of the first arrival was 3.1 to 3.5 km/sec.

The passive seismic experiment has recorded 30 prolonged signals with a gradual buildup and then a slow decrease in signal amplitude. Signals with these characteristics may imply transmissions with very low attenuation and intense wave scattering—conditions that are mutually exclusive on Earth. Because of the similarity with the signal from the impact of the LM ascent stage, the 30 recorded signals are thought to be produced by meteoroid impacts of shallow moonquakes. Most of the events that produced these signals appear to have originated within 100 km of the Apollo lunar surface experiments package (ALSEP). The occurrence of signals with similar characteristics during both the Apollo 11 and 12 missions greatly strengthens the present belief that at least some signals observed, including the 30 signals recorded by the seismometer, are likely to be of natural origin.

Magnetometer

The Apollo 12 magnetometer is a very sophisticated three-component fluxgate instrument. It is the first magnetometer to be operated on the lunar surface. A permanent magnetic field of 36 gammas and a gradient of 4×10^{-3} gammas/cm were measured at the Apollo 12 site. The magnitude of the gradient is interpreted to mean that the local magnetic body must be at least 0.2 km in size. The largest transient magnetic field measured in space at distances greater than a few Earth radii, approximately 96 gammas, was recorded on November 26, 1969, when the Moon was in the vicinity of the Earth magnetohydrodynamic bow shock.

Solar-Wind Spectrometer

Examination of the data obtained from the solar-wind spectrometer during the first 35 days of operation indicates that the solar plasma at the lunar surface is superficially indistinguishable from the solar plasma at some distance from the Moon, both when the Moon is ahead of and when the Moon is behind the plasma bow shock of the Earth. No detectable plasma appears to exist in the magnetospheric tail of the Earth or in the shadow of the Moon. Times of passage through the bow shock or through the magnetospheric-tail boundary, as indicated by the solar-wind spectrometer and by the lunar surface magnetometer, are in agreement when comparison of data has been possible. Highly variable spectra that may involve unexpected phenomena were observed on November 27, 1969, and at lunar sunrise; otherwise, observations have been as expected.

Suprathermal Ion Detector Experiment

Preliminary analysis of data from the suprathermal ion detector reveals the following features: a concentration of ions in the 18- to 50-amu/q (mass-per-unit-charge) range, the frequent appearance of ions in the 10- to several-hundred eV range, the sporadic appearance of 1- to 3-keV ions early in the lunar night, and the presence of solar-wind ions on the nightside of the Moon approximately 4 days before lunar sunrise. Energetic ion fluxes correlate well with the impact of the LM ascent stage into the lunar surface. There is a strong suggestion that the impact-released gases have been ionized and accelerated by the solar wind. High background count rates observed during the second lunar day may be indicative of large quantities of gas escaping impulsively from the LM descent-stage tanks.

Cold Cathode Gage

The ambient lunar atmospheric pressure is less than 8×10^{-9} torr. The gas cloud around an astronaut on the lunar surface exceeds the upper range of the gage (approximately 10^{-6} torr) when the gage is a distance of several meters from the astronaut; however, no perceptible residual contamination at the 10^{-8} torr lev remains around the gage for longer than a few minutes after the departure of the astronaut.

Multispectral Photography Experiment

The astronauts obtained a total of 142 black-and-white photographs, taken with blue-, green-, red-, and infrared-filtered cameras, that are suitable for color-difference analysis. Two existing image data-reduction methods are being expanded to produce images that display greatly enhanced three-color contrast. Two-color difference pictures have been produced, and the method is effective. The color enhancement of the Apollo 13 landing-site frame shows a lack of

color variation. The frame containing Lalande η exhibits color differences, the first such differences to be detected in high-resolution photography of the lunar surface, that can probably be attributed to compositional variations.

Lunar Surface Closeup Stereoscopic Photography

The almost complete absence of dust on the surfaces of rocks, clearly evident in several of the Apollo lunar surface stereoscopic camera photographs taken during the Apollo 12 mission and in several similar photographs taken during the Apollo 11 mission, is most remarkable. The absence of dust cannot be attributed to any cleansing effect of the exhaust gases from the descent engine because shadowing would have to be evident, and shadowing is not evident in any of the photographs. During the time required to form the many impact holes on the surface of the rock, a similar number of impacts on the neighboring powdery ground would have scattered much powder; and the average condition, if impacts were the only process, would have to be a substantial blanket of dust so that the loss from the dust blanket by impacts equaled, in the long run, the gain from material scattered from nearby impacts. The almost complete absence of dust on the rocks requires an explanation other than such an equilibrium. It must be assumed that there is either a general removal of dust from the lunar surface that dominates all other processes that distribute dust or that there is a dust-transportation process over the lunar surface that has a strong tendency for downhill flow and in which the particles are generally not lifted as high (i.e., more than 5 or 10 cm) as the surfaces of the rocks that exhibit the clean areas. The latter possibility is more in accord with other observations, such as the scarcity of trenches adjoining rocks whose distribution clearly indicates that they fell to their present positions. The trench and pileup that must have been common in the soft soil surrounding a fallen rock must thus be eradicated, yet at the same time, no significant amount of material must be deposited on the tops of the rocks. This is a strong indication for a process of surface creep that may be a major process in the long-term evolution of the lunar surface.

Experiments on Returned Materials

Returned Lunar Samples

Three categories of samples were collected on the lunar surface. The contingency sample was collected early in the first EVA period in the vicinity of the LM. The selected sample was collected, after deployment of the ALSEP, in the vicinity of the mounds and near Middle Crescent Crater; and a core tube was driven into the surface near the LM late in the first EVA period. The documented sample, collected along the geologic traverse during the second EVA period, included a variety of rock and soil samples, one single- and one double-core tube, the special environment and gas analysis samples, and several totebag samples that were brought back in a totebag. One sample was grapefruit size.

Igneous rocks and breccias were collected on this mission. The igneous rocks are basaltic and vary widely in both texture and modal composition. Most of the igneous rocks fit a fractional crystallization sequence that indicates either that they represent parts of a single intrusive sequence or that they are samples of a number of similar sequences.

The breccias and fines have a higher carbon content than the crystalline rocks, which is presumably largely due to contributions of meteoritic material and the solar wind. The level of indigenous organic material capable of volatilization or pyrolysis, or both, appears to be extremely low ($\leqslant$10 to 200 ppb).

The content of noble gas of solar-wind origin is less in the fines and breccias of the Apollo 12 rocks than in similar material from Tranquility Base. The breccias contain less solar-wind contribution than the fines, which indicates either that the breccias were formed from fines that were lower in solar-wind noble-gas content than the fines presently at the surface or that the gases escaped during the process of formation.

The presence of nuclides produced by cosmic rays shows that the rocks have been within 1 m of the lunar surface for 1 to 200 million years. The preliminary ^{40}K-^{40}Ar measurements on igneous rocks show that they crystallized 1.7 to 2.7 billion years ago.

The Apollo 12 breccias and fines are chemically similar and contain only half the titanium

content of the Apollo 11 fines. The composition of the crystalline rocks is distinct from that of the fines material in containing less nickel, potassium, rubidium, zirconium, uranium, and thorium. The Apollo 12 rocks contain less titanium, zirconium, potassium, and rubidium and contain more iron, magnesium, and nickel than the Apollo 11 samples. Systematic variations among the magnesium, nickel, and chromium contents occur in the crystalline rocks, but there are only small differences in the potassium and rubidium contents.

Comparison of the Apollo 12 samples from Oceanus Procellarum with the Apollo 11 samples from Mare Tranquillitatis shows that the chemistry at the two mare sites is clearly related. Both sites show the distinctive features of high concentrations of refractory elements and low contents of volatile elements; these two features most clearly distinguish lunar material from other material. This overall similarity indicates that the Apollo 11 sample composition is not unique. Taken in conjunction with the Surveyor 5 and 6 chemical data, this similarity is suggestive of a similar chemistry for the maria basin fill. Unlike the Tranquility Base samples, the element abundances in the fines of the Apollo 12 samples display a generally more fractionated character than the rocks. The fine material and the breccias are generally quite similar in composition and could not have formed directly from the large crystalline rock samples. The chemistry of the fine material is not uniform in the different maria.

The overall geochemical behavior of the lunar rocks is consistent with the patterns observed during fractional crystallization in terrestrial igneous rocks—a process that involves separation of olivine and pyroxene; depletion in the silicate melt of the elements such as nickel and chromium, which preferentially enter these mineral phases; and enrichment of the residual melt in such elements as barium and potassium, which are excluded from the early crystal fractions. The slight degree of enrichment of barium and potassium indicates an early stage of the fractional crystallization process. Whether these rocks form a related sequence or are a heterogeneous collection of similar origins cannot be answered from the chemical evidence.

The chemistry of the Apollo 12 samples does not resemble that of any known meteorite because nickel, in particular, is strikingly depleted. The Apollo 12 sample chemistry, however, has interesting similarities with the eucrites; and there now seems to be a fairly good possibility that rocks of chemistry similar to the eucritic meteorites are present on the Moon.

The Apollo 12 material is enriched in many elements by 1 to 2 orders of magnitude in comparison with estimates of cosmic abundances. The mare material is clearly strongly fractionated relative to most models of the composition of the primitive solar nebula.

The K-Ar age of the Apollo 12 rocks is most interesting scientifically. The ^{40}K-^{40}Ar age of these rocks reinforces the possibility recognized from the data obtained on the Apollo 11 rocks, that is, that the lunar maria are geologically very old. If the minimum ages established by the K-Ar method are indicative of the true age of the Apollo 12 rocks, then the mare material in Oceanus Procellarum at the Apollo 12 site is approximately 1 billion years younger than that at the Apollo 11 site. Although this K-Ar age is subject to various uncertainties, the younger age for the Apollo 12 material is consistent with geological observations. This large age difference indicates a prolonged period of mare filling.

Solar-Wind Composition Experiment

The Apollo 12 foil had the same dimensions, general makeup, and trapping properties as the Apollo 11 foil. Three small foil pieces were decontaminated by ultrasonic means. It was found that a piece of the foil that had been shielded from the solar wind had a ^4He concentration per unit area that was less than 1 percent of the concentrations found in the foil pieces exposed to the solar wind. There is good agreement between the concentrations and the $^4He/^3He$ ratios measured in two exposed foil pieces.

From the first two Apollo 12 foil pieces analyzed, the $^4HE/^3HE$ ratio is 2300 ± 200 for the Apollo 12 exposure period. This value is higher than the $^4He/^3He$ ratio obtained thus far from analyses of pieces of the Apollo 11 foil. Comparative analyses of pieces of foils from the two flights are being continued to confirm this differ-

ence. Actually, time variations in isotopic ratios in the solar wind can be expected, and the $^4He/^3He$ ratio has to be determined repeatedly to assess the range of occurring variations before an average for the present-day solar wind can be established. This average is of high astrophysical significance, because it can be compared with ancient $^4He/^3He$ ratios derived from solar-wind gases trapped in the lunar surface or in meteorites.

Preliminary results from the investigation of the returned Surveyor 3 components indicate a surprisingly low number (0 to 3) of high-velocity-impact pits of meteoritic origin. The majority of low-velocity-impact pits have been identified as resulting from the LM descent. The Surveyor 3 spacecraft was found to be covered with a light-brown coating that has been identified as lunar dust. Other investigations in progress are engineering (cold welding) investigations, radioactivity analysis of the Surveyor 3 TV camera, dust analysis, and alpha-particle measurements.

With permission, reprinted from Apollo 14: Preliminary Science Report, NASA SP-272, 1971.

Summary of Scientific Results

Philip K. Chapman, Anthony J. Calio,* and M. Gene Simmons**

The planned landing site for the Apollo 13 mission was in the Fra Mauro region, which is an area of prime scientific interest because it contains some of the most clearly exposed geological formations that are characteristic of the Fra Mauro Formation. The Fra Mauro Formation is an extensive geological unit that is distributed (in an approximately radially symmetric fashion around the Mare Imbrium) over much of the near side of the Moon. Stratigraphic data indicate that the Fra Mauro Formation is older than the Apollo 11 and 12 mare sites. The Fra Mauro Formation is thought to be part of the ejecta blanket that resulted from the excavation of the Imbrium Basin, which is the largest circular mare on the Moon. The Apollo 13 landing site thus offered an opportunity to sample material that had been shocked during one of the major cataclysmic events in the geological history of the Moon and thereby to determine the date of the event. Furthermore, because of the size of the Imbrium Basin, it was expected that some of the material had come from deep (tens of kilometers) within the original lunar crust. Thus, a landing at the Fra Mauro Formation, in principle, should offer an opportunity to sample the most extensive vertical section available of the primordial Moon.

After the Apollo 13 mission, which failed to achieve a lunar landing, the importance of the Fra Mauro landing site led to a decision to attempt a landing in the same area during the Apollo 14 mission. The final landing site was very close to that chosen for the Apollo 13 mission. The site was located in a broad, shallow valley between radial ridges of the Fra Mauro Formation and approximately 500 km from the edge of the Imbrium Basin. The major crater Copernicus lies 360 km to the north, and the bright ray material that emanates from Copernicus Crater covers much of the landing-site region. In the immediate landing-site area, an important feature is the young (Copernican age), very blocky Cone Crater, which is approximately 340 m in diameter and which penetrates the regolith on the ridge to the east of the landing site. Thus, Cone Crater would provide access to the excavated Fra Mauro Formation, despite the general overlying blanket of later deposits.

The lunar-surface experiments planned for the Apollo 14 mission differed somewhat from those of the Apollo 13 mission. The crew's traverse capability was improved by the addition of the modularized equipment transporter (MET), which is a light, hand-drawn cart that enabled the crew to transport tools and samples with greater ease. Two extravehicular activity (EVA) periods were planned, each of which was to last 4 hr 15 min. The principal objectives of the first EVA were to collect geological samples (including a contingency sample in case an early abort became necessary) and to deploy the Apollo lunar-surface experiments package (ALSEP). The second EVA was largely devoted to a geological sampling traverse toward Cone Crater, with several other experiments being conducted along the traverse.

This section summarizes the scientific results obtained to date from the Apollo 14 mission. It should be understood, however, that this is a preliminary report, and the results and, especially,

*NASA Manned Spacecraft Center.

the interpretations may change after further data collection and analysis.

Geology

The Apollo 14 crew traversed a smooth-terrain unit, a Fra Mauro ridge unit, and the ejecta blanket of Cone Crater. Descriptions, photography, and samples of the Cone Crater ejecta blanket were the major geological objectives of the Apollo 14 lunar-surface activity. It was anticipated that the Cone Crater event had resulted in the penetration of the lunar regolith and excavation of material from the Fra Mauro Formation. Samples returned from the Cone Crater ejecta blanket and the photography of boulders on the ejecta blanket indicate that the Fra Mauro Formation is comprised of breccias that contain abundant dark lithic clasts and less-abundant light clasts. Clasts of breccias within breccias may represent pre-Imbrian cratering in the Imbrium Basin region.

The Apollo 14 landing site is dotted with abundant craters that range in diameter from several hundred meters to the limit of resolution of the Hasselblad data cameras. Craters between 400 m and 1 km in diameter are more numerous and more subdued than craters on the maria; this distribution is consistent with the inferred greater age (relative to the maria) of the Fra Mauro Formation. Craters along the traverse range from the old and highly subdued craters that form the rolling topography in the smooth-terrain unit to the sharp 30-m-diameter crater on the Cone Crater ejecta blanket near station C'. Rock fragments greater than 2 to 3 cm in diameter are sparse in the immediate vicinity of the lunar module (LM) landing site, but the surface of the Cone Crater ejecta blanket is characterized by abundant rock fragments that measure up to several meters in diameter.

The albedo of the fine-grained material in the vicinity of the landing site ranges from 8.2 to 15 percent, with the lower albedo values typical of the smooth-terrain unit and the higher values typical of the Cone Crater ejecta blanket. The highest albedo values yet measured on the lunar surface are the values determined for the Cone Crater ejecta blanket in the vicinity of station C1 The albedo of the component parts of the fragmental rocks ranges from 9 to 36 percent.

Small-scale surface lineaments, although less well developed than at the Apollo 11 and 12 landing sites, are present at the Apollo 14 landing site. Two primary northwest and northeast trends and one secondary north trend agree well with the strongest trends observed at the Apollo 11 and 12 landing sites. The lineaments are less well developed on the Cone Crater ejecta blanket than on the smooth-terrain unit. Fillets of fine-grained material banked against rock fragments are common at the Apollo 14 landing site The variety of fillet geometries suggests that the fillets are probably formed by several different mechanisms.

The large number of boulders (most of which were probably ejected from Cone Crater) offered for the first time the opportunity to study textures and structures of lunar rocks at scales from tens of centimeters to a meter. All the boulders appear to be fragmental, with abundant clasts up to 10 cm across or larger. The clastic appearance of the rocks is somewhat similar to the appearance of ejecta deposits of impact origin on Earth. Planar features (some of which are systematic in their development) are visible in all the boulders. In some of the boulders, distinct lithologic layers are evident. The boulders show different degrees of rounding by lunar erosion; differences in shape are probably caused in part by internal fracture systems and possibly by differences in lithologies.

Approximately 43 kg of lunar samples were returned by the Apollo 14 crew, including 33 rocks that weigh more than 50 g each. Thirteen of the rock samples were sufficiently documented to determine lunar locations and orientations. The locations of most of the samples have been at least approximately determined.

Nearly all the returned samples are fragmental rocks. Some rocks are composed mostly of dark clasts and a lighter colored matrix; others consist of a mixture of light- and medium-gray clasts in a dark-gray matrix. Samples of both rock types were collected from widely separated points along the traverse.

Numerous similarities can be seen between the characteristics of the returned samples and of the boulders shown in the photographs. Closely spaced fractures (in some cases, two or more intersecting

fracture sets) are present in many of the returned rocks. Variations among the rocks suggest the possibility of considerable lateral or vertical variation within the Fra Mauro unit.

Returned Lunar Samples

Of the 43 kg of lunar material returned by the Apollo 14 crew, the Lunar Sample Preliminary Examination Team has examined portions of six soil samples and the surfaces of all rocks that weigh 1 g or more—approximately 150 rocks in all. Thin sections of 12 rocks were examined; optical spectroscopic analyses were performed on 16 samples; gamma-ray analyses for potassium, thorium, uranium, aluminum-26, sodium-22, and cobalt-56 were performed on 14 samples; and noble-gas analyses were performed on eight samples.

The ratio of fragmental rocks (including breccias and recrystallized clastic rocks) to igneous rocks (mostly basaltic) is approximately 9:1, which is much higher than the 1:1 and 1:9 ratios for the Apollo 11 and 12 rocks, respectively. The fragmental rocks returned from the Apollo 14 landing site also have larger and more abundant clasts and have a generally much more recrystallized matrix than the breccias from the previous missions. Three classifications of rocks from the Apollo 14 landing site were made for preliminary descriptive purposes:

(1) Rocks with predominantly lithic clasts in very friable matrices

(2) Rocks with predominantly light-colored and very abundant clasts in a matrix of moderate coherency

(3) Rocks with predominantly dark-colored clasts in a matrix of moderate to high coherency

The larger clasts are commonly clastic rocks themselves, but nonfragmental lithic clasts, which have been separated into six groups, are present. These groups are (1) clinopyroxene-plagioclase, (2) feldspar, (3) subophitic plagioclase-orthopyroxene, (4) olivine-glass, (5) granitic olivine, and (6) glass. Accessory minerals that are present include ilmenite, metallic iron, troilite, chromium spinel, ulvöspinel, metallic copper, armalcolite, zircon, apatite, and potassium-feldspar.

Only two homogeneous crystalline rocks that weigh more than 50 g were found. These rocks are basaltic, have typical igneous textures, and contain plagioclase, pyroxenes, olivine, and possibly opaques. Very-fine-grained granulitic-textured crystalline rocks were also found. Basaltic rock sample 14310, which weighs 3.4 kg, was the second largest rock returned. It is similar to terrestrial high-alumina basalts, but contains more highly calcic plagioclase and predominantly pigeonite pyroxenes. The occurrence of a solar flare on January 25, 1971, induced the formation of cobalt-56, which has been detected in the upper surface of the rock.

The soil samples collected at various locations vary in composition and grain size; and, within particular samples, a compositional variation exists among the grains of differing size. The finer grained portions have a higher glass content than the coarser grained portions. The soil collected from the immediate vicinity of Cone Crater has coarser grains than the soils from other locations and has a lower glass content and a higher content of fragmental-rock fragments. The core samples have thus far been studied only by X-ray radiography; however, definite layering and some grading of particle sizes have been observed.

Chemical analyses of the Apollo 14 material show it to be distinct from the material returned from the Apollo 11 and 12 landing sites in that lower concentrations of iron, titanium, manganese, chromium, and scandium and higher concentrations of silicon, aluminum, zirconium, rubidium, strontium, sodium, lithium, lanthanum, thorium, and uranium are present. The total carbon content of the soil samples falls within the carbon-content range found for material returned from the Apollo 11 and 12 sites. The rocks have carbon contents that range from 28 to 225 parts per million.

A noticeable difference in the noble-gas content of material from the Apollo 14 landing site was observed. The spallation-produced isotopes of these noble gases in four Apollo 14 rocks yielded exposure ages of 10 to 20 million yr, which is considerably lower than the 40- to 500-million-yr exposure ages of the rocks returned from previous missions. The solar-wind content of the fragmental rocks varies between the high values seen for the solar-wind content of fine material to essentially zero.

Soil Mechanics

Although the surface texture and appearance of the soil at the Apollo 14 landing site are similar to those at the Apollo 11 and 12 landing sites, a larger variation in the soil characteristics exists at depths of a few centimeters in both lateral and vertical directions than had previously been encountered. The walls of a trench that was dug by the commander collapsed at a shallower depth than had been predicted, evidently because of lessened soil cohesion. Calculations indicate that the soil cohesion value at the Apollo 14 trench site may be as small as 10 percent of the values calculated for soils at previous landing sites. The grain-size distributions of most of the soil samples returned from the Apollo 14 site are similar to the grain size distributions of soil samples from the Apollo 11 and 12 sites, with two significant exceptions: (1) a soil sample collected from near the rim of Cone Crater and (2) a soil sample from the bottom of the trench. At both of these locations, the soil was considerably coarse, with the median grain size as much as 10 times greater than at other Apollo 14 soil-sample locations.

The LM pilot was unable to push the Apollo simple penetrometer into the lunar surface near the ALSEP as deeply as had been expected. Similarly, the Apollo 14 crew encountered more difficulty in driving the core tubes than did the Apollo 12 crew. These results indicate that the soil at the Apollo 14 landing site is stronger with depth than had been previously supposed. The calculated bulk density of the soil in the lower half of the double core tube was significantly less than that determined for soil in the lower half of the Apollo 12 double core tube. Variations in the soil grain-size distribution or specific gravity (or both) may account for this difference in bulk density. The MET track observations confirm that the soil is less dense, more compressible, and weaker at the rims of small craters than in level intercrater regions.

Passive Seismic Experiment

Each lunar landing mission to date has included deployment of a passive seismometer. The Apollo 11 instrument produced useful data for approximately 1 month; however, the Apollo 12 instrument is still functioning satisfactorily. Deployment of the Apollo 14 passive seismometer as a part of the ALSEP thus represented a major step forward in the location and interpretation of lunar seismic events by providing a second instrument, one separated from the Apollo 12 passive seismometer by a baseline of 181 km.

The Apollo 14 seismometer has detected natural seismic events at more than twice the frequency recorded by the Apollo 12 instrument, and all seismic events that have been recorded at the Apollo 12 site have also been detected by the Apollo 14 instrument. It is hypothesized that the greater sensitivity at the Apollo 14 site is a result of the thick layer of unconsolidated material that blankets this region (the Fra Mauro Formation and the overlying regolith). This layer of unconsolidated material may provide a more efficient coupling of seismic energy with the lunar surface. The Apollo 14 instrument appears to be sufficiently sensitive to detect the impacts at any location on the Moon of meteoroids that have masses in excess of approximately 1 kg.

The detected natural events can be divided into two classes (on the basis of spectral characteristics and other characteristics of the signals) that correspond to meteoroid impacts and moonquakes. Moonquake occurrences correlate strongly with the time of perigee passage of the Moon in its orbit, which leads to the hypothesis that the release of internal strain, the origin of which is unknown, is triggered by tidal stresses. It is believed that not less than nine different locations are involved in the moonquakes that have been detected by both seismometers, although more than 80 percent of the total seismic energy detected has come from a single focal zone that is located perhaps 600 to 700 km from both stations and possibly at a considerable depth within the Moon. If the depth of the focal zone is confirmed by future data, fundamentally important information about the present state of the lunar interior will be made available.

A cumulative mass spectrum for meteoroids impacting the Moon has been tentatively constructed from the data. The cumulative mass spec-

trum indicates that the total meteoroid mass flux is a factor of 20 less than values from previous estimates. Approximately one meteoroid impact per year of kinetic energy equal to that of the SIVB impact is predicted. The Apollo 14 SIVB impact was detected by the Apollo 12 passive seismometer, and the LM ascent-stage impact was detected at both sites. These seismic events produced the characteristic, remarkably slow decay signals that had been previously detected by the Apollo 12 instrument; the signals persisted for several hours. The passive seismometer data have greatly increased the understanding of the lunar structure and of seismic energy transmission. A simple wave-propagation model of the entire Moon has now been derived; the model involves intensive scattering of waves in the outer shell of the Moon but very low energy absorption.

Crew activities produced detectable seismic signals for the Apollo 14 instrument throughout the EVA traverses. Venting gases from and thermoelastic stress relief within the LM caused the expected seismic signals, which are continuing. In view of the long-range detectability of lunar seismic events, it appears that a scattered network of passive seismometers can produce very valuable data. The deployment of a third passive seismometer at the Apollo 15 landing site will greatly increase the capability for accurately locating natural events that occur on the Moon.

Active Seismic Experiment

For the first time in the Apollo lunar-landing program, an active seismic experiment (ASE), in addition to the passive seismometer, was deployed on the lunar surface. The Apollo 14 crew deployed a string of three geophones across the lunar surface and used a thumper device with small explosive initiators to generate seismic signals. The active seismic instrument can also be used to monitor high-frequency natural seismic activity.

The data that were generated by the thumping operation indicate the existence of a surficial layer approximately 8.5 m thick at the ALSEP site. This layer, which exhibits a P-wave velocity of 104 m/sec, may be interpreted as the regolith in this area. The 8.5-m thickness of the regolith is in good agreement with the thickness estimated from geological studies of small craters. The seismic propagation velocity observed during the thumping operation is in remarkable agreement with the propagation velocity derived at the Apollo 12 landing site (108 m/sec), where the elapsed time between LM ascent-engine ignition and arrival of the generated seismic signal at the Apollo 12 passive seismometer was recorded.

Below the regolith at the Apollo 14 landing site is another layer, which exhibits a P-wave velocity of 299 m/sec. The thickness of this layer is estimated to be approximately 50 m. It is premature to speculate on the composition of this layer, but it is interesting to note that the estimated thickness of the layer is not in substantial disagreement with estimates of the thickness of the Fra Mauro Formation in this area. The relatively low compressional-wave velocities that have been measured in this experiment are evidence against the existence of substantial permafrost near the surface in the landing region.

The ASE also includes a rocket-grenade launcher that is capable of launching four grenades to impact at known times and at known distances (up to approximately 1500 m) from the seismometer. The rocket grenades will not be activated until data collection from the other ALSEP experiments is virtually complete.

Suprathermal Ion Detector Experiment (Lunar Ionosphere Detector)

The suprathermal ion detector experiment (SIDE), which was deployed as part of the Apollo 14 ALSEP, is essentially identical to the instrument deployed by the Apollo 12 crew. By correlation of data returned by the two SIDE instruments now operating on the Moon, discrimination is possible between moving ion clouds and temporal fluctuations of the overall ion distribution. For example, this discrimination capability enabled the interpretation of an ion event that was detected at both SIDE sites on March 19. This ion event was the passage of a large (approximately 130 km in diameter) ion cloud that moved westward at approximately 0.7 km/sec. The cloud was possibly associated with a relatively large

seismic event that was recorded by the Apollo 14 passive seismometer approximately 37 min earlier.

Ions in the 250- to 1000-eV energy range have been detected streaming down the magnetosheath of the Earth as the Moon entered the magnetospheric tail. In addition, approximately 2 days after sunrise, intermittent intense fluxes of 50- to 70-eV ions with masses in the 17- to 24-amu/unit-charge range were recorded. Energy and mass spectra were obtained during the venting of the oxygen atmosphere of the the LM cabin. After ascent-stage liftoff, the Apollo 14 LM ascent-engine exhaust was detected by the Apollo 12 SIDE, beginning 1 min after the vehicle passed the Apollo 12 landing site at a minimum slant range of 27 km. The Apollo 14 SIVB and LM ascent-stage impacts both produced useful signals at the Apollo 12 SIDE.

Cold-Cathode-Gage Experiment (Lunar Atmosphere Detector)

The cold-cathode-gage experiment, which is similar to the instrument deployed as a part of the Apollo 12 ALSEP, measures the concentration of neutral atoms (i.e., the density of the lunar atmosphere) in the vicinity of the ALSEP. During the lunar night, the concentration appears to be approximately 2×10^5 cm^{-3}, although transient increases by one to two orders of magnitude are fairly frequent and last from minutes to many hours. Some of these transient increases may be caused by venting or outgassing from the LM or from other equipment at the ALSEP site. As might be expected, the neutral-atom concentration rises rapidly at sunrise (two orders of magnitude in 2 min); the concentration then decays, over a period of approximately 50 hr, to a mean daytime level of less than 10^3 cm^{-3}. Numerous gas events have also been observed during the lunar day. The mean neutral-atom levels observed are thought still to be affected by outgassing from other ALSEP equipment, but the output of neutral atoms from this source should decrease with time in an identifiable way.

Charged-Particle Lunar Environment Experiment

The charged-particle lunar environment experiment (CPLEE) is designed to measure the ambient fluxes of charged particles, both electrons and ions, with energies in the range of 50 to 50 000 eV. One of the most stable features observed is the presence of low-energy electrons whenever the landing site is illuminated by the Sun. The variation in the low-energy-electron flux during the lunar eclipse of February 10 provided strong evidence that the electrons are photoelectrons liberated from the lunar surface. The solar-wind flux observed by the CPLEE has exhibited rapid time variations (periods of approximately 10 sec), both when the Moon is in interplanetary space and when it is immersed in the magnetospheric tail of the Earth. Passage of the Moon through the magnetopause and magnetospheric tail has produced some particularly interesting data, including rapidly fluctuating low-energy (50- to 200-eV) electrons, fluxes of medium-energy electrons lasting from a few minutes to tens of minutes, and electrons that have energy spectra remarkably similar to those observed above terrestrial auroras. Thus, auroral particles do appear to penetrate far into the magnetospheric tail, an observation that, if confirmed, contains important implications concerning the general topology of the magnetosphere.

After the Apollo 14 LM ascent-stage impact, two plasma clouds, which were separated in time by a few seconds, passed the CPLEE. If these plasma clouds were associated with the impact, they were traveling at approximately 1 km/sec and had diameters of 14 and 7 km.

Laser Ranging Retroreflector

Used in conjunction with the laser ranging retroreflector (LRRR) deployed during the Apollo 11 mission, the Apollo 14 LRRR array provides a capability for accurate monitoring of lunar librations in longitude. The LRRR scheduled for deployment during the Apollo 15 mission will complete the network by providing a long baseline separation of LRRR arrays in latitude as well. The deployment of a complete network is important not only because study of the lunar librations provides information about the internal structure of the Moon, but also because knowledge of lunar librations enables the errors that are introduced

by them to be eliminated when range measurements are needed in other studies (such as geophysics, general relativity, etc.).

Range measurements to the Apollo 14 LRRR were successfully accomplished on the day it was deployed by the crew. Range measurements taken after the LM liftoff indicate that the ascent-stage-engine burn caused no serious degradation of the LRRR reflective properties. Continued measurements over a period of years will be required before the full scientific value of this program is realized. Results to date indicate that the LRRR-array lifetime on the Moon will be long enough for all scientific objectives to be fulfilled.

Solar-Wind Composition Experiment

The solar-wind composition experiment was similar to the investigations conducted during the Apollo 11 and 12 missions. The aluminum foil was exposed to the solar wind at the Apollo 14 site for 21 hr. Five small samples from the upper part of the foil have been analyzed to date to determine noble-gas concentrations. The helium-4 flux observed is definitely lower than the flux detected during previous missions, but the helium-4/helium-3 ratio is similar to that obtained during the Apollo 12 mission and higher than that obtained during the Apollo 11 mission. Several isotopes of neon were detected, and their concentrations were measured. For the first time, the presence of argon in the solar wind has been detected. The accuracy of the isotopic ratios for argon will be improved when larger pieces of foil have been examined.

Lunar Portable Magnetometer

The Apollo 12 ALSEP included a magnetometer that measured the unexpectedly intense, steady magnetic field of 38 gammas at the ALSEP site. The Apollo 14 ALSEP does not include a stationary magnetometer; instead, a new instrument, the lunar portable magnetometer (LPM), was used during the second EVA to measure the magnetic field at two locations separated by 1.1 km. These measurements yielded values of 103 and 43 gammas, which indicated that the magnetic anomaly at the Apollo 12 landing site (181 km away) is by no means unique on the Moon. These results, together with the relatively high magnetic remanence found in returned lunar samples from all landing sites to date, give evidence that much of the lunar-surface material has been magnetized —perhaps even the entire crustal shell around the Moon. The LPM measurements enable a magnetic-field gradient of 54 gammas/km to be calculated, which is less than the upper limit of 133 gammas/km that was determined from measurements with the Apollo 12 magnetometer.

S-Band Transponder Experiment

The S-band transponder experiment used precision doppler tracking of the command and service module and the LM to provide detailed information about the near-side lunar gravity field. This technique was used with the Lunar Orbiter spacecraft and resulted in the discovery of the large gravity anomalies called mascons. The Apollo tracking system is capable of measuring line-of-sight velocity with a resolution of 0.65 m/sec.

Reduction of the data obtained during the Apollo 14 mission is in progress. Preliminary results show that the gravity-anomaly profile over the mascon in Mare Nectaris has a flat-topped appearance that is characteristic of a shallow plate-shaped mass anomaly. If other mascons exhibit this characteristic, it will be evidence that the mascons are near-surface features rather than deeply buried inhomogeneities. Results of the analysis of the crash orbit of the Apollo 14 LM ascent stage will be particularly interesting. Data were obtained at very low altitudes, which may enable small anomalies (a few kilometers in diameter) to be discerned.

Ancillary Experiments

In addition to the preceding experiments, several less formal investigations were conducted during the Apollo 14 mission. The details of these investigations will be published elsewhere.

The first such investigation concerned the light flashes that all crews since Apollo 11 have observed, when in the dark or when they closed their eyes, while in transit to and from the Moon and in lunar orbit. The Apollo 14 crew was briefed on

this phenomenon before the mission, and an observational schedule was suggested that was intended to test the various theories of the origin of the flashes. The most significant result obtained during the flight was the discovery that it is not necessary to be dark adapted to see the flashes. This observation indicates that Cerenkov radiation from energetic cosmic rays traversing the eyeball, which had been the most widely accepted explanation for the light flashes, probably does not cause all or most of the flashes because the light from this source is quite faint. Comparison with results of recent terrestrial experiments (in which human subjects were exposed to particle beams from accelerators) suggests that some of the flashes observed in space may be caused by direct ionization interactions of cosmic rays within the retina.

During transearth coast, the crew conducted a series of simple demonstrations with the objective of gathering design data for use in future scientific and engineering applications. These demonstrations were shown on television and were filmed, and samples were returned to Earth for analyses, which are presently in progress. The results to date are as follows.

Composite Casting

Eleven samples of various immiscible compositions were heated, mixed by shaking, and allowed to solidify by cooling in zero gravity. Laboratory analysis has not yet been completed, but X-ray examination of the samples indicates that more homogeneous mixing was achieved than is possible with similar samples on Earth. Further research in this area may result in the manufacture of new combinations of materials in the space environment (such as immiscible composites and supersaturated alloys) for structural, electronic, and other applications.

Electrophoretic Separation

Results to date indicate that electrophoresis (which is a technique commonly used on Earth for analysis or separation of chemical, especially organic, mixtures) provides a sharper separation in zero gravity because of a reduction of sedimentation and thermal convective mixing. This process may allow economical purification and separation of high-value biological materials in space.

Heat Flow and Convection

It was demonstrated that surface tension can produce Bénard cells in a liquid, independently of gravity-induced convection. Zone heating of liquid samples produced an unexpected cyclic heat-flow pattern that is now under study.

Liquid Transfer

The liquid-transfer demonstration clearly showed that suitable baffles inside a tank in zero gravity permit positive expulsion of liquid contents, taking advantage of the surface-tension properties of the liquid.

With permission, reprinted from Apollo 15: Preliminary Science Report, NASA SP-289, 1972.

2. Summary of Scientific Results

Joseph P. Allen[a]

The major scientific objectives of the Apollo 15 mission were to carry out extensive geological exploration, comprehensive sampling, and photographic documentation of the Apennine Front at Hadley Delta, Hadley Rille, and the mare plain; to emplace the Apollo lunar surface experiments package (ALSEP) near the landing site; and to perform a series of survey experiments with the scientific instrument module (SIM) equipment from lunar orbit and during transearth coast. The main scientific phase of the mission began when the Apollo 15 lunar module (LM) landed as planned on the mare plain at the eastern margin of the multiringed Imbrian basin just inside the arcuate Apennine mountain range. The scientific adventure by no means ended with command module (CM) splashdown in the Pacific Ocean, however; rather, the adventure continues as the returned samples and photographs are studied and as the data transmitted daily from the ALSEP and the orbiting subsatellite are analyzed. Only the initial results of these scientific investigations are contained in the Apollo 15 Preliminary Science Report. Whenever possible, data trends from each of the experiments are indicated in this summary, and tentative interpretations based on these trends are pointed out. It should be emphasized that, because the results are preliminary, the interpretations based on the results possibly will change as more data become available and the analyses continue.

GEOLOGIC INVESTIGATION

Because of the extended capability of the life-support equipment and the new mobility provided by the lunar roving vehicle (Rover), the Apollo 15 astronauts explored a much larger area than had been possible on previous missions. The three major geological objectives investigated during the traverses were the Apennine Front along Hadley Delta, Hadley Rille at locations west and southwest of the landing site, and the mare plain at various locations. Extensive information also was obtained about the secondary crater cluster near the Hadley Delta scarp and, although not visited, about the North Complex by photographing the south-facing exposures of this positive feature.

The Apennine Mountains, which rise above the Imbrian plain to heights of nearly 5 km, are thought to be fault blocks uplifted and segmented by the Imbrian impact. The frontal scarp of Hadley Delta, consequently, is interpreted as an exposed section of the pre-Imbrian lunar crust. For this reason, the frontal scarp of Hadley Delta was of highest priority for exploration during the mission. The mountain front was visited on both the first and second traverses; and it was sampled, photographed, and described extensively during this time. In general, the Apennine Mountains show gentle to moderate slopes and are sparsely cratered, with very subdued, rounded outlines. Large blocks are extremely scarce on the mountain flanks, which suggests a gravitationally transported, thick regolith cover on the lower portions of the mountain with a thinner cover of debris on the upper slopes. Sets of stark, sharply etched, parallel linear patterns, completely unexpected before the mission, appear on many of the mountain faces. These major lineaments may represent the expressions of sets of compositional layers or regional fractures showing through the regolith. However, the ambiguities introduced by the oblique lighting of the vertical exposures make difficult an unequivocal interpretation of these linear patterns. For example, the linear ribs clearly present in photographs of Silver Spur and vividly described in real time by the crew may be the expression of gently dipping massive rock layers, or they may reflect near-vertical geologic

[a]NASA Manned Spacecraft Center.

structure. The dark band observed by the crew near the base of Mt. Hadley is intermittently visible in both the surface photographs and the panoramic-camera photographs of the landing site. This feature is quite possibly the remnant of a high-lava mark left after the subsidence of the mare basalts following a partial lava drain-back or a cooling shrinkage during one episode of basin filling.

The rocks collected from the mountain front are mainly breccias; many are glass coated. The absence of clasts of older breccias within them distinguish the Apollo 15 rocks from the Apollo 14 samples. The samples from the mountain front are of three types: (1) friable breccias with clasts of nonmare-type basalt, of mare-type basalt, and of glass fragments; (2) coherent breccias with a vitreous matrix that contains clasts of nonmare-type basalt and granulated olivines and pyroxenes; and (3) well-lithified breccias with abundant granulated feldspathic clasts.

Hadley Rille, interpreted as one of the freshest sinuous rilles found on the Moon, was visited during the first and third traverses. The exposed rille walls, on both the near and far sides, were photographed in detail, and the rille rim and several massive outcrops on the near side were extensively sampled. The exposed bedrock strata visible in the photographs have thicknesses as great as 60 m, are distinctly layered, and exhibit varying surface textures and albedos. These characteristics are indicative of a number of individual flow units. All the layers are nearly horizontal. The talus deposits over the lower sections of the rille walls contain enormous blocks shed from the poorly jointed outcrops above. Unbroken blocks of the sizes seen (approaching 20 m in dimension) are uncommon on Earth. The detailed shape of the rille, the regolith cover of the rims, the lithologies of the outcrops and talus deposits, and the stratigraphy displayed in the rille walls are discussed in greater detail in sections 5 and 25.

The dark plain of the mare surface is generally smooth to gently undulating and hummocky. Rocks cover approximately 1 percent of the surface, except for the rougher ejecta blankets around the numerous subdued craters. The morphology of the craters in the surface indicates the mare age to be late Imbrian to early Eratosthenian, and the specific sampling sites visited by the crew span this age range. For example, a 15-m-diameter crater with a widespread glassy ejecta blanket probably represents the youngest surface feature (station 9) yet sampled on the Moon.

Initial study of the panoramic-camera photography of the landing site indicates a possible subdivision of the mare into four geological units characterized by differences in crater population and surface texture. The rocks collected from the mare and from the exposed outcrops at the rille edge consist mainly of basalts with abundant, coarse, yellow-green to brown pyroxene and olivine phyric basalts. In addition to the characteristics of the major geologic features, the optical properties of the surface materials, as recorded in the many photographs; a number of smaller scale features, such as the craters, fillets, and lineaments that are typical of the Hadley region; and the individual samples themselves are discussed in detail in section 5.

PRELIMINARY EXAMINATION OF LUNAR SAMPLES

A total of 77 kg of samples was returned from the Hadley area. These samples consist of rocks that weigh from 1 g to 9.5 kg, three core tubes, a deep-drill corestem, and a variety of soil samples taken from the two distinct selenologic regions at the Hadley site (the mare plain and the base of Hadley Delta). The Lunar Sample Preliminary Examination Team has made a macroscopic study of the more than 350 individual rock samples and additional petrographic and chemical studies of a selected few of these samples. The rocks from the mare plain fit into two categories: (1) extrusive and hypabyssal basalts and (2) glass-covered breccias. The rocks from the base of Hadley Delta exhibit a variety that ranges from breccias to possible metaigneous rocks.

The mare basalts appear to be fresh igneous rocks with textures that range from dense to scoriaceous. The chemical composition of these rocks is very similar to the compositions of those basalts returned from the Apollo 11 and 12 and Luna 16 mare sites. In particular, the mare basalts are high in iron, with a correspondingly high iron-oxide-to-magnesium-oxide ratio, and low in sodium oxide, in contrast to terrestrial basalts. Thin-section examinations of 13 of these basalts reveal four different textural types: (1) porphyritic-clinopyroxene basalt with 3- to 9-mm-long prisms, (2) porphyritic-clinopyroxene-basalt vitrophyre with 1- to 7-mm-long skeletal prisms, (3) porphyritic-olivine basalt, and (4) highly vesicular basalt.

A number of rock fragments from Spur Crater and

many of the clasts in breccias from the mountain front are basalts that are distinctly different from the mare basalts. Specific differences are: (1) The plagioclase-to-mafic-mineral ratio is 1, compared with a ratio of 0.5 for the mare basalts; (2) the pyroxene is light brown to tan with no zoning, compared with the cinnamon-brown, zoned pyroxene of the mare basalts; (3) the grain size of all mineral phases is less than 1 mm, compared with some grains as large as 1 cm in mare basalts; and (4) no vugs or vesicles are found in the nonmare basalts, in sharp contrast to the often highly vesiculated mare-basalt samples.

Many types of clastic and metamorphosed rocks were found along the traverse routes at the Hadley site, including several unique specimens that are discussed individually in section 6. The greatest variety of these rocks was concentrated along the base of Hadley Delta, where all the samples have undergone shock metamorphism and brecciation.

The soils returned from the Hadley-Apennine area are similar in most respects to soil samples returned from previous missions. The soil is composed primarily of the following particle types: (1) agglutinates plus brown-glass droplets, (2) basalt fragments of different textures, (3) mineral fragments, (4) microbreccias, and (5) glasses of varying color and angularity, including a particular component of green-glass spheres never before observed in lunar soils. The chemical composition of the soil samples, particularly from the mare regions, is distinctly different from the composition of the rocks from presumably the same locales. A linear correlation involving the iron oxide and aluminum oxide constituents of the soil and rocks from the Apollo sites suggests that the soil may be derived from a range of rock material, with the two end members being the iron-rich mare basalt and the aluminum-rich, iron-poor nonmare basalt.

A total of 4.6 kg of material was returned from the Hadley site in the form of core samples. A deep-drill corestem of six sections was driven to a depth of 2.4 m into the regolith near the landing site. All except part of the lowest section was returned completely full. Stereoscopic X-radiographs of this deep-drill core reveal significant variations in pebble concentration and in the density of the material along the core. These variations indicate the presence of more than 50 individual layers with thicknesses from 0.5 to 21 cm. In addition, three drive tubes with a maximum penetration as great as 70 cm were returned. As with the deep-drill core, X-radiographs of the lunar material within these tubes reveal distinct layering and a spectrum of soil textures and fragment sizes. The deep-drill core and the three drive cores all show that the lunar regolith has a substantial stratigraphic history.

The gamma-ray spectra of 19 samples have been measured to determine the concentrations of primordial radioactivity of potassium-40, uranium-238, and thorium-232 and of the cosmic-ray-induced radioactivity of aluminum-27 and sodium-22. In general, the radionuclide abundance is similar to that seen at previous sites. The potassium-to-uranium ratio of both the mare basalts and soils at the Hadley site is strikingly different from the ratio measured in terrestrial samples, which is further evidence in support of an earlier hypothesis concerning differences between Earth and Moon materials.

Concentrations of noble-gas isotopes measured in the samples from the Hadley-Apennine area are similar to the abundances previously measured in lunar materials. Variations in the argon-40 component of the soils are found at this site, as was the case for samples from previous sites, which suggests, for example, differing concentrations of argon-40 in the lunar atmosphere or differing argon-40 retention efficiencies of the soils. Concentrations of the spallation-produced isotopes, neon-21, krypton-80, and xenon-126, result in rock exposure ages in the range of 50 to 500 $\times 10^6$ yr, which is similar to the range of exposure ages measured in the Apollo 11 and 12 samples.

The total carbon content for several samples has been determined. As found for the materials from previous lunar sites, the total carbon content for the soils and breccias is higher than for the igneous samples. This continued systematic difference in carbon content seems to confirm the idea that much of the carbon in the lunar soil may originate in the solar wind.

SOIL-MECHANICS EXPERIMENT

The objectives of the soil-mechanics investigation are to examine the physical characteristics (such as particle sizes, shapes, and distributions) and the mechanical properties (such as particle density, strength, and compressibility) of the in situ lunar soil and to examine the variation of these parameters laterally over the areas traversed at the Hadley site. The longer duration of the extravehicular activities

and the correspondingly larger distances covered with the Rover, the variety of the geological units found at the Hadley-Apennine site, and the quantitative measurements provided by the self-recording penetrometer (a device carried for the first time on this mission) have resulted in a number of conclusions.

The lunar surface at the Hadley site is similar in color and texture to the surfaces at the previous landing sites. Although the variability of grain-size distribution of samples from the Apollo 15 site appears to be less than the variability found at the Apollo 12 and 14 sites, considerable variety exists, both with depth and laterally, in the soil properties of strength and compressibility. For example, the compressibility ranges from soft along the mountain front to much firmer near the rim of Hadley Rille. Evidence exists of downslope movement of surficial material on the walls of Hadley Rille; however, no evidence of deep-seated slope failures along the mountain front was found.

Soil densities derived from both the core-tube and the deep-drill corestem samples exhibit considerable variability that ranges from approximately 1.3 to 2.2 g/cm^3. The self-recording-penetrometer data indicate an in situ density of approximately 2.0 g/cm^3, a high soil strength, and a low soil compressibility. When coupled with additional data from the soil-mechanics trench dug near the ALSEP site, the penetrometer information can be used to estimate the cohesion and friction angle of the lunar soil. The values for both these parameters are higher than the values that resulted from experiments conducted during previous missions.

PASSIVE SEISMIC EXPERIMENT

The purpose of the passive seismic experiment is to study the lunar-surface vibrations, from which interpretations of the internal structure and physical state of the Moon can be determined. Sources of seismic energy may be internal (from moonquakes) or external (from impacts of both meteoroids and spent space hardware). In either case, a straightforward determination of the unambiguous source locations requires at least three vibration-sensing instruments monitoring the event of interest. The Apollo 15 passive-seismometer station represents the third of a network of seismometers now operating on the lunar surface, thus, the successful deployment of this instrument marked a vitally important step in the investigation of the Moon.

Seismic data accumulated over the first 45 days of operation have been analyzed, and the preliminary results are summarized as follows. Seismic evidence for a lunar crust and mantle has been found. The thickness of the crust is between 25 and 70 km in the region of the Apollo 12 and 14 landing sites. The velocity of compressional waves in the crustal material is between 6.0 and 7.5 km/sec, which is a range that spans the velocities expected for the feldspar-rich rocks found on the lunar surface. The transition the crustal material to the mantle material m gradual, starting at a depth of approximately 2 or rapid, with a sharp discontinuity at a depth o to 70 km. In either case, the compressional-wave velocity reaches 9 km/sec in the subcrustal mantle material, and the contrast in elastic properties of the rocks comprising these two major layers is at least as great as the contrast that exists between the materials comprising the crust and mantle units of the Earth.

The major part of the natural lunar seismic energy detected by the network is in the form of periodic moonquakes that occur near times of perigee and apogee and that originate from at least 10 separate locations. However, a single focal zone at a depth of approximately 800 km, with a dimension less than 10 km and with an epicenter approximately 600 km south-southwest of the Apollo 12 and 14 sites, accounts for 80 percent of the seismic energy detected. The release of seismic energy at these depths (which are slightly greater than any known earthquake sources) suggests that the lunar interior at these depths must be rigid enough to support appreciable stress. This fact, in turn, places strong constraints on realistic thermal models of the lunar interior.

In addition to the periodic moonquakes, episodes of frequent small moonquakes have been discovered. Individual events may occur as frequently as every 2 hr for periods lasting up to several days. The source of the moonquake swarms is at present unknown, but they may well result from continuing minor adjustments to stresses in the outer shell of the Moon.

The average rate of seismic-energy release within the Moon is far below that of the Earth. Thus, the outer crust and mantle of the Moon appear to be relatively cold and stable compared with that of the Earth, and significant internal convection currents causing lunar tectonism seem to be absent; however,

the discovery of moonquakes at great depths suggests the possibility of some very deep convective motion.

Seismic energy deposited at the lunar surface by an impacting meteoroid or manmade object is confined for a surprisingly long time in the near-source area by efficient scattering near the surface. Nevertheless, the energy slowly dissipates through interior propagation to more distant parts of the Moon, and, for this reason, all but the smallest of impact signals from all parts of the Moon are probably detected at the operating seismic stations.

LUNAR-SURFACE MAGNETOMETER EXPERIMENT

The Apollo 15 magnetometer, which is the third and all-important member of the magnetometer network now on the lunar surface, was deployed to study intrinsic remanent magnetic fields and to observe the global magnetic response of the Moon to large-scale solar and terrestrial magnetic fields imposed on it. Fundamental properties of the lunar interior, such as electrical conductivity, magnetic permeability, and temperature profile, can be calculated from these magnetic measurements. The measuring and understanding of these properties are obvious requirements for meaningful theoretical descriptions of the origin and evolution of the Moon.

The three fluxgate sensors of the Apollo 15 instrument show a steady magnetic field of approximately 5 γ at the Hadley site, which is considerably smaller than the 38-γ field measured at the Apollo 12 site and the 103- and 43-γ fields measured at the two locations at the Apollo 14 site. The bulk relative permeability of the Moon is calculated from the magnetometer data to be near unity. The electrical conductivity of the lunar interior is obtained from measurements of the response of the Moon to externally imposed, variable magnetic fields; and these measurements can be interpreted in terms of a spherically symmetric, three-layer model that has a thin outer crust (extending from the radius of the Moon to 0.95 the radius of the Moon) of very low conductivity, an intermediate layer (extending from 0.95 the radius of the Moon to 0.6 the radius of the Moon) with a conductivity of approximately 10^{-4} mho/m, and an inner core (of a diameter approximately 0.6 the radius of the Moon) of conductivity greater than 10^{-2} mho/m. In the case of an olivine Moon, these values correspond to a temperature profile of 440 K for the crustal layer, approximately 800 K for the intermediate layer, and greater than 1240 K for the central core.

SOLAR-WIND SPECTROMETER EXPERIMENT

Two identical solar-wind spectrometer experiments now operate 1100 km apart at the Apollo 12 and the Apollo 15 sites. Solar-wind plasma, magnetosphere plasma, and magnetopause crossings have been observed by both instruments, which show good internal agreement of observations; for example, simultaneous (within 15 sec) changes in proton densities and velocities are detected at both sites. As first measured with the Apollo 12 instrument, the solar plasma at the lunar surface is indistinguishable from the solar plasma some distance out from the surface (monitored by orbiting instruments), when the Moon is both ahead of and behind the magnetic bow shock of the Earth.

HEAT-FLOW EXPERIMENT

The heat-flow experiment is designed to make temperature and thermal-property measurements within the lunar subsurface in order to determine the rate at which heat is flowing out of the interior of the Moon. This heat loss is directly related to the rate of internal heat production and to the internal temperature profile; hence, the measurements result in information about the abundances of long-lived radioisotopes within the Moon and, in turn, result in an increased understanding of the thermal evolution of the body.

Emplacement of the first heat-flow experiment into the lunar surface was completed during the second period of extravehicular activity at the Hadley site. Initial measurements with this instrument show a subsurface temperature at 1.0 m below the surface of approximately 252.4 K at one probe site and 250.7 K at the other, which are temperatures that are approximately 35 K above the mean surface temperature. From 1.0 to 1.5 m below the surface, the temperature increases at the rate of 1.75 K/m. (±2 percent) In situ conductivity measurements result in values between 1.4×10^{-4} and 2.5×10^{-4} W/cm·K at depth and are found to be greater than the conductivity values of the surface regolith by a factor of 7 to 10.

which indicates that conductivity increases with depth as well

Preliminary analysis of these results indicates that the heat flow from below the Hadley-Apennine site is 3.3×10^{-6} W/cm^2 (±15 percent). This value is approximately one-half the average heat flow of the Earth. By assuming that this value is an accurate representation of the heat flow at the Hadley site (while realizing that data accumulation over a number of lunations will be required to establish this accuracy) and by further assuming that this value is representative of the moonwide heat-flow value, then consideration of the Moon as a sphere with uniform internal heat generation results in a picture of the Moon as a far more radioactive body than had been previously suspected, and a far more radioactive body than suggested by the ordinary chondrites and the type 1 carbonaceous chondrites that have been used to construct the standard models of the Earth and the Moon to date.

SUPRATHERMAL ION DETECTOR EXPERIMENT (LUNAR-IONOSPHERE DETECTOR)

The suprathermal ion detector experiment deployed at the Apollo 15 site is identical, except for the ion mass ranges covered, to the instruments operating at the Apollo 12 and 14 sites, and the Apollo 15 experiment is the third member of this ion-monitoring network. In the first days of operation, a number of energy and mass spectra of positive ions were measured, primarily from the gas clouds vented by the spacecraft and other mission-associated equipment. At lunar lift-off, for example, a marked decrease in the magnetosheath-ion fluxes was observed. This decrease lasted approximately 8 min and is attributed to either a change in the ion flow direction (because of the exhaust-gas cloud) or to energy loss of the ions passing through the exhaust-gas cloud. Some hours later, the ascent stage impacted the lunar surface nearly 100 km west-northwest of the Hadley site, and the ions that resulted from the impact-generated cloud were monitored.

Multiple-site observations of ion events that possibly correlate with seismic events of an impact character (recorded at the seismic stations) have resulted in information about the apparent motions of the ion clouds. Typical travel velocities have been calculated to be approximately 80 m/sec. Numbers of single-site ion events have been detected, some with ions in the mass range of 16 to 20 amu/Q, which corresponds quite possibly to the release of water vapor from deep below the lunar surface. The 500- to 1000-eV ions streaming along the magnetosheath have been observed simultaneously by all three suprathermal ion detectors. This ion flux is strongly peaked in the down-Sun direction, which is a fact established by the different look directions of the individual instruments.

COLD CATHODE GAGE EXPERIMENT (LUNAR-ATMOSPHERE DETECTOR)

The cold cathode gage experiment that was deployed at the Hadley site is similar to the instruments at the Apollo 12 and 14 sites and is intended to measure the density of the tenuous lunar atmosphere at the lunar surface. This anticipated thin concentration of gases is a result of the solar wind, the possible continued release of molecules from the lunar interior through the lunar crust, and certain venting and outgassing from the LM descent stage and other gear left on the Moon. The contamination, however, should decrease with time in a recognizable way.

As might be expected from cold cathode gage experiment results from the earlier missions, the gas concentrations observed during the lunar days appear to be overwhelmingly a result of contaminants released by the LM and associated equipment. However, during the lunar nights, the observed concentrations, which are typically less than 2×10^5 particles/cm^3, are lower even than the concentrations expected from the neon component of the solar wind alone. This fact suggests that the contaminant gases from spacecraft equipment remain adsorbed at the low nighttime temperatures and that the lunar surface itself is not saturated with neon, but rather absorbs this gas much more readily than releases it. Except for mission-associated phenomena, no easily recognizable correlations have been found between transient gas events, as seen on this instrument, and the response of the suprathermal ion detector or of the solar-wind spectrometer.

LASER RANGING RETROREFLECTOR

The third and largest U.S. laser ranging retroreflector was delivered to the lunar surface and deployed at

the Hadley site approximately 40 m from the ALSEP site. Successful range measurements to this 300-corner-cube array were made shortly after the LM lifted off several days later, and subsequent measurements indicate that no degradation of the reflective properties of the unit resulted from dust being kicked up during the extravehicular activities or by ascent-engine residue. The better signal-to-noise ratio available with this larger retroreflector will enable more frequent ranging measurements to be made and will enable measurements to be carried out by telescopes of smaller aperture than heretofore possible. Additionally, this third array now provides the important long north-south base-line separation with the Apollo 11 and the Apollo 14 retroreflectors. For the accumulation of data important to the planned astronomical, geophysical, and general relativity experiments, range measurements will be required over a period of years.

SOLAR-WIND COMPOSITION EXPERIMENT

The solar-wind composition experiment, which is similar to the experiments conducted during the Apollo 11, 12, and 14 missions, was deployed at the end of the first extravehicular activity and exposed to the solar wind for a period of 41 hr, nearly twice the exposure time obtained during the previous mission. Initial samples of the aluminum foil have been analyzed, and isotopes of helium and neon have been detected. The helium flux during the Apollo 15 exposure is nearly four times that detected during the Apollo 14 exposure; yet, interestingly enough, the relative abundance of helium and neon and the relative isotopic abundances of these elements are very similar to the earlier abundances. A positive correlation has been found between the general level of solar activity and the helium-4 to helium-3 ratio, a correlation first suggested perhaps by the helium-to-hydrogen ratio measurements of the Explorer 34 spacecraft.

GAMMA-RAY SPECTROMETER EXPERIMENT

The gamma-ray spectrometer experiment is designed to measure, from lunar orbit, the gamma-ray activity of the lunar-surface materials. The gamma-ray flux from the lunar surface is expected to contain two components, one resulting from naturally occurring radioisotopes (primarily of potassium, uranium, and thorium) and the other resulting from cosmic-ray-induced interactions at the lunar surface. The gamma-ray intensity from the naturally occurring radionuclides is a sensitive function of the degree of chemical differentiation undergone by the Moon; and, thus, the measured intensity relates directly to the origin and evolution of the planet.

Analysis of the very preliminary data printout (unfortunately the only data available for analysis before the preparation of this document) shows a strong contrast in gamma-ray count rates over different regions of the Moon. Specifically, the regions of highest activity are the western maria, followed by Mare Tranquillitatis and Mare Serenitatis. Considerably lower activity is found in the highlands of the far side, with the eastern portion containing nearly an order of magnitude less gamma-ray activity than that found in Oceanus Procellarum and Mare Imbrium. The preliminary data show intensity peaks that correspond to the characteristic energies of the isotopes of iron, aluminum, uranium, potassium, and thorium; however, more data than available in the preliminary printout are required to verify this identification unambiguously.

X-RAY FLUORESCENCE EXPERIMENT

The purpose of this experiment is to map the principal elemental constitutents of the upper layer of the lunar surface by measuring the fluorescent X-rays produced by the interaction of solar X-rays with the surface material. Secondarily, the experiment is used to observe X-radiation from astronomical objects during the transearth-coast phase of the mission. The X-ray detector assembly consists of three proportional counters, two X-ray filters (and associated collimators), temperature monitors, and the necessary support electronics. Inflight energy, resolution, and efficiency calibrations are made with X-ray sources carried with the instrument.

Preliminary analysis of the initial data from this experiment is very exciting. In general, the suspected major compositional differences between the two fundamental lunar features, the maria and the highlands, are confirmed by the X-ray data, and more subtle compositional differences within both the maria and the highlands are strongly suggested. For

example, the aluminum-to-silicon intensity ratio is highest over the terrae, lowest over the maria, and intermediate over the rim areas of the maria. The extremes for this ratio vary from 0.58 to 1.37, with a tendency for the value to increase from the western mare to the highlands of the eastern limb. Furthermore, a striking correlation exists between the aluminum-to-silicon intensity ratio and the values of surface albedo along the groundtrack surveyed by the X-ray experiment.

Although the data from the X-ray fluorescence experiment are still in the initial stages of analysis, a number of tentative conclusions may be drawn about the fundamental properties of the lunar surface. The sharply varying aluminum-to-silicon ratio confirms that the maria and the highlands are indeed chemically different, and the distinguishing albedo differences between these major features must be, in part, the signature of this difference. The anorthositic component of the returned lunar samples is certainly related to the high aluminum content measured in the highland regions, and the correspondingly low aluminum content of the returned mare basalts is consistent with the low measurement values over the maria. The experimental X-ray data, thus, further support the theory that the Moon, shortly after formation, developed a differentiated, aluminum-rich crust. The sharp change in the aluminum-to-silicon intensity ratio between the highland and mare areas places stringent limitations on the amount of horizontal displacement of the aluminum-rich material after the mare flooding. Indications definitely exist in the more gradual data trends that the circular maria have a lower aluminum content than the irregular maria; and within particular maria (for example, Crisium and Serenitatis), the centers have a lower aluminum content than the edges. Finally, the large ejecta blankets, such as the Fra Mauro formation, seem to be chemically different from the unmantled highlands.

During the transearth coast, X-ray data were obtained from three discrete X-ray sources and from four locations dominated by the diffuse X-ray flux. The count rate from two of the sources, Sco X-1 and Cyg X-1, did show significant changes in intensity of approximately 10 percent over time periods of several minutes; however, a final analysis of Apollo data is required to rule out completely the possibility that changes in spacecraft attitude during the counting periods might account for the counting-rate variations.

ALPHA-PARTICLE SPECTROMETER EXPERIMENT

The alpha-particle spectrometer experiment consists of 10 totally depleted silicon surface-barrier solid-state detectors of 3 cm^2 area each that are particularly sensitive to alpha particles in the energy range between 5 and 12 MeV. The experiment is designed to map, from lunar orbit, possible uranium and thorium concentration differences across the surface by measuring the alpha-particle emissions from the two gaseous daughter products of uranium and thorium, radon-222 and radon-220, respectively. Because trace quantities of these radioactive gases would be included in any outgassing of, for example, water or carbon dioxide from the lunar interior, detection of radon also would provide a sensitive probe of remanent volcanic activity or of local release of common volatiles.

Preliminary analysis of the alpha-particle data indicates that the alpha-particle activity of the Moon is at most equal to the observed count rate of 0.004 count/cm^2-sec-sr (±1 percent) in the energy band from 4.7 to 9.1 MeV. No significant difference in this count rate was observed between the dark and sunlit sides of the Moon. This measured alpha-particle activity is considerably less than was anticipated before the mission. For example, if the uranium and thorium concentrations measured in the samples returned from the Apollo 11 and 12 sites are typical moonwide values, then the alpha-particle counting rate that results from radon emission is at least a factor of 60 lower than the rate predicted by radon-diffusion models. Complete analysis of all the Apollo 15 alpha-particle data should result in another order of magnitude more sensitivity than reported here for the detection of alpha-particle emission from lunar sources.

LUNAR ORBITAL MASS SPECTROMETER EXPERIMENT

The lunar orbital mass spectrometer is designed to measure the composition and density of neutral gas molecules along the flight path of the command-service module (CSM) in order to better understand the origin of the lunar atmosphere and the related transport processes in planetary exospheres in general. The instrument was mounted in the SIM on a bistem boom and was operated from the CM. The

preliminary results indicate that a large number of gas molecules of many species exist near the spacecraft in lunar orbit; none, however, have an obvious lunar origin or a sufficient intensity to be detected above the background of molecules from all sources. The gas cloud apparently moves with the vehicle because the measured density is essentially independent of the angle of attack of the spectrometer entrance plenum. The spacecraft is thought to be the source of most of this cloud, even though the intensity of the apparent contamination is a strong function of the orbital parameters. For example, during the transearth coast, the detected amplitudes of all species of molecules were reduced by a factor of 5 to 10 from the amplitudes measured in lunar orbit.

S-BAND TRANSPONDER EXPERIMENT

During the last near-side pass before transearth injection, a small scientific spacecraft was launched into lunar orbit from the SIM bay of the service module. This subsatellite is instrumented to measure plasma and energetic-particle fluxes and vector magnetic fields and is equipped with an S-band transponder to enable precision tracking of the spacecraft. The S-band transponder experiment uses the precise doppler-tracking data of this currently orbiting satellite and the tracking data of the CSM and of the LM taken during the mission to provide detailed information about the gravitational field of the near side of the Moon. The data consist of the minute changes in the spacecraft speed, as measured by the Earth-based radio tracking system (which has a resolution of 0.65 mm/sec). The initial data indicate that the subsatellite is operating normally and, because the periapsis altitudes are following closely the predicted altitudes, suggest that the spacecraft will have an orbital lifetime of at least the planned one year. The subsatellite transponder experiment should provide data for a detailed gravity map for the area between ±95° longitude and ±30° latitude.

Analyses of the low-altitude CSM data have resulted in new gravity profiles of the Serenitatis and Crisium mascons; these results are in good agreement with the Apollo 14 data analysis and strongly suggest that the mascons are near-surface features with a mass distribution per unit area of approximately 500 kg/cm^2. The Apennine Mountains show a local gravity high of 85 mgal but have undergone partial isostatic compensation, and the Marius Hills likewise have a gravity high of 62 mgal.

SUBSATELLITE MEASUREMENTS OF PLASMAS AND SOLAR PARTICLES

The main objectives of the subsatellite plasma and particles experiment are to monitor the various plasma regimes in which the Moon moves, to determine how the Moon interacts with the fields and plasmas within these regimes, and to investigate certain features of the structure and dynamics of the Earth magnetosphere. The experiment consists of two solid-state particle-detector telescopes that are sensitive to electrons with energies as large as approximately 320 keV and to protons with energies as large as approximately 4 MeV, and of five electrostatic-analyzer assemblies that are sensitive to electrons in the energy range from 0.5 to 15 keV.

Detailed observations have been made of particle fluxes around the Moon as the Moon moves through interplanetary space, through the magnetosphere, and through the bow shock of the Earth. Analysis of these preliminary data leads to several tentative conclusions. Solar electrons were measured at the subsatellite following a large solar flare on September 1, 1971. In the energy range of 6 to 300 keV, the electron spectrum is reproduced by the power-law equation $dJ/dE = (3 \times 10^3) E^{-1.5}$ electrons/cm^2-sr-sec-keV. Additionally, an electron flux of 20 electrons/cm^2-sr-sec of energy from 25 to 30 keV is found to move predominantly in a sunward direction for several days while the Moon is upstream from the Earth. It is not known as yet whether this flux is of solar or terrestrial origin. Finally, a distinct shadow in the fast-electron component of the solar wind is formed by the Moon. For the case when the interplanetary magnetic field is nearly alined along the solar-wind flow, this electron shadow corresponds closely to the optical shadow behind the Moon. However, for the case when the interplanetary magnetic field alines more perpendicular to the solar-wind flow, the fast-electron shadow region broadens to a diameter much greater than the lunar diameter and becomes extremely complex.

SUBSATELLITE MAGNETOMETER EXPERIMENT

The major objectives of the subsatellite magnetometer experiment are to extend the measurements of the permanent and induced components of the lunar magnetic field by systematically mapping the remanent magnetic field of the Moon and by measuring

the magnetic effects of the interactions between cislunar plasmas and the lunar field. Initial data from the two subsatellite fluxgate sensors indicate that detailed mapping of the remanent magnetization, although complex, is entirely feasible with the present experiment. For example, preliminary analysis shows a fine structure in the magnetic field associated with the large craters Hertzsprung, Korolev, Gagarin, Milne, Mare Smythii I, and, in particular, Van de Graaff, which produces a 1-γ variation in the field measured by the subsatellite passing overhead. Furthermore, magnetic fields induced within the Moon by externally imposed interplanetary magnetic fields are detectable at the subsatellite orbit. Estimated variations of lunar conductivity as a function of latitude and longitude will be possible from magnetometer data. Finally, the data show that the plasma void that forms behind the Moon when it is in the solar wind extends probably to the lunar surface, and the flow of the solar wind is itself rather strongly disturbed near the limbs of the Moon.

BISTATIC-RADAR INVESTIGATION

The bistatic-radar experiment uses the S-band and the very high frequency (VHF) communication systems in the CSM to transmit toward the portion of the Moon that scatters the strongest echoes to Earth-based receivers. The echoes are received from an area approximately 10 km in diameter that moves across the lunar sufrace near the orbiting CSM. The characteristics of these echoes are compared to those of the directly transmitted signals in order to derive information about such lunar crustal properties as the dielectric constant, density, surface roughness, and average slope.

The VHF data obtained during this mission have approximately one order of magnitude higher signal-to-noise ratio than previously obtained, and the effects of the bulk electrical properties and slope statistics of the surface are clearly present in the data. The S-band data show the areas surveyed during the mission to be similar to those regions sampled at latitudes farther south during the Apollo 14 mission. Distinct variations in the slopes of the lunar terrain in the centimeter-to-meter range exist, and some areas contain an unusually heavy population of centimeter-size rock fragments. The bistatic-radar data are currently being combined with the CSM ephemeris data to correlate these results with orbital photography and corresponding geological interpretations in order to better distinguish between adjacent and subjacent geological units.

APOLLO WINDOW METEOROID EXPERIMENT

The Apollo window meteoroid experiment involves a careful study of the CM heat-shield window surfaces for pits caused by meteoroid impacts. These tiny craters, when identified, are further examined to obtain information on crater morphology and possible meteoroid residence. So far, 10 possible impacts of 50 μm diameter and larger have been identified in the windows of the Apollo 7, 8, 9, 10, 12, 13, and 14 spacecraft. These findings correspond to a meteoroid flux below that expected from theoretical calculations but are in good agreement with the flux value derived by an examination of the Surveyor shroud returned by the Apollo 12 mission.

ANCILLARY EXPERIMENTS

The numerous orbital-science and orbital-photography experiments conducted during the mission are discussed in a separate section (sec. 25) of this report. The individual experiments will not be discussed in this summary of scientific results.

Several other experiments and tests were conducted during the Apollo 15 mission that will not be discussed in detail in this report. The reader is particularly referred to the documents of the NASA Medical Research and Operations Directorate for the biomedical evaluation of the mission-related medical experiments (i.e., bone-mineral measurement, total-body gamma-ray spectrometry, and visual light-flash-phenomena experiment) and to the Apollo 15 Mission Report for a discussion of the many engineering tests conducted during the mission. Four additional experiments not reported elsewhere are discussed in the following paragraphs.

An ultraviolet (uv) photography experiment[1] was conducted primarily to obtain imagery of the Earth and Moon for comparison with similar photographs of Mars and Venus. Both of these latter planets show mysterious behavior in the uv-wavelength region; in particular, Mars exhibits a peculiar lack of detail in

[1] Private communication with T. Owen, Earth and Space Sciences Dept., State University of New York, October 1971.

this radiation region, and, in contrast, Venus exhibits major detail only in this part of the photographically accessible spectrum. Comparison of uv data for the Earth with corresponding data from the less well understood planets should aid in the understanding of these planets. The experiment equipment consisted of a Hasselblad camera fitted with a 105-mm uv lens, two filters with pass bands centered at 3400 and 3750 $\times 10^{-10}$ m, and a uv cutoff filter to obtain comparison photographs in visible light. A special uv-transmitting window is used in the CM. Photographs were taken of both the Earth and the Moon from a variety of distances throughout the mission. Preliminary examination of these photographs indicates that the surface of the Earth is still clearly visible down to 3400 $\times 10^{-10}$ m, and no large-scale changes in the detection of aerosols occur between 3750 and 3400 $\times 10^{-10}$ m. This experiment will be extended on subsequent missions in wavelength coverage and in imagery of the Earth over more land mass.

A lunar dust detector experiment[2] has been deployed as a part of the ALSEP central station on all of the manned lunar landings to date. The experiment has three purposes: (1) to measure the accumulation of dust from the LM ascent or from slow accretion processes, (2) to measure the lunar-surface brightness temperature from reflected infrared radiation, and (3) to measure long-term high-energy-proton radiation damage to solar cells in the lunar-surface environment.

The Apollo 15 dust detector experiment is mounted on top of the ALSEP central station sunshield, with the vertically mounted infrared temperature sensor facing west. Three solar cells (2 ohm-cm, N-on-P, 1- by 2-cm corner dart cells) are mounted on a horizontal Kovar metal mounting plate. For the purpose of determining radiation damage, one cell is bare; the other two cells each have 6-mil cover glasses attached. Solar-cell temperature is monitored by a thermistor on the cell mounting plate.

Results from the dust detectors deployed so far have shown (1) no measurable dust accumulation as a result of the LM ascent during the Apollo 11, 12, 14, and 15 missions; (2) a rapid surface-temperature drop of approximately 185 K during the August 6, 1971, lunar eclipse; and (3) no long-term radiation damage thus far to any of the dust detectors. However, a difference of approximately 8.5 percent in the amount of solar-radiation energy received at the lunar surface has been measured by the Apollo 12 dust detector; this variation is a result of the change of the Moon from lunar aphelion to perihelion.

During the time between spacecraft touchdown and the powerdown of the primary guidance, navigation, and control system of the LM, nearly 19 min of data[3] were obtained from the pulsed integrating pendulous accelerometers, which are instruments normally used with the inertial measurement unit for operational guidance and navigation of the LM. In this case, however, these data provide a direct measurement of the acceleration of gravity (g) at the Hadley site. The mean of the accelerometer data results in a value for g of 162 706 mgal, with a standard deviation of 12 mgal. If a spherical mass distribution is assumed for the Moon, this same quantity can be calculated from the familiar equation $g = GM/R^2$, where GM is the product of the universal gravitational constant and the lunar mass, and R is the lunar radius at the Hadley site, as determined from a combination of doppler-shift tracking of the spacecraft around the lunar center of mass and optical tracking of the landing site from the orbiting spacecraft. If the values $GM = 4902.78$ km^3/sec^2 and $R = 1735.64$ km are used in the equation, then a value for g of 162 752 mgal is obtained, which is in good agreement with the directly measured value of acceleration at the Hadley site.

During the final minutes of the third extravehicular activity, a short demonstration experiment was conducted. A heavy object (a 1.32-kg aluminum geological hammer) and a light object (a 0.03-kg falcon feather) were released simultaneously from approximately the same height (approximately 1.6 m) and were allowed to fall to the surface. Within the accuracy of the simultaneous release, the objects were observed to undergo the same acceleration and strike the lunar surface simultaneously, which was a result predicted by well-established theory, but a result nonetheless reassuring considering both the number of viewers that witnessed the experiment and the fact that the homeward journey was based critically on the validity of the particular theory being tested.

[2]Private communication with James R. Bates, NASA Manned Spacecraft Center, October 1971.

[3]Private communication with R.L. Nance, NASA Manned Spacecraft Center, October 1971.

With permission, reprinted from Apollo 16: Preliminary Science Report, NASA SP-315, 1972.

3. Summary of Scientific Results

Anthony W. England[a]

The exploration of the Descartes region by the Apollo 16 crewmen provides the best look at lunar highlands. As a result, many theories concerning lunar geologic structure and processes will be improved greatly. Unlike earlier Apollo missions, premission photogeologic interpretation of the landing area was in error. Far from diminishing the mission, however, discovery of the unexpected enhanced the scientific impact. The surprise at Descartes was the state of the rocks, not their composition. That is, breccias rather than volcanics were dominant. The compositions are near those of anorthositic gabbro and gabbroic anorthosite. This composition is consistent with the hypothesis that highlands are an early differentiate of a primitive lunar mantle. Aluminum-to-silicon (Al/Si) and magnesium-to-silicon (Mg/Si) ratios, as determined by the orbiting X-ray fluorescence experiment, indicate that the Descartes area differs compositionally from previous Apollo sites and that its chemical characteristics are representative of large regions of the lunar highlands. Thus, lessons learned at Descartes will support new generalizations potentially applicable to much of the lunar surface.

Although the dramatic phase of the Apollo 16 mission ended with the splashdown, the scientific adventure will continue for many years. This report presents the first fruits of the mission; and, inevitably, a number of its conclusions will be short lived. Few disciplines are as dynamic as the lunar sciences.

GEOLOGY EXPERIMENT

The two morphologically distinct units at the Apollo 16 site are the highland plains-forming unit, called the Cayley Formation, and the ridges and mountains of the Descartes highlands. The Cayley Formation was sampled extensively at nine stations spread over 7 km in a north-south direction. The goal was to construct a vertical section and lateral variation of the Cayley Formation based on samples from the rims of various-sized craters. Before the mission, the Cayley Formation was thought to be a sequence of lava flows interbedded with ancient regoliths. Instead, the Cayley Formation is composed dominantly of four types of heterogeneous fragmental rocks or breccias. Although the relative proportions of the four breccias varied over the traverse area, no basic differences in the rock assemblages were seen. Based on the sample distribution and Apollo 16 panoramic camera photographs of South Ray and Baby Ray Craters, the only stratification exhibited by the Cayley Formation is a crude, horizontal layering of alternating light and dark breccia units.

The Cayley Formation appears to be a thick (at least 200 m, possibly more than 300 m), crudely stratified debris unit, the components of which are derived from plutonic anorthosites and feldspathic gabbros and from metamorphic rocks of similar composition. The Cayley Formation has an elemental composition similar to that observed over large regions of the lunar highlands by the orbital X-ray experiments of the Apollo 15 and 16 missions (ref. 3-1 and sec. 19 of this report). The observed textures and structures of the breccias resemble those of impact breccias. The observed textures and structures of the breccias do not resemble those of volcanic rocks, nor do the plutonic or metamorphic source rocks of the breccias have the textures or compositions of terrestrial or previously sampled lunar volcanic rock.

Stations 4 and 5 on the northern flank of Stone Mountain were selected as sampling locales for the Descartes highlands. However, the documented samples and the soils collected on Stone Mountain are indistinguishable from those collected on the Cayley Plains. This similarity may be caused by a heavy mantle of ejecta from South Ray Crater. If so, the cores taken at station 4 and the rake samples collected from the inner slopes of small craters at stations 4 and 5 may contain unique Descartes highland material. However, the upper layers of the Descartes highlands may be lithologically identical to the bulk of the Cayley Formation.

[a]NASA Manned Spacecraft Center; now with U.S. Geological Survey.

Although caution dictates that a volcanic origin for the Cayley Formation not be eliminated as a possibility, all the evidence of the preliminary analysis argues against it. Several alternate hypotheses are suggested by the geology team and by various authors of the photogeologic sections contained in this report. The dominant theme is deposition of debris from combinations of the ejecta from the Imbrium and Nectaris Basins.

PRELIMINARY SAMPLE ANALYSIS

A preliminary characterization of the rocks and soils returned from the Apollo 16 site has substantiated most of the widely held inferences that the lunar terra is commonly underlain by plagioclase-rich or anorthositic rocks. The texturally complex rocks exhibit cataclastic textures with intergrowths of shock-induced glass, of devitrified glass, or of relict preexisting clasts that indicate a multistage history. In contrast to the complexity of the fabric, the chemical characteristics of the rocks and soils were comparatively simple. The dominant chemical feature is the high abundance of aluminum and calcium. In a number of rocks, the absolute and relative abundances of these elements approach those of pure calcic plagioclase. Each Apollo 16 rock falls into one of three groups, based on its alumina (Al_2O_3) content. Rocks in the first group are nearly pure plagioclase and can be called cataclastic anorthosites. The second group, characterized by Al_2O_3 contents of between 26 and 29 percent, consists of several breccias, two crystalline rocks, and all soil samples. The third group, all metamorphosed igneous rocks, has Al_2O_3 contents below 26 percent. Many samples in this third group are similar chemically to the basalts that are rich in potassium, rare-Earth elements, and phosphorus (KREEP) found at the Apollo 12, 14, and 15 sites. With a few qualifications, the chemistry of the Apollo 16 rocks can be accounted for by a rather simple geologic model consisting of a large igneous complex that is variably enriched in plagioclase and is intruded by a trace-element-rich liquid after its formation.

In addition to normal rock and soil samples, many special samples were collected. A few of the investigations based on these samples will be the study of small-scale stratigraphy in the regolith; the study of the interaction of solar wind and cosmic rays with the lunar surface; and the study of special processes such as erosion by micrometeorites, mobility of volatile elements, and darkening with time of freshly exposed lunar soil. Essentially all planned special samples were collected.

Lunar samples exhibit two components of remanent magnetism: (1) a "hard" component that can be erased only at temperatures near the Curie point of the sample and (2) a "soft" component, most of which can be lost by degaussing in a weak magnetic field. The implication of the hard component is that the sample cooled from a temperature above 850° C in the presence of a strong magnetic field. This hypothesis places stringent requirements on the early history of the Moon. Either the Moon once generated an internal field, or the Moon was once located near a strong external field. The soft component might reflect the lunar magnetic environment from the time the rock cooled to the present. An alternate hypothesis was that the soft component was largely an artifact of handling by the astronauts and of traveling in magnetically dirty spacecraft. The results of several tests, one involving a controlled sample sent on the Apollo 16 mission, indicate that much of the soft remanent magnetism in lunar samples was acquired from magnetic fields within the spacecraft.

SOIL MECHANICS EXPERIMENT

The mechanical properties of lunar regolith are governed by the distribution of grain sizes, by the angularity of the grains, and by packing density or porosity. The distribution of grain sizes for the soil samples from Descartes lies near the coarse boundary of a composite distribution composed of soils from all previous sites. Statistical analysis of bootprint depths indicates that the near-surface porosities at the Apollo 16 landing site were slightly higher than the average of those of the four previous missions, 45 percent compared with 43.3 percent. The average porosity on crater rims was 46.1 percent. The resistance to penetration measured with the self-recording penetrometer is highly variable on both regional and local (points as close as 1 m) scales. As a result, no general conclusion is possible concerning whether the soil on slopes is weaker or stronger than that on flat areas. However, the pattern of resistance as a function of depth correlates well with the stratigraphy observed in X-radiographs of the core tubes, and stratigraphic profiles of the lunar surface have been determined for the first time. The density and density

distribution in the 2.6-m core at Descartes differed significantly from those in the deep core taken at Hadley. The Apollo 16 densities were lower (by approximately 0.2 g/cm^3). The densities increased smoothly with depth. The density of the Apollo 15 deep core varied erratically with depth. The soils at the two locations must have experienced distinctly different histories.

PASSIVE SEISMIC EXPERIMENT

The activation of the Apollo 16 passive seismometer resulted in a four-station seismic network on the near side of the Moon. Because of a fortuitous impedance match between the Apollo 16 seismometer, the local regolith, and the underlying lunar crust, the seismic station at Descartes is an order of magnitude more sensitive than stations on the maria (Apollo 12 and 15) and five times more sensitive than the station at the Fra Mauro site (Apollo 14). The Apollo 16 seismometer is detecting moonquakes at the rate of 10 000/yr. One quake was the result of the largest meteoroid impact yet recorded. The event occurred 145 km north of the Apollo 14 station. The resulting seismic waves were well recorded at all four stations of the seismic network. Analysis of this single event has greatly improved the concept of the structure beneath the lunar crust. Measured seismic velocities are close to those expected for gabbroic anorthosites, which predominate in the highlands of the Descartes site. Analysis of data from the lunar orbiting X-ray fluorescence experiment suggests that this rock type is representative of the lunar highlands on a global scale. The combination of velocity information with laboratory data from returned samples suggests the following conclusions.

(1) The lunar crust in the highlands is approximately 60 km thick.

(2) The lunar crust in the highlands consists primarily of gabbroic and anorthositic material.

(3) The maria were formed by the excavation of the initial crust by meteoroid impacts and subsequent flooding by basaltic material.

(4) From seismic evidence, the basalt layer in the southeastern portion of Oceanus Procellarum may be 25 km thick, which is comparable to the thickness inferred for mascon maria.

The seismic velocities below the crust and to the maximum depth that was investigated (approximately 120 km) are roughly equivalent to velocities observed in the upper mantle of the Earth.

Although the Moon is seismically active, the total energy released is many orders of magnitude below that of the Earth. All seismic sources of internal origin are, apparently, discrete and are located below the lunar crust. Twenty-two source locations have been identified. In the five source regions in which focal depths have been determined, all quakes occurred in the range from 800 to 1000 km. The occurrence of these quakes correlates with maximum lunar tides. Either they represent a release of tidal energy or the tides trigger the release of internally generated stresses.

A new model for the meteoroid flux that is consistent with the seismically observed frequency of meteoroid impacts is proposed. This new flux estimate is from one to three orders of magnitude lower than models derived from photographic measurements of luminous trails striking the atmosphere of the Earth.

ACTIVE SEISMIC EXPERIMENT

The objective of the Apollo 16 active seismic experiment was to determine the local structure of the regolith and of the shallow lunar crust. The near-surface, compressional-wave velocity at the Descartes site was 114 m/sec; this value can be compared to 104, 108, and 92 m/sec at the Apollo 12, 14, and 15 sites, respectively. A refracting horizon at 12.2 m may be the base of the regolith. The velocity below this depth was 250 m/sec. A crustal velocity of 250 m/sec is comparable to the 299-m/sec velocity observed in the Fra Mauro breccias and is incompatible with the velocity of 800 m/sec or more expected for competent lava flows. This finding, along with the prevalence of breccias in the returned samples, argues that the Cayley Formation is composed of low-velocity brecciated material and impact-derived debris. Preliminary analysis indicates that this brecciated zone is more than 70 m thick.

LUNAR SURFACE MAGNETOMETER EXPERIMENT

The activation of the Apollo 16 lunar surface magnetometer resulted in a network of three active magnetic observatories on the lunar surface. The objective of this network is to observe the global response of the Moon to variations in the magnetic field carried

by the solar wind. Variations in the solar wind magnetic field generate eddy currents within the Moon. These currents create a magnetic field that suppresses the change in the total field observed on the surface of the Moon, and the charac' of this suppression can be related to the electrical conductivity of the lunar interior. Because this electrical conductivity is dominantly a function of temperature, these temporal studies of the magnetic field can be used to infer temperature distributions for the lunar interior. For the model of a peridotite Moon, preliminary analysis indicated a temperature profile that rises sharply to 850° to 1050° K at a depth of approximately 90 km, then increases gradually to 1200° to 1500° K at approximately 1000 km, and may be above 1500° K at greater depths. Greater detail as well as a comparison of the response of the Moon under maria (Apollo 12), under the edge of a large basin (Apollo 15), and under highlands (Apollo 16) should be possible as more data are received.

LUNAR PORTABLE MAGNETOMETER

The lunar portable magnetometer was used at four sites along the traverse route. These measurements and the magnetic measurement by the lunar surface magnetometer yield a total of five spatial measurements at Descartes. The remanent magnetic field was the largest yet observed on the Moon. Its strength was 180 gammas near Spook Crater, 125 gammas on Stone Mountain, and 313 gammas at station 13 near North Ray Crater. Not only were the field strengths higher at Descartes than at other Apollo sites, the gradients were significantly greater: 370 gammas/km maximum observed at Descartes compared to less than 133 gammas/km (resolution limit of the lunar surface magnetometer) at the Apollo 12 and 15 sites and a measured 54 gammas/km at the Apollo 14 site.

FAR UV CAMERA/SPECTROGRAPH EXPERIMENT

The far UV camera/spectrograph was operated from the lunar surface for the first time on Apollo 16. The instrument was sensitive to light in the 50- to 160-nm range and "blind" to ordinary visible light. The experiment was completely successful in that the experiment team obtained 178 photographic frames of far UV data on the airglow and polar auroral zones of the Earth and the geocorona; on over 550 stars, nebulae, or galaxies; and on the nearest external galaxy, the Large Magellanic Cloud. The detailed analysis will take many months. However, the lack of quantitative results in time for this preliminary report cannot dull the accomplishment of emplacement of the first lunar astronomical observatory.

SOLAR WIND COMPOSITION EXPERIMENT

The solar wind composition experiment was designed to measure with high precision the abundances and isotopic compositions of noble gases in the solar wind. It has been demonstrated that both elemental abundances and isotopic ratios varied with time. The Apollo 16 experiment hardware is composed of aluminum and platinum foils that were exposed on the lunar surface for periods of several hours to trap various components of the solar wind. The relative elemental and isotopic abundances of helium and neon measured for the Apollo 12, 14, 15, and 16 exposure times are quite similar and differ from those obtained during the Apollo 11 mission. Particularly noteworthy is the absence of any indication of electromagnetic separation effects that might have been expected at Descartes because of the relatively strong local magnetic field.

COSMIC RAY EXPERIMENT

The relative abundances and energy spectra of heavy solar and cosmic rays convey a wealth of information about the Sun and other galactic particle sources and about the acceleration and propagation of the particles. In particular, the lowest energy range from a few million electron volts per nuclear mass unit (MeV/nucleon) down to 1 keV/nucleon (a solar wind energy) is largely unexplored. The cosmic ray experiment contained a variety of detectors designed to examine this energy range. The precise nature of the experiment is dependent on the radiation environment during the mission. If the Sun were relatively quiescent, the objective was to determine whether the low-energy nuclei are primarily solar or galactic in origin. If the Sun were active, the objective was to study the composition of solar cosmic rays and the solar acceleration processes. Because a solar flare occurred during the mission, the latter objective was served.

A preliminary analysis indicates that the spectrum for iron-group cosmic rays is given by an $(\text{energy})^{-3}$ relation in the energy range from 30 MeV/nucleon

down to 0.04 MeV/nucleon and flattens to $(energy)^{-1}$ from 0.04 to 0.01 MeV/nucleon. The higher energy relation is identical to previous results for the 0.16- to 100-MeV/nucleon range. A striking aspect is the relative enrichment of iron at the lower energies during a solar flare. This enrichment is estimated to be a factor of approximately 450 greater than the photospheric value. Although the precise value of the enhancement might be in question, the data do strongly suggest that the heavier particles are appreciably more abundant in the solar flares than in the surface of the Sun. At higher energies, however, the abundances were normal for galactic cosmic rays.

Mica and feldspar were included as detectors in addition to Lexan and glass. By comparing the sensitivities of the natural materials against those of the Lexan, a calibration will be established applicable to studies of particle tracks in lunar samples.

GEGENSCHEIN EXPERIMENT

Gegenschein is the phenomenon of sky brightness in the antisolar region as viewed from the Earth. A possible mechanism for this brightness might be backscatter of light by particles lingering in the Moulton region, a libration point of the Earth-Sun system. The objective of the experiment was to use fast film and long exposures in lunar orbit to map the luminance of the gegenschein. If it were a result of particles in the Moulton region, the gegenschein would be displaced 15° from the antisolar point as viewed from the Moon. Preliminary analysis indicates that the gegenschein as viewed from the Moon appears at the antisolar point and, thus, argues against the Moulton region as a source.

GAMMA RAY SPECTROMETER EXPERIMENT

The gamma ray spectrometer is one of the three instruments in a geochemical remote-sensing package flown for the second and last time on Apollo 16. The spectrometer is sensitive primarily to gamma rays produced by natural radioactivity in the lunar soil. The secondary emissions induced by galactic cosmic rays constitute a second source. The experiment team's initial conclusions, based upon the natural rather than the induced radiation, are as follows.

(1) In agreement with the Apollo 15 results, the western maria are generally more radioactive than other regions of the Moon.

(2) Detailed structure exists within the high-radioactivity regions. The high observed in the Fra Mauro area is at approximately the same level as those seen around Aristarchus and south of Archimedes on the Apollo 15 mission. Those levels are comparable to that observed in the soil returned on the Apollo 14 mission.

(3) Radioactivity is lower and more variable in the eastern maria.

(4) The lunar highlands are regions of low radioactivity. The Descartes area appears to have undergone some admixing of radioactive material.

A second objective of the experiment was to map the anisotropies in the galactic cosmic ray fluxes by using the spacecraft as an occulting disk. Although the analysis has just begun, a preliminary look at the data indicates that discrete, celestial gamma ray sources were, in fact, detected.

X-RAY FLUORESCENCE EXPERIMENT

The X-ray spectrometer was the second of the three geochemical remote sensors flown on the Apollo 16 mission. By analyzing the characteristic secondary X-ray emissions produced by solar X-rays impinging on the lunar surface, maps of the Al/Si and Mg/Si ratios can be constructed for the sunlit portions of the Moon. Preliminary conclusions reaffirmed the validity of the Apollo 15 result and extended the interpretation over new areas. Most important, and the objective of all the orbiting geochemical sensors, is the ability to compare the compositions of returned lunar samples to those of remote areas of the Moon. The Al_2O_3 concentration in the Descartes soil inferred from the X-ray measurements (26 to 27 percent) was confirmed by the preliminary analysis of the returned soil (26.5 percent). Descartes soils appear to be similar to those of the eastern limb and the far-side highlands. Remotely sensed Al/Si and Mg/Si ratios for Descartes are 0.67 ± 0.11 and 0.19 ± 0.05 and those of the eastern limb and the far-side highlands are approximately 0.60 to 0.71 and 0.16 to 0.21, respectively. Generally, the highlands are high in aluminum and low in magne-

sium, whereas the reverse is true for the maria. However, there are exceptions, such as Ptolemaeus, where both magnesium and aluminum are high. The emerging picture of the lunar highlands is one of an ancient lunar crust composed of materials with a composition varying between anorthositic gabbro and gabbroic anorthosite.

During transearth coast, the Apollo 16 X-ray spectrometer was used to observe the temporal behavior of two pulsating X-ray stars, Scorpius (Sco X-1) and Cygnus (Cyg X-1). Sco X-1 may be characterized by quiet periods and by periods of up to a day in length in which 10- to 30-percent changes in X-ray intensity occur in a few minutes. These changes in intensity are concurrent but not necessarily simultaneous with changes in optical and radio intensity. Cyg X-1 can double in intensity within a day or so. The increase occurs in all three energy ranges, 1 to 3 keV, 3 keV, and 7 keV. The time variability of the two sources does not appear to be similar at time scales of several seconds to 2 hr.

ALPHA PARTICLE SPECTROMETER EXPERIMENT

The third of the remote geochemical sensors, the alpha particle spectrometer, is sensitive to radioactive radon gas emanating from the lunar surface. Because radon itself is a product of the decay of uranium and thorium, mapping the concentration of radon gas is tantamount to mapping regions of high radioactivity. This capability is especially significant where the radioactivity lies below the lunar surface yet might be detected by its escape through fissures. Results from a still incomplete analysis of Apollo 15 data indicate that the region including Aristarchus, Schröter's Valley, and Cobra Head is an area of relatively high radon emanation. Because of the limited spatial resolution of the technique, only general source regions can be designated. Another area that has been identified is the broad region from west of Mare Crisium to the Van de Graaff-Oriov area. A real-time analysis of Apollo 16 data indicates a strong high centered on Mare Fecunditatis.

MASS SPECTROMETER EXPERIMENT

The objectives of the lunar orbital mass spectrometer carried on both the Apollo 15 and 16 missions were to detect a lunar atmosphere and to search for active lunar volcanism. The instrument covered the mass range from 12 to 67 amu and was sensitive to partial pressures as low as 1×10^{-14} torr. Unfortunately, contamination from the spacecraft tends to mask the lower concentrations of the atmospheric gases. However, shortly after the plane change and rendezvous of the Apollo 16 command and service module (CSM) and lunar module (LM), the contamination levels as recorded by the mass spectrometer were the lowest yet observed in lunar orbit. During this period, data were obtained on the partial pressure of neon-20. A preliminary analysis indicates that, at the orbital altitude of 100 km, the concentration of neon-20 is 8.3 (± 5) $\times 10^3$ atoms/cm^3. Because 100 km is 4 scale heights above the lunar surface at night, the nighttime surface concentration would be 4.5 (± 3) $\times 10^5$ atoms/cm^3. This value is approximately a factor of 3 less than previous estimates.

SUBSATELLITE MEASUREMENTS OF PLASMA AND ENERGETIC PARTICLES

Along with a magnetometer and an S-band tracking function, plasma and energetic particle detectors were carried on the subsatellite launched into lunar orbit by the Apollo 16 CSM. These detectors were included to observe the various plasmas in which the Moon moves, to study the interaction of the Moon with the solar wind plasma, and to observe certain features of the structure and dynamics of the magnetosphere of the Earth. The detectors were sensitive to electrons in the 0.5- to 15- and 20- to 300-keV ranges and to protons in the 40-keV to 2-MeV range.

A first look at the data indicates that the sensors experienced passage of a hydromagnetic shock wave in the solar wind. The magnetometer recorded a sharp discontinuity at the time of electron onset, and, 10 min later, Earth-based magnetometers observed a similar disturbance. This magnitude corresponds to a shock-propagation velocity that is greater than 400 km/sec. The rise times for the proton and electron increases yield profiles for the region of shock discontinuity. The inferred thickness of this region is approximately 4000 km. Solar wind electrons maintained abnormally high temperatures for 12 hr following the shock.

At the time of the Apollo 16 subsatellite launch, the Moon was just entering the geomagnetic tail. During the time the Moon was in the magnetotail, the subsatellite returned 22 orbits of data on the high-latitude magnetotail and nine orbits of data on the plasma sheet. From these data, the fluxes and the energy spectra were constructed. A continuing feature of the plasma sheet is a large flux of energetic protons. Plasma-sheet protons greater than 40 keV often have flux an order of magnitude greater than electrons of the same energy. This difference is in contrast to the high-latitude magnetotail, in which the electron and proton fluxes are approximately the same.

S-BAND TRANSPONDER EXPERIMENT

S-band transponder tracking of the LM-CSM and of the Apollo subsatellites is used to map the lunar gravitational field. The degree of correlation between the gravity map and physiographic features such as craters or mountains is used to infer density contrasts or to detect buried structures.

Unlike spacecraft on previous Apollo missions, the Apollo 16 LM-CSM did not traverse any known completely visible mascons. However, several features do appear in the new gravity profiles. An extensive gravity that does not correlate well with the surface feature was found in the area of the Riphaeus Mountains. The mountains may be associated with a much larger subsurface structure. The Nubium and Fra Mauro areas are gravity lows; and the Descartes area, although essentially a gravity high, is flanked on the east by a definite negative anomaly. Although the detailed analysis continues, several generalizations may be made.

(1) All unfilled craters are negative anomalies.

(2) All filled "craters" and circular seas with diameters greater than approximately 200 km are positive anomalies, or mascons. The smallest is Grimaldi at 150 km; an exception is the unique Sinus Iridum.

(3) Filled craters less than 200 km in diameter are negative anomalies; an example is Ptolemaeus.

(4) Part of the central highlands appears as a positive anomaly.

(5) Mountain ranges observed so far have positive anomalies (Marius, Apennines); whether isostatic equilibrium has been achieved is undetermined.

(6) Gravitational anomalies associated with the ring structure of Orientale are verified independently; the suggestion of ring structure for some of the other mascons is consistent with the additional data.

(7) There are definable features not correlated with obvious surface features of geologic blocks, and these features presumably represent subsurface characteristics.

BISTATIC RADAR EXPERIMENT

The bistatic radar experiment uses CSM S-band and very-high-frequency (VHF) transmissions to probe the electromagnetic and structural properties of the lunar surface. Radio signals from the CSM are reflected by an approximately 10-km-diameter area of the Moon and recorded by radiotelescopes on the Earth. As the CSM orbits, the reflecting spot scans the lunar disk. The characteristics of that reflecting area can be interpreted in terms of dielectric properties, block sizes, and slopes.

Initial conclusions are that the oblique geometry scattering properties of the lunar surface are wavelength dependent in the decimeter to meter range. At a given wavelength, the scattering law is highly dependent on local topography. Furthermore, there are systematic differences in the average scattering properties of mare and highland units. Generally, reflections off maria at the S-band wavelength are uniform and consistent with a lunar surface dielectric constant of 3.1 ± 0.1. The VHF reflection is not as easily interpreted. Evidently, the maria are not simple half-space reflectors at VHF wavelengths. Both the Apennines and the central highlands show a reduction in the dielectric constant from 3.1 for S-band to 2.8 for VHF. Typical root-mean-square slopes for the highlands are 5° to 7° for both S-band and VHF wavelengths, whereas, for the maria, the data are consistent with 2° to 4° slopes at S-band but only to 1° or 2° at VHF wavelengths.

ADDITIONAL EXPERIMENTS

A continuation of an experiment flown on the Apollo 15 mission, the ultraviolet photography of the Earth and Moon, was to allow comparison of ultraviolet and color photographs under equivalent circumstances. The results will be applied to telescopic observations of the planets. A 70-mm camera was

used with four filters having passbands between 255 and 400 nm. A survey of the returned images of the Moon shows little of the loss of detail at the shorter wavelengths observed in telescopic ultraviolet photographs of Mars. The photographs of the Earth show the expected diminution of detail with shorter wavelengths caused by the increased opacity of the atmosphere of the Earth at ultraviolet wavelengths.

The Apollo command module heat shield windows are studied to obtain information about the flux of meteoroids with masses of 1×10^{-7} g down to the detection limit of 1×10^{-11} g for optical studies or of meteoroids of much lower masses for anticipated electron microscope studies. The resulting estimate of mass flux is in good agreement with Surveyor III data and with models generated from near-Earth studies.

Three biomedical experiments were flown on the Apollo 16 mission. These were the biostack, an experiment to study the biological effects of galactic cosmic radiation; the Apollo light flash moving emulsion detector, to study the subjective observation of faint light flashes seen by nearly all Apollo crewmen while in space; and the microbial ecology evaluation device, to study the response of various microbes to a space environment. All three experiments were executed successfully. Although a few qualitative results are included in this report, the detailed analyses have just begun.

An impressive array of cameras was flown in the Apollo 16 CSM. These ranged from the highly sophisticated 24-in. panoramic camera and the 3-in. mapping camera with its laser altimeter and star-field recorder to the 16-, 35-, and 70-mm cameras used for astronomical photography, earthshine lunar photography, and solar corona photography and to support crew observations of lunar features. The more than two dozen sections in this report resulting from this Apollo 16 photography are ample testimony of its value. These sections, as well as summaries of Earth-based radar and infrared studies, are included as valid products of the Apollo 16 effort.

REFERENCE

3-1. Adler, I.; Trombka, J.; Gerard, J.; Schmadebeck, R.; et al.: X-Ray Fluorescence Experiment. Sec. 17 of Apollo 15 Preliminary Science Report. NASA SP-289, 1972.

With permission, reprinted from Apollo 17: Preliminary Science Report, NASA SP-330, 1973.

3. Summary of Scientific Results

Robert A. Parker[a]

The first phase of man's active exploration of the Moon came to an end with the Apollo 17 mission. Many questions about lunar science have been answered during the intensive activity of the last decade, but many more remain to be answered. Some of the unanswered questions will be answered in the future from data already returned but as yet not fully analyzed, and some will have to wait for data yet to be returned from instruments already in place on the lunar surface. Still other questions must await further exploration.

The basic objective of the Apollo 17 mission was to sample basin rim highland material and adjacent mare material and investigate the geological evolutionary relationship between these two major units. In addition to achieving this general geological objective, it has also been possible to measure directly the thermal neutron flux in the regolith, to explore geophysically the subsurface structure of the valley floor, to determine the constituents of the lunar atmosphere and observe their variations during the lunar day and night, and to explore even more of the lunar surface remotely from orbit.

These initial results and others will someday be combined into a coherent picture of the evolution of the Moon that will reflect more light on both the abstract and specific problems of the evolution and current conditions of the Earth and other planets. That will be the true legacy of the Apollo Program—not just the sometimes apparently fragmented preliminary results seen here.

LUNAR FIELD GEOLOGY

Premission photogeology of the Taurus-Littrow valley and its environs led to the expectation of sampling five different major stratigraphic units: the light mantle, the dark mantle, the subfloor, the Sculptured Hills, and the massifs.

The light mantle unit was sampled at stations 2, 2A, and 3 and at two lunar roving vehicle (LRV) sampling stops. Preliminary indications from these samples are that the light mantle is primarily fine-grained debris that includes cataclasites and breccias similar to those attributed to the South Massif and different from the regolith elsewhere on the valley floor. These observations are in agreement with the hypothesis that the light mantle unit resulted from a slide down the northern face of the South Massif that occurred approximately 10^8 yr ago as indicated by crater counts. The slide perhaps was caused by the impact of some secondary ejecta at the top of the South Massif.

The dark mantle unit remains one of the enigmas of the Apollo 17 mission. Photogeological observations of the subdued appearance of the larger craters and the general paucity of craters on the valley floor had led to the expectation of a "mantling" unit which covered the valley floor sometime after most of the regolith formation had taken place and which was perhaps Copernican in age. Because of dark areas in depressions in the surrounding highlands, the mantling unit was expected to have also covered at least part of the highlands. No such unit has so far been detected in situ. Instead, everywhere on the valley floor except in the area of the light mantle, the soil appears to be regolith largely derived from the underlying subfloor basalt unit. A possible dark mantle component in the regolith is the dark glass sphere unit of unknown origin but possibly related to the orange glass of station 4. The age of the dark glass, however, is 3.7×10^9 yr, and it is apparently well mixed into the regolith, which seems to rule it out as the mantling unit.

The subfloor unit was well sampled at a number of stations (the Apollo lunar surface experiments package (ALSEP) site and stations 1A, 4, 5, and 9?) and

[a]NASA Lyndon B. Johnson Space Center.

was shown to be a 3.8×10^9-yr-old, massive, light-colored mare basalt unit containing 10 to 15 percent vesicles, 30 to 40 percent plagioclase, together with clinopyroxene and ilmenite as rock-forming plagioclase. Some local variations in texture, mineralogy, and chemistry exist. Geophysical experiments on the mission also indicate the existence of such a layer with a thickness of approximately 1 km. Samples of the subfloor basalt were primarily taken from boulder-size ejecta at large craters that penetrated the regolith to the underlying unit. Samples of the basalt were also obtained from the regolith that has been developed on top of it, notably in a widespread series of LRV samples as well as at the major geological stations. Samples from station 9 in particular may be from deep in the regolith (but not quite to the depth of the basalt unit).

The Sculptured Hills unit was investigated at station 8. Because of the lack of any identifiable material that has moved downslope, sampling of the Sculptured Hills unit consists of samples of the regolith from the lower part of the slope. Because the soil undoubtedly is composed of material from both the valley regolith and the Sculptured Hills regolith, identification of the Sculptured Hills rock types will have to be delayed until a comparison can be made between the valley regolith and the soil collected at station 8. At the moment, no more is known about the Sculptured Hills unit than that it is a highland unit morphologically different from the massifs and the reasons for this difference are unknown.

The massif unit was sampled at three locations at the bases of the South and North Massifs (station 2 and stations 6 and 7, respectively) and also in the light mantle. Five different boulders (one of which, at station 6, had broken into five boulder-size pieces) as well as soils were sampled at the three stations. The boulders undoubtedly represent units in place higher up the massif slopes (in the upper half of the South Massif and the lower third of the North Massif). All the boulders are breccias of a moderately complex nature, similar to those from the Apollo 15 and 16 sites, and are indicative of more than one brecciation event. There is indication of a correlation of breccia types between the North and South Massifs, but definitive conclusions on this must wait for additional geochemical analyses and detailed petrologic examination. In the meantime, it can be concluded that the massif unit, probably raised by the Serenitatis event, is composed of breccias that probably were produced by one or more basin-forming events.

An event of great interest during the geological exploration of the valley of Taurus-Littrow was the discovery of deposits of orange glass on the rim of Shorty Crater. Present indications are that the orange glass is fairly old (3.7×10^9 yr); that shortly after its formation, it was well buried; and that only recently (20 to 30×10^6 yr ago), it was excavated by the Shorty Crater impact. Some traces of the orange glass spheres exist in the regolith elsewhere in the valley.

The general premission model of a graben valley that was formed as part of the Serenitatis event, perhaps reactivated since then, and later partly filled with a basalt flow (or flows) during the episode of mare filling is corroborated and more tightly defined by the data analyzed to date.

PRELIMINARY SAMPLE ANALYSIS

The suite of rock samples returned from the Apollo 17 mission is a quite varied one. Included in the samples are basalts, dark-matrix breccias and agglutinates, green-gray breccias, blue-gray breccias, light-gray breccias, brecciated gabbroic rocks, and others (including a dunite clast composed of more than 95 percent olivine).

The basalts are quite uniform in composition and are generally similar to the Apollo 11 basalts. They are generally vesicular, have variable grain sizes as large as 2 mm, and consist of approximately 25 to 30 percent plagioclase. The basalts are high in titanium like the Apollo 11 basalts but are much lower in nickel. In detail, chemical differences within the Apollo 17 basalt suite argue for at least two different basalt types.

The dark-matrix breccias and agglutinates are derived from the basalt regolith of the valley floor and contain clasts of basalt. The green-gray breccias are predominantly matrix with a small percentage of mostly mineral clasts. The matrix is coherent, is rich in poikilitic orthopyroxene, and has vesicles as large as several centimeters in diameter. The blue-gray breccias are matrix breccias with a more varied population of clasts than the green-gray breccias. The blue-gray matrix is slightly vesicular with some fine-scale banding and a recrystallized texture. The light-gray breccias are layered and foliated, have a higher percentage of clasts, and are less coherent than

the green-gray and blue-gray types. The clasts, both lithic and mineral, are generally feldspar rich and include first- and second-order breccias. The light-gray matrix texture is fragmental. The brecciated gabbroic rocks are similar to the crushed cataclastic anorthosites returned on the Apollo 15 and 16 missions.

The breccias can be divided chemically into two groups: the blue-gray, green-gray, and light-gray breccias with approximately 50 percent normative plagioclase and the brecciated gabbroic rocks with approximately 70 percent normative plagioclase. The blue-gray, green-gray, and light-gray breccias have strikingly more potassium, phosphorus, rubidium, yttrium, zirconium, and niobium than the brecciated gabbroic rocks. Based on analysis of one light-gray breccia, they appear to have slightly higher rubidium, yttrium, and zirconium contents and a slightly lower strontium and nickel content than the blue-gray and green-gray breccias. Both the major- and trace-element compositions of the blue-, green-, and light-gray breccias are very similar to those of the KREEP-like rocks (those that are rich in potassium, rare-earth elements, and phosphorus) from Descartes and are especially similar to those of the brown-glass-matrix breccia from Hadley-Apennine. The brecciated gabbroic rocks chemically resemble similar rocks from the Apollo 16 mission and especially closely resemble Apollo 15 sample 15418.

The Apollo 17 soils are generally divided into two types: soils on the valley floor derived as regolith from the underlying basalt and soils from the massifs and light mantle derived as regolith from the breccias. At the transition zones between the two units and at the foot of the Sculptured Hills, the soils are a mixture of the two types. Exotic glasses (orange and black glass spherules), first noticed at Shorty Crater, are present in soils throughout the valley. The orange soil is generally basaltic but has a higher percentage of magnesium and a very strikingly high abundance of zinc as well as other trace-element differences (e.g., high chromium oxide). The orange soil also contains more low-temperature volatiles than do other soil samples.

SURFACE ELECTRICAL PROPERTIES EXPERIMENT

The surface electrical properties (SFP) experiment was used to measure the dielectric constant of the lunar regolith in situ and also to provide information on the subsurface structure in the region covered by the geology traverses. Electromagnetic radiation at six frequencies between 1 and 32 MHz was transmitted from a fixed crossed-dipole antenna and received through an antenna attached to the LRV. Preliminary indications are that useful data were received only during the traverse from the SEP site to station 2. On the basis of early analysis of the signals recorded during that traverse, two different models can be developed. One model explains the observations in terms of a dielectric constant that increases as a function of depth, in particular with a marked discontinuity at a depth of approximately 50 m. The other model includes two layers having different dielectric constants the interface of which decreases in depth from approximately 20 m at the lunar module (LM) site to 15 m at station 2.

LUNAR TRAVERSE GRAVIMETER

By the comparison of measurements made on the Earth and at the Apollo 17 landing site with the same instrument, the lunar traverse gravimeter, the value of gravity at the LM site was found to be 162 695 ± 5 mgal. Relative gravity measurements were obtained for a network of 12 stations spread across the valley floor. At four stations near the LM (the LM, ALSEP, and SEP sites and station 1A), the 10 measurements agree within approximately ± 3 mgal. At four other stations on the valley floor located as far as 5 km from the LM (stations 3, 4, 5, and 9), the Bouguer anomaly is generally small and slightly negative (−5 to −10 mgal). At four other stations either at or very near the massifs (stations 2, 2A, 6, and 8), the Bouguer anomaly increases rapidly to between −20 and −25 mgal. Between stations 2A and 3, a distance of less than 1.5 km, the Bouguer anomaly changes from −20 to −5 mgal. The Bouguer anomaly curve has been interpreted in terms of a model with a 1-km-thick plate of basalt for the valley floor, assuming a density contrast of 0.8 g/cm^3 with respect to the material on either side.

LUNAR SEISMIC PROFILING EXPERIMENT

The lunar seismic profiling experiment is an extension of the active seismic experiment carried on the Apollo 14 and 16 missions. Eight explosive

charges (ranging in size from 57 to 2722 g) were deployed at distances between 100 and 2700 m from a triangular geophone array. These charges were later detonated on command from the Earth, and travel-time measurements were obtained that, together with the LM-impact signals, indicate a three-layer model for the valley floor at Taurus-Littrow. The first 248-m-thick surface layer has a seismic velocity of 250 m/sec. The second layer, extending to a depth of approximately 1200 m, has a seismic velocity of 1200 m/sec. Below 1200 m, the third layer, with a seismic velocity of approximately 400 m/sec, begins. A reasonable model, with basalt flows filling the valley of Taurus-Littrow to a depth of 1.2 km, can be derived from these observations. The 4000-m/sec velocity for the third layer is a valuable tie point between the shallow surface velocities measured earlier and the deeper velocities measured by the passive seismometers from distant events.

LUNAR SURFACE GRAVIMETER

The lunar surface gravimeter was designed to make very accurate (1 part in 10^{11}) measurements of the acceleration of lunar gravity and of its variation with time. These measurements should allow investigations of gravitational waves by using the Moon as an antenna and also investigations of tidal distortions of the shape of the Moon. Following deployment of the gravimeter, problems occurred in trying to balance the beam. These problems were probably caused by an incorrect mass of the beam and have at least partly been overcome by applying pressure on the beam with the mass-changing mechanism. Data in the form of seismic events at sunrise and sunset have been received, and it is hoped that the instrument can be used in its off-nominal mode to obtain the data for which it was designed.

LUNAR EJECTA AND METEORITES EXPERIMENT

The objectives of the lunar ejecta and meteorites experiment, which is part of the ALSEP, are to detect secondary particles that have been ejected by meteorite impacts on the lunar surface and to detect primary micrometeorites themselves. The particle detectors of the instrument are multilayered arrays that are capable of measuring the velocity and energy of incident particles. No meaningful results are yet available from this instrument.

LUNAR ATMOSPHERIC COMPOSITION EXPERIMENT

The lunar atmospheric composition experiment is designed to identify the various gases in the lunar atmosphere and to determine the concentration of each species. Previous measurements using the cold cathode ion gages have been limited to total gas concentrations. Preliminary results for the first three lunations indicate the presence of (1) three native species in the lunar atmosphere (helium, neon, and argon) and (2) a large number of other species, some of which are undoubtedly contaminants (e.g., atomic hydrogen, nitrogen, oxygen, chlorine, hydrochloric acid, and carbon dioxide). The measured concentrations of these contaminants has continued to decline with the passage of time.

The measured helium concentrations and their behavior as a function of phase in the lunation (increasing by a factor of 20 toward lunar midnight) are in agreement with predictions that helium does not freeze out on the surface at night and that its source is the solar wind. The concentration of neon, measured only at night, is a factor of 20 lower than predicted, and the results are not understood. The concentration of argon also decreases (in fact, becomes undetectable) during the night as expected for a gas that freezes out on the surface during the lunar night. Shortly before dawn, the argon concentration begins to rise, apparently indicative of the migration of argon across the approaching sunrise terminator (a predawn argon breeze); the behavior of the contaminants is markedly different in that they show a sharp rise just at local sunrise.

HEAT FLOW EXPERIMENT

The deployment of a second heat flow experiment on the lunar surface as a part of the Apollo 17 ALSEP allows comparison of lunar heat flow measured at two different stations, the Apollo 15 and 17 landing sites. Both Apollo 17 probes were successfully inserted to their full depth of 2.36 m.

Preliminary results indicate that the heat flow at the Apollo 17 site is 2.8×10^{-6} W/cm^2 for the first probe and 2.5×10^{-6} W/cm^2 for the second probe.

These values can be compared with a revised value for the Apollo 15 site of 3.1×10^{-6} W/cm^2. The uncertainty for all three values is ± 20 percent. The heat flow gradient for probe 1 is uniform in agreement with a similar observation made at the Apollo 15 site. For probe 2, however, the gradient is definitely not uniform and the difference is believed to be due to insertion of the probe very near a buried boulder.

Corrections for topography have not yet been applied to the heat flow values. Although the size of these corrections is not clear at this time, it would appear that they will result in a reduction of the present values by a factor of 15 to 25 percent for the Apollo 17 measurements and an uncertainty of ± 10 percent for the Apollo 15 measurements. The possible resulting difference between the heat flow values measured at the two different sites may be explainable in terms of higher thorium abundances, observed by the Apollo 15 gamma ray instrument, in southeastern Mare Imbrium as compared with southeastern Mare Serenitatis. In any case, values of the heat flow between 2.4×10^{-6} and 3.0×10^{-6} W/cm^2 are confirmed as characteristic of more than one site of the Moon. If applied generally to the entire Moon, those values argue for relatively large quantities of radioisotopes in the outer layers of the Moon.

LUNAR NEUTRON PROBE EXPERIMENT

Time-integrated fluxes of thermal neutrons ($\lesssim$ 1 eV) as a function of depth in the regolith were measured using the lunar neutron probe. These measurements were accomplished with targets of boron-10 and uranium-235 placed at intervals along a 2-m rod that was inserted into the hole left by the deep drill core when it was extracted. Preliminary analysis of tracks in the mica detectors that were used in conjunction with the uranium-235 targets agrees with both the magnitude and shape of previous theoretical work on the neutron flux as a function of depth in the lunar regolith. Therefore, the problem concerning the fact that integrated neutron dosages for soil samples indicate more rapid and/or deeper regolith turnover than geological evidence indicates is not resolved. Hence, neither the mixing depth nor the time scale of the regolith model, both of which are needed to fully interpret the gadolinium ratios, has been defined.

PASSIVE SEISMIC EXPERIMENT

A passive seismometer station was not included in the Apollo 17 ALSEP. The impacts of the Apollo 17 LM and SIVB were observed by the four stations already in place at distances as great as 1750 km. These impacts and the occurrence of other natural events since the Apollo 16 mission (especially an impact on the far side near Mare Moscoviense) have helped to further define the lunar seismic model below the "crust" as being characterized by a thick, seismically inactive, relatively homogeneous lithosphere that encloses an asthenospheric zone of partial melting. Moonquake activity appears to be concentrated at the boundary between these two zones at a depth of approximately 1000 km. Evidence has also been found for the existence of two belts of seismic activity as plotted by epicenter locations. Seismic observations to date cannot be used to either confirm or deny the possible existence of a small iron-rich core.

COSMIC RAY EXPERIMENT

A new set of cosmic ray detectors was carried to the surface of the Moon on the Apollo 17 mission. Two sets of detectors (including mica, quartz, glass, plastic, and foil) were exposed, one set facing the Sun and one set in the shade facing away from the Sun. During the time that the detectors were exposed, no significant solar activity occurred. Although the absolute flux levels for the 0.02- to 1-MeV/amu energy range were considerably lower than those for the Apollo 16 mission, the shape of the spectrum is similar to that for the flare that occurred during the Apollo 16 mission and indicates that proportionate numbers of energetic particles are emitted by the Sun even during quiet periods. Heavy-element enrichment noted during flares is also present during the quiet periods. Tracks were also noted in the detectors facing away from the Sun. Because these particles also have a "solar energy" spectrum and presumably come from the Sun, the "antisolar" tracks indicate the existence of irregularities in the interplanetary magnetic field outside the orbit of the Earth that are capable of "reflecting" these solar cosmic rays.

SOIL MECHANICS EXPERIMENT

Although there is considerable local variability in the properties of the soil, large-scale averages have

been very similar for all Apollo landing sites with the exception of Descartes, where the relative density is notably lower than at the other sites. Although the soil density in the Apollo 17 double-core sample obtained from the orange soil is the highest yet found on an Apollo mission, the difficulty in driving the core tube was not exceptional, leading to the conclusion that it is not a low mean porosity but a high specific gravity of the individual grains that causes the observed high density. Because of the long-term stability of the deep drill hole, it is concluded that the soil strength is relatively high at depths on the order of 1 to 2 m.

APOLLO LUNAR SOUNDER EXPERIMENT

The Apollo lunar sounder experiment carried in the scientific instrument module (SIM) bay was a three-frequency (5, 15, and 150 MHz) chirped radar sounder. Depth of subsurface exploration, in terms of features defined by changes in the dielectric constant, decreased with increasing frequency.

The Apollo lunar sounder was designed for three primary modes of operation: sounding, profiling, and imaging. The sounding mode pertains to the detection and mapping of subsurface features such as a probable 100-m-deep interface detected in western Mare Serenitatis. The profiling and imaging modes, which are similar to conventional surface return radars, can provide quantitative metric and topographic data as well as albedo measurements.

Preliminary results obtained by processing some small selected portions of the data indicate that useful data were obtained.

ULTRAVIOLET SPECTROMETER

The ultraviolet spectrometer flown in the SIM bay of the Apollo 17 spacecraft was a single-channel scanner having a 12° by 20° field of view and covering a spectral range of 1180 to 1680 Å (118 to 168 nm). The entire spectral range was repetitively scanned every 12 sec. The primary objective of the instrument was to measure the lunar atmosphere using resonance line scattering. No lunar atmospheric constituents were detected except for a short-lived (2 to 4 hr) "cloud" just after the descent of the LM. Among new lower limits that were established is one of $\leqslant 10$ atoms/cm^3 for atomic hydrogen at the lunar surface. This low value (at least 10 times lower than predicted for a transient lunar atmosphere resulting from the solar wind) implies that during diffusion at the lunar surface, hydrogen molecules are formed. The upper limits for hydrogen molecules from the current observations are not inconsistent with this idea. Xenon is also less abundant than predicted as a native constituent of the lunar atmosphere.

INFRARED SCANNING RADIOMETER

The infrared scanning radiometer, carried in the SIM bay, was used to map the lunar surface in 352-km-wide strips centered on the groundtracks with a resolution of better than 10 km. This mapping was accomplished by sweeping the 1° instantaneous field of view in contiguous strips perpendicular to the orbital groundtrack. The spectral bandpass extended from 1.2 to 70 μm.

In addition to a number of individual thermal anomalies, preliminary examination of the data shows, among other things, a great concentration of nighttime thermal hot spots in the Oceanus Procellarum region, particularly in contrast to the relative smoothness of nighttime scans of highland areas. The nighttime thermal picture of the far side of the Moon is relatively featureless compared to that of the near side.

S-BAND TRANSPONDER

The general similarities of the Apollo 15 and 17 groundtracks allowed good comparisons to be made between gravity data obtained on the two separate missions. Agreement in many areas (e.g., over Mare Crisium) was good. The model for the Serenitatis mascon, however, was shown to be inadequate; the Apollo 17 observations were 1.6 times larger than those predicted for the Apollo 17 groundtrack by the Apollo 15 model. Because the new Apollo 17 data increase the areal coverage of Mare Serenitatis, it is obvious that an improved model can be expected. Very good areal coverage was also obtained of Grimaldi Crater, and there is evidence that this mascon has the largest mass distribution yet observed for any mascon (approximately 1000 kg/cm^2).

An estimate derived from these observations for the value of lunar gravity at the landing site (162 722 mgal) compares very well with that obtained by the lunar traverse gravimeter (162 695 mgal).

BIOSTACK EXPERIMENT

The Apollo 17 biostack experiment (biostack II) was of very similar configuration to the Apollo 16 biostack experiment (biostack I). The total radiation dose received by biostack II was approximately 15 percent higher than that received by biostack I. The primary difference between the two experiments was the different set of species flown on the two missions. (Three of the four species flown on Apollo 16 were flown again on Apollo 17 as well as three other species.) Initial results, using organisms not hit by cosmic rays, show that, as on the Apollo 16 mission, viability is apparently not affected by other factors related to space flight. The Apollo 16 results showed markedly different sensitivity to radiation between different strains of the same species. These aspects will be further investigated as work is continued on biostacks I and II.

BIOCORE EXPERIMENT

Five pocket mice were flown in a self-contained unit in the Apollo 17 command module to study the effects of cosmic rays on living tissues, especially the brain. Four of the five mice survived the trip. Processing of the bodies of all five Apollo mice and of a number of control mice is underway. Sectioning of the brains has been delayed pending full analysis of the cosmic ray tracks in the subscalp monitors. An average of 16 tracks/monitor was found for the monitors on the mice that survived the trip. Portions of the scalp of one Apollo mouse have been examined and found to contain some lesions, but a direct relationship between these lesions and cosmic ray hits will have to await further analysis and comparison between locations in the scalp and in the monitors. Other organs are also being examined, but no results are yet available.

VISUAL LIGHT PHENOMENON

Observations of the light flash phenomenon continued during the Apollo 17 mission. As on Apollo 16, the Apollo light flash moving emulsion detector was worn by one crewman for a 1-hr observing session during translunar coast. No results are yet available on the time history of tracks in these emulsions. When available, these data should define the particles responsible for the light flashes.

Some statistical data are available now on observations made during the last four Apollo missions. In particular, two items stand out. First, a relatively long period of time is required before the perception of the first event compared to the time between events thereafter. This fact would indicate that dark adaptation is involved and that the events occur in the eye. Second, the length of time before the observation of the first event was longer during transearth coast than during translunar coast; also, the rate of observed events, after the first one, was lower during transearth coast than during translunar coast. The cause of the greatly reduced ability to see the light flashes during transearth coast as opposed to translunar coast is not clear.

ORBITAL GEOLOGY

More than a score of individual investigations of surface and spatial features have been performed so far based on the Apollo 17 crew orbital observations and panoramic and metric camera photographs. The scope of these investigations ranges from studies of the structure of individual craters to studies of the sequences of mare stratigraphy and mare ridges to studies of the solar corona and zodiacal light.

CHAPTER XI – MARS

THE GEOLOGY OF MARS

Michael H. Carr
U.S. Geological Survey, Menlo Park, Calif. 94025

The Mariner 9 mission revealed Mars to be a much more diverse planet geologically than had been anticipated. Unlike the Earth and the Moon, the planet preserves on its surface a seemingly continuous record of dynamic activity from the late stages of accretion to the present day. Large volcanoes of widely different ages and extensive fracture systems attest to a long history of internal activity while the preservation of large areas of primitive densely cratered terrain indicates that crustal mobility and erosional processes have been far less effective than on Earth in destroying the early record. Perhaps the greatest surprise of Mariner 9 was the discovery of fluvial-like features. Since liquid water is unstable under present conditions at the Martian surface, the presence of the channels indicates either an origin other than aqueous or climatic conditions in the past that were quite different from those that presently prevail. The great canyons and numerous cliff-like features suggestive of active erosion were also surprises, as were the widespread layered deposits at the poles. The significance of these unexpected results is still far from understood, and the planet remains a fertile field for speculation.

The surface of Mars can be divided into two hemispheres: one exhibiting nearly all the primitive cratered terrain; the other, nearly all the young shield volcanoes and volcanic plains. The division is not exclusive but generally holds. At the boundary between the two hemispheres, the primitive cratered terrain appears dissected and broken into numerous buttes and mesas. At greater distances from the boundary into the young plains, the mesas become smaller and more dispersed until finally none remain. Although the present boundary appears to be the product of erosion, it may have resulted initially from early fractionation of the crust.

The large, young shield volcanoes are concentrated into two regions, Tharsis and Elysium. The Tharsis shields are enormous by terrestrial standards, Olympus Mons being 23 km above the surrounding plains. The large size compared to terrestrial counterparts is believed to result from an absence of crustal plate motion and the great depth of magma origin. Lines of strato volcanoes are absent on Mars, but since on Earth these are generally located above subduction zones, their absence on Mars is not surprising. The NE-SW alignment of the Tharsis shield may be related to a general updoming of the Tharsis region. The dome, approximately 4000 km across and 7 km high at the summit, is at the center of a vast fracture system that encompasses almost half the planet. The fractures are crudely radial to the Tharsis region and appear to have formed before the onset of the main shield building period in Tharsis. Shield volcanoes older than the fracture system do occur but do not achieve heights comparable to the shields that post-date the fractures. Although the shield volcanoes are the most spectacular examples of volcanism, the plains may be more significant volumetrically. On high-resolution frames of the plains, long subdued lobate scarps are common. They resemble those found on the lunar maria and are widely interpreted as flow fronts. Older plains units that occur in the intercrater areas of the primitive cratered terrain, also may be volcanic in origin, but because they lack the characteristic flow features, their origin is much more uncertain. Less ambiguous examples of volcanism in the primitive cratered terrain are subdued, heavily cratered shield-like structures.

The large canyon of Mars (Valles Marineris) is aligned along the direction of the Tharsis fractures; thus, its orientation appears to be fracture controlled. It is not, however, purely tectonic in origin; secondary processes such as aeolian and fluvial action almost have certainly contributed to its present dimensions. At the eastern end of the canyon (downslope) are wide areas of chaotic terrain. The surface has been broken into numerous blocks by seemingly randomly oriented fractures, and each fractured area has subsided 1-2 km as though support had been withdrawn from beneath. Issuing from the chaotic region are the largest channels on Mars. By comparison with terrestrial periglacial flood features, these channels have been attributed to massive release of subsurface water. Large channels occur elsewhere particularly in the primitive cratered terrain. Their wide spacing and absence of distributary systems with dimensions comparable to the size of the main channels make origin by surface runoff of rainfall unlikely. However, myriads of fine channels throughout the equatorial region argue for an atmospheric origin for water.

The polar regions are quite unlike the rest of the planet. The caps, composed mostly of CO_2, advance and recede with the seasons. As the caps recede in the spring, they uncover a series of distinctively polar deposits. Because the imagery is difficult to interpret, there is considerable uncertainty about the geometric relations, but the following general picture has emerged. Sitting unconformably on the underlying nonpolar materials are the "etch-pitted deposits" whose surface is smooth and level except for irregularly shaped pits and craters. In most places, the etch-pitted terrain is overlain by laminated deposits whose surface is smooth and crater free. The fine layering of the laminated deposits are exposed mainly at their equatorward edge. Overlying the laminated deposits is the present emphemeral cap. Both the laminated and the etch-pitted deposits have been interpreted as a residuum of less volatile components of the cap, mixed with aeolian debris. The layering may preserve a record of past climatic changes.

With permission, reprinted from Journal of Geophysical Research, vol. 78, no. 20, July 1973, pp. 4031–4036.

A Generalized Geologic Map of Mars

M. H. Carr

U.S. Geological Survey, Menlo Park, California 94025

Harold Masursky

U.S. Geological Survey, Flagstaff, Arizona 86001

R. S. Saunders

Jet Propulsion Laboratory, California Institute of Technology, Pasadena, California 91103

A geologic map of Mars has been constructed largely on the basis of photographic evidence. Four classes of units are recognized: (1) primitive cratered terrain, (2) sparsely cratered volcanic eolian plains, (3) circular radially symmetric volcanic constructs such as shield volcanoes, domes, and craters, and (4) tectonic erosional units such as chaotic and channel deposits. Grabens are the main structural features; compressional and strike slip features are almost completely absent. Most grabens are part of a set radial to the main volcanic area, Tharsis.

A generalized geologic map of Mars has been constructed largely on the basis of differences in the topography of the surface. The success with which the geology can be deduced from surface topography depends on how distinctively the original topography of a feature reflects its mode of origin and the extent to which subsequent modification can be recognized and assessed. We are fortunate in having a number of topographic features on Mars whose forms are highly diagnostic of their origin. Of particular note are the shield volcanoes and lava plains. In some areas the original features have been considerably modified by subsequent erosional and tectonic processes. These have not, however, resulted in homogenization of the planet's surface but rather have emphasized its variegated character by leaving a characteristic imprint in specific areas. The topography of the planet therefore lends itself well to remote geologic interpretation.

The map (Figure 1) is an outgrowth of an earlier version of the equatorial belt [*McCauley et al.*, 1972]. The techniques and conventions used are similar to those used for the moon and have been fully described elsewhere [*Wilhelms*, 1972]. The surface has been divided into several units, each of which has a specific range of topographic characteristics. In the map explanation (Figure 2) the units are arranged according to their age as inferred from superposition and transection relations, crater counts, and so forth. The map also provides a generalized indication of tectonic deformation. Most of the units represent materials of a specific origin deposited within a restricted period of time. Other units, such as the chaotic and knobby materials, are not strictly geologic deposits but are modifications of preexisting materials. The modifications, however, have been so drastic as to, in effect, create new geologic units, and they are mapped as such.

For this early version of the map, data from the various spectral instruments have been largely ignored because of the difficulty in obtaining the data in a form readily correlatable with the visual image. However, we would not expect that, at the scale at which the map is depicted here, the spectral data would significantly affect delineation of the various units. The scale was dictated by journal format and should not be taken as indicative of a present level of knowledge. The map is a very coarse generalization of the information available. A more detailed map that will do justice to the wealth of information in the Mariner photography will be published in the not too distant future.

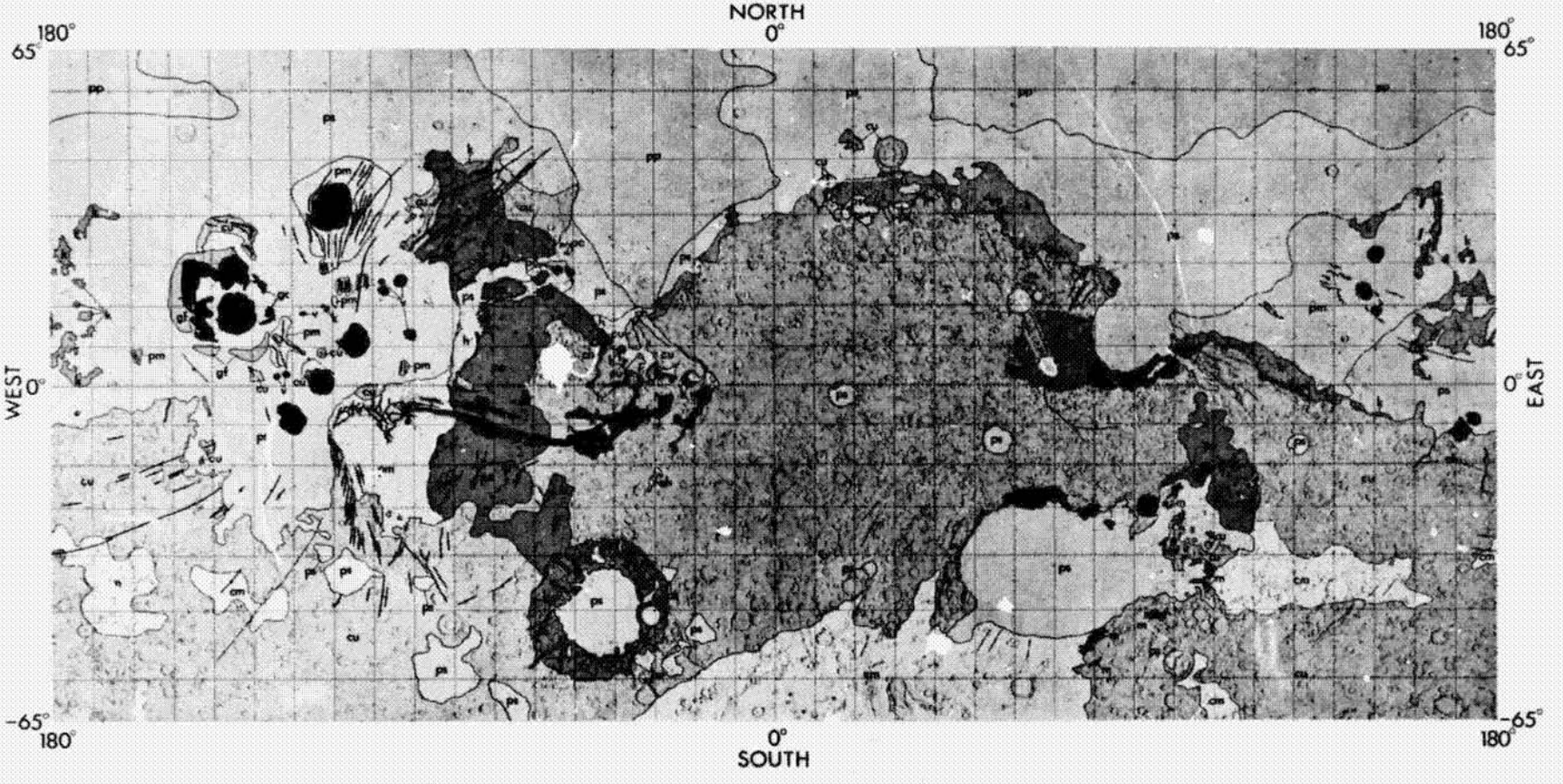

Fig. 1. Generalized geologic map of the region of Mars between 65°N and 65°S.

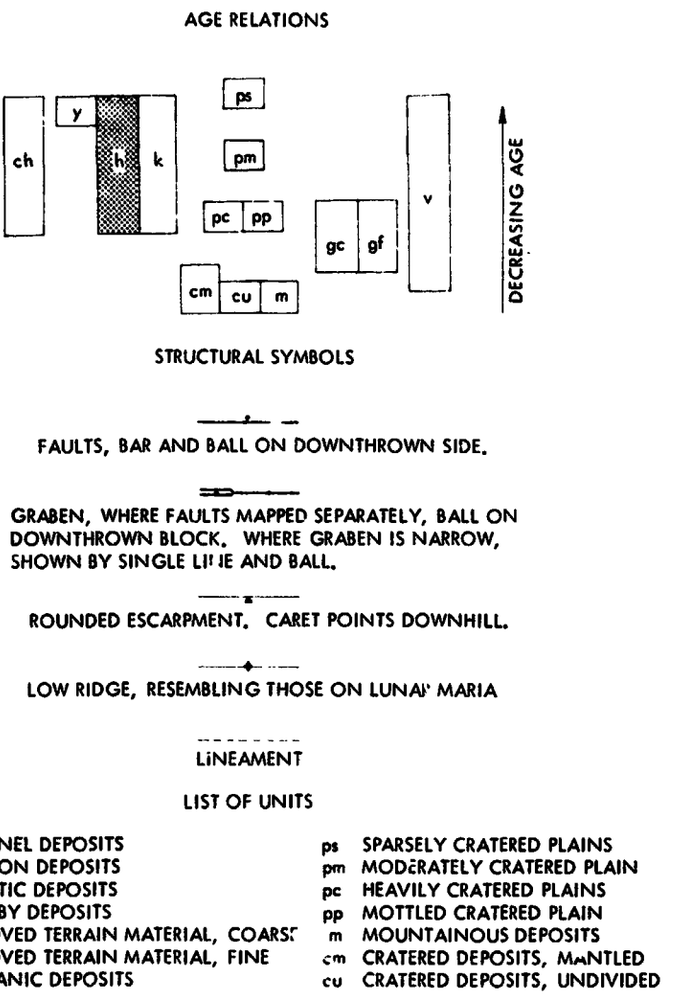

Fig. 2. Age relations and explanations of map symbols.

Description of Units

Densely Cratered Units

Densely cratered terrain covers approximately one half of the planet's surface, including most of the central and southern parts of the map and the south polar regions. The cratered area was photographed by Mariner 4, 6, and 7 in 1964 and 1969 and has been described in detail [*Murray et al.*, 1971]. The surface is almost saturated with large (>20 km) flat-floored craters; the density of smaller craters, which are mostly bowl shaped, falls short of saturation by a factor of 10. Several large ring structures resembling lunar basins occur within the densely cratered terrain [*Wilhelms*, 1973]. The character of the cratered terrain varies both locally and on a regional scale. Around the large impact basins, positive relief features are more common than elsewhere, providing the basis for discriminating a mountainous unit (m). In other areas the cratered terrain appears to be partly mantled, so that fewer intermediate and small (<20 km) craters are present and the larger craters appear subdued. A unit termed 'cratered deposits, mantled' (cm) has therefore been designated; the rest of the densely cratered deposits are left undivided (cu).

Cratered deposits, undivided (*cu*). This unit forms the primitive accretionary surface of the planet. It occurs primarily in the southern midlatitudes but extends to 40°N around the

330°W meridian. Isolated areas occur in the volcanic province. The unit is saturated with large flat-floored commonly rimless craters. Intercrater areas are flat and featureless except for scattered small bowl-shaped craters. Locally they may be partly covered by younger deposits, so that the topography has a muted appearance. Ridges, resembling those on the lunar maria, occur in some of the muted areas. The unit probably consists mostly of reworked impact breccias but locally includes younger volcanic and eolian deposits.

Cratered deposits, mantled (*cm*). This unit is mapped only where extensive areas appear mantled. Fewer intermediate and small craters (<20 km) occur than in unit cu. The unit occurs primarily in high southern latitudes and is interpreted as cratered deposits mantled by various thicknesses of younger material. Lobate flow fronts indicate volcanic materials in some areas, but the mantling material almost certainly includes significant portions of eolian debris.

Mountainous deposits (*m*). This unit forms the rugged parts of the rims of the three largest recognized impact basins, Argyre, Libya, and Hellas. Argyre (50°S, 43°W) is surrounded by rugged terrain cut by graben. The Libya basin (15°N, 270°W) rim is preserved as a distinct mountainous unit only at the south side of the basin. The Hellas (45°S, 295°W) rim is subdued. Mountainous terrain with relief comparable to Argyre is preserved only in isolated areas, particularly to the east where there is a complex array of isolated mountains. The mountainous unit is interpreted as remnants of parts of the primitive crust uplifted during the formation of the impact basins. Remnants of basin ejecta are also included.

Plains-Forming Materials

Plains, showing various degrees of cratering, occur over most of the planet not covered by the densely cratered units. The plains-forming materials are thought to be largely volcanic and eolian in origin. They have been divided into three units on the basis of the number and character of the superimposed craters.

Heavily cratered plains materials (*pc*). This unit is the most heavily cratered of the plains units but has fewer large craters than the densely cratered units described. It is equivalent to unit mc of *McCauley et al.* [1972] and occurs mainly in the areas north and south of Lunae Palus and in Hesperia. Ridges resembling those on the lunar maria are common. This material is interpreted as old lava plains similar to the lunar maria. (Small areas of material similar to this are present widely throughout the densely cratered area; they are not mapped because of scale limitations.)

Moderately cratered plains materials (*pm*). This unit has fewer craters in the size range 2–20 km than unit pc but more than unit ps [*Carr*, 1973]. It occurs in Elysium around the major shield volcanoes, in the Arcadia-Tharsis region, where it is exposed mainly as islands surrounded by unit ps, and in the region of Phoenicus Lacus. In the Arcadia-Tharsis region the unit is almost everywhere intensely fractured. It is interpreted as volcanic lava plains intermediate in age between units ps and pc.

Sparsely cratered plains materials (*ps*). This unit occurs mainly in the Amazonis-Tharsis region and in the large impact basins in the densely cratered province. Unit ps is the least cratered and presumably the youngest of the plains units. At wide-angle resolution it is relatively featureless, except in places close to its contact with the densely cratered terrain, where indistinct ridges and low rounded hills are common. At narrow-angle resolution irregular lobate scarps suggestive of flow fronts are common, especially in the Tharsis region. Low hills, islands of highly fractured terrain, sinuous channels, and polygonal fractures occur in other areas. More rarely, the narrow-angle pictures are featureless. In the Tharsis region the plains appear to be composed mainly of volcanic flows, since lobate flows are detectable on nearly all narrow-angle pictures. In the Amazonis region and in the large impact basins, Argyre, Hellas, and Libya, volcanic features are rare, and the eolian component probably dominates. The unit embays all other units, confirming the young age inferred from the crater counts.

Mottled cratered plains materials (*pp*). This unit occurs only at high northern latitudes where it forms an annulus around the pole. The density of large (>20 km) craters is comparable to that of unit pc, but the density of smaller craters is substantially lower. Large craters are subdued and apparent mainly because of an albedo contrast between the light crater floors and the dark surrounding materials. The local albedo

contrasts give the unit a mottled appearance. The albedo of the unit as a whole is lower than that of unit ps, with which it is generally in contact to the south. It is interpreted as cratered plains material (pc) overlain by a mantle of eolian debris.

Volcanic Units

Included under this heading are all volcanic units associated with roughly circular volcanic structures, as distinct from the extensive plains units. Because of limitations of scale, only two categories are depicted: a general unit v and another unit consisting of two facies (gc and gf), which form some very distinctive terrain around Nix Olympica.

Volcanic materials (*v*). This unit includes materials associated with shield volcanoes, volcanic domes, and volcanic craters (units vs, vd, and vc of *McCauley et al.* [1972]). Most of these features are circular and radially symmetric and have a central crater and gently sloping flanks. They occur primarily outside the densely cratered region, although two features within the densely cratered province are indicated on the map. The volcanic deposits have a wide range of ages. Those associated with Nix Olympica are relatively young [*Hartmann*, 1973]; those within the cratered province are relatively old [*Carr*, 1973].

Grooved terrain materials (*gf and gc*). Two facies of grooved terrain are recognized: a unit gc with a coarse surface topography that occurs close to Nix Olympica and a unit gf with a finer surface texture that occurs farther away. The coarse unit gc is characterized by linear mountains 1–5 km wide and typically 100 km long. The mountains are commonly separated by valleys that have flat floors with a fine striation parallel to the length of the valleys. The unit appears to be broken into blocks along arcuate faults that tilt the blocks gently inward toward Nix Olympica. The fine-textured unit gf is characterized by closely spaced equidimensional mountains whose horizontal and vertical dimensions decrease outward from Nix Olympica until the mountains merge with the surrounding plains. Both units are complex embayed by the surrounding plains deposits.

The grooved terrain deposits may represent old volcanic materials derived from the Nix Olympica center and since complexly fractured by the continual tectonic activity associated with the formation of the central shield. An alternative hypothesis is that the grooved terrain represents the outer remnants of a once much larger Nix Olympica that has been reduced in size by whatever process has formed the bounding scarp

Other Units

In several areas erosional and tectonic processes have resulted in the formation of distinctive geologic units. Four categories have been identified.

Channel deposits (*ch*). These have all the characteristics of terrestrial stream deposits. They occur in long, linear, sometimes sinuous channels that commonly have well-developed tributaries. Narrow-angle pictures show terraces, bars, finely braided networks of channels, and superimposed meanders. The most prominent channels head in the area of chaotic terrain around 2°N, 30°W and run northwest to the Chryse basin. Most, but not all, other channels occur in the densely cratered terrain near its contact with the plains. The unit is interpreted as materials deposited by a fluid, presumably water [*Milton*, 1973].

Canyon deposits (*y*). This unit includes materials that are exposed on the floor of the major rift system that extends 4000 km across the surface close to the equator between 30° and 100°W. The talus on the canyon walls is excluded. In most places the floor appears smooth, but locally jumbled blocks are present. At the eastern end of the canyon the unit merges with the chaotic terrain. At the western end the unit is pinched out as the canyon grades into a zone of branching troughs.

Chaotic deposits (*h*). Chaotic deposits have been described in detail previously [*Sharp et al.*, 1971]. The surface of the unit is crossed by numerous intersecting cracks that break the surface into blocks that have a wide range of sizes and that may be tilted slightly in different directions. The chaotic deposits normally occur in locally low areas, occasionally in completely closed basins. The outcrop areas are usually surrounded by an inward-facing scarp. The main area of occurrence is a broad region around 5°S latitude, 35°W longitude. The origin of the unit is obscure. Some process of sapping from below and subsequent collapse is required.

Knobby deposits (*k*). The unit is characterized

by irregular rounded hills and intervening plains. The hills are all sizes, from several hundred kilometers down to the limit of resolution (<1 km). The unit occurs mostly in a zone up to 500 km wide between the cratered terrain and the plains units. In general, the individual hills are larger and have more rectilinear outlines and flatter tops closer to the cratered terrain. Farther from the cratered terrain they become rounded and smaller in both horizontal and vertical dimensions until they merge with the surrounding plain. The unit includes the unit kt of *McCauley et al.* [1972] and the fretted terrain of *Sharp* [1973].

Structural Features

Mars is characterized by an abundance, if not a great variety, of structural features. The most common are graben, typically 1–5 km wide. They may occur as closely spaced parallel arrays, as in the Arcadia region, or as isolated fractures several thousand kilometers long, as in the Mare Sirenum region. The distribution of graben is markedly nonuniform. Most grabens are part of a system of faults approximately radial to the Tharsis ridge. The western part of the Coprates canyon also appears to be part of this set. The focal point of this vast system of fractures is the Phoenicus Lacus area, which is also the highest part of the ridge. The pattern appears to have formed as a result of the extension associated with the broad domical uplift of the Tharsis region.

Elsewhere fractures occur concentric and radial to the large impact basin of the densely cratered province [*Wilhelms*, 1973]. Fractures also occur locally around the large shield volcanoes [*Carr*, 1973] and at and parallel to the margin of the densely cratered terrain to form the knobby and fretted terrains [*Sharp*, 1973].

Mare ridges are the other common structural feature. They occur primarily on the most heavily cratered plains unit (pc). West of the Tharsis ridge they are aligned along directions concentric with the center of the Tharsis ridge.

Acknowledgment. Publication authorized by the Director, U.S. Geological Survey.

References

Carr, M. H., Volcanism on Mars, *J. Geophys. Res.*, *78*, this issue, 1973.

Hartmann, W. K., Martian cratering, 4, Mariner 9 initial analysis, *J. Geophys. Res.*, *78*, this issue, 1973.

McCauley, J. F., M. H. Carr, J. A. Cutts, W. K. Hartmann, H. Masursky, D. J. Milton, R. P. Sharp, and D. E. Wilhelms, Preliminary Mariner 9 report on the geology of Mars, *Icarus*, *17*, 289, 1972.

Milton, D. J., Water and processes of degradation in the Martian landscape, *J. Geophys. Res.*, *78*, this issue, 1973.

Murray, B. C., L. A. Soderblom, R. P. Sharp, and J. A. Cutts, The surface of Mars, 1, Cratered terrains, *J. Geophys. Res.*, *76*, 313, 1971.

Sharp, R. P., Mars: Fretted and chaotic terrain, *J. Geophys. Res.*, *78*, this issue, 1973.

Sharp, R. P., L. A. Soderblom, B. C. Murray, and J. A. Cutts, The surface of Mars, 2, Uncratered terrains, *J. Geophys. Res.*, *76*, 331, 1971.

Wilhelms, D. E., Geologic mapping of the second planet, *Astrogeology 55*, interagency report, 36 pp., U.S. Geol. Surv., Washington, D.C., 1972.

Wilhelms, D. E., Comparison of lunar and Martian multiring basins, *J. Geophys. Res.*, *78*, this issue, 1973.

(Received January 4, 1973;
revised March 14, 1973.)

With permission, reprinted from Journal of Geophysical Research, vol. 78, no. 20, July 1973, pp. 4009–4030.

An Overview of Geological Results from Mariner 9

HAROLD MASURSKY

U.S. Geological Survey, Flagstaff, Arizona 86001

Mariner 9 acquired pictures of all of Mars at a resolution of 1–3 km; 1–2% of the planet is covered by pictures of 100- to 300-meter resolution. From these data, preliminary 1:5,000,000 scale photomosaics have been made of the entire planet, and a 1:25,000,000 scale shaded relief map published. Geologic maps of the planet have also been made at a variety of scales. The more than 7300 pictures acquired indicate that Mars is more varied and dynamic than previously inferred. About one half of the surface consists of ancient cratered terrain; the largest circular feature, Hellas, is almost twice the size of the largest basin on the moon, Imbrium. The remainder of the surface is covered either by younger volcanic rocks and constructs that stand as much as 17 km above the mean level or by extensive tracts of plains deposits, some of which are sedimentary in origin. The volcanic piles with summit calderas have fresh flank flows and appear to be geologically young. The great equatorial chasm or canyon system, comparable in size to the East African rift valley system, terminates in a complexly faulted plateau to the west and in large patches of chaotic terrain on the east. Large fluvial channels originate in this chaotic terrain possibly by melting of permafrost and appear to flow northward into the Chryse region. Other large sinuous channels with many tributaries have no such obvious source areas and many small dendritic channel networks abound in the equatorial regions and imply possible collection of rainfall. In addition, many small lava channels with distinctive characteristics are present like those on the moon and earth. Many of the basin floors are underlain by lava flows inferred to be basaltic from the form of the flows, ridges, and domes that characterize their surface. The polar regions are covered by glacio-eolian layered sediments that appear to be still forming under the present climatic regime. Older, layered, somewhat different deposits are being eroded into large pits and troughs around the margins of the poles. A mantle of eolian debris presumably derived from these eroded circumpolar zones thins equatorward. Both eolian erosional features such as yardangs and depositional features such as dunes have been identified. Eolian erosion and deposition processes are currently active, as is seen by numerous changes in the albedo patterns that were monitored after the clearing of the planet-wide dust storm. The largest planetary scale differences in crustal style are between the southern highlands, presumably underlain by less dense rocks, and the northern lowlands or 'oceanic' basins, underlain by more dense rocks. The greatest difference along the equator is between the high 'continental' block of the Tharsis ridge with its volcanoes aligned along its margin and the oceanic floor of the Amazonis basin in which the Nix Olympica volcanic pile lies.

This paper provides a summary of Mariner 9 mission operations insofar as they affected acquisition of geologic data. Selected results with a minimum of supporting evidence are presented to give, as briefly as possible, the geologic highlights of the mission. More detailed discussions of various regional and topical problems are given in other papers by various members of the television team. Also included are hypotheses inferred from preliminary evidence that will have to await the test of later geologic mapping and detailed topical studies. These hypotheses are included to call attention to areas in which potentially valuable work can be performed. It should be emphasized that many of the observations and hypotheses given have developed during discussions with many of the members of the Mariner 9 television team. My purpose here is to attempt a first distillation from the enormous body of facts and theory generated by the mission as a guide to the other papers in this issue and to present the most salient geologic results that distinguish Mars as a planet from both earth and the moon.

Mariner 9 was launched from Cape Kennedy on May 30, 1971, and was inserted into Mars orbit on November 13; the spacecraft continued to take pictures and to make measurements

until October 27, 1972. More than 54 billion bits of information were transmitted to earth. More than 7300 pictures were taken of Mars and its satellites; about 1500 pictures of the planet were obtained by the 50-mm focal length wide-angle television camera, which has a resolution of 1–3 km [cf., *Masursky et al.*, 1970]. A preliminary map of the entire surface of Mars at a scale of 1:25,000,000 has been made from a mosaic of these pictures; a preliminary shaded relief map, the first detailed complete map of Mars, has been published at the same scale [*U.S. Geological Survey*, 1972].

The narrow-angle camera (500-mm focal length) acquired high-resolution pictures (100–300 meters) of between 1 and 2% of the surface. Geodesy pictures taken with the wide-angle camera from higher altitudes cover most of the southern hemisphere. These low-resolution pictures (4–9 km) were taken to provide control points for maps to be made from the high-resolution pictures. Thirty photomosaic maps at a scale of 1:5,000,000 have also been made for preliminary analysis and plotting of various types of data; later editions, based on improved control and use of enhanced pictures, have been made [*Batson*, 1973]; final maps will be made over the next several years.

Many pictures were taken to show time variations in cloud cover, polar cap frost, and the light and dark surface markings [*Sagan et al.*, 1973] on the planet. The infrared interferometer spectrometer [*Hanel et al.*, 1972] and ultraviolet spectrometer experiments [*Barth et al.*, 1972; *Hord et al.*, 1972], in addition to acquiring the atmospheric data, made pressure measurements from which the cartographers will attempt to compare integrated contour maps with occultation measurements [*Cain et al.*, 1973; *Kliore et al.*, 1972] and earth-based radar [*Downs et al.*, 1971; *Pettengill et al.*, 1971]. Systematic geologic mapping will be performed on the final cartographic products. Rectification, scaling, and additional enhancement of pictures and their integration with numerical results from the other experiments, such as gravity measurements provided by the celestial mechanics experimenters [*Lorell et al.*, 1973], will allow more sophisticated analysis, particularly of the thickness and density of the crust.

Because Mars is a low-contrast object, the pictures must be extensively computer enhanced to bring out surface detail. Suppression of electronic noise in the television subsystem and upgrading of enhancement techniques, especially early in the mission when dust in the atmosphere obscured the surface, allowed the image detail to be made visible [*Levinthal et al.*, 1973].

With the loss of Mariner 8, the extensively preplanned different but complementary objectives established for both spacecraft had to be integrated into a new mission plan for Mariner 9. On the arrival of Mariner 9 at Mars, the planetwide dust storm that had been observed in late September was still raging [*Capen and Martin*, 1971], so that this complex postlaunch mission plan also had to be abandoned. Reconnaissance pictures were taken until January 1, when the dust storm subsided sufficiently to begin mapping sequences, along with selected pictures taken for geodesy, variable features, atmosphere, and satellite studies. This mode continued with numerous successive modifications brought on by operational constraints until 70% of the planet had been mapped.

After a period of 2 months, during which pictures could not be taken because of solar occultation, the mapping mission was resumed. During this period the northern spring season progressed, and the north polar hood disappeared. Two new stars (Arcturus and Vega) were used for the first time in any space program to orient the spacecraft into more favorable picture-taking attitudes, thus allowing the remaining 30% of the planet in the northern hemisphere to be mapped. Some candidate landing sites for the Viking program in 1976 [*Soffen and Young*, 1972] also were photographed. After another interruption of 6 weeks during superior conjunction (Mars and the spacecraft passed behind the sun), the final extended mission picture sequences were taken to fill gaps in the photographic coverage, to photograph areas of special interest, to monitor the retreat of the north polar cap [*Soderblom et al.*, 1973*a*], and to study cloud formation over the volcanic constructs such as Nix Olympica [*Leovy et al.*, 1973].

Volcanic Features

The first features that emerged through the dust pall that blanketed the planet were four

dark spots visible in high-altitude reconnaissance pictures; these spots later proved to be the four highest peaks on the planet, each of which is surmounted by a summit crater or complex of craters [*Masursky et al.*, 1972*a*, Figure 1]. Gradual atmospheric clearing revealed first the full extent of the great volcanic pile of Nix Olympica, which rises high above the Amazonis basin floor [*McCauley et al.*, 1972, Figure 10; *Carr*, 1973]. (Estimates of its height by various methods of altimetry vary from 8 to 27 km.) This single volcanic edifice is about twice as wide as the largest of the Hawaiian volcanic piles and is about equal in volume to the total extrusive mass of the Hawaiian Islands chain. The form of the flank flows and the lava channels with natural levees is strikingly similar to the form of those in Hawaii and the Galapagos, suggesting that the flows also may be basaltic in composition, as are those on these comparable terrestrial structures [*Simkin and Howard*, 1970; *Masursky et al.*, 1972*a*].

The three other volcanoes, also of surprisingly large size, lie along the Tharsis ridge. The summit of South Spot from current altimetry data lies more than 17 km above the floor of the Amazonis basin to the west. This estimated elevation difference almost equals the maximum relief on earth, which amounts to about 20 km. The lava flows that radiate from the summit caldera of South Spot are not long and thin, as are those of Nix Olympica, but rather are short and stubby [*Masursky et al.*, 1972*a*; *Carr*, 1973]. This difference in form suggests probable differences in the composition of the flank flows. Those of South Spot were clearly less fluid than those of Nix Olympica and may be more silicic, possibly andesitic in composition. Short, stubby flows of similar appearance are common in the upper parts of some continental volcanoes such as Mt. Hood and Mt. Rainier.

It is possible that variation in temperature and gas content, rather than a difference in original composition, could account for these differences in flow morphology. The lack of

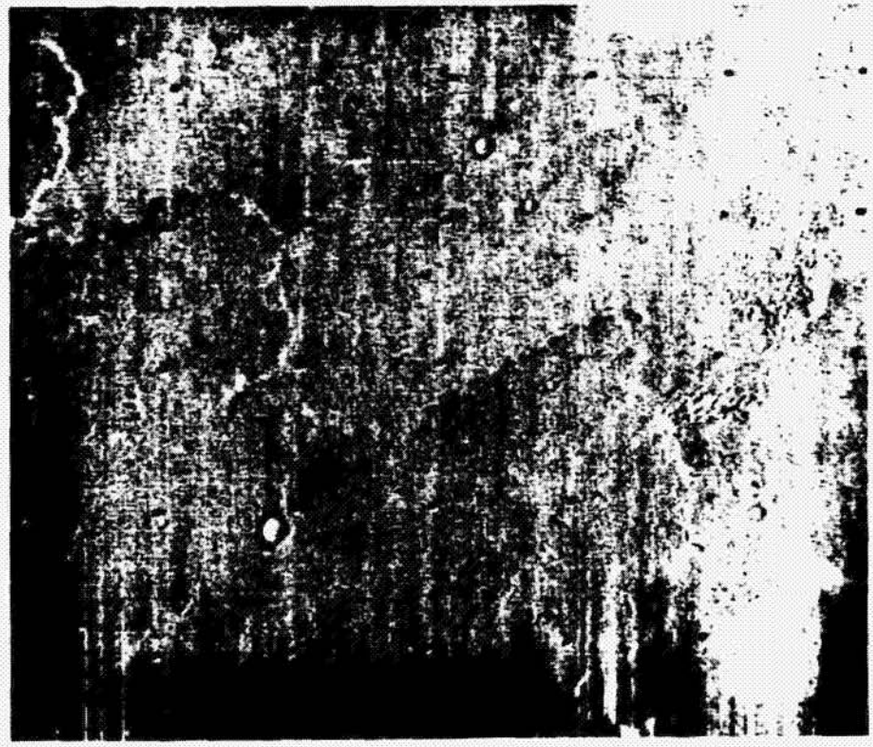

Fig. 1*a*. Lobate lava flow front on basin floor similar to basaltic flows on earth and the moon. (MTVS 4179-30, DAS 6966608.)

craters and the morphologic crispness of the lava flows indicate that the upper layers of these volcanoes are relatively young geologically, whatever their composition. The discovery of geologically youthful, large volcanic structures clearly indicates that Mars has been internally active. These features also provide a plausible source for much of the carbon dioxide and water in the atmosphere.

The Amazonis basin floor is covered in many places by a succession of lobate-fronted flows (Figure 1*a*) that resemble terrestrial basalt flows and the basalt flows that fill the mare basins on the moon (Figures 1*b* and 1*c*). Low mare-type domes with summit craters resemble basaltic shield volcanoes common on both the earth and the moon. Domes of this type are scattered over the basin floors in the Amazonis and Elysium regions [*McCauley et al.*, 1972; *Carr*, 1973].

In some areas the plains are slightly uplifted and transected by faults. Some of these closely spaced horsts and grabens are modified and often assume a streamlined appearance attributed to the long-term effects of eolian erosion [*McCauley*, 1973, Figures 2*a* and 2*b*]. Craters are more abundant in these structured terrains than on unfaulted plains; the most obvious of these faulted areas forms a large aureole around Nix Olympica. These rocks may represent an earlier generation of lava flows related to ancestral Nix Olympica volcanism [*Carr et al.*, 1973].

Another type of volcanic feature is exemplified in the Hesperia region (22°S, 253°W) [*Masursky et al.*, 1972*a*]. This feature is characterized by a line of calderas in the center of a pattern of circular and radiating faults and channels with irregularly distributed volcanic blankets. This unusual feature lies within an area of plains, and no large volcanic pile or constructional edifice is evident [*Carr*, 1973]. The channels closely resemble terrestrial and lunar lava channels. Another example of a volcanic

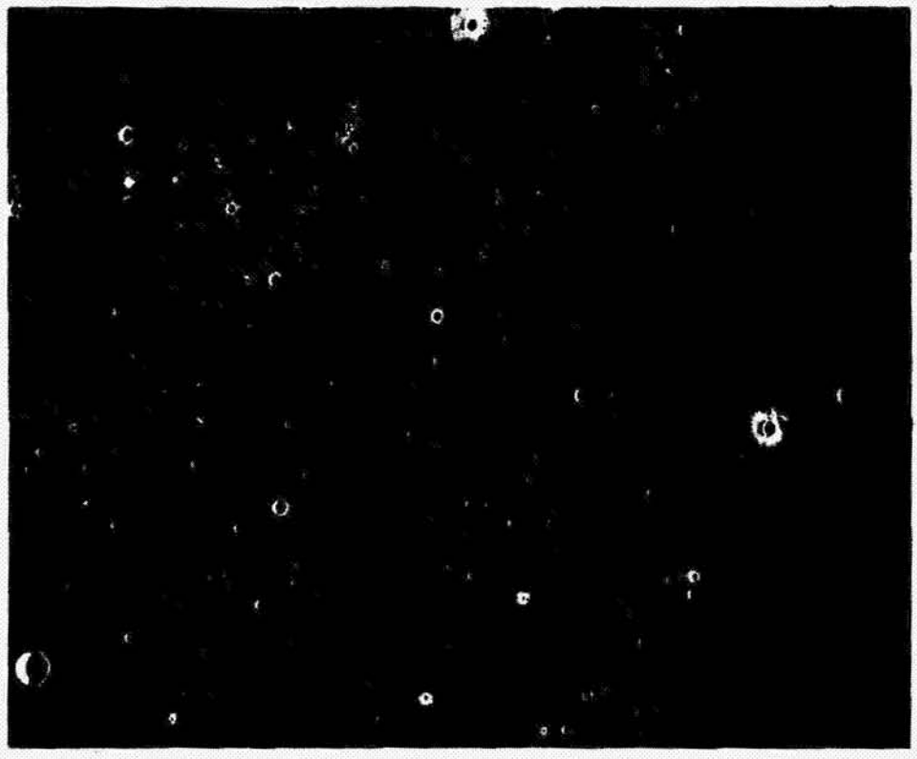

Fig. 1*b*. Lunar Orbiter 5 photograph showing lobate flow front on the moon in central part of Imbrium basin. Similar flows collected at the Apollo 15 landing site are basaltic in composition.

Fig. 1c. Elongate lava flows in northern Oceanus Procellarum photographed by the metric camera on Apollo 15.

feature lies in the Alba region (40°N, 110°W) (Figure 2*a*). Here an array of faults encircles a large depression in the central part of a very low prominence. This depression resembles a cauldron rather than a caldera. The morphology of these deposits and their relation to the tectonic features resemble those of terrestrial intracontinental volcanic centers such as those of Scotland [*Bailey et al.*, 1924; *Anderson*, 1937; *Richey*, 1961], Norway [*Oftedahl*, 1960], New England [*Kingsley*, 1931], and Africa [*Korn and Martin*, 1954] that contain more differentiated rocks of more variable composition than flood basalts and shield volcanoes. These terrestrial volcanic centers, when they are deeply eroded, commonly display ring and radial dikes, cone sheets, and evidence of cauldron subsidence.

Three other types of volcanic features are well developed. The first is typified by lines of craters 2–10 km in diameter along structural breaks parallel to major grabens [*McCauley et al.*, 1972, Figures 25 and 26]. Lines of volcanic vents such as the craters along the southwest rift zone of Mauna Loa, Hawaii [*McDonald and Hubbard*, 1970], are common in terrestrial areas with a similar structural pattern. The second type, which occurs in the floors of some Martian craters (Figure 2*b*) along fault zones, consists of polygonal blocks segmenting what appear to be frozen lava lakes in pit craters like those near the summit of Kilauea, Hawaii. Craters of this type also occur on the moon, where they have been called 'turtleback' craters (Figure 2*c*). The third type of volcanic feature consists of complex ridges that are commonly steeper on one side (Figures 3*a* and 3*b*). They occur in areas where lobate flow fronts and broad low domes imply basaltic volcanism. They resemble the lunar mare ridges that are interpreted as faults along which basaltic lava has squeezed upward. Similar squeezeups are common on terrestrial basalt flows but on a much smaller scale.

Fig. 2*a*. Mosaic of wide-angle pictures showing the complex of faults surrounding the volcanic structure in the Alba region. It resembles terrestrial volcanic complexes with central cauldrons. (MTVS 4224-63, DAS 8443019; MTVS 4222-69, DAS 83771129; MTVS 4222-57, DAS 83710849.)

Tectonic Features

Sloping eastward from the Tharsis ridge crest is a large equatorial plateau or tableland. This plateau is broken by three sets of fractures trending east-west, northwest, and northeast. The paucity of craters indicates that the rocks underlying the plateau are geologically young. East of the mosaic of fault blocks, the grabens between blocks coalesce into the great equatorial canyon or rift valley system (Figure 4), 6 km deep in places, that extends almost 5000 km to the east (Figure 5*a*). Some volcanism associated with the inferred faulting that initiated these unanticipated Martian structures is suggested by the previously mentioned lines of craters along fractures parallel to the main rift valley system. These chain craters, however, lack obvious rim deposits and, alternatively, could be the product of collapse of surficial materials into subsurface fissures. The steep lateral valleys in places appear to be debris channels for mass wasted material. In other channels there are closed depressions that may be degraded volcanic vents. The upper reaches of the shallow sinuous valleys along the southern margin of the rift valley system appear to require formational processes other than mass wasting [*Masursky et al.*, 1972*b*]. Along the cliffs bounding the high plateau, layers and deposits are exposed that average about 100 meters in thickness. The uppermost

Fig. 2*b*. Polygonally broken filling of crater cut by fault. Filling is inferred to be volcanic and resembles terrestrial lava lakes that have solidified. (MTVS 4174-27, DAS 6822588.)

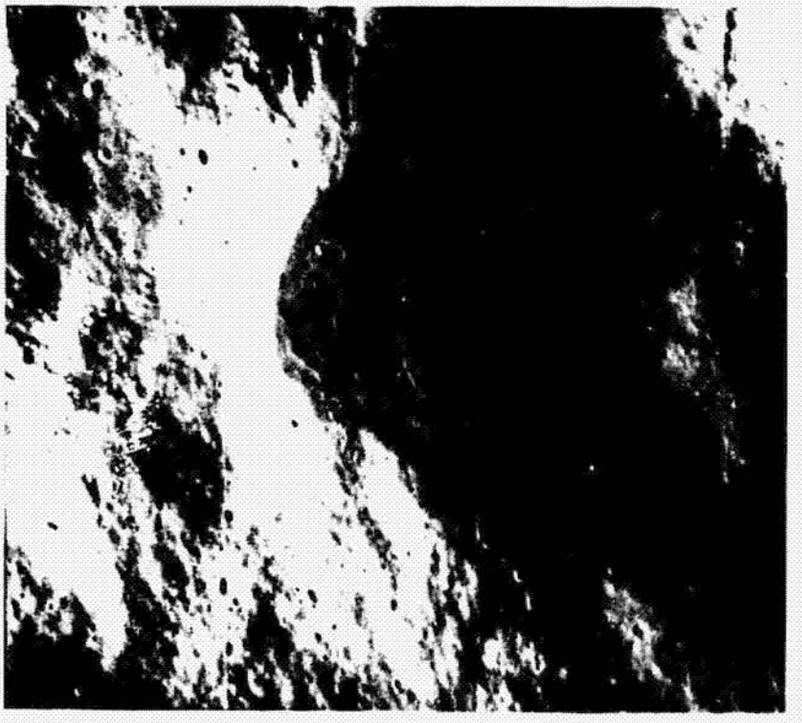

Fig. 2*c*. Turtleback lunar crater near crater Tycho photographed by Lunar Orbiter 5. Filling of crater inferred to be volcanic.

Fig. 3*a*. Wide-angle view of Middle Spot caldera. (MTVS 4081-3, DAS 3930239.)

Fig. 3*b*. Narrow-angle view of Middle Spot showing radiating fracture with accompanying extrusives similar to lunar mare ridges. (MTVS 4096-81, DAS 4402170.)

layer usually seems to be the most resistant and forms a rocky rim. The rocks may be volcanic, since they lie adjacent to the lines of craters that could be the feeder vents. In places, markedly eroded layers are visible within the canyon floors, and many layers of light and dark rocks are exposed (Figure 5*b*). The layers within these presumed valley fill deposits do not seem to match the more obscure and thicker layering in the canyon walls; thus these more

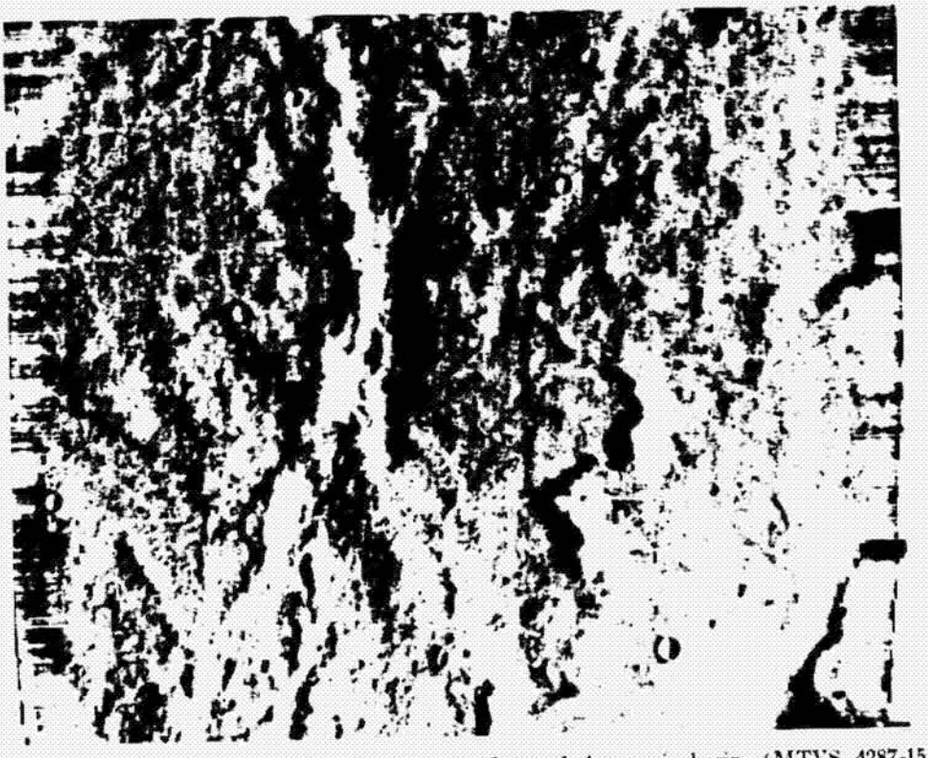

Fig. 3*c*. Complex fracture with extrusives on floor of Amazonis basin. (MTVS 4287-15, DAS 11443439.)

Fig. 4. Mosaic of Mariner 9 wide-angle pictures of the rift valley system.

finely layered deposits could represent earlier generations of valley fill now being stripped out by erosion. In many areas the cliffs are bordered by masses of debris that apparently have slid into the adjacent lowlands. In other areas the material retains its coherence and descends in a series of terraces similar in appearance to the chaotic terrain described in pictures taken by Mariner 6 and 7 [*Sharp*, 1973; *Sharp et al.*, 1971*a*, *b*].

Channels

Emerging from the northern plateau lands, a complex array of broad sinuous channels descends into a regionally depressed area (Figures 6*a* and 6*b*). As the channels merge on the border of the flat low Chryse area, the channel floors show multiple braided channels and streamlined islands (Figure 6*c*) that confirm the northward direction of flow consistent with the regional slope of the surface determined from infrared and ultraviolet spectral data.

Lying on the level high plateau surface are other channels; these are sinuous and have many tributaries [*Masursky et al.*, 1972*c*, *d*; *Milton*, 1973]. The channels descend to the east and north, becoming broader and more clearly defined. The tributaries and the form of the braided channels are unlike those of terrestrial and lunar volcanic sinuous rilles and closely resemble terrestrial intermittent stream channels. Their form and degree of freshness strongly suggest flow of liquid water in the recent geologic past of Mars (Figure 7).

Some channels originate in great masses of hummocky to broken slabby material at the base of cliffs and may be related in origin to this chaotic terrain, as was proposed by *McCauley et al.* [1972] and *Masursky et al.* [1972*a*]. *Sharp et al.* [1971*a*] proposed from the Mariner 6 and 7 pictures that the collapse of these rocks and the formation of large-scale landslides may be caused by melting of permafrost. The more extensive photographic coverage leads to the logical extension of the permafrost proposal; that is, water derived from the melting of the permafrost seeped out from under the slides, formed the broad sinuous channels, and flowed into the northern lowlands. The only terrestrial analogs to these enormous channels, which are 30–60 km wide, are the channeled scablands of the Columbia plateau in the United States and the sandur plains (glacial outwash) of Iceland, which fringe the large glaciers [*Milton*, 1973]. In both areas, great volumes of glacial meltwater result in

torrential floods with accompanying fluviatil: erosion and deposition.

Two proposals have been made to account for the melting of permafrost over large areas. The first hypothesis is that local heating by volcanic activity would mobilize the fluids; the second proposes planetwide heating as a result of secular or cyclical changes in climate. A climate interglacial episode conceivably could melt the permafrost in the large equatorial region and thus be the cause not only of the chaotic terrain but also of the channels.

Somewhat different, very *sinuous* valleys with many tributaries lie on the high-level plateau surface in the Rasena, Mare Erythraeum, and Memnonia regions. The channels with braided floors descend to the east and north, becoming broader and more clearly defined [*Masursky et al.*, 1972*b*]. They apparently are formed by a different process than the broad chaos-related channels. Their primary and secondary tributaries, dendritic patterns, and lack of apparent source areas seem to require rainfall collected into integrated channels along with both surface erosion and deposition in alluvial basins.

Another type of channel is widespread in the ancient cratered terrain such as that near Sinus Sabaeus (8°S, 334°W). Complex networks of tiny coalescent channels run down the sides of many craters. Their origin is not unequivocal, but they also resemble fluvial channels and imply formation of precipitation collection. If this origin is correct, widespread rainfall is

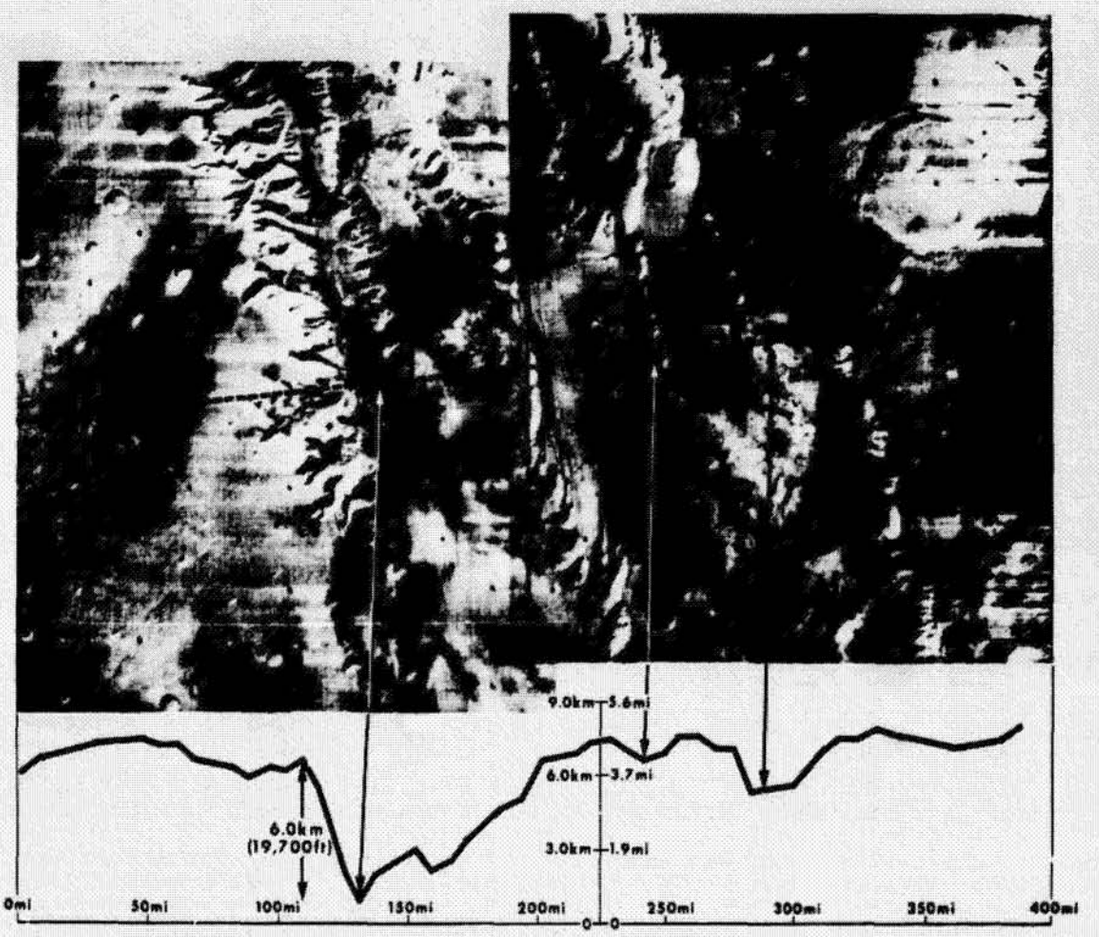

Fig. 5*a*. Inferred elevation profile across the rift valley system using pressure measurements made by the ultraviolet spectrometer [*Hord et al.*, 1973].

Fig. 5*b*. Light and dark layers in equatorial zone. Layers do not match the layers in the adjacent walls of the canyon and may be later fill now being stripped by erosion. (MTVS 4282-11, DAS 1049 2589.)

necessary to feed the channels. The occurrence of the channels in the equatorial zone suggests that only a slight temperature rise may be necessary to produce liquid water there, if the water partial pressure were to be raised at the same time. An 'interglacial' episode that melted the polar caps and planetwide permafrost should be adequate to allow flowing water to exist in the equatorial zone on the surface of Mars.

Another type of channel is associated with volcanic centers (Figure 8*a*). The channels start on the flanks of volcanic craters and are less well defined downstream. This relationship is the opposite of that generally observed in fluviatile channels. These features closely resemble lunar sinuous rilles such as the Hadley and Prinz rilles (Figure 8*b*) and are now generally thought to be collapsed lava channels in basaltic rocks, as is inferred from the samples and photographs returned by the Apollo 15 mission.

In summary, channels can be divided into four groups: the three varieties discussed with characteristics that imply a fluviatile origin in which water must be the transport medium (broad and sinuous, narrow with braided floors and tributaries, and small and closely spaced) and a fourth variety with characteristics that imply a volcanic origin involving molten lava flows.

Polar Features

Monitoring of the polar regions allowed observation of the rapid retreat of the frost cover from its maximum extent of more than 50° across when it was photographed in 1969 to a minimum of less than 10° across in 1972 [*Masursky et al*, 1972*a*; *Soderblom et al.*, 1973*a*]. Ancient cratered terrain extends from north of the equator southward to the south polar region, where it is overlapped by two younger units (L. A. Soderblom, personal communication, 1972). The older of these overlying units is moderately cratered and has many closed depressions that appear to be deflation hollows (Figure 9*a*). This 'etch-pitted' unit is composed of alternating resistant and nonresis-

Fig. 6*a*. Mosaic of wide-angle pictures showing broad sinuous channels emerging from the base of the landslide debris and flowing north into the lowland.

tant rock layers that produce numerous topographic benches and slopes along exposed edges. The exposures of etch-pitted terrain surrounding the polar region indicate a zone of high wind velocity that is stripping the surface and forming deflation hollows. The etch-pitted unit is overlain by layered rocks originally termed the 'laminated terrain' (Figure 9*b*). The two units of young layered deposits do not overlie the ancient terrain in a platelike fashion. Although they total about 6 km in thickness, the central part lies at a lower elevation than the surrounding ancient cratered terrain covered by ice at the pole [*Hord et al.*, 1972]. Thus these layered rocks occupy a saucer-shaped depression that defines a discrete basin in both polar regions. It may be that the polar rocks have been depressed by formerly thicker polar ice. A quantitative measure of the degree of this deformation could be an indicator of the mobility of the Martian suberust.

The uniformly bedded layers best observed in the laminated terrain are estimated to range from 10 to 30 meters in thickness (L. A. Soderblom and J. A. Cutts, personal communication, 1972). There are about 20 layers in each cuestalike ridge, of which there are 6–12 encircling the pole. The individual thin layers appear to be cyclical deposits, as the groups of layers that form the ridges that showed in the Mariner 1969 pictures may be [*Sharp et al.*, 1971*b*]. The ledges are being eroded; the edges are smoothly rounded, unlike the sharp-edged ridges in the etch-pitted and central plateau

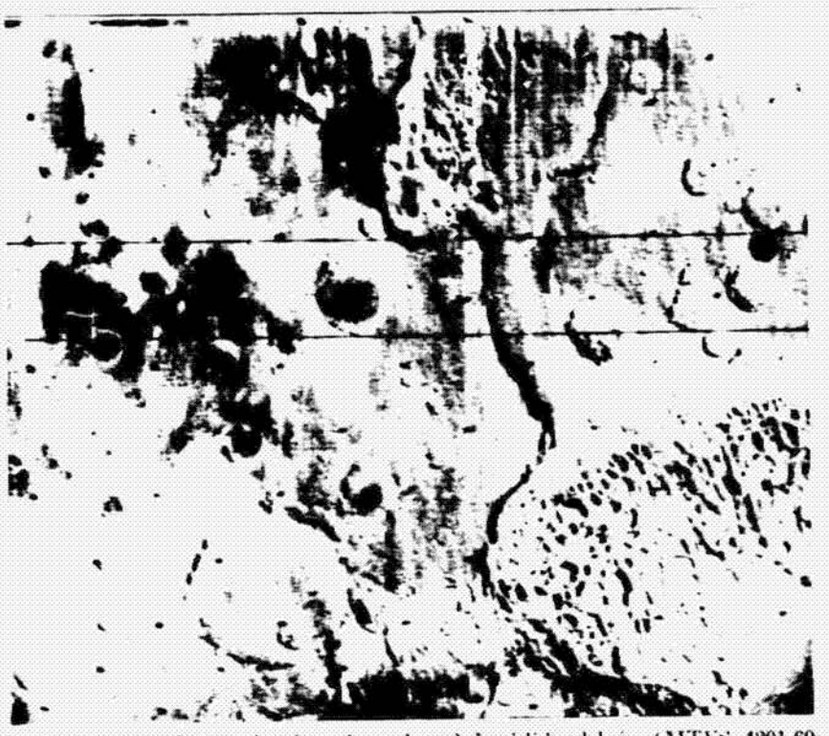

Fig. 6*b*. Wide-angle picture showing channel and landslide debris. (MTVS 4201-60, DAS 07686808.)

Fig. 6*c*. Braided channel with its source near the toe of a hummocky debris landslide. (MTVS 4206-63, DAS 07830588.)

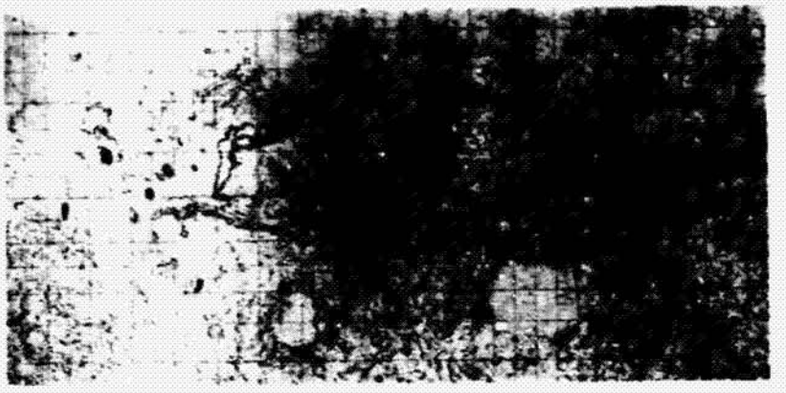

Fig. 7. Map showing the distribution of three fluviatile-type Mars channels.

regions. Subjacent craters are partially covered in many places; apparently they are being reexhumed after burial. The upper surfaces of these deposits on which the remnant polar ice cap lies are grooved radial to the pole [*Murasky et al.*, 1972b; *Cutts*, 1973]. These grooves may have been formed by wind erosion or perhaps even by glacial scour.

The south and north polar regions are similar (Figures 10 and 11) and apparently have acted

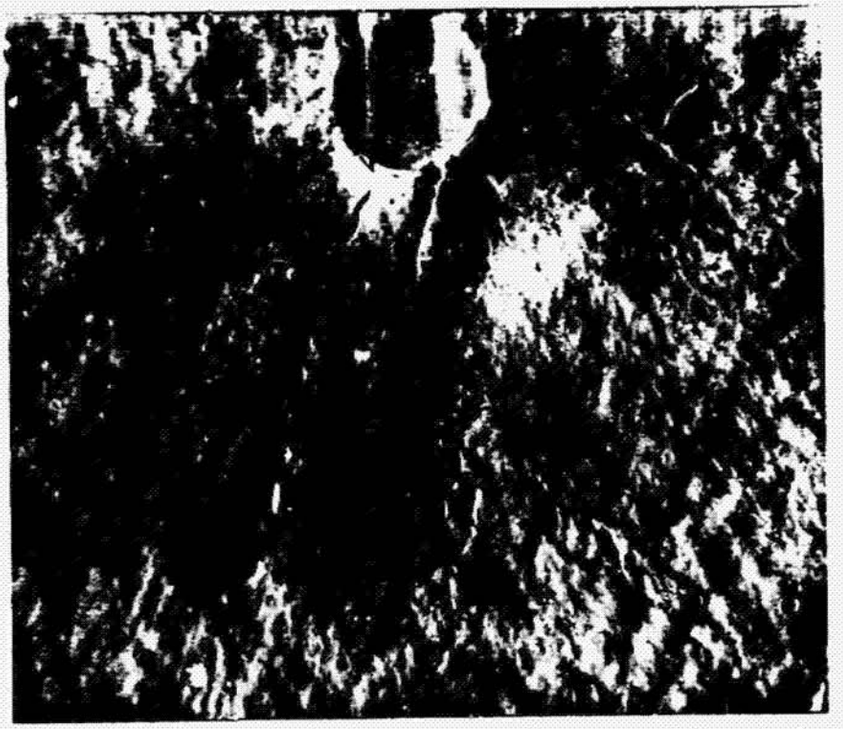

Fig. 8*a*. Lava channel on flank of crater; starts in crater and descends, becoming smaller in contrast to the fluviatile-type channels that grew downstream. (MTVS 4298-39, DAS 13496088.)

Fig. 8*b*. Priaz rilles in northwest part of moon photographed by Lunar Orbiter 5. The crater at the head of the rille is the side of the crater Priaz. It descends to the north, becoming narrower and shallower in contrast with the fluviatile-type channels on Mars.

as sediment traps throughout much of Mars history. Sedimentation in these areas must have started when the planet cooled enough to initiate frost accumulation in the polar region. Pervasive wind erosion in the equatorial regions took place; these sediments were then transported, principally in suspension, and deposited into the polar regions. The polar deposits may be thought of as glacio-eolian, formed when the dust particles acting as nuclei around which the snow crystals form are laid down as horizontal layers. A similar process takes place on earth when rain, wind, and snow sweep the atmosphere clean of dust particles. Alternatively, descending air currents in the polar high-pressure zone may abet the entrapment of dust particles on the surface ice, in much the same way as dust is entrapped in terrestrial ice fields and glaciers.

Eolian Features

The planetwide dust storm appears to have blanketed much of the surface with bright silt and clay-sized particles, obscuring most of the dark markings normally observed telescopically. Since the end of the storm, bright material has been locally scoured from the surface and reveals the darker, presumably coarse-grained, underlying surface. During the mission a local dust storm was observed, and after its passage a dark track was visible [*Leovy et al.*, 1973]. As the mission progressed, the classic dark sur-

Fig. 9*a*. Etch-pitted terrain in the south polar region that overlies the ancient cratered terrain and is overlain by the laminated terrain. The closed depressions probably were made by deflation. The winds are particularly strong adjacent to the polar ice, as they are on earth in Antarctica and Greenland. (MTVS 4132-21, DAS 05453843.)

Fig. 9*b*. Laminated terrain in the south polar region overlain by residual ice. It eroded with rounded edges and was deposited cyclically. The short cycles comprise 8-10 layers, which make up ledges that form the circumpolar features. (MTVS 4213-21, DAS 08080243.)

face markings began to reemerge as the fine-grained and brighter surficial materials were scoured and redeposited [*Sagan et al.*, 1973].

Uniformly distributed deposits that fringe the polar regions and blanket the plains may correspond to terrestrial loess (widespread deposits of silt and clay-sized particles). Their redistribution reveals dark irregular markings and light and dark tails emanating from craters and other topographic obstacles. The light tails appear to be wind-deposited material; the dark tails appear to be mostly wind-scoured zones in the lee of various topographic obstacles. In other cases some dark streaks appear to be dark deposits.

In some areas dark markings in wide-angle pictures have been resolved into sand dune fields in the narrow-angle pictures [*Cutts and Smith*, 1973]. This dune field, about 50 km across, lies in the bottom of a crater. The spacing of the crests of individual dunes is of the order of 1–2 km. In size and shape this feature is similar to many dune fields and sand sheets in terrestrial deserts such as the Mojave Desert in southern California, within which the Kelso dune field is a good analog [*Sharp*, 1963]. Adjacent to the etch-pitted south polar terrain is an area of 'riffles,' which resemble longitudinal or seif dunes. Equatorward, in addition to the dune fields, the mottled cratered plains and smooth plains are areas of irregular to uniform eolian loesslike deposits that indicate even lower wind velocities. The identification of dunes is significant because dunes indicate that saltation is operative on the surface despite the tenuous atmosphere. With saltation occurring, numerous eolian erosion and deposition features should be expected at larger scales; some of these features are described by *McCauley* [1973] and compared with pure erosion forms in the coastal desert of Peru

Impact Craters

Although impact craters are common on about one half of the planet's surface, fresh craters with well-developed ejecta blankets are

Fig. 10. Mosaic of wide-angle pictures of the south polar region showing the terrain units and residual cap. The polar deposits stand higher and overlie the ancient continental cratered terrain. The laminated deposits are deep inward and are topographically lower than the surrounding cratered terrain forming the polar basin.

Fig. 11. Mosaic of wide-angle pictures of the north polar region showing the terrain and residual cap. The region lies 3 km lower than the south pole. The polar deposits lie on plains deposits of ocean basin type. The topography is not yet well enough known to determine whether the deposits are in a basin.

rare [*Masursky et al.*, 1972*d*]. A few small craters show hummocky continuous ejecta blankets and well-developed rays. Most small craters, however, exhibit degraded ejecta blankets and no ray patterns.

Interpretation of lunar craters indicates that the first crater-related feature that disappears by erosion is the ray material, which originally extended outward for many crater diameters. The continuous ejecta blankets, up to two crater diameters in width, are more resistant to wind erosion. These deposits eventually lose their hummocky character, but the outer irregular edges remain as low ridges. The very slow degradation of craters on the moon is largely by impact gardening; on Mars the erosion is probably dominantly eolian. Most of the ray material of lunar craters and terrestrial experimental craters is fine grained; such material on Mars would be subject to degradation and transportation by winds. Thus the paucity of ray craters is an indicator of the effectiveness of the eolian erosional and depositional processes on Mars.

Prominent in the southern hemisphere of the planet are craters ranging from the limit of resolution (200–300 meters) up to the Hellas and Argyre basins. (Hellas is 2000 km in diameter and one half again the size of the Imbrium basin on the moon.) The cratering in this hemisphere is similar to that in the southern highlands of the near side and much of the far side of the moon [*Masursky et al.*, 1972*d*; *Wilhelms*, 1973]. The abundance of craters here is such that this terrain must be relatively older geologically. The crater frequency is less, however, than that on Phobos, the satellite of Mars, and in the most heavily cratered of the lunar uplands [*Hartmann*, 1973]. This lower crater frequency probably indicates destruction of some craters by various processes that include all previously mentioned (i.e., volcanism, tectonism, channel generation, and eolian erosion and deposition).

The Argyre basin is ringed by radially and concentrically textured mountainous terrain that indicates its similarity to the lunar multiringed impact basins such as Imbrium and

Orientale [*Hartmann and Kuiper*, 1962; *Hartmann and Wood*, 1971]. However, the deposits are altered by subsequent events, including eolian modification, so that they do not display the structural and depositional textures still preserved in the drastically less dynamic lunar environment [*Wilhelms and McCauley*, 1971]. Rough-textured, externally and internally terraced, generally circular craters with central peaks are thought, like those on the moon, to be of impact origin if they are not so degraded as to have these diagnostic characteristics obliterated.

Craters of impact type are clearly distinct from the smooth-rimmed volcanic craters with their commonly attendant radiating lava channels and flows. Secondary crater arrays are visible in several areas and are distinct from the linear arrays of volcanic craters along structural lineaments. They are, however, far less abundant than on the moon and generally cannot be identified as to source.

Planetwide Distribution of Geologic Units

The cratered terrain apparently is the most ancient on Mars and probably records, as it does on the moon, the impact of cosmic debris on the early differentiated planet [*Masursky*, 1973; *Carr et al.*, 1973, Figure 1]. Preliminary correlation of gravity mapping achieved by tracking the Mariner 9 spacecraft with topography from several sources indicates that the lowlands and plateau regions previously described are largely isostatically compensated. This result is in agreement with the distribution of rocks on the moon, where the highlands are underlain by low-density crustal rocks with high Al/Si ratios and the lowlands are underlain by basalts that may rest directly on mantle rocks. For Mars, the cratered terrain that occupies most of the southern hemisphere may represent the more siliceous 'continental' crustal rocks. The Amazonis and adjacent Elysium basin and the northern lowlands may be underlain by basalts resting on the mantle and may be the gross equivalents of the terrestrial ocean basins and Oceanus Procellarum on the moon. Within the primitive cratered terrain are areas filled by smoother, younger material with lower, but still substantial, crater populations. These cratered plains are overlain by smooth deposits that form the plains, which comprise several different units. The smooth plains locally exhibit lobate laval flow fronts and broad low shield volcanoes attesting to the probable basaltic nature of the smooth deposits.

Mantling the smooth lava plains are possible alluvial deposits at the mouths of the channels in the Chryse and Lunae Palus regions. These deposits probably form piedmont alluvial and possibly playa sequences near where the channels debouche into the lowlands, so that some of the smooth plains may consist of sedimentary deposits. Pediplanation may have taken place in a few areas along channel margins and where plateau edges and isolated hills and mesas seem to be retreating [*Milton*, 1973].

Eolian deposits derived from the polar-eolian sediment traps may have been spread equatorward [*Soderblom et al.*, 1973*b*]. The thickness of these loess and dune deposits on the northern lava plains can be estimated from their apparent thickness in the south polar region. Here the mantling eolian material cannot exceed tens to hundreds of meters in thickness, for it partly but does not completely mask the south polar cratered terrain. Thinner deposits of eolian sediments (possibly silt and sand) cover the central part of the planet in places. Apparently these deposits in the central part of the planet are mobile, as the continually changing light and dark patterns monitored after the great dust storm attest. They must be only a few meters in thickness, as they do not obscure textural detail in the cratered and faulted terrain. Thicker loess deposits probably lie within Hellas and other similar large circular basins and craters, but their thickness cannot be determined; such regions do appear, however, to be the source areas for many Martian dust storms, including that of 1971 [*Capen and Martin*, 1971].

The south polar glacio-eolian deposits overlie the cratered terrain; the north polar deposits overlie smooth and cratered plains. The north polar region is about 3 km lower than the southern region (A. J. Kliore, personal communication, 1972). This observation is consistent with the morphology of the terrain, which suggests that the south polar region is part of the continental mass; the north polar region is part of the 'ocean' basin floor.

The margins of the central continental block are varied. At 100° to 130°W the margin is

abrupt and the slopes are steep; the crest of the Tharsis ridge is marked by the three aligned volcanic structures. Perhaps this continental margin is the site of incipient plate tectonic movement; alternatively, the volcanoes may lie along a zone of vertical movement bounding the continental block. The northern margin is irregular with gentler slopes. The contact between the cratered plains and the low-lying smooth plains is gradational and has many irregularly disposed hills and mesas. The central canyon or troughed zone may mark a rift zone developed by the highland rocks sliding into the northern lowlands; again alternatively, the canyons may mark complex vertical faulting, the most complex faulting being in the area of greatest uplift and adjacent to the thickest young volcanic rocks that overlie the continental crust.

Geologic History

The various topical studies presented in this issue and the regional geologic mapping accomplished to date permit an expansion and synthesis of the earlier preliminary geologic histories presented for the equatorial belt [*McCauley et al.*, 1972; *Carr et al.*, 1973]. The principal data used are overlap relations between geologic units and differences in their crater populations. These relations show that Mars has a decipherable history that dates far back in time. This history may place some boundary conditions on theories about the evolution of its atmosphere and the development of an ice regime. The heavily cratered generally high-standing rocks that lie predominantly in the mid-latitudes and southern latitudes are the most ancient on the planet, as has been recognized since Mariner 6 and 7 [*Leighton and Murray*, 1971].

Large lunar basins such as Imbrium formed after the initial differentiation of the entire moon. Ejecta from these basins contain norites, anorthositic gabbros, and anorthosites that form the crustal rocks, which stand high because of their lesser density. A similar process probably took place on Mars, so that the high-standing heavily cratered rocks may be part of the early differentiated continental crust.

During a time of rapidly decreasing flux of impacting bodies, the many large flat-floored craters formed, as well as the large impact basins, Hellas, Argyre, and Libya. Hellas appears to be the oldest, as its rim has been almost completely destroyed and the number of superimposed craters around its edge is comparable to the rest of the heavily cratered terrain. Argyre and Libya are more rugged than Hellas and have fewer superimposed craters. They probably formed later.

Impact presumably continued at a decreasing rate, but volcanism started early in this episode. The oldest volcanic feature recognized is a volcano on the northeast rim of the Hellas basin (M. H. Carr, personal communication, 1972). This heavily cratered (it has twice as many craters as the oldest of the plains units) and eroded feature at first was difficult to recognize; other features may be found as systematic geologic analysis continues. The ancient volcano is of particular significance because it indicates that volcanism of the type observed in the Amazonis region began early in Mars history and within the ancient cratered terrain. Old plains units mantle parts of the ancient cratered terrain and are marked by lower crater frequencies. They are difficult to delineate because erosion and deposition have obscured their contacts. The oldest plains unit that can be mapped satisfactorily occurs in the Lunae Palus area and overlies part of the volanic structures in the Hesperia region. It has a greater crater density than most of the lunar maria. Its absolute age, like that of the other Martian units, is difficult to assess because the relative contributions to the flux of cometary and asteroidal impacts are not known.

Next younger in age are the heavily faulted plains around Nix Olympica, in Arcadia, and in Alba. They appear to be basalt flows, similar to those in the surrounding smooth plains, that have been slightly uplifted, faulted, heavily modified by eolian erosion, and moderately cratered. Mottled cratered terrain underlies large areas in the northern regions. It is moderately cratered and partly covered by eolian deposits. Volcanism probably started in the Nix Olympica area about the same time that these plains formed. The erosional scarp at the base of Nix Olympica suggests that these layers were being eroded while the upper part of the mountain was still being constructed. The next youngest plains unit occurs in the Phoenicis Lacus and Elysium areas. It is moderately cratered and faulted; the number of craters is

comparable to that on most lunar maria. It embays knobby terrain, indicating that the process forming the latter unit began before deposition of the moderately cratered plains.

Upwarping or epeirogeny then took place in the Tharsis region and resulted in mosaiclike fault patterns as well as the extensive rifting to the east in the main part of the Coprates canyon system. The upper part of the Nix Olympica as well as the Tharsis shield volcanoes then formed. Contemporaneously, the young lava plains with their abundant flow fronts and lava domes were extruded. Chaotic terrain developed later along the margins of the equatorial plateau. Broad channels then formed, apparently over a considerable time, since some of their floors are moderately cratered and others are little cratered. Their development may have paralleled the construction of the large volcanoes.

Eolian deposition and erosion extended over a considerable time up to the present; in the polar regions the laminated terrains were being deposited and eroded and redeposited in great mantles of sand and loesslike deposits that thin equatorward. Etch-pitted plains surrounding the poles attest to the intensity of eolian erosion of earlier deposits in the vicinity of the polar caps. This erosion raises the possibility that earlier generations of laminated terrain have been redistributed. The present polar deposits may record only the latest episode of deposition of layered materials.

The possible fluviatile channels may record episodes when water was much more abundant in the atmosphere than it is at present. Planet-wide warmer interglacial periods would release not only the water locked in the polar caps but also that frozen in the subsurface as permafrost. Similar warmer and colder periods also are characteristic of terrestrial history. Still continuing is the erosional modification of landforms and deposition of widespread silt and clay loess deposits and local sand dunes.

Acknowledgments. Members of the television team were H. Masursky (leader), D. Arthur, R. Batson, W. Borgeson, G. Briggs, M. Carr, P. Chandeysson, J. Cutts, M. Davies, G. de Vaucouleurs, W. Hartmann, J. Lederberg, R. Leighton, C. Leovy, E. Levinthal, J. McCauley, D. Milton, B. Murray, J. Pollack, C. Sagan, R. Sharp, E. Shipley, B. Smith, L. Soderblom, J. Veverka, R. Wildey, D. Wilhelms, and A. Young. Publication authorized by the Director, U.S. Geological Survey.

This work was done under the auspices of the Jet Propulsion Laboratory, California Institute of Technology contract WO-8122.

References

Anderson, E. M., Cone-sheets and ring dykes: The dynamical explanation, *Bull. Volcanol., 1,* 35, 1937.

Bailey, E. B., C. T. Clough, W. B. Wright, J. E. Richey, and G. V. Wilson, Tertiary and post-Tertiary geology of Mull, Loch Aline, and Oban, *Mem. Geol. Surv. Scot.*, 445 pp., 1924.

Barth, C. A., A. I. Stewart, C. W. Hord, and A. L. Lane, Mariner 9 ultraviolet spectrometer experiment: Mars airglow spectroscopy and variations in lyman alpha, *Icarus, 17,* 457, 1972.

Batson, R. M., Cartographic products from the Mariner 9 mission, *J. Geophys. Res., 78,* this issue, 1973.

Cain, D. L., A. J. Kliore, B. S. Seidel, M. J. Sykes, and P. M. Woiceshyn, Approximations to the near surface of Mars and Mars atmosphere using Mariner 9 occultation, *J. Geophys. Res., 78,* this issue, 1973.

Capen, C. F., and L. J. Martin, The developing stages of the Martian yellow storm of 1971, *Bull. Lowell Observ., 157,* 211, 1971.

Carr, M. H., Volcanism on Mars, *J. Geophys. Res., 78,* this issue, 1973.

Carr, M. H., H. Masursky, and R. S. Saunders, A generalized geologic map of Mars, *J. Geophys. Res., 78,* this issue, 1973.

Cutts, J. A., Wind erosion in the Martian polar regions, *J. Geophys. Res., 78,* this issue, 1973.

Cutts, J. A., and R. S. U. Smith, Eolian deposits and dunes on Mars, *J. Geophys. Res., 78,* this issue, 1973.

Downs, G., R. M. Goldstein, R. R. Green, and G. A. Morris, Mars radar observations: A preliminary report, *Science, 174,* 1324, 1971.

Hanel, R. A., B. Conrath, W. Hovis, V. Kunde, P. Lowman, W. Maguire, J. Pearl, J. Pirraglia, C. Prabhakara, B. Schlachmann, G. Levine, P. Straat, and T. Burke, Investigation of the Martian environment by infrared spectroscopy on Mariner 9, *Icarus, 17,* 423, 1972.

Hartmann, W. K., Martian cratering, 4, Mariner 9 initial analysis of cratering chronology, *J. Geophys. Res., 78,* this issue, 1973.

Hartmann, W. K., and G. P. Kuiper, Concentric structures surrounding lunar basins, *Commun. Lunar Planet. Lab., 1,* 51, 1962.

Hartmann, W. K., and C. A. Wood, Moon: Origin and evolution of multi-ringed basins, *Moon, 3,* 4, 1971.

Hord, C. W., C. A. Barth, A. I. Stewart, and A. L. Land, Mariner 9 ultraviolet spectrometer experiment: Photometry and topography of Mars, *Icarus, 17,* 443, 1972.

Kingsley, L., Cauldron subsidence of the Ossipee Mountains, *Amer. J. Sci., 22,* 139, 1931.

Kliore, A. J., D. L. Cain, G. Fjeldbo, B. L. Seidel, M. J. Sykes, and S. I. Rasool, The atmosphere of Mars from Mariner 9 radio occultation measurements, *Icarus, 17*, 484, 1972.

Korn, H., and H. Martin, The Messum igneous complex in south-west Africa, *Trans. Geol. Soc. S. Afr., 57*, 83, 1954.

Leighton, R. B., and B. C. Murray, One year's processing and interpretation—An overview, *J. Geophys. Res., 76*, 293, 1971.

Leovy, C. B., G. A. Briggs, and B. A. Smith, Mars atmosphere during the Mariner 9 extended mission: Television results, *J. Geophys. Res., 78*, this issue, 1973.

Levinthal, E. C., W. B. Green, J. A. Cutts, E. D. Jahelka, R. A. Johansen, M. J. Sander, J. B Seidman, A. T. Young, and L. A. Soderblom, Mariner 9 image processing products, *Icarus, 18*, 75, 1973.

Lorell, J., G. Born, E. Christensen, P. Esposito, J. F. Jordan, P. Laing, W. Sjogren, S. Wong, R. Reasenberg, I. Shapiro, and G. Slater, Gravity field of Mars from Mariner 9 tracking data, *Icarus, 18*, 304, 1973.

Masursky, H., An Apollo view of lunar geology, in *Lunar Science*, vol. 4, edited by J. W. Chamberlain, and C. Watkins, pp. 511–512, Lunar Science Institute, Houston, Tex., 1973.

Masursky, H., et al., Television experiment for Mariner Mars, 1971, *Icarus, 12*, 10, 1970.

Masursky, H., et al., Mariner 9 television reconnaissance of Mars and its satellites: Preliminary results, *Science, 175*, 395, 1972*a*.

Masursky, H., et al., A planet-wide view of the geology of Mars (abstract), *Geol. Soc. Amer. Abstr. Programs, 4*, 584, 1972*b*.

Masursky, H., et al., Mariner 9 Mars television experiment (abstract), *Bull. Amer. Astron. Soc., 4*, 356, 1972*c*.

Masursky, H., et al., A planet-wide view of the geology of Mars as observed from Mariner 9, paper presented at 15th meeting of COSPAR, Madrid, May 10–24, 1972*d*.

McCauley, J. F., Mariner 9 evidence for wind erosion in the equatorial and mid-latitude regions of Mars, *J. Geophys. Res., 78*, this issue, 1973.

McCauley, J. F., M. H. Carr, J. A. Cutts, W. K. Hartmann, H. Masursky, D. J. Milton, R. P. Sharp, and D. E. Wilhelms, Preliminary Mariner 9 report on the geology of Mars, *Icarus, 17*, 289, 1972.

McDonald, G. A., and D. H. Hubbard, *Volcanoes of the National Parks in Hawaii*, 5th ed., 56 pp., Hawaii National Historical Association, Hawaii National Park, 1970.

Milton, D. J., Water and processes of degradation in the Martian landscape, *J. Geophys. Res., 78*, this issue, 1973.

Oftedahl, C., Permian igneous rocks of the Oslo graben, Norway, *Int. Geol. Congr. 21st*, 1960.

Pettengill, G. H., A. E. E. Rogers, and I. I Shapiro, Martian craters and a scarp as seen by radar, *Science, 174*, 1321, 1971.

Richey, J. E., *Scotland: The Tertiary Volcanic Districts*, 3rd ed., revised by A. G. MacGregor and F. W. Anderson, 119 pp., Department of Scientific and Industrial Research, Geological Survey and Museum, Edinburgh, Scotland, 1961.

Sagan, C., J. Veverka, P. Fox, R. Dubisch, R. French, P. Gierasch, L. Quam, J. Lederberg, E. Levinthal, R. Tucker, B. Eross, and J. B. Pollack, Variable features on Mars, 2, Mariner 9 global results, *J. Geophys. Res., 78*, this issue, 1973.

Sharp, R. P., Wind ripples, *J. Geol., 71*, 617, 1963.

Sharp, R. P., Mars: Fretted and chaotic terrains, *J. Geophys. Res., 78*, this issue, 1973.

Sharp, R. P., L. A. Soderblom, B. C. Murray, and J. A. Cutts, The surface of Mars, 2, Uncratered terrains, *J. Geophys. Res., 76*, 331, 1971*a*.

Sharp, R. P., B. C. Murray, R. B. Leighton, L. A. Soderblom, and J. A. Cutts, The surface of Mars, 4, South polar cap, *J. Geophys. Res., 76*, 357, 1971*b*.

Simkin, T., and K. A. Howard, Caldera collapse in the Galapagos Islands, 1968, *Science, 169*, 429, 1970.

Soderblom, L. A., M. C. Malin, J. A. Cutts, and B. C. Murray, Mariner 9 observations of the surface of Mars in the north polar region, *J. Geophys. Res., 78*, this issue, 1973*a*.

Soderblom, L. A., T. J. Kreidler, and H. Masursky, The latitudinal distributions of erosional debris on the Martian surface, *J. Geophys. Res., 78*, this issue, 1973*b*.

Soffen, G. A., and A. T. Young, The Viking mission to Mars, *Icarus, 16*, 1, 1972.

U.S. Geological Survey, Shaded relief map of Mars, *Atlas of Mars*, MM 25 MIR I 810, scale 1: 25,000,000, Washington, D.C., 1972.

Wilhelms, D. E., Comparisons of Martian and lunar multiringed circular basins, *J. Geophys. Res., 78*, this issue, 1973.

Wilhelms, D. E., and J. F. McCauley, Geologic map of the nearside of the moon, *Geologic Atlas of the Moon, I-703*, U.S. Geol. Surv., Washington, D.C., 1971.

(Received February 2, 1973;
revised March 22, 1973.)

CHAPTER XII – EDUCATIONAL RESOURCES

Educational Programs and Services – *G. A. Hull*

EDUCATIONAL PROGRAMS AND SERVICES

Garth A. Hull
Ames Research Center, NASA, Moffett Field, Calif. 94035

NASA's Ames Research Center is responsible for providing to colleges and universities in the eleven Western states – including California and Oregon – speakers, films, publications, and center visits to augment school curriculums.

For information about these services, please contact the Educational Programs Office, NASA–Ames Research Center, Moffett Field, CA 94035, or call 415/965-5543. The personnel responsible are Garth Hull, Mike Donahoe, and Barbara Busch.

Films

The National Aeronautics and Space Administration provides films describing NASA research and development programs in space and aeronautics, and documents the results of this research. Approximately 75 titles are currently being loaned, including documentaries on each Apollo lunar exploration. There is no rental charge; however, borrowers must pay for the cost of return postage and insurance. Please order at least 30 days in advance (see Appendix H).

Publications

Educational Publications are designed to present and explain NASA's goals and projects and to document new knowledge generated by these programs. These publications are free-of-charge to teachers, upon request. Additional copies can be ordered from the Superintendent of Documents, U. S. Government Printing Office, Washington, D. C. 20402. The foldout (black-and-white) flyers are available free-of-charge to all requestors, in single or bulk quantities.

Educational Publications Mailing List

A mailing list maintained by NASA Headquarters in Washington, D. C., provides teachers with a sample copy of new educational publications. An application form for that mailing list can be obtained through NASA-Ames.

Special Publications

NASA's Scientific and Technical Information Division publishes detailed reports on NASA's accomplishments. These publications are also available from the Superintendent of Documents. The Federal Book Store, 450 Golden Gate Avenue, San Francisco, provides the same ordering service in a shorter period of time. Library reference copies are available for the entire series at major library depositories, located at the University of California/Berkeley, the Los Angeles and San Diego Public Libraries, and at Ames Research Center.

Speakers

NASA provides speakers, including education specialists as well as its scientists. The specialists provide special lectures to audiences at community colleges, augmented by audio-visual materials, models, etc. These specialists, in their mobile vans, move throughout the Western states providing this service. NASA scientists and engineers, when time and travel funds permit, enjoy the opportunity to address community college students and faculty in their subject fields. When an on-site lecture is not practical, lectures are sometimes given from Ames by telelecture. The telelecture is a technique whereby visual aids are sent ahead to the requesting organization, and the speaker then addresses the audience via a two-way audio hook-up.

In addition, the Jet Propulsion Laboratory, Pasadena, California, provides speakers concerned with JPL's missions, particularly to Southern California audiences.

Slides and Audio Visuals

Ames Research Center maintains a varied collection of 35-mm slides on various aspects of the space program. In addition, Ames provides slide-copying service. The users, bringing their own film, can reproduce these resources during Ames' working hours. In addition, our Earth Resources Data Facility encourages users to copy their resources, mostly high-altitude photographic coverage of the Western United States. The entire Earth Resources Photographic Collection is located at EROS (Department of the Interior), Sioux Falls, South Dakota 57198. The telephone number is 605/594-6511. ERTS, Skylab, and high-altitude aircraft photography in various spectra are available at cost.

Library Resources

The Ames Research Center Library is open to students and faculty. The Library specializes in aeronautics, astronautics, and life sciences collections. An excellent periodical and abstract service collection is available. These materials are available for reference use.

Work-Experience Programs

Ames Research Center provides work experience opportunities for college students. The Foothill and San Mateo Community College Districts currently have 107 students working at Ames in eighteen career categories.

Center Visits

Ames Research Center hosts college and university students and faculty whenever possible. Programs are normally scheduled for approximately two hours, at 10:00 a.m., 1:00 p.m., and 2:45 p.m., Monday through Friday. Briefings are normally associated with our wind tunnels, motion simulations, and research aircraft. If possible, special programs are arranged for specific interest areas. Please contact us at least one month in advance to arrange for these programs.

APPENDIX

SOURCES OF INFORMATION AND MATERIAL

A. *Lunar and Planetary Geology Text Books*

Hartmann, W. K., 1972. *Moons and Planets*, Bogden and Quigley, Inc., Tarrytown-on-Hudson New York, and Belmont, California.

Mutch, T. A., 1972. *Geology of the Moon: A stratigraphic view.* Princeton University Press, Princeton, New Jersey. College-level text and reference, well written and illustrated. Extensively revised from th 1970 first edition. $22.50.

B. *Reference Books and Papers*

Carr, M. H., ed. 1970. *A strategy for the geologic exploration of the planets*, U. S. Geological Survey Circular 640. Free from U. S. Geol. Survey, Washington, D.C. 20242. General account of the methods and rationale of planetary geology.

Baldwin, R. P., 1949. *The Face of the Moon*, Chicago, Univ. of Chicago Press, 273 p.

Baldwin, R. P., 1963. *The Measure of the Moon*, Chicago, Univ. of Chicago Press, 488 p.

Davies, M. E. and B. C. Murray, 1971. *The View from Space*, Columbia Univ. Press, New York. College-level reference on lunar and planetary spacecraft that carried imaging systems. Excellent review of advantages and disadvantages of different systems. $14.95

Fielder, G. ed., 1971. *Geology and Physics of the Moon*, American Elsevier Publ. Co., New York. A collection of papers on different aspects of lunar geology. $25.50

Fielder, G., 1965. *Lunar Geology*, Dufour Editions, Inc., Chester Springs, PA. $10.00

Guest, J. E., ed., 1971. *The Earth and Its Satellite.* Rupert Hart-Davis, Ltd., London. Excellent collection of papers by various authors on the geology of the Earth and Moon, illustrated with color and black and white photographs. $10.00

Kopal, Z., 1966. *An Introduction to the Study of the Moon*, New York, Gordon and Breach, Dordrecht-Holland, D-Reidel, 464 p.

Kosofsky, L. J. and F. El-Baz, 1969. *The Moon as Viewed by Lunar Orbiter*, NASA SP-200. An excellent collection of annotated lunar photographs from the Lunar Orbiter series. *GPO $7.50

Lowman, P. D. 1969. *Lunar Panorama*, Pulb. Weitflugbild, R. A. Muller-Feldmeilen, Zurich. Collection of lunar photographs from unmanned missions, with annotations of the geology. $12.45

*GPO = Superintendent of Documents, Government Printing Office, Washington, D. C. 20402.

Schultz, P. H. 1974 (in press). *Moon Morphology*. Univ. Texas Press, Austin, Texas. College-level text on the geomorphology of the Moon. Profusely illustrated with Lunar Orbiter images and arranged such that the text and illustrations can be examined separately without losing continuity.

Whipple, F. L. 1968. *Earth, Moon and Planets*. Harvard Univ. Press, Cambridge. Excellent general treatment of the Solar System; very little geology. Paperback edition, $3.00

Wilhelms, D. E. 1970. *Summary of Lunar Stratigraphy-Telescopic Observations*, U. S. Geological Survey Professional Paper 599-F, 47 p. Good account of the methods of lunar geologic mapping. *GPO 60¢

C. *Atlases of Lunar and Planetary Photographs*

Alter, Dinsmore, 1967. *Pictorial Guide to the Moon*, Thom Y. Crowell Co., New York, 199 p. Primarily an atlas of telescopic photographs with an extensive text. $8.95

Alter, Dinsmore, ed., 1964. *Lunar Atlas* Dover Publications, Inc., New York. Collection of telescopic lunar photographs. 154 plates. Paperback $6.00

Bowker, D. E. and J. K. Hughes. *Lunar Orbiter Photographic Atlas of the Moon*, NASA SP-206 (675 plates). Collection of selected Lunar Orbiter photographs. *GPO $19.25

Collins, S. A., 1971. *The Mariner 6 and 7 pictures of Mars*, NASA SP-263, 159 p. Complete collection of photographs with a short explanation of the missions. *GPO $4.25

Cortwright, E. M., 1968. *Exploring Space with a Camera*, NASA SP-168, 214 p. Collection of the best space photographs taken until the publication date; includes scenes from Gemini (of Earth, in color), Ranger, Surveyor, Lunar Orbiter, with descriptions of the spacecraft and missions. *GPO $4.25

Kuiper, G. P., 1960, ed. *Photographic Lunar Atlas*, Chicago, Univ. of Chicago Press.

Musgrove, R. G., 1971. *Lunar Photographs from Apollo 8, 10, and 11*, NASA SP-246, 119 p. Selected photographs from the earliest manned lunar missions; some pictures in color. *GPO $3.00

D. Public information bulletins on lunar and planetary missions, informative, well written and illustrated; excellent teaching materials. Available from *GPO

Lunar Orbiter, NASA Facts-32/ vol. 4, no. 4 15¢
The view from Ranger, NASA EP-38 40¢
Journey to the Moon NASA Facts-40/11-67 (wall chart) 30¢
Log of Apollo 11 (first lunar landing), NASA EP-72 35¢
The first lunar landing, as told by the astronauts, NASA EP-73 75¢
Mariner Spacecraft, NASA Facts-39/2-68 20¢

*GPO = Superintendent of Documents, Government Printing Office, Washington, D. C. 20402.

E. *Maps and Charts*

The Earth's Moon, 1969. National Geographic Society, Washington, D.C. 20036, $1.00. 40" X 27". Nearside and farside, with index to named features; information on lunar shape and motion on the margins; the best general lunar chart available.

The Red Planet, MARS, 1973. National Geographic Society, Washington, D.C. 20036. $1.00. Excellent map prepared from Mariner 9 data.

Wilhelms, D. E. and J. K. McCauley, 1971. Geologic Map of the nearside of the Moon, U. S. Geol. Survey Map I-703, 54" X 36" *GPO $1.00

Lunar Chart LEM – frontside. Available in three scales from *GPO:
66" X 66" (1:2,500,000 scale) two sheets, $2.00
35" X 36" (1:5,000,000 scale) $1.00
19" X 17" (1:10,000,000 scale) $0.50

Lunar Chart LPC-1 Frontside, backside, and polar regions, 1:10,000,000 38" X 26", *GPO 50¢

F. *Globes*

Denoyer – Geppert Lunar Globe. Times Mirror, 5235 Ravenswood Ave., Chicago, Ill. 60640. 16" diameter ($68.00 – hand mounted, $27.24 mass produced); highly detailed and well produced.

Denoyer – Geppert Mars Globe. Times Mirror, 5235 Ravenswood Ave., Chicago, Ill. 60640. 16" diameter, $60.00 hand mounted. Excellent globe, shows the named features as of 1973.

Rand McNally Lunar Globe. 12" diameter, surface detail not as accurate as Denoyer-Geppert, but it includes more names of surface features and crater depth for selected craters.

G. *Photographs* – most of the following agencies and institutions will supply indices of available photographs, with prices, on request.

Public Affairs Office, Ames Research Center, National Aeronautics and Space Administration, Moffett Field, California 94035.

National Space Science Data Center, Goddard Space Flight Center, National Aeronautics and Space Administration, Greenbelt, Maryland 20771. Source for photographic prints and negatives of research quality for Lunar Orbiter, Surveyor, Apollo, Mariner, etc. missions. Individual catalogs for missions are available. Photographs are supplied at cost.

---

*GPO = Superintendent of Documents, Government Printing Office, Washington, D. C. 20402.

Observatory telescopic photographs of the Moon, planets, and stars:

Lick Observatory, Univ. of California at Santa Cruz, Santa Cruz, Calif. 95060

Hale Observatories, Calif. Inst. Tech. Bookstore, 1201 E. California Blvd., Pasadena, Calif. 91109. Also sells NASA photographs from Apollo, Surveyor, Ranger, and Mariner missions.

Yerkes Observatory, Williams Bay, Wisconsin 53193. 35¢ for a catalog.

H. *Motion Pictures*

NASA film catalog—available from Ames Research Center, NASA, Moffett Field, Calif. 94035. Films are available free to bonafide representatives of educational, industrial, professional, youth activity and governmental organizations for group showings.

U. S. Geological Survey-Astrogeology Branch films -- listing is available from The Information Office, Geological Survey, Washington, D.C. 20242.

CHAPTER XIII – TEACHING METHODS

APPROACHES FOR TEACHING PLANETOLOGY

Ronald Greeley
University of Santa Clara, Santa Clara, Calif. 95035

I. INTRODUCTION

The primary objective of the "Short Course in Lunar Geology" is to provide information and ideas for instructors so that aspects of planetology can be introduced or expanded in their earth-science curriculum. Although the ways that this is accomplished are probably as varied as the number of participants, I would like to offer some suggestions for incorporating planetology into earth-science programs. Three general possibilities are: 1) supplemental instruction in existing courses, 2) introduction of special projects or formal courses in planetology, and 3) introduction of short-courses for high school instructors, or as community affairs programs.

II. PLANETOLOGY IN EXISTING COURSES

Community college earth-science instructors generally teach a variety of courses (physical geology, historical geology, physical science, astronomy) in which the solar system, "Earth's place in space," and the early history of the Earth are discussed. A great deal of the recent information on the characteristics of the solar system and ideas of its origin has come from lunar and planetary programs. Thus, it would be appropriate to expand and supplement lectures with the data gained through their short course in regard to geochemistry, ages of lunar material, and characteristics of the terrestrial planets. Now that lunar landings have been accomplished and large photographic libraries are being compiled from detailed views of other planets, Solar System astronomy has changed drastically. The study of surface features is basically the field of the geologist, not the astronomer. Consequently, the topics in Solar System astronomy over the last decade have been redirected to the outer planets, to meteorological problems, to comets, and to the relatively "inaccessible" (as yet) planetary objects. The study of planetary surfaces is typically approached by astronomers as an aside. However, this topic is closest to the field of the geologist.

In one form or another, earth-science courses discuss *geological processes.* One approach for planetology is to show that the same geological processes are (or have been) operative on all terrestrial planets. Impact cratering as a geological process is usually neglected in general geology, even though it has been significant in the evolutionary history of most planets, including the primitive Earth. Comparisons of the relative effects of impact cratering as well as other processes (volcanism, gradation, and tectonism) for each planet could be discussed and supplemented with spacecraft imagery.

The basic concepts and principles of geology (superposition, uniformity, etc.) are used to decipher the geology of the other planets, just as they are used for Earth. As these topics are discussed, extraterrestrial cases could be cited. For example, the Imbrium lava flows photographed by Lunar Orbiter and Apollo 15 demonstrate superposition on a grand scale! Or, craters cut by

linear rilles (graben) show cross-cutting age relations for the formation of the crater and lunar crustal faulting. In addition, extrapolation of meteoritic flux data and "real-time" cratering events backwards through geologic time permits an understanding of the geological history and evolution of the Moon, demonstrating *geological uniformity*.

III. PLANETOLOGY AS A COURSE

Some schools have already initiated separate courses in space science, or lunar and planetary geology. These courses often start as reading projects or seminars (e.g., "Geological Exploration of the Moon and Planets"), and evolve into formal courses. Depending on the background of the instructor and the student population, the theme of the courses varies from photogeology, geochemistry, or geophysics to general space sciences, etc. Some courses are restricted to the Moon; others cover the Solar System.

This short course could serve as a core for a lunar geology course of about four (4) quarter units. With laboratory, it could satisfy State requirements as a physical science laboratory course. A sample class schedule for the Planetary Geology course that I teach at Foothill College is included here.

IV. SHORT COURSES

A general function of community colleges is to offer public service programs. Most communities have a ready-made audience for short courses in lunar and planetary geology through local and campus astronomy clubs. Short courses and special lecture series organized as community programs are particularly effective when they coincide with planetary probes (e.g., Pioneer 11, 1974; Viking-Mars, 1976; etc.).

Nearly all high schools teach physical science and many have initiated earth-science courses. They, too, could offer aspects of planetology in their normal curriculum. Short courses could be organized for high school instructors and offered for extension credit along the same general theme as this short course.

V. LABORATORY EXERCISES

Regardless of the approach taken to introduce planetology in the earth-science programs, laboratory exercises should be an integral part of the curriculum. We traditionally use the "do and learn" method in geology and this is true of planetology as well. Exercises in addition to those that are part of this short course are given in the accompanying material. Most of these can be adapted directly to the classroom, depending upon student level and instructor interest.

Material for the exercises (photographs, maps, etc.) can be obtained from the sources listed in the Appendix of the chapter, "Educational Resources."

Planetary Geology

SELENOLOGY EXERCISE

Ronald Greeley
University of Santa Clara, Santa Clara, Calif. 95035

OBJECTIVE: To become acquainted with the physical characteristics of the Moon.

METHOD: Analysis of lunar photographs, charts and reference materials.

The following questions refer to the full-disc photograph of the Moon.

1. Is the surface of the Moon homogeneous, that is, is it composed of material that appears to be the same everywhere?

2. Separate the Moon into two main geographic areas and list the characteristics for each.

AREA 1	AREA 2

3. What physical properties of the lunar surface (that can be distinguished on the photographs) did you employ in characterizing the areas?

4. Attempt to subdivide each area into sub-areas. What is the basis for your subdivisions?

5. Examine Lunar Chart LPC-1 and the National Geographic map of the Moon (frontside, backside, and polar regions). How does the backside differ from the front side?

6. In your opinion, what is the most common type of surface feature on the Moon?

The Lunar Charts, prepared (from telescope photos) at a scale of 1:1,000,000 and contoured at an interval of 300 meters, were drawn (using an air brush technique in which shading aids in simulating surface relief) by specialists of the U.S. Air Force Aeronautical Chart and Information Center. Parts of LAC 40 and 96 are reproduced on the following pages. Chart LAC 40 shows a region in the southern part of Mare Imbrium consisting of relatively flat lava flows into which a large, young crater (Timocharis) has been excavated. Chart LAC 96 displays a topography typical of the old central highlands.

7. Using the graphical layout provided on the next page, construct a topographic profile across each of these surfaces along the lines A - A′, B - B′, C - C′, and D - D′. In order to emphasize differences in relief, the vertical scale for each section has been exaggerated by a factor of four.

   Normal contours are shown as long dashed lines. Depression contours are indicated by hachured lines. For the larger craters, the number above the crater name represents the maximum elevation in meters (rounded off to the nearest 10 or 100 m value, depending on the control available). The number enclosed in parentheses refers to the total average depth in meters from the high point of the crater rim to the low point in the central crater floor.

   a. Contrast the topographic relief of LAC 40 and LAC 96.

   b. Compare and contrast the linear relief features of LAC 40 and LAC 96.

   c. Is the "flat" mare terrain of LAC 40 really flat? Explain.

   d. To what *geological process* would you attribute the rugged relief of LAC 96?

PART II

To be completed at home before the next meeting. From the list below, locate and write-in each feature on the attached full disc photos. Suggested references include the National Geographic Society Moon map, Lunar Atlases by Dinsmore Alter, Lunar Charts LEM and LPC-1, etc.

A. Maria

1. Oceanus Procellarum
2. Mare Imbrium
3. Sinus Aestuum
4. Mare Serenitatis
5. Mare Tranquillitatis
6. Mare Humorum
7. Mare Nubium
8. Mare Fecunditatis
9. Mare Crisium
10. Mare Frigoris
11. Mare Orientale
12. Mare Muscoviense
13. Mare Vaporum
14. Mare Nectaris
15. Sinus Iridum
16. Mare Smithii
17. Sinus Roris

B. Craters

1. Copernicus
2. Tycho
3. Aristarchus
4. Alphonsus
5. Bailly
6. Langrenus
7. Kepler
8. Messier
9. Gassendi
10. Archimedes
11. Timocharis
12. Theophilus
13. Plato
14. Ptolemaeus
15. Arzachel
16. Clavius
17. Grimaldi
18. Riccioli
19. Schiller
20. Hipparchus

C. Miscellaneous

1. Alpine Valley
2. Marius Hills
3. Schroeters Valley
4. Apennines
5. Hyginus Rille
6. Ariadaeus Rille
7. Taurus Mts.
8. Southern Highlands
9. Jura Mts.
10. Alpine Mts.
11. Central Highlands
12. Haemus Mts.
13. Pyrenees Mts.
14. Rheita Valley
15. Cordillera Mts.

D. Space Probe Sites

1. Rangers 6, 7, 8, 9
2. Surveyors 1, 2, 3, 5, 6, 7
3. Apollos 11, 12, 14, 15, 16, 17

Planetary Geology

LUNAR PHOTO EXERCISE

Peter H. Schultz
Ames Research Center, NASA, Moffett Field, Calif. 94035

OBJECTIVE: To be introduced to lunar surface features and to learn problems of photo-interpretation.

METHOD: Interpretations of lunar crater origin based on observation and personal experience.

MATERIALS: Photographs of lunar crater with increasing resolution, map of the Moon, scratch paper, tracing paper (optional).

INTRODUCTION FOR INSTRUCTORS

There are two basic methods for laboratory exercises. First is the "lead-through" or "spoon-feed" approach; the second, the "self-discovery" approach. Selenology lends itself to both techniques but several lessons in the scientific method can be learned by permitting the student to discover for himself plausible models of lunar surface processes. At one extreme, he is given a lunar photograph and only enough background to recognize the proper photographic scale and the lighting conditions at the surface (Exercise A). At the other extreme, he is provided with questions that generally guide him through the exercise (Exercise B). The choice of extremes typically depends on the experience of the student. However, if enough warning is given to what is expected of the student, he should be able to wade through either approach. A necessary part of the exercise is a summary and discussion period in which the student recognizes what was pertinent, what assumptions did he make (perhaps without knowing), and what was he supposed to learn about the Moon. If the student is left only to his own resources, then he must be given credit for ingenuity and approach rather than for the correct answer. In this sense, the exercise is not really conducive to a grading system but is used as a learning exercise.

The primary goals in a self-discovery approach are both the encouragement of independent thinking and the exposure of preconceived ideas. Whether the student is a science or humanities major, he probably will recognize the thin line between observation and interpretation. For example, a surface feature might be labeled on the basis of personal experience, and this label might carry with it a connotation or origin. Less philosophical goals include the appreciation of the type of data and restrictions in photo interpretation. In addition, the student will be exposed to a variety of surface features, a variety that will become more apparent the longer he looks at the photographs.

INSTRUCTIONS AND DISCUSSION

These two alternative selenology exercises are designed for groups of four students working together on the same set of lunar photographs. Larger working groups tend to stifle different ideas from the more timid students. Both exercises depend on their formulating a theory of the origin of lunar craters based on what they see and that they know from previous experience. This is basically the approach used by a photo-geologist; the difference is that the student might not have a geological background.

Two craters will be examined (see accompanying illustrations). Two or three working groups will be given one crater, Copernicus; other groups, a different crater, Gassendi. These craters have been selected because they are significantly different in appearance, indicating a difference in origin or modification. The theme is: "Based on the crater you have studied, what is the origin of lunar craters?" Each working group will select a spokesman to present their conclusions. Because the working groups independently examine two different craters and because the question of origin was made in a very general sense, a debate may result. This is intended and should be encouraged. In particular, it is likely that the groups will fall into two camps: those advocating an impact origin and those advocating a volcanic origin.

Division of opinion illustrates several problems in photo interpretation:

1. The dependence of the interpreter on his own past experience, regardless of training.

2. The danger of over applying a process recognized for one crater to all other lunar craters.

3. The necessity of maintaining a list of alternative origins and checking their plausibility as new information becomes available.

4. The difficulty in demonstrating one theory over another theory.

5. The ease with which dogmatic statements can slip into a discussion.

The instructor should watch for these problems in photo interpretation as they are exposed in the classroom, problems that characterized the early history of selenology.

A very important point is that seemingly wild ideas suggested by a student should not be summarily discarded. Remember, the students were asked to base their interpretation on their own experience, regardless of background. Such ideas should be examined for processes analogous to currently more popular theories of lunar crater formation and should be discussed in terms of both confirmable tests and your own knowledge of conflicting evidence.

If the students have sufficient geological background or if the level of questions and suggestions indicate that they are on the "right" track, then you might develop a line of questioning:

1. Could you see evidence for degradation or smoothing of surface features? What processes could do this smoothing on the Moon?

2. What features are similar to both Copernicus and Gassendi? What features are dissimilar?

3. Do you think Copernicus and Gassendi were formed by the same mechanism?

4. Could Gassendi be a degraded version of Copernicus?

Discussion of these questions probably will lead to three alternatives (also see table 1). First, Gassendi was once similar to Copernicus, an impact crater, but meteoritic erosion produced extensive degradation. Second, Gassendi is a volcanic caldera, whereas Copernicus is a relatively recent impact crater. Third, Gassendi was originally formed by impact, but volcanic processes associated with the emplacement of the lunar maria produced extensive modification. I prefer the last alternative based on the following evidence:

1. Craters exist (Taruntius, Atlas) that exhibit floor features resembling those in Gassendi but an ejecta blanket resembling that of Copernicus.

2. Most Gassendi-type craters (those with extensive floor fractures) occur along the borders of the maria and commonly have mare units emplaced on the floor.

3. Central peak height within Gassendi-type craters is comparable to that in Copernicus-type craters; however, several Gassendi-type craters have shallow floors with the central peaks extending above the rim. Thus it appears that the floor and central peak complex were raised *en masse*.

4. Craters with a wide variety of inferred stratigraphic ages exhibit Gassendi-type floors, yet floor features suggest a degree of preservation comparable to the maria.

The impact origin for Copernicus is generally accepted. This is based on the extensive evidence from returned Apollo samples for impact processes acting on the lunar surface over a long period of time; the massive blanket of material and secondary impact craters that surround the crater to enormous distances; and the absence of significant preferred associations of such craters with volcanic terrains. The argument that there is no volcano of comparable size on the Earth only can be used as supporting evidence. Any stronger stand may bring up the comment that scientists, too, have limitations in their experience or knowledge of the early history of the Earth.

EXERCISE

(Instructor: Suggest that each participant keep a record of the observations on a piece of paper)

In this investigation you will be divided into four groups. Each group is to study the geologic features associated with the crater shown in the lunar photographs. You have been given four sets of photographs that have progressively increasing resolutions:

1. Lunar Orbiter IV, medium resolution (framelet width approximately 100 km)
2. Lunar Orbiter IV, high resolution (framelet width approximately 12 km)
3. Lunar Orbiter V, medium resolution (framelet width between 3.3 and 4 km)
4. Lunar Orbiter V, high resolution (framelet width between 0.44 and 0.5 km)

The photographic scale, the north direction, the direction of the sun, and the elevation of the sun above the horizon are marked on each photograph.

Each group is to study the crater in order to derive a list of plausible origins. The intent of the exercise is not to arrive at a correct answer. Rather, it is for you to examine the surface features and deduce conclusions from your observations based on your experience. Select a spokesman to present briefly your findings to the rest of the groups. Be prepared to defend your conclusions for the origin of lunar craters.

In order to provide some direction for the study, consider the following questions:

EXERCISE A
(self-discovery, minimum guidance)

1. What are the relative ages of the geologic features you see; in particular, the crater of interest?
2. What evidence for geologic processes do you see on the floor, wall, and rim regions of the crater?
3. What geologic features are found on the Earth that appear analogous to the ones you see on the Moon?
4. What origin do you propose for the different features you see?
5. Based on your observations, what process do you feel is responsible for lunar craters?

You will be given about forty-five minutes to consider these questions.

ALTERNATE EXERCISE B
(guided self-discovery exercise)

A. From the distant view (Lunar Orbiter IV, medium resolution)

1. What are the most obvious features of the crater that are visible at this resolution (a resolution comparable to telescopic views from the Earth)?

2. Are there other similar craters visible? If so, using a map, identify these craters by name.

3. What is the relation of the crater to the surrounding terrain?

B. From a closer view (Lunar Orbiter IV, high resolution)

1. Divide the crater into three areas: floor, wall, and rim (beyond the rim crest) . . .s. List characteristic surface features in each zone.

2. Is the crater rim outline circular, polygonal, irregular, or scalloped? What about other craters in the area? Do you see any significance to similarities or differences in crater plan?

3. What do you think the crater looks like in cross section? Draw a rough profile based on your impression. What criteria did you use?

4. At this increased resolution, what other relations do you see between the crater and the surrounding terrain?

C. Still closer view (Lunar Orbiter V, medium resolution)

1. Compare the floor and wall zones; list characteristic features.

2. In general, what is the age relation between the wall and the floor? Are there any exceptions?

3. Can you divide the floor into different regions based on morphology? If so, list the most characteristic features that make these regions different.

D. Closest view (Lunar Orbiter V, high resolution)

1. Describe the floor in this high resolution photograph (smallest feature visible is approximately 10 m) with respect to crispness of detail, types of small craters, and types of other features.

2. Are any of the features you recognize similar to features on the Earth?

E. On the basis of the observations and your own background (whether geology or home economics) list the different origins you can imagine for lunar craters. Which do you feel is the most plausible? Which do you feel is the most implausible?

Opposite:

Figure 1.– The crater Copernicus. The distant view, (a) (LO-IV-126-M), reveals the bright ray system, and an extensive ejecta blanket with numerous secondary craters is shown in (b) (LO-IV-121-H2). The width of (a) corresponds to 770 km; the width of (b), 200 km (frameiet width 12 km). The stereo pair, (c) and (d), focuses on the crater floor and central peaks. These are medium-resolution images from Lunar Orbiter V (LO-V-154-M and LO-V-152-M) in which the framelet width corresponds to 3.3 km. See figure 10, Selenology, for further discussion.

a

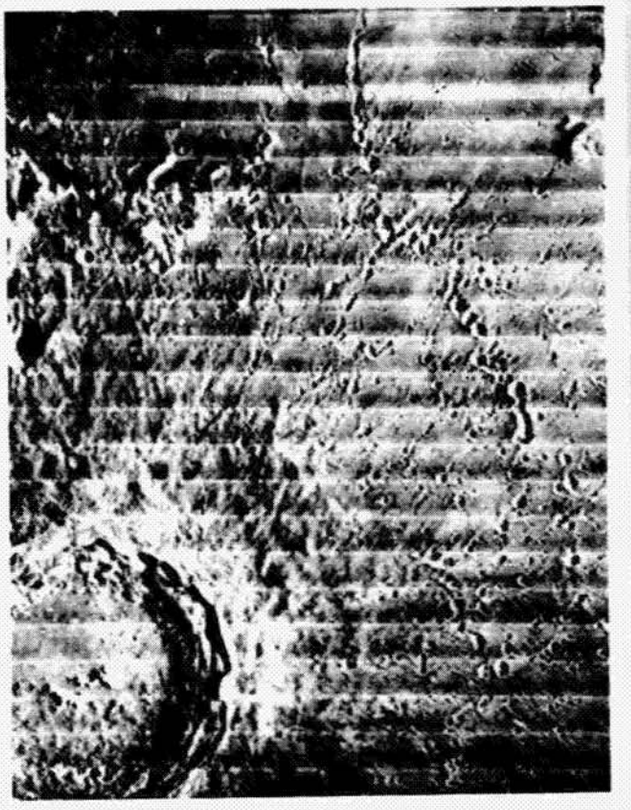

b

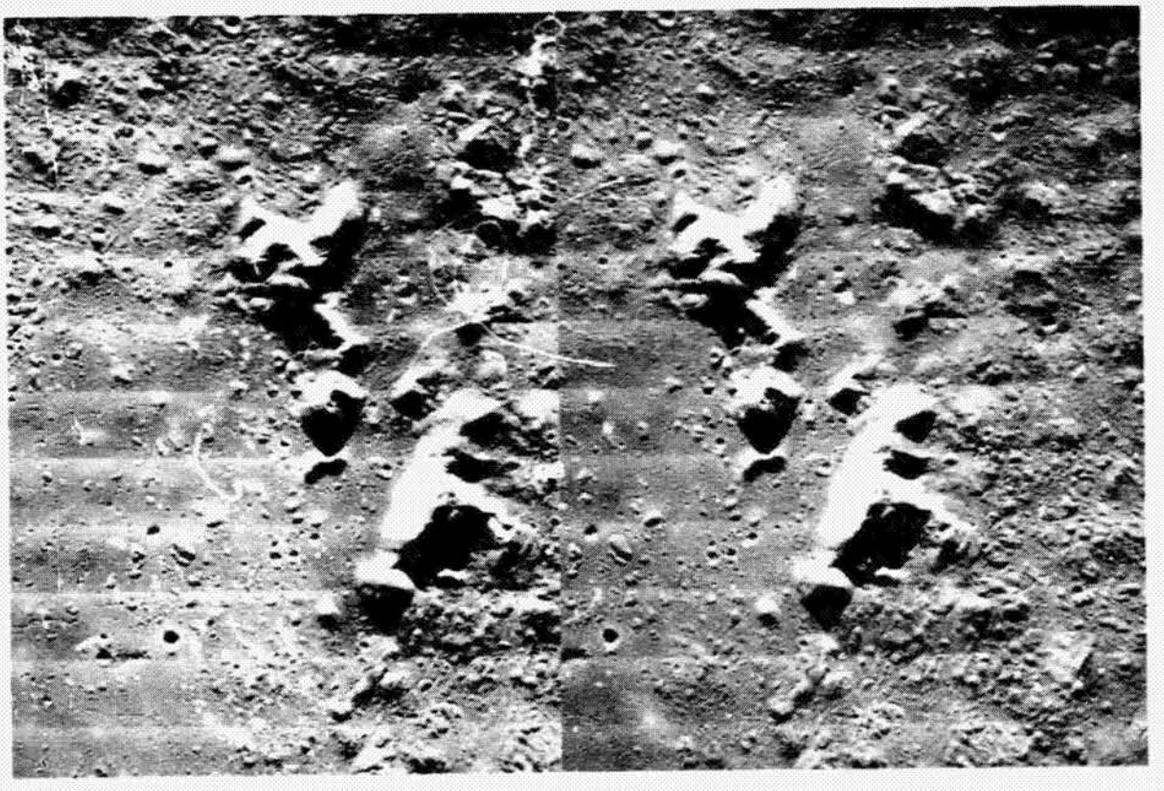

c d

Opposite:

Figure 2.– The wall and floor of Copernicus as seen in LO-V-151-M. Solar illumination is from the east (top). Frame/et width corresponds to 3.3 km.


CRATER COPERNICUS
LO II H-162 3/3

Opposite:

Figure 3.– High-resolution view of the floor of Copernicus (LO-V-152-H2). Solar illumination is from the top (east) and the framelet width corresponds to 0.43 km. This view shows an area approximately 12 km to the north of the southern central ridge. Note the rimless pit (upper left), the narrow depression or "moat" surrounding several domal structures (left, upper left), the dome complex with radial fractures (lower right), and the variation in surface textures and local crater densities.

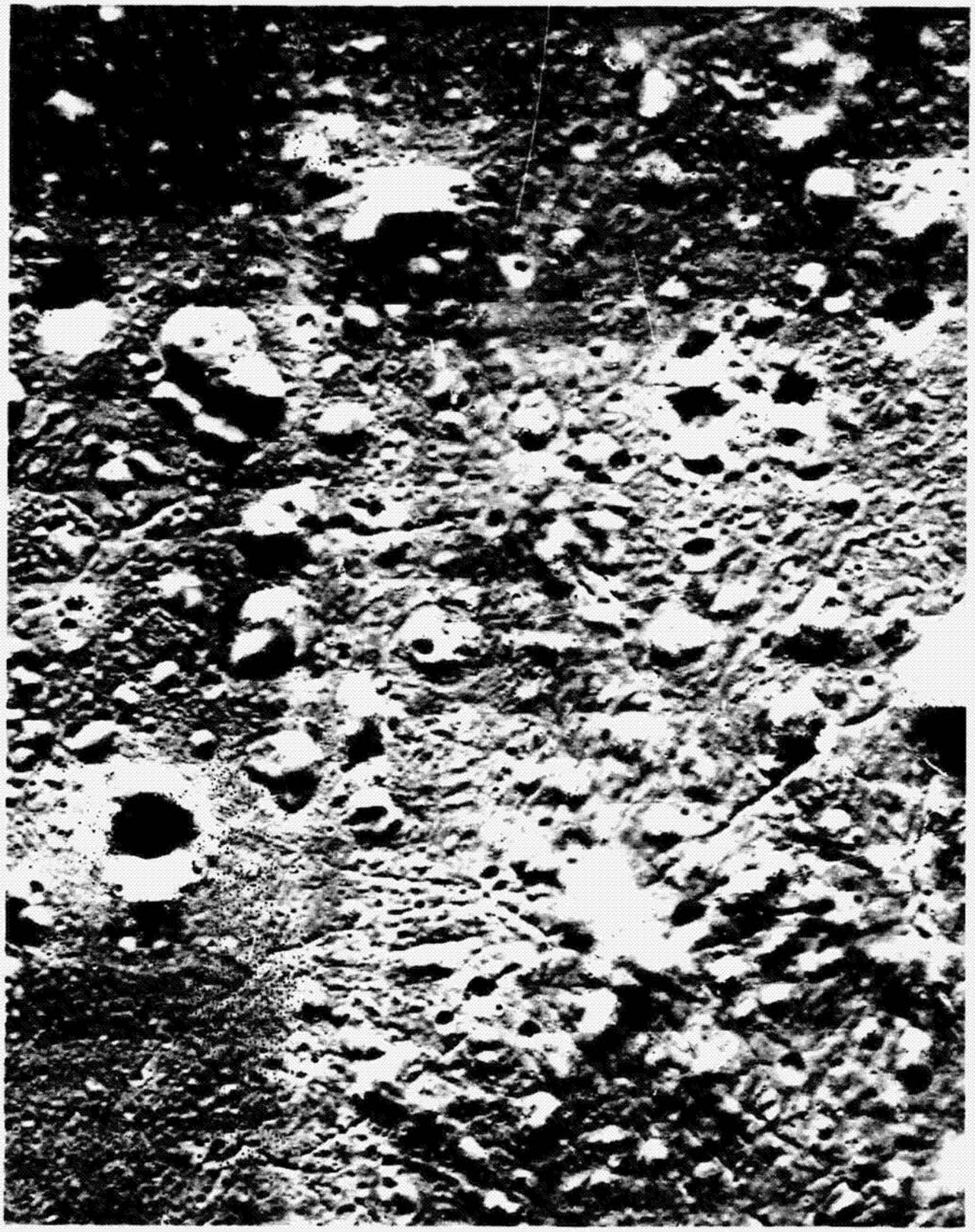

Opposite:

Figure 4. – High-resolution view of the central peaks (LO-V-151-H1) showing the talus slopes of the peaks and the floor surface between the peak complex.

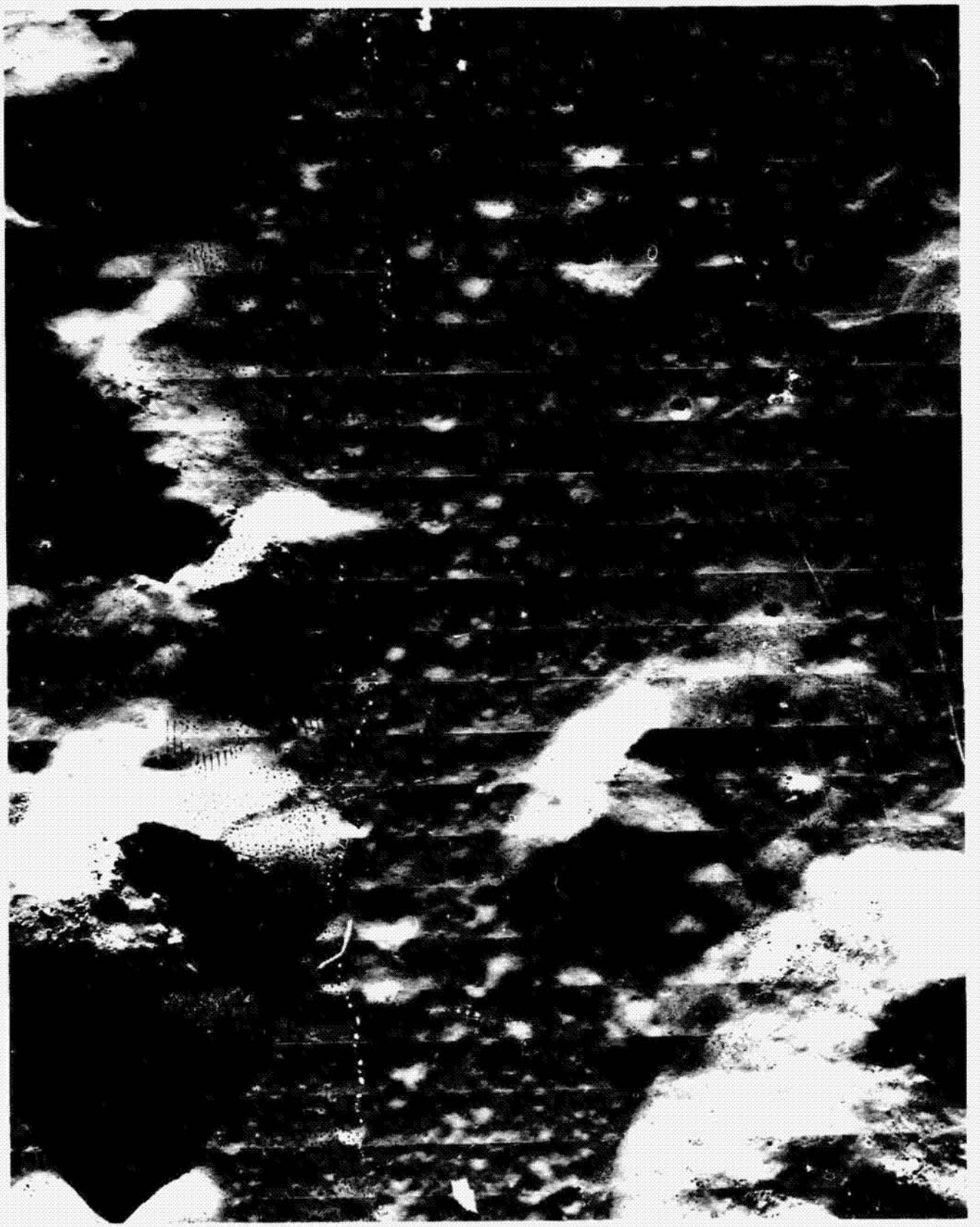

Opposite:

Figure 5.– The crater Gassendi. The low resolution view establishes its location, (a) (LO-IV-143-M), and the higher resolution view, (b) (LO-IV-143-H2), reveals its relation to the adjacent maria. The stereo pair, (c) and (d), provides a closer look at the central peaks and crater floor. The framelet width in (b) corresponds to 12 km; those in (c) and (d), to 4.0 km. The width of (a) represents 770 km on the lunar surface. See figure 12, Selenology, for discussion.

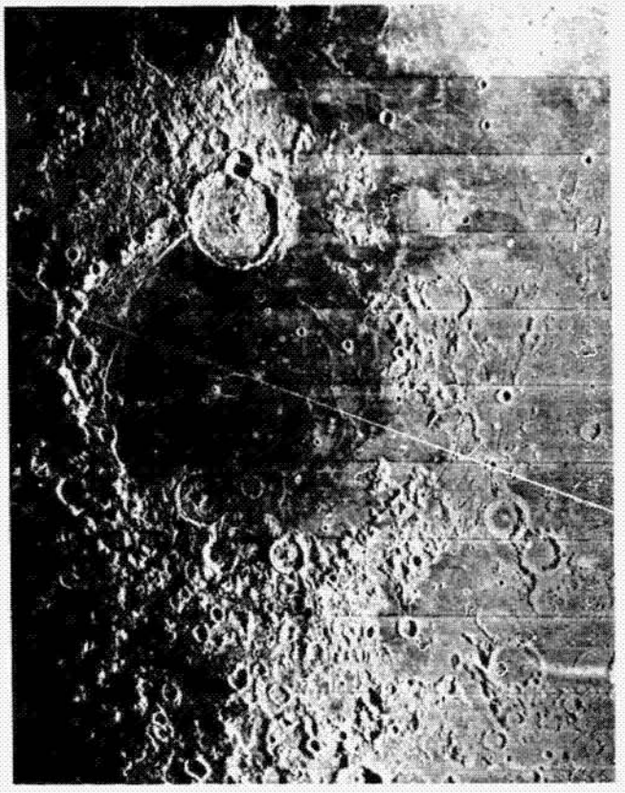

a

b

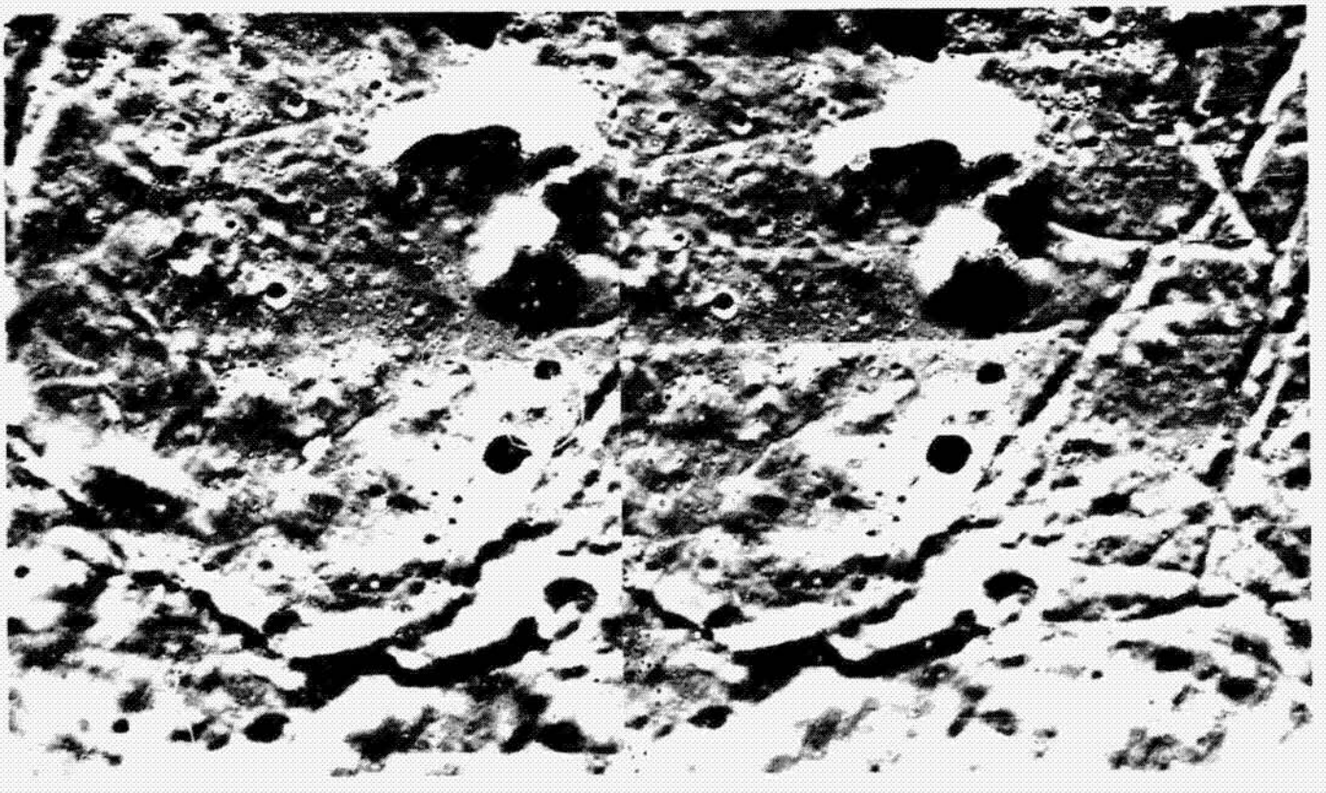

c d

Opposite:

Figure 6. – The southern half of Gassendi (LO-V-177-M; framelet width is 4 km). The complex fracture system is in contrast to the small narrow cracks on the floor of Copernicus. Mare material has been emplaced between the wall/rim and the edge of the floor. The source of this lava is believed to have been derived through vents within Gassendi. Illumination is from the top (east).

Opposite:

Figure 7.– A close-up of the mare-filled regions and the hummocky floor (LO-V-177-H1), situated in the upper center of figure 6. The relatively smooth mare surface is in contrast to the highly textured floor. The density of small craters is variable across both surfaces, but in many regions, it is lower on the crater floor than on the mare units. This contradiction between stratigraphic age and apparent cratering age is probably the result of more rapid degradation on the textured floor unit. Framelet width corresponds to approximately 0.55 km; illumination is from the top (east).

Opposite:

Figure 8.– Central peak and fractures within Gassendi (LO-V-178-H3). The textured floor at this resolution (framelet width, 0.53 km) should be compared to the floor of Copernicus (fig. 3). Note the highly subdued appearance of the fracture and the ropelike feature on its floor (upper right).

TABLE 1.– COMPARISON OF COPERNICUS AND GASSENDI

	COPERNICUS	GASSENDI
FLOOR	1. Multiple central peaks (ridges). 2. Two distinct floor units: one relatively flat, the other hummocky. 3. The floor generally overlaps the wall. 4. Volcanolike cones and rimless pits on the flat floor, suggesting volcanic processes (see medium and high resolution photographs). 5. Small fractures (high-resolution photos), several surrounded by smooth-surfaced deposits (thought to represent pyroclastic debris). 6. Numerous domes surrounded by depressions or "moats" (high resolution photos). 7. Boulder trails down central peak. 8. Variety of small crater appearances: from blocky to highly subdued.	1. Shallow floor with numerous fractures. 2. Central peaks (elevation is just below crater rim). 3. Smooth mare units within moatlike depression closest to mare. 4. Contrasting floor surfaces with markedly different crater densities. 5. Highly textured surfaces (high-resolution photos). 6. Ridge on edge of floor adjacent to mare-filled depression (remnants of base of wall).
WALL	1. Extensive slumping and slides. 2. Flow features extending down the wall and apparently originating in rimless elongate depressions. Flows may have been molten or landslide debris. 3. Smooth-surfaced "pools" on the terraces, several of which exhibit flow patterns and fractures.	1. Highly subdued wall slumps on western and northern walls. 2. Absence of wall slumps in moat region.
RIM	1. Division into three zones: first zone nearest rim crest characterized by annular fractures and smooth-surfaced units in local depressions. 2. Second zone: annulus around first zone; hummocky dunelike terrain. 3. Third zone: beyond second zone; numerous secondary craters with "herringbone" pattern; extensive ray system (not always radial to Copernicus).	1. Absence of ray system and ejecta sequence comparable to Copernicus. 2. Relatively symmetric rim/wall ridge adjacent to mare – in contrast to subdued rim profile adjacent to highlands.

TABLE 1.– COMPARISON OF COPERNICUS AND GASSENDI

	COPERNICUS	GASSENDI
FLOOR	1. Multiple central peaks (ridges). 2. Two distinct floor units: one relatively flat, the other hummocky. 3. The floor generally overlaps the wall. 4. Volcanolike cones and rimless pits on the flat floor, suggesting volcanic processes (see medium and high resolution photographs). 5. Small fractures (high-resolution photos), several surrounded by smooth-surfaced deposits (thought to represent pyroclastic debris). 6. Numerous domes surrounded by depressions or "moats" (high resolution photos). 7. Boulder trails down central peak. 8. Variety of small crater appearances: from blocky to highly subdued.	1. Shallow floor with numerous fractures. 2. Central peaks (elevation is just below crater rim). 3. Smooth mare units within moatlike depression closest to mare. 4. Contrasting floor surfaces with markedly different crater densities. 5. Highly textured surfaces (high-resolution photos). 6. Ridge on edge of floor adjacent to mare-filled depression (remnants of base of wall).
WALL	1. Extensive slumping and slides. 2. Flow features extending down the wall and apparently originating in rimless elongate depressions. Flows may have been molten or landslide debris. 3. Smooth-surfaced "pools" on the terraces, several of which exhibit flow patterns and fractures.	1. Highly subdued wall slumps on western and northern walls. 2. Absence of wall slumps in moat region.
RIM	1. Division into three zones: first zone nearest rim crest characterized by annular fractures and smooth-surfaced units in local depressions. 2. Second zone: annulus around first zone; hummocky dunelike terrain. 3. Third zone: beyond second zone; numerous secondary craters with "herringbone" pattern; extensive ray system (not always radial to Copernicus).	1. Absence of ray system and ejecta sequence comparable to Copernicus. 2. Relatively symmetric rim/wall ridge adjacent to mare – in contrast to subdued rim profile adjacent to highlands.

Planetary Geology

IMPACT CRATER EXPERIMENTS

Ronald Greeley
University of Santa Clara, Santa Clara, Calif. 95053

OBJECTIVE: To learn the mechanics of impact cratering.

METHOD: Observations of laboratory-produced craters and film of hypervelocity experiments; comparative analyses of lunar craters.

MATERIAL: Sand-filled tray,* supply of dyed sand, slingshot, projectiles, scale, cross-sections of hypervelocity-produced craters, and lunar photographs.

Prepare a smooth, flat sand surface by scraping the board across the sand tray. Ask instructor to emplace a layer of dyed sand over the prepared surface. Divide the target area into four (4) sections.

1. In one quarter-section, produce a crater using the slingshot to launch a 6 mm projectile fired normal (at 90°, or vertical) to the target surface. Sketch a plan (map) view and cross section of the crater. Be sure to sketch the pattern of the light-colored sand around the crater. This material is *ejecta*. Where did it come from?

What would you expect to find beneath the ejecta?

Would you expect the ejecta to be of equal thickness everywhere? What is its distribution and thickness in relation to the crater?

2. In the second quarter-section, produce a crater with a 6 mm projectile launched at about 65° to the surface (estimate the angle). Sketch the crater. Is there a *marked* difference between the two craters or ejecta patterns?

3. In the third quarter-section, produce a crater with a 6 mm projectile launched at about 40° to the surface. Be sure no one is "down range" in case the projectile ricochets. Sketch the crater.

4. In the fourth quarter-section, produce a crater with a 6 mm projectile launched at about 5–10° to the surface. Be sure no one is "down range" in case the projectile ricochets. Sketch the crater. Note the *asymmetric* cross section.

---

*100μ sand is recommended. Sand can by dyed easily by mixing it with *dry* powdered tempera paint.

5. Examine the sand craters and your sketches. What are the relationships between impact angle, crater morphology (shape, form), and ejecta distribution?

6. Examine the photograph of the lunar crater Messier.* What interpretations can you make concerning its formation? Did the projectile which formed Messier enter from the east or west?

The next section deals with the relationships of projectile mass (weight) and velocity (average speed) to crater size.

7. Recover the projectiles from the experiments above and thoroughly mix the dyed and undyed sand to produce a uniform mixture. Smooth the target surface with the board. The remaining experiments will be performed *without* a dyed upper layer of sand.

Produce four (4) craters on the smooth target surface, using 8 mm projectiles. Make the first crater by dropping the projectile from a height of 10 cm above the surface, the second crater from a height of 2 m. The third projectile should be launched from the slingshot extended 23 cm (9"); the fourth, from the slingshot extended 36 cm (14"). Mass of projectile = 2 grams.

Complete the following table:

	*Velocity***	*Crater diameter*
Shot 1	2 cm/sec	_____
Shot 2	200 cm/sec	_____
Shot 3	1000 cm/sec	_____
Shot 4	3000 cm/sec	_____

8. Recover the projectiles and smooth the target surface with the board. Produce three (3) craters by dropping 4 mm, 9 mm, and 18 mm steel projectiles from a height of 2 m above the target surface. Record the crater diameter.

*See figure 18 "Impact Craters."
**Approximate

	Mass	*Crater diameter*
Shot 1 (4 mm)	.34	_____
Shot 2 (9 mm)	3.52	_____
Shot 3 (18 mm)	28.14	_____

9. Recover the projectiles and smooth the target surface with the board. Produce three (3) craters by dropping 18 mm steel, glass, and hollow aluminum projectiles* from a height of 2 m above the target surface. Record the crater diameter.

	Mass	*Crater diameter*
Shot 1 (steel)	28.14	_____
Shot 2 (glass)	8.07	_____
Shot 3 (hollow aluminum)	2.37	_____

10. From observations of your experiments, answer the following questions concerning impact cratering:

a. In producing craters, which is more important, projectile *diameter* or projectile *mass*?

b. What is the relationship between projectile velocity and crater size?

Impacts involve the transfer of energy from the projectile to the target. *Kinetic energy* (energy in motion), K.E. = ½ mv^2, where m = mass (weight) and v = velocity. The above exercises involved *iow velocity* impacts (maximum velocities of only a few *meters* per second). Natural impact events commonly occur at velocities of more than 10 *kilometers* per second (22,500 mph!); "projectile" mass (meteorites) may be several kilotons.

11. Determine the amount of energy involved in producing the crater for "Shot 2" of Question 7.

$$K.E. = \tfrac{1}{2} mv^2$$

*Projectiles available from Industrial Techtronics, P.O. Box 1128, Ann Arbor, Michigan 48106.

12. Determine the kinetic energy for an iron meteorite 20 m in diameter (mass = 3.34×10^{10} g), impacting at a velocity of 10 km/sec. For comparison, 1 kiloton of TNT = 4.2×10^{19} ergs.

13. Investigation of *hypervelocity* (high velocity) impacts requires extensive laboratory equipment. Your instructor will explain hypervelocity impact studies performed at NASA-Ames and show high speed motion pictures of impact events produced by a *Hydrogen Gas Gun.*

View the film and note the sequence of events in crater formation. The flash of light seen during the initial stage of impact resulted from "impact-shocked" electrons shifting from one orbit to another within the molecular structure of the sand. A significant part of the kinetic energy of impacting projectiles is transformed to *heat*. This heat often melts part of the target or planetary surface. Explain the geological significance of this fact.

Examine the slabs* prepared from targets impacted in the NASA-Ames light gas gun. In the space below sketch the "rock" layers.

a. Is the crater rim higher, lower, or the same level as the original target surface?

b. Trace the uppermost "formations" (colored sand layers) through the rim. What happens to these units?

c. Are the units in the crater walls of uniform thickness?

d. What happens to the units beneath the crater floor?

14. Examine the film† and photograph** of "Mare Exemplum" produced at NASA-Ames Research Center.

a. Pick out a large crater and describe the changes that occur as it "ages" with time.

*See figure 10(a) "Impact Craters."

**See figure 17 "Impact Craters."

†Film "Mare Exemplum" available from Public Affairs, NASA-Ames, Moffett Field, CA.

b. Select a large crater formed late in the sequence. How does its ejecta alter the surrounding surface?

c. Is impact-cratering an effective erosive process? Would it be as effective on Earth as on the Moon? On Mars?

d. Considering the lunar surface, would it be possible to obtain "relative" age dates for different geological units on the basis of crater statistics? Could you obtain "absolute" age dates? Explain.

Planetary Geology

GEOLOGIC MAPPING EXERCISE

Ronald Greeley

OBJECTIVE: To produce a lunar photogeologic map.

METHOD: Following the procedures, mapping methods, and time scale outlined by Wilhelms (1970, 1972), a geologic map is to be made for a part of the lunar surface. Units should be placed in the lunar time scale, described, and their possible origins discussed.

The instructor will show the solution at the conclusion of the exercise.

MATERIALS: Glossy photographs of the map site (DO NOT MARK OR MAR!), lithographic copy of map site, chart for unit descriptions.

1. Examine the photographs of the mapping site and determine tentative geologic units.

2. Sketch possible contacts on one copy of the map site.

3. Place units in relative time sequence. Check contact relations against the age sequence.

4. Check the validity of the map by drawing cross-sections through the area. Remember that a geologic map (in contrast to a *geomorphic* map) shows three-dimensional rock units.

5. Finalize contacts on second copy of map. Complete the chart for unit descriptions, placing units in proper age sequence. Use the appropriate symbols for the units on the map and chart. Offer possible explanations for the origin of each unit.

Produce a geologic sketch map on the attached lithographic copy of a lunar photograph; draw the *contacts* (lines, or boundaries) between the major formations. At least five *major* units are to be defined. Identify the units with appropriate symbols and complete the chart below:

youngest ↑

↓ oldest

Unit (symbol)	Relative lunar age (Copernican, etc.)	Physiographic feature (mare, craters, etc.)	Physical description	Possible origin

Planetary Geology

LUNAR SAMPLES

Ronald Greeley

OBJECTIVE: To become familiar with the mineralogy and petrology of lunar surface rocks.

METHOD: Familiarization with common rock textures and structure as related to their mode of formation; comparison of terrestrial rocks with lunar samples through the use of thin sections and "pseudo-sections."

The instructor will review the main categories of rocks and processes leading to their formation as illustrated through the *Rock Cycle*. In addition, he will discuss the technique of *thin sections* to analyze rocks.

1. Using both normal and polarized light, examine thin sections A, B, C, and D (common terrestrial rocks) and record your observations on the chart. When you are completed, ask instructor to check your results, then be certain that you can recognize the characteristic textures for igneous (plutonic and volcanic), sedimentary, and metamorphic rocks.

2. Examine pseudo-section 3 and record your observations on the chart. This is a section through a pyroxene crystal (cross polarizers) taken from the rock *suevite* from the Ries Basin, Germany. The deformation *lamellae* (linear structures) resulted from high-pressure shock waves generated by the impact that created the Ries Basin (size of original 0.32 X 0.22 mm).

3. Examine pseudo-section 4 and record your observations on the chart. This is a section of a glass bomb from the Ries Basin, found within suevite. It shows schlieren (yellow flow patterns), bubbles (round, white areas) and mineral fragments (white, angular material). (Size of original 0.79 X 0.55 mm.)

Explain how this material could form during impact:

4. Examine photographs AS 11-45-6707 and AS 11-45-6708 through the stereoviewer. These were taken by the Apollo 11 astronauts of the lunar surface; each photo covers an area a few centimeters square. Describe the physical character of the lunar surface:

Where did the fragmental material come from?

The shiny material coating the rock fragments is glass. Where did it come from?

Explain the origin of the irregular vesicles in the rocks in the bottom of photographs AS 11-45-6708.

5. Examine lunar sample pseudo-sections 122, 125, and 126. The round objects were recovered from the lunar "fines," or soil; they are commonly 1.0 mm or less in diameter. The lack of internal structure (crystal form) identifies them as glass objects. Why do they have a rounded shape; how might they have formed?

Notice the small pock-marks on slide 122. What might they be?

6. Examine pseudo-section 135 (crossed polarizers) and note your observations on the chart. Size of original 0.97 X 0.64 mm. It is a thin section of lunar material and contains feldspar (plagioclase) pyroxene.

It most closely matches terrestrial rock _____.

7. Examine pseudo-section 142 (crossed polarizers) and note your observations on the chart. Size of original 0.09 X 0.06 mm. It is a thin section of lunar material.

It most closely matches terrestrial rock _____.

8. Examine pseudo-section 123 (original 0.38 X 0.25 mm), section 141 (original 2.9 X 1.9 mm), and strew slide 121, all of lunar material. Describe sections 123 and 141 and record your observations on the chart.

Do you see a possible genetic relation between 123, 141 and 121? Explain.

How might the rock of sections 141 and 123 have formed?

9. From your examination of this material, give a summary of the rock types found on the lunar surface and the geologic processes that led to their formation.

Thin Section Analysis.
Fill in as much of the chart as you can. Some of the information you will not be able to determine. Sketches should show grain-to-grain relations, gross texture, and characteristic structure, if any.

Slide no.	Sketch	Texture (clastic, crystalline, etc.)	Structure (lineations, etc.)	Origin	Name

Planetary Geology

APOLLO LANDING SITE EXERCISE

Ronald Greeley

INSTRUCTOR NOTES

1. This exercise enables the student to use the information gained in lunar geology toward the solution of a practical problem. To be effective, the exercise should be given toward the end of the course so that the students have sufficien' background in lunar geology.

Using reference materials for a *general* landing site (e.g., the crater Copernicus), a specific landing site is to be selected and geological traverses planned.

2. The exercise can be handled several different ways, depending upon the class and available time:

Option A. Students work individually, all on the same general site (e.g., Copernicus, Marius Hills, etc.).

Option B. Students work individually, each on a different general site.

Option C. Students work in groups of 3 to 5, all on the same general site.

Option D. Students work in groups of 3 to 5, each group on a different general site.

3. Regardless of option selected, the assignment could be made for either outside work or as lab work for two or three lab periods.

4. If time permits, the last lab session could be used for the presentation of various sites selected, during which the site and scientific rationale of the selection could be defended and debated as an open forum.

5. The main part of the exercise should be the photogeologic analysis and mapping, from which the specific landing site and geological traverses are derived. The listing of the "capabilities" of the Orbiting CM-SM and the surface experiments are secondary to the photogeology. The inclusion of this material is twofold: *first*, it requires the student to gain some understanding of remote sensing techniques and geophysical instruments, and *second*, the type of geological data that can be gained with the various instruments (heat flow, subsurface structure, etc.) will influence the site selection.

Student level and capability as well as available time will determine the emphasis placed on the "non-photogeologic" aspects of the exercise.

6. Candidate sites are presented in the material that follows. These are some of the general sites that were considered during the Apollo program as potential landing areas. For each site, lists are given for available maps and photographs. Material best suited for the exercise is indicated with an asterisk and the best photographs are reproduced. Photographs can be obtained at cost from the National Space Science Data Center and maps from the Superintendent of Documents.

7. Site material for each student or group should consist of:

A. U.S.G.S. Geological Map, 1:1,000,000, covering the general area.

B. LAC 1:1,000,000 charts for general area.

C. Base Map or Lunar Orbiter Photograph. Students prepare their geologic map, landing site, and geological traverses on this base, using tracing paper.

D. Reference photos and maps (other Orbiter and Apollo photos, etc.).

8. An abbreviated and modified form of this exercise could be given as a final examination (probably a "take-home" examination).

Planetary Geology

APOLLO LANDING SITE EXERCISE

Ronald Greeley

I. OBJECTIVES

To select an Apollo landing site by applying your current knowledge of lunar geology to the analysis of lunar data, photographs, and maps.

II. MATERIALS

Sets of photographs, lunar charts, 1:1,000,000 geological map(s) and reference material.

III. HYPOTHETICAL SITUATION

Assume that there have been only three lunar landings (Apollo 11, 12, and 14) and that there is to be only one more landing – the one that you are to plan. You must select the site and plan the mission to derive maximum geological data and to solve as many lunar problems as possible.

IV. CAPABILITIES

(See reference material for instrument descriptions.)

A. *Orbiting CM-SM (Command module – service module) will have the following instruments*:

Gamma-ray spectrometer, X-ray spectrometer, mass spectrometer, infrared scanning spectrometer, lunar sounder, panoramic camera, mapping camera.

B. *Lunar module (LM)*

1. ALSEP (Apollo lunar surface experiment package): lunar active and passive seismometers, lunar heat flow, triaxis magnetometer, lunar atmosphere composition.

2. Other experiments: geology investigation, surface electrical properties.

3. Lunar rover: 3 EVA (extravehicular activity) traverses, each cannot be more than 10 km long, round trip.

C. *Engineering constraints*:

The Apollo spacecraft travels in an inclined equatorial orbit from east to west. The LM separates from the CM-SM and begins its descent hundreds of miles from the landing site,

bringing the LM into the site on a very low approach angle. The astronauts must have a clear view of the landing site during approach. Therefore, the landing site must not have high, steep mountains on its east side. The site must be fairly smooth, level, and free of large boulders.

V. REQUIREMENT

Under the conditions described above, you are to prepare a report, "Geological Analysis of Apollo Landing Site." The report should consist of the following parts:

A. *Objective.*

A simple statement of the mission objective(s). What specific lunar problems potentially could be solved?

B. *Regional Geology.*

Describe the broad geologic, physiographic and structural setting of the area.

C. *Site Selection.*

Select the exact landing site within the general area indicated. Use the clear plastic sheet with the 10 km diameter circle (range of the Lunar Rover) to select the best site.

D. *Site Geology.*

Describe the local geology of the site (physiography, stratigraphy, structure). Prepare a detailed geologic map showing landing site.

E. *Detailed Plan.*

Devise 3 Rover EVA's (10 km round trip) and 2 foot EVA's (1.5 km round trip) on the site map. Describe the specific objectives of each EVA, show stations along each traverse and discuss the duties to be carried out for each station.

F. *Summary.*

Which of the following geological, geochemical and geophysical problems will this site potentially solve:

1. Chronology
    a. "Original crust"
    b. Origin of major mare basins
    c. Mare flooding
    d. Post-mare time scale

2. Composition
    a. "Primitive" rocks
    b. Deep-seated rocks

c. Differentiated rocks
d. Transient events
e. Atmosphere

3. Processes
   a. Cratering
      (1) Impact
      (2) Volcanic
      (3) Chain
   b. Transport
      (1) Ejecta
      (2) Gravity
   c. Volcanic-Tectonics
      (1) Fault
      (2) Dome
      (3) Flows
      (4) Rilles
      (5) Ridges
      (6) Seismicity

COPERNICUS

Geological Description

Copernicus (9°52'N, 19°55'W) is a relatively young, very large bright-rayed probable impact crater approximately 95 km in diameter and located south of Mare Imbrium. The primary objective of the mission to the floor of the crater, 4 km below the crater rim is the examination of the central peaks and the crater floor material. The central peaks (800 meters high) probably are composed of deep-seated material. Samples from the central peaks could aid in determining the internal characteristics of the moon. Examination of the domes and textured material of the crater floor could provide an understanding of the process of crater floor filling and help to clarify the role of volcanism in post-impact crater modification. Age determinations of the central peak material, the cratering event, and the subsequent crater fill material will aid in understanding the origin and modification of large impact craters.

Scientific Objectives

1. Sampling the central peaks materials with emphasis on variations in texture or appearance.
2. Study the structures within the central peaks and the relationships between the peaks and floor materials.
3. Sample the floor materials.
4. Sample and study domical hills within the floor.
5. Emplace geophysical instruments and monitering experiments of the distant wall terraces.

Reference Material

Photography:

Mission	Frame Number
Orbiter II	M, H-162 (oblique)
Orbiter IV	H-121 (2/3)
	-121 (1/3)
	-126 (2/3)
	-126 (1/3)
Orbiter V	M, H-150
	-151
	-152
	-153
	-154
	-155
	-156
	-157

Mission	Magazine	Frames	Film Size
Apollo 12	Q	7535	70 mm
Apollo 12	Q	7541	70 mm

Cartography:

Type Map	Item	Scale
Topographic	LAC 58	1,000,000
Geological	Copernicus (LAC 58) H. H. Schmitt, N. J. Trask and E. M. Shoemaker, 1967. USGS Map I-515	1,000,000
Photomosaic	Copernicus V-37	200,000
TOPOCOM	Orb V-37 (200)	

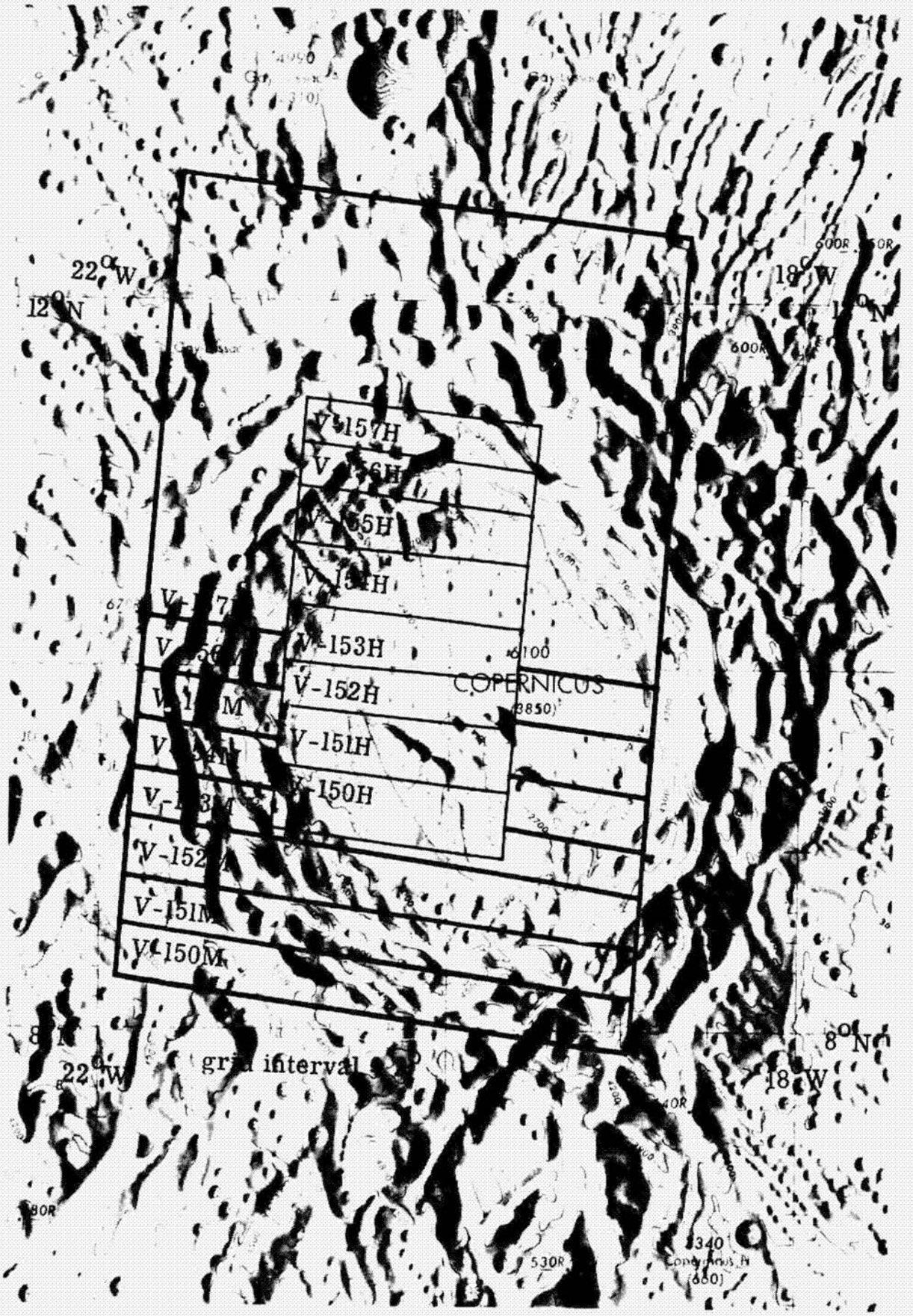
22°W
12°N
18°W
8°N
V-157H
V-154H
V-153H
V-152H
V-151H
V-150H
V-151M
V-150M
COPERNICUS
(3850)
grid interval

Site V–37.


CRATER COPERNICUS
LO II H-162 3/3


CRATER COPERNICUS
LO V SITE 57 M-151
NORTH

MARIUS HILLS

Geological Description

The Marius Hills (14°36'N, 56°34'W) are a series of domes, cones and rilles of Eratosthenian material located northwest of the crater Marius near the center of Oceanus Procellarum. The morphologic units which comprise these hills are analogous in form and sequence to terrestrial volcanic complexes which display a wide spectrum of rock compositions and ages. The various geologic units suggest that a prolonged period of volcanic activity has occurred in the Marius Hills area and that magmatic differentiation has produced a spectrum of rock types and a series of volcanic landforms displaying characteristic structural relationships. Therefore, the primary objectives of a mission to the Marius Hills are to study the geologic units in order to establish the extent and age of possible magmatic differentiation and to determine the structural relationships of volcanic landforms in the maria.

Scientific Objectives

1. Sampling the variety of volcanic domes and cones present in the area to collect evidence for differentiation of lunar materials and its extent.
2. Sampling and studying the structures of the mare (wrinkle) ridges, sinuous rilles, and rimless depressions in the area.
3. Sampling the plateau plains material.
4. Emplacing and conducting geophysical experiments.
5. Obtaining high resolution photography on this high inclination mission of the western part of the moon's nearside.

Reference Material

Photography:

Mission	Frame Number
Orbiter IV	M-150 (2/3)
Orbiter IV	M-157 (2/3)
Orbiter V	M, H-210
↓	H-211
	H-212
	H-213
	H-214
	H-215
	H-216
	H-217

Cartography:

Type Map	Item	Scale
Topographic	LAC 56	1,000,000
Geologic	Hevelius (LAC-56) J. F. McCauley, 1967 USGS Map I-491	1,000,000
Photomosaic TOPOCOM	Marius F (V51)	1:250,000

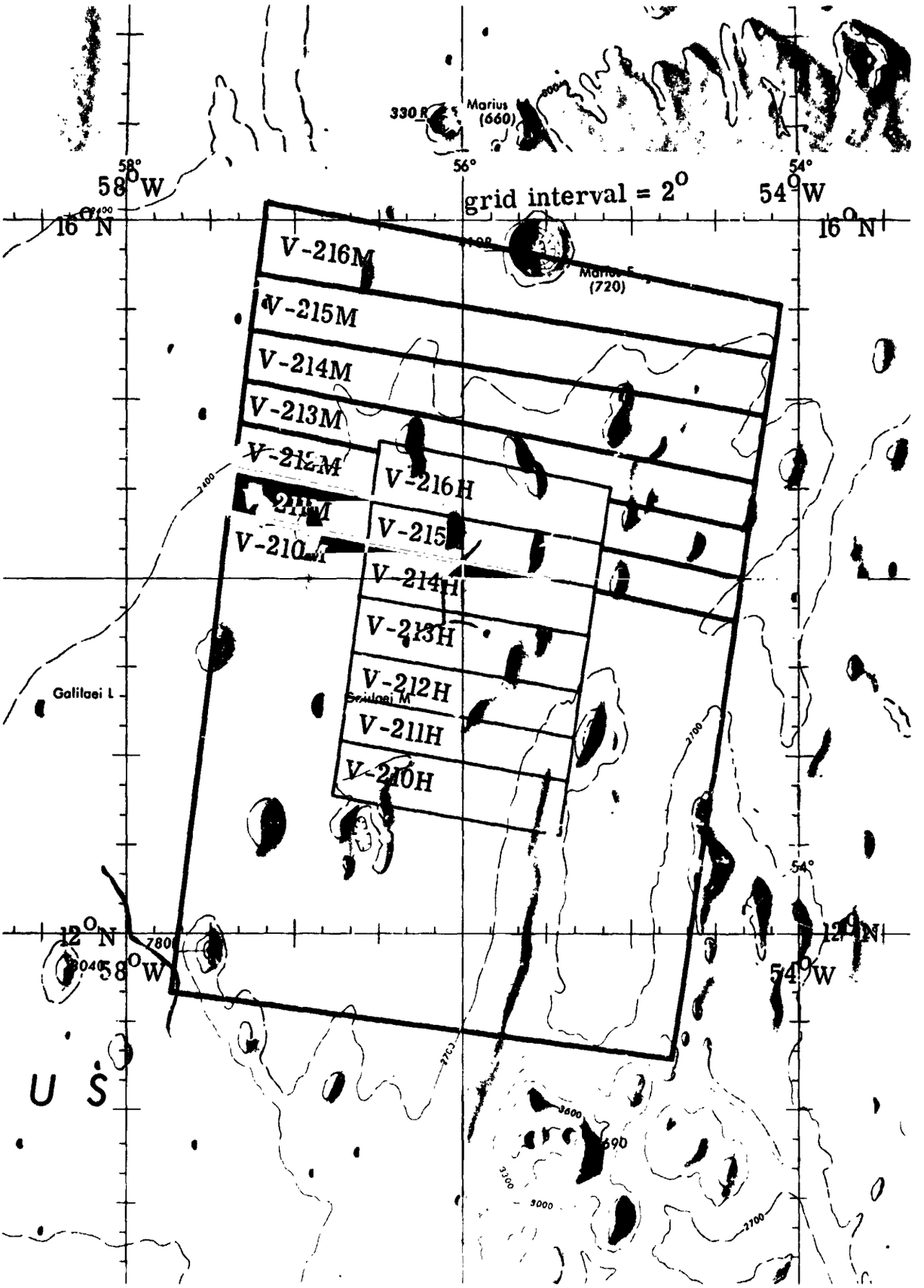
grid interval = 2°
58° W
54° W
16° N
12° N
V-216M
V-215M
V-214M
V-213M
V-216H
V-215H
V-214H
V-213H
V-212H
V-211H
V-210H
Marius
(660)
(720)
Galilaei L
Galilaei M
U S

Site V-51.

MARIUS HILLS
LO V SITE 51 M-214
NORTH

HYGINUS RILLE

Geological Description

The crater Hyginus (8°08'N, 6°24'E) is located south-southeast of Mare Vaporum at the juncture of the two branches of the Hyginus linear rille. The crater is 10 km in diameter and is characterized by a very low rim and numerous domical hills on the crater floor. Two linear rille branches of *Rima Hyginus* trend northwest and east and are characterized by associated chains of low-rimmed craters. *Rima Hyginus* appears to be a structural graben, formed in Imbrium plains-forming units. The northwest rille segment is in the Cayley Formation. Smooth plains-forming units surrounding Hyginus Crater may be of volcanic origin and closely related to the origin of the crater. The eastern rille segment is in a widespread upland plains-forming unit (possibly Cayley) whose origin is not well understood. The craters associated with Hyginus rille are morphologically similar to terrestrial volcanic craters known as maars. On Earth, deposits associated with this type of volcanic crater often contain samples brought up from deep within the mantle. The primary objectives at this landing site are the sampling of possible deep-seated material and the plains-forming material in the vicinity of Hyginus crater and rille.

Scientific Objectives

1. Sampling the ejecta fields of the crater Hyginus or the associated lobate crater.
2. Sampling the ejecta fields of the crater chains associated with Rima Hyginus in search for xenoliths or deep-seated rock fragments.
3. Sampling the plains-forming (Cayley Formation) materials in the vicinity.
4. Studying the structures along the walls of Rima Hyginus in search for layering or banding.
5. Emplacing geophysical experiments.

Reference Material

Photography:

Mission	Magazine	Frame Number
Orbiter III		H-73 (oblique)
Orbiter IV		-97 (2/3)
		-97 (3/3)
		-102 (2/3)
		-102 (3/3)
Orbiter V		M and H-94
		-95
		-96
		-97
Apollo 10	S	4811* (oblique)
↓	S	4813 ↓
	R	4648
	R	4649
	R	4650
	R	4651*
	R	4652

*Recommended

Cartography:

Type Map	Item	Scale
Topographic	LAC 59	1,000,000
Topographic	AIC 59B	500,000
Topographic	AIC 59C	500,000
Geologic	Mare Vaporum (LAC 59) D. Wilhelms, 1968 USGS Map I-548	1,000,000
Photomosaic	Rima Hyginus (V-23.1)	200,000
Topocom		
Photomap	Rima Hyginus	250,000
Topocom		

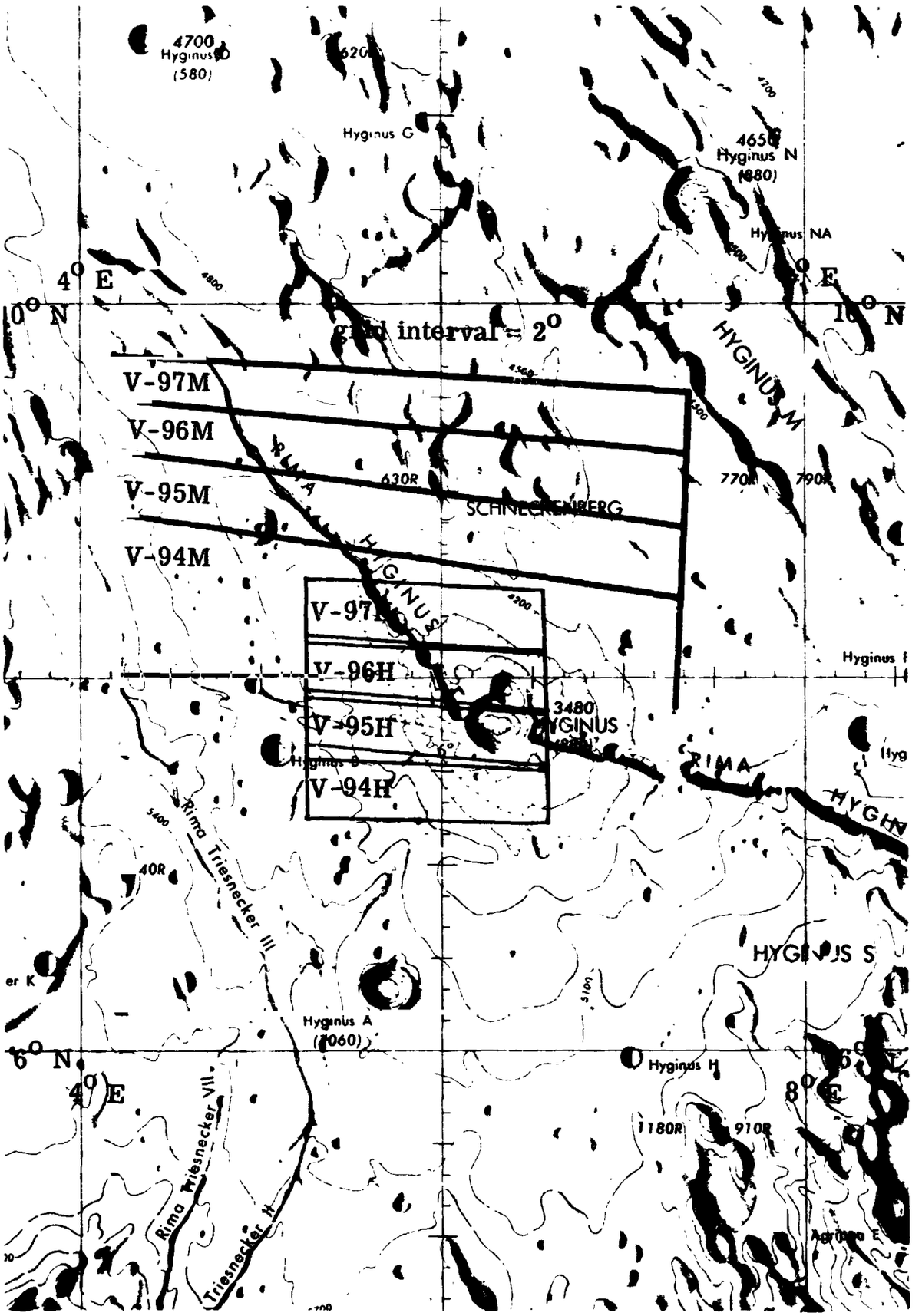
4700
Hyginus D
(580)
Hyginus G
4650
Hyginus N
(880)
Hyginus NA
4° E
0° N
grid interval = 2°
V-97M
V-96M
V-95M
V-94M
RIMA HYGINUS
630R
SCHINEEBERG
770R
790R
HYGINUS M
V-97H
V-96H
V-95H
V-94H
3480
HYGINUS
Hyginus F
Hyginus B
RIMA
HYGINUS
Rima Triesnecker III
40R
HYGINUS S
Hyginus A
(1060)
6° N
4° E
Hyginus H
8° E
1180R
910R
Rima Triesnecker VII
Triesnecker H

Site V–23.1.


RIMA HYGINUS
LO V SITE 25.1 M-46

TYCHO

Geological Description

Crater Tycho (40°56'S, 11°15'W) is a very young impact crater 85 km in diameter in the southern lunar highlands. Bright rays from Tycho spread across the near side of the Moon. A mission to the northern crater rim of Tycho would land in the vicinity of the Surveyor VII spacecraft. Principal mission objectives include investigation of highland composition and of features associated with a young large impact crater. The origin and nature of the ejecta, flows, and associated volcanism located on the crater rim are of interest in this regard. Since Tycho is approximately 4 km deep, the ejecta material should provide samples from deep within the highlands. The composition and age of this material will provide important information about the formation and evolution of the lunar highlands. Establishment of the age of the relatively young event which produced Tycho will add an important point to the lunar time scale.

Geological Description

Scientific Objectives

1. To sample the highland material excavated and ejected by the impact event that created the crater Tycho.
2. To sample and study the post-impact flows and ponds of dark material.
3. To study and sample the Surveyor VII Spacecraft and its vicinity including the rocks it analyzed and the trenches it dug.
4. To emplace geophysical instruments.
5. To obtain metric and high resolution photography on this high inclination orbit mission to the "southern highlands."

Reference Material

Photography:

Mission	Frame Number
Orbiter IV	H-119 (2/3)
	-124 (2/3)
Orbiter V	M, H-125
	-126
	-127
	-128+

Cartography:

Type Map	Item	Scale	Type Copy
Topographic	LAC-112	1,000,000	Litho

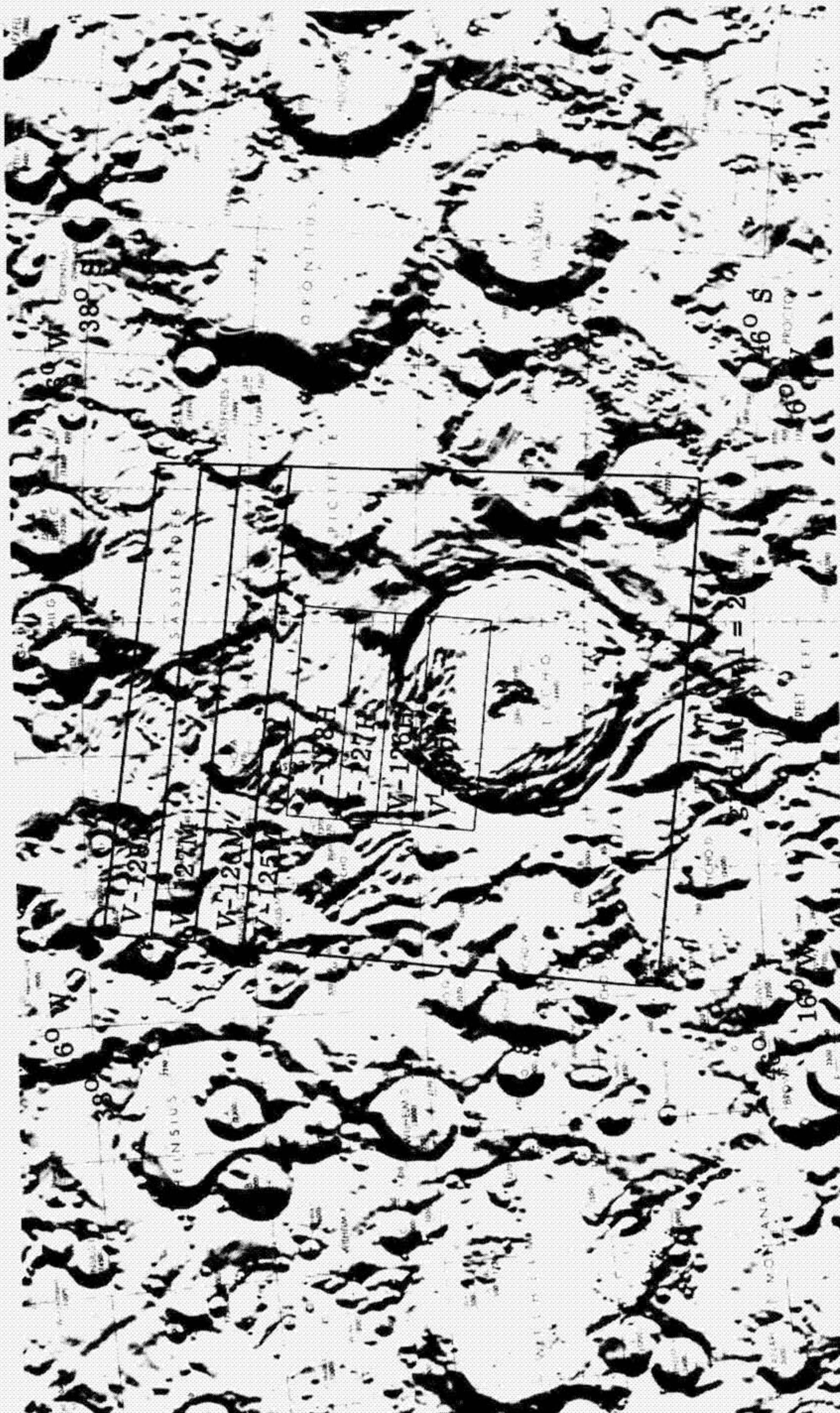

SITE V-30.

CRATER TYCHO
LO V SITE 30 M-126
NORTH

CRATER TYCHO
LO V SITE 301 H-127 1/3
NORTH

HADLEY-APENNINES

Geological Description

Rima Hadley (24°57′N, 2°27′E) is a V-shaped lunar sinuous rille which parallels the Apennine Mountain front along the eastern boundary of Mare Imbrium. The rille is in mare material of Eratosthenian age. The rille apparently originates in an elongate depression in an area of associated volcanic domes and generally maintains a width of about 1 km and a depth of 200 meters until it merges 100 km to the north with a second rille of apparent structural origin. The origin of sinuous rilles such as Rima Hadley is enigmatic but is probably due to some type of fluid flow. The Apennine Mountains rise up to 2 km from the area of Rima Hadley and probably contain ancient material exposed during the excavation of the Imbrium basin. The determination of the nature and origin of a sinuous rille and its associated elongate depression and deposits will provide information on an important lunar surface process and may yield data on the history of lunar volatiles. Sampling of Apenninian material should provide very ancient rocks whose origin predates the formation and filling of the major mare basins.

Scientific Objectives

1. Sampling the pre-Imbrium materials of the Apennine Mountain front and studying the structures and textures displayed.
2. Sampling and studying the material within the sinuous rille (Rima Hadley).
3. Sampling the material surrounding the Hadley C crater for clues of its origin.
4. Sampling the mare material of Palus Putredinis for comparison with other mare samples.
5. Emplacing and conducting geophysical experiments and atmosphere detection devices.

Reference Material

Photography:

Mission		Frame Number
Orbiter IV		H-102 (3/3)
		-103 (1/3)
		-109 (3/3)
		-110 (1/3)
Orbiter V		M-H-104
		-105
		-106
		-107
		Stereo Pan Frames
Apollo 15	Rev 27	9425 and 9430
		9427 9432
		9429 9434
		9431 9436

Cartography:

Type Map	Item	Scale
Topographic	LAC-41	1,000,000
Geologic	Montes Apenninus Region (41) R. J. Hackman, 1966 USGS Map I-463	1,000,000
Geologic	Apennine-Hadley Region Apollo 15 pre-mission M. H. Carr, K. A. Howard, F. El-Baz, 1971 USGS Map I-723	
Photomosaic	Rima Hadley (V26.1b)	200,000
TOPOCOM Topographic Orthophotomap NASA	Hadley	250,000

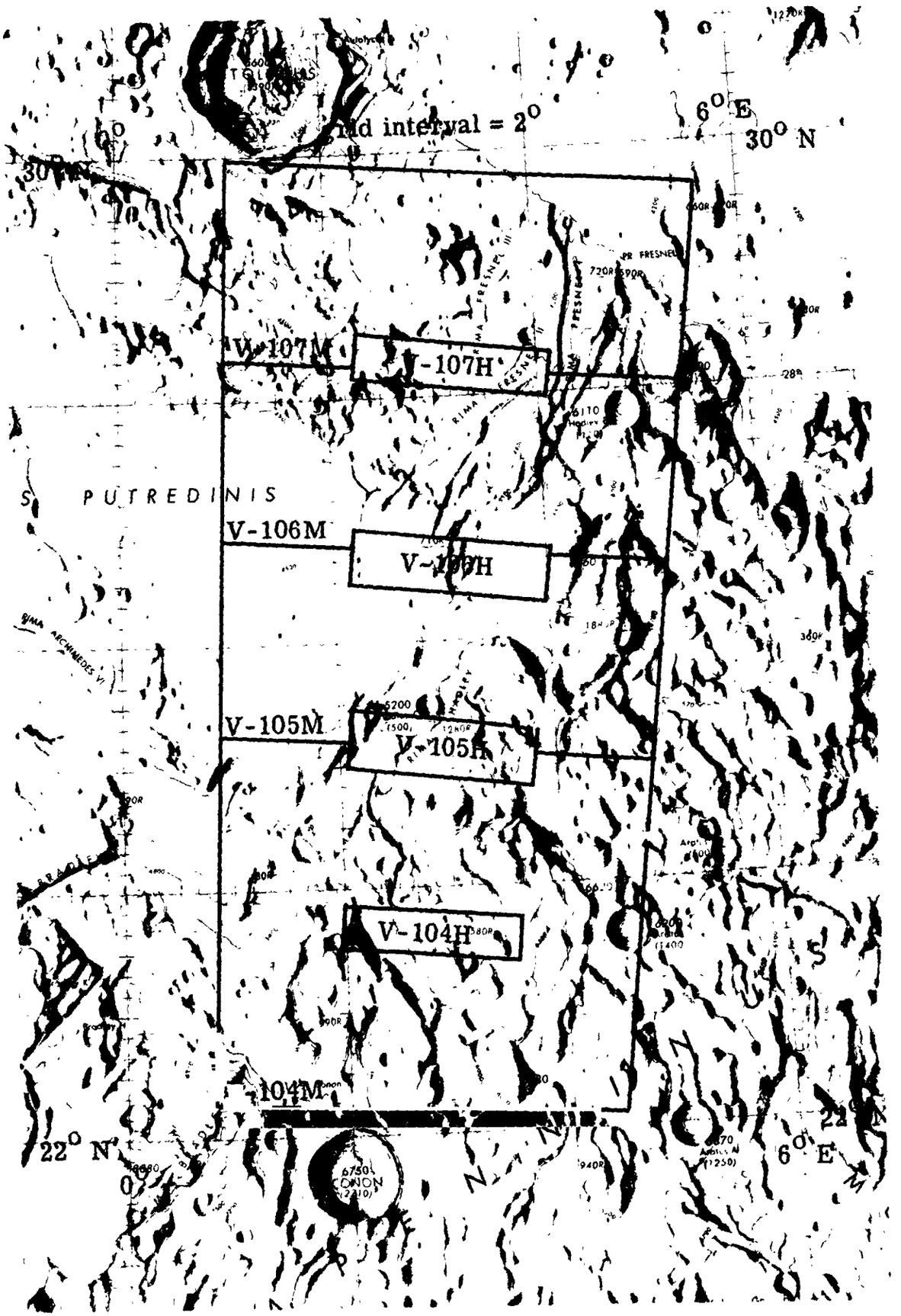
Grid interval = 2°
6° E
30° N
V-107M
V-107H
PUTREDINIS
V-106M
V-106H
V-105M
V-105H
V-104H
104M
22° N
6° E

Site V-26.1.

RIM HADLEY
LO V SITE 26.1 M-105 NORTH

With permission, reprinted from Journal of Geological Education, vol XIX, no. 1, Jan. 1971

Use of Lunar Orbiter Photographs In Earth Science Courses

George E. McGill and Paul A. Chizook, University of Massachusetts, Amherst

INTRODUCTION

In recent years, the national Aeronautics and Space Administration has generated a large volume of material of interest to earth scientists. Much of it is eminently suitable for use in elementary earth science and geology courses, or in more advanced courses such as stratigraphy. This material is generally not difficult to obtain, but it is almost impossible for someone not actively using it to know which of the many thousands of photographs are best for geologic studies.

This paper suggests a very small number of Lunar Orbiter photographs that we believe are superior for illustrating geologic features and the principles of stratigraphy and historical geology. Only Orbiter photographs are considered. Some of the Apollo pictures currently becoming available are certainly spectacular, but few are as suitable as the Orbiter photographs for general geologic purposes. Reference to available Apollo photographs is included in the appendix, which also includes information on ordering Orbiter photographs, lunar maps, and other useful materials.

Three books and one general geologic map are particularly useful, and should be available to students for reference. These are: Mutch (1970), Kosofsky and El-Baz (1970), Lowman (1969), and Wilhelms and McCauley (in press).

Mutch's book is an excellent survey of lunar geology which strongly emphasizes stratigraphy and historical geology, and which has a good bibliography. The Kosofsky and El-Baz book contains many Orbiter pictures organized to show the classical features of the lunar surface, as well as a lucid section on the technology of the Orbiter missions. Its only drawback is the poor reproduction of many of the pictures. The Lowman book is similar, but with more emphasis on geologic features and much better reproduction of photographs. It has a particulary good section on crater characteristics. Finally, the geologic map provides an excellent overview of lunar geology.

The usefulness of Orbiter photographs is greatly enhanced if their locations are known. Consequently, indexes for each Orbiter mission plus some sort of lunar chart are desirable (see appendix). Other basic information such as scale, location of north etc. must be determined for each photograph by the user. Even though lengthy data sheets are provided with each photograph, some small but important details are omitted and some definitions could be clearer. Consequently, the most important parameters and conventions are defined and discussed in the following paragraphs.

PHOTOGRAMMETRY

The pictures from each Lunar Orbiter mission are cataloged by frame numbers, each frame number including a low-resolution (or medium-resolution or moderate-resolution; the terms seem to be used interchangeably), and three high-resolution photographs. The high-resolution photographs cover a small area in the center of the larger area included in the low-resolution photograph. Actually, the high-resolution photographs are one long, narrow photograph cut into three pieces for convenience. Thus photograph IV-109M is a Lunar Orbiter Mission Four low-resolution photograph, and photographs IV-109H_1, IV-109H_2, and IV-109H_3 are the three high-resolution photographs centered within the area of IV-109M. "High resolution" is strictly a relative term, and is based on a comparison with other pictures taken on the same mission. Orbiter V medium-resolution pictures provide a higher resolution than Orbiter IV high-resolution pictures.

Every photograph is divided into many long, narrow, numbered framelets which are 18.2mm wide on

the standard 20"x24" print. These framelets are artifacts of the system used to transmit the photographic images from the spacecraft to earth. On Orbiter V photographs, the framelet boundaries are oriented approximately north-south whereas on most Orbiter I, II, III, and IV photographs they are oriented approximately east-west. On pictures taken of the visible face of the moon, illumination is from the east. For a more complete discussion of the photographic system, see Kosofsky and El-Baz (1970) or Beeler and Michlovitz (1969).

Locations are given in terms of a lunar latitude and longitude system exactly analagous to the one used on earth; that is, the equator divides the moon into northern and southern hemispheres, and an arbitrary prime meridian passing through the center of the visible face of the moon divides it into eastern and western hemispheres. East is defined, as on earth, as being to the right of an observer standing on the moon facing north. On the data sheets, positive values of latitude are north; positive values of longitude are east. South and west values are thus recorded as negative. Latitude and longitude coördinates of the corners, and lengths of the sides in kilometers are given for each photograph. Figure 1 illustrates this, using frame IV-109 high-resolution as an example. It is important to orient the photographs as shown so that the corners are properly matched to the data-sheet print-out. Note also that dimensions and coördinates given are for all three high-resolution photographs reassembled into one long, narrow photograph.

Of the thirty-four photogrammetric parameters defined on the data sheets, six are of major importance for our purposes. These are:

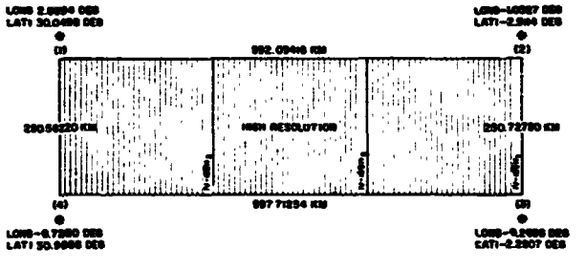

Figure 1: Orientation of photographs for determination of corner co-ordinates. Low-resolution photographs also oriented with legend to right. This orientation places north approximately to the left on L.O. IV photographs, north approximately up on L.O. V photographs. The array of numbers is copied from the data sheet for frame 109; the outlines of the pictures have been added by the writers for clarity. Numbers (1 to 3 from right to left) for the three parts of the photograph follow the NASA-LRC system.

1) SCALE FACTOR: The number of meters *on the film in the spacecraft* equal to one kilometer on the lunar surface. Two listings are included on the data sheets, one for high-resolution, and the other for low-resolution photographs. For the standard 20"x24" prints, these must be multiplied by the enlargment factor of 7.18. For example, the scale on a 20"x24" print for frame IV-109, high-resolution, would be:

SCALE = 7.18 x SCALE FACTOR (HIGH)
= (7.18) (0.0002265M/Km)
= 0.001627M/Km = 1.627mm/Km
or, 1mm = 0.615Km = 615M

2) NORTH DEVIATION ANGLE: the angle, measured *clockwise* from the *normal* to framelet boundaries, to north (see Figure 2 for proper orientation of photograph and measurement of angle).

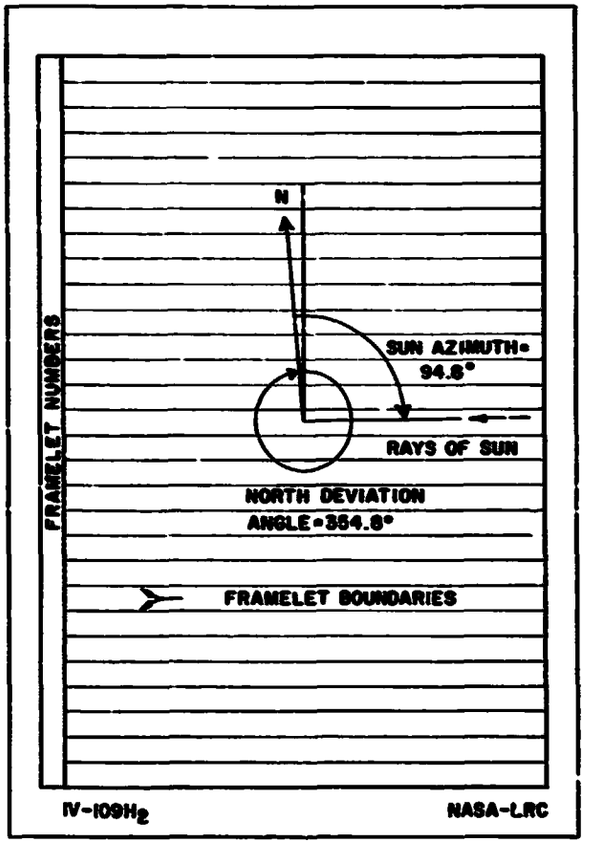

Figure 2: Determination of north and sun azimuth on Orbiter photographs.

3) SUN AZIMUTH at PRINCIPAL GND. PT.: the angle measured *clockwise* from north to the direction from which the sun's rays are coming (see Figure 2).

4) EMISSION ANGLE: the angle between camera axis and the normal to the moon's (idealized) surface at the point where the camera axis intersects the ground (see Figure 3). The *EMISSION ANGLE* provides a measure of obliqueness of the photograph (a 0° *EMISSION ANGLE* means a vertical photograph). On photographs with an *EMISSION ANGLE* of more than a few degrees, surface features are distorted and accurate measurement becomes very difficult.

5) RESOLUTION CONSTANT: the theoretically determined diameter of the smallest object distinguishable on the high-resolution photographs. The smallest distinguishable object on the low-resolution photograph has a diameter eight times larger than the listed *RESOLUTION CONSTANT*.

6) INCIDENCE ANGLE: the vertical angle between the rays of the sun and the normal to the lunar surface (Figure 3).

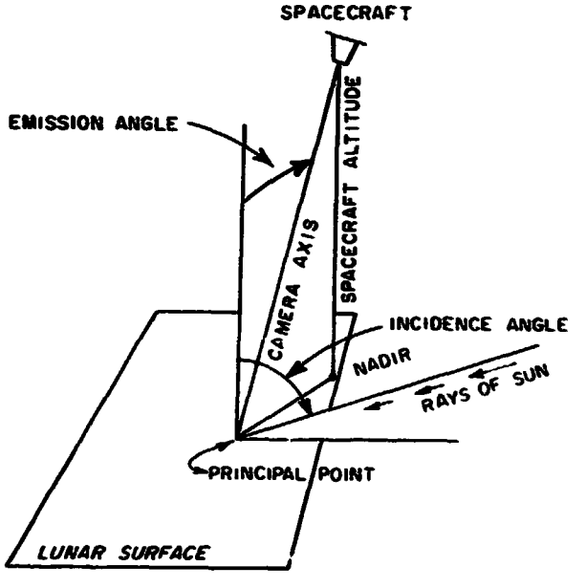

Figure 3: Geometrical definitions of some photogrammetric parameters.

Once the scale has been computed (see above), the *INCIDENCE ANGLE* may be used in conjunction with Figure 4 to determine the height of mountains and walls above adjacent lowlands (see explanation to Figure 4).

SELECTED PHOTOGRAPHS

Introduction

Twenty-six photographs are recommended for use in courses. These are either single photographs or nested sets considered superior for a particular feature or use, or nested sets that illustrate a wide range of features at different scales. The descriptions which follow are intended to provide a general idea of the features illustrated. Exhaustive decriptions are unnecessary and undesirable in the present context.

Most of the photographs are from Lunar Orbiter Mission IV and V, a not surprising result considering that these missions were specifically designed to yield information of geologic value. These provide a wide range in scale, from Orbiter IV low-resolution pictures which show a major portion of the lunar disk at scales of several kilometers per millimeter, to Orbiter V high-resolution pictures with scales on the order of 25 meters to the millimeter.

General Nested Sets

The general nested sets may be used with reasonable success for a number of different purposes. For those with limited time for lunar geology or limited budgets, use of one of these sets is probably the best approach. Both nests include an Orbiter IV low-resolution photograph approximately centered on the area covered by the higher resolution photographs. These low-resolution photographs not only clearly show well-known

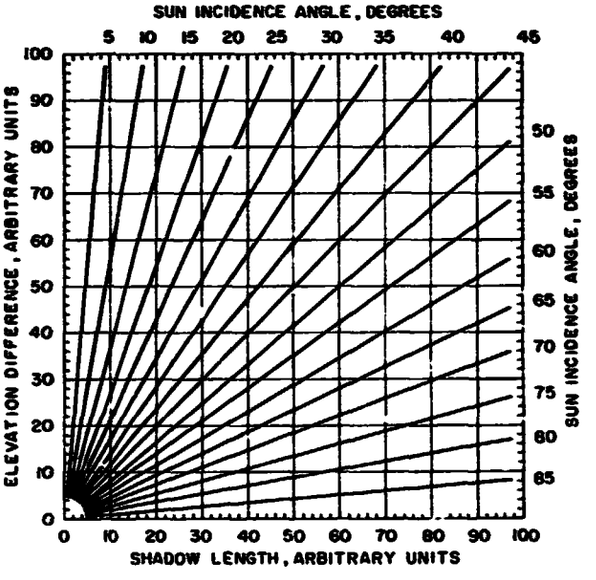

Figure 4: Diagram for determining relative heights from shadow length. Follow shadow length upward until proper incidence angle value (lines radiating from origin) is intersected, and read corresponding relative height value along left margin in same units used to measure shadow length. Shadow length must be measured directly down sun. It is easier to use the diagram if the decimal point is placed in scales so that determination is as close to the right-hand margin as possible. Decimal point in scales may be moved from one measurement to the next because units are arbitrary. It is, in fact, permissible to multiply shadow length by any factor needed to move reading away from congested lower-left corner of diagram. Elevation difference obtained must, of course, be divided by the same factor.

craters, mountain ranges, maria, etc., but are also sharp enough to permit recognition of the major mappable stratigraphic units. Moreover, they provide a regional framework for the more detailed pictures in the nested set.

1) *Fra Mauro nest*: Photographs IV-114M; IV-120H_3; V-139M; V-139H_1; V-139H_2; V-139H_3. Centered on junction of craters Fra Mauro, Perry, and Bonpland (8° S. Lat., 17° W. Long.). Included on Riphaeus Mountains quadrangle (LAC 76), geology by Eggleton (1965).

Photograph IV-120H_1 is usable for stratigraphic studies, showing pre-Imbrian material on the crater rims, part of the Imbrian ejecta blanket (Fra Mauro Formation), and smooth plains divisible into two or three stratigraphic units. A wide range of crater ages is also present. Some of the dark material is associated with and covers a rille, and may be volcanic. This material is shown in greater detail on V-139M and V-139H_2. Age relationships between graben-like rilles and stratigraphic units are well shown on IV-120H_3 and V-139M. The Orbiter V high-resolution photographs illustrate such surficial details as variation in morphology of small craters (presumably a function of age), patterned ground on slopes, concentrations of large blocks of rock (not a very good example for this feature), and variation in crater density.

2) *Alphonsus nest*: Photographs IV-108M; IV-108H_2; V-117M; V-118H_2; V-118H_3. Centered on western rim of crater Alphonsus (14° S. Lat., 4° W. Long.). Largely included on the Ptolemaeus quadrangle (LAC 77), geology by Howard and Marsursky (1968).

Photograph IV-108H_2 shows pre-Imbrian material in the rims of old craters modified by the Imbrian "sculpture," and younger smooth plains materials divisible into two or three mappable units. A moderately good range of crater ages is present. The three major craters—Ptolemaeus, Alphonsus and Arzachel—show different degrees of rim degradation, suggesting that they are of different ages.

Alphonsus has several dark spots on its floor spatially related to rilles and pits. One of these spots is shown in detail on V-117M and V-118H_2. The latter photography clearly illustrates the difference in crater density between the dark spot and a lighter area of crater floor in the northwestern corner of the photograph. These dark spots are suggestive of volcanic activity, as is a crater chain in the northwestern corner of IV-108H_2.

Photographs V-118H_2 and V-118H_3 also provide an excellent example of patterned ground, and show variation in morphology of small craters. The crater Arzachel illustrates large-scale slumping of crater walls (photograph IV-108H_2). Both Arzachel and Alphonsus have central peaks.

If only one nest is obtained, the one to get will depend on the user's primary objectives. The Fra Mauro set includes the better low-resolution Orbiter IV photograph because it is centered near the southern margin of Mare Imbrium which is used as the type area for lunar mapping by the U.S. Geological Survey. In addition, photograph IV-120H_3 is better for stratigraphic studies than is IV-108H_2. On the other hand, the Alphonsus set includes more convincing examples of volcanic features and deposits, as well as better examples of patterned ground, slumping of crater walls, and the correlation of crater density with relative age.

Photographs for Stratigraphic Studies

On the basis of clarity of superposition and cross-cutting relationships, the number of mappable units, and the total relative age range present, three photographs (IV-109H_3, IV-169H_2, and IV-97H_2) are considered superior single photographs for stratigraphic studies. Mapping units may be distinguished from each other by albedo (relative brightness), crater density, and topographic texture. They may be arranged in stratigraphic sequence by superposition, embaying relationships, crater density, and contrasting relationships with structural features such as craters and rilles. Good general summaries of the lunar stratigraphic scheme are those by Shoemaker (1964), McCauley (1967b), Mutch (1970, p. 117-139), and Wilhelms (in press). The scheme has changed somewhat with time, as best explained by McCauley (1967b) and Wilhelms (in press).

Photograph IV-109H_3, which is probably the best of the three, is in the southeastern part of Mare Imbrium and includes most of the crater Archimedes. The area is included on the Montes Apenninus quadrangle (LAC 41), geology by Hackman (1966). Photograph IV-169H_2 is next best and is along the southwestern edge of Oceanus Procellarum. No published quadrangle includes this area. The third photograph, IV-97H_2, is included on four quadrangles: Mare Vaporum (LAC 59), geology by Wilhelms (1968); Julius Caesar (LAC 60), geology by Morris and Wilhelms (1967); Mare Serenitatis (LAC 42), geology by Carr (1966); and Montes Apenninus (LAC 41), geology by Hackman (1966).

Photograph IV-114M from the Fra Mauro nest may be used to provide a regional frame for both IV-109H_3 and IV-97H_2.

Photographs of Specific Features

1) *Volcanic landforms*: Photographs IV-157H_2, V-214M; and V-216H_3, on Hevelius quadrangle (LAC

56), geology by McCauley (1967a) constitute a nested set showing the Marius Hills in the center of Oceanus Procellarum. This area provides the most convincing evidence of volcanism on the moon (McCauley, 1967a; Mutch, 1970, p. 217-231). The Orbiter IV photograph is covered with domes and steep-sided peaks, many with summit pits, plus sinuous rilles and wrinkle ridges. The higher resolution pictures supply many interesting details, including crater types directly comparable to types associated with terrestrial volcanism. Photograph II-213M is an interesting oblique view of this area, but because this picture has been reproduced by Mutch (1970, p. 218), by Kosofsky and El-Baz (1970, p. 122), and by Lowman (1969, plate 86), it is probably not necessary to buy it.

2) *Impact crater morphology*: Photographs V-197; V-199H_2; and V-201H_3, on Aristarchus quadrangle (LAC 39), geology by Moore (1965). The medium-resolution photograph clearly shows the radial zoning of the raised rim of Aristarchus, slumping of the inner wall of the rim, the radial array of secondary craters, the central peak, and numerous minor characteristics. Shoemaker (1962) presents a discussion of the characteristics and probable origin of craters similar to Aristarchus. Photograph V-199H_2 is a close-up of the northern portion of the inside of the crater showing numerous concentrations of large boulders, the peculiar "blistery" topography of much of the crater floor, and patterns suggestive of the flow of some fluid material down the inner wall of the rim. Photograph V-201H_3 is a close-up of a portion of the outer rim. It includes some of the most convincing flows on the moon—features with lobate forms raised above the surroundings, smoother and darker surfaces than surrounding terrain, and very low crater densities.

3) *Sinuous rille*: V-204M and V-204H_3 on Aristarchus and Seleucus quadrangles (LAC 39 and 38), geology by Moore (1965 and 1967), are a nested pair of photographs of a portion of Vallis Schröteri on the Aristarchus Plateau in Oceanus Procellarum. This sinuous rille has a smaller, meandering rille within it which shows what appears to be a cut-off meander and partial burial of a meander loop by talus from the wall of the larger rille. This meandering inner rille is particularly controversial because it so closely resembles terrestrial stream channels, yet may have a totally different origin (e.g., Schumm, 1970).

Photograph V-204M includes a small segment of the crater Aristarchus in the southeastern corner, and the radial array of secondary impacts from this crater covers nearly half the photograph. Patterned ground and boulder concentrations at the bases of slopes are visible on V-204H_3, with one visible track left by a rolled boulder in framelet 202.

4) *Crater chain*: Photographs V-94M and V-95H_1, on Mare Vaporum quadrangle (LAC 59), geology by Wilhelms (1968). This is a nested pair of the Hyginus Rille, near the center of the visible disk. This feature is large enough to be clearly visible on the low-resolution Orbiter IV photographs listed under the nested sets. Rima Hyginus is the classic example of a rille that is also a crater chain. The craters of the chain have been interpreted as volcanic by Wilhelms (1968). The lunar surface appears darker and possibly slightly less cratered near the rille than elsewhere, perhaps due to a covering of pyroclastic deposits. The high-resolution photograph shows a portion of the largest crater (Hyginus) along the rille, a crater very different in appearance from those generally explained as due to impact. The walls of this crater show patterned ground, boulder concentrations, and some good examples of tracks left by rolled boulders.

5) *Maria vs. terrae*: Photographs III-213M and IV-161H_3, on Grimaldi quadrangle (LAC 74) illustrate the contrasts between maria and terrae in topography, albedo, smoothness, and fracture patterns. Photograph III-213M is an oblique picture of a portion of the western shore of Oceanus Procellarum, whereas IV-161H_3 is a partially overlapping vertical photograph. Although the primary purpose of these photographs is to illustrate the differences between the two major types of terrain on the moon, they also provide excellent views of wrinkle ridges, graben-like rilles, a crater with a floor webbed by branching rilles, and a systematic grid-like alignment of small topographic forms on the terrae. The photographs are also useful for illustrating the distortion created by oblique views.

ACKNOWLEDGMENTS

Lunar Orbiter photographs were supplied by the National Space Science Data Center. L. M. Hall and K. Michlovitz kindly read the manuscript; however, the writers are responsible for any remaining errors. The study was partially supported by NSA Grant NGR-22-010-052.

APPENDIX: SOURCES OF MATERIAL

Lunar Orbiter Photographs

The photographs and supporting data are obtained from:
Data Services Branch
National Space Science Data Center
Goddard Space Flight Center
Code 601.4
Greenbelt, Maryland 20771

The first step is to request the following guide to ordering
Beeler, M. and Michlovitz, K., 1969, *Lunar Orbiter Photographic Data*: NASA, NSSDC 69-05.

This publication includes complete Orbiter index maps as

well as instructions for ordering photographs. The 20"x24" prints of the Orbiter photographs referred to in the text of this paper are the NASA-LRC enhancements, which cost about $4.00[1] each. The Data Center will provide all Orbiter photographs on microfilm for $27.00[1]. Although the microfilm versions of the photographs were noticeably degraded in quality, they are very convenient as an aid to ordering additional full-sized prints.

When ordering Orbiter photographs, it is important to emphasize that high resolution pictures are being identified according to the NASA-LRC numbering system (1 to 3 from south to north for L.O. IV. 1 to 3 from east to west for L.O. V). Many people order according to the AMS numbering system which is exactly opposite this one. It may be helpful to tell the Data Center which end of the strip (north or south, east or west) you want in addition to giving them the proper NASA-LRC number. The microfilm set we have is numbered according to the AMS system, so care must also be exercised in placing orders for additional pictures.

Apollo Lunar Photographs

The Data Center also provides copies of Apollo pictures, for which various indexes have been published. Available on request as of October, 1970, are:

1) *Apollo 8 Lunar Photography; 70mm Frame Index*: NASA, NSSDC 69-06.
2) *Apollo 10 Photography Index; 70mm and 16mm Frame Index*: NASA, NSSDC 69-14.
3) *Apollo 11 Photography; 70mm, 16mm, and 35mm Frame Index*: NASA, NSSDC 70-72.
4) *Apollo 11 70mm Photographic Catalog*: NASA, NSSDC 70-07.
5) *Apollo 12 Lunar Photography*: NASA, NSSDC 70-09.
6) *Apollo 12 70mm Photographic Catalog*: NASA NSSDC 70-10.
7) *Apollo 12 Photography; 70mm, 16mm, and 35mm Frame Index*: NASA, NSSDC 70-11.

Charts and Maps

Except for number 1, all the following items are obtainable from:

Superintendent of Documents
U.S. Government Printing Office
Washington, D.C. 20402

1) *U. S. Geological Survey geologic quadrangle maps of the moon*: These are sold by the U.S. Geological Survey, Washington, D.C. for $1.00 each.

2) *U.S. Air Force Lunar Reference Mosaic:* An orthographic projection of the lunar near side identifying major features. Available in two sizes:

a) LEM-1, scale 1:5,000,000 lunar diameter =27 inches, price, $1.00.
b) LEM-1B, scale 1:2,500,000, lunar diameter =54 inches, two sheets, price $2.00.

Both sizes are suitable for hanging on the wall for reference and display.

3. *NASA lunar charts*: The entire moon is covered on three sheets at a scale of about 1:5,000,000. The Earthside and Farside charts (covering a belt between 48°N. and 48° S. latitudes) are Mercator projections, the Polar chart is a polar stereographic projection.

a) Lunar Earthside Chart (LMP-1): price, 50¢.
b) Lunar Farside Chart (LMP-2): price, 50¢.
c) Lunar Polar Chart (LMP-3): price, 50¢.

d) *LAC Charts*: These are a series of 1:1,000.000 charts of the near side of the moon, by quadrangles. Quadrangles are identified both by number and by the name of a prominent feature included. Each chart includes an index to the locations of all charts, price, 50¢ each.

5) *Other charts and publications relating to the moon*: Request from the Superintendent of Documents, the price list for publications dealing with "space."

[1]These prices should be checked with the Data Center before ordering.

REFERENCES CITED

Beeler, M. and Michlovitz, K., 1969, Lunar Orbiter photographic data: Nat. Aeronautics and Space Admin., NSSDC 69-05.

Carr, M. H., 1966, Geologic map of the Mare Serenitatis region of the moon: U.S. Geol. Survey Misc. Inv. Map I-489.

Eggleton, R. E., 1965, Geologic map of the Riphaeus Mountains of the moon: U.S. Geol. Survey Misc. Inv. Map I-458.

Hackman, R. J., 1966, Geologic map of the Montes Apenninus region of the moon: U. S. Geol. Survey Misc. Inv. Map I-463.

Howard, Keith A. and Masursky, Harold, 1968, Geologic map of the Ptolemaeus quadrangle of the moon: U.S. Geol. Survey Misc. Inv. Map I-566.

Kosofsky ,L. J. and El-Baz, Farouk, 1970, *The Moon as Viewed by Lunar Orbiter*. Nat. Aeronautics and Space Admin., NASA SP-200, 152 p.

Lowman, Paul D., Jr., 1969, *Lunar Panorama*. Zurich, Weltflugbild Reinhold A. Müller.

McCauley, John F., 1967a, Geologic map of the Hevelius region of the moon: U.S. Geol. Survey Misc. Inv. Map I-491.

....., 1967b, The nature of the lunar surface as determined by systematic geologic mapping: *Mantles of the Earth and Terrestrial Planets*, Runcorn, S. K., editor, Interscience, p. 431-460.

Moore, H. J., 1965, Geologic maps of the Aristarchus region of the moon: U.S. Geol. Survey Misc. Inv. Map I-465.

....., 1967, Geologic map of the Seleucus quadrangle of the moon: U.S. Geol. Survey Misc. Inv. Map I-527.

Morris, Elliott C. and Wilhelms, Don E., 1967, Geologic map of the Julius Caesar quadrangle of the moon: U.S. Geol. Survey Misc. Inv. Map I-510.

Mutch, T. A., 1970, *The Geology of the Moon*. Princeton Univ. Press, 324 p.

Schumm, S. A., 1970, Experimental studies on the formation of lunar surface features of fluidization: *Geol. Soc. America Bull.*, v. 81, p. 2539-2552.

Shoemaker, Eugene M., 1962, Interpretation of lunar craters: *Physics and Astronomy of the Moon*, Kopal, Z., editor, London, Academic Press, p. 283-359.

....., 1964, The geology of the moon: *Sci. American*, v. 211, no. 6, p. 38-47.

Wilhelms, Don E., 1968, Geologic map of the Mare Vaporum quadrangle of the moon: U.S. Geol. Survey Misc. Inv. Map I-548.

....., Summary of lunar stratigraphy telescopic observations: U. S. Geol. Survey Prof. Paper 599-F, in press.

....., and McCauley, John F., Geologic map of the near side of the moon: U.S. Geol. Survey Misc. Inv. Map, in press.